

# Investigation into the interaction of Dantocol in polymer bonded explosives and bonding agent development

Christopher Allen Williams (BSc.Hons)

Thesis submitted to the School of Chemical and Physical Sciences of the Flinders University of South Australia in partial fulfilment of the requirements for the degree of

Doctor of Philosophy in Chemistry





# Investigation into the Interaction of Dantocol in Polymer Bonded Explosives and Bonding Agent Development

Mr. Christopher Williams\*<sup>1,2</sup>

Assoc Prof Stewart Walker,<sup>1,2</sup> Dr Ian Lochert,<sup>2,3</sup> Dr Stephen Clarke,<sup>4</sup> Prof Paul Kirkbride<sup>1,2</sup>

<sup>1</sup> Centre of Expertise in Energetic Materials

<sup>2</sup> Flinders University, School of Chemical and Physical Sciences

<sup>3</sup> Defence Science & Technology Organisation, Weapon and Combat Systems Division

<sup>4</sup> University of South Australia, Division of Information, Engineering and the Environment

## Abstract

The call for increased safety in explosive ordnance has driven the requirement for improved design of Insensitive Munitions (IM). Cast-cured Polymer Bonded Explosives (PBXs) are often used as an approach to achieving IM compliance. Incorporation of bonding agents is often employed to improve adhesion between particulates and the binder system, however the exact mechanism by which this occurs is poorly understood. In the absence of an appropriate bonding agent, the PBX system is susceptible to mechanical failure via dewetting. This degradative process occurs when the adhesion between filler and binder is poor, causing failure under stress and allowing the binder to break free or ‘dewet’ from the filler surface.

One of the forerunners in bonding agent technology for nitramine-based composites is the Hydantoin derivative 1,3-*bis*(2-hydroxyethyl)-5,5-dimethylhydantoin, known also as Dantocol. This promotes successful interaction between the filler and binder within polymer composites. Investigations revealed non-polar binder matrices applied in this process enable polar Dantocol molecules to adsorb onto the nitramine filler via secondary bonding. Subsequent reaction with the binder system produces primary bonds involving the diisocyanate curative. This reacts with free hydroxyl groups to form urethane linkages, facilitating integration of Dantocol within the binder matrix. The strength of these bonds

dictates the mechanical properties of respective systems, through prevention of deformation mechanisms.

Knowledge of surface characteristics and interacting mechanisms was consequently applied to the design of novel bonding agents. Development of bonding agents focussed on improving mechanical properties of PBXs, with flow-on benefits for explosive ordnance. These advances have the potential to eliminate conjecture regarding the selection of bonding agents and provides viable alternatives for inclusion in cast-cured composite energetic materials.



## Acknowledgments

I would like to take this opportunity to thank the many people that contributed towards the work depicted herein, without whom this would not be possible. First and foremost, the supervision provided by Assoc Prof Stewart Walker, Dr Stephen Clarke, Dr Ian Lochert and Prof Paul Kirkbride went above and beyond expectations. This resulted in a rewarding postgraduate experience, through the provision of intellectual freedom, supporting my attendance at numerous conferences and demanding a high standard of work in all my endeavours.

For stepping into the role of primary supervisor, I am indebted to Assoc Prof Stewart Walker, whose expertise, understanding, and patience was greatly appreciated. Likewise, I would like to extend my gratitude to members of the Walker research group, in particular Paul McCurry who provided valuable insight into the characterisation of energetic materials. Acknowledgments also extend to the Clarke research group, with whom I commenced my postgraduate study. The opportunities provided by Dr Stephen Clarke have shaped my scientific career thus far, and for that I'm inherently grateful. Furthermore, the intellectual contributions of Dr Neil Trout were fundamental to performing the synthesis of novel bonding agents. During our time in the laboratory, his expertise in organic chemistry enabled me to acquire a wealth of related knowledge.

I recognise this research would not have been possible without the financial support of the Centre of Expertise in Energetic Materials (CEEM). I therefore offer my sincere thanks to members of the technical committee, for the opportunity to undertake this project. This extends to the Defence Science and Technology Organisation (DSTO), based upon which CEEM was funded. Practical and intellectual support was also provided by Dr Ian Lochert, Dr Phil Davies, Dr Chad Prior, Craig Wall and Praveen Gangadharan from the Weapon and Combat Systems Division. Further credit is due in relation to work conducted by Dr Merran

Daniels, whose tireless efforts concerning PBX processing and the evaluation of mechanical properties was critical toward conclusions.

I'm also indebted to Dr Andrew Jane, without whose motivation and encouragement, this path may not have been pursued. I must also acknowledge the team at Flinders Analytical, Dr Daniel Jardine, Jason Young and Belinda Wade. The exceptional training and technical support provided by these members was pivotal in expanding my knowledge of analytical chemistry. All mechanical requirements were addressed by Chris Price, from consulting on fittings to fabricating replacement parts for my cherished office chair. His skill and experience regularly proved invaluable in ensuring equipment performed as required. The administrative support provided by Jennie Brand, Dr Sean Graney, Tricia Butterfield and Janette Wale was also pivotal in enabling work to progress without delay.

Finally, I would like to extend my deepest gratitude and appreciation to my friends and family that offered support throughout my time at Flinders University. The faith and encouragement bestowed by my parents and brother was none shy of overwhelming, thereby facilitating this achievement.

## Declaration

I hereby declare all work completed in this thesis was carried out within the School of Chemical and Physical Sciences at Flinders University of South Australia, under the supervision of Assoc Prof Stewart Walker, co-supervised by Dr Stephen Clarke, Dr Ian Lochert and Prof Paul Kirkbride.

I certify that this thesis does not incorporate, without my knowledge, any material previously submitted for a degree or diploma in any university and that, to the best of my knowledge and belief, does not contain any previously published or written by another person except where reference is made in the text.

.....

Mr Christopher. A. Williams

1<sup>st</sup> April 2015

<b>Abstract</b> .....	I
<b>Acknowledgments</b> .....	III
<b>Declaration</b> .....	V
<b>Contents</b> .....	VI
<b>1. Introduction</b> .....	1
1.1 Introduction .....	2
1.1.1 History of Insensitive Munitions .....	3
1.1.1.1 Solid Propellant Systems.....	3
1.1.1.2 Polymer Bonded Explosives.....	3
1.1.1.3 Bonding Agents .....	4
1.1.2 Polymer Bonded Explosives.....	4
1.1.2.1 Binder Systems .....	5
1.1.2.2 Energetic Filler .....	7
1.1.2.3 Bonding Agents .....	8
1.1.2.4 PBX Additives .....	10
1.1.3 Propellant Systems.....	12
1.1.3.1 Propellant Binder Systems .....	12
1.1.3.2 Oxidiser and Metal Fuels .....	13
1.1.3.3 Propellant Bonding Agents .....	13
1.2 Deformation Mechanisms.....	13
1.2.1 Dewetting .....	14
1.2.2 Dewetting of Propellant Systems.....	16
1.2.3 Hydrostatic Tension .....	17
1.2.4 Thermal Expansion .....	17
1.2.5 Diffusion of Moisture.....	18
1.2.6 Trapped Gas.....	18
1.2.7 Deformation Twinning.....	19
1.2.8 Molecular Slip .....	19
1.3 Bonding Agents .....	20
1.3.1 Function of bonding agents .....	20
1.3.2 Commercial Bonding Agents .....	21
1.3.2.1 Polyfunctional Aziridine Amides .....	22
1.3.2.2 HX-752.....	22
1.3.2.3 Tepanol.....	23
1.3.2.4 Tepan.....	24
1.3.2.5 MAPO.....	25

1.3.2.6	BITA .....	26
1.3.2.7	Ferrocene Based Bonding Agents.....	27
1.3.2.8	Dantocol.....	28
1.3.3	Bonding Agent Selection.....	29
1.3.4	Problems Associated With Current Technologies .....	31
1.4	Methods of Evaluating Bonding Agent Activity.....	32
1.4.1	Investigation of Mechanical Properties .....	32
1.4.1.1	Modelling of Interfacial Dewetting .....	32
1.4.1.2	Critical Stress.....	34
1.4.1.3	Surface and Interfacial Tension .....	35
1.4.1.4	Swelling Ratio .....	36
1.4.1.5	Poisson's Ratio .....	37
1.4.1.6	Young's Modulus .....	38
1.4.2	Surface Characterisation .....	38
1.4.2.1	X-Ray Photoelectron Spectroscopy .....	39
1.4.2.2	Infrared Spectroscopy .....	40
1.4.2.3	Microscopy Analysis .....	41
1.4.3	Supplementary Analysis Techniques .....	42
1.4.3.1	Thermal Analysis.....	42
1.4.3.2	Compatibility, Sensitiveness and Mechanical Properties.....	43
1.5	Conclusion.....	43
1.6	References .....	45
<b>2.</b>	<b>Coatings and Characterisation of Dantocol.....</b>	<b>53</b>
2.1	Introduction .....	54
2.2	Experimental.....	56
2.2.1	Preparation and Characterisation of Compounds.....	56
2.2.1.1	Recrystallisation of Dantocol .....	56
2.2.1.2	Recrystallisation of RDX .....	56
2.2.1.3	Nuclear Magnetic Resonance .....	57
2.2.1.4	Fourier Transform Infrared Spectroscopy .....	57
2.2.1.5	Raman Spectroscopy.....	58
2.2.1.6	Scanning Electron Microscopy of Surface Coatings .....	58
2.2.2	Coating Techniques .....	58
2.2.2.1	Slurry Technique .....	59
2.2.2.2	Reverse Slurry Technique .....	59
2.2.2.3	Starved Addition Technique.....	59

2.2.2.4	Solvent/Antisolvent Technique .....	60
2.2.2.5	Aqueous Suspension/Melting Technique.....	60
2.2.2.6	Microencapsulation.....	60
2.3	Results .....	61
2.3.1	Characterisation of Dantocol and RDX.....	61
2.3.1.1	Characterisation of Dantocol.....	61
2.3.1.2	Characterisation of RDX.....	63
2.3.2	Coating Techniques .....	64
2.3.2.1	Slurry Technique .....	64
2.3.2.2	Reverse Slurry Technique .....	67
2.3.2.3	Starved Addition Technique.....	68
2.3.2.4	Solvent/Antisolvent Technique .....	69
2.3.2.5	Aqueous suspension-melting technique.....	71
2.3.3	Microencapsulation.....	71
2.3.3.1	Solvent Evaluation.....	72
2.3.3.2	Mixing Conditions .....	75
2.3.3.3	Solvent Removal.....	77
2.3.3.4	Surfactant additives.....	78
2.3.3.5	Microencapsulation Procedure .....	79
2.4	Conclusion.....	79
2.5	References .....	81
<b>3.</b>	<b>Characterisation of interfacial interactions by FTIR.....</b>	<b>83</b>
3.1	Introduction .....	84
3.1.1	Comparison of FTIR Techniques .....	84
3.1.1	Attenuated Total Reflectance.....	86
3.1.2	Transmission Infrared Spectroscopy .....	86
3.1.3	Photoacoustic Spectroscopy.....	87
3.1.4	Diffuse Reflectance Infrared Fourier Transform Spectroscopy .....	88
3.2	Experimental.....	89
3.2.1	Fourier Transform Infrared Spectroscopy Techniques .....	89
3.2.1.1	Attenuated Total Reflectance .....	89
3.2.1.2	Transmission Spectroscopy .....	90
3.2.1.3	Photoacoustic Spectroscopy .....	90
3.2.1.4	Diffuse Reflectance Infrared Fourier Transform Spectroscopy.....	91
3.2.2	Advanced Signal Processing in the Resolution of Spectral Bands .....	91
3.2.2.1	Fourier Self-Deconvolution.....	91

3.2.2.2	Curve-Fitting .....	92
3.3	Results .....	92
3.3.1	Characterisation of Interfacial Interactions by FTIR .....	92
3.3.1.1	Attenuated Total Reflectance .....	93
3.3.1.2	Transmission Spectroscopy .....	97
3.3.2	Hydrogen Bonding .....	99
3.3.2.1	Fourier Self-Deconvolution.....	100
3.3.2.2	Curve Fitting.....	102
3.3.2.3	Bonding Index .....	104
3.3.3	Highly Surface Sensitive Techniques .....	106
3.3.3.1	Investigation of Interfacial Interactions via PAS .....	106
3.3.3.2	Investigation of interfacial interactions via DRIFTS.....	110
3.3.4	Dipole Interactions.....	113
3.3.5	Investigation of RDX Particle Size.....	115
3.3.6	Interaction of Dantocol and HMX .....	116
3.4	Conclusion.....	118
3.5	References .....	122
<b>4.</b>	<b>Hydroxyl protection of Dantocol .....</b>	<b>127</b>
4.1	Introduction .....	128
4.1.1	Silylation of Hydroxyl Groups .....	128
4.1.2	Intermolecular Forces.....	129
4.2	Experimental.....	131
4.2.1	Synthesis of Hydroxyl Protected Dantocol .....	131
4.2.1.1	1,3- <i>bis</i> (2-trimethylsilyloxyethyl)-5,5-dimethylhydantoin.....	131
4.2.1.2	<i>N</i> -(2-hydroxyethyl)- <i>N</i> -(2- <i>tert</i> -butyldimethylsilyloxyethyl)-5,5-dimethyl- hydantoin.....	132
4.2.2	Characterisation of Hydroxyl Protected Dantocol .....	134
4.2.2.1	Fourier Transform Infrared Spectroscopy .....	134
4.2.2.2	Nuclear Magnetic Resonance .....	134
4.2.2.3	Scanning Electron Microscopy.....	134
4.3	Results .....	134
4.3.1	1,3- <i>bis</i> (2-trimethylsilyloxyethyl)-5,5-dimethylhydantoin.....	135
4.3.1.1	Characterisation of Disilylated Dantocol .....	135
4.3.1.2	Interaction of Disilylated Dantocol and RDX .....	137
4.3.2	<i>N</i> -(2-hydroxyethyl)- <i>N</i> -(2- <i>tert</i> -butyldimethylsilyloxyethyl)-5,5-dimethyl- hydantoin .....	140
4.3.2.1	Characterisation of Monosilylated Dantocol .....	140

4.3.2.2	Interaction of Monosilylated Dantocol and RDX .....	143
4.3.3	Intermolecular Forces Between Dantocol and RDX.....	146
4.4	Conclusion.....	147
4.5	References .....	149
<b>5.</b>	<b>Thermal analysis of bonding agent interaction .....</b>	<b>153</b>
5.1	Introduction .....	154
5.1.1	Differential Scanning Calorimetry.....	155
5.1.1.1	Glass Transition Temperature .....	155
5.1.1.2	Melting Point.....	155
5.1.1.3	Sublimation .....	156
5.1.1.4	Thermal Stability and Compatibility.....	157
5.1.1.5	Critical Temperature .....	158
5.1.2	Thermogravimetric Analysis .....	158
5.2	Experimental.....	159
5.2.1	Differential Scanning Calorimetry.....	159
5.2.2	Pressure Differential Scanning Calorimetry .....	159
5.2.3	Thermogravimetric Analysis .....	160
5.3	Results .....	160
5.3.1	Differential Scanning Calorimetry of Coated RDX.....	161
5.3.1.1	Sublimation Temperature.....	164
5.3.1.2	Thermal Stability and Compatibility.....	167
5.3.1.3	Critical Temperature .....	170
5.3.2	Thermogravimetric Analysis .....	171
5.4	Conclusion.....	173
5.5	References .....	175
<b>6.</b>	<b>Polymerisation of polyurethane binder system .....</b>	<b>179</b>
6.1	Introduction .....	180
6.1.1	Polymerisation of Polyurethanes .....	180
6.1.2	Polymerisation of Dantocol.....	184
6.2	Experimental.....	185
6.2.1	Polymerisation of Polyurethane Binder System .....	185
6.2.2	Investigation of Dantocol and HTPB Blends .....	186
6.2.3	Polymerisation of Dantocol and Isophorone Diisocyanate .....	186
6.2.4	Characterisation Techniques.....	187
6.2.4.1	Hydroxyl Number Determination .....	187
6.2.4.2	Nuclear Magnetic Resonance .....	188



6.2.4.3	Fourier Transform Infrared Spectroscopy .....	188
6.2.4.4	Differential Scanning Calorimetry.....	188
6.2.4.5	Thermal Gravimetric Analysis .....	189
6.2.4.6	Rheology .....	189
6.2.4.7	Gel Permeation Chromatography .....	190
6.3	Results .....	190
6.3.1	Polymerisation of Polyurethane Binder System .....	190
6.3.1.1	Hydroxyl Number Determination.....	191
6.3.1.2	Nuclear Magnetic Resonance .....	192
6.3.1.2.1	NMR Spectroscopy of Hydroxyl-Terminated Polybutadiene .....	192
6.3.1.2.2	NMR Spectra of Polyurethane .....	196
6.3.1.3	Fourier Transform Infrared Spectroscopy .....	198
6.3.1.3.1	FTIR Spectroscopy of Hydroxyl-Terminated Polybutadiene .....	198
6.3.1.3.2	FTIR Spectroscopy of Polyurethane .....	200
6.3.1.4	Thermal Analysis.....	201
6.3.1.4.1	Differential Scanning Calorimetry of HTPB .....	202
6.3.1.4.2	Differential Scanning Calorimetry of Polyurethane.....	203
6.3.1.4.3	Thermal Gravimetric Analysis of HTPB .....	204
6.3.1.4.4	Thermal Gravimetric Analysis of Polyurethane.....	205
6.3.1.5	Rheological Properties of Polyurethane Cure.....	206
6.3.2	Investigation of Dantocol and HTPB Blends .....	209
6.3.2.1	Characterisation of Blends .....	210
6.3.3	Polymerisation of Dantocol and Isophorone Diisocyanate .....	212
6.3.3.1	Catalyst.....	213
6.3.3.2	Nuclear Magnetic Resonance .....	214
6.3.3.2.1	NMR Spectroscopy of Isophorone Diisocyanate .....	214
6.3.3.2.2	NMR Spectroscopy of Polyurethane .....	216
6.3.3.3	Fourier Transform Infrared Spectroscopy .....	220
6.3.3.4	Thermal Analysis.....	221
6.3.3.5	Rheological Behaviour.....	222
6.3.3.6	Gel Permeation Chromatography .....	223
6.4	Conclusion.....	224
6.4.1	Polyurethane Binder System .....	225
6.4.2	Dantocol and HTPB Blends .....	226
6.4.3	Dantocol and IPDI Polymerisation .....	227
6.5	References .....	228

<b>7. Polymerisation of the binder system and PBX composites</b> .....	233
7.1 Introduction .....	234
7.1.1 Influence of Hydrogen Bonding Within the Binder System.....	235
7.1.2 Cast-Cured PBX Composites .....	238
7.2 Experimental.....	240
7.2.1 Copolymerisation of Polyurethane Binder System .....	240
7.2.2 Curing of Polymer Bonded Explosives .....	242
7.2.3 Characterisation of Composites .....	243
7.2.3.1 Fourier Transform Infrared Spectroscopy .....	243
7.2.3.1.1 Spectral Subtraction .....	243
7.2.3.2 Differential Scanning Calorimetry.....	244
7.2.3.3 Rheology .....	244
7.2.3.4 Scanning Electron Microscopy.....	245
7.3 Results .....	245
7.3.1 Copolymerisation of Polyurethane Blend .....	245
7.3.1.1 Fourier Transform Infrared Spectroscopy of Polyurethane blend .....	246
7.3.1.1.1 Spectral Subtraction .....	250
7.3.1.2 Polyurethane of Increasing Dantocol concentration .....	252
7.3.1.3 Thermal Analysis of Polyurethane Blend .....	255
7.3.1.4 Rheology of Polyurethane Blend.....	259
7.3.2 Cast-Cured PBX Composites .....	261
7.3.2.1 Scanning Electron Microscopy.....	261
7.3.2.2 Fourier Transform Infrared Spectroscopy .....	263
7.3.2.2.1 Intermolecular Interaction of Dantocol .....	263
7.3.2.2.2 Hydrogen Bonding of Dantocol and RDX.....	265
7.3.2.2.3 Dipole Interaction of Dantocol and RDX .....	267
7.3.2.2.4 Copolymerisation of Urethane Linkage.....	268
7.3.2.3 Thermal Analysis.....	269
7.3.2.4 Theoretical Chemistry Behind Resistance to Hydrogen Bond Dissociation .....	272
7.3.2.5 Promotion of Bonding Agent Interaction.....	273
7.3.2.5.1 Isocyanate Selectivity .....	273
7.3.2.5.2 Implications of Mixing Procedure.....	275
7.4 Conclusion.....	276
7.4.1 Copolymerisation of Polyurethane Blend .....	276
7.4.2 Cast-Cured PBX Composites .....	278
7.5 References .....	279

---

<b>8. Synthesis of novel bonding agents</b> .....	285
8.1 Introduction .....	286
8.2 Experimental.....	290
8.2.1 Adduct Characterisation.....	290
8.2.1.1 Difunctional Isocyanate Terminated Bonding Agent.....	290
8.2.1.2 Trifunctional Isocyanate Terminated Bonding Agent.....	291
8.2.2 Synthesis of 1,3- <i>Bis</i> (2,3-dihydroxypropyl)-5,5-dimethylhydantoin .....	293
8.2.3 Synthesis of Hydroxyalkyl Ureas .....	294
8.2.3.1 Synthesis of 1,3- <i>Bis</i> (2-hydroxyethyl)urea.....	294
8.2.3.2 Synthesis of 1,1,3- <i>Tris</i> (2-hydroxyethyl)urea.....	295
8.2.3.3 Synthesis of 1,1,3,3- <i>Tetrakis</i> (2-hydroxyethyl)urea .....	295
8.2.3.4 Synthesis of 1,3- <i>Bis</i> [3-hydroxy-1,1- <i>bis</i> (2-hydroxyethyl)propyl]urea.....	296
8.2.4 Synthesis of Polycarbamate Dendrimer .....	297
8.2.5 Hydroxyalkylation of Heterocyclic Compounds .....	298
8.2.5.1 Preparation of 1,3,5- <i>Tris</i> (2-hydroxyethyl)isocyanurate .....	298
8.2.5.2 Synthesis of 1,3- <i>Bis</i> (2-hydroxyethyl)parabanate.....	299
8.2.5.3 Synthesis of 1,2,4- <i>Tris</i> (hydroxyethyl)urazole .....	300
8.2.5.4 Synthesis of 1,3,4,6- <i>Tetra</i> (2-hydroxyethyl)glycoluril .....	300
8.3 Results .....	301
8.3.1 Bonding Agent Adducts .....	302
8.3.1.1 Difunctional Isocyanate Terminated Bonding Agent.....	302
8.3.1.2 Trifunctional Isocyanate Terminated Bonding Agent.....	304
8.3.2 Synthesis of 1,3- <i>Bis</i> (2,3-dihydroxypropyl)-5,5-dimethylhydantoin .....	304
8.3.3 Synthesis of Hydroxyalkyl Ureas .....	306
8.3.4 Synthesis of Dendrimeric Bonding Agents .....	308
8.3.5 Synthesis of Hydroxyalkyl Heterocycles .....	311
8.3.5.1 Preparation of 1,3,5- <i>Tris</i> (2-hydroxyethyl)isocyanurate .....	312
8.3.5.1 Synthesis of 1,3- <i>Bis</i> (2-hydroxyethyl)parabanate.....	312
8.3.5.2 Synthesis of 1,2,4- <i>Tris</i> (2-hydroxyethyl)urazole .....	314
8.3.5.4 Synthesis of 1,3,4,6- <i>Tetra</i> (2-hydroxyethyl)glycoluril .....	315
8.4 Conclusion.....	316
8.5 References .....	319
<b>9. Mechanical Properties of PBXs</b> .....	323
9.1 Introduction .....	324
9.2 Experimental.....	326
9.2.1 Processing of Polymer Bonded Explosives .....	326

9.2.1.1	Mixing Procedure .....	326
9.2.1.2	Casting .....	328
9.2.2	Compatibility Testing .....	329
9.2.2.1	Differential Scanning Calorimetry.....	329
9.2.2.2	Vacuum Thermal stability .....	329
9.2.3	Sensitiveness Testing .....	330
9.2.3.1	Rotter Impact Sensitiveness .....	330
9.2.3.2	BAM - Friction Test.....	331
9.2.3.3	Temperature of Ignition .....	331
9.2.3.4	Electrostatic Discharge.....	331
9.2.4	Mechanical Testing.....	332
9.3	Results .....	332
9.3.1	Compatibility Testing .....	332
9.3.1.1	Differential Scanning Calorimetry.....	333
9.3.1.1.1	Hydroxyalkyl Ureas .....	333
9.3.1.1.2	Hydroxyalkyl Heterocycles .....	334
9.3.1.1.3	Bonding Agent Adducts .....	335
9.3.1.2	Vacuum Thermal Stability Testing.....	336
9.3.2	Sensitiveness Testing .....	338
9.3.3	Mechanical Testing.....	339
9.3.3.1	Dantocol.....	339
9.3.3.2	1,3,5- <i>Tris</i> (2-hydroxyethyl)isocyanurate.....	341
9.3.3.3	Bonding Agent Adducts .....	342
9.3.3.3.1	Difunctional Isocyanate Terminate Bonding Agent .....	343
9.3.3.3.2	Trifunctional Isocyanate Terminated Bonding Agent .....	344
9.4	Conclusion .....	345
9.4.1	Compatibility and Sensitiveness Testing .....	346
9.4.2	Mechanical Properties .....	347
9.5	References .....	348
<b>10. Conclusion</b>	.....	<b>351</b>
10.1	Introduction .....	352
10.2	Interaction of Dantocol and RDX .....	352
10.2.1	Coatings and Characterisation of Dantocol .....	353
10.2.2	Characterisation of interfacial interactions by FTIR.....	353
10.2.3	Hydroxyl protection of Dantocol .....	354
10.2.4	Thermal analysis of bonding agent interaction.....	355

10.3	Polymerisation of Dantocol and the Binder System.....	356
10.3.1	Polyurethane Binder System .....	356
10.3.2	Dantocol and HTPB Blends .....	357
10.3.3	Dantocol and IPDI Polymerisation .....	357
10.3.4	Copolymerisation of Polyurethane Blend .....	358
10.4	Dantocols mode of action .....	359
10.5	Synthesis of Novel Bonding Agents .....	360
10.5.1	Synthesis of 1,3- <i>bis</i> (2,3-dihydroxypropyl)-5,5-dimethylhydantoin .....	360
10.5.2	Synthesis of Hydroxyalkyl Ureas .....	361
10.5.3	Synthesis of Polycarbamate Dendrimer .....	361
10.5.4	Synthesis of Hydroxyalkyl Heterocycles .....	361
10.6	Mechanical Properties of PBXs .....	362
10.6.1	Compatibility and Sensitiveness Testing .....	362
10.6.2	Mechanical Properties .....	363
10.7	Future Developments .....	3624
10.8	References .....	365
	<b>Appendix</b> .....	38269
	Abbreviations.....	382
	Laboratory Reagents .....	386
	List of Figures.....	396
	List of Tables .....	401
	List of Schemes.....	403



# Chapter 1

---

Introduction

## 1.1 Introduction

The call for increased safety in explosive ordnance has driven the requirement for improved design of Insensitive Munitions (IM). Cast-cured Polymer Bonded Explosives (PBX) are often used as an approach to achieving IM compliance. PBX formulations typically comprise a nitramine explosive (e.g. RDX or HMX), suspended in a polymer matrix, with additional components such as fuels, oxidisers and stabilisers added depending on the application. These PBX's demonstrate favourable mechanical properties, reducing the likelihood of unexpected detonation resulting from external stimuli such as friction, shock loading, heat or electrical charge. Since their introduction, cast-cured energetic materials have seen widespread application in the field of munitions, on account of energetic performance, coupled with a neutral response to external stimuli.<sup>1</sup>

Damage resulting from external stimuli is not limited to mechanical properties, but further influences the sensitivity, combustion and detonation behaviour of energetic materials.<sup>2</sup> Work exerted on cast-cured energetic materials by external stimuli can be converted to thermal energy through a process known as hot spot ignition.<sup>3, 4</sup> In response, the binder system functions to adsorb and dissipate energy, preventing transition to unexpected detonation on account of hot spots. This requires strong interfacial adhesion between the filler and binder to accommodate the process.

Cast-cured energetic materials are particularly susceptible to degradation, resulting from dewetting. This occurs when adhesion between the filler and binder is poor, causing adhesive failure under stress and allowing the binder to break free or “dewet” from the filler surface. Dewetting is a rapidly occurring event, which leads to significant drop in tensile strength. This adversely affects both performance and sensitivity characteristics of energetic composites. Voids evolved during dewetting act as initiation sites when adiabatically compressed by impact or shockwave.<sup>4</sup> This may result in catastrophic failure of cast-cured energetic materials.



Formulations incorporate bonding agents to improve adhesion between particulates and the binder system. This is crucial in avoiding degradation of mechanical properties, caused by propagation of dewetting.<sup>5</sup> One of the forerunners in bonding agent technology for nitramine based composites is the hydantoin derivative 1,3-*bis*(2-hydroxyethyl)-5,5-dimethylhydantoin (Dantocol). Although invaluable in its application, the mechanism in which this promotes interfacial adhesion is poorly understood.

Current demands on safety and design have brought about the need to understand bonding agent's mode of action.<sup>4</sup> Knowledge of surface characteristics and interacting mechanisms is critical to further development of cast-cured energetic materials. Specifically, this will enable improved design of adhesion through advancements in bonding agent technology, improving both insensitivity and mechanical properties.

## **1.1.1 History of Insensitive Munitions**

### **1.1.1.1 Solid Propellant Systems**

The concept of binder systems, which today forms the backbone of cast-cured energetic materials, was originally developed for application in propellants at the California Institute of Technology. In 1942, members from Guggenheim Aeronautical Laboratory developed a simple asphalt-pitch mixture, which became the first cast-cured propellant composite.<sup>1</sup> Two years later, the group went on to trial the first liquid polymer, which formed a rubbery solid upon reaction. Produced by Thiokol Chemical Company, the product involved reaction of a polysulfide, with thiol end groups to form disulfide linkages.

### **1.1.1.2 Polymer Bonded Explosives**

Based on advances in propellant technology, the first cast-cured PBX composite was developed in 1947 at Los Alamos involving polystyrene.<sup>1</sup> This was the first example of an energetic filler encapsulated within a binder system. Since then, binder systems based on a range of polymers have emerged for PBX application. Polyurethanes are now recognised as

a forerunner in PBX technology, since their introduction in the 1950s. Recognised for producing a clean, reproducible cure, these characteristics established the popularity of polyurethane based systems. Initial formulations were known to experience complications resulting from moisture sensitivity, crystallization temperature and aging properties. Technical advances soon rectified these issues, with the development of additives targeting such problems. Inclusion of plasticisers, bonding agents and antioxidants demonstrated vast improvements in the mechanical properties of energetic materials.

### **1.1.1.3 Bonding Agents**

Of these additives, arguably the most significant breakthrough was the discovery of bonding agents by Oberth & Bruenner.<sup>6, 7</sup> The first bonding agent applied to a polyurethane based propellant system, demonstrated remarkable improvements. Mechanical testing revealed addition of bonding agents dramatically enhanced aging characteristics, broadened the operational temperature range and eliminated moisture embrittlement.<sup>6</sup> This discovery contributed to improving the mechanical properties of cast-cured propellants and PBXs alike, whilst addressing the stringent requirements for space and munitions application. The significance of this innovation is reflected in the presence of bonding agents within the majority of all modern formulations.<sup>6</sup>

## **1.1.2 Polymer Bonded Explosives**

The term PBX refers to an explosive composite consisting of an energetic filler, suspended within a solid polymer matrix.<sup>8</sup> Encapsulation of filler particles serves to absorb and dissipate energy caused by hazardous stimuli. Ideally, PBXs should aim to provide maximum explosive force, whilst maintaining minimal sensitivity. To achieve these requirements, inclusion of non-energetic components must be minimised. This is accomplished through application of binder systems, which enable high filler loading to optimise the Velocity of Detonation (VoD). Along with the primary components, various

additives are combined to formulations. These additives function to improve curing, processing, sensitivity and explosive properties of the PBX.

### 1.1.2.1 Binder Systems

The choice of binder system for application in PBX formulations is relatively complex, involving consideration of mechanical and surface properties.<sup>9</sup> Along with the requirements of being both chemically and physically stable, binders must maintain good mechanical properties over a wide range of temperatures. Other favourable characteristics include high elasticity and low glass transition temperature ( $T_g$ ).<sup>10</sup> Additionally, the pot life should ensure the submix remains processable for several hours at working temperatures, without significant viscosity increase.<sup>11</sup> Research into the development of suitable binder systems has produced numerous polymers for application in cast-cured energetic materials. Of those investigated, several polymers have demonstrated favourable properties, including polyamides, polystyrene, polyethylene and polyurethanes. Polytetrafluoroethylene has also been applied to pressed energetic materials.

The ability of polyurethanes to satisfy requirements has contributed to widespread use throughout cast-cured energetic materials. Organic polymers are produced by formation of carbamate linkages, resulting from the reaction of isocyanates with a polymeric diol/triol. In terms of the polyol content, common examples include hydroxyl-terminated polyether (HTPE), hydroxyl-terminated (poly)caprolactone ether (HTCE) and the popular hydroxyl-terminated polybutadiene (HTPB).

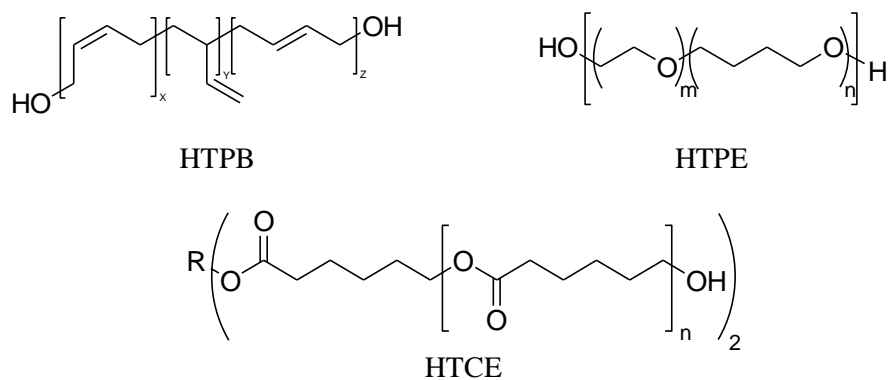
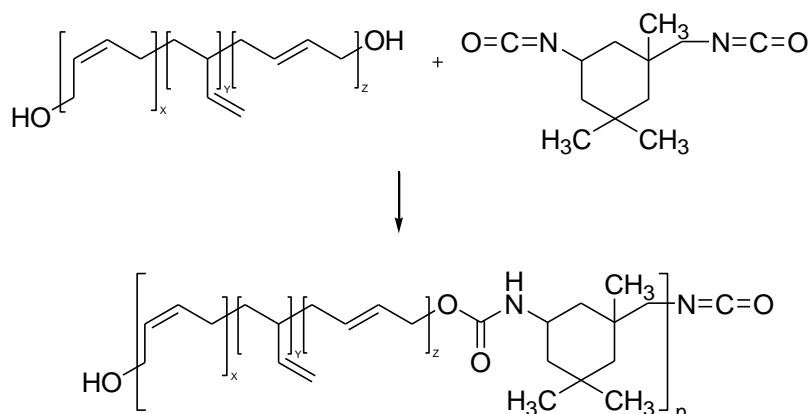


**Figure 1.1.** Polyol prepolymers

Depending on the polyol employed, arrangement of repeating units are either linear in the case of diols, or crosslinked in the case of triols. Linear polymer chains contain no chemical crosslinking, however large chains become entangled producing an elastomeric polymer network. This enables the polymer to deform under applied stress, returning to its original dimensions when the imposing stress is removed. Mechanical strength can be increased by introducing crosslinking. This is achieved by incorporating a prepolymer containing functionality  $\geq 3$ , or crosslinker additive.<sup>1</sup>

In principle, any combination of reactive prepolymers will yield a polymer network, however specific conformations are known to increase performance. Current PBX formulations typically employ elastomeric, or rubbery prepolymers such as HTPB.<sup>10</sup> This imparts superior mechanical properties, hydrolytic stability, ageing stability, viscosity and loading properties, establishing the popularity of HTPB. Termination in primary end groups demonstrate advantages over secondary and tertiary alcohols, due to their increased reactivity towards isocyanates.<sup>12</sup> Upon reaction with a diisocyanate curative such as isophorone diisocyanate (IPDI), the prepolymer forms a polyurethane matrix according to Scheme 1.1.



**Scheme 1.1.** Reaction of HTPB with IPDI to form a Urethane linkage.

Application of long chain diols as the primary building blocks of the binder system satisfies many of the operational requirements demanded of cast-cured energetic materials. The prepolymer also ensures the isocyanate concentration is minimised, avoiding problems with

cure shrinkage and hardening of the composite.<sup>13</sup> Other examples of isocyanates which display favourable properties include toluene diisocyanate (TDI), diphenylmethan-4,4'-diisocyanate (MDI), hexamethylene diisocyanate (HDI), bis(4-isocyanatocyclohexyl)methane (HMDI) and poly(hexamethylene diisocyanate) (N 100).

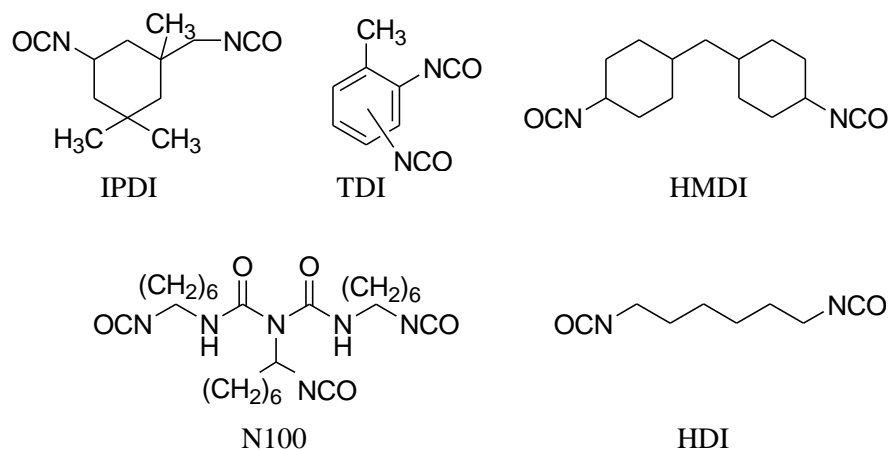


**Figure 1.2.** Triisocyanate/Diisocyanate curatives.

### 1.1.2.2 Energetic Filler

PBXs demonstrate high VoD while maintaining a neutral response to external stimuli. Secondary explosives are responsible for imparting the energetic characteristics of formulations. Nitramines such as cyclotrimethylene trinitramine (RDX) and cyclotetramethylene tetranitramine (HMX) are common fillers, due to their ability to meet energetic demands. Of these crystalline explosives, RDX remains the most widely used in military application. This trend is the result of RDX's energetic performance, relative insensitivity and low manufacturing cost.<sup>14</sup>

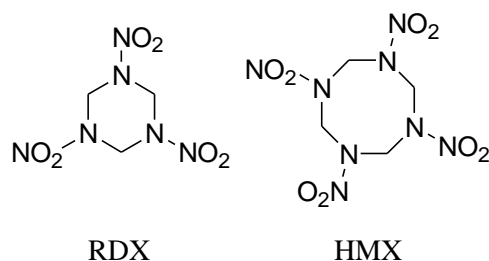


**Figure 1.3.** Nitramine fillers.

The explosive energy of cast-cured PBX composites is further improved by increasing the degree of filler loading. Although varying between formulations, filler content typically accounts for between 80-90% of the mass.<sup>15</sup> Consequently, the degree of filler loading also affects the mechanical performance of composites. This may result in deformation mechanism such as dewetting, stress concentration and the presence of friction between filler particles.<sup>16</sup>

### **1.1.2.3 Bonding Agents**

Cast-cured energetic materials are known to exhibit an intrinsic flaw in terms of the poor compatibility between the energetic filler and binder system. Weak adhesion originates from the typically smooth, inert surface of filler particles, which hinders binder adsorption.<sup>17</sup> Separation of the polymeric binder from filler particles leads to severe deterioration in mechanical properties, impacting the service life, sensitivity and performance of composites.<sup>18</sup> In order to improve properties, bonding agents are incorporated within the polymer matrix at concentrations of 0.5-3.0% (w/w). Addition of bonding agents is imperative to formulations, as this enables improved adhesion at the binder-filler interface.<sup>19</sup> This occurs via formation of a tear resistant layer surrounding filler particles, with which the binder system readily adheres to.<sup>20</sup> Limited data exists regarding this interaction of bonding agents, with no definitive explanation reported as to the mechanism involved in nitramine based composites. Insufficient knowledge of the mode of action has resulted in difficulties associated with selection of compatible bonding agents.

Adsorption of bonding agents is primarily dependent on their solubility within the binder phase. Systems in which bonding agents are readily soluble, may cause them to remain within the binder, rendering them ineffective.<sup>21</sup> In the presence of non-polar binder systems, polar bonding agents undergo adsorption to polar fillers. Polyurethane-based systems are a common example where highly polar bonding agents, such as organic diols or triols are applied.<sup>13</sup> This enables bonding agents to accumulate at the filler surface, forming a polymeric shell which encapsulates polar fillers such as nitramines.

Contrary to this, application of polar binder systems including nitro and nitrate plasticizers cause polar bonding agents to become highly soluble.<sup>22, 23</sup> This prompts bonding agents to undergo phase separation at the processing temperature, causing them to remain within the submix. Therefore systems involving bonding agents that are readily soluble within the binder system, fail to migrate and adsorb onto the surface of filler particles.<sup>24</sup> Surface adsorption becomes even less likely for nitramine fillers, which may have a cohesive energy density close to that of the binder matrix.<sup>23</sup> Consequently the application of alkanolamines, alkanolamides, polyamides and amine salts used as bonding agents for PBX formulations, are limited to use in non-polar binder systems. Neutral polymeric bonding agents (NPBA) have been found to improve interfacial adhesion within polar environments.<sup>8, 19, 25</sup> Examples of NPBA and other commercial bonding agents are listed in Table 1.1.

Chemical Name	Commercial Name
1,3- <i>bis</i> (2-hydroxyethyl)-5,5-dimethylhydantoin	Dantocol
Butyliminodiethanol	BIDE
1,1',1''-(1,3,5-benzenetriyltricarboxyl) <i>tris</i> (2-ethylaziridine)	BITA
1,1'- <i>bis</i> (trimethylsilyloxymethyl) ferrocene	BTMF
1,1-diacetylferrocene disemicarbazone	DAFS
1,1'-ferrocenediyl diethylidene <i>bis</i> (thiocarbonohydrazide)	DAFT
1,1-diacetylferrocenebenzoyl hydrazone	FDBAH
1,1-diacetylferrocene- <i>p</i> -nitrobenzoyl hydrazone	FDNBAH
1,1'-(1,3-phenylenedicarbonyl) <i>bis</i> -2-methyl-aziridine	HX-752
Tris-1-(2-methyl aziridinyl) phosphine oxide	MAPO
Cyanoacrylated tetraethylenepentamine	Tepan
Tetraethylenepentaamine acrylonitrile glycidol adduct	Tepanol
<i>P</i> -toluenesulfonic acid 1,1'-ferrocenediyl diethylidene dihydrazide	TFDD

**Table 1.1.** Commercially available bonding agents.

One of the forerunners in bonding agent technology for nitramine based composites is the hydantoin derivative Dantocol. Unlike other bonding agents identified, Dantocol is applied to cast-cured PBX composites due to its ability to interact with energetic fillers; RDX and HMX. This has led to extensive use in the munitions industry.

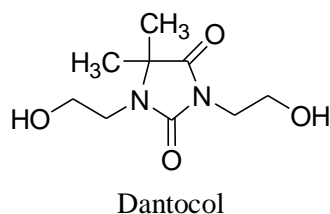


**Figure 1.4.** Hydantoin bonding agent.

The affinity of bonding agents for the energetic filler must also be greater than that of other components. Additional to the filler, binder components and bonding agent, typical PBX formulations also comprise of plasticiser, cure catalyst, antioxidant, stabilisers and metal fuel, which may compete for bonding sites.<sup>23</sup> Therefore the solubility parameters of bonding agents should reside between that of the filler and submix.

#### 1.1.2.4 PBX Additives

Formulations may contain a number of components combined at low concentrations to improve mechanical properties and stability. This includes plasticisers which are used to reduce the rigidity of composites. These additives are responsible for imparting the rubbery characteristics of the binder, which improves tensile strength, elongation and flexibility of the system.<sup>26</sup> Plasticisers also play an important role in the cure response, reducing viscosity of the cast to enable satisfactory pot life. Examples of plasticisers used within PBX formulations include dioctyl adipate (DOA), phthalates and isodecyl pelargonate (IDP).

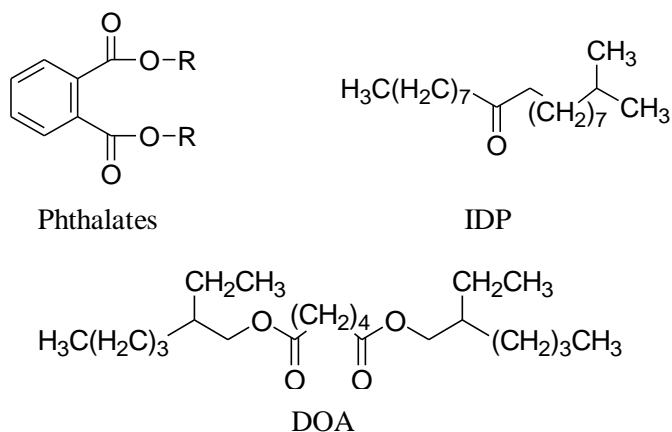


**Figure 1.5.** Plasticisers.



Curing of binder systems can occur over a period of minutes, hours or days depending on the reactants and cure temperature. Prolonged curing is addressed by the addition of catalyst such as triphenyl bismuth (TPB) or dibutyltin dilurate (DBTDL). This can increase the cure rate from a scale of days, to a matter of hours. Catalyst therefore resolves problems with lengthy cure times at elevated temperatures, which are both expensive and impractical.

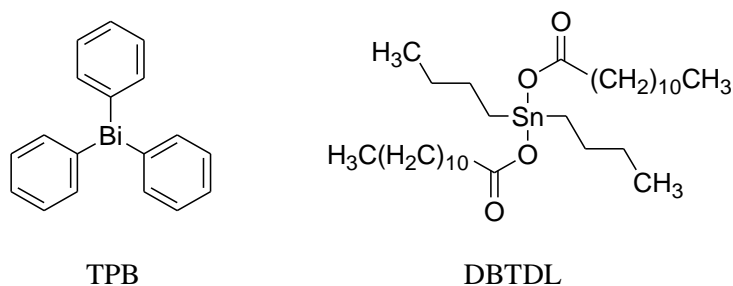


**Figure 1.6.** Cure catalyst.

A popular additive used in countless applications for slowing or preventing oxidation of molecules is the range of antioxidants. When applied to explosive composites, antioxidants inhibit oxidation of the binder, resulting in increased cross-linking to improve binder strength. Typically 2,2'-methylene-bis[6-t-butyl-4-methyl phenol] (AO2246) is applied for this purpose.

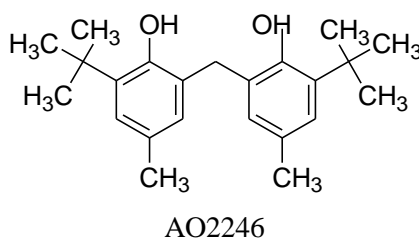


**Figure 1.7.** Antioxidant.

Metal fuels are commonly used in formulations to increase blast duration.<sup>26</sup> Aluminium is one example used to increase blast effects, by providing additional high temperature burning. This occurs following initial detonation, whereby the metal fuel is exposed to an oxygen source.

### **1.1.3 Propellant Systems**

Cast-cured propellant composites consist of a complex mixture of oxidising and reducing agents, that upon ignition, burn in a homogeneous and controlled manner.<sup>27</sup> Formulations contain an oxidiser and fuel source, dispersed within a polymer matrix. Ammonium perchlorate (AP) and HTPB often constitute the main ingredients of cast-cured propellant composites. The remaining components reflect that of PBX formulations, both of which include bonding agents, cure catalyst, plasticisers, metal fuel and curing agent. Propellant composites often require additional antifoaming agents and burn rate modifiers, in order to satisfy service requirements. The function of these additives is to stabilise the submix, maintain desirable mechanical properties and improve both processing and handling of the propellant.

#### **1.1.3.1 Propellant Binder Systems**

Binder systems perform two critical tasks when applied to propellant composites. Firstly the polymer must undergo continuous burn, throughout the propellant's service life. This requires the binder to provide an oxygen source, which facilitates burning of fuel particles embedded within the matrix. Secondly the binder must also impart mechanical stability.<sup>28</sup> This is necessary to survive the rigours of environmental loads, imposed by mechanical and climatic conditions such as temperature, humidity, vibration and impact. Binder systems capable of addressing these issues include polysulfides, polybutadieneacrylic acid, polybutadieneacrylonitrile and polyurethanes.

Polyurethanes are predominantly applied as the binder system for propellant composites, consistent with trends observed in PBX formulations. This commonly involves the use of HTPB and IPDI, which polymerises to form a polyurethane matrix. Hocaoglu<sup>29</sup> investigated the ratio of NCO:OH necessary to achieve minimum stress, modulus and hardness. This determines the degree of crosslinking within the polyurethane, which contributes towards mechanical properties.

### **1.1.3.2 Oxidiser and Metal Fuels**

High performance propellants typically comprise a metal fuel and oxidiser, which deflagrates to produce thrust. AP is largely applied as the oxidiser component, according to its ability to undergo complete conversion into gaseous reaction products.<sup>15</sup> The oxidiser is typically coupled with aluminium, due to the metals fuels heat of combustion.<sup>30</sup> Upon deflagration, aluminium oxide and hydrochloric acid are released as exhaust products. Emission of heat trails are often unfavourable, and have led to the introduction of alternative oxidising agents such as ammonium nitrate, ammonium dinitramine and other nitramines to limit heat signal.<sup>30</sup>

### **1.1.3.3 Propellant Bonding Agents**

Cast-cured propellant composites also experience poor adhesion at the oxidiser-binder interface. Bonding agents are therefore incorporated to improve adhesion between components. Due to differences in the chemical environment of propellants and PBX composites, bonding agents are generally incompatible between the two.

Although the structure of bonding agents applied to propellant formulation may vary from PBXs, their principle function remains. Common bonding agents associated with AP based propellants include HX-752, MAPO, Tepanol and Tepan. These compounds comprise multiple functional groups, capable of interaction with both the oxidiser and binder system. The ability to incorporate solid oxidiser particles within the polymeric binder system results in improved mechanical properties. This extends to the stress and strain characteristics, as well as resistance to moisture and reduced brittleness.<sup>27</sup>

## **1.2 Deformation Mechanisms**

The mechanical behaviour of cast-cured energetic materials is driven by the complicated microstructure and physical processes occurring within the system, particularly under mechanical loading. External stimuli can initiate any number of degradative processes within

energetic materials. Consideration of failure mechanisms is critical in the design and safety evaluation of energetic materials. Propagation of deformations is known to result in catastrophic failure, with potentially devastating consequences. The implications of this have led to demands for increased stability to prevent onset of deformation.

Damage resulting from mechanical failure is not confined to a particular point, rather it diffuses throughout the larger area.<sup>31</sup> Independent of whether damage is incurred during the manufacturing process or from service loads, development of localised damage is redistributed, causing additional damage to unconfined locations. The cumulative damage process is time dependant, with stress diffusing further into the polymer matrix over time.<sup>32</sup> This predominantly accounts for the degradation of strength over time.

Energetic composites are particularly prone to degradation mechanisms on account of their composition. These highly filled polymeric materials display high interface area per unit volume, causing interface behaviour to have a pronounced effect on the mechanical properties. Across the interface exists a region of instability due to differences in the chemical and physical properties of constituents.<sup>33</sup> Consequently, onset of deformation mechanisms often stems from poor compatibility of the binder and filler particles.

### **1.2.1 Dewetting**

Potentially the most hazardous failure mechanism involving cast-cured energetic materials is that of dewetting, sometimes referred to as debonding or blanching.<sup>34</sup> This phenomenon evolves from adhesion failure between filler particles and the binder system. Adhesion failure causes the binder to break free or “dewet” from the filler, resulting in the formation of voids.<sup>5</sup> Onset of dewetting originates from cohesive failure of the binder phase, generating detachment of filler particles.

Studies into the mechanism of dewetting has identified the process occurs in two stages, beginning with cohesive failure of the binder.<sup>20, 35</sup> When incorporated within a polymer matrix, filler particles generate regions of highly concentrated stress. This produces localised

stress at the poles of the involved particles, in excess of twice the magnitude applied. Exceeding the critical stress causes cohesive failure to manifest in the form of microscopic cavities near the interface. Further increase in stress causes the cavity to propagate towards the filler-binder interface. The second stage then commences, whereby cavity formation causes modifications in the stress field. This promotes adhesive failure, resulting in dewetting of the binder system. Initiation of dewetting is dependent on the strength of interfacial adhesion, and the magnitude of stress exerted. Once dewetting occurs, no discernible rehealing process can occur at ambient temperature.

The degree of interaction at the interface is influenced by numerous factors. Differences in chemical composition are primarily responsible for poor compatibility between constituents. The smooth, inert surface of fillers such as nitramines, significantly hinder binder adsorption.<sup>17</sup> Crystalline particles also display rigid properties in comparison to the elastic binder matrix, which creates a modulus gradient, or soft boundary layer surrounding the filler.<sup>20</sup> Under these conditions, the interface between soft and hard materials is vulnerable to dewetting as a result of the high stress gradient.<sup>36</sup>

Often binder systems initially adhere to the filler, while proceeding to deteriorate over time. Strong interfacial adhesion, introduced by bonding agents, resolves issues of dewetting and produces filler reinforcement leading to high tensile strength.<sup>20</sup> Contrary to this, non-reinforcing fillers are by definition, those which fail to raise the tensile strength on account of insufficient interfacial adhesion. Exposure to stress is redistributed to adhered particles, promoting dewetting in the absence of bonding agents.<sup>16, 37</sup> Detachment from the binder relieves stress imposed on filler particles and is dispersed amongst neighbouring particles, thereby causing tear propagation. Following complete detachment of filler particles, additional strain serves to enlarge voids.

The presence of dewetting within energetic composites is accompanied by significant decline in tensile and compressive strengths. This occurs due to the adverse effects of decreasing filler reinforcement.<sup>38</sup> The modulus is impaired as a consequence of this phenomenon,

influencing the degree of stress composites absorb, before experiencing permanent damage. Deterioration of properties is proportional to the extent of dewetting which constitutes void formation. These voids act as initiation sites if adiabatically compressed by impact or shockwave.<sup>5</sup> During collapse, hot spots account for increase in temperatures, which remains a key factor in transition to accidental detonation.<sup>39,40</sup>

## 1.2.2 Dewetting of Propellant Systems

Dewetting poses an equal threat to the stability and performance of propellant systems. Problems associated with interfacial adhesion represents one of the primary causes of propellant failure.<sup>34</sup> Poor interaction between the binder and filler particles predominantly involves oxidiser particles, with metal fuels exonerated due to their irregular surface and increased reactivity. By comparison, oxidisers exhibit smooth surfaces which hinder formation of intermolecular forces.<sup>41</sup> Therefore dewetting originates at the surface of oxidiser particles, as observed in Figure 1.8.

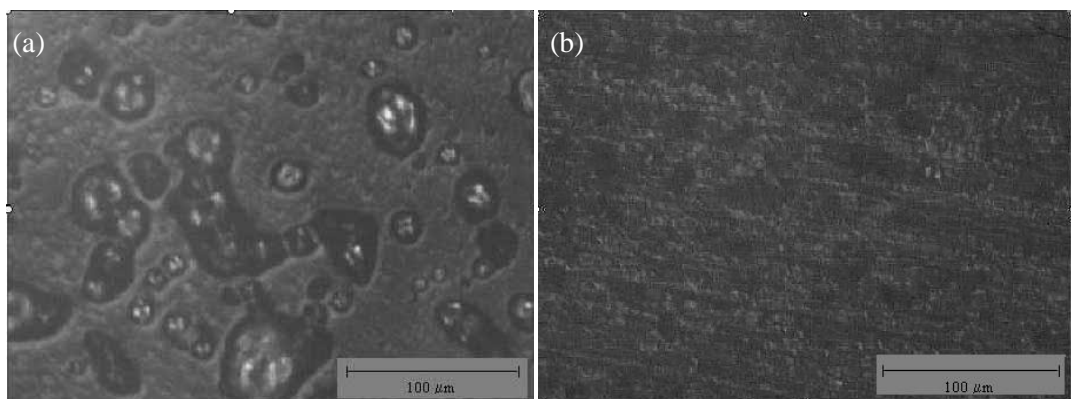


**Figure 1.8.** SEM image outlining (a) dewetting of AP from the binder matrix, and contrasting (b) incorporation of AP within the matrix.<sup>41</sup>

Dewetting manifests in propellants via the same process involved in cast-cured PBX composites. Differences arise in the consequences of dewetting, with erratic burn rates being of primary concern during operation of propellants. Cast-cured propellant composites rely on controlled burn in order to function effectively. In contradiction to this, the presence of dewetting produces increased surface area, along with allowing the flame front to propagate

below the burning surface. The combination of these events contributes toward a rapid increase in burn rate. In response, the internal pressure of the propellant is increased, producing cracks which may cause catastrophic failure.<sup>28,41</sup> Therefore the impact of dewetting on combustion has major implications towards the safety and reliability of propellants.

### **1.2.3 Hydrostatic Tension**

Crystalline filler particles such as nitramines are capable of producing regions of high hydrostatic tension within the binder matrix. This results from uneven stretching of the binder surrounding filler particles, which creates a triaxial stress field. Under these conditions, the binder develops a state of hydrostatic tension, which is neutralised by tearing of the binder system.<sup>20</sup> Hydrostatic stress is only tensile over a small fraction of the inclusion radius, therefore limiting the size of void growth. This translates to decreased damage in composites containing small filler particles.<sup>9</sup> Regardless of size, void formation may become sufficient to cause dewetting, as cavities under strain approach the interface.

### **1.2.4 Thermal Expansion**

Throughout the service life of cast-cured energetic materials, exposure to varying degrees of temperature cycling and climatic conditions is almost certain.<sup>42</sup> Even under mild environmental exposure, slow chemical reactions may occur resulting in embrittlement and eventual formation of voids. Composites may also experience softening, which cause filler particles to slump, or the failure of propellants to withstand acceleration upon service.<sup>13</sup>

The response of cast-cured energetic materials to environmental factors is particularly concerning, due to occurrence of thermal expansion causing irreversible damage. Differences in the thermal expansion coefficient between the binder and filler particles introduce stress. This facilitates void formation, which further impacts mechanical properties.<sup>33, 43</sup>

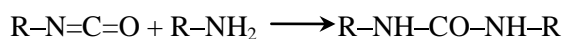
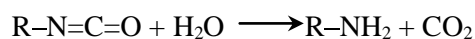
### 1.2.5 Diffusion of Moisture

Propagation of voids has the capacity to trigger diffusion of moisture into the binder matrix.<sup>28</sup> Although H<sub>2</sub>O is potentially unreactive following cure of binder components, mechanical properties deteriorate irrespectively in its presence. This occurs due to accumulation of moisture at the filler surface, creating a layer of liquid which envelops the particles. Interfacial adhesion is then caused to fail under the slightest stress input, resulting in almost immediate propagation of dewetting.<sup>41</sup>

Prior to service of cast-cured energetic composites, moisture poses significant concern during the cure process. Presence of moisture may react to produce unwanted side products, such as those observed in polyurethane based composites. Under moist conditions, water is found to react with the isocyanate component producing CO<sub>2</sub> gas.

### 1.2.6 Trapped Gas

Presence of trapped gas within energetic composites generates voids during cure, which result from absorption of moisture. This remains a common problem associated with polyurethane chemistry. Isocyanates react with H<sub>2</sub>O, generating urea and carbon dioxide gas which remains trapped within the submix. This occurs throughout the binder system, with evolution of gas expressed as follows:



**Scheme 1.2.** Reaction of isocyanates and moisture forming carbon dioxide and urea.

Exposure to stress causes voids to undergo coalescence, resulting in size increase.<sup>41</sup> Voids expand towards the filler, exposing the surface upon contact. This alone affects the performance and safety of energetic materials, while adiabatic compression of voids promote hot spots capable of transitioning to detonation.<sup>28, 44</sup>



### 1.2.7 Deformation Twinning

Unlike other nitramine crystals, exposure of  $\beta$ -HMX to stress may result in a phenomenon known as deformation twinning. The crystalline structure of  $\beta$ -HMX consist of planar molecules stacked in layers parallel to the (101) plane. Introduction of stress causes intermolecular rotation of adjacent nitramine groups.<sup>45</sup> This alters the lattice orientation, forming twin bands.<sup>45</sup> At low stress, these bands are elastic, enabling crystals to return to their original conformation upon relaxing. At higher stresses, the number of twin bands increases, causing crystal fracture to initiate according to Figure 1.9.<sup>9</sup>

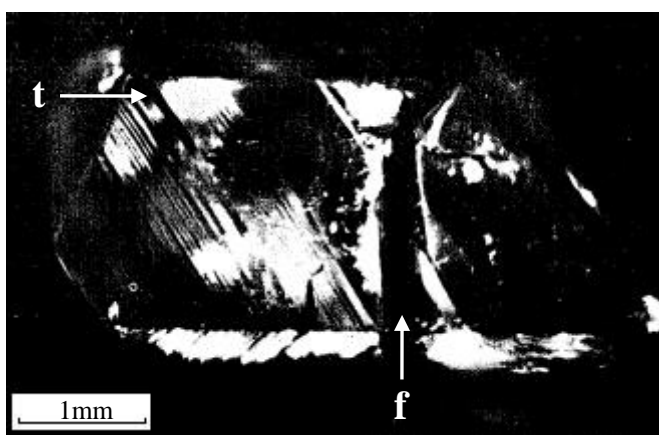


**Figure 1.9.**  $\beta$ -HMX crystal fracture (*f*) due to deformation twinning (*t*).<sup>45</sup>

Twin deformation ultimately causes  $\beta$ -HMX to undergo change in configuration. This results in disruption to the binder system and breakdown of interfacial adhesion.<sup>45</sup> Disruptions at the interface of crystals experiencing deformation twinning promotes dewetting of particles. Lateral elongation also lowers the crack initiation threshold by forming surface steps that increase stress concentration.<sup>9</sup> These effects present threats to the stability and performance of  $\beta$ -HMX based composites.

### 1.2.8 Molecular Slip

Binders temporarily adsorbed to the surface of filler particles experience a destructive interaction known as molecular slip. Exposure to deforming forces transmits energy through

the matrix to the region nearby the interface. This causes a portion of the binder to dewet from the surface, enabling neighbouring polymer strands to occupy the vacant region. Spatial occupation prevents reattachment of the original strand, therefore establishing a new equilibrium condition.<sup>46</sup>

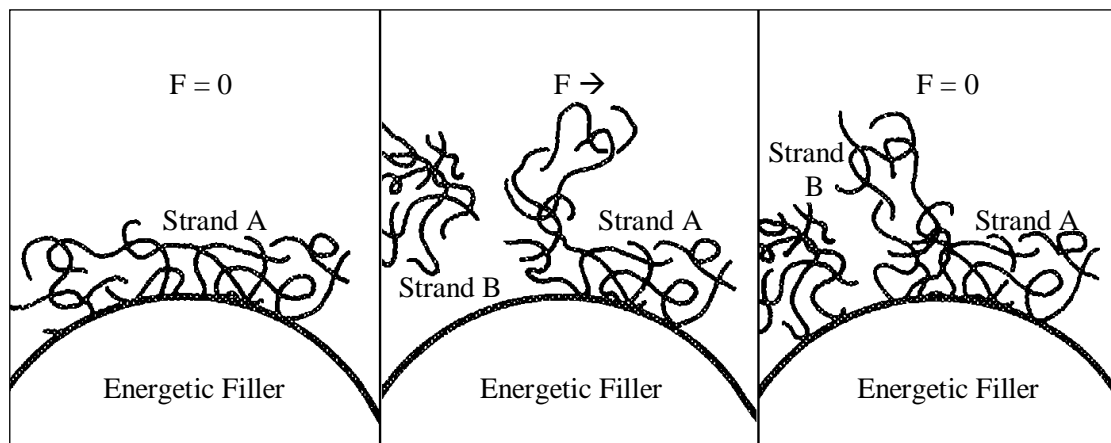


**Figure 1.10.** Mechanism of molecular slippage and reformation.<sup>46</sup>

As the force ( $F$ ) applied is increased, so too does the degree of slippage. However, increased adhesion at the interface has the potential to eliminate this occurrence. Deformation sustained by the binder system on account of molecular slippage, again influences mechanical properties. This impedes the ability of cast-cured energetic material to remain neutral on exposure to external stimuli.

## 1.3 Bonding Agents

### 1.3.1 Function of bonding agents

Application of bonding agents within cast-cured energetic materials is common practice in the majority of modern formulations. These additives are indispensable in terms of their ability to improve the mechanical properties of propellant and PBX composites alike. Incorporation of compatible bonding agents minimises, if not prevents the onset of deformation mechanisms outlined in Section 1.2. Failure mechanisms are resolved through

improved adhesion at the binder-filler interface. This remains the primary function of bonding agents, which provides filler reinforcement to increase the strength of the system.<sup>19</sup> Upon inclusion to formulations, bonding agents perform three important steps to achieve interfacial adhesion:

- I. Migrate towards filler particles within the submix.
- II. Form strong adhesion at the surface of filler particles.
- III. Contain functional groups available to undergo cross-linking reactions with the binder.

In order to fulfil this criterion, bonding agents must contain a minimum of two reactive sites. Functionality must be capable of initiating interaction with the filler, whilst providing moieties which crosslink with the binder system. This ensures formation of a tough coating encapsulating filler particles, while the homopolymer extends into the binder and strengthens the matrix. Bonding agents are therefore able to assist with incorporating filler particles into the polymeric binder systems, improving mechanical properties and preventing degradative mechanisms.

The impact of strengthening adhesion between the binder and filler particles, improves stress and strain characteristics, aging properties, resistance to moisture and reducing brittleness.<sup>27</sup> This enables high filler loading employed in modern composites, without increasing the risk of mechanical failure.

### **1.3.2 Commercial Bonding Agents**

Within the munitions field, a small number of commercial bonding agents are available for application in cast-cured energetic composites. The dilemma with these options is the selection of compatible bonding agent for a particular formulation. Limited knowledge of their mode of action dictates that choice of bonding agent is relatively hit and miss. Following selecting of an appropriate bonding agent, considerations should be made to ensure the compound contributes to improved mechanical properties and decreased sensitivity. The range of bonding agents described in the following section were developed

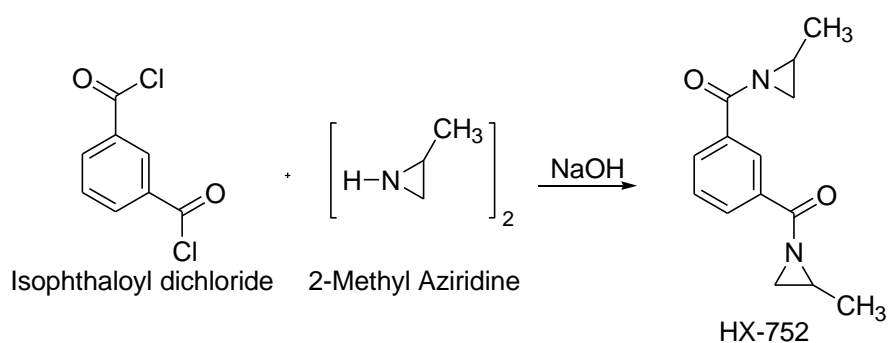
with the ambition of satisfying these requirements. This resulted in various structures, each performing at different efficiency, dependant on the system to which their applied.

### 1.3.2.1 Polyfunctional Aziridine Amides

Aziridine derivatives are one class of compounds known to perform as bonding agents, which boast the potential to improve mechanical properties of cast-cured propellant composites.<sup>47</sup> These compounds include polyfunctional aziridene amides with an isophthalic, trimesic, isocyanuric, or trimethyladipic backbone. Structures also often comprise 2-methyl or 2-ethyl aziridene groups.

### 1.3.2.2 HX-752

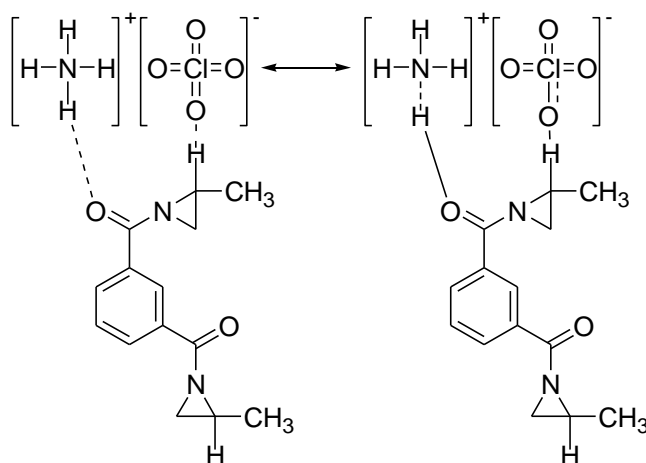
Of those aziridine bonding agents, 1,1'-(1,3-phenylenedicarbonyl) *bis*-2-methyl-aziridine is widely used amongst propellant composites. Produced in the United States by 3M, this has been commercially available since 1962 as HX-752. Synthesis of the compound in racemic form is prepared by reaction of methyl aziridine and isophthaloyl dichloride, as illustrated in Scheme 1.3.



**Scheme 1.3.** Synthesis of HX-752.<sup>48</sup>

HX-752 is one of the few bonding agents in which the mode of action at the filler-binder interface is published. However, the mechanism described is relevant only to propellants containing AP as the oxidiser. This involves the abstraction of protons from AP, producing a HX-752 cation. The cation acts as an initiator for reaction with other HX-752 molecules in a ring opening reaction that forms polyethyleneimine. Secondary aziridine groups are then free

to undergo crosslinking with the binder.<sup>49</sup> This results in formation of a polymeric coating surrounding AP particles, which extends into the binder to form crosslinking reactions.



**Scheme 1.4.** Proposed intermolecular interaction between AP and HX-752.<sup>48</sup>

Storage of HX-752 must be maintained at  $-18^{\circ}\text{C}$  or below, to prevent rearrangement of the compound to the mono-oxazoline or di-oxazoline product.<sup>50</sup> This complicates handling of the bonding agent, imparting unfavourable characteristics.

### 1.3.2.3 Tepanol

Similar in application to HX-752, the reaction product of tetraethylenepentamine, acrylonitrile and glycidol known as Tepanol (or HX-878), is another example produced by the 3M Company. This dark yellow liquid is also compatible as the bonding agent for propellants containing AP. The adduct contains multiple functionality, consisting of amine and hydroxyl groups as shown in Figure 1.11. Amine groups function to abstract protons from the AP, producing a Tepanol cation and ammonium gas. Once converted to the cation, Tepanol forms an ionic bond with the surface crystals of AP. This leaves the remaining amines and hydroxyl groups to form covalent bonds with the binder matrix.<sup>49</sup> Again this results in the formation of polymeric coatings, whilst establishing crosslinking with the binder system.

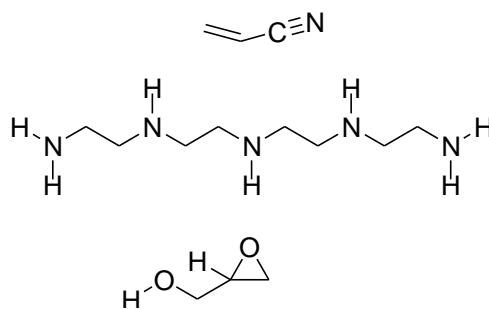


**Figure 1.11.** Tetraethylenepentamine, acrylonitrile and glycidol adduct.

#### 1.3.2.4 Tepan

3M produces a variation of Tepanol, consisting of the reaction product of tetraethylenepentamine and acrylonitrile known as Tepan. This differs from Tepanol, in that it excludes the glycidol component and therefore contains no hydroxyl groups. The amine component reacts similarly to Tepanol, regarding interaction with AP particles. In the absence of hydroxyl functionality, amine groups are also required to interact with the binder matrix.

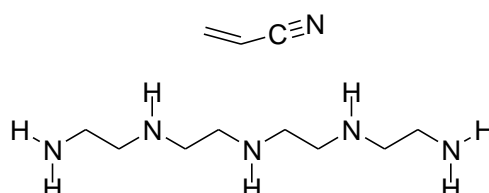
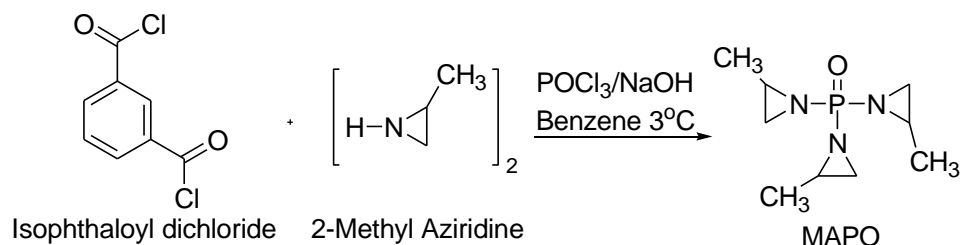


**Figure 1.12.** Tetraethylenepentamine and acrylonitrile adduct.

The consistency of Tepan is much less viscous than Tepanol, while both emit a strong odour of ammonia. Due to the basicity of Tepanol and Tepan, a considerable amount of ammonia gas is produced in the presence of AP. This requires removal during processing of propellant composites to prevent trapping bubbles.<sup>51</sup> Evolution of gas presents highly unfavourable conditions, as this requires extended vacuum removal, creating longer mix time and higher labour costs.

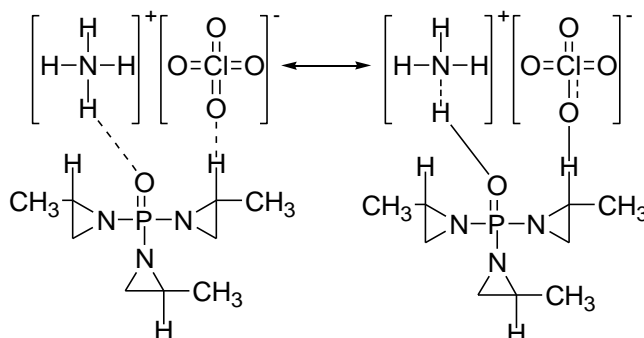
## 1.3.2.5 MAPO

Of the aziridine derivatives applied to cast-cured propellant composites, *tris*-1-(2-methyl aziridinyl) phosphine oxide (MAPO) has demonstrated the greatest success.<sup>48</sup> This has seen production of the bonding agent expand to France, India, Japan, Russia and the United States. Synthesis of MAPO occurs via reaction of methyl aziridine and isophthaloyl dichloride, producing the racemic compound shown in Scheme 1.5. This produces a slightly viscous amber liquid, having a distinct acrid odour. The structure comprises three aziridine moieties arranged in a pyramidal shape around a central phosphorus atom.



**Scheme 1.5.** Synthesis of MAPO.<sup>48</sup>

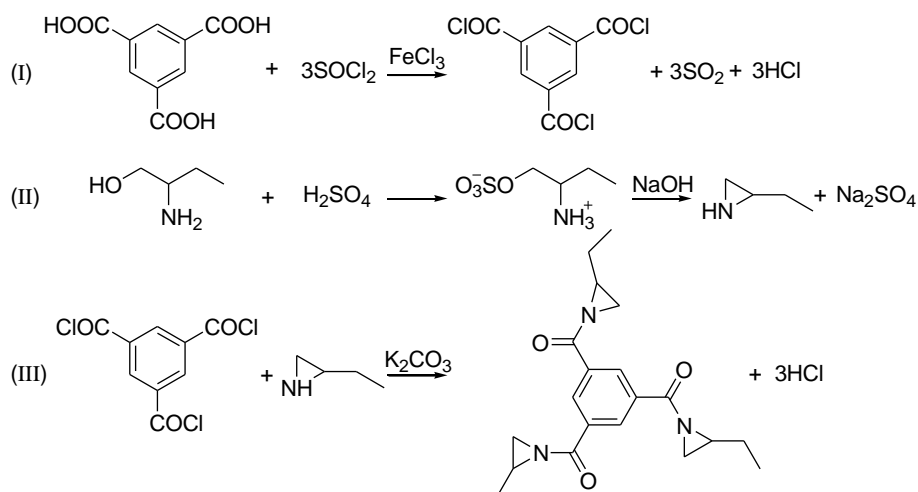
The interaction between MAPO and AP was originally investigated by Wei et al.<sup>52</sup> Evaluation involved density functional theory, calorimetry experiments, infrared spectroscopy and mass spectroscopy, to elucidate the interaction between constituents. According to conclusions, only one of three aziridine rings participates in interaction with AP.<sup>52</sup> Wei et al. proposed that AP catalyses homopolymerisation of MAPO, according to lone ring opening, in the presence of limited acidity associated with AP.<sup>20</sup> Although, no hard evidence was produced to confirm the presence of homopolymerisation. Contrasting theories suggest steric hindrance is responsible for ring opening of the single moiety.<sup>52</sup>



**Scheme 1.6.** Proposed intermolecular interaction between AP and MAPO.

## 1.3.2.6 BITA

Distributed by the Hangzhou Sage Chemical Company under the commercial name BITA or HX-868, the aziridine derivative 1,1',1''-(1,3,5-benzenetriyltricarboxyl) tris(2-ethylaziridine) is commonly applied to AP based propellant composites. Synthesis involves a three stage process, illustrated in Scheme 1.7.



**Scheme 1.7.** Synthesis of 1,1',1''-(1,3,5-benzenetriyltricarboxyl) tris(2-ethylaziridine).

Initially trimesic acid is converted to trimesoyl chloride using thionyl chloride in the presence of ferric chloride. Secondly, butylene amine is produced by cyclization of the sulfate ester of 2-amino-1-butanol. The two products are reacted in potassium carbonate to produce the final product.<sup>53</sup> This compound comprises a planner arrangement of three aziridine moieties, increasing the three-dimensional networking ability. In comparison, the pyramidal conformation of MAPOs aziridine groups is spatially restricted, with functional groups orientated in one direction. This provides BITA with the advantage of being spatially more effective than MAPO.

Although gaps exist in the literature regarding the interaction of BITA, the major reaction pathway of aziridine-based bonding agents is known to involve ring opening reactions.<sup>54</sup> Binder systems comprising hydroxyl functionality facilitate ring opening, including that of HTPB. The accompanying diisocyanate curative react with the imino groups generated upon



ring opening of aziridines.<sup>55</sup> Beyond these descriptions, remaining theories involving the interaction of BITA are considered speculative.

### 1.3.2.7 Ferrocene Based Bonding Agents

Investigation of ferrocene based compounds by Kishmore et al. identified the potential for application in cast-cured propellant composites.<sup>56</sup> Compounds applied to formulations included, 1,1-diacetylferrocene disemicarbazone (DAFS), 1,1'-ferrocenediyl diethylidene *bis*(thiocarbohydrazide) (DAFT), 1,1-diacetylferrocene-benzoyl hydrazone (FDBAH), 1,1-diacetylferrocene-*p*-nitrobenzoyl hydrazone (FDNBAH), *P*-toluenesulfonic acid 1,1'-ferrocene-diyl diethylidene dihydrazide (TFDD) and 1,1'-*bis*(trimethylsilyloxymethyl) ferrocene (BTMF).

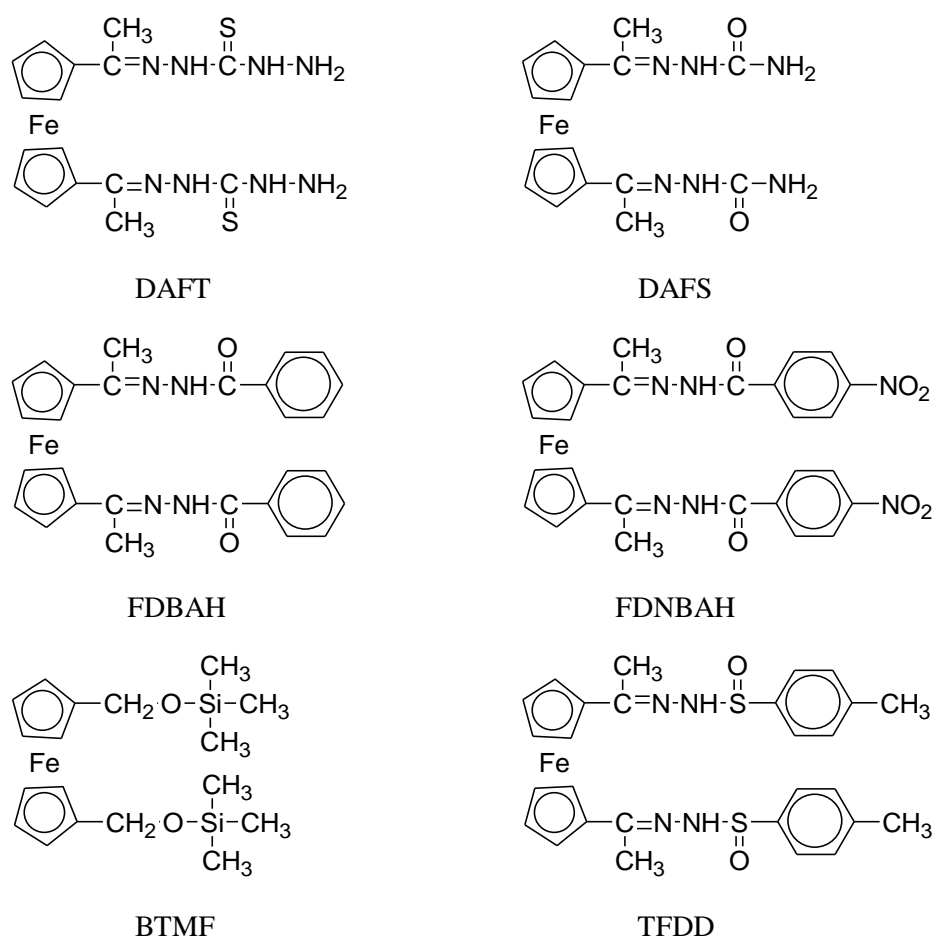
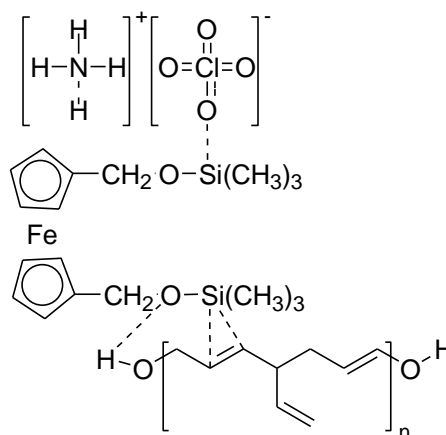


**Figure 1.13.** Structures of ferrocene based bonding agents.

Ferrocene bonding agents were found to increase tensile strength and elongation properties, as well as functioning as burning-rate modifiers. These properties arise from the presence of multiple functional groups, which enable interfacial adhesion, along with performing secondary functions as burning-rate modifiers. The ability to modify the burn rate of propellant composites is attributed to the ferrocene component, which is recognised as an effective burning-rate modifier.<sup>56</sup>

Of the available ferrocene bonding agents, Kishore & Rajalingam investigated the interaction of BTMF within AP/HTPB based formulations.<sup>57</sup> This involved application of IR spectroscopy, revealing spectral shifts in the -Si-CH<sub>3</sub> stretching vibration indicative of interaction. The silyl ether responsible for interaction functions also as the energy supply during combustion. Coupled with the ferrocene components ability to perform as a burning-rate modifier, this establishes BTMF as a dynamic bonding agent for AP/HTPB based propellants.



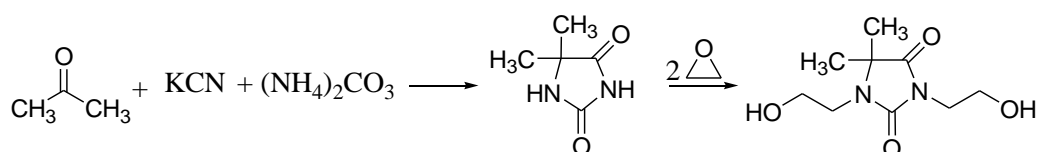
**Scheme 1.8.** Interaction of BTMF with AP and HTPB.<sup>57</sup>

### 1.3.2.8 Dantocol

One of the few bonding agents available for application in nitramine based cast-cured PBX composites, is the hydantoin based derivative 1,3'-bis(2-hydroxyethyl)-5,5-dimethylhydantoin. Known also as Dantocol. the bonding agent was trademarked by Glycol

Chemicals Inc in 1974. Since its inception, Dantocol has become one of the forerunners in bonding agent technology for nitramine composites.

The hydantion glycol is synthesised from 5,5-dimethylhydantoin, prepared by Bucherer synthesis involving potassium cyanide, ammonium carbonate and propan-1-one.<sup>58,59</sup> Dantocol is then produced by hydroxyethylation of 5,5-dimethylhydantoin via reaction of ethylene oxide.<sup>60</sup>



**Scheme 1.9.** Synthesis of 1,3'-bis(2-hydroxyethyl)-5,5-dimethylhydantoin.

Unlike previously mentioned bonding agents which are compatible with AP based propellants, Dantocol is designed for application in nitramine based PBXs. This highlights the importance of Dantocol, which is renowned for its capabilities in energetic composites based on RDX or HMX. Incorporation of Dantocol within formulations is known to improve interfacial adhesion, preventing the onset of dewetting and other deformation mechanisms.<sup>19</sup> Previous investigations suggest interaction occurs through hydrogen bonding of the hydroxyl groups with the nitramines multiple nitro moieties.<sup>61</sup> Surface sensitive IR techniques were used to characterise the interaction through observation of peak shifts between coated and uncoated RDX samples. However, research in this area remains in its infancy.

### 1.3.3 Bonding Agent Selection

Selection of an appropriate bonding agent is primarily dependent on the composition of the material. Therefore, the chemical environment to which it's applied must be evaluated to ensure the bonding agent functions efficiently. Due to significant variations between formulations, bonding agents that perform well in one composite may be ineffective in another.

The polarity of a submix remains a critical factor in determining the compatibility of bonding agents. An effective bonding agent must exhibit high affinity for the filler component, whilst demonstrating the capability to interact with both the filler and binder system. The first consideration is to ensure the bonding agent contains functionality capable of forming primary chemical bonds with the binder system.<sup>23</sup> This enables it to crosslink with the polymer chain during cure. Consaga et al. went further to suggest bonding agents should preferably contain the same functional group as the prepolymer.<sup>38, 41</sup>

Limited knowledge of the mechanism in which bonding agents interact make it difficult to select bonding agents compatible with both the filler/binder. This has introduced an element of trial and error in the selection of bonding agent for novel formulations. Greater understanding of the mechanisms occurring at the interface region will enable informed decisions regarding the selection of bonding agents.

In addition to functionality, particular qualities are recognised to increase the performance of bonding agents. This extends to the size of the molecule, with those displaying increased mass demonstrating advantages over smaller bonding agents. Increasing the molecular mass can provide more adsorption points per molecule. This produces greater surface activity in comparison to bonding agents of low molecular mass.<sup>8, 23, 62</sup> The extent of adsorption is therefore increased, even at dilute concentrations. Secondly, an increase in size also produces greater flexibility in modifying the solubility characteristics of the bonding agent. This is necessary to ensure the bonding agent remains insoluble within the binder phase.

Bonding agents should avoid impacting on the rheological behaviour of the submix. An increase in viscosity above 50% of the initial value in the first 3 hours of curing is generally considered unacceptable.<sup>56</sup> Beyond this point the bonding agent's effect on pot life becomes detrimental to the casting process.

### 1.3.4 Problems Associated With Current Technologies

The majority of commercial bonding agents, although improving interfacial adhesion also display various unfavourable properties. Propellant composites based on alternative oxidisers to AP, impede the performance of Tepan, Tepanol and HX-752. Common substitutes include ammonium dinitramide, ammonium nitrate and bismuth trioxide, which inhibit the function of bonding agents on account of their weak ionisation properties.<sup>49</sup> This prevents proton transfer between the oxidiser and bonding agents, thereby failing to provide interfacial adhesion.

Tepanol and Tepan are also susceptible to the production of ammonia during cure of AP based propellants.<sup>63</sup> This requires extended mixing in vacuo to ensure complete removal of gas, thus increasing cost and mix time. Although avoiding problems of gas evolution, HX-752 presents additional complications regarding viscosity.<sup>51</sup> This considerably increases viscosity of the submix, which impedes processing and reduces the pot life. Further to this the cost of HX-752 is exceedingly high, along with speculation the bonding agent is carcinogenic.

The stability of bonding agents is yet another element requiring consideration. Bonding agents must exhibit chemical and thermal stability, in order to maintain mechanical properties. This is complicated by the presence of aziridine rings, common in bonding agents due to their high reactivity. Although the ring opening reaction provides strong interfacial adhesion, this also triggers instability within the bonding agent.<sup>27</sup> This implicates BITA, MAPO, HX-752 and other polyfunctional aziridines, which account for the majority of bonding agents applied to propellant formulations.

The development of second generation bonding agents that overcome limitations encountered in current bonding agents, would present a significant discovery. Contributions towards lower production costs, shorter mixing times, enhanced insensitivity and improved mechanical properties would also further substantiate this achievement.

## **1.4 Methods of Evaluating Bonding Agent Activity**

In order to evaluate the integrity and reliability of cast-cured energetic materials, knowledge of degradation mechanisms and their impact on the system is required. Consideration of the microstructure, mechanical properties and failure mechanisms is critical in the development of novel formulations. This facilitates design of highly insensitive energetic composites, able to resist changes in the microstructure upon exposure to external stimuli. Damage incurred during compression, tension or impact disrupts not only mechanical properties, but also interferes with sensitivity, combustion and even detonation behaviour of energetic materials.<sup>2</sup>

### **1.4.1 Investigation of Mechanical Properties**

#### **1.4.1.1 Modelling of Interfacial Dewetting**

A number of mathematical descriptions which attempt to quantify dewetting behaviour have been published, predicting the nonlinear stress-strain behaviour induced by the dewetting of filler particles.<sup>64-74</sup> This enables expression of the stress of dewetting in terms of the modulus, particle size, filler volume fraction, work of adhesion and Poisson's ratio.

Tan et al. applied a linear cohesive zone model to study the micromechanical properties of the filler-binder interface. The model conveys a linear relation between the stress traction and displacement discontinuity across the interface during dewetting.<sup>66</sup> However, results yield an unphysical infinite cohesive energy which is unable to characterise nonlinear behaviour, such as softening and other phenomena associated with dewetting. These parameters influence the degree of nonlinearity associated with the binder-filler interface.<sup>46,</sup>

<sup>67</sup> Granted application of an effective bonding agent limits the occurrence of nonlinear behaviour.

Improved accuracy can be achieved by using the nonlinear cohesive law, that combines experimental and micromechanics modelling.<sup>65, 66</sup> The cohesive law displays three stages of dewetting defined as:

Stage I - Linear hardening

Stage II - Softening

Stage III - Complete dewetting

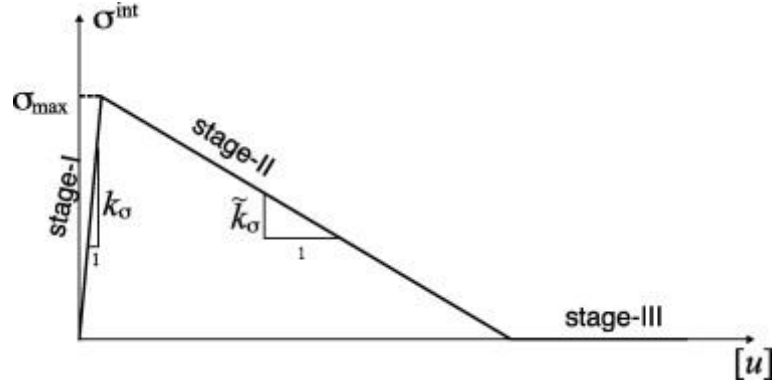


**Figure 1.14.** Interface cohesive model.<sup>65</sup>

The interfacial cohesion law describes the relation between the interface cohesive strength  $\sigma_{max}$ , linear modulus  $k_\sigma$  and the softening modulus  $\tilde{k}_\sigma$ . The normal traction  $\sigma^{int}$  is described in terms of the opening displacement  $[u_r]$  across the interface, as indicated in the following equations:

$$\begin{aligned}
 \sigma^{int} &= k_\sigma [u_r] & [u_r] < \sigma_{max}/k_\sigma & & \text{Stage I} \\
 \sigma^{int} &= \left(\frac{1+\tilde{k}_\sigma}{k_\sigma}\right) \sigma_{max} - \tilde{k}_\sigma [u_r] & \sigma_{max}/k_\sigma < [u_r] < \sigma_{max} \left(\frac{1}{k_\sigma} + \frac{1}{\tilde{k}_\sigma}\right) & & \text{Stage II (1.1)} \\
 \sigma^{int} &= 0 & [u_r] \geq \sigma_{max} \left(\frac{1}{k_\sigma} + \frac{1}{\tilde{k}_\sigma}\right) & & \text{Stage III}
 \end{aligned}$$

Calculations based on the Mori-Tanaka method demonstrates the constitutive relation of cast-cured energetic materials in terms of viscoelasticity and the nonlinear cohesive law.<sup>64</sup>

This method determines the average stress  $\sigma_N^p$  and displacement discontinuities  $[u_r]_N$  of the interface in terms of the macroscopic stress  $\bar{\sigma}$ . Values relate both the average stress  $\sigma_N^p$  of particles and the average stress  $\sigma^m$  to the macroscopic stress  $\bar{\sigma}$  within the matrix. Energetic composites containing a range of particle sizes implicate Equation 1.2 in calculating stress components, with  $f$  representing the total particle volume fraction.<sup>74</sup>

$$\bar{\sigma} = (1 - f)\sigma^m + \sum_N f_N \sigma_N^p \quad (1.2)$$

Numerous equations derived from the cohesive law have proposed theory for predicting a range of macroscopic properties. However, these theoretical calculations remain largely irrelevant to the application of bonding agents.

#### 1.4.1.2 Critical Stress

The critical stress of dewetting indicates the stress required to promote onset of dewetting. Consequently, the extent of dewetting is dependent on the magnitude of stress and interaction at the interface. Critical stress is influenced by the Young's modulus  $E$  of the binder system and filler particle size.<sup>75</sup> Gent et al approached the mechanics of dewetting according to Equation 1.3:

$$t_a = \left( \frac{8\pi E G_a}{3d \sin 2\theta} \right)^{1/2} \quad (1.3)$$

Where  $t_a$  is the critical stress at which dewetting occurs, and  $G_a$  denotes the energy required for the binder to dewet per unit area of the interface. The angle  $2\theta$  represents that subtended by a hypothetical dewetting area on the inclusion.<sup>75, 76</sup>

Inspection of Equation 1.3, suggests  $t_a$  will increase proportional to  $E$ . Contrary to this, an increase in  $E$  has the effect of decreasing  $t_a$ , due to an anomaly occurring between  $E$  and  $G_a$ . This emerges from the dependence of  $G_a$  on the binders dissipative properties, which increases with the materials tendency to dissipate. Rigid binder systems containing increased crosslinking are less dissipative than softer equivalents, decreasing the strength of adhesion. Therefore an increase in  $E$  has the overall effect of decreasing the critical stress of dewetting.<sup>75</sup>

Theoretical investigations by Nicholson<sup>77</sup> and Gent<sup>76</sup> predicted the stress required to cause dewetting is inversely proportional to the square root of the radius of filler particles. Based



on an energy balance approach, Nicholson's analysis predicts dewetting occurs according to Equation 1.4:

$$\sigma_d^2 = \frac{4E\gamma(1 + \nu)}{9r(1 - \nu)^2} \quad (1.4)$$

This represents the radial tension  $\sigma_d$  of dewetting, in terms of both Young's modulus  $E$  and Poisson's ratio  $\nu$  of the binder. Further to this, the inclusion radius  $r$  and interfacial fracture surface energy  $\gamma$  are also represented.<sup>77</sup> Failure is assumed to occur at the interface, with the value of  $\gamma$  measuring lower than that of cohesive failure.<sup>9</sup> Implementing these equations has proven successful in predicting the critical stress associated with the detachment of filler particles.

#### **1.4.1.3 Surface and Interfacial Tension**

The performance of bonding agents can be evaluated based on the interfacial adhesion demonstrated by cast-cured energetic materials. This involves investigation of the interfacial bond strength, by measuring the maximum mechanical stress. Results describe the strength of interfacial adhesion, expressed in terms of force per unit area.

The energy required to promote dewetting also provides useful information regarding deformation. This is expressed as the work of adhesion  $W_a$ , which is defined as the energy required to separate the interface between two components.<sup>24</sup> The value of  $W_a$  is equivalent to the product of the adhesive strength and the distance between the binder and filler immediately following detachment.<sup>78</sup> Investigation of  $W_a$  therefore provides a measure of bonding agent efficiency, with increased values representing stronger interfacial adhesion. The Wilhelmy plate method is commonly applied to determine  $W_a$ . Rivera et al. developed a modified technique which measured  $W_a$ , along with the interfacial tension between a pressed triaminotrinitro-benzene (TATB) plate and the binder.<sup>79</sup> This identified the work of wetting/dewetting, also known as adhesion tension  $\tau$ , by measuring the force exerted on the

plate, upon emersion from liquid of known surface tension. Adhesion tension over height  $dh$  is expressed in terms of force  $f$ , according to Equation 1.5:

$$\tau p dh = f dh \quad (1.5)$$

Where  $p$  is the perimeter of the plate, thus:

$$\tau = \frac{f}{p} \quad (1.6)$$

The wetting and dewetting value of  $\tau$  relates the known liquid surface tension  $\gamma_L$  with both the advancing  $\theta_A$  and receding contact angles  $\theta_R$  as follows:

$$\tau = \gamma_L \cos \theta \quad (1.7)$$

Work of adhesion between the liquid and solid plate is then given as:

$$W_a = \gamma_L + \gamma_L \cos \theta \quad (1.8)$$

The experimental component of this technique involves immersing a thin rectangular plate in liquid, which is slowly immersed while measuring the force exerted on the plate.<sup>80</sup> Emersion creates a meniscus, which leans on the upper edge of the plate. Liquid is withdrawn from the plate at a specific height, and the meniscus retains a constant contact angle with the solid beyond this point. Prior to this moment, no work is done against surface tension or hydrostatic forces; therefore  $W_a$  originates exclusively from dewetting of the plate.

#### **1.4.1.4 Swelling Ratio**

Growth of voids causes a noticeable increase in the volume of cast-cured energetic composites. Dilation in volume was investigated by Wenhui et al. to determine the adhesive properties of the binder-filler interface.<sup>81</sup> This involved measurement of swelling ratios for PBX composites in relation to the presence of bonding agents. The performance of bonding agents were evaluated in terms of their ability to decrease the swelling ratio, indicative of interaction at the interface. This occurs as the polymeric shell encapsulating filler particles

limits swelling of the binder system.<sup>24</sup> Lack of interfacial adhesion or failure to withstand swelling stresses results in the formation of voids surrounding filler particles. This translates to an increase in the swelling ratio of the system, indicating failure of proposed bonding agents.<sup>16</sup>

The method for determining the swelling ratio  $R_s$  involves measurement of the initial sample length  $L_o$ , and the swelling length  $L$  after immersion in solvent.<sup>24</sup> Calculation of  $R_s$  is then performed according to Equation 1.9:

$$R_s = \left( \frac{L}{L_o} \right)^3 \quad (1.9)$$

#### 1.4.1.5 Poisson's Ratio

Perhaps one of the most efficient methods for investigating dewetting is by measurement of volume for filled system as a function of elongation.<sup>37</sup> The process of stretching unfilled systems observes constant volume, provided crystallisation fails to occur. Conversely, upon stretching filled systems voids are produced, causing an increase in volume. Evolution of voids resulting from dewetting appear as a macroscopic increase in volume.<sup>34</sup> Measurement of this volume provides an indication of the elongation value at which dewetting initiates and reaches completion.<sup>37</sup>

Poisson's ratio is applied to measure fluctuations in volume. This is defined as the relationship between the strain produced by tensile force and the contraction that occurs perpendicular to its directions.<sup>37</sup> Poisson's ratio  $\nu$  is therefore represented according to the equation:

$$\nu = \frac{\text{lateral strain}}{\text{axial strain}} = -\frac{W/W_o}{L/L_o} = -\frac{\epsilon_c}{\epsilon} \quad (1.10)$$

Where  $W$  and  $L$  represent width and length, while  $\epsilon$  denotes strain.

Poisson's ratio has previously been applied to investigate the degree of dewetting at the filler-binder interface.<sup>34, 37, 82</sup> Smith concluded that plotting Poisson's ratio as the logarithm of the extension ratio, interfacial behaviour of filled systems can be evaluated.<sup>37</sup> Beyond a critical strain  $\epsilon_c$ , changes in volume were established to represent dewetting at the interface.<sup>82</sup> This is expressed as a negative slope in the plot of lateral strain vs axial strain, according to the rate of void formation. In addition to causing a decrease in Poisson's ratio, dewetting also introduces nonlinearity to the stress-strain curve.<sup>33</sup>

#### 1.4.1.6 Young's Modulus

Decrease in Young's modulus, subsequent to filler loading, serves as an indication of the fraction of debonded particles within composites.<sup>83</sup> This enables interpretation of Young's modulus to describe the degree of dewetting within cast-cured energetic materials. Theory focuses on determining the fraction of debonded filler  $\phi_x$ , depending on the mechanical stress  $\sigma_o$  of samples exposed to dewetting.<sup>83</sup> Methodology is based on that developed by Zgaewsky,<sup>84</sup> according to which:

$$\frac{E_f}{E_o} = (2/3)(1 - \phi_f) \quad (1.11)$$

Where  $E_f$  and  $E_o$  represents the Young's modulus of the filled and unfilled polymer, and  $\phi_f$  is the concentration of filler particles experiencing dewetting.<sup>84</sup> Deviation in modulus following deformation occurs as the result of dewetting, which initiates void formation. As the volume of voids is determined by the fraction of debonded particles  $\phi_f$ , this implies that the modulus is proportional to  $\phi_f$  as indicated in Equation 1.11.<sup>83</sup>

### 1.4.2 Surface Characterisation

Stability and sensitivity of energetic materials is greatly influenced by the morphology and chemical composition of the surface.<sup>85</sup> Surface analysis is consequently regarded as an important area of explosives and propellant research. Variations in surface characteristics

dramatically affect the behaviour of both filler and binder components. Numerous surface sensitive techniques have seen application in the investigation of cast-cured energetic materials and their surface properties. This includes the influence of bonding agents which operate within the surface region, providing interfacial adhesion between filler particles and the binder system.

#### 1.4.2.1 X-Ray Photoelectron Spectroscopy

X-ray photoelectron spectroscopy (XPS) is employed throughout the field of energetics, with application in explosive characterisation, coating studies, reactivity of materials and compatibility studies. Binding energies of surface electrons provide data on the oxidation state of metals, along with identifying elements bonded to the surface of organic material.<sup>85</sup> This enables XPS to determine the surface elementary mass fraction of samples, which is interpreted to reveal the coating degree  $R$ . Results indicate the extent of coating, whereby an increase in  $R$  represents greater coating efficiency. An et al.<sup>49</sup> described  $R$  in terms of the mass fraction  $N$  of RDX, and the sample coating:

$$N_{RDX}(1 - R) + N_C R = N_{sam} \quad (1.12)$$

This technique is limited by its inefficiency to distinguish between organic materials of similar elemental composition. Runan et al. applied XPS to investigate the occurrence of hydrogen bonding at the surface of 3-nitro-1,2,4-triazol-5-one (NTO) and various polymer coatings.<sup>86</sup> Selection of polymers was primarily based on their ability to participate in hydrogen bonding with NTO. This included fluoro rubber, polyvinyl butyral, acrylonitrile styrene copolymer and polystyrene. Interaction between NTO and polymer coatings was distinguished by XPS and FTIR, according to evolution of spectral features.

The effect of boron-containing bonding agents on the interfacial behaviour of TATB composites was similarly investigated by XPS.<sup>87</sup> The bonding agents active hydrogen was found to participate in hydrogen bonding with the nitro functionality of TATB. A series of bonding agents including trioctyl borate, boric acid/aminopropyltriethoxysilane complex,

triethanolamine borate and lauric acid diethanolamine were applied to form a thin film at the surface of TATB. This involved heating 5g of TATB and respective bonding agents (20% w/w) in 20mL ethyl acetate. After stirring, coated particles were filtered, washed and dried at 60°C under vacuum.<sup>87</sup> Binding energies of TATB surface elements before and after coating were then measured by XPS. The oxygen atom of TATBs nitro functionality and nitrogens associated with the bonding agents amino groups were observed to decrease in binding energy. This represents hydrogen bonding, with the electron cloud density migrating toward TATB from the bonding agent, whereby the nitramine withdraws electrons causing decrease in the binding energy.

Weiishang et al. similarly employed XPS to investigate interfacial bonding of novel bonding agents and HMX.<sup>88, 89</sup> This revealed decrease in the binding energy of nitrogen atoms at 402.2eV, associated with the nitro functionality of HMX. Hydrogen bonding was established as being responsible for shoulder formation at 400.8eV. Studies involving wax-coated RDX and surface coating of RDX with a composite of TNT and energetic polymer further applied XPS analysis.<sup>90, 91</sup> This identified the extent of coatings, while characterising the interaction mechanism.

#### **1.4.2.2 Infrared Spectroscopy**

IR spectroscopy is fundamental in its ability to focus on characterisation of the surface region. This is facilitated by the diverse range of IR accessories, which exhibit differing surface sensitivities. Consequently, the majority of these techniques have been applied to the surface analysis of energetic materials, often investigating the interaction of surface coatings.<sup>87-92</sup> This has included application of attenuated total reflectance (ATR), diffuse reflectance infrared fourier transform spectroscopy (DRIFTS), photo-acoustic spectroscopy (PAS) and transmission spectroscopy. Advantages to these techniques include minimal sample preparation, rapid results and high surface sensitivity.

The capacity of ATR to perform surface analysis resides with the impinging infrared beam, displaying a penetration depth of approximately 0.5-2.0 $\mu\text{m}$ . Application also offers the advantage of requiring fewer scans and eliminates the need for sample preparation. DRIFTS meanwhile provides increased surface sensitivity, due to infrared light reaching the detector having reflected from the particle surface. Although predominantly a bulk sampling technique, surface sensitivity is also achieved by transmission spectroscopy when conditions enable the particle bulk to completely absorb incident light. This allows only light passing through the outermost surface to arrive at the detector.<sup>92</sup> PAS features the unique ability to perform depth profiling. Altering the mirror velocities provides control over the penetration depth, thus enabling compilation of depth profiles.<sup>93-95</sup>

#### **1.4.2.3 Microscopy Analysis**

Microscopy offers an effective means for studying the microstructure of energetic materials, revealing mechanical deformation and surface characteristics. Scanning electron microscopy (SEM) is commonly applied to investigate energetic materials.<sup>2</sup> This is complimented by a diverse selection of instrumentation, including atomic force microscopy (AFM) and transmission electron microscope (TEM). Techniques enable visual identification of defects within energetic materials, revealing the presence of voids, dewetting, crystal fractures and deformation twinning. This provides an indication of bonding agent performance, while surface inspection also reveals the degree of coating and efficiency of adhesion.<sup>90, 96</sup>

Examination of the microstructure is enhanced by pre-treatment of energetic composites. Palmer et al. developed a method whereby the surface of PBXs are etched with iso-methyl butyl ketone, then washed with water to reveal the underlying microstructure.<sup>9</sup> The surface is then polished using silicon carbide, followed by application of an automated polishing machine. Polishing involves use of 2 $\mu\text{m}$  cerirouge powder, while exerting a 50g load under water. If required, samples are stained to accentuate the interface region. Exposure to ruthenium tetroxides vapour for a period of several hours causes the binder to react, forming a thin black film of ruthenium oxide. In contrast the energetic filler is unreactive, creating

distinction between components.<sup>9</sup> This functions to enhance the visibility of dewetting and other deformations occurring at the surface.

### 1.4.3 Supplementary Analysis Techniques

#### 1.4.3.1 Thermal Analysis

The thermal behaviour of cast-cured energetic materials has previously been investigated by differential scanning calorimetry (DSC) and thermal gravimetric analysis (TGA). This provides information on the thermal stability of energetic material, which is defined as the ability to resist onset of reaction under thermal action. Thermal stability can be expressed in terms of the self ignition temperature  $T_b$ , according to Equation 1.13:<sup>91</sup>

$$\frac{E}{RT_b}(T_b - T_e) = 1 \quad (1.13)$$

Where  $T_e$  represents the onset temperature of thermal decomposition. Both activation energy  $E$ , and the pre-exponential factor  $A$ , are derived using the Kissinger's method:

$$\ln \frac{\beta_i}{T_{ei}^2} = \ln \frac{AR}{E} - \frac{E}{RT_{ei}} \quad (1.14)$$

Whereby  $T_{ei}$  at a given heating rate  $\beta_i$  is determined experimentally by DSC.

DSC is also applied to identify the glass transition temperature  $T_g$ . This parameter was investigated by Nema et al. to evaluate the performance of bonding agents in cast-cured propellant composites.<sup>97</sup> Incorporation of bonding agents within propellant formulations was found to impart an increase in  $T_g$ . The influence of molecular mobility on  $T_g$ , enables DSC to provide an indication of interfacial interaction.<sup>16</sup> This occurs due to the impact of filler particles on mobility, resulting from changes in viscosity or crosslinking density. Therefore, shifts in  $T_g$  can be interpreted to represent interactions occurring at the interface, following incorporation of bonding agents.



TGA provides an alternative method for determining thermal stability, along with decomposition behaviour.<sup>98</sup> This functions by measuring weight loss of samples either upon heating, or at constant temperature as a function of time.<sup>99</sup> Combined, DSC and TGA provide a wealth of information pertaining to thermal stability, melting points, decomposition temperature and glass transition temperatures of cast-cured energetic material.

#### **1.4.3.2 Compatibility, Sensitiveness and Mechanical Properties**

Evaluation of mechanical properties is necessary to interpret the performance of additives such as bonding agents.<sup>100</sup> This involves investigation into the density, hardness, sensitiveness and thermal characteristics of cast-cured energetic materials. Techniques involved in determining these characteristics include:

- Rotter impact sensitiveness
- BAM friction test
- Temperature of ignition
- Electrostatic discharge
- Vacuum stability
- Hardness
- Instron mechanical testing

Data collated indicates the performance of proposed bonding agents following incorporation within novel composites. This provides a means for understanding the role of bonding agents within the bulk material. Bonding agents are consequently evaluated in terms of their ability to improve mechanical properties and insensitivity.

## **1.5 Conclusion**

Application of bonding agents within cast-cured energetic materials has provided dramatic improvement in mechanical properties. The significance of these additives is highlighted by their extensive use throughout the field of cast-cured propellant and PBX composites, with

the majority of modern formulation containing bonding agents.<sup>6</sup> Popularity stems from the additives ability to enhance interfacial adhesion, promoting filler reinforcement. This resolves issues relating to poor compatibility of constituents, which has long been problematic to cast-cured energetic materials.

Bonding agents ability to prevent dewetting remains of fundamental importance to the insensitivity of energetic composites. Propagation of dewetting is often regarded as the most detrimental deformation mechanism observed in energetic materials.<sup>28, 34</sup> This is known to cause weakening of the material, decrease in modulus, increased potential for fracture and production of voids which act as initiation sites if adiabatically compressed.<sup>5</sup> Incorporation of compatible bonding agents has the capacity to prevent these issues, contributing towards highly insensitive material.

Contrary to the importance of bonding agents, limited literature exists regarding their mode of action, or selection for novel formulation. Of the commercial bonding agents available for application in cast-cured energetic materials, the choice of compound for differing systems is considered speculative. Providing a comprehensive understanding of the bonding mechanism stands to benefit the selection of bonding agent, along with the development of novel compounds.

## 1.6 References

1. Daniel, M. A. *Polyurethane binder systems for polymer bonded explosives*; DSTO-GD-0492; DSTO: Weapons Systems Division, **2006**.
2. Chen, P.; Huang, F.; Ding, Y., Microstructure, mechanical properties and mechanical failure of polymer bonded explosives. In *New Trends in Research of Energetic Materials 7th*, Vagenknecht, J., Ed. Pardubice: Czech Republic, **2004**; Vol. 1, pp 142-149.
3. Mellor, A. M.; Boggs, T. L.; Convino, J.; Dickinson, C. W.; Dreitzler, D.; Thorn, L. B.; Frey, R. B.; Gibson, P. W.; Roe, W. E.; Kirshenbaum, M.; Mann, D. M., Hazard initiation in solid rocket and gun propellants and explosives. *Progress in energy and combustion science* **1988**, *14* (3), 213-244.
4. Shim, J. S.; Kim, H. S.; Lee, K. D.; Kim, J. K., A study of the interfacial characteristics of nitramine explosive-polymer binder. In *American Institute of Chemical Engineers Annual Meeting*, Agency for Defense Development: Austin, Texas, **2004**; p 169.
5. Bellerby, J. M.; Kiriratnikom, C., Explosive-binder adhesion and dewetting in nitramine-filled energetic materials. *Propellants, Explosives, Pyrotechnics* **1989**, *14* (2), 82-85.
6. Klager, K., Polyurethanes, the most versatile binder for solid composite propellants. In *20th Joint Propulsion Conference*, American Institute of Aeronautics and Astronautics: Cincinnati, Ohio, **1984**.
7. Oberth, A. E.; Bruenner, R. S., Binder-filler interaction and propellant physical properties. In *4th Meeting, Intergency Chemical Rocket Propulsion Group, Mechanical Behaviour Working Group*, CPIA Publication: 1965; Vol. 2, pp 45-97.
8. Kim, C. S. Filler reinforcement of polyurethane from addition of neutral polymeric bonded explosive. US Patent 4,915,755, **1987**.
9. Palmer, S. J. P.; Field, J. E.; Huntley, J. M., Deformation, Strengths and Strains to Failure of Polymer Bonded Explosives. *Proceedings of the Royal Society of London. Series A: Mathematical and Physical Sciences* **1993**, *440* (1909), 399-419.
10. Akhavan, J.; Koh, E.; Waring, S.; Kronfli, E., Effect of UV and thermal radiation on polyNIMMO. *Polymer* **2001**, *42* (18), 7711-7718.
11. Shimp, D. A. Polyol/imidazole curing agents for epoxy resins. US Patent 4,417,010, **1983**.
12. Provatas, A. *Energetic polymers and plasticisers for explosive formulations - a review of recent advances*; DSTO-TR-0966; DSTO: Weapons Systems Division, **2000**.
13. Oberth, A. E.; Bruenner, R. S., Polyurethane-based propellants. *Advances in Chemistry* **1969**, *88* (5), 84-121.
14. Lochert, I. J.; Franson, M. D.; Hamshere, B. L., Reduced sensitivity RDX (RS-RDX) Part I: Literature review and DSTO evaluation. **2003**, (DSTO-TR-1447), 1-14.
15. Meyer, R.; Koher, J.; Homburg, A., *Explosives, Sixth Edition*. Wiley: Weinheim, Germany, **2007**.

16. Diamant, Y.; Folman, M., Influence of dewetting on the damping properties of a filled polymer system: 1. Static characterization. *Polymer* **1979**, *20* (8), 1025-1033.
17. Consaga, J. P. Bonding agents for composite propellants. US Patent 4,944,815, **1990**.
18. Hori, K., On the adhesion between hydroxyl-terminated polybutadiene fuel binder for composite solid propellants. *Propellants, Explosives, Pyrotechnics* **1985**, *21* (1), 43-50.
19. Kim, C. S.; Noble, P. N.; Youn, C. H.; Tarrant, D.; Gao, A., The mechanism of filler reinforcement from addition of neutral polymeric bonding agents to energetic polar propellants. *Propellants, Explosives, Pyrotechnics* **1992**, *17* (2), 51-58.
20. Oberth, A. E.; Bruenner, R. S., Tear phenomena around solid inclusions in castable elastomers. *Transactions of the Society of Rheology* **1965**, *9* (2), 165-185.
21. Bruenner, R. S.; Oberth, A. E. Bonding agents for polyurethanes. US Patent 4,410,376, **1983**.
22. Yueping, J.; Guangming, Q.; Yuxiang, Z.; Yi, Y., Synthesis and application of novel bonding agents. In *26th International Pyrotechniques Seminar*, Xi'an Modern Chemistry Research Institute: China, **1999**; pp 187-194.
23. Kim, C. S.; Youn, P. H.; Noble, P. N.; Gao, A., Development of neutral polymeric bonding agents for propellants with polar composites filled with organic nitramine crystals. *Propellants, Explosives, Pyrotechnics* **1992**, *17* (1), 38-42.
24. Wenhui, W.; Weishang, Y.; Bin, Z., Surface and interfacial properties of polymeric bonding agents and nitramine crystal fillers. *Journal of Beijing Institute of Technology* **1997**, *6* (4), 369-375.
25. Kim, H.-S., Improvement of mechanical properties of plastic bonded explosive using neutral polymeric bonding agents. *Propellants, Explosives, Pyrotechnics* **1999**, *24* (2), 96-98.
26. Hamshere, B. L.; Lochert, I. J.; Dexter, R. M. *Evaluation of PBXN-109: The explosive fill for the penguin anti-ship missile warhead*; DSTO-TN-0440; DSTO: Weapons Systems Division, **2003**.
27. Sciamareli, J.; Holanda, J. A. S.; Dutra, R. C. L.; Lourenco, V. L.; Iha, K., RX bonding agent - study of its natural aging. In *34th International Annual Conference of ICT*, Fraunhofer-Institut fuer Chemische Technologie: **2003**; pp 63/1 - 63/11.
28. Geibler, E.; Eisenreich, N.; Geibler, A.; Hubner, C., Analysis and test methods for service life prediction of energetic materials. In *31st International Annual Conference of ICT*, Fraunhofer-Institut für Chemische Technologie: **2000**; pp 149/1 - 149/11.
29. Hocaoglu, O.; Ozbelge, T.; Pekel, F.; Ozkar, S., Fine-tuning the mechanical properties of hydroxyl-terminated polybutadiene/ammonium perchlorate-based composite solid propellants by varying the NCO/OH and triol/diol ratios. *Journal of Applied Polymer Science* **2002**, *84* (11), 2072-2079.
30. Teipel, U., *Energetic Materials*. Wiley: Weinheim, Germany, **2005**.
31. Liu, C. T., Three-Dimensional Finite Element Analysis of Crack-Defect Interaction. *Journal of Spacecraft and Rockets* **1992**, *29* (5), 713-717.

32. Liu, C. T., Effect of predamage on crack growth behavior in a particulate composite material. *Journal of Spacecraft and Rockets* **1995**, 32 (3), 533-537.
33. Hubner, C.; Geibler, E., Finite element modelling of matrix-filler debonding of energetic materials. In *30th International Annual Conference of ICT*, Fraunhofer-Institut für Chemische Technologie: **1999**; pp 99/1 - 99/15.
34. Lohrmann, M.; Hubner, C. In *The influence of the matrix-filler-interaction on the mechanical properties of filled elastomers*, 27th International Annual Conference of ICT, Fraunhofer-Institut für Chemische Technologie: **1996**; pp 140/1-140/7.
35. Farris, R. J., Dilatation of granular filled elastomers under high rates of strain. *Journal of Applied Polymer Science* **1964**, 8 (1), 25-33.
36. Sih, G. C., A model of debonding instability for solid propellant rocket motor: Part I - Uniform longitudinal and transverse stress rate. *Theoretical and Applied Fracture Mechanics* **1996**, 24, 93-113.
37. Smith, T. L., Volume changes and dewetting in glass bead-poly(vinyl chloride) elastomeric composites under large deformations *Transactions of the Society of Rheology* **1959**, 3 (1), 113-136.
38. Consaga, J. P. Dimethyl hydantoin bonding agents in solid propellants. US Patent 4,214,928, **1980**.
39. Frey, R. B., Cavity collapse in energetic materials. In *8th International Symposium on Detonation*, Naval Surface Weapons Centre: **1985**; pp 68-82.
40. Field, J. E.; Bourne, N. K.; Palmer, S. J. P.; Walley, S. M., Hot-spot ignition mechanisms for explosives and propellants. *Philosophical Transactions: Physical Sciences and Engineering* **1992**, 339 (1654), 269-283.
41. Dostanić, J.; Ušćumlić, G.; Husović, T. V.; Heinemann, R. J.; Mijin, D., The use of image analysis for the study of interfacial bonding in solid composite propellant. *Journal of the Serbian Chemical Society* **2007**, 72 (10), 1023-1030.
42. Berghout, H. L.; Son, S. F.; Asay, B. W., Convective Burning in Gaps of PBX 9501. In *Proceedings of the Combustion Institute*, Los Alamos National Laboratory: Scotland, **2000**; Vol. 28, pp 911-917.
43. Voigt, W. H.; Stranhope, N. J. Castable explosive containing TNT and a reaction product of diisocyanate and 1,4-butyleneoxide polyglycol. US Patent 3,447,980, **1969**.
44. Ramaswamy, A. L.; Field, J. E., Lazer-induced ignition of single crystals of the secondary explosive cyclotrimethylene trinitramine. *Journal of Applied Physics* **1995**, 79 (8), 488-502.
45. Palmer, S. J. P.; Field, J. E., The deformation and fracture of  $\beta$ -HMX. *Proceeding of the Royal Chemistry Society of London: Series A* **1982**, 383, 399-407.
46. Stacer, R. G.; Hubner, C.; Husband, D. M., Binder/filler interaction and the nonlinear behaviour of highly filled elastomers. *Rubber chemistry and technology* **1990**, 63 (4), 488-502.

47. Kawamoto, A. M.; Campbell, M. M.; Mahon, M. F., Isophthalic dimethyloxaziridine as a potential bonding agent for rocket solid propellants. *Journal of Energetic Materials* **1999**, *17*, 393-402.
48. Kawamoto, A. M.; Wills, M., Enantioselective synthesis of aziridines using asymmetric transfer hydrogenation as a precursor for chiral derivatives used as bonding agent for rocket solid propellants. *Química Nova* **2002**, *25*, 921-925.
49. Zarras, P.; Dean, D.; Ciaramitaro, D.; Nguyen, S.; Dodson, F. J.; Cambrea, L. R.; Baldwin, L., Dendritic-based bonding agents for high density insensitive munitions (IM) propellant formulations. *Polymer Preprints* **2008**, *49* (1), 27-28.
50. Aiello, P. F.; Hunter, R. W.; Manzara, A. P., Room-temperature storable bonding agent. In *27th International Annual Conference of ICT*, Fraunhofer-Institut fuer Chemische Technologie: **1996**; pp 153/1-153/10.
51. Hamilton, R. S.; Wardle, R. B.; Hinshaw, J. C. Oxazoline bonding agents in composite propellants. US Patent 5,366,572, **1993**.
52. Wei, H.; Shenhui, L.; Shengliang, X.; Gen, T.; Hongxu, L., Investigation on the interaction between bonding agent MAPO and oxidizer AP. In *39th International Annual Conference of ICT*, Fraunhofer-Institut fuer Chemische Technologie: **2008**; pp 74/1-74/7.
53. Scigliano, J. J.; Weyland, H. H.; Hamel, E. E. Preparation of trimesoyl chloride. US Patent 3,364,259, **1968**.
54. Hori, K.; Fukuda, T.; Yamamoto, A.; Aoyagi, S.; Iwama, A., Simple evaluation method of the bonding agents for HTPB/AP propellant. *Internationale Jahrestagung - Fraunhofer-Institut fuer Treib- und Explosivstoffe* **1983**, (Guetesicher. Ueberwach. Treib-Sprengm.), 711-726.
55. Gercel, B. O.; Uner, D. O.; Pekel, F.; Ozkar, S., Improved adhesion properties and bonding performance of HTPB-based polyurethane elastomer by using aziridine-type bond promoter. *Journal of Applied Polymer Science* **2001**, *80*, 806-814.
56. Kishore, K.; Prema, S.; Iyanar, K.; Pandureng, L. P., Mechanistic studies on the effect of ferrocene bonding agents in composite solid propellants. *Fuel* **1994**, *73* (10), 1583-1593.
57. Kishore, K.; Rajalingam, P., The bonding ability and bonding site of a new ferrocene based silicon compound in composite solid propellants. *Journal of Polymer Science Part C: Polymer Letters* **1986**, *24* (9), 471-476.
58. Kormachev, V. V.; Kolyamshin, O. A.; Mitrasov, Y. N.; Bratilov, B. I.; Kozyrev, S. V. Method of obtaining 1,3-di(2-oxyethyl)-5,5-dimethylhydantoin. SU Patent 1,555,327, **1990**.
59. Zussman, H. W.; Knell, M.; Dexter, R. M. Unsaturated hydantoin coagents. US Patent 4,091,223, **1978**.
60. Ušćumlić, G.; Kshad, A. A.; Mijin, D., Synthesis and investigation of solvent effects on the ultraviolet absorption spectra of 1,3-bis-substituted-5,5-dimethylhydantoins. *Journal of Serbian Chemistry Society* **2003**, *68* (10), 699-706.
61. Williams, C. A.; Clarke, S. R.; Lochert, I. J. Binding interaction between dantocol and RDX. Honours Thesis, Flinders University, Adelaide, **2008**.

62. Takahashi, A.; Kawaguchi, M., The structure of macromolecules adsorbed on interfaces. *Advances in Polymer Science* **1982**, *46*, 1-65.
63. Hamilton, R. S.; Wardle, R. B.; Hinshaw, J. C. Vinyl ethers as nonammonia producing bonding agents in composite propellant formulations. US Patent 5,336,343, **1994**.
64. Tan, H.; Huang, Y.; Liu, C., The viscoelastic composite with interface debonding. *Composites Science and Technology* **2008**, *68* (15-16), 3145-3149.
65. Tan, H., Effect of interface debonding on the viscoelastic behaviour of plastic-bonded explosives. In *Proceedings of the 2007 International Autumn Seminar on Propellants, Explosives and Pyrotechniques*, School of Mechanical, Aerospace and Civil Engineering: Beijing, **2007**; pp 290-296.
66. Tan, H.; Huang, Y.; Liu, C.; Geubelle, P. H., The Mori-Tanaka method for composite materials with nonlinear interface debonding. *International Journal of Plasticity* **2005**, *21* (10), 1890-1918.
67. Inglis, H. M.; Geubelle, P. H.; Matous, K.; Tan, H.; Huang, Y., Cohesive modeling of dewetting in particulate composites: micromechanics vs. multiscale finite element analysis. *Mechanics of Materials* **2007**, *39* (6), 580-595.
68. Metzner, A. P., Yielding of polymers filled with large-diameter particles. *Journal of Applied Polymer Science* **2002**, *85* (3), 455-466.
69. Vratsanos, L. A.; Farris, R. J., A predictive model for the mechanical behaviour of particulate composites. Part I: Model derivation. *Polymer Engineering and Science* **1993**, *33* (22), 1458-1465.
70. Vratsanos, L. A.; Farris, R. J., A predictive model for the mechanical behaviour of particulate composites. Part II: Comparison of model predictions to literature data. *Polymer Engineering and Science* **1993**, *33* (22), 1466-1474.
71. Matous, K.; Inglis, H. M.; Gu, X.; Rypl, D.; Jackson, T. L.; Geubelle, P. H., Multiscale modeling of solid propellants: From particle packing to failure. *Composites Science and Technology* **2007**, *67* (7-8), 1694-1708.
72. Sih, G. C., A model of debonding instability for solid propellant rocket motor: Part I - Uniform longitudinal and transverse stress rate. *Theoretical and Applied Fracture Mechanics* **1996**, *24* (2), 63-113.
73. Sih, G. C., A model of debonding instability for solid propellant rocket motor: Part II - Unequal longitudinal and transverse stress rate. *Theoretical and Applied Fracture Mechanics* **1996**, *24* (2), 115-134.
74. Mori, T.; Tanaka, K., Average stress in matrix and average elastic energy of materials with misfitting inclusions. *Acta Metallurgica* **1973**, *21* (5), 571-574.
75. Gent, A. N.; Park, B., Failure processes in elastomers at or near a rigid spherical inclusion. *Journal of Materials Science* **1984**, *19* (6), 1947-1956.
76. Gent, A. N., Detachment of an elastic matrix from a rigid spherical inclusion. *Journal of Materials Science* **1980**, *15* (11), 2884-2888.
77. Nicholson, D. W., On the Detachment of a Rigid Inclusion from an Elastic Matrix. *The Journal of Adhesion* **1979**, *10* (3), 255 - 260.

78. Tracton, A. A., *Coating Technology Handbook*. Third edition ed.; Taylor & Francis Group: Florida, **2006**; p 6/3.
79. Rivera, T.; Matuszak, M. L., Surface properties of potential plastic-bonded explosives (PBX). *Journal of Colloid and Interface Science* **1983**, *93* (1), 105-108.
80. Rosano, H. L.; Gerbacia, W.; Feinstein, M. E.; Swaine Jr, J. W., Determination of the critical surface tension using an automatic wetting balance. *Journal of Colloid and Interface Science* **1971**, *36* (3), 298-307.
81. Smith, J. C.; Kermish, G. A.; Fenstermaker, C. A., Separation of Filler Particles from the Matrix in a Particulate-Loaded Composite Subjected to Tensile Stress. *The Journal of Adhesion* **1972**, *4* (2), 109 - 122.
82. Kugler, H. P.; Stacer, R. G.; Steimle, C., Direct measurement of poisson's ratio in elastomers. *Rubber chemistry and technology* **1990**, *63*, 473-487.
83. Babich, V. F.; Lipatov, Y. S.; Todosijchuk, T. T., Filler Debonding in Particulate-Filled Composites. *The Journal of Adhesion* **1996**, *55* (3), 317 - 327.
84. Zgaevsky, V. E., Elastic and viscoelastic properties of polymers filled with solid particles. *International Journal of Polymeric Materials* **1977**, *6* (1), 109 - 124.
85. Van Gruijthuijsen, L.; Duvalois, W.; Eerligh, R.; Van Ham, H., Surface characterization of energetic materials. In *25th International Annual Conference of ICT*, Fraunhofer-Institut fuer Chemische Technologie: 1994; pp 30/1 - 30/7.
86. Runan, D., Study on the polymer-bonded 3-nitro-1,2,4-triazol-5-one. In *4th, International autumn seminar on propellants, explosives and pyrotechnics*, Shaoxing, China, **2001**; pp 93-96.
87. Li, F.; Ye, L.; Nie, F.; Liu, Y., Synthesis of boron-containing coupling agents and its effect on the interfacial bonding of fluoropolymer/TATB composite. *Journal of Applied Polymer Science* **2007**, *105* (2), 777-782.
88. Weishang, Y.; Wenhui, W.; Zhanning, J.; Jianwu, D.; Huiming, T., Investigation on interfacial bonding in HMX-containing model propellant composite. *Propellants, Explosives, Pyrotechnics* **1995**, *20* (6), 327-329.
89. Weishang, Y.; Jianwu, D., Interfacial interaction of bonding agents with HMX. *Journal of Beijing Institute of Technology* **1992**, *12* (1), 88-92.
90. Cowey, K.; Day, S.; Fryer, R., Examination of Wax-Coated RDX by scanning electron microscopy and X-ray photoelectron spectroscopy. *Propellants, Explosives, Pyrotechnics* **1985**, *10* (3), 61-64.
91. An, C.-W.; Li, F.-S.; Song, X.-L.; Wang, Y.; Guo, X.-D., Surface Coating of RDX with a Composite of TNT and an Energetic-Polymer and its Safety Investigation. *Propellants, Explosives, Pyrotechnics* **2009**, *34* (5), 400-405.
92. Eva Roedel; Atsushi Urakawa; Sven Kuretiw; Baiker, A., On the local sensitivity of different IR techniques: Ba species relevant in NO<sub>x</sub> storage-reduction. *Physical Chemistry Chemical Physics* **2008**, *10* (40), 6190-6198.
93. Tracton, A. A., *Coating Technology Handbook*. Third ed.; Marcel Dekker: 2005; p 936.



94. Yongling. L.; Yuan. W.; Shaoxuan. R.; Chengwei. J., An investigation of interfacial interactions between RDX and polymer binders by FTIR photoacoustic spectroscopy. In *17th International Pyrotechnics Seminar Xi'an Modern Chemistry Research Institute: Beijing, China, 1991*; pp 347-352.
95. Chaudhary, A. K.; Bhar, G. C.; Das, S., Low-limit photo-acoustic detection of solid RDX and TNT explosives with carbon dioxide laser. *Journal of Applied Spectroscopy* **2006**, 73 (1), 123-129.
96. Mattos, E. C.; Moreira, E. D.; Diniz, M. F.; Dutra, R. C. L.; Silva, G.; Iha, K.; Teipel, U., Characterization of Polymer-Coated RDX and HMX Particles. *Propellants, Explosives, Pyrotechnics* **2008**, 33 (1), 44-50.
97. Nema, S. K.; Nair, P. R.; Francis, A. U., The effects of oxidizer bonding agents on the low temperature properties of HTPB. In *AIAA/SAE 13th Propulsion Conference, AIAA: Florida, 1977*; Vol. 77, pp 1-6.
98. Lee, J.-S.; Hsu, C.-K.; Chang, C.-L., A study on the thermal decomposition behaviours of PETN, RDX, HNS and HMX. *Thermochimica Acta* **2003**, 392-392, 173-176.
99. Quintana, J. R.; Ciller, J. A.; Serna, F. J., Thermal behaviour of HMX/RDX mixtures. *Propellants, Explosives, Pyrotechnics* **1992**, 17 (3), 106-109.
100. Provatas, A. *Formulation and performance studies of polymer bonded explosives (PBX) containing energetic binder systems. Part I*; DSTO-TR-1397; DSTO: Weapons Systems Division, **2003**.



# Chapter 2

---

## Coatings and Characterisation of Dantocol

---

Sections of this chapter were presented at: Williams, C. A.; Walker, G. S.; Lochert, I. J.; Clarke, S. R., Investigation into the interaction of Dantocol in polymer bonded explosives and the impact on mechanical properties. *Parari 10th Australian Explosive Ordnance Symposium*, Brisbane, Australia, 2011; 9, pp 1-7.

Williams, C. A.; Walker, G. S.; Lochert, I. J.; Clarke, S. R., Application of Dantocol in polymer bonded explosives and determination of the mode of action. *2<sup>nd</sup> Australian energetic materials symposium*, Adelaide, Australia. 2010.

## 2.1 Introduction

Investigation of bonding agent interaction involves the characterisation of filler particles encapsulated within a thin film of Dantocol. This requires development of an effective method to ensure formation of interfacial adhesion between constituents. Such procedures are called upon to deliver individually coated particles resistant to aggregation, while imposing negligible impact on crystal morphology. These properties are dependent on coating conditions which further influence thickness, particle size distribution and surface conditions.<sup>1</sup> Previous attempts at coating energetic particles have identified a number of techniques, demonstrating mixed success.<sup>1-6</sup>

Previous coatings of energetic crystals involved procedures based on the widely used slurry technique.<sup>1-6</sup> Methodology behind this technique involves mixing solid particles with a dilute solution of the coating agent. This is concentrated by solvent removal, causing precipitation of the coating agent at the particle surface.<sup>7</sup> Problems associated with this procedure are known to include; partial coatings, flocculation of the coating agent, insufficient interaction and agglomeration of coated particles. Requirements also stipulate that additives possess sufficiently low viscosity, enabling dispersion amongst filler particles.<sup>2</sup> However, excessively low viscosities may result in coatings experiencing surface shear. These concerns require individual consideration, enabling optimisation of coatings prior to characterising interactions.

Microencapsulation is considered a popular variation of the slurry technique, often applied to achieve uniform coatings of crystalline particles.<sup>1</sup> This exploits physical methods, phase separation and interfacial reactions to establish superior coatings. Aspects that influence the efficiency of microencapsulation include the solvent conditions, force of attraction, constituents applied and subsequent concentrations.

Irrespective of the methodology applied, coating procedures typically involve two fundamental steps. Firstly, additives dissolved in the solvent phase participate in wetting of

solid particles. Wetting behaviour is recognised to depend on the surface tension, or surface energy between constituents. Lower surface tension results in greater wetting efficiency of the coating agent applied. Polarity then promotes migration towards solid particles, from where intermolecular forces are responsible for surface adsorption. Upon removal of solvent, content adsorbed at the surface undergoes solidification respective of its physical properties. This constitutes the second step, forming a thin uniform coating as illustrated in Figure 2.1.

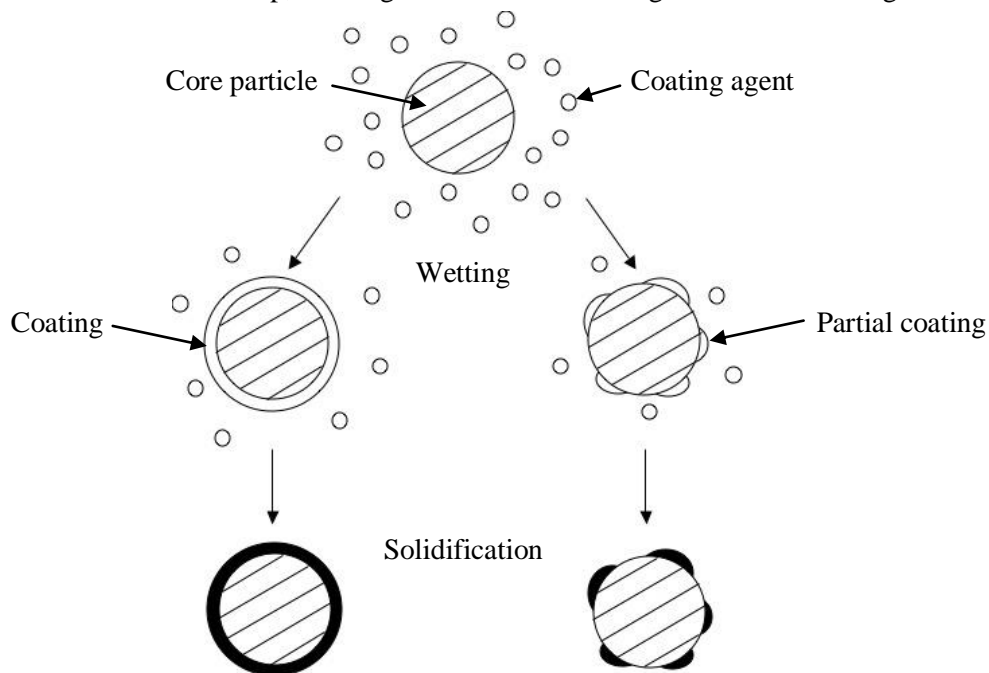


**Figure 2.1.** Coating mechanism of particles suspended in an emulsion.

These principles were employed by Eerligh<sup>1</sup> and Reed,<sup>8</sup> to perform coating of RDX crystals in ethylene and vinyl acetate copolymers. Results indicated the polar vinyl acetate groups caused wetting of RDX, whilst Lewis Acid/Base interactions of the ester groups further enhanced interfacial adhesion. These conclusions were realised due to the efficiency of coatings, establishing the presence of interaction. This translates to current investigations, with the ability to maximise interaction of the bonding agent and nitramine particles considered of critical importance. Improving the extent of intermolecular forces ensures the response to such interactions is increasingly pronounced. This benefits subsequent investigations through optimising features associated with Dantocol interaction.

## 2.2 Experimental

### 2.2.1 Preparation and Characterisation of Compounds

#### 2.2.1.1 Recrystallisation of Dantocol

Dantocol supplied by Interchem Pty Ltd was purified prior to use, removing impurities such as moisture and ethylene glycol. Due to the bonding agent's hygroscopic behaviour, H<sub>2</sub>O is absorbed which competes for active sites associated with RDX. Recrystallisation was performed to resolve purity issues, with Dantocol (20g) charged to a 250mL round bottom flask with propan-2-ol (30mL). This was dissolved at 80°C while stirring for 30mins. Potassium carbonate (3g) was combined as a drying agent and removed by filtration. The solution was then quenched at -5°C in benzene (70mL), promoting recrystallisation. After 3-4 days the solvent was decanted leaving crystals adhered to the flask. Residual solvent was removed by vacuum at 0.5mmHg, with the purified bonding agent stored under nitrogen at 5°C. The purity of Dantocol was confirmed by spectroscopic techniques, with regular assessments conducted to identify moisture adsorption.

<sup>1</sup>H NMR 600MHz, Chloroform-*d*,  $\delta$  (ppm): 1.42 (s, 6H, CH<sub>3</sub>); 2.67 (t, 1H, OH); 2.98 (t, 1H, OH); 3.43 (t, 2H, CH<sub>2</sub>-N); 3.74 (t, 2H, CH<sub>2</sub>-N); 3.73-3.82 (t, 4H, CH<sub>2</sub>-O).

<sup>13</sup>C NMR 600MHz, Chloroform-*d*,  $\delta$  (ppm): 23.02 (2CH<sub>3</sub>); 41.76, 42.88 (CH<sub>2</sub>-N); 60.44, 61.21 (CH<sub>2</sub>-OH); 62.39 (C); 157.03, 177.18 (C=O).

FTIR,  $\nu$  (cm<sup>-1</sup>): 3412.9 ( $\nu$ OH); 2937.6 ( $\nu$  aliphatic CH<sub>2</sub>); 1687.9, 1761.8 ( $\nu$ C=O); 1452.8, 1384.0 ( $\nu_{as}$ CH<sub>2</sub>-N); 1126.2, 1047.4 ( $\nu$ OH stretch); 767.9 ( $\nu$ CH<sub>2</sub>).

Raman Spectroscopy,  $\nu$  (cm<sup>-1</sup>): 2942.7 ( $\nu$  aliphatic CH<sub>2</sub>); 1760.5 ( $\nu$ C=O); 1439.7 ( $\nu_{as}$ CH<sub>2</sub>-N); 1047.4 ( $\nu$ OH stretch).

#### 2.2.1.2 Recrystallisation of RDX

RDX Type 1 Class 1 and Class 5 were applied for the purposes of this research. Samples provided by DSTO were dried at 60°C prior to use. Recrystallised RDX was acquired by dissolving crystals (0.02g) in acetone, until a homogenous solution was obtained. Methylene

chloride (50.0mL) was then charged to the flask, and stored overnight at  $-5^{\circ}\text{C}$ . This initiated precipitation of RDX, after which crystals were filtered and dried.

$^1\text{H}$  NMR 600MHz, Acetonitrile- $d_3$ ,  $\delta$  (ppm): 6.16 (s, 2H,  $\text{CH}_2\text{-N}$ ).

$^{13}\text{C}$  NMR 600MHz, Acetonitrile- $d_3$ ,  $\delta$  (ppm): 61.92 ( $\text{CH}_2\text{-N}$ ).

FTIR,  $\nu$  ( $\text{cm}^{-1}$ ): 3074.1 ( $\nu\text{CH}_2$ ); 1591.3, 1572.40, 1532.2 ( $\nu_{\text{as}}\text{NO}_2$ ); 1458.5, 1433.3 ( $\delta_{\text{s}}\text{CH}_2$ ); 1350.7, 1310.3 ( $\nu_{\text{a}}\text{NO}_2 + \text{N-N}$ ); 1267.0, 1232.9, 1217.2 ( $\nu_{\text{a}}\text{NO}_2 + \text{N-N}$ ); 1039.1, 1017.5, 945.9, 922.8 (ring stretching); 781.5, 753.4 ( $\delta \text{NO}_2 + \gamma \text{N-N}$ ).

Raman Spectroscopy,  $\nu$  ( $\text{cm}^{-1}$ ): 1592.1 ( $\nu_{\text{as}}\text{NO}_2$ ); 1428.0 ( $\text{CH}_2$  stretch); 1383.5, 1306.8, 1270.6, 1213.4 ( $\nu_{\text{s}}\text{NO}_2 + \nu\text{N-N}$ ); 1028.3, 940.0, 879.6, 844.5 (ring stretch); 664.0, 599.6 ( $\text{NO}_2$  stretch); 456.8, 409.6 (ring deformation).

### 2.2.1.3 Nuclear Magnetic Resonance

Characterisation was performed using a Bruker 600MHz NMR spectrometer.  $^1\text{H}$  and  $^{13}\text{C}$  spectra employed model parameters comprising standard units of chemical shift (ppm) and J-coupling constant (Hz). Proton acquisitions were collected over a spectral width of 6009Hz, with a relaxation delay of 1.0sec and acquisition time of 2.726sec.  $^{13}\text{C}$  NMR comprised a minimum acquisition of 500 scans, while employing a spectral width of 24038Hz, relaxation delay of 2.0sec and acquisition time of 1.363sec. Sample preparation involved use of chloroform- $d$ , referenced to  $^1\text{H} = 7.26\text{ppm}$  and  $^{13}\text{C} = 77.16\text{ppm}$ . Acetonitrile- $d_3$  was also applied, with peaks referenced to  $^1\text{H} = 2.05\text{ppm}$  and  $^{13}\text{C} = 29.84\text{ppm}$ .

### 2.2.1.4 Fourier Transform Infrared Spectroscopy

Infrared spectroscopy was performed using a Nicolet Nexus 8700 FT-IR Spectrophotometer, equipped with MCT/A detector. Spectra were acquired over 128 scans, at a resolution of  $2.0\text{cm}^{-1}$ . This was applied over a wavenumber range of  $650\text{-}4000\text{cm}^{-1}$ , using a sample gain of 2.0. Subsequent data analysis was supported by OMNIC version 7.3 software.

### **2.2.1.5 Raman Spectroscopy**

Raman spectra were obtained using a DeltaNu Advantage 200A Raman Spectrometer. Instrumentation comprised a He-Ne laser of wavelength  $\lambda = 633\text{nm}$ , equipped with focal adjustment. This provided spectral data between the range of  $200\text{-}3400\text{cm}^{-1}$ , at an integration time of 35sec. Resulting spectra were interpreted using the Thermo-Galactic Industries GRAMS software.

### **2.2.1.6 Scanning Electron Microscopy of Surface Coatings**

Coating efficiency was determined by Scanning Electron Microscope (SEM) employing a CamScan MX2500 SEM equipped with Energy Dispersive X-ray (EDX). Samples were pretreated with 5nm of platinum deposited using a Quorumtech K757X Sputter Coater. Prepared samples were exposed to an acceleration voltage of 10kV, over a spot size of 4.00nm. This was controlled using MaXim 4 software to produce high resolution images of surface coatings.

## **2.2.2 Coating Techniques**

Coating of nitramine particles involved modified application of the slurry technique, in pursuit of uniform Dantocol coverage. The principle behind this technique involves dissolving coating agents within an organic solvent, while enabling core particles to remain insoluble. Appropriate solvents should display low polarity to facilitate adsorption of polar compounds and high vapour pressure to assist in removal. Solid components are introduced as a slurry which experience wetting upon displacement of solvent from the coating solution. This provides coatings which solidify, following adhesion to the surface of solid particles.

Several variations of the slurry technique were applied to identify an appropriate means for coating nitramine particles. Attempts to optimise methodology called for investigation of individual techniques in regards to improving coating efficiency. This involved evaluation of



solvent conditions, mix time, nitramine extraction and concentration of constituents. Results led to the development of techniques described in the following sections.

### **2.2.2.1 Slurry Technique**

Initial adaptation of the standard slurry technique was applied to coating of nitramine particles. This called for the addition of RDX (0.02g) and H<sub>2</sub>O (0.3mL) to a 10mL round bottom flask, equipped with magnetic stirrer. A dilute solution of Dantocol (0.002g) and chloroform (0.2mL) was then prepared in a 10mL flask. This was combined with the nitramine slurry and mixed vigorously for 30mins. The flask was then heated at 70°C to evaporate the layer of chloroform, after which crystals were allowed to cool. Finally, the aqueous layer was removed by filtration, with coated RDX dried overnight at 60°C under nitrogen purge.

### **2.2.2.2 Reverse Slurry Technique**

The reverse slurry technique follows a differing approach to that of the original method. Contrary to the slurry technique, RDX is dissolved in conjunction with Dantocol to produce a homogenous solution. This enables components to interact in the liquid phase, prior to precipitation of coated crystals. Preparation includes dissolution of RDX (0.02g) and Dantocol (0.002g) in 0.3mL of acetone. Crystals were then precipitated by addition of H<sub>2</sub>O (1.5mL) at reduced temperature. Coated RDX crystals were lastly filtered and dried overnight in a vacuum desiccator.

### **2.2.2.3 Starved Addition Technique**

Focused on improving the coating distribution, the starved addition technique was applied to encapsulate filler particles. The fundamental variable of this method relates to the dropwise addition of Dantocol in solution. This involves mixing RDX (0.01g) in a 0.75mL solution, comprising equal parts ethanol and H<sub>2</sub>O. The slurry was diluted in H<sub>2</sub>O (7.5mL) and stirred for an additional 15mins. Dantocol (0.001g) and methylene chloride (0.8mL) was then

prepared for dropwise addition to the aqueous slurry. Following transfer of bonding agent, solvent was removed by rotary evaporation and coated crystals dried under desiccation.

#### **2.2.2.4 Solvent/Antisolvent Technique**

Alternative coatings were performed based on the coacervation principle.<sup>9</sup> This involved a solvent/antisolvent technique, whereby Dantocol (0.001g) was dissolved in chloroform (3.0mL), followed by the addition of RDX (0.01g). The slurry was then mixed for 15mins, prior to combining 5.0mL of *n*-hexane as the antisolvent. Further to mixing, the slurry was cooled to -5°C, causing precipitation of the coating layer. The final product was filtered and washed with *n*-hexane, prior to overnight drying under vacuum desiccation.

#### **2.2.2.5 Aqueous Suspension/Melting Technique**

The concept of applying heat to disperse Dantocol throughout an aqueous suspension of RDX was also applied in preparation of coatings. This promotes droplets to collide with crystals, thereby undergoing adhesion as the result of intermolecular forces.<sup>10</sup> Subsequent reduction in temperature causes the bonding agent to solidify at the surface, thus forming uniform coating. The suspension was prepared by heating RDX (0.02g) in H<sub>2</sub>O (2mL) at temperatures of 60°C. Dantocol (0.002g) was then charged to a flask containing 2.0mL of equal parts ethanol/ether. This was introduced to the RDX slurry under vigorous stirring. Elevated temperatures were maintained until evaporation of low boiling point solvents was complete. Following removal from heat, coated particles were collected by filtration and dried using a vacuum desiccator.

#### **2.2.2.6 Microencapsulation**

Final attempts to improve surface coatings involved application of a microencapsulation procedure. This was adapted to facilitate coating of RDX crystals and the hydantoin bonding agent. Methodology involved the addition of RDX (0.020g) and Dantocol (0.002g) to a 5mL pear shaped flask. The concentration of bonding agent was increased for subsequent experiments, providing a series of Dantocol coatings ranging from 5%-100% mass of RDX.

Solvent, capable of dissolving Dantocol while enabling RDX to remain insoluble, was then introduced. Solvents included ethanol, methylene chloride and chloroform, applying each to independent systems in 0.3mL volumes. Slurries were agitated for 60mins to facilitate interaction, followed by the removal of solvent. Encapsulated particles were then dried overnight under vacuum desiccation.

## **2.3 Results**

### **2.3.1 Characterisation of Dantocol and RDX**

#### **2.3.1.1 Characterisation of Dantocol**

Purification of Dantocol involved a recrystallisation procedure, yielding high purity crystals, as confirmed by spectroscopic techniques. Recrystallisation from isopropanol/benzene occurred over several days at reduced temperatures. This was necessary to remove impurities such as ethylene glycol and moisture due to the hygroscopic properties of Dantocol. The compounds amine functionality was likely responsible for this behaviour, according to its affinity for water. If exposed to atmosphere over an extended period the bonding agent is caused to deliquesce, therefore requiring storage under anhydrous conditions. This was observed in the IR spectra as a broad hydroxyl peak, indicating the presence of hydrogen bonding.

Recrystallisation was found to remove such impurities, as indicated by NMR and IR spectroscopy. Figure 2.2 illustrates the IR spectrum of purified Dantocol, highlighting separation of the broad hydroxyl peak into three distinct bands. Resolution of bands at 3468, 3413 and 3332cm<sup>-1</sup>, confirms removal of hydrogen bonding between impurities and hydroxyl groups.

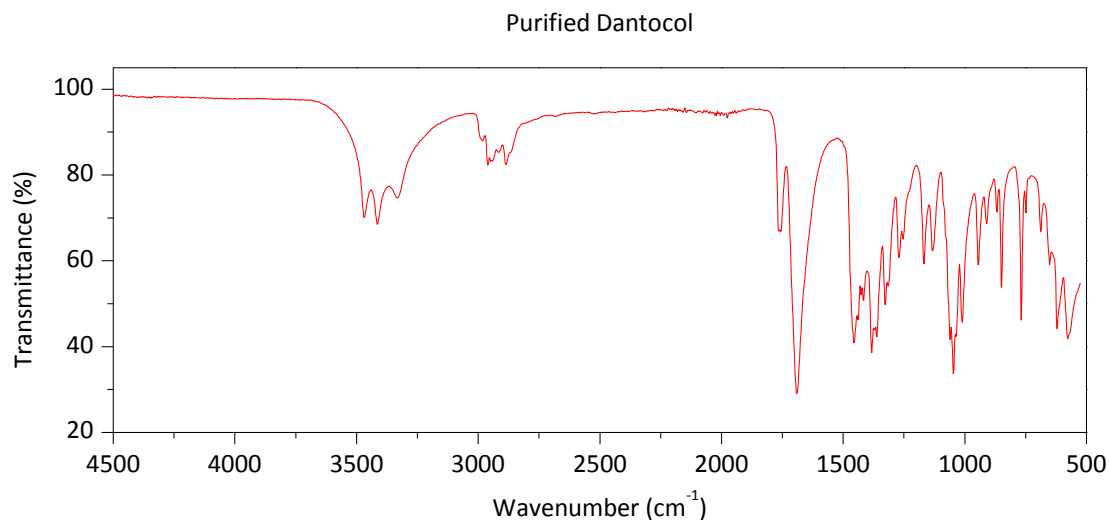


**Figure 2.2.** IR spectrum of purified Dantocol.

The purity of Dantocol was substantiated by NMR, according to removal of unassigned peaks. This was particularly evident in the chemical shift region 3.5-3.7ppm, having initially displayed a series of multiplets associated with impurities. Presence of H<sub>2</sub>O at 1.56ppm originates from chloroform-*d*, while an absence of solvents involved in recrystallisation indicates effective removal.

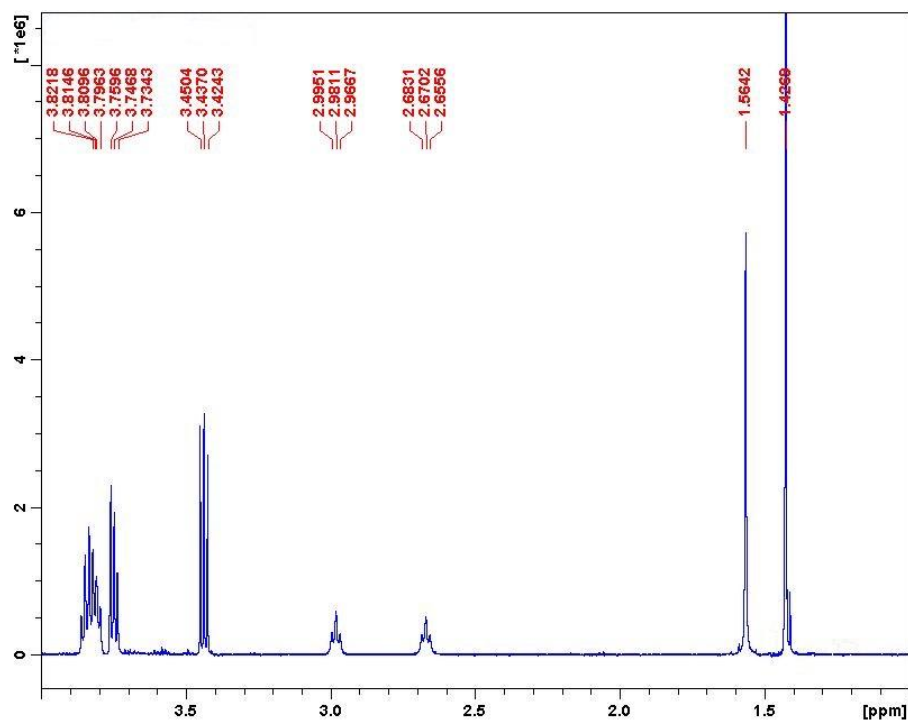


**Figure 2.3.** <sup>1</sup>H NMR of purified Dantocol in chloroform-*d*.

Purification required to isolate the interaction of Dantocol and RDX was therefore satisfied by recrystallisation. This demonstrated benefits over kugelrohr and alternative methods,

which were slower and less effective. Consequently recrystallised Dantocol was applied to all future experiments.

### 2.3.1.2 Characterisation of RDX

To ensure the purity of RDX, recrystallisation was repeated for nitramine crystals. This was found to improve surface area, due to changes in particle size and increase binding sites impeded by impurities. These properties assist in maximising the potential for intermolecular interaction with Dantocol. Spectroscopic techniques were again employed to confirm purity and provide a reference from which to compare coated samples.

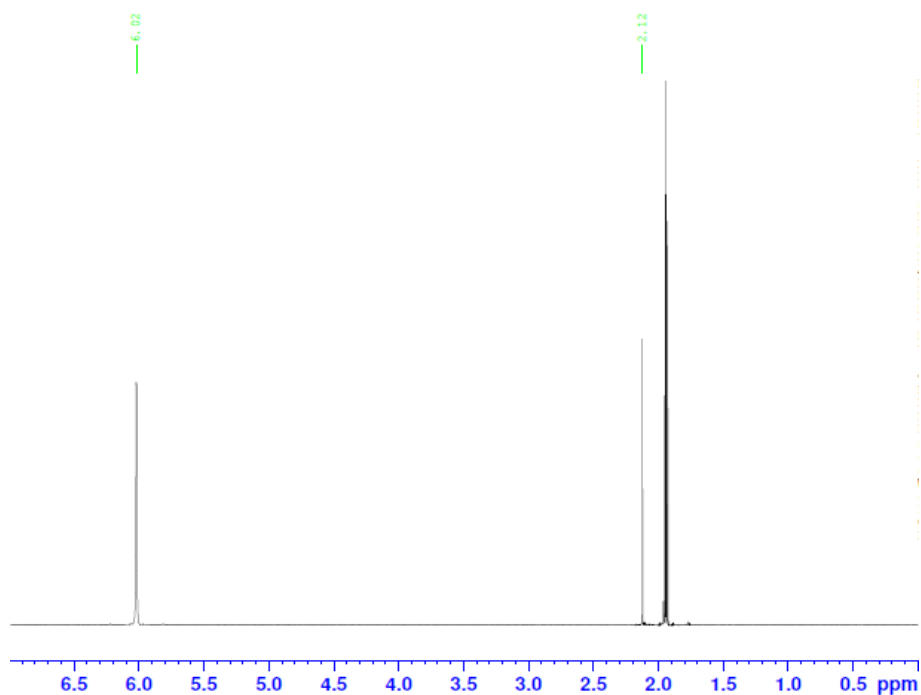


**Figure 2.4.** <sup>1</sup>H NMR of recrystallised RDX in acetonitrile-*d*<sub>3</sub>.

Initial characterisation of recrystallised RDX involving IR spectroscopy revealed increased resolution of vibrational bands. Assignment of bands is described in detail throughout Section 3.3, indicating consistency with the literature. Further analysis by NMR confirmed the purity of nitramine crystals. This revealed a lone singlet in the <sup>1</sup>H spectrum at  $\delta = 6.16$  ppm, representing the aromatic  $\text{CH}_2\text{-N}$  peak. Again the  $\text{H}_2\text{O}$  peak at 2.12 ppm reflects that introduced by acetonitrile-*d*<sub>3</sub>. These results were verified by <sup>13</sup>C NMR which displayed

the  $\underline{\text{C}}\text{H}_2\text{-N}$  peak at  $\delta = 61.92\text{ppm}$ . The absence of residual peaks indicates removal of impurities, required for application.

Investigation of crystals revealed a reduction in the original particle size of approximately  $\sim 150\text{-}200\mu\text{m}$ , with recrystallised RDX measuring  $20\text{-}50\mu\text{m}$ . This was determined using SEM, which also identified consistency in the surface morphology of commercial and recrystallised RDX. Replication of surface morphology is favourable in limiting variables between that occurring under typical PBX conditions. Consequent improvements in purity and surface area led to the assignment of recrystallised RDX for future applications.

### **2.3.2 Coating Techniques**

Evaluation of surface coatings was similarly investigated through SEM, providing information on the quality of coatings. This enabled images to be captured on a scale of several microns, depicting the surface of coated crystals. Interpretation of physical properties was used to assess the efficiency of coating procedures. The ability to monitor surface conditions identified the impact of adjusting variables, enabling optimisation of techniques. These observations were considered in developing an effective method for coating nitramine particles.

Potentially the most influential variable in respect to coating efficiency is that of solvent selection. This determines the affinity of Dantocol for RDX, with polar solvents capable of participating in intermolecular interactions competing for binding sites.<sup>11</sup> For this reason intermolecular forces are typically investigated in non-polar solvents such as toluene, chloroform, methylene chloride or linear and cyclic alkanes.<sup>11</sup> Choice of solvent therefore requires consideration, if interaction between constituents is established.

#### **2.3.2.1 Slurry Technique**

Application of the standard slurry technique was initially investigated to determine coating efficiency. This involved use of chloroform to dissolve Dantocol, due to its immiscibility

with the aqueous RDX slurry. The result is illustrated in Figure 2.5, indicating complete coverage of the nitramine surface. However, this was disrupted by formation of pores in the coating layer. This occurred during the preliminary drying process, whereby coated particles were heated at 60°C.

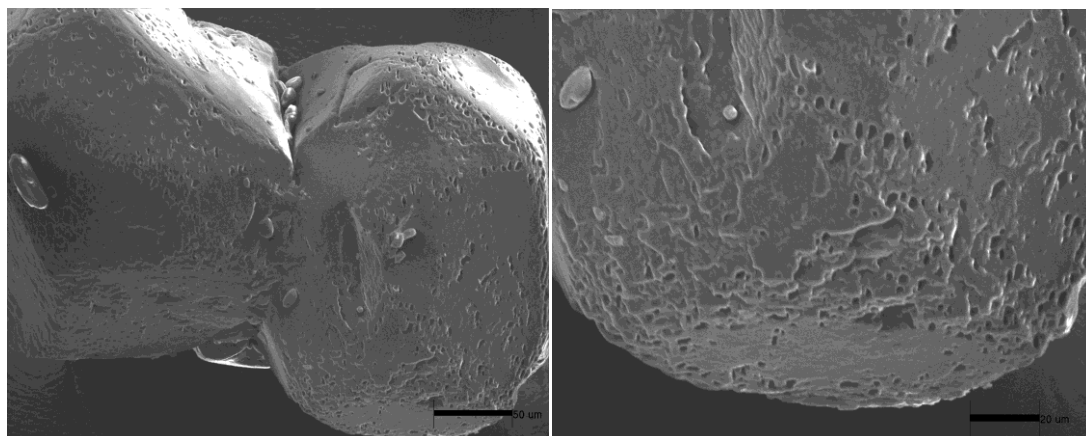


**Figure 2.5.** Slurry coating of RDX in 10% Dantocol.

Drying at elevated temperatures was therefore substituted for overnight storage under vacuum desiccation. The consequence of implementing gentle drying conditions resulted in the elimination of pore formation. This is observed in Figure 2.6, indicating improved coverage following resolution of drying issues.

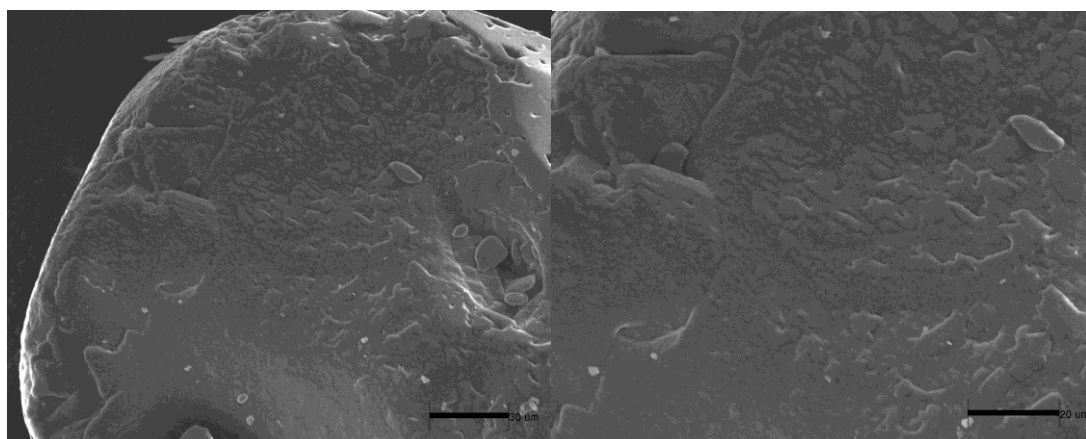


**Figure 2.6.** Slurry coating of RDX in 10% Dantocol through subtle drying.

Further investigation of the slurry technique involved focus on mixing conditions. This compared the efficiency of heterogeneous mixing to determine appropriate parameters and ensure interaction. The impact of prolonged mixing was evaluated over the course of 7 days.

Coated particles were sampled at regular intervals, employing a gyratory mixer to facilitate mixing. Inspection of surface coatings revealed the gyratory mixer failed to improve coating efficiency over this period. The results of mixing conditions are further discussed in Section 2.3.3.

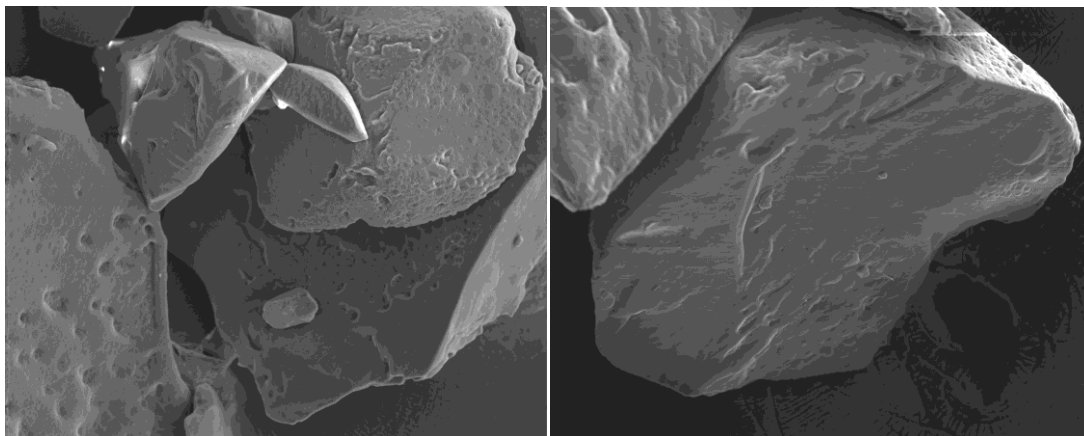


**Figure 2.7.** Slurry coating of RDX in 10% Dantocol using gyratory mixer.

Evaluation of solvent conditions and removal, identified implications towards methodology. Initially, the ratio of organic solvent to water was examined, with negligible impact on coating efficiency. Solvent removal was then attempted using a centrifuge technique, whereby an internal sample reservoir was applied to centrifuge tubes. Samples were mixed, then spun at 3500rpm for 30mins, allowing solvent to pass through the reservoir membrane. Figure 2.8 highlights coatings generated which consist of incomplete surface coverage. NMR analysis identified the presence of Dantocol within the supernatant extracted from centrifuge tubes, confirming partial failure of adhesion.

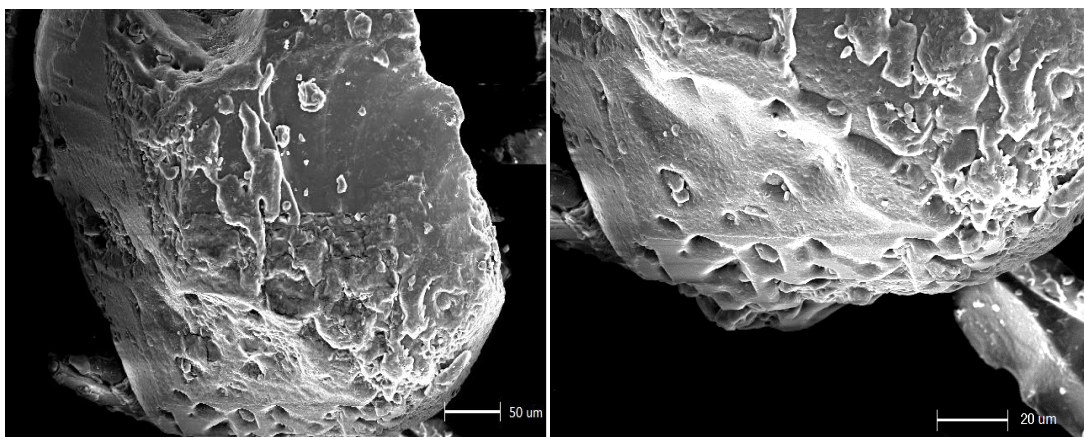


**Figure 2.8.** Slurry coating of RDX in 10% Dantocol using centrifugation.



### 2.3.2.2 Reverse Slurry Technique

The principle behind the reverse slurry technique differs from previous methods, in that RDX is dissolved to allow reduction in particle size. Although disruption to crystal morphology is otherwise avoided, the influence of increased surface area was investigated in this example. Increasing the concentration of binding sites was expected to improve intermolecular interaction, relaying benefits in characterising the bonding agent's mode of action. In contrast, the reverse slurry technique was found to develop particle aggregation. Collapse of the fragile formations exposed the surface of uncoated RDX, further detracting from the technique's performance.

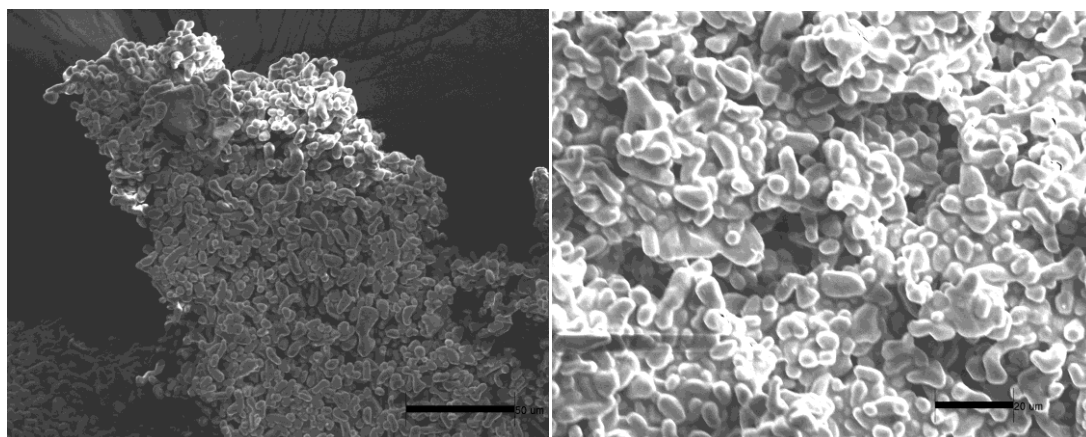


**Figure 2.9.** Reverse slurry coating of RDX in 10% Dantocol.

Attempts to resolve these issues involved the addition of Dantocol, following recrystallisation of RDX. Regardless of this, negligible improvements were observed in Figure 2.10. The desired changes in particle size were again apparent, generating coated crystals of 5-10 $\mu\text{m}$ . Meanwhile, the reoccurrence of agglomerate formation and associated issues, denied the possibility of applying the technique.

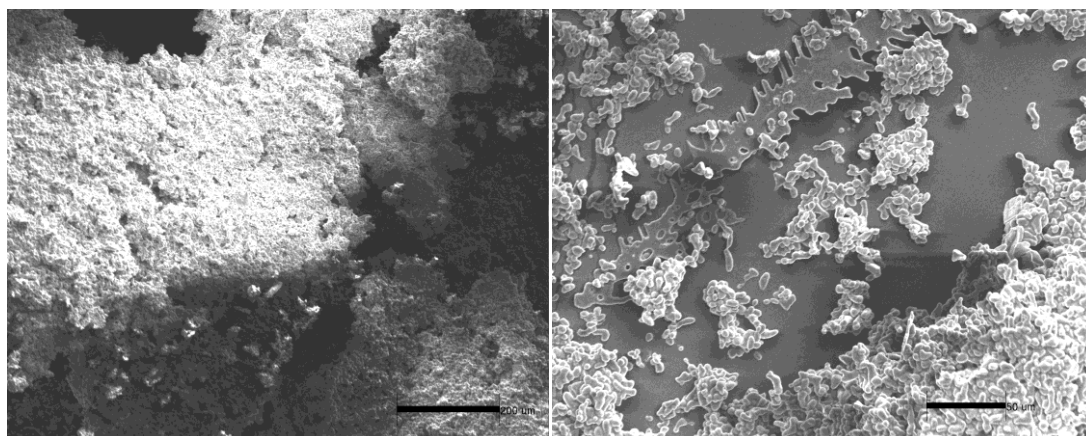


**Figure 2.10.** Reverse slurry coating of RDX in 10% Dantocol post recrystallisation.

### 2.3.2.3 Starved Addition Technique

Limiting the rate at which coating agents are introduced to slurries often provides an even coating distribution at the surface of particles.<sup>12</sup> The addition of coating agents in low concentration therefore assists in forming uniform coatings of individual suspended crystals.<sup>13</sup> When applied to the current system, dropwise addition of Dantocol enables complete coverage of RDX. Figure 2.11 highlights this occurrence, while deviations in topography indicate the presence of irregular thickness.

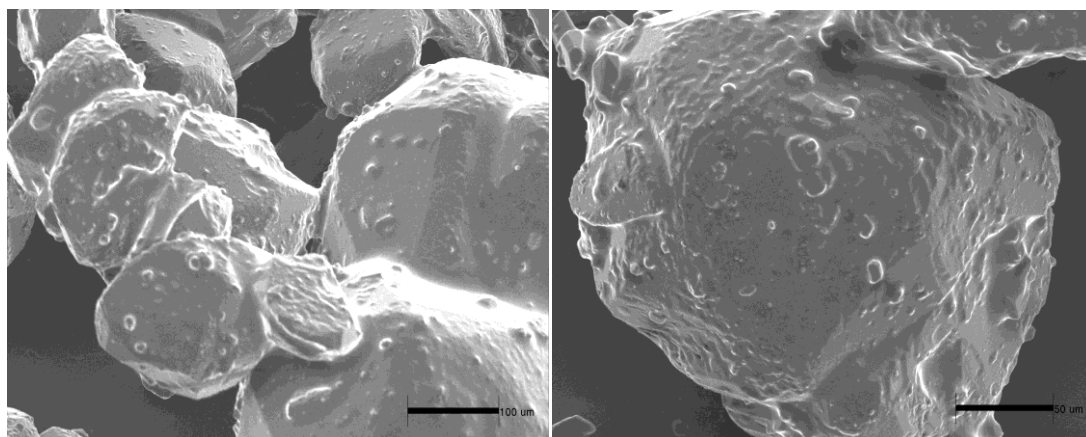


**Figure 2.11.** Starved addition coating of RDX in 10% Dantocol.

Separate issues arise from the length of time taken to achieve starved addition. Contributing to this is the dropwise addition of Dantocol and prolonged removal of H<sub>2</sub>O. This translates to highly laborious conditions, unfavourable in application.

To address these concerns a modified technique developed by Dagley et al. was implemented.<sup>2</sup> This involved substitution of solvents, with toluene and H<sub>2</sub>O replacing that applied to the RDX slurry. Isopropanol was also exchanged in regards to the bonding agent solution, due to its ability to function as a surfactant. Changes to solvent conditions provided mixed results, with aggregation resolved following addition of isopropanol. This introduced flow on benefits for solvent removal, according to the reduction in boiling point. However, coatings observed in Figure 2.12 indicates revised solvent conditions impede surface coverage. Changes to the surface morphology of RDX generate multi-faceted crystals, hindering adhesion of Dantocol in response to the smooth inert surface.

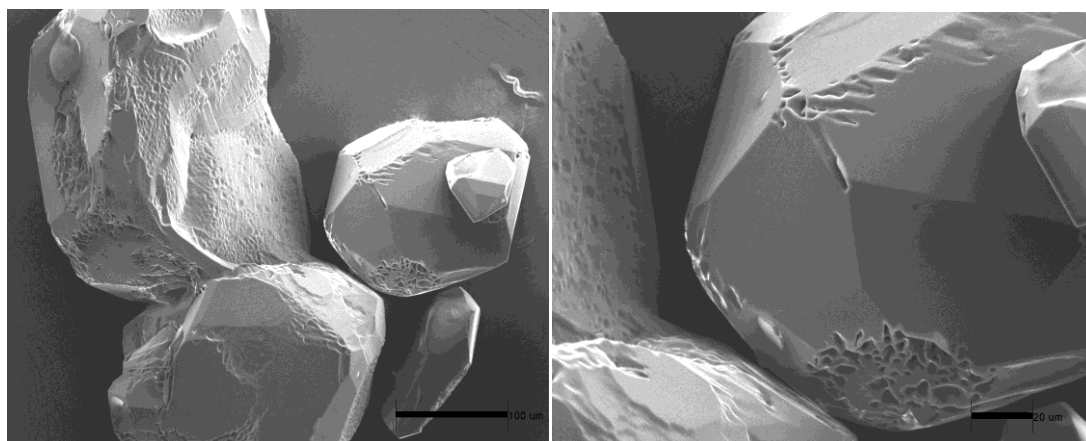


**Figure 2.12.** Starved addition coating of RDX in 10% Dantocol using alternative solvent conditions.

#### 2.3.2.4 Solvent/Antisolvent Technique

The solvent/antisolvent technique provides the unique ability to ensure precipitation of Dantocol. This employed chloroform and *n*-hexane, to promote precipitation onto the surface of RDX. The efficiency of precipitation was confirmed from the <sup>1</sup>H NMR of filtered solvents, as indicated by the absence of Dantocol. This also appeared absent from the filter membrane. Although this demonstrates the ability to ensure Dantocol adsorbs onto the surface of RDX, the distribution of surface coatings generated inconsistencies. This emerged as regions of intermittent thickness, as depicted in Figure 2.13.

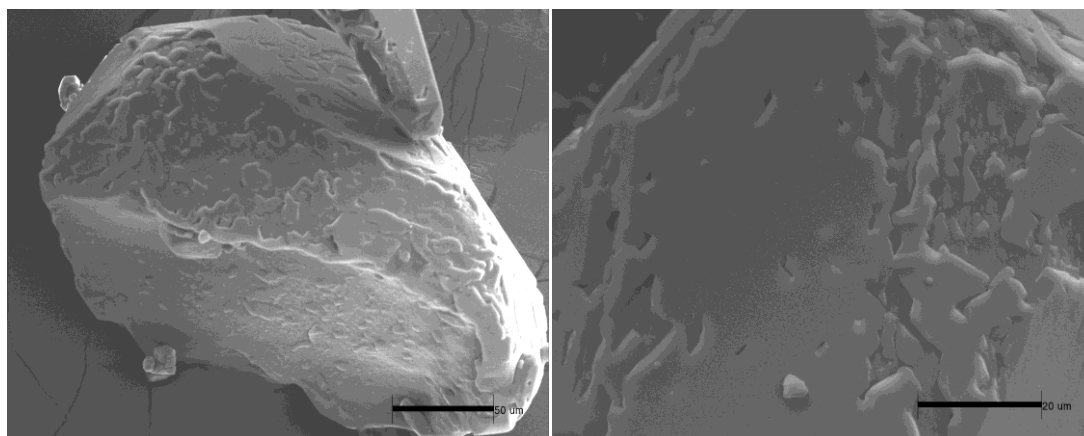


**Figure 2.13.** Solvent/antisolvent coating of RDX in 10% Dantocol.

Further investigation of the solvent system focused on improving the uniformity of coatings. This involved preparing a solution of Dantocol and chloroform, while RDX was dissolved by dropwise addition of tetrahydrofuran. Solutions were combined and recrystallised overnight at reduced temperature. This provided conditions necessary to establish uniform RDX coatings.

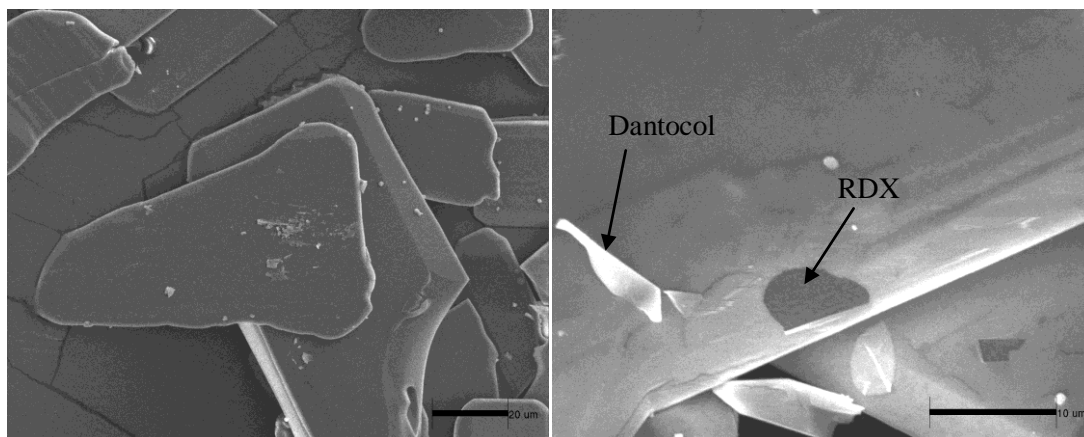


**Figure 2.14.** Solvent/antisolvent coating of RDX in 10% Dantocol, involving chloroform/tetrahydrofuran.

Inspection of the coating layer at high resolution revealed an area of dewetting measuring  $5\mu\text{m}$  in length. This manifests as a darkened area representing the exposed surface of RDX. Onset of this event was observed following bombardment of the surface with electrons, originating from the SEM electron beam. This indicates the impinging electrons provide

sufficient energy to cause propagation of dewetting. Observation of this phenomenon offers insight into the physical properties of dewetting. This also suggests the formation of planar crystals creates a smooth inert surface, responsible for dewetting. The susceptibility towards removal of Dantocol impedes characterisation, rendering the procedure flawed.

### 2.3.2.5 Aqueous suspension-melting technique

An aqueous suspension-melting technique was originally developed by Chong-Wei, for application in RDX coatings.<sup>10</sup> Interpretation of the procedure to facilitate use of Dantocol revealed only partial coverage of RDX. Adverse changes in crystal morphology were also incurred during the coating procedure. This involved deviation from rounded particles, towards that of multi-faced crystals observed in Figure 2.15. Further disruption in the form of crevices was identified at the surface of treated RDX. These changes in crystal morphology can be attributed to crystalline growth, as confirmed by the increase in particle size. Consequently, this technique was found to provide an inaccurate representation of processes occurring within a typical PBX submix.

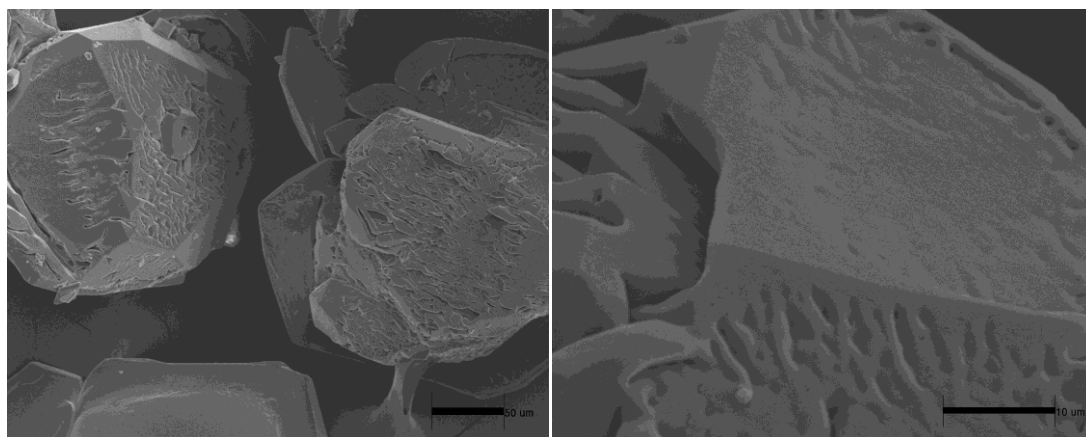


**Figure 2.15.** Aqueous suspension/melting coating of RDX in 10% Dantocol.

### 2.3.3 Microencapsulation

The process of microencapsulation is commonly applied in the pharmaceutical industry to isolate medication from its surroundings, or control the rate of its release. This was adapted

to coating energetic particles, with initial results indicating potential. Further investigations demonstrated advantages over previous methods, leading to its adoption for coatings.

Microencapsulation delivered individually coated particles of uniform thickness, while maintaining the crystal morphology of RDX. This also resolved issues associated with peeling, and the formation of pores. The ability to overcome these problems is decisive in optimising the interaction of Dantocol prior to characterisation. Based on this success, steps involved in microencapsulation were investigated to improve coating efficiency.

### **2.3.3.1 Solvent Evaluation**

In response to microencapsulation, the solvent system is required to perform three primary functions. The first involves the ability to disperse and suspend energetic crystals without influence on crystal morphology or chemistry. Secondly, the solvent must dissolve the bonding agent, whilst enabling adhesion to crystals. Finally, a preferred embodiment suggests the solvent acts as a surfactant, lowering the interfacial tension between liquid and solid components.

Solvent polarity is similarly as important to that of the binder system in PBX formulations. This determines the bonding agent's ability to migrate towards filler particles and adsorb to the surface. As evident in polar binder systems, the bonding agent's high polarity prevents Dantocol from accumulating at the filler surface if too soluble. This causes the bonding agent to remain in solution, highlighting the importance of solvent selection. Consequent efforts were made to identify solvents displaying favourable chemical properties.

Of those solvents evaluated, three were found to dissolve Dantocol while enabling RDX to remain in suspension. Ethanol, chloroform and methylene chloride each satisfied these requirements, while carbon tetrachloride was considered in accordance with work conducted by Marmo et al.<sup>14</sup> This suggests carbon tetrachloride displays superior capabilities for enabling adsorption of polar compounds at the surface of polar particles.

In the interest of optimising coatings, prospective solvents were evaluated in terms of their performance in microencapsulation. This required elucidation of interactions between solvents and RDX to isolate that occurring with Dantocol. Characterisation of RDX washed in respective solvents employed NMR, FTIR and SEM to determine compatibility. This involved mixing solvent and RDX over an extended period, followed by distillation. Washed samples were then compared with untreated RDX to identify inconsistencies. Spectroscopic techniques confirmed the absence of peak shift, indicating negligible interaction between RDX and proposed solvents. Figure 2.16 also highlights removal of solvents, as confirmed by the absence of peak formation.

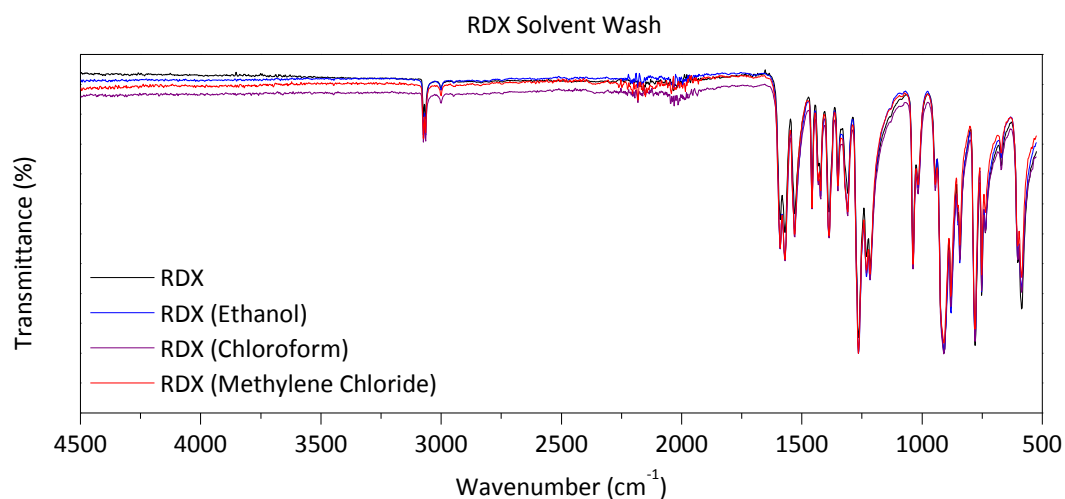


**Figure 2.16.** IR spectra of RDX washed in solvent.

In contrast to spectroscopic analysis, inspection of the crystal surface via SEM revealed inconsistencies in washed samples. This involved disruption to the nitramines smooth crystalline surface, following exposure to chloroform and ethanol. Observations suggest partial dissolution of RDX results in the abrasive surfaces depicted in Figure 2.17. An advantage of disrupting the nitramines smooth inert surface involves the potential improvements in bonding agent adhesion. This is otherwise known to contribute towards dewetting in cast-cured PBX composites.

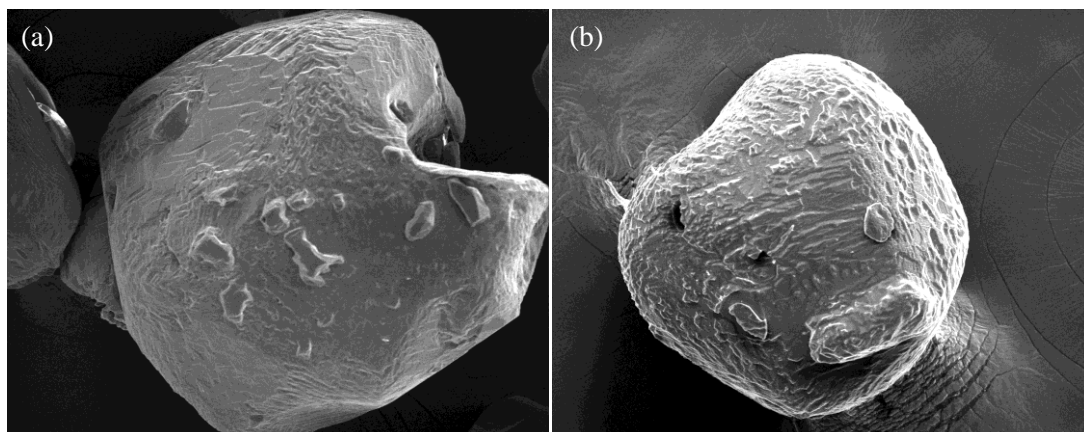


**Figure 2.17.** RDX crystals washed in (a) chloroform and (b) ethanol.

Evidently the remaining solvents have no discernible impact on the surface morphology of RDX. Inspection of crystals washed in carbon tetrachloride and methylene chloride, reflected that of untreated RDX. This indicates limited interaction with filler particles, satisfying initial solvent requirements. The ability to eliminate competing interactions is crucial in isolating the interaction of RDX and Dantocol.

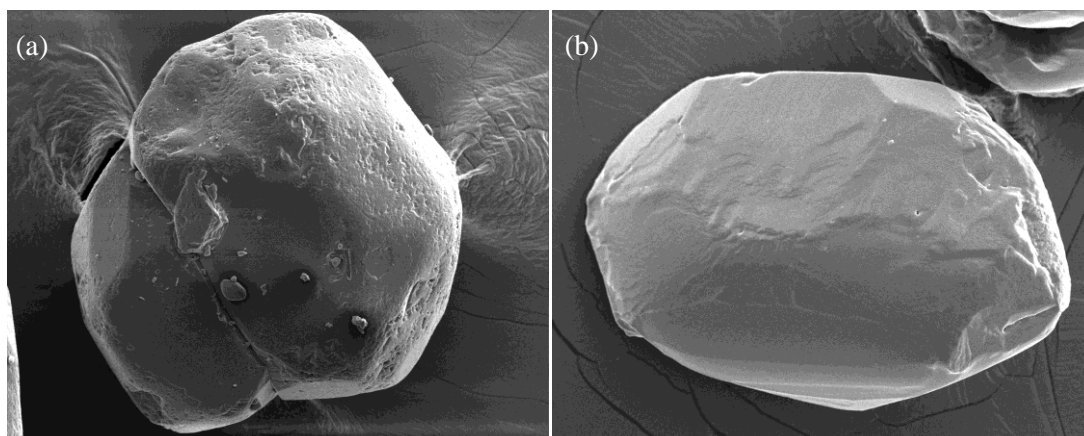


**Figure 2.18.** RDX washed in (a) carbon tetrachloride and (b) methylene chloride.

The influence of solvent polarity may prevent Dantocol from adsorbing to filler particles if exceeding that of the bonding agent. Of the available solvents, polarity increases as follows; carbon tetrachloride < chloroform < methylene chloride < ethanol. Both carbon tetrachloride and chloroform represent non-polar solvents, suggesting improved ability to perform microencapsulation. As methylene chloride is considered only slightly polar, this is also



likely to result in adsorption of Dantocol at the surface of RDX. The polar aprotic solvents inability to participate in hydrogen bonding also creates an advantage over ethanol. Protic solvents able to engage in such interaction may potentially compete for binding sites. Irrespective of these details, the bonding agent high polarity was sufficient to enable adsorption within ethanol.

### **2.3.3.2 Mixing Conditions**

Investigations continued into the conditions necessary to accommodate solvents identified, within the current procedural method. This involved monitoring the timeframe constituents were mixed during microencapsulation. Results indicated an appropriate duration for coating, while avoiding the onset of surface disruption due to ethanol. The influence of mixing times was repeated for chloroform and methylene chloride, with Dantocol coatings evaluated at various intervals.

Mixing in ethanol was initially performed over 1-7 days, to gauge the effect of prolonged exposure on the quality of coatings. As the duration of mixing was increased, coatings failed to show appreciable improvements. In contrast, the surface of RDX was found to deteriorate in line with previous observations. Disruption to coatings suggests reduced mixing times are required. Figure 2.19 demonstrates the coating efficiency at 15, 30 and 60min intervals, with negligible deviation observed. During this period, Dantocol was successfully dispersed amongst RDX particles, while migrating towards the nitramines binding sites.

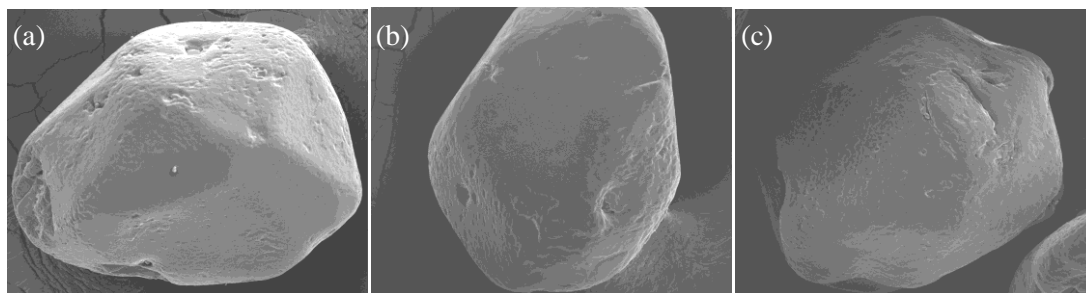


**Figure 2.19.** RDX coated with 10% Dantocol in ethanol, applying mixing times of  $T =$  (a) 15mins (b) 30mins (c) 60mins.

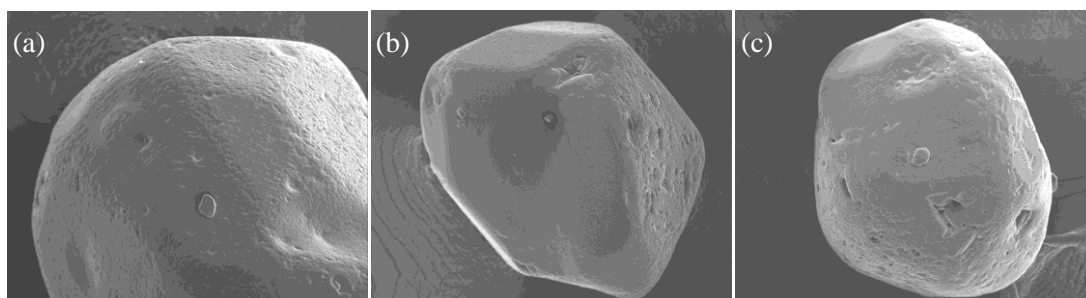


**Figure 2.20.** RDX coated with 10% Dantocol in chloroform, applying mixing times of  $T =$  (a) 15mins (b) 30mins (c) 60mins.

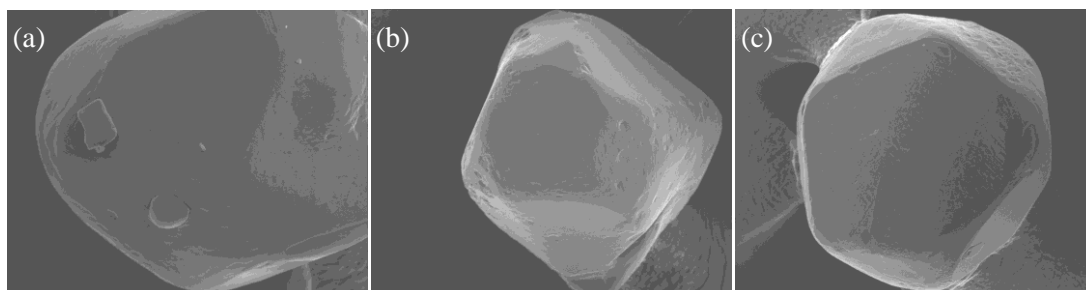


**Figure 2.21.** RDX coated with 10% Dantocol in methylene chloride, applying mixing times of  $T =$  (a) 15mins (b) 30mins (c) 60mins.

Substitution of chloroform and methylene chloride similarly displayed uniform coatings after  $T \leq 60$ mins. Carbon tetrachloride was omitted from investigations due to its toxicity and inability to dissolve Dantocol without heat. The remaining solvents applied were considered to yield superior coating efficiency within the prescribed timeframe.

Additional requirements stipulate particles are continuously agitated, ensuring separation necessary to produce individually coated particles. Investigations revealed inefficiencies in

this regard are capable of prompting agglomerate formation. Conversely, exposure to excessive agitation increased particle collisions, potentially damaging the coating layer and crystal structure. This observation was originally reported by Dagley et al. following use of agitation to limit the particle size of coated energetic crystals.<sup>2</sup> Increasing the solvent volume further minimised particle collisions, assisting in maintaining uniform surface coverage. Consideration of these results led to modification of coating procedures, thus incorporating experimental findings.

### 2.3.3.3 Solvent Removal

Microencapsulation typically employs filtration, often coupled with heating to remove solvents. However, exposure of Dantocol to elevated temperatures caused the bonding agent to soften, while promoting pore formation. This also allows for loss of Dantocol upon filtering the solution. An alternative method was therefore developed, involving distillation to remove only the solvent content. This provides the additional benefit of concentrating the bonding agent solution, causing precipitation onto the surface of RDX. Solvent volatility is therefore an advantage to assist with removal.

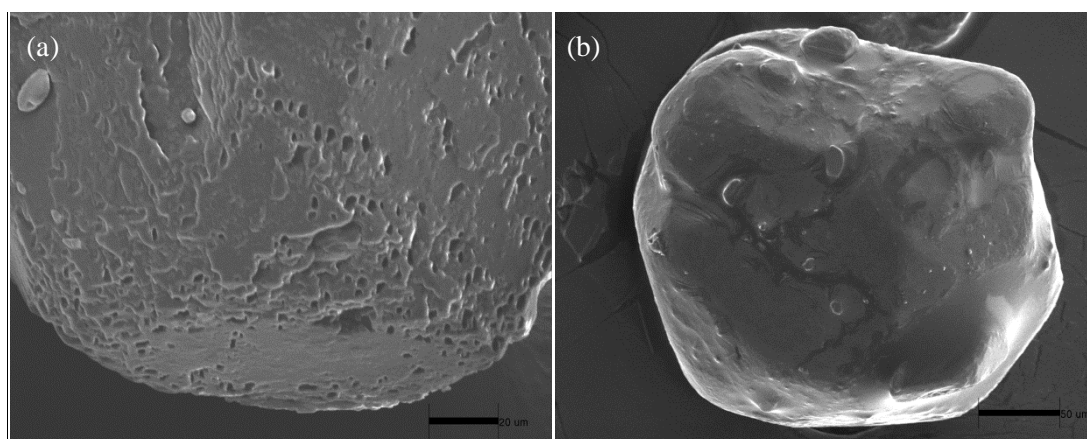


**Figure 2.22.** Coating of RDX in 10% Dantocol, involving use of (a) filtration/heat and (b) distillation to remove solvent.

Following distillation of solvents, coated RDX was stored under silica gel to maintain anhydrous conditions. Solvent removal was confirmed according to the  $^1\text{H}$  NMR of coated RDX. This indicated an absence of impurities in the chemical shift region of ethanol ( $\delta =$

1.12 , 2.47, 3.54ppm), chloroform ( $\delta = 7.58\text{ppm}$ ) and methylene chloride ( $\delta = 5.44\text{ppm}$ ).<sup>15</sup> Based on these findings an effective method for solvent removal was identified, with distillation incorporated into the standard procedure.

#### 2.3.3.4 Surfactant additives

Addition of surfactants was investigated to prevent the onset of agglomeration. Resolution of this issue ensures particles are individually coated, avoiding the occurrence of partial encapsulation. This was achieved by lowering both surface and interfacial tension between particles and the bonding agent solution. Vannet et al. previously applied polyvinyl alcohol as a surfactant to assist in coating energetic crystals.<sup>13</sup> Polyvinyl alcohol was found to prevent agglomeration resulting from adhesion of particles through the course of wet coating. Introduction of protective colloids provides shielding to prevent coated particles from contacting, thus forming agglomerates.<sup>7</sup> This was also exploited by Dagley et al. to provide uniform coating of RDX through incorporating non-ionic and cationic surfactants.<sup>2</sup>

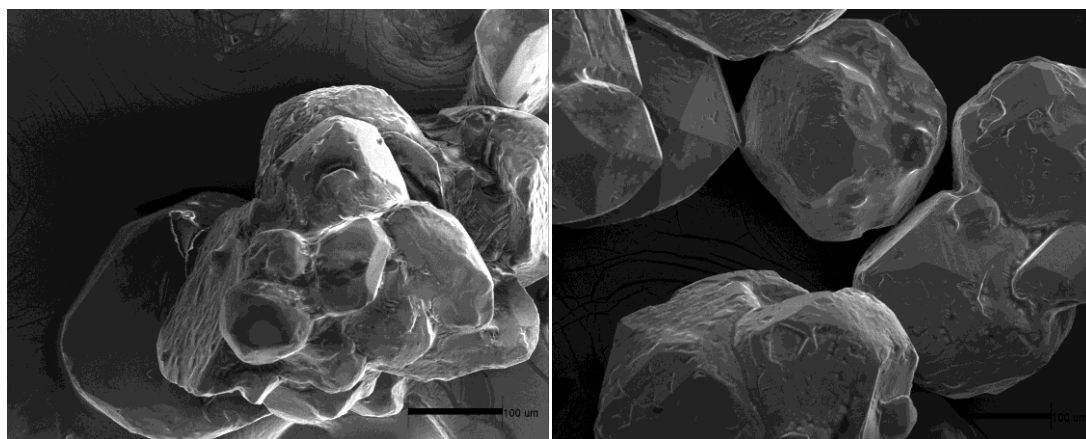


**Figure 2.23** Coatings of RDX in 10% Dantocol (a) before and (b) after surfactant addition.

Based on the success of previous studies, the addition of surfactants was investigated in terms of their ability to improve coatings. Dantocol's low molecular weight suggests the inclusion of surfactants is likely to benefit microencapsulation. Figure 2.23 demonstrates the impact of adding polyvinyl alcohol 0.1% (w/w) in resolving issues associated with agglomerate formation.

Although polyvinyl alcohol was found to resolve aggregation, the role of surfactants can also be performed by an appropriate solvent. The ability of solvents to function as surfactants is highly advantageous, as this negates the potential for additives to interrupt characterisation of interactions. Inspection of coatings involving proposed solvents displayed equivalent ability to prevent aggregation, compared with additives such as polyvinyl alcohol.

### 2.3.3.5 Microencapsulation Procedure

Optimisation of microencapsulation led to developing an effective means of providing uniform coatings. This emerged as the leading method to facilitate characterisation of bonding agent interaction. Investigation of variables identified the conditions necessary to optimise microencapsulation. This served to provide individually coated particles, while maintaining crystal morphology. Along with contributing to undisrupted surface coatings, microencapsulation displayed superior capabilities over alternative methods. Consequently this procedure was adopted for all further coatings, unless otherwise indicated.

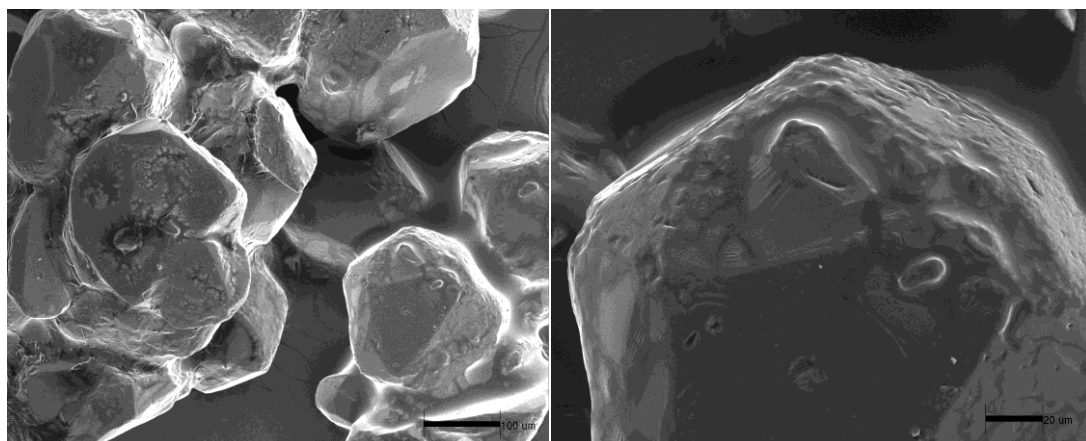


**Figure 2.24.** Microencapsulation of RDX in 10% Dantocol.

## 2.4 Conclusion

Numerous coating techniques were investigated to determine a method capable of delivering uniform coatings, while limiting agglomerate formation. Of those based on the slurry technique, the majority were found to provide a level of surface coating. However, these

failed to provide complete coverage, while often displaying issues pertaining to aggregation, coating thickness and disruption to surface morphology. These observations highlighted the need to devise an alternative method for providing quality coating of RDX. Achieving this represents the first critical step in characterising the interaction of RDX and bonding agents, thus providing the basis for future work.

Implementing microencapsulation established superior coatings, exceeding that of previous efforts. This has formerly been applied to protective coating, preventing exposure of core particles to the adverse effects of UV rays, moisture and oxygen.<sup>9</sup> The adaptation for nitramine particles involved suspending RDX in a bonding agent solution, followed by removal of solvent to cause precipitation of Dantocol. In addition to delivering uniform coatings, microencapsulation has no measurable impact on the structure, crystal morphology or particle size of RDX crystals. This is necessary to characterise the interaction of Dantocol and RDX as it occurs in PBX formulations.

The role of solvent is critical towards satisfying these requirements. In the presence of acidic or basic conditions, solvents may inhibit interaction of energetic particles and coating agents.<sup>14</sup> This stipulates the adsorption of Dantocol proceeds only when interaction with RDX is favoured over the solvent system. Methylene chloride was nominated based on its ability to dissolve Dantocol, while enabling RDX to remain insoluble. The bonding agent's solubility eliminated the need for heating, while the polarity of methylene chloride promoted constituent interaction. Demonstration of low boiling point also assisted with the removal of solvent during the latter stages of microencapsulation.

Interactions were enhanced, as the result of purifying constituents to remove impurities competing for binding sites. In particular, drying hygroscopic components was shown to eliminate residual water, capable of occupying hydrogen bonding sites. Addition of the purification step, coupled with coating optimisation delivered the means necessary to promote interfacial interaction. The significance of this is apparent throughout following chapters, which characterise Dantocol's mode of action.

## 2.5 References

1. Eerligh, R.; Van Gool, M. A.; Kramer, R. E.; Van Ham, N. H. A., Investigation of the result of coating techniques of high explosives with the aid of scanning electron microscope / energy-dispersive X-ray spectrometry. *17th Annual International ICT Conference* **1986**, 10-1.
2. Dagley, I. J.; Spencer, H. J.; Louey, C. N.; Parker, R. P., An Evaluation of Ethylene-Vinyl Acetate Copolymers as Desensitizers for RDX in Insensitive Booster Compositions Prepared by the Slurry Coating Technique. **1989**, (MRL-TR-89-33), 1-49.
3. Dagley, I. J.; Spencer, H. J.; Louey, C. N.; Parker, R. P., Pressed booster compositions prepared by coating RDX using polymer dispersions. *Journal of Energetic Materials* **1992**, *10* (2 & 3), 127-149.
4. Wright, S. B. Granular explosive moulding. US Patent 3,173,817, **1965**.
5. Wright, S. B. Granular crystalline plastic bonded explosives. US Patent 3,296,041, **1967**.
6. Hildebrant, F. J.; Banker, B. R. Process for coating crystalline high explosives. US Patent 4,092,187, **1978**.
7. Meulenbrugge, J. J.; Kramer, R. E.; Leeuwenburgh, A. B., Investigation into the microencapsulation of RDX in viton. *Technology of Energetic Materials* **1987**, *18*, 32/1 - 32/13.
8. Reed, R.; Stanton, H. D. Mouldable ethylene/vinyl acetate copolymer. US Patent 4,090,894, **1978**.
9. Eslami, A.; Hosseini, S. G.; Shariaty, S. H. M., Stabilization of ammonium azide particles through its microencapsulation with some organic coating agents. *Powder Technology* **2010**.
10. An, C.-W.; Li, F.-S.; Song, X.-L.; Wang, Y.; Guo, X.-D., Surface Coating of RDX with a Composite of TNT and an Energetic-Polymer and its Safety Investigation. *Propellants, Explosives, Pyrotechnics* **2009**, *34* (5), 400-405.
11. Kuo, S.-W., Hydrogen-bonding in polymer blends. *Journal of Polymer Research* **2008**, *15* (6), 459-486.
12. Worley, C. M.; Vannet, M. D.; Ball, G. L.; Moddeman, W. E., Surface chemistry of a microcoated energetic material, pentaerythritoltetranitrate (PETN). *Surface and Interface Analysis* **1987**, *10* (6), 273-279.
13. Vannet, M. D.; Ball, G. L., Pourability enhancement of PETN explosive powders. *Journal of Energetic Materials* **1987**, *5* (1), 35-55.
14. Marmo, M. J.; Mostafa, M. A.; Jinnal, H.; Fowkes, F. M.; Manson, J. A., Acid-base interaction in filler-matrix systems. *Industrial & Engineering Chemistry Product Research and Development* **1976**, *15* (3), 206-211.
15. Fulmer, G. R.; Miller, A. J. M.; Sherden, N. H.; Gottlieb, H. E.; Nudelman, A.; Stoltz, B. M.; Bercaw, J. E.; Goldberg, K. I., NMR Chemical Shifts of Trace Impurities: Common Laboratory Solvents, Organics, and Gases in Deuterated Solvents Relevant to the Organometallic Chemist. *Organometallics* **2010**, *29* (9), 2176-2179.





# Chapter 3

---

## Characterisation of interfacial interactions by FTIR

---

Sections of this chapter were published in: Williams, C. A.; Walker, G. S.; Lochert, I. J.; Clarke, S., Investigation into the interaction of Dantocol in polymer bonded explosives and the impact on mechanical properties. *Parari 10th Australian Explosive Ordnance Symposium*, Brisbane, Australia, 2011; 9, pp 1-7.

Williams, C. A.; Walker, G. S.; Lochert, I. J.; Clarke, S., Investigation into the interaction of Dantocol in polymer bonded explosives and bonding agent development. *16th New trends in energetic materials*, Pardubice, Czech Republic, 2013; Vol. I, pp 399-406.

### **3.1 Introduction**

Fourier Transform Infrared spectroscopy (FTIR) was used to evaluate interfacial interactions, owing to its high signal to noise ratio and ability to analyse samples in any phase. This is particularly advantageous as RDX interacts with bonding agents while in the solid phase, whereas Dantocol exists as either liquid or solid at room temperature. Crystalline RDX is known to exhibit favourable scattering properties, which in turn produce sharp spectral peaks.

Numerous FTIR techniques of differing surface sensitivities were applied to investigate the interaction between Dantocol and RDX. This involved application of Diffuse Reflectance Infrared Fourier Transform Spectroscopy (DRIFTS), Photoacoustic Spectroscopy (PAS), Attenuated Total Reflectance Spectroscopy (ATR) and transmission spectroscopy. Each displays unique qualities suitable for surface analysis, which enables investigation of the interface region. Combined, these methods provide complimentary information pertaining to vibrational bands involved in intermolecular interaction. This provides a comprehensive representation of both surface and bulk properties for coated RDX, within the mid infrared region.

#### **3.1.1 Comparison of FTIR Techniques**

Infrared spectroscopy represents the most widely used technique for investigating surface interactions. This is due to the surface sensitivity of FTIR techniques, which are highly sensitive to surface adsorbates. Consequently, vibrational modes exhibit shifts proportional to the interaction of surface terminal groups. This provides an effective means for detection and characterisation of intermolecular forces within infrared spectra.

Employing multiple FTIR techniques provided a comprehensive representation of the interface region between constituents. Typically, this involves transmission, reflectance and photoacoustic spectroscopy to evaluate the source of interfacial interactions. Techniques

display variation in wavenumber and intensity of a particular sample, with vibrational bands often found to disappear entirely, depending on sensitivity. Spectral deviations signify the range of surface and bulk sensitivities between methods. Subsequently, fewer bands evolve for ATR and transmission spectrums compared to DRIFTS and PAS, which exhibit increased surface sensitivity.

The ability of PAS to perform depth profiling provides a valued tool with which to probe the interface region. This was achieved by detection of the acoustic signal generated by absorption of incident infrared radiation.<sup>1</sup> DRIFTS meanwhile provides increased surface sensitivity, due to infrared light impinging upon the detector having reflected from the particle surface. Similar surface sensitivity can be achieved by transmission spectroscopy, when conditions enable the particle bulk to completely absorb incident light, allowing only that which passes through the outermost surface to arrive at the detector.<sup>2</sup>

In comparison, ATR involves infrared light passing through an internal reflection element such that it reflects off the internal surface in contact with the sample. Infrared light is absorbed causing the beam to penetrate a thin surface layer. The penetration depth of radiation is typically between 0.5-2.0 $\mu\text{m}$ , producing a spectrum representative of the surface region. Factors which determine the surface sensitivity of ATR include the refractive index of the internal reflection element, sample composition and wavelength of incident light.<sup>2</sup> The contribution of surface or bulk detection is further influenced by particle size and surface gradient of samples. Consequently, these conditions have been exploited in order to optimise characterisation of the surface region.

The combined capabilities of FTIR techniques provide a comprehensive spectral profile of the interface. This is achieved by exploiting the surface sensitivity of each to obtain a series of spectra depicting the region. The role of individual techniques is described in the following section, outlining advantages as relevant to the investigation. Applying these attributes to characterisation of surface interactions provides a definitive response to the bonding agent's mode of action.

### 3.1.1 Attenuated Total Reflectance

ATR was implemented to identify functional groups responsible for interaction between RDX with Dantocol. This involves incident light passing through a high refractive index diamond stage, allowing radiation to penetrate the surface and reflect within the sample. Incident light penetrates a thin layer of the surface, losing energy characteristic of the wavelength absorbed by the material. This generates a surface spectrum, which was previously applied to characterise HMX coated with a Viton fluoroelastomer.<sup>3,4,5</sup>

ATR has the advantage of negligible sample preparation, increased surface sensitivity and requires fewer scans than alternative techniques. In relation to current investigation, ATR also eliminates the need for grinding during sample preparation which may disrupt coatings. Samples are applied directly to the stage, producing both sharp peaks and reproducible spectra. The capability of ATR to characterise both solids and liquids enabled the analysis of RDX crystals, along with Dantocol which exists in liquid or solid state at room temperature.

### 3.1.2 Transmission Infrared Spectroscopy

Although uncommon in surface analysis, application of transmission IR has previously been applied to investigate interactions between ammonium perchlorate and bonding agents with considerable success.<sup>6,7</sup> Typically, reflectance techniques are employed for the purpose of surface analysis, due to their increased surface sensitivity. Despite this trend, current advances in FTIR spectrometers has seen sensitivity improved to a point where spectra are now measurable from even a single surface monolayer.<sup>8</sup> Such capabilities have prompted further application in coating chemistry, including use of transmission spectroscopy in the characterisation of polymer coated RDX and HMX particles.<sup>5,9,10</sup> These citations combined reflection and photoacoustic spectroscopy to validate the results of transmission spectra.

As previously described, when conditions enable the particle bulk to completely absorb incident light, this allows only that passing through the outermost surface layer to arrive at

the detector.<sup>2</sup> In addition to increasing the surface area of particles, these properties are often exploited to improve the surface sensitivity of transmission spectroscopy.

Increasing the surface area also impacts the portion of incident light originating from the surface, as opposed to the bulk. This improves the quality of spectra, with particles greater than 20 $\mu\text{m}$  absorbing excess light, causing a sloping baseline. Sample preparation therefore involves grinding in order to lower the particle size. Solid samples are mixed with potassium bromide (KBr), which is pressed into discs used to obtain transmission spectra. KBr is employed due to its infrared transparency which enables sample dilution. The challenge with preparing KBr discs lies in optimising thickness, sample concentration and particle size to improve surface sensitivity.

### 3.1.3 Photoacoustic Spectroscopy

In providing a complete assessment of coated RDX crystals, PAS was applied to characterise samples. PAS is a non-destructive method which can be used for surface depth profiling through varying the mirror velocity. The technique operates by detection of an acoustic signal, generated during absorption of infrared radiation.<sup>1</sup> Infrared light is focused on samples within the PAS chamber, whereby light characteristic of the absorption spectrum of the material is absorbed, causing fluctuation in surface temperature. The change in surface temperature produces periodic variation in gas pressure within the cell. This results in the development of soundwaves, detected by microphone to record the frequencies of infrared absorption. The depth from which thermal waves originate is described in Equation 3.1.<sup>5</sup>

$$\mu_s = \left(\frac{2\alpha}{\pi f}\right)^{1/2} \quad (3.1)$$

Whereby  $\mu_s$  is the thermal diffusion length of the sample being studied, which represents the distance below the surface that the heat generated can convey with the surface. The thermal diffusivity is assigned  $\alpha$ , while  $f$  represents the fourier frequency as described by Equation 3.2.

$$f = 2Vv \quad (3.2)$$

The mirror velocity of the interferometer is given by  $V$ , with  $v$  defined as the wavenumber of incident radiation. The depth of penetration is therefore dependant on the thermal diffusion length which is varied by selection of the fourier frequency. This is achieved through adjusting the mirror velocity to provide spectral data from altering depths. Decreasing the mirror velocity produces an increase in thermal diffusion length, causing the photoacoustic signal to penetrate greater depths. This forms the basis of depth profiling, enabling collection of IR spectra at varying sample depths.

### 3.1.4 Diffuse Reflectance Infrared Fourier Transform Spectroscopy

DRIFT spectroscopy was employed as the primary method for analysing shifts in the vibrational modes of coated RDX. This yields significant advantages over conventional IR methods, owing to superior surface sensitivity. Consequently, DRIFTS is regularly applied in the analysis of solid particles to identify coatings and elucidate interaction between adsorbates and surface functional groups. This is facilitated by reflection of the infrared light from the surface of particles. Light is additionally transmitted through particles, whereby the process is repeated amongst neighbouring particles. This increases the path length of scattered IR light, before being focused onto the detector by an ellipsoidal mirror. The partially absorbed signal reaching the detector consequently conveys information originating from the surface region. Diffuse reflectance also has advantages over internal reflectance and ATR, as problems associated with optical contact are avoided.<sup>9</sup>

The most widely used model for quantitatively describing the process of diffuse reflectance was developed by Kubelka and Munk.<sup>11</sup> This assumes a plane parallel layer of particles is illuminated randomly with monochromatic radiation. For an infinitely thick layer occurring at penetration depths of  $\geq 3$  mm, diffuse reflectance ( $R_\infty$ ) becomes:

$$\frac{(1-R_\infty)^2}{2R_\infty} = \frac{k}{s} \quad (3.3)$$

This is known as the Kubelka-Munk expression, which defines the units of DRIFT spectroscopy. Like the Beer-Lambert law, the absorption coefficient  $k$  is proportional to the product of the absorptivity  $a$  and concentration  $c$  therefore:

$$R_{\infty} = \frac{(1-R_{\infty})^2}{2R_{\infty}} = k'ac \quad (3.4)$$

Assuming the scattering coefficient  $s$  is constant, this expression relates the reflectance of a sample to its concentration in the same way Beer's Law relates absorbance to concentration.<sup>12</sup>

## **3.2 Experimental**

### **3.2.1 Fourier Transform Infrared Spectroscopy Techniques**

#### **3.2.1.1 Attenuated Total Reflectance**

ATR was operated in conjunction with a Nicolet Nexus 8700 FT-IR Spectrophotometer. Alignment of the ATR stage was performed using bench diagnostics and a sample gain of 2.0 specified. Scans amounting to 128 per acquisition were recorded on a MCT/A detector, measuring the intensity of reflected light at a resolution of  $2.0\text{cm}^{-1}$ . RDX samples were added neat to the diamond stage and optical contact maintained using the sample press affixed. The spectrum acquired was recorded in standard units of transmittance (%) and wavenumber ( $\text{cm}^{-1}$ ) using Omnic 7.3 computer software.

During the coating process, secondary bonding is greatly affected by the solvent content. Various solvents were therefore evaluated with the view of optimising coating efficiency. The stability of secondary bonded complexes are usually highest in non-polar organic solvents and lower in solvents that act as a hydrogen bond donor or acceptor.<sup>13</sup> To form a stable intermolecular complex, solvation of the receptor-substrate complex should be favoured over that of the associating species. Three solvents were identified as displaying the properties necessary for microencapsulation of RDX with Dantocol. This necessitated the

ability to dissolve Dantocol, whilst enabling RDX to remain insoluble within solution. Ethanol, chloroform and dichloromethane were deemed capable of performing this function, albeit to differing degrees of success. Each solvent was evaluated as per the coating process outlined in Section 2.3.3.1, and characterised by ATR and SEM. Dichloromethane was found to provide optimal conditions for application of coatings, according to the solvents polarity.

### **3.2.1.2 Transmission Spectroscopy**

Coated RDX samples (5.0mg) were mixed with KBr (500mg) purified and dried according to methodology described by Armarego et al.<sup>14</sup> Diluted samples were pressed into discs under loads of 20MPa for 2mins in vacuo. Once prepared, discs were stored over silica gel to prevent adsorption of moisture.

The transmission stage was used to align discs with the IR beam. This was purged with N<sub>2</sub> prior to collection of spectra. Vibrational data was recorded at a resolution of 2cm<sup>-1</sup> using a MCT/A detector. This was acquired over 128 scans, between a wavenumber range of 4000-650cm<sup>-1</sup>. The resulting spectra were reported in absorbance, expressed as Arbitrary Units (a.u).

### **3.2.1.3 Photoacoustic Spectroscopy**

PAS Spectra were obtained using a MTEC photoacoustic accessory for the Nicolet Nexus 8700 FT-IR Spectrophotometer. The cell was purged with helium gas and the dark spectrum acquired using carbon black over 4000-450cm<sup>-1</sup> wavenumbers. Experimental parameters engaged a resolution of 2cm<sup>-1</sup> fixed at 256 scans. Spectra of RDX samples were collected at mirror velocities of 0.1581, 0.3165, 0.4747, 0.6329, 0.9494 and 1.2659cm s<sup>-1</sup>, facilitating depth profiling. Coated RDX consisting 5-25% Dantocol were loaded into a 5mm sample tray for acoustic analysis.



#### **3.2.1.4 Diffuse Reflectance Infrared Fourier Transform Spectroscopy**

Reflectance spectra were recorded on a Nicolet Nexus 8700 FT-IR Spectrophotometer, with liquid nitrogen cooled MCT/A detector. The DRIFTS accessory was aligned using diagnostic software and the spectral resolution set at  $2.0\text{cm}^{-1}$ . Background spectra of KBr were collected over 256 scans, having dried the optical material at  $180^{\circ}\text{C}$  overnight to remove moisture. Sample preparation involved grinding  $\approx 5\text{mg}$  of coated RDX in  $100\text{mg}$  KBr, ensuring an even distribution of particles. Data collated from reflected light was measured in the standard Kubelka-Munk units.

Modifications to standard sample prep were performed, with the intent of preserving surface coatings, while optimising the signal to noise ratio. Difference in particle size is recognised as impacting transmission spectra, with large particles causing scattering which leads to shifts in the baseline and broadening of peaks. This occurrence is magnified in respect to DRIFTS, as infrared light travels within samples for an extended period, resulting in collection of a large portion of distorted energy. Grinding is therefore necessary to obtain satisfactory spectra, however this introduces potential for removing the bonding agent coating. Pre-grinding was therefore performed prior to coating RDX, in order to limit this occurrence. Coated samples ( $5\text{mg}$ ) were then combined with ground KBr ( $100\text{mg}$ ) and mixed by agitation to disperse particles. The resulting mix was transferred to the sample tray for analysis via reflectance methodology.

### **3.2.2 Advanced Signal Processing in the Resolution of Spectral Bands**

#### **3.2.2.1 Fourier Self-Deconvolution**

Fourier Self-Deconvolution (FSD) was applied to FTIR spectra as a means of resolving overlapping bands contributing towards the  $\text{NO}_2$  vibration of RDX. Spectra were converted to absorption units prior to performing deconvolution, processed using Thermo Electron Omnic 7.3 software. Deconvolution of the  $\text{NO}_2$  region employed a Lorentzian line shape function, with a resolution enhancement factor of 2.4 and bandwidth of  $13\text{-}18\text{cm}^{-1}$ .

### **3.2.2.2 Curve-Fitting**

Curve fitting was performed using the peak resolve feature, available from the Omnic 7.3 software suite. Application of Gaussian profile was employed according to its suitability for fitting solid samples. Iterations were repeated until a best fit was achieved.

## **3.3 Results**

### **3.3.1 Characterisation of Interfacial Interactions by FTIR**

FTIR is recognised as one of the most effective techniques for investigating intermolecular interactions, owing to its versatility and depth of information provided. The location of peaks is derived from the vibrational frequency of the molecule, causing evolution of characteristic bands. Importantly, the wavenumber of vibrational bands is also dependent on interactions occurring within the chemical environment. Presence of hydrogen bonding between molecules effectively lowers the bond energy by spreading the bonding energy over a greater area. This causes shifts towards lower energy, known as a bathochromic or red-shift.<sup>15</sup> Conversely, molecules experiencing repulsion forces exhibit blue-shifts towards higher energy.

Variation in position and intensity of bands associated with a particular compound result from participation of functional groups in intermolecular interaction. The presence of interaction may result in multiple spectroscopic scenarios. Weak interactions could also result in the formation of a small shift or shoulder in participating bands. Strong interactions produce a well-defined peak shift relative to the band involved. Alternatively, broad peak resulting from evolution of multiple peak shift may also occur.<sup>16</sup> The size of compounds may further influence the magnitude of peak shifts. Small compounds are known to exhibit greater shifts in comparison to peaks derived from that of greater mass.<sup>16</sup>

### 3.3.1.1 Attenuated Total Reflectance

ATR spectroscopy is an internal reflection method, involving infrared light passing through an ATR crystal, such that it reflects off the internal surface in contact with the sample. The beam penetrates a thin layer in the order of a few microns. This produces surface spectra, enabling investigation of near surface layers.<sup>17</sup>

To eliminate the possibility dichloromethane used in the coating process causes shifts in the spectra of coated RDX, investigation of RDX washed in dichloromethane was completed. Figure 3.1 depicts the overlay of RDX samples, indicating negligible solvent effect on washed RDX. Dichloromethane was therefore deemed suitable for application in coating procedures.

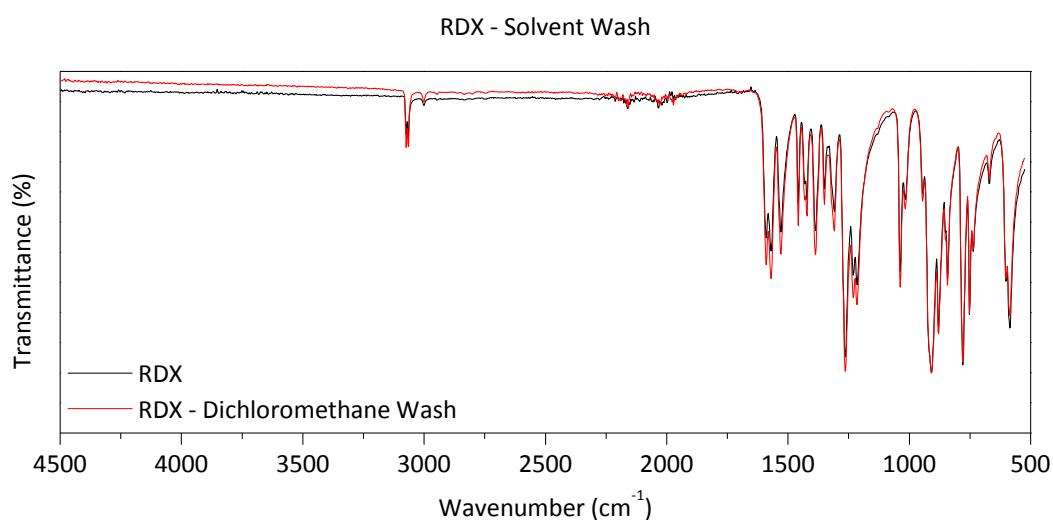


**Figure 3.1.** IR spectra of RDX and dichloromethane washed RDX.

Comparison of RDX spectra and coated samples were exploited to identify fundamental changes in vibrational bands. Of significance is the asymmetrical stretching vibration of the NO<sub>2</sub> group within the 1600-1500cm<sup>-1</sup> range. The location of RDX peaks at 1589cm<sup>-1</sup>, 1570cm<sup>-1</sup> and 1532cm<sup>-1</sup> is consistent with previous literature.<sup>5</sup> Inspection of the  $\nu_{as}$ NO<sub>2</sub> peak at 1532cm<sup>-1</sup> revealed a fundamental shift towards lower wavenumber in respect to coated RDX. Bathochromic shifts in the  $\nu_{as}$ NO<sub>2</sub> band are flagged in Figure 3.2.

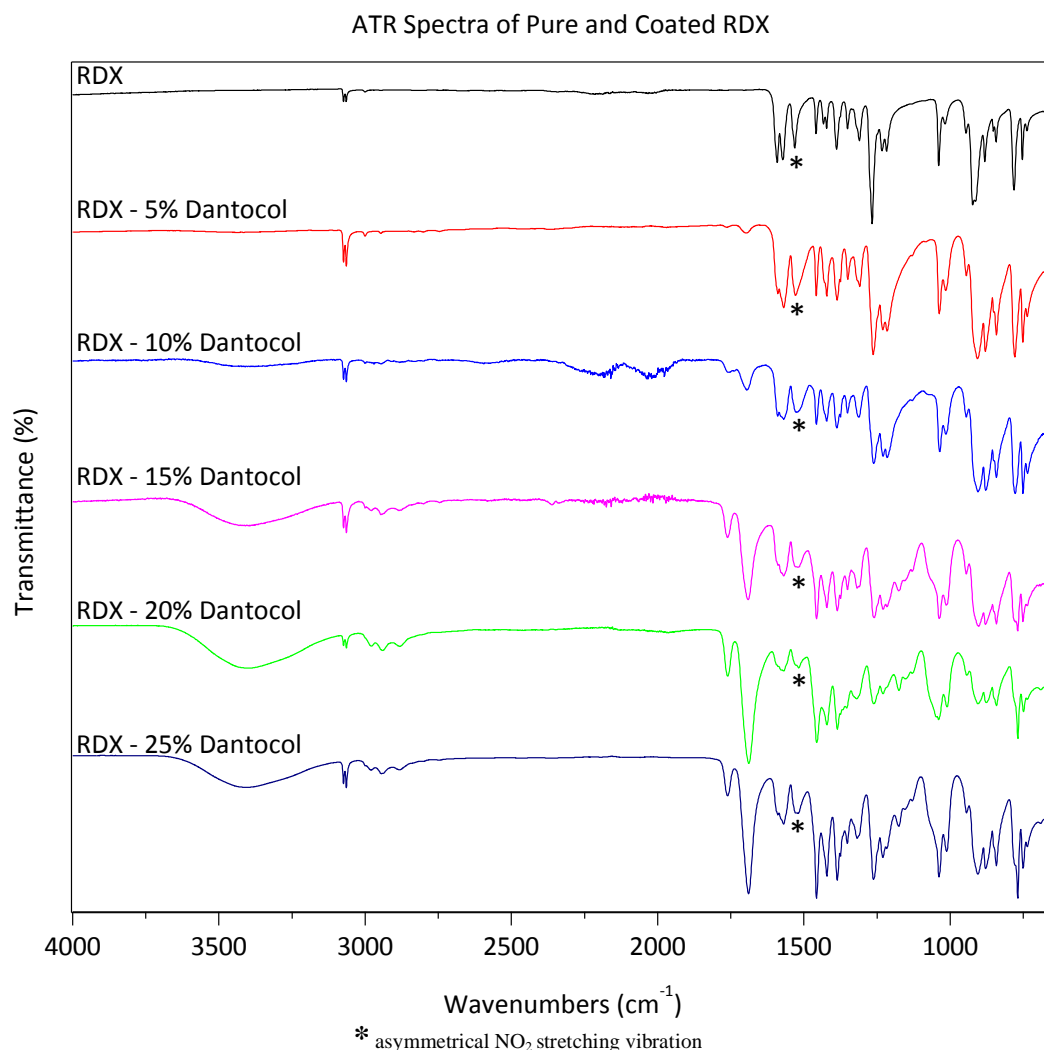


**Figure 3.2.** IR spectra of RDX and Dantocol 5-25% coated samples.

Bathochromic shifts in excess of  $\Delta\nu_{\text{as}}\text{NO}_2$   $15\text{cm}^{-1}$  were observed for Dantocol coatings  $\geq 20\%$  mass of RDX. The location of peak shifts negates the possibility of bands arising from Dantocol. Shifts are therefore indicative of hydrogen bond formation, occurring between NO<sub>2</sub> and OH functionality. Deviation in the asymmetrical NO<sub>2</sub> vibrational band is also accompanied by peak broadening. This is known to occur on account of the hydrogen bonded NO<sub>2</sub> peak overlapping that of the free NO<sub>2</sub> band.<sup>18</sup> Failure of the NO<sub>2</sub> wagging vibration to undergo peak shift suggests the orientation of the hydrogen bonding occurs along the N-O bond axis. Likewise, the absence of shift in peaks assigned to the CH<sub>2</sub> deformation at  $1433\text{cm}^{-1}$  and  $1459\text{cm}^{-1}$ , along with the N-N bond vibration at  $1310\text{cm}^{-1}$  confirms the NO<sub>2</sub> functionality is responsible for interaction with Dantocol. Minor deviation

in wavenumber of the remaining vibrational bands occur within the range of spectral resolution ( $2.0\text{cm}^{-1}$ ) and is therefore attributed to experimental error.

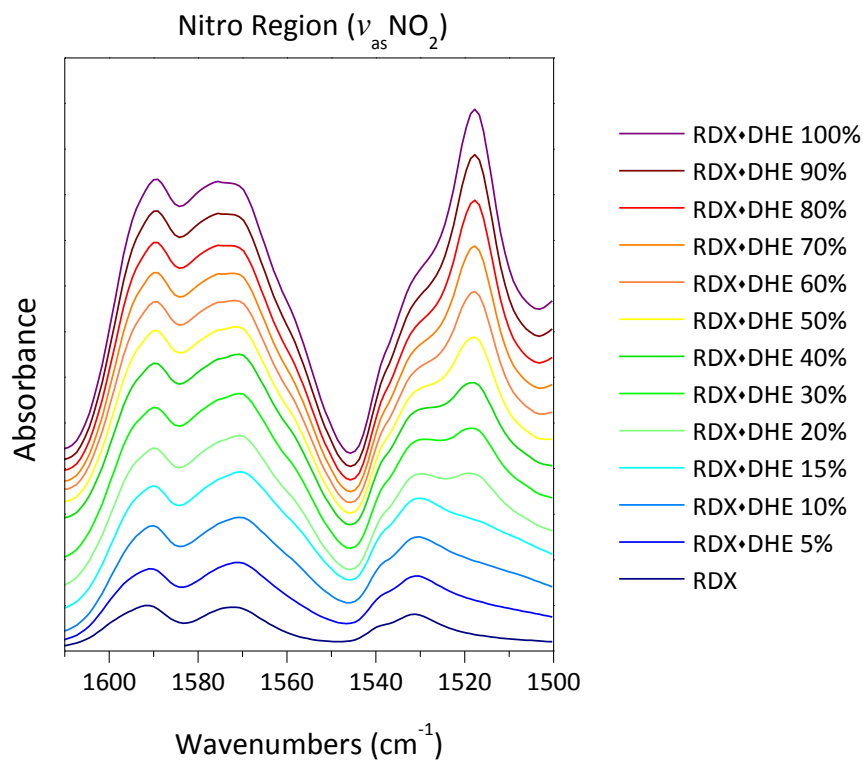


**Figure 3.3.** Cumulative offset of asymmetrical  $\text{NO}_2$  stretching vibration.

Sample	$\nu_{\text{OH}}$	$\nu_{\text{as}}\text{NO}_2$	$\Delta\nu_{\text{as}}\text{NO}_2$
RDX	-	1532	-
RDX·DHE 5%	3393	1527	5
RDX·DHE 10%	3397	1522	10
RDX·DHE 15%	3397	1519	13
RDX·DHE 20%	3398	1517	15
RDX·DHE 25%	3406	1519	13
RDX·DHE 30%	3397	1517	15
RDX·DHE 40%	3407	1517	15
RDX·DHE 50%	3411	1517	15
RDX·DHE 60%	3423	1517	15
RDX·DHE 70%	3426	1517	15
RDX·DHE 80%	3429	1517	15
RDX·DHE 90%	3430	1517	15
RDX·DHE 100%	3431	1517	15

**Table 3.1.** RDX peak shifts of OH and asymmetrical stretching  $\text{NO}_2$  vibration ( $\text{cm}^{-1}$ ).

The magnitude of bathochromic shifts are collated in Table 3.1, revealing an initial increase with Dantocol concentration. This indicates a maximum of  $\Delta\nu_{\text{asNO}_2}$   $15\text{cm}^{-1}$  at  $\geq 20\%$  Dantocol, constituting the highest concentration of  $\text{NO}_2$  groups participating in bonding agent interaction. The extent of interaction is limited by availability of active sites and the presence of steric hindrance. This is responsible for the plateau effect on  $\Delta\nu_{\text{asNO}_2}$  which restricts further interaction of  $\text{NO}_2$  groups.

Shifts in the  $\nu_{\text{asNO}_2}$  band imply interfacial bonding forces originate from interaction of the  $\text{NO}_2$  functionality. Literature indicates  $\text{NO}_2$  compounds are capable of interacting with proton donors, which gives rise to hydrogen bonding.<sup>19, 20</sup> Hydroxyl groups are known to be strong proton donors, presenting capability for interaction with RDX. This observation is particularly relevant to primary alcohols. The structure of Dantocol contains two such groups, producing broad hydroxyl peaks in the IR spectra. Figure 3.4 highlights the hydroxyl region of coated RDX samples that contains the broad  $\nu_{\text{OH}}$  band associated with the hydantoin.

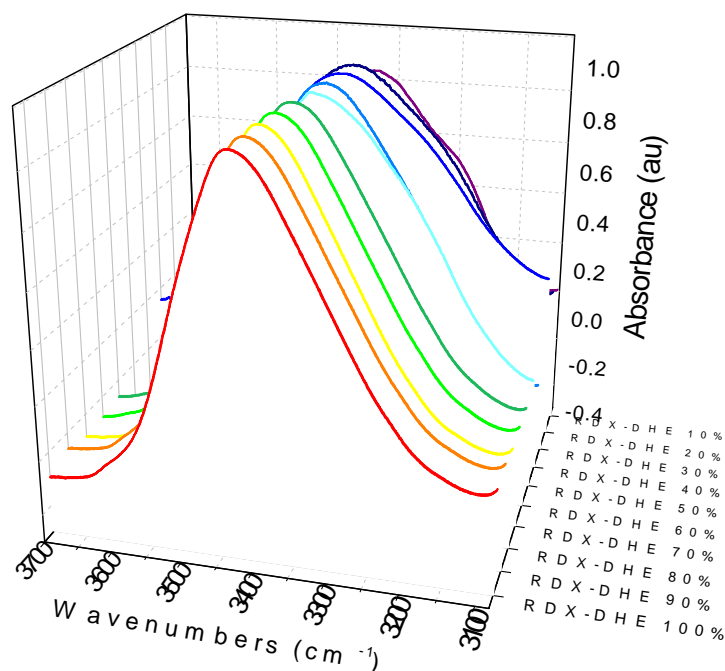


**Figure 3.4.** Normalised OH peak data of RDX and Dantocol 10-100%.

The OH peak appears in the IR spectra of coated RDX at Dantocol concentrations  $\geq 10\%$ . The immediate difference in the hydroxyl peak of Dantocol shown in Figure 2.2 and that observed in coated samples, is the shape of its peaks. Dantocol coatings display a broad hydroxyl peak, in contrast to neat Dantocol which consists of three distinct peaks. This indicates the absence of hydrogen bonding within the neat sample, as opposed to Dantocol applied in coatings. This provides initial indications of the hydroxyl's involvement in hydrogen bonding with RDX.

Following coating of RDX, the bonding agent's OH band was found to undergo significant shift in peak location. As the concentration of Dantocol is decreased, hydroxyl peaks exhibit greater bathochromic shift. This indicates increased participation of OH groups in hydrogen bonding with the nitramine's  $\text{NO}_2$  functionality. As the concentration of Dantocol is increased, the number of OH groups participating in secondary bonding approaches its limit, according to the availability of active sites. Increasing the coating concentration beyond this point yields a higher percentage of non-bonded OH groups. This causes the  $\nu\text{OH}$  peak to revert back to the frequency of neat Dantocol. These findings replicate the effects increasing the RDX concentration has on shifts in the  $\nu_{\text{as}}\text{NO}_2$  bands.

Increasing the monolayer coating of Dantocol from 10% to a bulk thickness of 100% reduces shift in hydroxyl peaks from  $3392\text{cm}^{-1}$  to  $3431\text{cm}^{-1}$ . The magnitude of shifts at 10% Dantocol exceeds  $\Delta\nu\text{OH } 39\text{cm}^{-1}$ , indicative of the strength of hydrogen bonding. This is highlighted in Figure 3.4, along with the  $\nu\text{OH}$  bands of the remaining RDX coatings.

### 3.3.1.2 Transmission Spectroscopy

Shifts involving the asymmetrical  $\text{NO}_2$  stretching vibration were observed to diminish within the transmission spectra of coated samples. This demonstrated the constraints of both particle size and IR transparency towards the surface sensitivity of transmission spectroscopy. Roedel et al. described the manner in which absorption within the bulk is reduced for highly absorbing materials.<sup>2</sup> This should be considered when performing surface analysis, as

decrease in sample transparency provides greater surface information. This is particularly relevant to transmission spectroscopy, whereby KBr is applied to dilute samples.

The potential for grinding to remove surface coatings further complicates investigations. Although necessary for sample preparation, grinding results in fragmentation of RDX crystals, causing exposure of the uncoated surface. This results in the spectra depicted in Figure 3.5, which observes limited deviation from  $\nu_{\text{as}}\text{NO}_2$   $1536\text{cm}^{-1}$  of untreated RDX. Although peaks involved are consistent with the reflectance spectra, the magnitude of shifts suggests improvement in surface sensitivity is required.

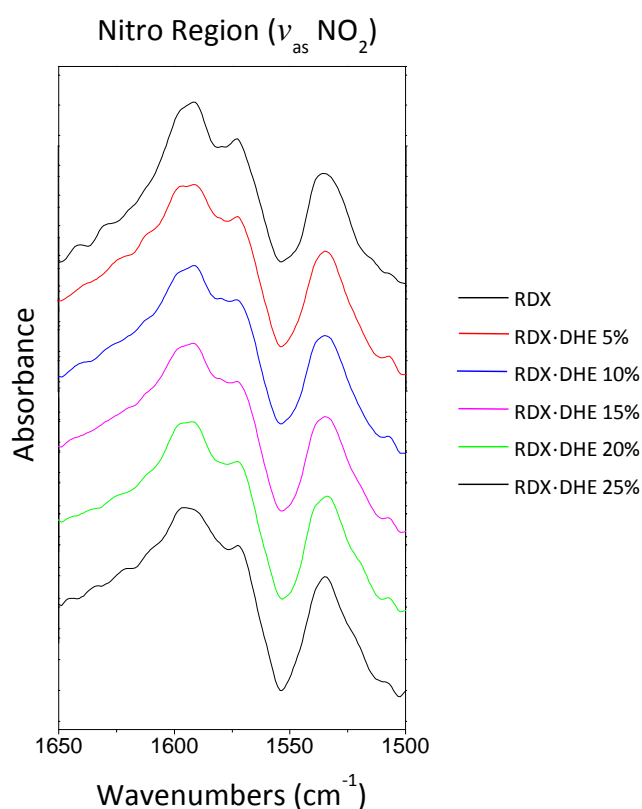


**Figure 3.5.** FTIR spectra of RDX and Dantocol 5-25% coated samples.

The extent of bathochromic shifts are highlighted in Table 3.2, with maximum shift observed for coatings  $\geq 20\%$  Dantocol. As the coating concentration decreases, so too does the shift in wavenumber. However, these figures reside only marginally outside the range of spectral resolution, therefore proving inconclusive in characterising intermolecular forces.



Sample	$\nu_{\text{as}}\text{NO}_2$ ( $\text{cm}^{-1}$ )
RDX	1536
RDX·DHE 5%	1535
RDX·DHE 10%	1534
RDX·DHE 15%	1534
RDX·DHE 20%	1533
RDX·DHE 25%	1533

**Table 3.2.** Transmission assignment of asymmetrical  $\text{NO}_2$  stretching vibration.

Attempts were made to resolve issues associated with grinding and its effect on the removal of surface coatings. This involved pre-grinding RDX particles prior to performing microencapsulation. Application of the Dantocol monolayer provides an increase in particle size, impacting the signal to noise ratio. Although this enables coatings to remain intact, the effect on signal to noise ratio limits conclusions regarding the nature of interactions.

### 3.3.2 Hydrogen Bonding

Hydrogen bonding within FTIR spectra is known to impart a number of characteristic features arising from intermolecular forces. The covalent bond between nitrogen and oxygen atoms of  $\text{NO}_2$  groups contain a lone pair electron that stretches according to the strength of hydrogen bonding experienced.<sup>21</sup> A small amount of electron density is also transferred from the oxygen of the  $\text{NO}_2$  group to the proton donating hydroxyl. As indicated by FTIR results, the absorbance band of functional groups involved in hydrogen bonding shift towards lower frequency. The  $\text{NO}_2$  band to which this relates was found to broaden, whilst increasing in intensity upon formation of hydrogen bonds. Although changes in bond length, energy and electron densities resulting from hydrogen bonding are relatively small, the sensitivity of IR spectroscopy enables detection of chemical changes. For this reason, FTIR is regarded as one of the most effective techniques for investigating hydrogen bonding. Shift observed in the hydroxyl band provides decisive evidence of hydrogen bonding between Dantocol and RDX, displaying shifts upwards of  $\Delta\nu_{\text{OH}} 39\text{cm}^{-1}$ . The strength of hydrogen bonding is such that

the covalent bond of the adjacent NO<sub>2</sub> group experiences similar shifts, further substantiating hydrogen bond formation.

### 3.3.2.1 Fourier Self-Deconvolution

IR spectra of multiple component systems are often difficult to analyse, due to the presence of overlapping bands. Peaks displaying shoulder formation resulting from overlap are often resolvable via application of FSD. This function separates spectral features when unable to improve overlapping by increasing the number of scans or resolution.

FSD resolves spectral peaks by adjusting the bandwidth and enhancement in order to optimise results. Bandwidth settings estimate the width of overlapping bands, while enhancement determines the degree to which features are amplified.<sup>22</sup> Adjusting the enhancement settings determines the scale of the resolving power applied to spectral data. Application of FSD subsequently enables reduction in the width of bands such that overlapping bands are resolved.<sup>23</sup>

Overlapping occurs when the spectral region between two peaks of wavenumber  $\nu_1$  and  $\nu_2$  exceeds the number of bands  $N$ , divided by the average width at half the value of each band.

$$N > \frac{|\nu_1 - \nu_2|}{2 \sum \gamma_i} \quad (3.5)$$

Decreasing the width of spectral bands  $\gamma_i$ , enables resolution of individual bands, thus providing additional information. Data manipulation including spectral subtraction, curve fitting and second derivative calculations are commonly applied to resolving peaks. Such techniques rarely produce useful quantitative information without resulting in significant spectral distortion. Application of FSD was found to provide an effective means of enhancing resolution, enabling reduction in  $\gamma_i$  values of NO<sub>2</sub> bands.

FSD is typically applied to a narrow spectral range, inclusive of a single overlapping vibrational mode. Selection of  $\gamma_i$  values which provide maximum band narrowing and minimum noise interference, were determined by manual adjustments. This improved peak

resolution over that of automated FSD programming. Adjustments to bandwidth and enhancement settings were applied to rectify the appearance of negative peaks, indicative of over resolved spectra.

Complications arise from the presence of background noise, limiting the extent of band narrowing achieved by FSD. Excessive background noise manifests as side lobes which continue to complicate spectra. To identify situations whereby peaks result from noise interference, repetition of scans may be employed to confirm bands reflect vibrational modes.

This technique was applied to resolve overlap of free and bonded  $\text{NO}_2$  bands within coated samples. Figure 3.6 demonstrates the efficiency with which FSD rectifies the issue. Resolution of free and bonded  $\text{NO}_2$  bands into two discernible peaks enables measurement of their respective wavenumbers.

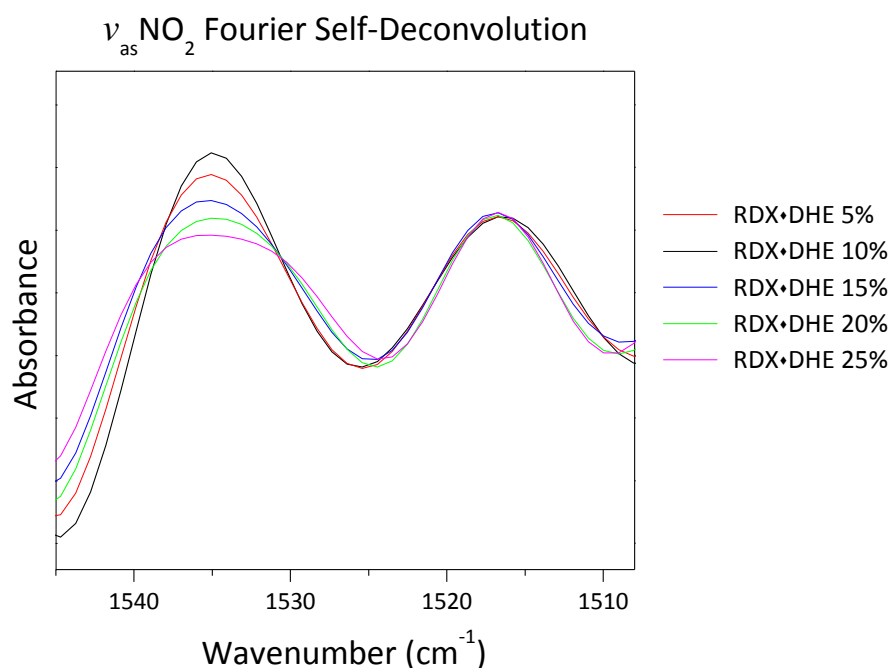


**Figure 3.6.** Fourier self-deconvolution of asymmetrical nitro stretching vibration.

Results of FSD reveal free  $\text{NO}_2$  bands are consistent with that of untreated RDX. Bonded  $\text{NO}_2$  bands, subsequently appear around  $\nu_{\text{as}}\text{NO}_2$   $1516\text{cm}^{-1}$  as collated in Table 3.3.

Sample	$\nu_{as}\text{NO}_2$ (cm <sup>-1</sup> )		
	Free	Bonded	$\Delta\nu$
RDX	1532	-	-
RDX·DHE 5%	1534	1517	17
RDX·DHE 10%	1535	1516	19
RDX·DHE 15%	1534	1516	18
RDX·DHE 20%	1534	1516	18
RDX·DHE 25%	1534	1516	18

**Table 3.3.** FSD data for asymmetrical nitro stretching vibration.

### 3.3.2.2 Curve Fitting

Curve fitting was applied as a complementary technique to resolve the asymmetric NO<sub>2</sub> vibration bands into free and bonded NO<sub>2</sub> bands. The summation of bands resolved by curve fitting equates to that of the original band. This is known as convergence, to which OMNIC software applies the Fletcher-Powell-McCormick algorithm.<sup>15</sup> The fitting process enables resolution of peak position, shape, width and height of bands to produce a best fit of calculated and experimental bands. This is performed by selection of line shape and baseline handling. As previously discussed, the Gaussian profile is best suited to solids and is therefore applied to curve fitting of coated RDX. Single Gaussian bands are expressed by the following equation.

$$f(\nu) = \frac{2A\sqrt{\ln 2}}{\gamma G\sqrt{\pi}} \exp\left(-\left(\frac{2\sqrt{\ln 2}(\nu-\nu_0)}{\gamma G}\right)^2\right) \quad (3.6)$$

Where  $\gamma G$  is the full width at half height,  $\nu$  represents the wavenumber and  $\nu_0$  the position.<sup>24</sup> In the presence of multiple bands, this is expressed as a summation, according to the equation:

$$f(\nu) = A \exp\left(-\left(\frac{\pi\gamma G x}{2\sqrt{\ln 2}}\right)^2\right) \exp(i2\pi x \nu_0) \quad (3.7)$$

Whereby  $A$  is the band area,  $x$  corresponds to distance and  $i$  represents  $\sqrt{-1}$ .<sup>24</sup> The later equation is therefore applied to curve-fitting of  $\nu_{as}\text{NO}_2$  bands.

In terms of baseline handling, selection of minimum baseline correction is preferable as this limits the impact on the fit. If required, baseline correction was performed prior to fitting to assist processing. Following adjustment of operating parameters, the  $\text{NO}_2$  region was selected thereafter. Minimization was then performed, whereby the fit routine minimizes the peak location, height and width.<sup>15</sup> Optimising these steps ensure the accuracy of curve fitting, providing information regarding free and bonded functional groups.

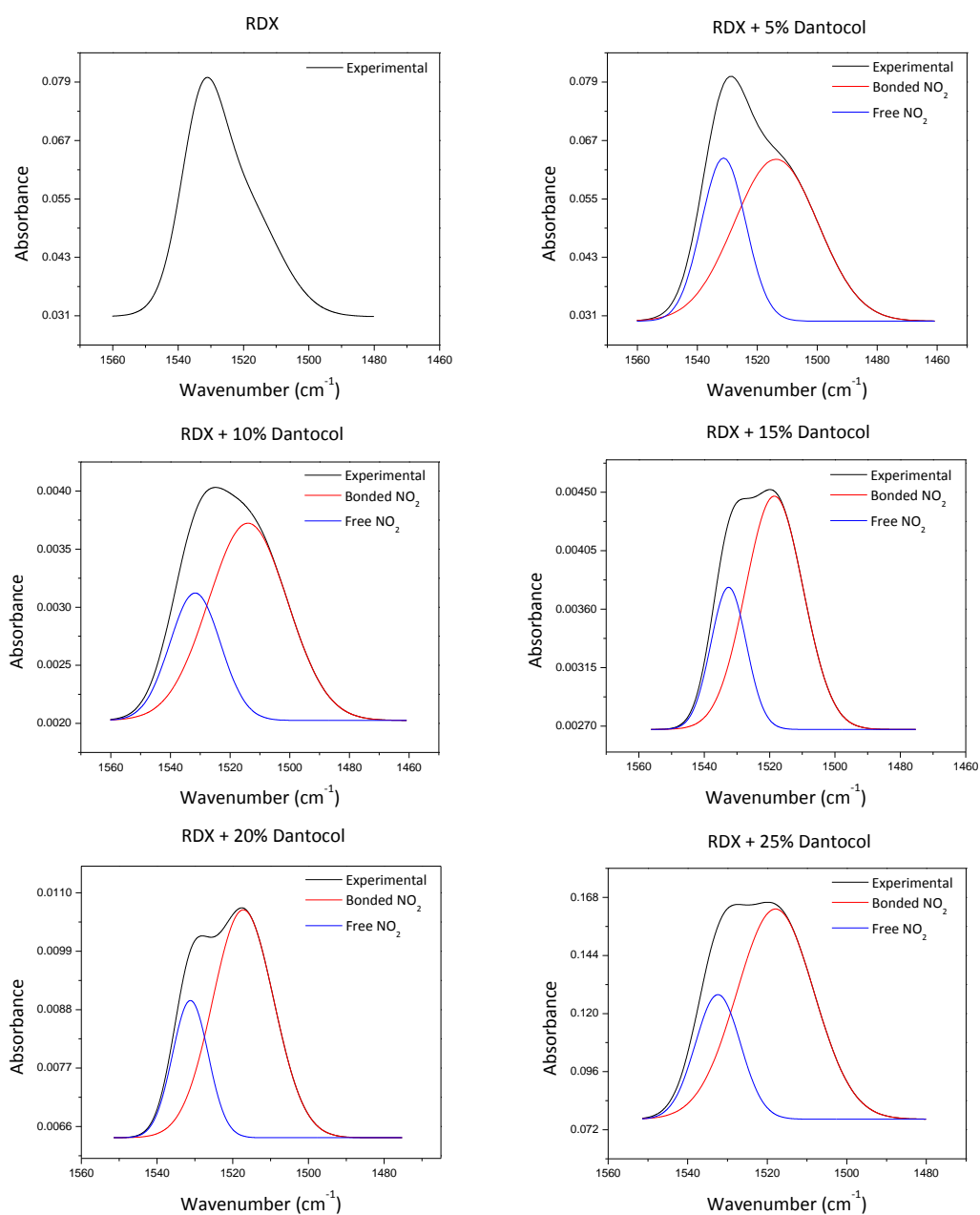


**Figure 3.7.** Peak resolution of  $\text{NO}_2$  groups.

Also critical in performing curve fitting is the signal to noise ratio of spectral data. Although possible to acquire a curve fit in the presence of minor background noise, as this increases, noise may contribute towards convergences unrelated to the signal. This manifests as curve fitting attempts to fit noise spikes within unsatisfactory spectra. Smoothing can be applied to resolve this issue, however this may slightly alter the peak shape. Therefore 5-9 point smoothing should not be exceeded to prevent distortion.<sup>15</sup> Efforts were made to optimise the signal to noise ratio, negating requirements for use of smoothing. This ensures good agreement of curve fitting data as observed in Figure 3.7.

Discrepancies in the NO<sub>2</sub> vibration of coated RDX are attributed to changes in the chemical environment of the NO<sub>2</sub> group. This originates from intermolecular forces between the energetic filler and bonding agent monolayer. The NO<sub>2</sub> region of RDX displays the characteristic asymmetrical stretching NO<sub>2</sub> band centred at 1532cm<sup>-1</sup>. Minor interaction between RDX molecules causes the appearance of shoulder formation, however this remains negligible by comparison to that resulting from bonding agent interaction. The position of the RDX peak at 1532cm<sup>-1</sup> was fixed during the curve fit, with movement limited to peak height and width. Microencapsulation of RDX crystals produces a secondary band appearing as a lower wavenumber shoulder. This remained unrestricted in terms of peak height, position and width. Evolution of the secondary band is primarily attributed to hydrogen bonded NO<sub>2</sub> groups, indicating formation of intermolecular interactions.

Division of experimental data into multiple peaks representing free NO<sub>2</sub> groups and those involved in interaction, coincides with the results of deconvolution. Correlation with deconvolution data validates the number of peaks present in the overlapping band, indicating the peak source does not result from background noise.

### **3.3.2.3 Bonding Index**

Curve fitting reveals an increase in Dantocol concentration relative to the absorbance of bonded NO<sub>2</sub> bands. Conversely, the free NO<sub>2</sub> band is observed to decrease with Dantocol

concentration. This is indicative of a decrease in the percentage of free NO<sub>2</sub> groups, relative to that undergoing intermolecular interactions. The extent of interactions can be expressed by the bonding index (BI), which is defined as the ratio of the bonded and free NO<sub>2</sub> absorbance peaks area.<sup>18</sup>

$$BI = \frac{C_{bonded}\epsilon_{bonded}}{C_{free}\epsilon_{free}} = \frac{A_{bonded}}{A_{free}} \quad (3.8)$$

Whereby  $C$  represents the concentration of NO<sub>2</sub> groups and  $\epsilon$  is the extinction coefficient of the bonding effect. Peak fitting is applied to determine the peak area  $A$  of the vibrational band, with the subscript “bonded” and “free” indicating bonded and non-bonded NO<sub>2</sub> groups.

Sample	$\nu_{asl}NO_2$ (cm <sup>-1</sup> )	BI
RDX·DHE 5%	1528.76	1.87
RDX·DHE 10%	1524.90	2.43
RDX·DHE 15%	1519.89	2.67
RDX·DHE 20%	1517.60	2.82
RDX·DHE 25%	1519.83	2.89

**Table 3.4.** Bonding index of Dantocol coated RDX.

Data regarding the BI is summarised in Table 3.4. Values increase with bonding agent concentration, indicating greater participation of NO<sub>2</sub> groups in interaction involving hydrogen bonding. This occurs as result of the OH:NO<sub>2</sub> ratio, which impacts the number of NO<sub>2</sub> groups engaged in interaction. The extent of NO<sub>2</sub> groups involved in hydrogen bonding is therefore limited by the availability of the adsorbate. Consequently, the intensity of free NO<sub>2</sub> bands decrease with increasing Dantocol content, as opposed to the bonded NO<sub>2</sub> band which increases. This relationship confirms previous conclusions, and indicates the consistency of results. Satisfactory agreement of curve fitting data relays the reliability of the technique, providing a quantitative outlook on the relative integrated intensities of the free and bonded NO<sub>2</sub> bands. This experimental data is depicted in Figure 3.8, showing the BI as a function of Dantocol concentration.

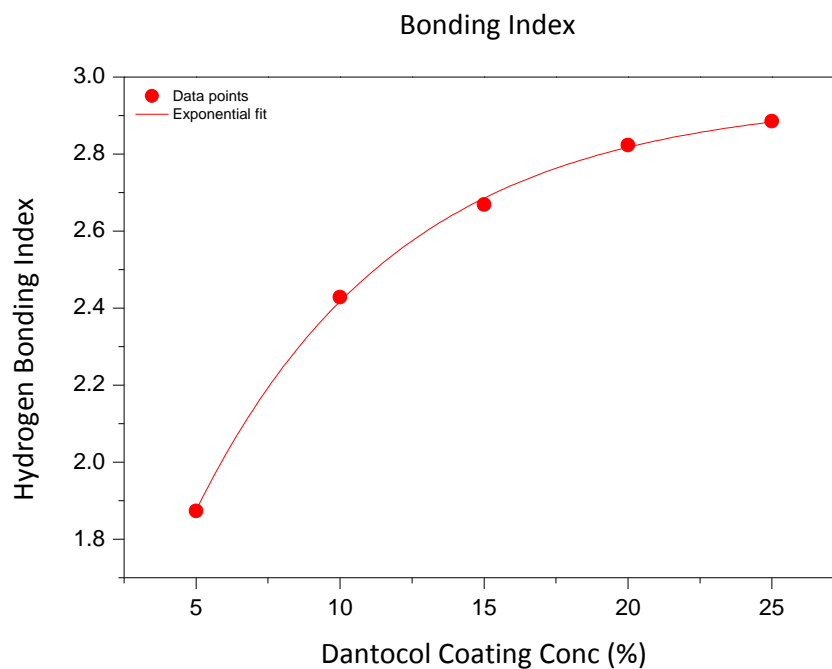


**Figure 3.8.** Relationship between BI and Dantocol coating concentration of RDX.

Plotting the BI vs concentration, reveals a logarithmic increase associated with bonding agent interaction. The logarithmic fit of data points observed in Figure 3.8 generates an R-square value of 0.99. This indicates limited trendline deviation, demonstrative of the results accuracy. Evaluation of the initial increase in BI with the introduction of Dantocol coating promotes rapid incline, consistent with the onset of hydrogen bond formation. As the coating concentration increases, the availability of free  $\text{NO}_2$  groups are reduced causing the BI to plateau.

### 3.3.3 Highly Surface Sensitive Techniques

#### 3.3.3.1 Investigation of Interfacial Interactions via PAS

PAS was employed as a complementary IR technique, owing to its high surface sensitivity and depth profiling capabilities. Acoustic detection of absorbed light is exceptionally useful for near-surface characterisation of solid materials, with PAS previously employed in the analysis of RDX coatings. Yongliang et al. investigated interactions between RDX and various polymer binders through use of PAS.<sup>25</sup> This enabled identification of acid-base interactions between components located within the near-surface region.



Applying this methodology to the current system, the acoustic spectra of RDX encapsulated with 5-25% Dantocol was acquired. The spectra of pure and coated RDX were recorded at mirror velocities of 0.1581, 0.3165, 0.4747, 0.6329, 0.9494 and 1.2659  $\text{cm s}^{-1}$ . These settings provided a series of six spectra per sample, originating from differing penetration depths, when combined provide a depth profile of coated samples. As the mirror velocity is increased, the ensuing spectra originate from nearer the surface. This provides structural information on the near-surface region, inclusive of the interface.

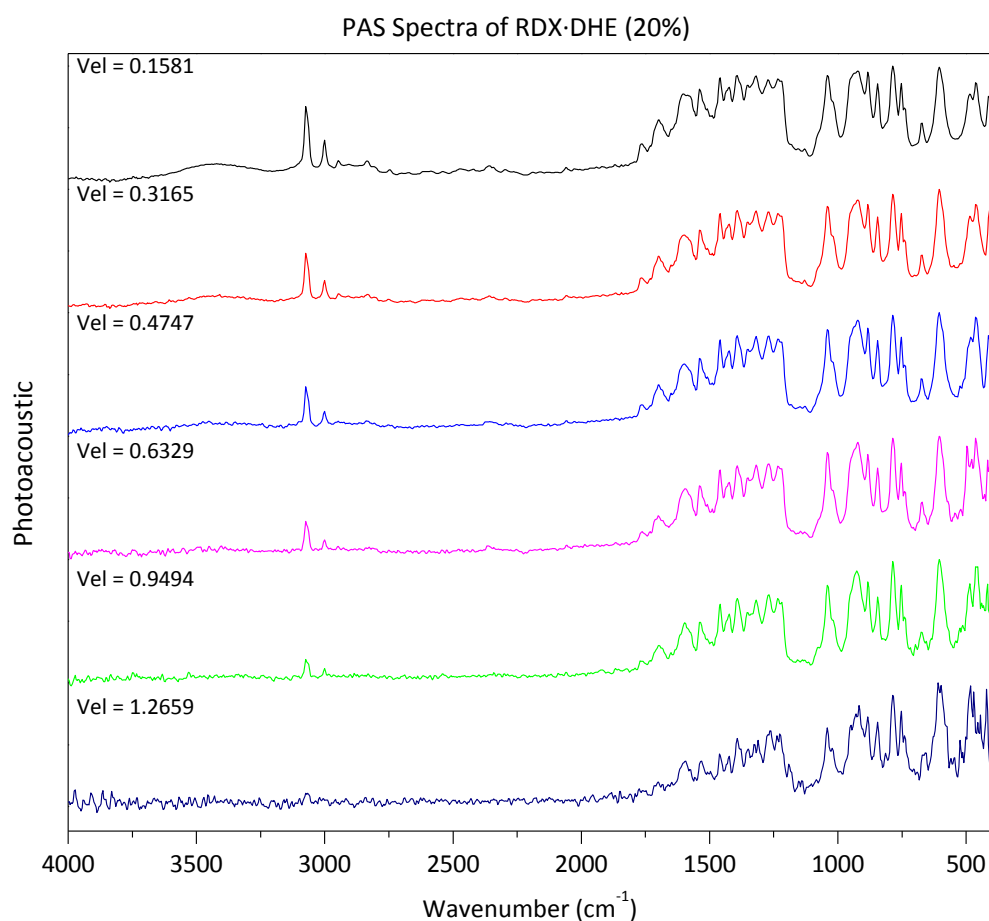


**Figure 3.9.** PAS spectra of RDX·DHE 20% conc at increasing mirror velocities.

The impact of mirror velocity on the spectra of coated RDX particles is evident in Figure 3.9. Of significance is the variation in intensity of the  $\nu\text{CH}_2$  band at  $3072\text{cm}^{-1}$ . Through monitoring the intensity of this band as a function of mirror velocity, the intensity of the  $\nu\text{CH}_2$  band of RDX is observed to decrease as the mirror velocity is increased. This confirms an increase in mirror velocity translates to lower penetration of light into the surface of coated RDX.

Comparisons between the spectra of neat RDX and coated samples reveal shifts in the  $\text{NO}_2$  asymmetrical stretching vibration, consistent with that of previous IR techniques. As the mirror velocity is increased, the wavenumber of the  $\nu_{\text{as}}\text{NO}_2$  band steadily decreases. As evident in Figure 3.9, low mirror velocity ( $0.1581\text{cm s}^{-1}$ ) generates spectra comparable to neat RDX, as spectral information originates from the bulk. Increasing the mirror velocity causes the  $\nu_{\text{as}}\text{NO}_2$  peak to shift progressively towards lower wavenumber. This represents shallow sampling, which introduces difficulties due to signal generation becoming weaker at high frequency. In response, the acoustic signal commences deterioration at a mirror velocity of  $1.2659\text{cm s}^{-1}$ . For this reason a mirror velocity of  $0.9494\text{cm s}^{-1}$  was chosen to represent the PAS spectra of coated RDX. The penetration depth at this velocity targets the interface region while optimising the signal to noise ratio. These conditions reveal the degree of interaction occurring within the near surface region, with  $\nu_{\text{as}}\text{NO}_2$  bands shifting towards lower wavenumber upon increased coating concentration. Maximum shift of  $\Delta\nu_{\text{as}}\text{NO}_2$   $5\text{cm}^{-1}$  was acquired at 20% Dantocol concentration.

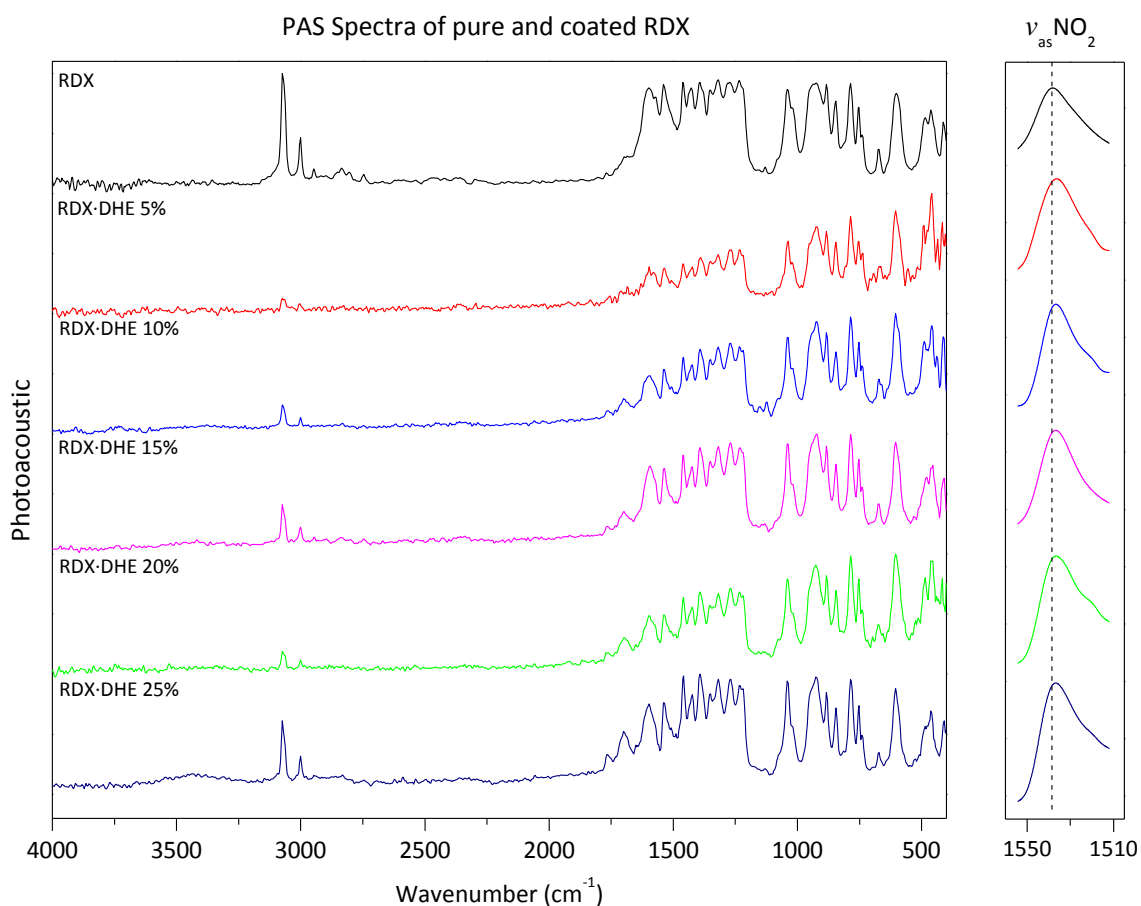


**Figure 3.10.** PAS spectra of pure and Dantocol coated RDX ( $vel = 0.9494\text{cm s}^{-1}$ ).

The assignment of functional groups listed in Table 3.5, highlight the relationship between coating concentration and the extent of bathochromic shift in the  $\nu_{as}NO_2$  peak. In comparison to the  $NO_2$  band, negligible deviation is observed amongst the remaining vibrational bands. This substantiates evidence hydrogen bonding involves  $NO_2$  groups and Dantocol's OH functionality. As the bonding agent approaches 20% concentration, the asymmetrical  $NO_2$  stretching vibration displays a maximum shift of  $\Delta\nu_{as}NO_2$   $5cm^{-1}$ . This represents the strongest hydrogen bonding amongst coatings, signifying a greater degree of constituent interaction. Additionally, as the coating concentration of Dantocol is increased, the intensity of peaks arising from the bonding agent becomes more pronounced. In particular, the hydroxyl peak at  $3400cm^{-1}$  and carbonyl peaks at  $1700$  and  $1765cm^{-1}$  show increased intensity. Fortuitously, the location of peaks representing Dantocol avoids overlap of the  $NO_2$  band. This negates the possibility of shifts in the  $NO_2$  peak arising from bands associated with the bonding agent.

Vibrational Band	RDX	RDX•Dantocol (%)				
		5%	10%	15%	20%	25%
$\nu$ $CH_2$	3072	3074	3073	3073	3073	3073
$\nu_s$ $C=O$	-	1767	1765	1765	1764	1764
$\nu_{as}$ $C=O$	-	<b>1700</b>	<b>1698</b>	<b>1697</b>	<b>1696</b>	<b>1696</b>
$\nu_{as}$ $NO_2$	1598	1597	1595	1593	1595	1596
	1572	1575	1574	1573	1574	1754
	<b>1538</b>	<b>1535</b>	<b>1534</b>	<b>1534</b>	<b>1533</b>	<b>1535</b>
$\delta_s$ $CH_2$	1460	1459	1460	1460	1459	1459
	1427	1423	1425	1425	1424	1424
$\nu_a$ ( $NO_2$ ) + (N-N)	1351	1350	1351	1351	1352	1352
	1319	1319	1319	1319	1319	1319
$\nu_a$ ( $NO_2$ ) + (N-N)	1272	1271	1271	1270	1270	1270
	1234	1232	1233	1232	1234	1233
	1218	1220	1220	1219	1220	1220
Ring Stretching	1040	1038	1039	1040	1040	1040
	1023	1022	1022	1020	1019	1019
	924	923	923	923	925	924
$\delta$ ( $NO_2$ ) + $\gamma$ ( $NO_2$ )	786	786	786	786	786	785
	753	754	753	753	753	753
$\tau$ + $\gamma$ ( $NO_2$ )	602	604	604	605	604	605

**Table 3.5.** PAS assignment of pure and Dantocol coated RDX ( $vel = 0.9494cm\ s^{-1}$ ).

Previous articles indicate PAS has successfully been applied to provide high quality analysis of energetic materials, relative to associated FTIR techniques.<sup>26</sup> The primary advantage of PAS over associated methods relates to the exclusion of contributions from scattered or reflected infrared radiation. This avoids complications arising from other methods and provides an alternative information source. Sample preparation is unnecessary, unlike DRIFTS and transmission spectroscopy which requires grinding with KBr, along with the requirements of ATR samples to engage perfect optical contact with the diamond stage. For this reason, PAS is frequently applied in circumstances where sample preparation becomes difficult, or when other techniques fail to provide adequate spectral information.<sup>5</sup> Of particular advantage towards the current research is the ability to alter the depth of penetration of incident radiation. Investigations of coated RDX at differing sample regions generate variation in spectra according to penetration depth. This enables targeting of the filler/bonding agent interface, providing spectra information regarding functional groups responsible for interaction.

Inspection of Dantocol's C=O region provides initial indications of interaction complementary to hydrogen bonding. The increased surface sensitivity of PAS over prior techniques suggests involvement of  $\nu_{as}C=O$  bands in dipole-interactions. Bathochromic shifts are highlighted in Table 3.5, indicating maximum divergence of  $\Delta\nu_{as}C=O$   $4\text{cm}^{-1}$ . This occurs just outside the spectral resolution of  $2.0\text{cm}^{-1}$ , requiring further investigation via DRIFTS.

### **3.3.3.2 Investigation of interfacial interactions via DRIFTS.**

DRIFTS provides the greatest potential for investigating interfacial interactions, owing to its superior surface sensitivity. This was applied to encapsulated RDX particles in determining the origin of secondary bonding associated with the bonding agent. Analysis of untreated RDX was initially performed to gauge a baseline from which to compare bands. This was reported in Kubelka-Munk units, which represents data of the form linear in concentration, such as relates to absorption spectra.<sup>12</sup>

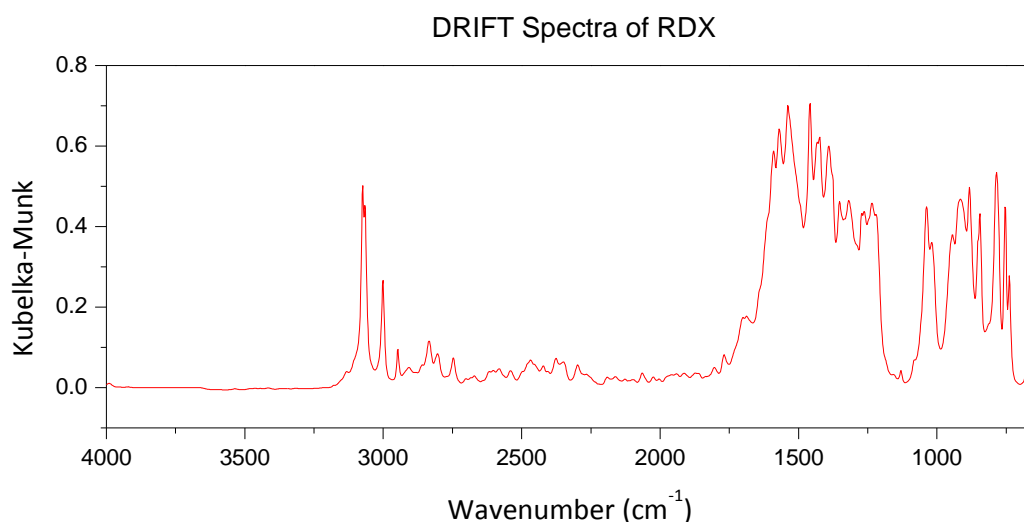


**Figure 3.11.** DRIFT spectrum of pure RDX.

Following characterisation of functional groups depicted in Figure 3.11, coated RDX was investigated at increasing Dantocol concentrations. Coated samples readily display fundamental changes in the IR spectrum relevant to bands involved in interfacial interactions. Bathochromic shifts upwards of  $\Delta\nu$  19cm<sup>-1</sup> are evident in the asymmetrical NO<sub>2</sub> vibration of coated RDX. This occurrence is illustrated in Figure 3.12, outlining the decrease in wavenumber.

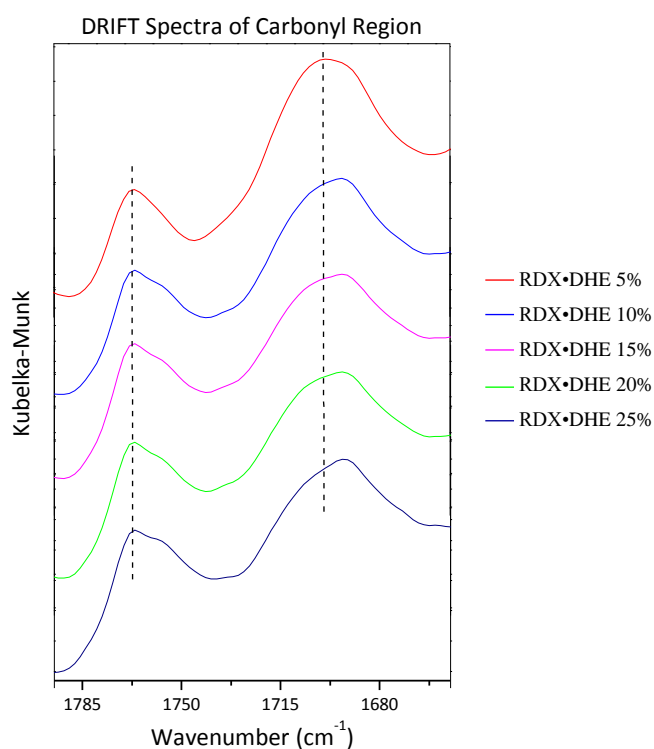


**Figure 3.12.** DRIFT spectra of RDX•DHE (5-25%) carbonyl region.

Consequent deviations from the fundamental  $\nu_{as}\text{NO}_2$  band of RDX ( $1538\text{cm}^{-1}$ ), indicate the presence of strong intermolecular interactions involving functional groups residing at the interface. This substantiates evidence that the mechanism of filler reinforcement occurs through interfacial effects and is not simply due to an overall increase in the crosslink density of the binder.

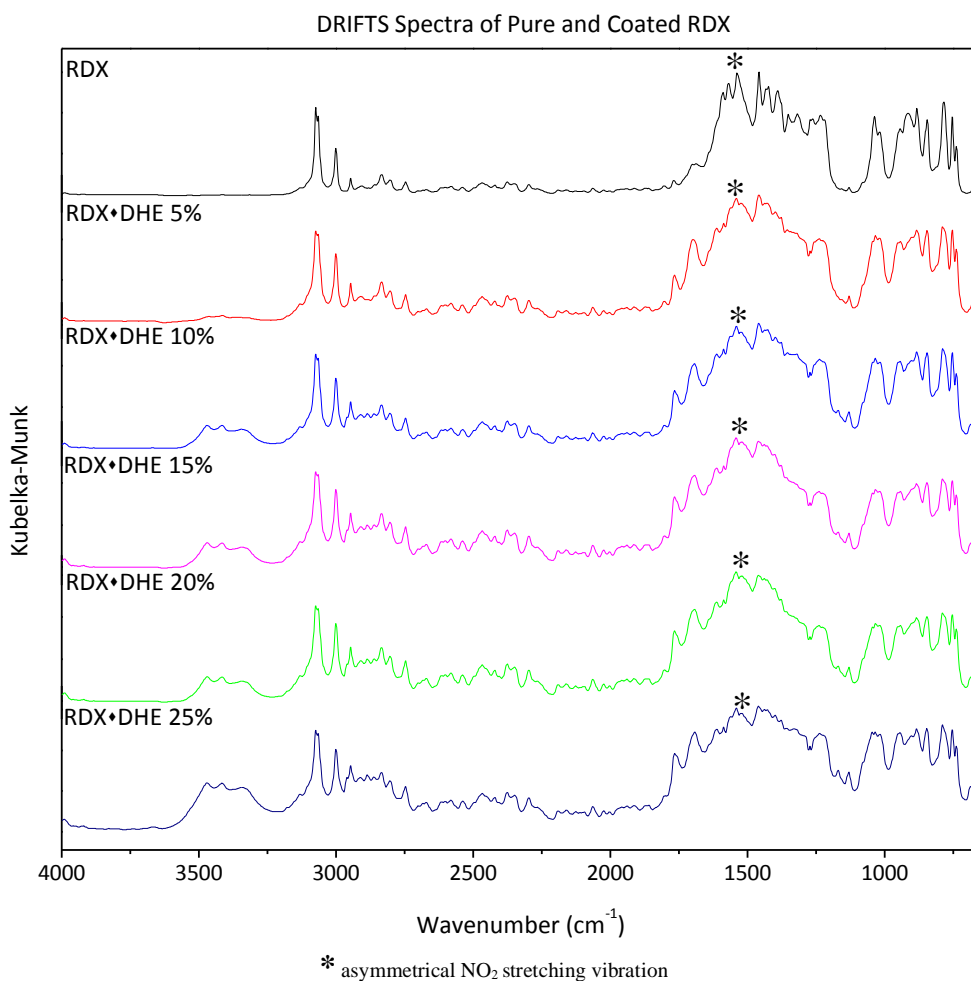


**Figure 3.13.** DRIFT spectra of pure and coated RDX at Dantocol conc 5-25%.

Shifts in wavenumber of the asymmetrical  $\text{NO}_2$  vibrations are outlined in Table 3.6, relative to coating concentrations. Increasing the concentration of Dantocol impedes the ability of photons to reflect the RDX bulk. This promotes an increase in the degree of  $\text{NO}_2$  bands originating from the surface region, inclusive of the RDX interface. Conversely, excess Dantocol concentration may inhibit the ability of photons to penetrate coatings and cause vibration of surface  $\text{NO}_2$  groups. Therefore coating concentrations were limited to prevent

shielding of RDX particles from incident photons, which may create spectra representative of neat Dantocol.

The improved surface sensitivity of DRIFTS revealed an important shift in addition to that of the NO<sub>2</sub> band. Subtle variation in Dantocol's C=O bands provided evidence of an interaction complementary to hydrogen bonding. The significance of shifts within the carbonyl region is critical in completing our understanding of the bonding agent's mode of action, with observations consistent with dipole interactions.

Vibrational Band	RDX	RDX•DHE (%)				
		5%	10%	15%	20%	25%
$\nu$ CH <sub>2</sub>	3074	3074	3074	3075	3075	3075
$\nu_s$ C=O	-	1767	1767	1767	1767	1766
$\nu_{as}$ C=O	-	<b>1699</b>	<b>1694</b>	<b>1693</b>	<b>1692</b>	<b>1692</b>
$\nu_{as}$ NO <sub>2</sub>	1590	1587	1588	1587	1587	1587
	1569	1569	1565	1566	1565	1562
	<b>1538</b>	<b>1525</b>	<b>1524</b>	<b>1522</b>	<b>1519</b>	<b>1520</b>
$\delta_s$ CH <sub>2</sub>	1459	1459	1460	1461	1462	1461
	1432	1438	1438	1438	1438	1438
$\nu_a$ (NO <sub>2</sub> ) + (N-N)	1352	1355	1354	1354	1355	1357
	1319	1322	1321	1320	1320	1319
$\nu_a$ (NO <sub>2</sub> ) + (N-N)	1272	1272	1273	1273	1273	1273
	1235	1239	1238	1240	1240	1238
	1220	1225	1223	1223	1223	1223
	1037	1034	1034	1033	1033	1035
Ring Stretching	1019	1019	1017	1019	1019	1018
	944	943	945	944	944	945
	915	-	-	-	-	-
$\delta$ (NO <sub>2</sub> ) + $\gamma$ (NO <sub>2</sub> )	785	789	789	790	790	790
	753	753	753	753	753	753

**Table 3.6.** Peak assignment of RDX and Dantocol coated samples.

### 3.3.4 Dipole Interactions

The presence of dipole interactions was alluded to in previous FTIR techniques, however results were unable to provide conclusive evidence of such interaction, due to shifts occurring just outside the spectral resolution. In contrast, the increased surface sensitivity of

DRIFTS enables detection of weak intermolecular forces. This provides further evidence towards the occurrence of dipole interactions, as the reduced magnitude of carbonyl shifts is consistent with the decreased strength of such interactions.

Assignment of the hydantoin's duplicate C=O bands has been the topic of much debate, with the low frequency signal previously attributed to carbonyls at both the C-2 and C-4 position.<sup>27</sup> In recent years, this conjecture was addressed, with numerous authors concluding these bands originate from symmetrical and asymmetrical vibrations of the coupled C=O system.<sup>28-32</sup> This assignment is observed throughout the spectra of imide-containing compounds. Accordingly, the wavenumber of C=O bands are outlined in Table 3.7, revealing the degree of shift between differing FTIR techniques. DRIFTS displayed the greatest spectral shift, consistent in its involvement of the NO<sub>2</sub> band. Further to this, the asymmetrical C=O vibration observed increased shift in comparison to the symmetric band. The  $\nu_{as}C=O$  band approached a minimum wavenumber 1692cm<sup>-1</sup> at 20% Dantocol concentration. Meanwhile at lower concentrations, evolution of the  $\nu_{as}C=O$  band appears at 1699cm<sup>-1</sup> in the 5% Dantocol sample, displaying reduced shift. The  $\nu_{as}C=O$  band also displays greater intensity due to the geometry of the bonding agent. As the angle between the two carbonyls increases, the net dipole moment charge of  $\nu_sC=O$  decreases, causing this appearance.<sup>33</sup> In the case of azetidinediones and *p*-quinones where dipoles are opposed, C=O vibrations become IR-inactive. The intensity ratio of  $\nu_{as}C=O$  :  $\nu_sC=O$  therefore increases as the ring size decreases.<sup>33</sup>

Sample	ATR		Trans		DRIFTS		PAS	
	$\nu_sC=O$	$\nu_{as}C=O$	$\nu_sC=O$	$\nu_{as}C=O$	$\nu_sC=O$	$\nu_{as}C=O$	$\nu_sC=O$	$\nu_{as}C=O$
RDX·DHE 5%	1764	1696	1766	1703	1767	1699	1767	1700
RDX·DHE 10%	1761	1695	1765	1703	1767	1694	1765	1698
RDX·DHE 15%	1761	1690	1765	1703	1767	1693	1765	1697
RDX·DHE 20%	1760	1689	1765	1703	1767	1692	1764	1696
RDX·DHE 25%	1761	1689	1765	1703	1766	1692	1764	1696

**Table 3.7.** DRIFT Spectra of RDX·DHE carbonyl region at resolution 2cm<sup>-1</sup>.



Molecules with dipole moments tend to orientate in such a way that negative poles align with that of positive poles. Such interactions may occur in synergy with hydrogen bonding, effectively increasing interfacial adhesion. Those OH groups involved in hydrogen bonding comprise a highly concentrated positive charge associated with the hydrogen atom, which determines both the amount and rate of adsorption at the filler surface. Hydrogen bonding therefore dominates filler/bonding agent interaction, in agreement with consideration as the strongest intermolecular force between covalent compounds.

Hydrogen bonding also has the potential to promote similar bathochromic shifts in participating carbonyl bands. Therefore, further investigation is required to confirm shifts originate from dipole-interactions, rather than self-association between hydroxyl and carbonyl groups. To justify these findings, hydroxyl protection will be investigated in Chapter 4.

### **3.3.5 Investigation of RDX Particle Size**

The impact of particle size was evaluated in regards its potential for increasing interfacial adhesion. This is relevant to PBX formulations PBXN-109, which contains a mixture of RDX type 1 class 1 (59%) and class 5 (5%). Increasing the surface area, as achieved by the addition of RDX class 5, may be expected to improve interaction with Dantocol. This theory was evaluated by FTIR analysis of coated RDX at differing particle size.

The morphology of RDX type 1 class 5 exhibits a mean particle size of  $\sim 20\mu\text{m}$ , whilst RDX type 1 class 1 typically ranges from  $\sim 150\text{-}200\mu\text{m}$ .<sup>34</sup> Particles of increased size are susceptible to crystal fracture during FTIR sample preparation, exposing uncoated RDX. Therefore to remove impurities and optimize particle size, recrystallised RDX type 1 class 1 was applied to prior FTIR experiments. This process yields a mean particle size of  $\sim 20\text{-}50\mu\text{m}$ , within the dimensions of RDX type 1 class 5. Reduction in particle size resolves limitations associated with surface analysis of larger particles, enabling satisfactory evaluation of interactions.

Subsequent investigation of interactions between Dantocol and RDX type 1 class 5 displayed results consistent with that of recrystallised RDX. Comparison of FTIR spectra, involving multiple grades of RDX encapsulated with Dantocol, each display shifts in nitro, carbonyl and hydroxyl bands. Deviation in the magnitude of wavenumber shifts between RDX grades lie within the limits of spectral resolution, while variation in intensity results from day to day variables. The extent of these deviations is evident in the overlay spectra depicted in Figure 3.14.

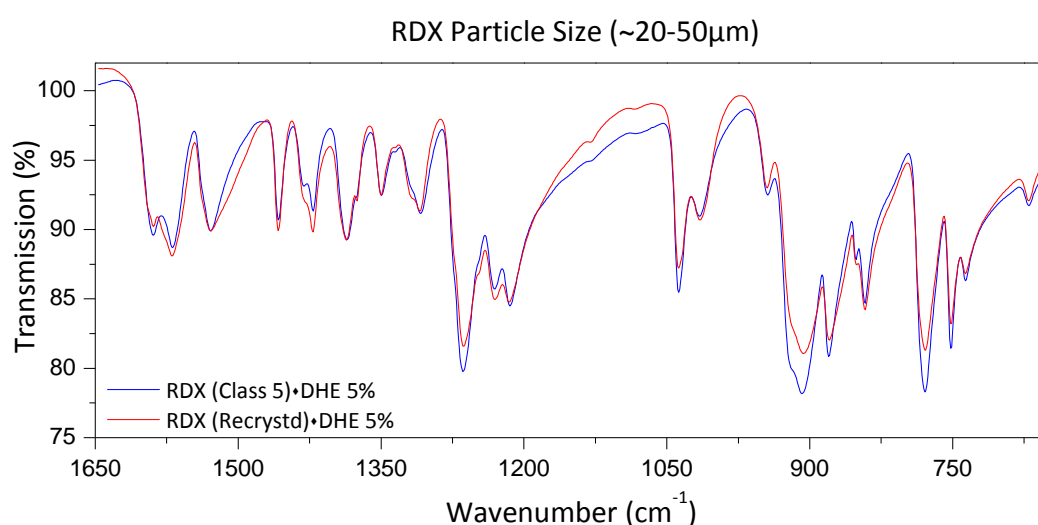


**Figure 3.14.** Spectra of Class 5 and recrystallised RDX coated with 5% Dantocol.

Further evaluation of untreated RDX revealed uniform bands amid the various grades of RDX. This is expected, as the structure of RDX remains consistent, with both surface and bulk information reflecting equivalent bands. This generates matching spectra for RDX type 1 class 1, RDX type 1 class 5 and recrystallised RDX. Resulting bands also provide a reference for measuring the extent of spectral shifts relevant to coated RDX.

### 3.3.6 Interaction of Dantocol and HMX

The second most widely used filler in cast-cured PBX formulations is the nitramine explosive HMX. This is a common replacement for RDX, possessing the added benefit of increased VoD, due to its additional nitro functionality and higher density. Increasing the concentration of nitro groups attached to the ring structure may be expected to provide

additional active sites capable of participating in secondary bonding. The potential for this to occur was investigated by FTIR, in a parallel study focused on identifying secondary bonding between Dantocol and HMX.

Confirmation of spectra shifts revealed the presence of interaction at the interface region. Initially, the  $\nu_{\text{as}}\text{NO}_2$  bands were investigated to determine the extent of secondary bonding between HMX and Dantocol. Bathochromic shifts were consistent with coated RDX, although the magnitude of shifts was found to decrease at the equivalent coating concentration. Maximum deviation in wavenumber was recorded at  $\geq 20\%$  Dantocol, producing shifts of  $\Delta\nu_{\text{as}}\text{NO}_2$   $11\text{cm}^{-1}$ . Steric hindrance is likely responsible for the inability of HMXs additional nitro group to increase participation in interaction.

Correlating shifts in the  $\nu\text{OH}$  band, confirmed the occurrence of hydrogen bonding at the interface. The initial Dantocol monolayer provides the greatest percentage of hydroxyl groups involved in hydrogen bonding. This generates a minimum wavenumber of  $\nu\text{OH}$   $3393\text{cm}^{-1}$  for 5% Dantocol coatings. As the concentration is increased, the number of hydroxyl groups participating in secondary bonding is limited to those located at the interface. This causes an increase in free hydroxyl groups unable to align with surface active nitro group, leading to a decrease in  $\Delta\nu\text{OH}$ . These observations are mirrored in the  $\nu_{\text{as}}\text{NO}_2$  band, whereby increasing the HMX concentration causes the peak to approach that of untreated HMX. Importantly the  $\nu\text{OH}$  band avoids overlay with the  $\nu\text{C}=\text{O}$  overtone occurring at  $\sim 2938\text{cm}^{-1}$ . This negates the possibility carbonyl groups are responsible for deviations in the hydroxyl band.

Sample	$\nu\text{OH}$	$\nu\text{C}=\text{O}$	$\nu_{\text{as}}\text{NO}_2$
HMX	-	-	1529
HMX·DHE 5%	3393	1695	1527
HMX·DHE 10%	3397	1695	1524
HMX·DHE 15%	3399	1690	1520
HMX·DHE 20%	3407	1688	1518
HMX·DHE 25%	3412	1687	1518

**Table 3.8.** Assignment of OH, C=O and  $\text{NO}_2$  peaks displaying spectral shift.

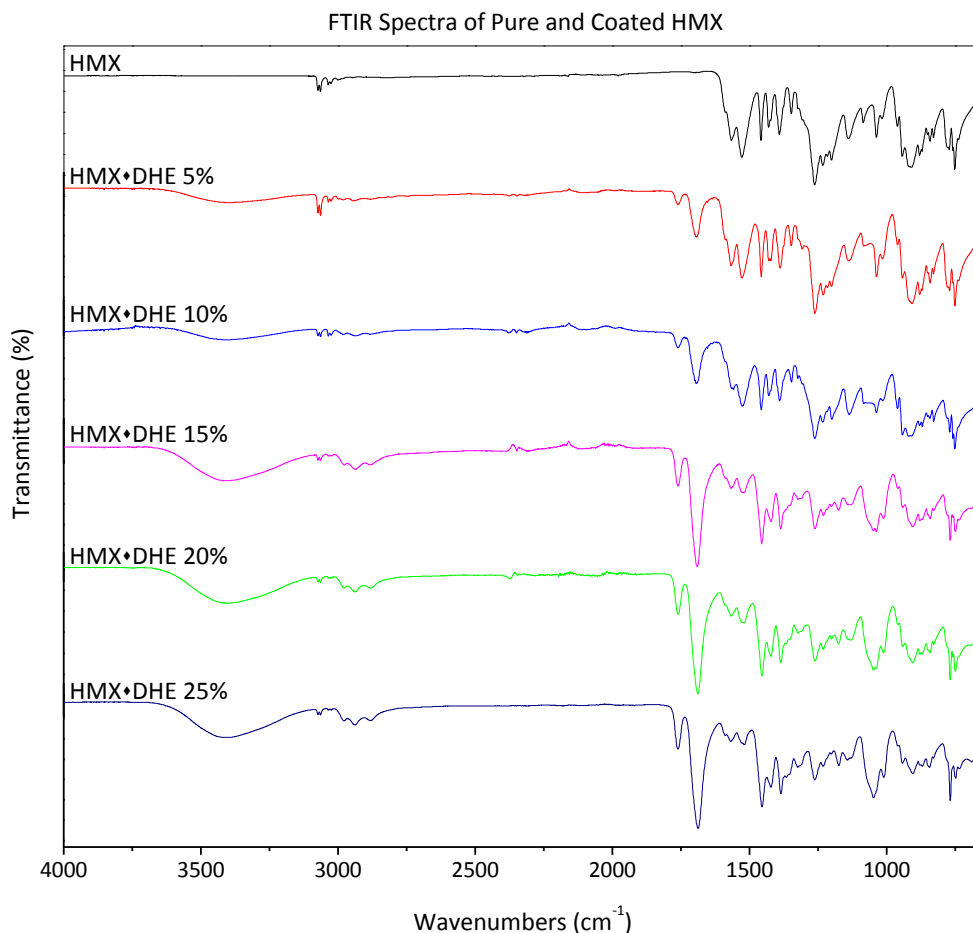


**Figure 3.15.** Spectra of pure and coated HMX of 5-25% Dantocol conc.

In addition to shifts in the  $\nu_{\text{as}}\text{NO}_2$  bands, Figure 3.15 also revealed bathochromic shifts in the  $\nu\text{C}=\text{O}$  peaks. This is consistent with dipole interactions described in Section 3.3.4. Unlike the  $\nu_{\text{as}}\text{NO}_2$  band, shifts were slightly greater for coated HMX compared with RDX. As the dipole moment of HMX is greater than that of RDX, this may account for the increased shift in  $\nu\text{C}=\text{O}$  bands of coated HMX.<sup>35</sup> The magnitude of referenced shifts are collated in Table 3.8, indicating the strength of interactions. These results confirmed the presence of hydrogen bonding and dipole interactions at the interface of Dantocol and HMX. This was expected given the similarity in structure of HMX and RDX, both comprising nitro functionality.

### 3.4 Conclusion

Application of a diverse range of FTIR techniques provided the means necessary for effective evaluation of secondary bonding between RDX and Dantocol. The combined

capabilities of ATR, DRIFTS, PAS and transmission spectroscopy facilitated investigation of the interface region at differing penetration depths while employing an alternative signal method. Each was exploited to provide spectral data from a range of sample depths, by altering measurement conditions. This detailed the interface region from all perspectives, along with the interactions occurring there.

The combined results of FTIR analysis indicate the presence of spectral shifts within the asymmetrical  $\text{NO}_2$  stretching vibration of RDX. Extensive evaluation of the  $\text{NO}_2$  region, revealed participation of  $\text{NO}_2$  groups in hydrogen bonding with the bonding agent's OH functionality. Coating concentrations of 20% Dantocol provided maximum shifts in the nitramines  $\nu_{\text{as}}\text{NO}_2$  band. This remained consistent throughout the applied techniques, displaying shifts in excess of  $\Delta\nu_{\text{as}}\text{NO}_2$   $18\text{cm}^{-1}$ . The magnitude of  $\nu_{\text{as}}\text{NO}_2$  shifts represents the strength of hydrogen bonding occurring at the interface. Beyond concentrations of 20% Dantocol, spectral shift cease to increase, due to limited availability of active sites required for hydrogen bonding.

Coinciding with the appearance of  $\text{NO}_2$  shifts, was the formation of shifts in Dantocol's broad hydroxyl peak. This verified correlations between the  $\text{NO}_2$  and OH functionality, from which hydrogen bonding originates. Shifts in excess of  $\Delta\nu\text{OH}$   $39\text{cm}^{-1}$ , confirmed the presence of hydrogen bonding between Dantocol and the nitramine's proton accepting nitro groups.

The improved surface sensitivity of DRIFTS presented the greatest capability for investigation of surface interactions. This provides an accurate measure of the relative strength and concentration of intermolecular interactions between Dantocol and RDX. Consequently the surface sensitivity of DRIFTS is often capable of detecting interactions other techniques are unable to discern.<sup>36</sup> This is relevant to weak interactions, such as the dipole interaction observed within coated samples. Although only trace evidence of dipole interactions manifests within supporting techniques, interpretation of DRIFTS spectra demonstrates definitive evidence of such interaction. Shifts in the carbonyl bands validate

this finding, with the dipole moment responsible for interaction occurring complimentary to hydrogen bonding.

Differences between the two intermolecular forces include the amenability of hydrogen bonding towards infrared studies. Unlike dipole-interactions, hydrogen bonding is readily observed in the FTIR spectra, making it the most widely used source of information on hydrogen bonding. This provides an efficient means of acquiring both quantitative and qualitative data pertaining to intermolecular forces. In response to this, DRIFTS readily affirmed the presence of hydrogen bonding which promoted shifts in wavenumber, peak broadening and increased absorption intensity. Bands attributed to this interaction remain well separated and unambiguous, eliminating conjecture regarding intermolecular forces between hydroxyl and nitro moieties. This is consistent with the literature, which describes participation of alternative nitro compounds in hydrogen bonding with proton donors.<sup>19, 37-44</sup>

Depth profiling of coated RDX samples was successfully demonstrated through application of PAS. This was achieved by altering the mirror velocity to investigate various layers below the sample surface. A mirror velocity of  $0.9494\text{cm s}^{-1}$  was deemed most effective in providing shallow surface depth, while maintaining good signal strength. Results confirmed the presence of secondary bonding described, which supports information derived from previous FTIR techniques. In addition to identifying functional groups responsible for interaction, PAS provided the means for acquiring a comprehensive depth profile of coated RDX samples. Depth profiling of coated RDX revealed spectral variation coinciding with change in the depth of penetration. This depicted transition from spectra resembling neat RDX at high penetration depths, towards spectra displaying peaks representative of Dantocol under shallow sampling conditions.

As infrared spectra containing bands participating in intermolecular interactions are difficult to quantitatively analyse, spectral resolution was applied to resolve peaks involved. This enabled evaluation of bands comprising both free and bonded functionality. Curve-fitting was therefore applied to elucidate parameters of individual bands, including position, width

and area. Information derived from this data was fundamental in performing quantitative spectral analysis. To facilitate data manipulation, the number of overlying bands is required prior to curve-fitting. Deconvolution is therefore necessary to identify the number of bands residing within a particular band, ensuring the accuracy of results. This provides a partial resolution of otherwise overlapped bands, while identifying the presence of free and bonded bands within the current system. These results confirmed characterisation of secondary bonding, through resolution of functional bands participating in intermolecular interaction.

### 3.5 References

1. Mattos, E. d. C.; Viganó, I.; Dutra, R. d. C. L.; Diniz, M. F.; Iha, K., Aplicação de metodologias FTIR de transmissão e fotoacústica à caracterização de materiais altamente energéticos: parte II. *Química Nova* **2002**, *25*, 722-728.
2. Eva Roedel; Atsushi Urakawa; Sven Kuretiw; Baiker, A., On the local sensitivity of different IR techniques: Ba species relevant in NO<sub>x</sub> storage-reduction. *Physical Chemistry Chemical Physics* **2008**, *10* (40), 6190-6198.
3. Graf, R. T.; Koenig, J. L.; Ishida, H., Introduction to Optics and Infrared Spectroscopic Techniques. In *Fourier Transform Infrared Characterization of Polymers*, Ishida, H., Ed. Springer US: **1987**; Vol. 36, pp 1-32.
4. Pandley, G. C.; Kulshreshtha, A. K., Fourier transform infrared spectroscopy as a quality control tool. *Process Control and Quality* **1993**, *4*, 109-123.
5. Mattos, E. C.; Moreira, E. D.; Diniz, M. F.; Dutra, R. C. L.; Silva, G.; Iha, K.; Teipel, U., Characterization of Polymer-Coated RDX and HMX Particles. *Propellants, Explosives, Pyrotechnics* **2008**, *33* (1), 44-50.
6. Hori, K.; Iwama, A., FTIR spectroscopic study on the interaction between ammonium perchlorate and bonding agents. *Propellants, Explosives, Pyrotechnics* **1990**, *15* (3), 99-102.
7. Kishore, K.; Prema, S.; Iyanar, K.; Pandureng, L. P., Mechanistic studies on the effect of ferrocene bonding agents in composite solid propellants. *Fuel* **1994**, *73* (10), 1583-1593.
8. Bart, J. C. J., In-Polymer Spectroscopic Analysis of Additives. In *Plastic Additives: Advanced Industrial Analysis*, Amsterdam, **2006**; pp 1-132.
9. Mattos, E. C.; Dutra, R. C.; Diniz, M. F.; Iha, K., Evaluation of the use of FT-IR techniques for characterisation of polymeric coating material energy. *Polymers* **2004**, *12* (2).
10. Mattos, E. d. C.; Viganó, I.; Dutra, R. d. C. L.; Diniz, M. F.; Iha, K.; Luis, H. D., Application of FT-IR techniques for identification of different polymers used in the coating process of energetic materials. In *Energetic Materials: Structure and Properties 35th International Annual Conference of ICT*, Karlsruhe, Germany, **2004**; pp 147/1-147/13.
11. Kubelka P.; Munk F., An Article on Optics of Paint Layers. *Zeitschrift für Technische Physik* **1931**, *12*, 593-601.
12. Suzuki, E. M.; Gresham, W. R., Forensic Science applications of diffuse reflectance infrared Fourier transform spectroscopy (DRIFTS): I. Principles, sampling methods, and advantages. *Journal of Forensic Sciences* **1986**, *31* (3), 931-952.
13. Al-Sayah, M. H.; Branda, N. R., Calorimetric and NMR binding studies of hydrogen-bonding receptors for carboxylates. *Thermochimica Acta* **2010**, *503-504*, 28-32.
14. Armarego, W. L. F.; Chai, C. L. L., *Purification of Laboratory Chemicals*. Fifth ed.; Butterworth Heinemann: **2003**.
15. Bradley, M. *Curve fitting in raman and IR spectroscopy: basic theory of line shapes and applications*; Thermo Fisher Scientific: Madison, USA, **2007**; pp 1-4.



16. Oldak, R. K.; Pearson, R. A., Evaluation of infrared spectroscopic techniques to determine the Drago constants of a cycloaliphatic epoxy. *Journal of Adhesion Science and Technology* **2007**, *21* (9), 775-793.
17. Oelichmann, J., Surface and depth-profile analysis using FTIR spectroscopy. *Fresenius' Journal of Analytical Chemistry* **1989**, *333* (4), 353-359.
18. Yin, H.; Chen, H.; Chen, D., Hydrogen bond interaction in poly(acrylonitrile-co-methylacrylate)/attapulgitite nanocomposites. *Polymer Engineering & Science* **2010**, *50* (2), 312-319.
19. Baitinger, W. F.; Schleyer, P. v. R.; Murty, T. S. S. R.; Robinson, L., Nitro groups as proton acceptors in hydrogen bonding. *Tetrahedron* **1964**, *20* (7), 1635-1647.
20. Baitinger, W. F.; Schleyer, P. v. R., Hydrogen Bonding in 1,4-Substituted Butane-1,4-diols. *J. Org. Chem.* **1964**, *29* (4), 989-990.
21. He, Y.; Zhu, B.; Inoue, Y., Hydrogen bonds in polymer blends. *Progress in Polymer Science* **2004**, *29* (10), 1021-1051.
22. *Omnic user's guide, Version 7.3*. Thermo Electron Corporation: Madison, USA, **2006**; p 1-471.
23. Griffiths, P. R.; Pariente, G. L., Introduction to spectral deconvolution. *TrAC Trends in Analytical Chemistry* **1986**, *5* (8), 209-215.
24. Lórenz-Fonfría, V. c. A.; Padrós, E., Curve-fitting of Fourier manipulated spectra comprising apodization, smoothing, derivation and deconvolution. *Spectrochimica Acta Part A: Molecular and Biomolecular Spectroscopy* **2004**, *60* (12), 2703-2710.
25. Yongling, L.; Yuan, W.; Shaoxuan, R.; Chengwei, J., An investigation of interfacial interactions between RDX and polymer binders by FTIR photoacoustic spectroscopy. In *17th International Pyrotechnics Seminar Xi'an Modern Chemistry Research Institute*: Beijing, China, **1991**; pp 347-352.
26. Deeley, C.; Sellors, J.; Spragg, R. A., Comparison of FT near-IR Raman spectroscopy with FTIR photoacoustic and reflection measurements of solids. In *7th International Conference on Fourier Transform Spectroscopy*, Fairfax, Virginia, **1989**; Vol. 1145, pp 195-0.
27. Avendaño, C.; Menendez, J. C., Hydantoin and Its Derivatives. In *Kirk-Othmer Encyclopedia of Chemical Technology*, John Wiley & Sons, Inc.: **2000**.
28. Katritzky, A. R.; Taylor, P. J., *Physical Methods in Heterocyclic Chemistry*. Academic Press: New York, **1971**; Vol. 4.
29. Ušćumlić, G.; Kshad, A. A.; Mijin, D., Synthesis and investigation of solvent effects on the ultraviolet absorption spectra of 1,3-bis-substituted-5,5-dimethylhydantoins. *Journal of Serbian Chemistry Society* **2003**, *68* (10), 699-706.
30. Ušćumlić, G.; Mišić- Vuković, M., Substituent effect on C=O stretching vibrations in hydantoin derivatives. *Journal of Molecular Structure* **1992**, *266* (0), 315-320.
31. Ušćumlić, G.; Krstic, V. V.; Dramanic, S. Z., Reversal of Substituent Effect on C = O Stretching Vibrations in Hydantoin Derivatives. Part 2. *ChemInform* **1999**, *30* (16).

32. Ušćumlić, G.; Krstic, V. V.; Dramanic, S. Z., Reversed substituent effect on C=O stretching in hydantoin derivatives. *Indian Journal of Chemistry* **1997**, *36B*, 193-195.
33. Katritzky, A. R.; Taylor, P. J., Infrared Spectroscopy of Heterocycles. In *Physical Methods in Heterocyclic Chemistry*, **1971**; Vol. 4, pp 265-341.
34. Lochert, I. J.; Franson, M. D.; Hamshere, B. L., Reduced sensitivity RDX (RS-RDX) Part I: Literature review and DSTO evaluation. **2003**, (DSTO-TR-1447), 1-14.
35. Qasim, M. M.; Moore, B.; Taylor, L.; Honea, P.; Gorb, L.; Leszczynski, J., Structural Characteristics and Reactivity Relationships of Nitroaromatic and Nitramine Explosives – A Review of Our Computational Chemistry and Spectroscopic Research. *International Journal of Molecular Sciences* **2007**, *8*, 1234-1264.
36. Hapner, G.; Nease, A. *Study of explosives by diffuse reflectance FT-IR spectroscopy*; Monsanto Research Corp., Miamisburg, OH (USA). Mound: **1985**.
37. Forlani, L., Hydrogen Bonding and Complex Formation Involving Compounds with Amino, Nitroso and Nitro Groups. In *PATAI'S Chemistry of Functional Groups*, John Wiley & Sons, Ltd: **2009**.
38. Li, F.; Ye, L.; Nie, F.; Liu, Y., Synthesis of boron-containing coupling agents and its effect on the interfacial bonding of fluoropolymer/TATB composite. *Journal of Applied Polymer Science* **2007**, *105* (2), 777-782.
39. Granzhan, V. A.; Semenenko, S. V.; Zaitsev, P. M., The susceptibility of the nitro group to hydrogen bond formation. *Journal of Applied Spectroscopy* **1968**, *9* (3), 929-932.
40. Granzhan, V. A.; Semenenko, S. V.; Zaitsev, P. M., Sensitivity of a nitro group to the formation of a hydrogen bond. I Intramolecular hydrogen bonding in phenols. *Zhurnal Prikladnoi Spektroskopii* **1968**, *9* (3), 407-411.
41. Urbański, T., A study of the hydrogen bonds between the nitro-group and the hydroxyl or amino-groups in substituted nitroparaffins. *Tetrahedron* **1959**, *6* (1), 1-9.
42. Kamlet, M. J.; Taft, R. W., Linear solvation energy relationships. 20. Intra- vs. intermolecular hydrogen bonding by some 2-nitroaniline and 2-nitrophenol derivatives. *The Journal of Organic Chemistry* **1982**, *47* (9), 1734-1738.
43. Johnstone, R. A. W.; Loureiro, R. M. S.; Cristiano, M. L. S.; Labat, G., Bond energy/bond order relationships for N-O linkages and a quantitative measure of ionicity: the role of nitro groups in hydrogen-bonding. *Archieve of Organic Chemistry* **2010**, (5), 142-169.
44. T. Dubis, A.; Lotowski, Z.; Siergiejczyk, L.; Z. Wilczewska, A.; W. Morzycki, J., Study of Hydrogen Bonding in Nitro Enamides. *Journal of Chemical Research, Synopses* **1998**, (4), 170-171.





# Chapter 4

---

Hydroxyl protection of Dantocol

---

Sections of this chapter were presented at: Williams, C. A.; Walker, G. S.; Lochert, I. J.; Clarke, S. R., Application of Dantocol in polymer bonded explosives and determination of the mode of action. 2<sup>nd</sup> *Australian energetic materials symposium*, Adelaide, Australia. 2010.

## 4.1 Introduction

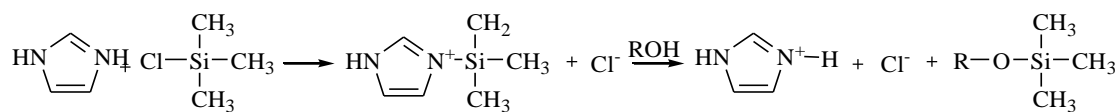
Until now, limited features have been established to identify the functional groups responsible for interaction of Dantocol and RDX. Consequently, modifications were made to the structure of Dantocol to prevent the interaction of hydroxyl groups. The intent of synthesis focussed on clarifying the bonding agent's involvement in hydrogen bonding.

An effective method for engaging hydroxyl protection is to initiate conversion of alcohol to the corresponding silyl ether. Consequently, silyl compounds are amongst the most commonly used protecting agents relevant to hydroxyl compounds. This response is due to the ease in which reaction is achieved under mild conditions, along with the ability to modulate stability through silyl compound selection.<sup>1</sup> Incorporation of bulkier compounds typically demonstrates greater stability towards acid-base hydrolysis, redox reactions and associated mechanisms. This is further influenced by electronic effects, which are exploited to differentiate stability under acidic or basic conditions.<sup>2</sup>

### 4.1.1 Silylation of Hydroxyl Groups

Various silyl compounds are available for application in hydroxyl silylation. This includes trimethylsilyl (TMS) and *tert*-butyldimethylsilyl (TBS), which are commonly employed in the protection of polar non-volatile compounds.<sup>2</sup> Formation of silyl ethers is achieved by reaction of alcohol and an appropriate silylation agent, comprising a necessary leaving group. This involves use of chlorosilanes, including trimethylsilyl chloride, recognised for its stability and ease with which it facilitates protection.<sup>3, 4</sup> This displays favourable properties, including the ability to remain stable under a range of conditions, while easily introduced and removed from reactions. Addition of trimethylsilyl chloride is performed in the presence of base, due to production of hydrochloric acid. Imidazole is often introduced to neutralise the pH, removing hydrogen chloride formed during silylation. Furthermore, the use of imidazole as a base is known to increase yield, as reported by Khalafi-Nwzhad et al.<sup>5</sup>

Subsequent reaction of trimethylsilyl chloride proceeds via formation of trimethylsilyl imidazole, indicated in reaction Scheme 4.1.



**Scheme 4.1.** Hydroxyl protection via formation of trimethylsilyl imidazole.

#### 4.1.2 Intermolecular Forces

Hydroxyl protection was intended to provide insight into the bonding agent's mode of action. This will enable confirmation of results obtained in Chapter 3, identifying intermolecular forces responsible for interaction of Dantocol. Comparisons drawn with silyl ethers will reflect involvement of hydrogen bonding, given the situation interactions are reduced. Meanwhile, under the circumstances weak interactions persist following hydroxyl removal, dipole interactions will also be confirmed. The presence of dipole interactions was initially proposed due to implications of the hydantoin's carbonyl functionality. This exhibits a dipole moment, according to the ring's nitrogen content.

Molecules with dipole moments tend to orientate in such a way that negative poles align with that of positive poles. The interaction between permanent dipoles are typically within the order of 1-3kcal mol<sup>-1</sup>. In comparison, hydrogen bonding exhibits a bond-dissociation energy of 3-103kcal mol<sup>-1</sup>. Consequently, hydrogen bonding is considered the strongest intermolecular interaction occurring between covalent compounds.<sup>6</sup>

The molar attraction constant ( $F$ ), is often applied to describe the attractive force of functional groups responsible for such interaction. Constants derived by Small, Van Kravlen and Hoy highlight the difference in attractive forces between the bonding agent's hydroxyl and carbonyl functionality.<sup>7-10</sup> These values are collated in Table 4.1, along with the molar attraction constants of Dantocol's remaining functional groups. Derivation of  $F$ , according to Small and Van Kravlen, was determined from the heat of vaporisation, as indicated in Equation 4.1.

$$F = (\Delta E_{i,j}^v V_{i,j})^{1/2} \quad (4.1)$$

Where  $\Delta E_{i,j}^v$  is the energy of vaporisation contribution associated with group  $j$ , and  $V_{i,j}$  represents the molar volume. Alternatively, Hoy employed vapour pressure measurements to determine the energy of vaporisation  $\Delta E_i^v$  prior to substitution.<sup>7</sup> Data collated indicates hydroxyl groups provide a greater attractive force than that of carbonyl groups. Alternatively the molar attraction constant of cyano groups has also lead to application within bonding agents.<sup>10</sup>

Group	Structure	F (Mpa <sup>1/2</sup> cm <sup>3</sup> mol <sup>-1</sup> )		$\Delta E_i^v$ (J mol <sup>-1</sup> )
		Small	Van Kravelen	Hoy
Methyl	-CH <sub>3</sub>	438	420	303
Carbon	>C<	-190	0	65.5
Carbonyl	C=O	563	685	538
Tertiary amine	>N-	-	-	125
Hydroxyl	-OH	-	754	462

**Table 4.1.** Molar attraction constants of functional groups at 25°C.<sup>7</sup>

Following interaction of two or more compounds, complexes may evolve between the above functionality. Fowkes investigated complex systems participating in hydrogen bonding derived from hydroxyl groups. This revealed superior surface adhesion, in comparison to that achieved by dipole interactions.<sup>11</sup> Literature also reports complex formation involving equimolar equivalents of HMX and dimethylformamide (DMF).<sup>12-15</sup> This calls for the recrystallisation of HMX dissolved in solution with DMF. While the resulting complex remains stable at room temperature, heating above 93°C promotes dissociation of components.<sup>15</sup> IR spectroscopy revealed the solvent's carbonyl band undergoes small bathochromic shifts, relative to its position in absolute DMF.<sup>13</sup> This is indicative of the solvents increased polarity within the complex. Presence of electron-donating groups adjacent to the carbonyl provides further complex stability. This suggests dipole-dipole interactions are in part responsible for the bond energy.<sup>12, 15</sup> These results imply dipole interactions are likely to occur within the current system.



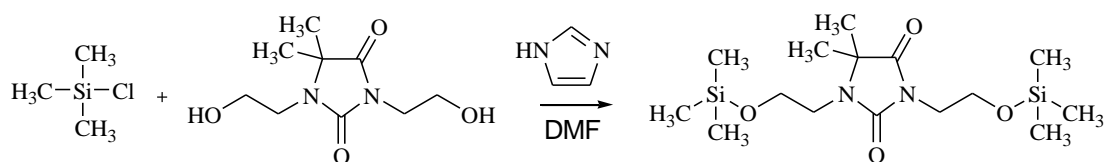
## 4.2 Experimental

Selective protection of Dantocol's multiple hydroxyl groups was achieved by silylation. This employed trimethylsilyl chloride on the grounds of its hydrolytic stability. Alternately, *tert*-butyldimethylsilyl chloride was substituted for the monosilylation reaction in response to its selective capabilities. Both protecting agents were used in conjunction with imidazole and polar aprotic solvents. Chemicals were purchased of highest commercial purity and used without further purification. However, Dantocol was recrystallised according to the method described in Section 2.2.1.1.

### 4.2.1 Synthesis of Hydroxyl Protected Dantocol

#### 4.2.1.1 1,3-*bis*(2-trimethylsilyloxyethyl)-5,5-dimethylhydantoin

Silylation of Dantocol's multiple hydroxyl groups was performed by reaction of Dantocol (1eq, 2.0g), trimethylsilyl chloride (2.4eq, 2.41g) and imidazole (5.0eq, 3.15g). Reagents were stirred overnight in DMF (40mL) at room temperature. Formation of a white precipitate indicates reaction onset, representing the imidazolium chloride by-product. Aqueous workup is therefore required to ensure its removal. A secondary wash in brine solution was performed to remove water content. The organic phase was further dried over sodium sulphate, followed by filtration. Residual solvent was removed under vacuum, yielding 1,3-*bis*(2-trimethylsilyloxyethyl)-5,5-dimethylhydantoin (TMSDHE) as a colourless oil.



**Scheme 4.2.** Synthesis of 1,3-*bis*(2-trimethylsilyloxyethyl)-5,5-dimethylhydantoin.

$^1\text{H}$  NMR 600MHz, Chloroform-*d*,  $\delta$  (ppm): 0.09 (s, 9H,  $\text{CH}_3$ ); 0.011 (s, 9H,  $\text{CH}_3$ ); 1.37 (s, 6H,  $\text{CH}_3$ ); 3.36 (t, 2H,  $\text{CH}_2\text{-N}$ ); 3.63 (t, 2H,  $\text{CH}_2\text{-N}$ ); 3.74 (t, 2H,  $\text{CH}_2\text{-O-Si}$ ); 3.75 (t, 2H,  $\text{CH}_2\text{-O-Si}$ ).

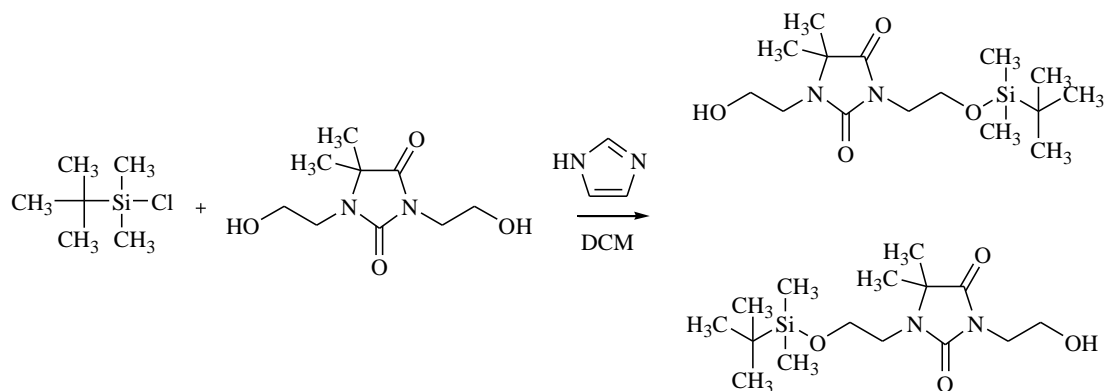
$^{13}\text{C}$  NMR 600MHz, Chloroform-*d*,  $\delta$  (ppm): -0.69, -0.61, 23.22 ( $\text{CH}_3$ ); 40.52, 42.30 ( $\text{CH}_2\text{-N}$ ); 58.85, 60.13 ( $\text{CH}_2\text{-O}$ ); 61.70 ( $\text{C-CH}_3$ ); 155.61, 176.91 ( $\text{C=O}$ ).

FTIR,  $\nu$  ( $\text{cm}^{-1}$ ): 835 ( $\text{Si-CH}_3$ ); 1101 ( $\text{Si-O-C}$ ); 1249 ( $\text{Si-CH}_3$ ); 1383, 1451 ( $\text{CH}_2$ ,  $\text{CH}_3$ ); 1704, 1770 ( $\text{C=O}$ ); 2874-2956 ( $\text{CH}_2$ ,  $\text{CH}_3$ ).

#### 4.2.1.2 *N*-(2-hydroxyethyl)-*N*-(2-*tert*-butyldimethylsilyloxyethyl)-5,5-dimethylhydantoin.

Synthesis of the monosilylated Dantocol derivative was performed to investigate the impact of reducing hydroxyl groups to single functionality. A similar protection technique was applied, substituting trimethylsilyl chloride in response to its limited ability to initiate selectivity.<sup>16</sup> Replacement with *tert*-butyldimethylsilyl chloride enables selective protection of similar hydroxyl arrangements.<sup>16</sup> This is possible due to the steric bulk of *tert*-butyldimethylsilyl chloride, which promotes attachment to the less hindered hydroxyl. Reaction conditions are equally critical to facilitate selectivity, requiring use of base to moderate the reactivity of *tert*-butyldimethylsilyl chloride. Selectivity is further enhanced by replacing the solvent with methylene chloride to reduce the reaction rate.<sup>16</sup> This is often coupled with a decrease in reaction temperature, in order to promote silylation of the less hindered hydroxyl group.<sup>17</sup> These efforts are assisted by attachment of the initial silyl ether side chain, which acts to impede reaction of Dantocol's secondary hydroxyl group.

Fundamentally, the adjustment of hydroxyl to silyl equivalents is required to achieve monosilylation of Dantocol. This involved charging *tert*-butyldimethylsilyl chloride (1.0eq, 1.39g), Dantocol (1eq, 2.0g) and imidazole (2.5eq, 1.57g), to a round bottom flask equipped with stirrer. Reactants were combined with methylene chloride (20mL) and mixed overnight at 0°C. The resulting silyl ether was washed in  $\text{H}_2\text{O}$ , followed by saturated NaCl solution (brine) to extract impurities. Residual  $\text{H}_2\text{O}$  was removed over sodium sulphate with *N*-(2-hydroxyethyl)-*N*-(2-*tert*-butyldimethylsilyloxyethyl)-5,5-dimethylhydantoin (TBSDHE) collected following filtration of the drying agent.



**Scheme 4.3.** Synthesis of N-(2-hydroxyethyl)-N-(2-*tert*-butyldimethylsilyloxyethyl)-5,5-dimethylhydantoin.

FTIR,  $\nu$  ( $\text{cm}^{-1}$ ): 833 (Si-CH<sub>3</sub>); 1104 (Si-O-C); 1253 (Si-CH<sub>3</sub>); 1384, 1451 (CH<sub>2</sub>, CH<sub>3</sub>); 1703, 1769 (C=O); 2857-2953 (CH<sub>2</sub>, CH<sub>3</sub>); 3467 (OH).

1-(2-hydroxyethyl)-3-(2-*tert*-butyldimethylsilyloxyethyl)-5,5-dimethyl-hydantoin.

<sup>1</sup>H NMR 600MHz, Chloroform-*d*,  $\delta$  (ppm): 0.02 (s, 6H, CH<sub>3</sub>); 0.85 (s, 9H, CH<sub>3</sub>); 1.39 (s, 6H, CH<sub>3</sub>); 3.02 (t, 1H, OH); 3.35 (t, 2H, CH<sub>2</sub>-N); 3.63 (t, 2H, CH<sub>2</sub>-N); 3.74 (t, 2H, CH<sub>2</sub>-OH); 3.79 (t, 2H, CH<sub>2</sub>-O-Si).

<sup>13</sup>C NMR 600MHz, Chloroform-*d*,  $\delta$  (ppm): -5.33, 23.05, 25.92 (CH<sub>3</sub>); 18.27 (C-Si); 41.1, 42.5 (CH<sub>2</sub>-N); 61.19, 61.78 (CH<sub>2</sub>-O); 59.61 (C-CH<sub>3</sub>); 155.79, 176.97 (C=O).

1-(2-*tert*-butyldimethylsilyloxyethyl)-3-(2-hydroxyethyl)-5,5-dimethyl-hydantoin.

<sup>1</sup>H NMR 600MHz, Chloroform-*d*,  $\delta$  (ppm): 0.06 (s, 6H, CH<sub>3</sub>); 0.89 (s, 9H, CH<sub>3</sub>); 1.37 (s, 6H, CH<sub>3</sub>); 2.63 (t, 1H, OH); 3.41 (t, 2H, CH<sub>2</sub>-N); 3.65 (t, 2H, CH<sub>2</sub>-N); 3.77 (t, 2H, CH<sub>2</sub>-OH); 3.83 (t, 2H, CH<sub>2</sub>-O-Si).

<sup>13</sup>C NMR 600MHz, Chloroform-*d*,  $\delta$  (ppm): -5.28, 23.39, 26.06 (CH<sub>3</sub>); 18.46 (C-Si); 40.91, 43.30 (CH<sub>2</sub>-N); 60.96, 61.65 (CH<sub>2</sub>-O); 59.49 (C-CH<sub>3</sub>); 155.79, 176.97 (C=O).

## 4.2.2 Characterisation of Hydroxyl Protected Dantocol

### 4.2.2.1 Fourier Transform Infrared Spectroscopy

Infrared spectroscopy was performed using a Nicolet Nexus 8700 FT-IR Spectrophotometer equipped with MCT/A detector. Spectra were acquired over 128 scans, at a resolution of  $2.0\text{cm}^{-1}$ . This was applied over a wavenumber range of  $650\text{-}4000\text{cm}^{-1}$ , using a sample gain of 2.0. Subsequent data analysis was supported by OMNIC version 7.3 software.

### 4.2.2.2 Nuclear Magnetic Resonance

Characterisation was performed using a Bruker 600MHz NMR spectrometer.  $^1\text{H}$  and  $^{13}\text{C}$  spectra employed model parameters comprising standard units of chemical shift (ppm) and J-coupling constant (Hz). Proton acquisitions were collected over a spectral width of 6009Hz, with a relaxation delay of 1.0sec and acquisition time of 2.726sec.  $^{13}\text{C}$  NMR comprised a minimum acquisition of 500 scans, while employing a spectral width of 24038Hz, relaxation delay of 2.0sec and acquisition time of 1.363sec. Sample preparation involved use of chloroform-*d*, referenced to  $^1\text{H} = 7.26\text{ppm}$  and  $^{13}\text{C} = 77.16\text{ppm}$ .

### 4.2.2.3 Scanning Electron Microscopy

Coatings of RDX in silyl ethers were evaluated by SEM, employing a CamScan MX2500 SEM equipped with EDX. Samples were pretreated with 5nm of platinum deposited using a Quorumtech K757X Sputter Coater. Prepared samples were exposed to an acceleration voltage of 10kV, over a spot size of 4.00nm. This was controlled using MaXim 4 software, to produce high resolution images of surface coatings.

## 4.3 Results

Selective protection of the bonding agent's multiple hydroxyl groups was applied to establish the functional groups responsible for interaction with RDX. Suppression of hydrogen bonding served to identify the ability to undergo interaction in the absence of hydroxyl

groups. This is necessary to confirm the presence of dipole interactions involving the bonding agents carbonyl functionality. Presence of multiple interaction was determined by FTIR investigation, involving RDX encapsulated in silyl ether compounds. Bathochromic shifts in vibrational bands indicate the functional groups responsible for interaction, therefore elucidating the bonding agents mode of action.

### 4.3.1 1,3-bis(2-trimethylsilyoxyethyl)-5,5-dimethylhydantoin

#### 4.3.1.1 Characterisation of Disilylated Dantocol

Silylation of Dantocol was initially directed towards removal of both hydroxyl side chains. This was achieved via reaction of Dantocol and trimethylsilyl chloride in the presence of base. Functionality ratios were previously investigated to maximise yield, whilst excess imidazole ensured complete conversion of the silyl ether.<sup>3,4</sup> This was characterised by proton NMR, indicating reaction of trimethylsilyl chloride and Dantocol's multiple hydroxyl functionality. Disilylation coincides with the formation of methyl peaks at  $\delta = 0.09\text{ppm}$  and  $0.011\text{ppm}$ . The difference in chemical environment from which trimethylsilyl groups reside, cause methyl peaks to appear at separate chemical shifts, therefore confirming protection of both hydroxyls. Absence of peaks within the hydroxyl region ( $\delta = 3-3.5\text{ppm}$ ) provides further evidence of reaction completion.

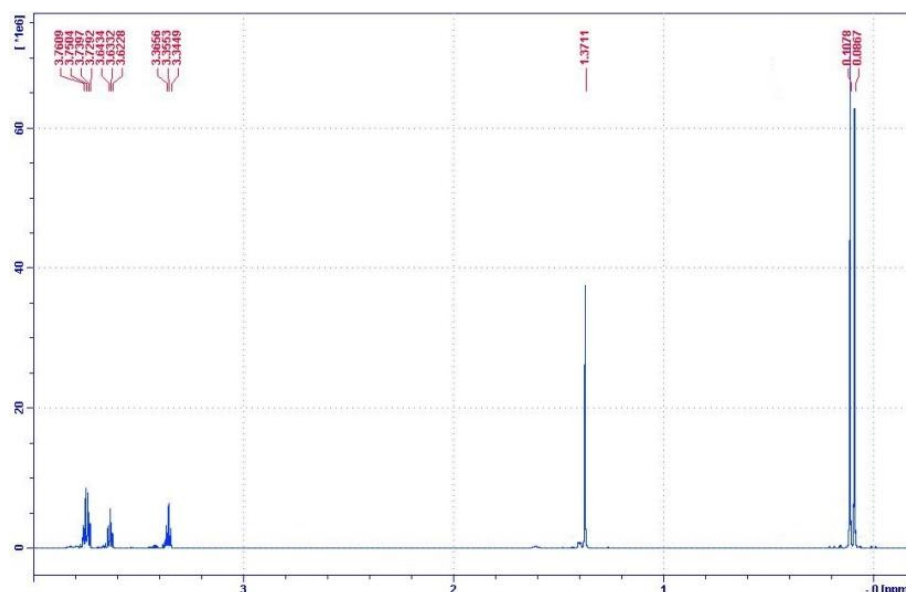


**Figure 4.1.** <sup>1</sup>H NMR of 1,3-bis(2-trimethylsilyoxyethyl)-5,5-dimethylhydantoin in CDCl<sub>3</sub>.

Investigation of  $^{13}\text{C}$  NMR confirms multiple attachment of silyl ethers, as indicated by methyl peaks consistent with the proton spectrum. Peaks occurring at  $\delta = -0.69\text{ppm}$  and  $-0.6\text{ppm}$  represent methyls associated with silyl ether formation. This occurs upfield from the hydantoin's methyl functionality, due to shielding of the silicon atom. Remaining peaks are consistent with Dantocol, while displaying minor deviation in chemical shift, due to proximity of the silyl ether.

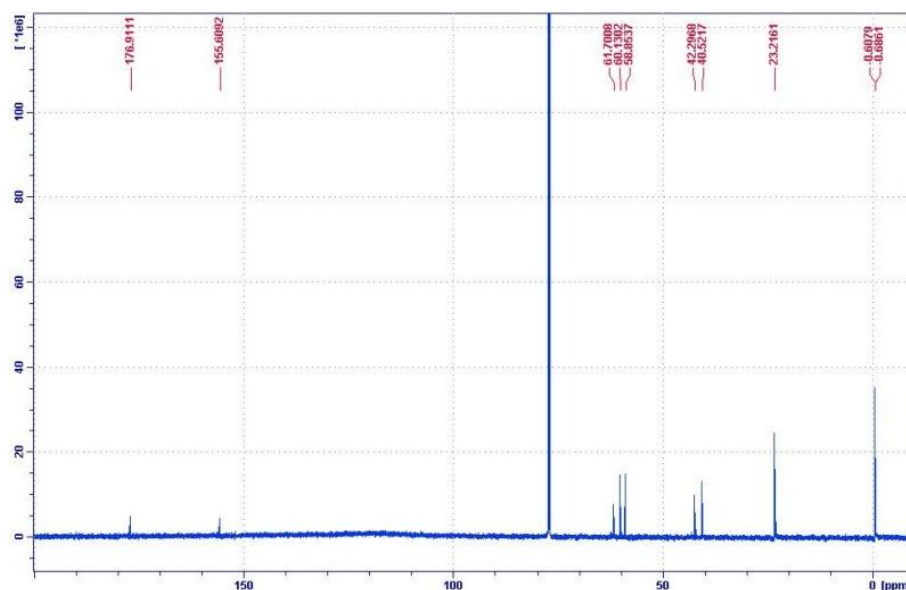


**Figure 4.2.**  $^{13}\text{C}$  NMR of 1,3'-bis(2-trimethylsilyloxyethyl)-5,5-dimethylhydantoin in  $\text{CDCl}_3$ .

FTIR analysis of TMSDHE was performed prior to characterising potential interactions of the modified bonding agent. The acquired spectrum functioned as a reference from which coated RDX was compared to identify shifts arising from interaction. Characterisation of TMSDHE demonstrated removal of the broad hydroxyl peak, typically located around  $3400\text{-}3300\text{cm}^{-1}$ . This coincides with the formation of  $\text{Si-CH}_3$  bands at  $\nu = 835\text{cm}^{-1}$  and  $1383\text{cm}^{-1}$ . Such features confirm reaction as indicated by silylation of the hydroxyl functionality.

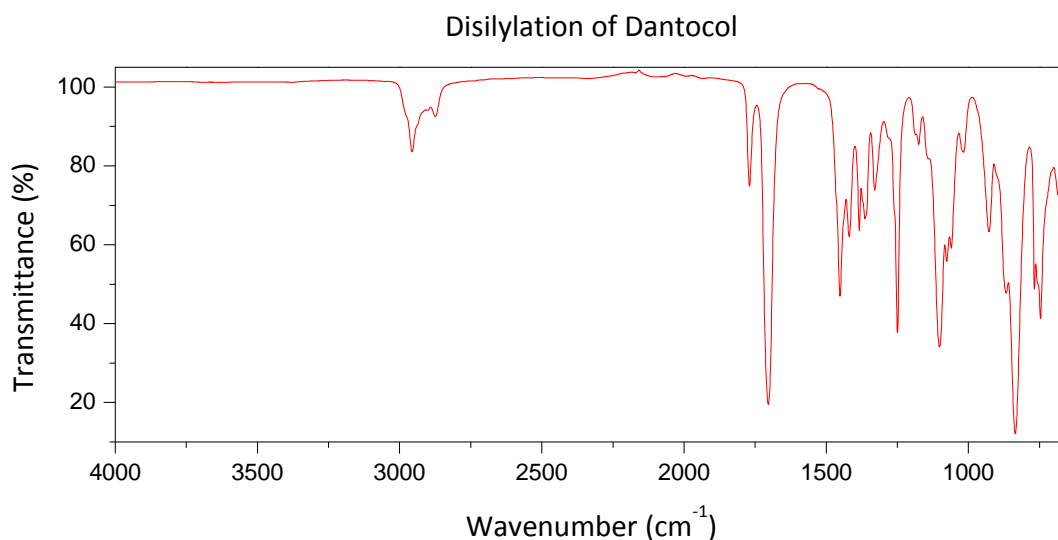


**Figure 4.3.** FTIR spectrum of 1,3-*bis*(2-trimethylsilyloxyethyl)-5,5-dimethylhydantoin.

#### 4.3.1.2 Interaction of Disilylated Dantocol and RDX

Following synthesis of TMSDHE, investigations shifted to the impact of hydroxyl protection on Dantocol's ability to participate in interaction. Preparation involved microencapsulation of RDX to provide uniform TMSDHE coatings. Concentrations of 5–25% TMSDHE were applied, according to procedures described in Section 2.2.2.6. Assessment of nitramine coatings involved SEM to identify the extent of surface coverage. This demonstrates the proficiency of microencapsulation, as hydroxyl protection is expected to hinder coating techniques.

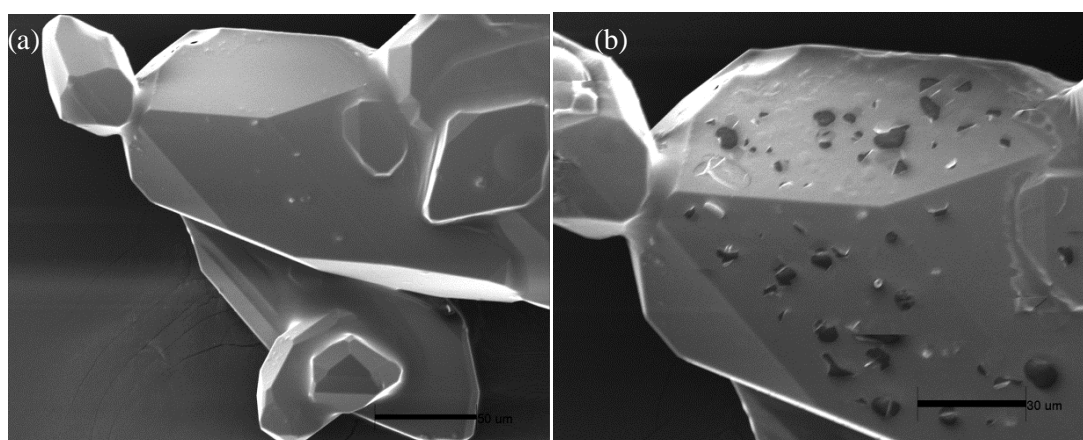


**Figure 4.4.** SEM of RDX coated in TMSDHE (a) before and (b) after electron ablation.

The tendency of coating to undergo ablation was also observed, following irradiation of the SEM electron beam. Figure 4.4 highlights disruption of the silyl ether coating, exposing the surface of RDX. This is represented by darkened regions, as the disilylated bonding agent appears to lift from the surface. The extent of this occurrence is unprecedented amongst coatings, therefore providing initial indications surface adhesion is impeded by hydroxyl protection.

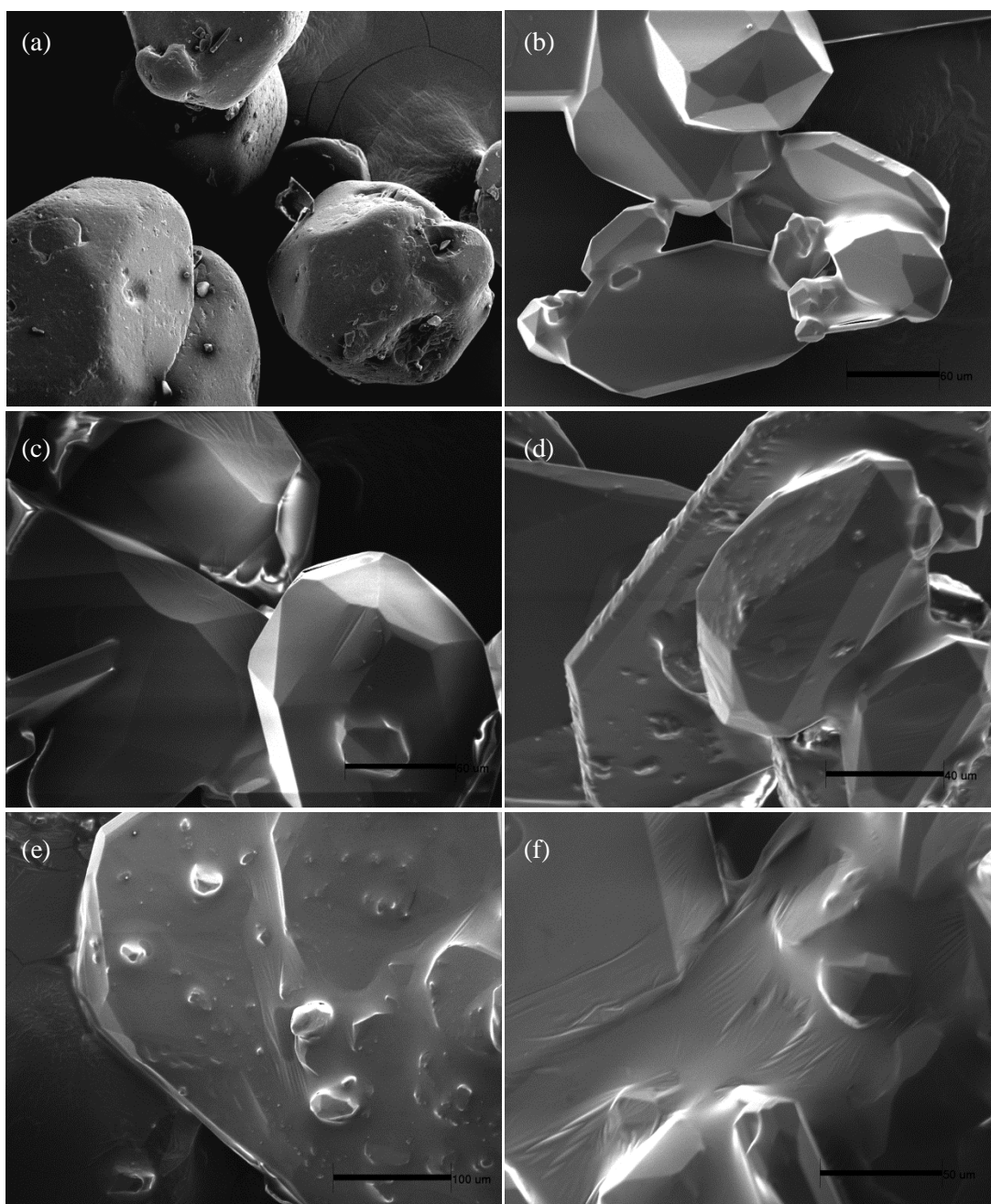


**Figure 4.5.** SEM images of (a) RDX at coating concentrations of (b) 5% TMSDHE (c) 10% TMSDHE (d) 15% TMSDHE (e) 20% TMSDHE (f) 25% TMSDHE.



Interpretation of RDX coatings reveals an increase in surface coverage, proportional to the concentration of disilylated bonding agent. Following confirmation of surface coatings, investigations commenced in relation to the impact of hydroxyl protection on interaction.

FTIR spectroscopy was employed to determine the presence of interaction as indicated by spectral shifts. This displayed a reduction in magnitude, compared with  $\nu_{as}NO_2$  shifts involving Dantocol and RDX indicated in Table 4.2. The connotations of this imply involvement of Dantocol's hydroxyl groups in interaction with RDX. Although impeded upon hydroxyl protection, the extent of shifts suggests the occurrence of weak interactions indicated in Figure 4.6. This concurs with the formation of dipole interactions, involving the bonding agents carbonyl functionality and RDX.

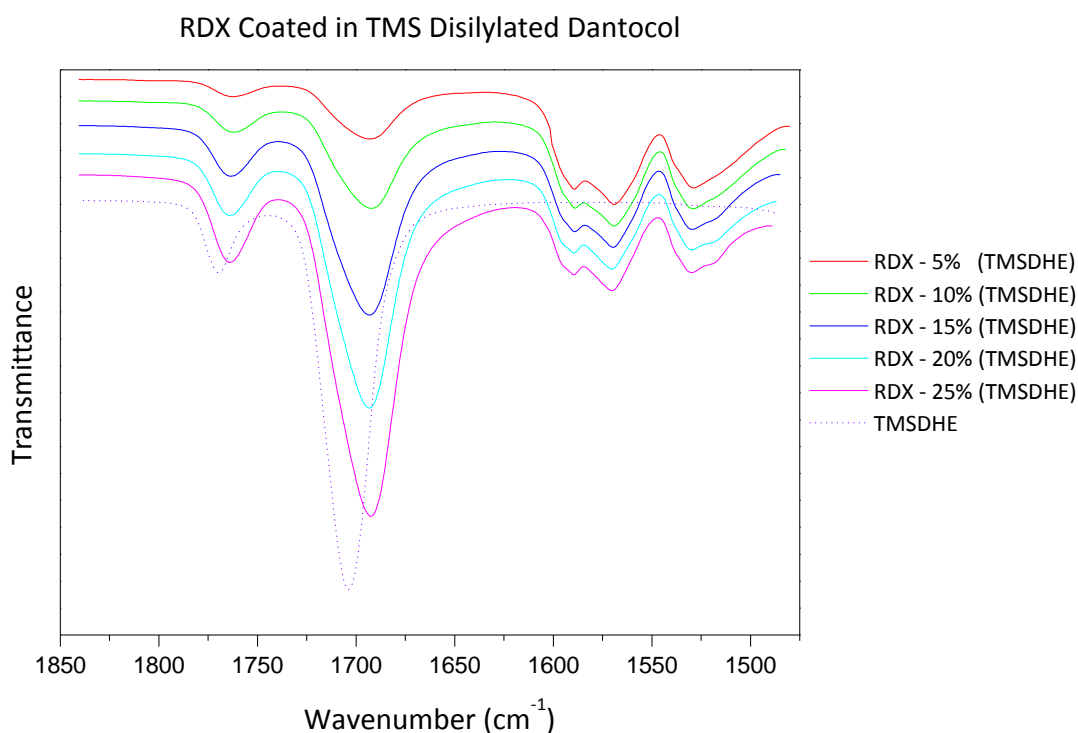


**Figure 4.6.** IR spectra of RDX coated in TMSDHE 5-25%.

Inspection of carbonyl peaks demonstrates increased intensity proportional to the concentration of TMSDHE. This was accompanied by wavenumber shifts, resulting from participation in interaction. Shifts in excess of  $\Delta\nu_s C=O$   $8\text{cm}^{-1}$  and  $\Delta\nu_{as} C=O$   $13\text{cm}^{-1}$ , were observed in the spectra of coated RDX. The ability of hydroxyl-protected Dantocol to

undergo weak interactions leads to the conclusion dipole interactions play an important role in the bonding agents mode of action. Investigation of the hydantoin ring deformation and C-N stretching vibration which may substantiate these findings, experience overlay associated with the nitramine bands. Consequently, this limits information obtained from such bands.

Conc %	TMSDHE Coated RDX (cm <sup>-1</sup> )			Dantocol Coated RDX (cm <sup>-1</sup> )		
	$\nu_s\text{C=O}$	$\nu_{as}\text{C=O}$	$\nu_{as}\text{NO}_2$	$\nu_s\text{C=O}$	$\nu_{as}\text{C=O}$	$\nu_{as}\text{NO}_2$
Pure	1770	1704	1532	1770	1704	1532
5%	1763	1694	1530	1764	1696	1527
10%	1763	1693	1529	1761	1695	1522
15%	1763	1693	1529	1761	1690	1519
20%	1762	1692	1529	1760	1689	1517
25%	1762	1691	1529	1761	1689	1519

**Table 4.2.** FTIR assignment of TMSDHE microencapsulated RDX.

### 4.3.2 *N*-(2-hydroxyethyl)-*N*-(2-*tert*-butyldimethylsilyloxyethyl)-5,5-dimethylhydantoin

#### 4.3.2.1 Characterisation of Monosilylated Dantocol

In addition to disilylation of Dantocol's hydroxyl functionality, the monosilylated alternative was synthesised to provide depth of analysis. *Tert*-butyldimethylsilyl chloride was subsequently exchanged as the protecting agent, due to advantages in selectivity. This was supported through optimising reaction conditions in promotion of monosilylation. Considerations include the ratio of molar equivalents, reduced reaction temperature and substitution of methylene chloride. Benefits associated with solvent replacement stem from the ability of methylene chloride to moderate the reactivity of *tert*-butyldimethylsilyl chloride.<sup>16</sup> Selectivity is further enhanced by decreasing the reaction temperature, thus reducing the reaction rate.

Efforts resulted in synthesis of the monosilylated bonding agent, with silyl ether attachment occurring at either the C-1 or C-3 position. This generated isomers described in Scheme 4.3 following reaction of Dantocol and TBS in equimolar quantities. Following silylation of the

initial hydroxyl group, the silyl ether inhibits reaction of the remaining hydroxyl group, due to steric hindrance.<sup>16</sup> This ensures hydroxyl protection is limited to single functionality, leaving the remaining hydroxyl unreacted.

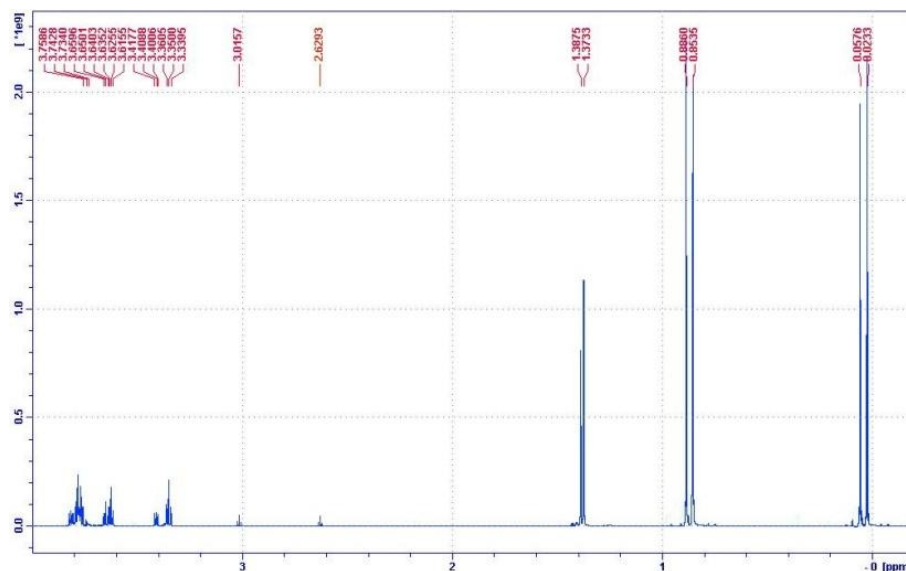


**Figure 4.7.** <sup>1</sup>H NMR of *N*-(2-hydroxyethyl)-*N*-(2-*tert*-butyldimethylsilyloxyethyl)-5,5-dimethylhydantoin in chloroform-*d*.

Characterisation of the monosilylation product revealed the presence of isomers as determined by NMR spectroscopy. Isomers were identified as 1-(2-*tert*-butyldimethylsilyloxyethyl)-3-(2-hydroxyethyl)-5,5-dimethylhydantoin and 1-(2-hydroxyethyl)-3-(2-*tert*-butyldimethylsilyloxyethyl)-5,5-dimethylhydantoin. This represents single attachment of TBS to the bonding agent's hydroxyl functionality. Chemical shifts associated with hydroxyl peaks appear at  $\delta = 3.02$ ppm and 2.63ppm, occurring downfield due to attachment of the silyl ether. This also represents the absence of unreacted Dantocol from the proton spectra. Methyl groups associated with the *tert*-butyldimethylsilyl side-arm evolve at Si-CH<sub>3</sub> ( $\delta = 0.02$ ppm, 0.06ppm) and CH<sub>3</sub>-C ( $\delta = 0.85$ ppm, 0.89ppm). Again, presence of multiple peaks confirms isomer formation which develop according to the chemical environment of the silyl ether.

The  $^{13}\text{C}$  NMR substantiates isomer formation, with downfield shift in the remaining CH-OH peaks indicating attachment of the silyl ether. Methyl peaks associated with the *tert*-butyldimethylsilyl side-arm appear at  $\text{CH}_3\text{-Si}$  ( $\delta = -5.33\text{ppm}$ ,  $-5.28\text{ppm}$ ) and  $\text{CH}_3\text{-C}$  ( $\delta = 25.92\text{ppm}$ ,  $26.06\text{ppm}$ ). The occurrence of duplicate peaks represents methyl groups correlating with isomer conformations. This is justified by the tertiary carbon attached to the silicon, appearing as multiple peaks at  $\text{C-Si}$  ( $\delta = 18.27\text{ppm}$ ,  $18.46\text{ppm}$ ).

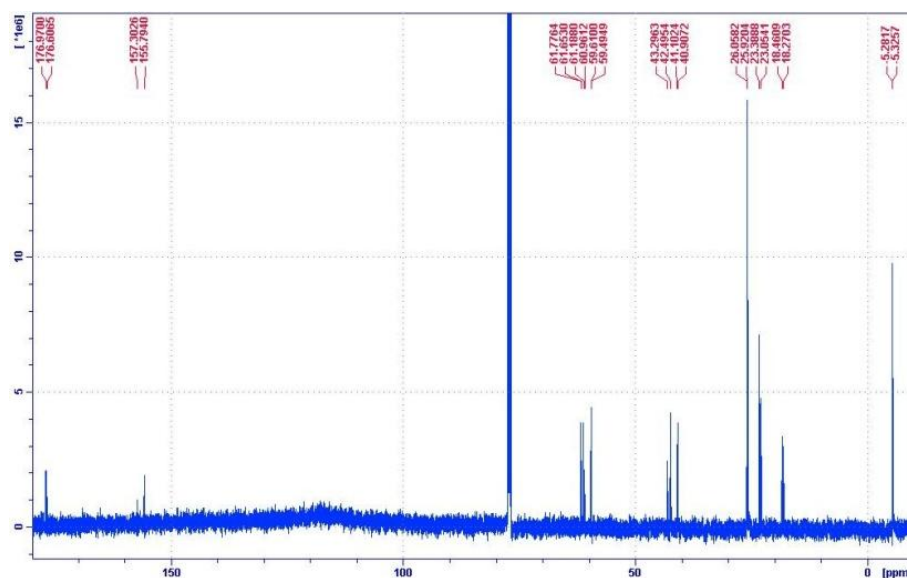


**Figure 4.8.**  $^{13}\text{C}$  NMR of *N*-(2-hydroxyethyl)-*N*-(2-*tert*-butyldimethylsilyloxyethyl)-5,5-dimethylhydanto in chloroform-*d*.

Inspection of the IR spectra revealed similar features to the disilylation product. This occurs due to the repetition of functional groups, with exception to the hydroxyl region. Monosilylation of Dantocol ensures the broad hydroxyl band remains present at  $\nu_{\text{OH}} = 3467\text{cm}^{-1}$ . This confirms selective protection of an isolated hydroxyl group, while that remaining exists unimpeded. As expected, peak intensity declines following monosilylation with the hydroxyl concentration reduced by half. Other notable variations include the shift in ring deformation which evolves at  $\nu = 768\text{cm}^{-1}$ . This appears at increased wavenumber, as the strain imposed by reduction in silyl ether functionality is decreased. These findings are consistent with NMR results, indicating successful monosilylation of the bonding agent.

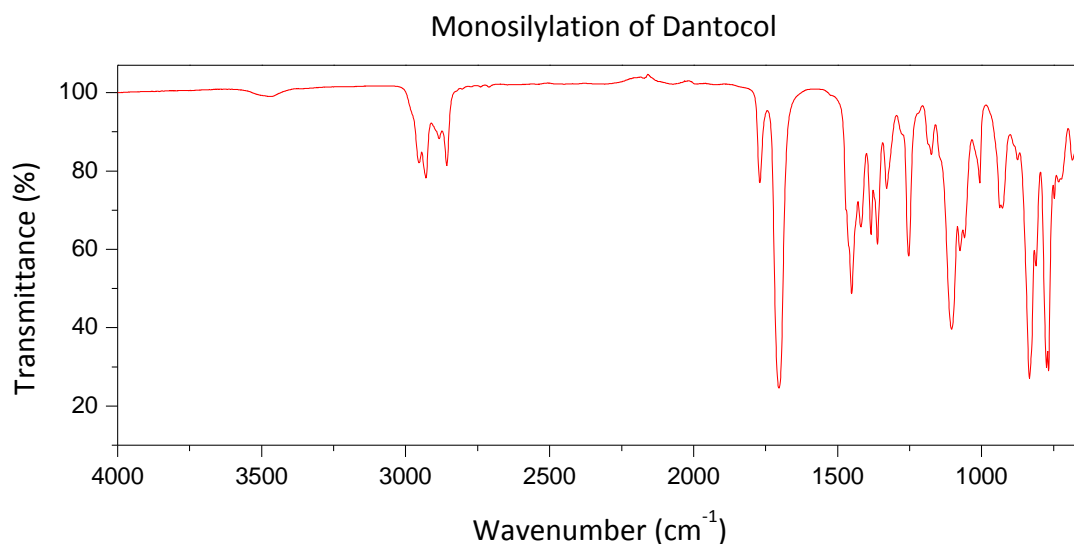


**Figure 4.9.** FTIR spectrum of *N*-(2-hydroxyethyl)-*N*-(2-*tert*-butyldimethylsilyloxy-ethyl)-5,5-dimethylhydantoin.

#### 4.3.2.2 Interaction of Monosilylated Dantocol and RDX

Monosilylated Dantocol was investigated for interaction with RDX following microencapsulation of nitramine particles. Coatings were monitored using electron microscopy to confirm application of surface coverage. Figure 4.10 reveals the extent of RDX coating at concentrations of 5-25% TBSDHE. As the potential for adhesion is improved in line with the remaining hydroxyl group, this could be expected to influence surface coatings. Comparison of the monosilylated and disilylated bonding agents suggest TBSDHE provides superior coatings at equivalent concentrations. Superior adhesion is achieved through the combined ability to participate in hydrogen bonding, whilst engaging in dipole interactions previously observed. This was supported by resistance of coating to participate in electron beam ablation, thus implying greater interfacial adhesion.

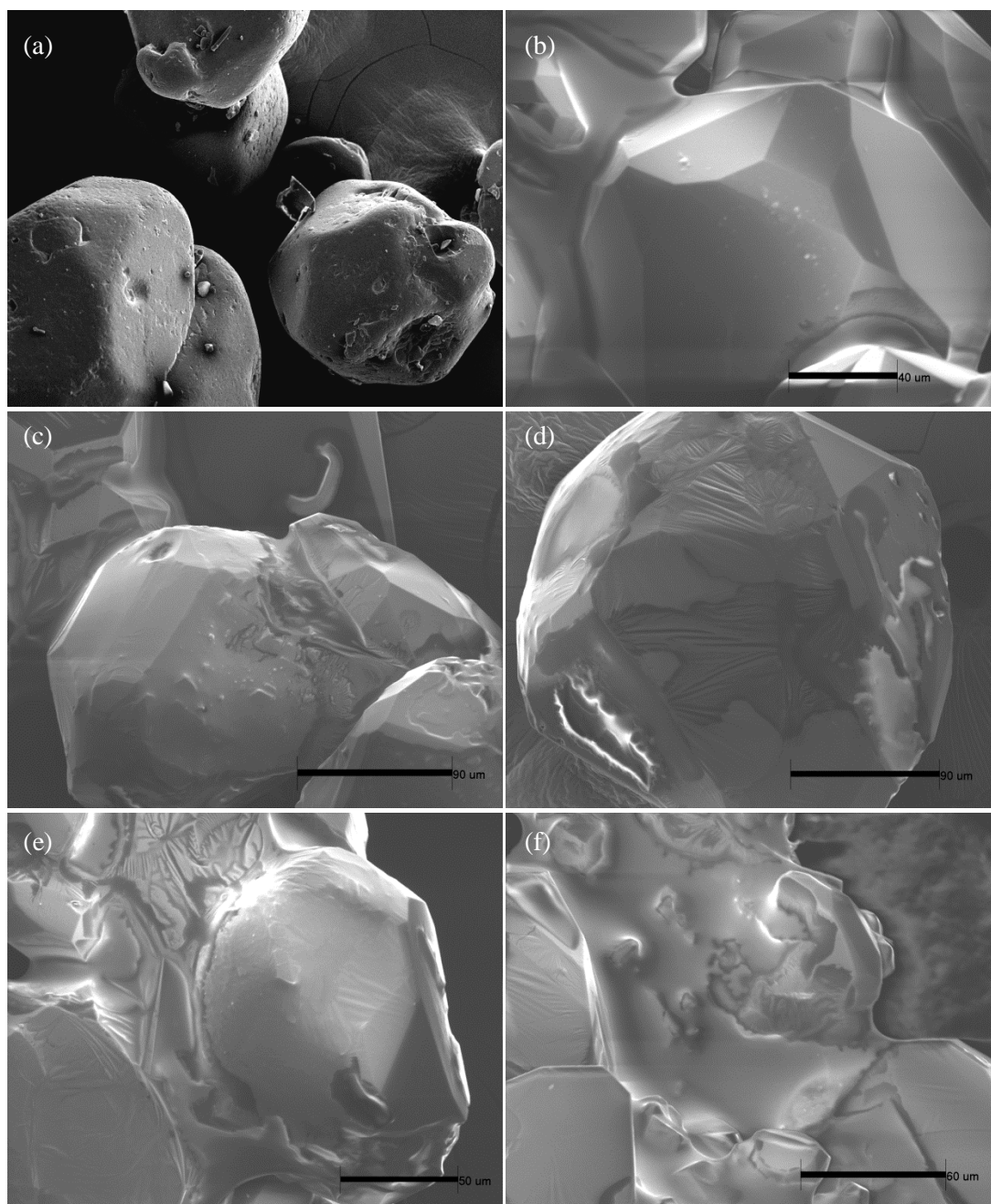


**Figure 4.10.** SEM images of (a) RDX at coating concentrations of (b) 5% TBSDHE (c) 10% TBSDHE (d) 15% TBSDHE (e) 20% TBSDHE (f) 25% TBSDHE.

Confirmation of surface coverage justified FTIR investigations into bonding agent interaction. Spectral interpretation presented definitive evidence of the monosilylated bonding agent's ability to participate in hydrogen bonding. Results illustrated in Figure 4.11 indicate shift in the  $\nu_{\text{as}}\text{NO}_2$  band increased, compared with RDX and the disilylated bonding agent. The band originating at  $\nu_{\text{as}}\text{NO}_2$   $1532\text{cm}^{-1}$  for untreated RDX proceeds to shift towards

lower wavenumber upon coating with TBSDHE. As the remaining hydroxyl group is available to participate in interaction, shifts in excess of  $\Delta\nu_{\text{asNO}_2} 9\text{cm}^{-1}$  manifest within the nitro region. This is limited by comparison to Dantocol coatings which comprises two hydroxyl groups. Reduction in  $\Delta\nu_{\text{asNO}_2}$  is therefore consistent with protection of functionality responsible for hydrogen bonding.

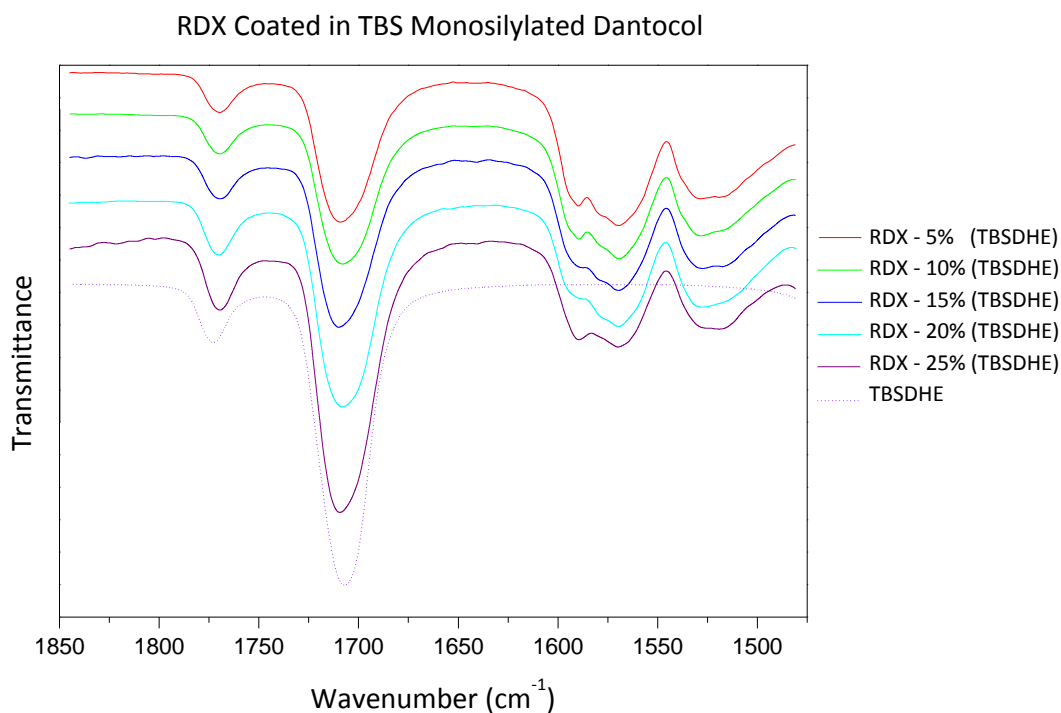


**Figure 4.11.** FTIR spectra of RDX coated in TBSDHE 5-25%.

Coupled with shifts involving nitro bands, the carbonyl region shows further deviation following interaction of TBSDHE. This remains comparable with the disilylated bonding agent, which is limited to participating in dipole interactions. Minor deviations in wavenumber arise due to steric hindrance of the *tert*-butyldimethylsilyl. This hinders carbonyl groups from engaging in dipole interactions with the nitramines nitro functionality. While *tert*-butyldimethylsilyl exhibits increased bulk, attachment of multiple trimethylsilyl side-arms also impedes interaction. The relatively weak forces exerted due to dipole interactions are responsible for shifts in excess of  $\Delta\nu_{\text{sC=O}} 3\text{cm}^{-1}$  and  $\Delta\nu_{\text{asC=O}} 4\text{cm}^{-1}$ . Compared with that resulting from hydrogen bonding, the magnitude of shifts are considerably reduced. As interaction of the remaining hydroxyl group is favoured over

dipole interaction, this influences carbonyl shifts relative to the disilylated bonding agent. These findings confirm both hydrogen bonding and dipole interactions occur in synergy within the system.

Conc %	TBSDHE Coated RDX (cm <sup>-1</sup> )			Dantocol Coated RDX (cm <sup>-1</sup> )		
	$\nu_s\text{C=O}$	$\nu_{as}\text{C=O}$	$\nu_{as}\text{NO}_2$	$\nu_s\text{C=O}$	$\nu_{as}\text{C=O}$	$\nu_{as}\text{NO}_2$
Pure	1770	1704	1532	1770	1704	1532
5%	1770	1709	1528	1764	1696	1527
10%	1769	1708	1527	1761	1695	1522
15%	1769	1708	1526	1761	1690	1519
20%	1768	1707	1525	1760	1689	1517
25%	1768	1708	1523	1761	1689	1519

**Table 4.3.** FTIR assignment of TBSDHE microencapsulated RDX.

### 4.3.3 Intermolecular Forces Between Dantocol and RDX

Prior to contact between Dantocol and RDX, interaction evolves due to atomic forces occurring at the surface.<sup>18</sup> Consequently, nitro groups were identified as highly efficient proton acceptors, while the bonding agent's hydroxyl functionality served as the proton donor. Presence of hydrogen bonding between constituents dictates both the rate and extent of surface adsorption. Therefore acid-base interactions dominate that involving Dantocol and RDX.

Johnstone et al. investigated the energy of hydrogen bonding between amides and aromatic nitro groups in both solid and liquid state.<sup>19</sup> Within the crystalline state, intermolecular hydrogen bonding is sufficient to disrupt self-association of amides. However, in solution the energy of hydrogen bonds diminishes between constituents. As nitramines remain solid throughout PBX mixing, hydrogen bonding of Dantocol and RDX crystals proceeds according to Figure 4.12.

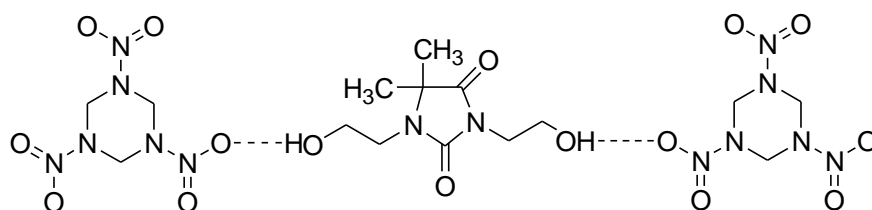


**Figure 4.12.** Hydrogen bonding of Dantocol and RDX.



Alternatively, amides provide a dipole moment capable of association with the nitramines nitro functionality. This develops due to non-uniform distribution of charge, enabling polar nitramines to align with Dantocol's carbonyl functionality. Although weak compared with hydrogen bonding, the presence of dipole interactions is integral towards the bonding agents mode of action. This becomes relevant as hydroxyl groups are consumed during reaction with diisocyanate curatives, occurring within the binder system of cast-cured energetic materials.

Such interaction occurs in synergy with hydrogen bonding, effectively increasing interfacial adhesion. As the angle between the two carbonyls decreases the net dipole moment is increased.<sup>20</sup> Scheme 4.5 illustrates the delocalisation of electrons within the bonding agents ring structure. This results in formation of dipole interactions, involving the nitro functionality of RDX.

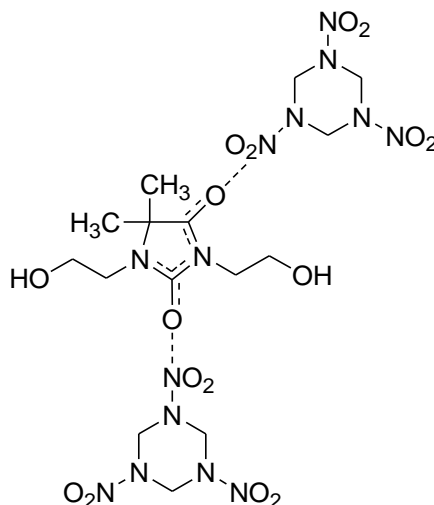


**Figure 4.13.** Dipole interaction of Dantocol and RDX.

## 4.4 Conclusion

Functional groups responsible for interaction of Dantocol and RDX were investigated through manipulating the bonding agents hydroxyl functionality. Selective protection of hydroxyl groups provided the means necessary to confirm the presence of hydrogen bonding, in addition to supplementary dipole interactions. Protection of Dantocol's hydroxyl

functionality was achieved via silylation, thereby suppressing the hydrogen bonding interaction. Disilylation engaged reaction with trimethylsilyl chloride, while selective protection was necessary to attain the monosilylated bonding agent. This introduced an element of complexity, ensuring single attachment of the silyl ether. Synthesis of non-isomeric compounds are often possible for structures containing multiple hydroxyl functionality.<sup>16</sup> However, as the bonding agent's hydroxyl groups are both primary alcohols and experience similar steric environments, isomer formation was unavoidable.

Investigation of hydroxyl-protected bonding agents revealed silylation impedes interaction involving RDX. This justified the hypothesis that the nitramine's polar oxygen atoms undergo hydrogen bonding with Dantocol's proton donating hydroxyl groups. However, IR spectroscopy confirmed weak interactions occur in the absence of hydrogen bonding. This is consistent with dipole interaction, involving the hydantoin's electronegative carbonyl functionality.

In the absence of acid-base interactions, interfacial adhesion is significantly reduced.<sup>21</sup> Energy associated with such interaction is dependent on the acidity of the hydrogen donor and basicity of the hydrogen acceptor.<sup>22</sup> Consequently, the attractive force introduced by the hydroxyl functionality exceeds that of dipole interactions. Interfacial contributions of dipoles are less conducive to adhesion, as dipole-dipole interactions generate an endothermic heat of mixing and enhance cohesive interactions at the interface.<sup>11, 22, 23</sup> Although comparatively weak, local dipoles are responsible for contributing towards improved interfacial adhesion. Multiple intermolecular forces also enable Dantocol to perform with greater efficiency in the presence of diisocyanate curatives. Reinforcing interactions therefore ensures optimisation of interfacial adhesion, focused on improving the sensitiveness of cast-cured energetic materials.

## 4.5 References

1. Wuts, P. G. M.; Greene, T. W., Protection for the Hydroxyl Group, Including 1,2- and 1,3-Diols. In *Greene's Protective Groups in Organic Synthesis*, John Wiley & Sons, Inc.: **2006**; pp 16-366.
2. Kocienski, P., Hydroxyl Protecting Groups. In *Protecting Groups*, Georg Thieme Verlag: **2003**; pp 187-350.
3. Corey, E. J.; Venkateswarlu, A., Protection of hydroxyl groups as tert-butyldimethylsilyl derivatives. *J. Am. Chem. Soc.* **1972**, *94* (17), 6190-6191.
4. Bastos, E. L.; Ciscato, L. F. M. L.; Baader, W. J., Microwave-Assisted Protection of Phenols as tert-Butyldimethylsilyl (TBDMS) Ethers under Solvent-Free Conditions. *ChemInform* **2005**, *36* (42), no-no.
5. Khalafi-Nezhad, A.; Fareghi Alamdari, R.; Zekri, N., Efficient and Selective Protection of Alcohols and Phenols with Triisopropylsilyl Chloride/Imidazole Using Microwave Irradiation. *Tetrahedron* **2000**, *56* (38), 7503-7506.
6. Ege, S. N., *Organic Chemistry: Structure and Reactivity* Fifth ed.; **2003**; p 30–33, 67.
7. Brandrup, J.; Immergut, E. H.; Grulke, E. A.; Abe, A.; Bloch, D. R., *Polymer Handbook* (4th Edition). John Wiley & Sons: **2005**; p 684.
8. Hoy, K. L., New values of the solubility parameters from vapor pressure data. **1970**, *42*, 76-118.
9. Small, P. A., Some factors affecting the solubility of polymers. *Journal of Applied Chemistry* **1953**, *3* (2), 71-80.
10. Van-Krevelen, D. W., Structure and Properties of Coal. XXVIII. Coal Constitution and Solvent Extraction. *Fuel* **1965**, *44*, 229.
11. Mittal, K. L., *Acid-base interactions: relevance to adhesion science and technology*. **1991**.
12. Lenchitz, C.; Velicky, R. *A thermochemical investigation of the complex formed by cyclotetramethylenetetranitramine (HMX) and dimethylformamide (DMF)*; DTIC Document: **1964**.
13. George, R.; Cady, H.; Rogers, R.; Rohwer, R., Solvates of Octahydro-1, 3, 5, 7-Tetranitro-1, 3, 5, 7-tetrazocine (HMX). Relatively Stable Monosolvates. *Industrial & Engineering Chemistry Product Research and Development* **1965**, *4* (3), 209-214.
14. Selig, W., A cyclomethylenetrinitramine: hexamethylphosphoramide complex. *Explosivstoffe* **1966**, *14*, 174-177.
15. Bedard, M.; Huber, H.; Myers, J. L.; Wright, G. F., The crystalline form of 1,3,5,7-tetranitro-1,3,5,7-tetrazacyclooctane (HMX). *Canadian Journal of Chemistry* **1962**, *40* (12), 2278-2299.
16. White, J. D.; Carter, R. G., Silyl Ethers. In *Science of Synthesis*, Georg Thieme Verlag: **2002**; pp 371-412.

17. Ye, B.; Nakamura, H.; Murai, A., Total Synthesis of (+/-)-Halipanicine. *Tetrahedron* **1996**, 52 (18), 6361-6372.
18. Gercel, B. O.; Uner, D. O.; Pekel, F.; Ozkar, S., Improved adhesion properties and bonding performance of HTPB-based polyurethane elastomer by using aziridine-type bond promoter. *Journal of Applied Polymer Science* **2001**, 80, 806-814.
19. Johnstone, R. A. W.; Loureiro, R. M. S.; Cristiano, M. L. S.; Labat, G., Bond energy/bond order relationships for N-O linkages and a quantitative measure of ionicity: the role of nitro groups in hydrogen-bonding. *Archieve of Organic Chemistry* **2010**, (5), 142-169.
20. Katritzky, A. R.; Taylor, P. J., Infrared Spectroscopy of Heterocycles. In *Physical Methods in Heterocyclic Chemistry*, **1971**; Vol. 4, pp 265-341.
21. Drago, R. S.; Vogel, G. C.; Needham, T. E., Four-parameter equation for predicting enthalpies of adduct formation. *Journal of the American Chemical Society* **1971**, 93 (23), 6014-6026.
22. Fowkes, F. M., Role of acid-base interfacial bonding in adhesion. *Journal of Adhesion Science and Technology* **1987**, 1 (1), 7-27.
23. Fowkes, F. M., Attractive forces at interfaces. *Industrial & Engineering Chemistry* **1964**, 56 (12), 40-52.





# Chapter 5

---

Thermal analysis of bonding agent interaction

---

Sections of this chapter were published in: Williams, C. A.; Walker, G. S.; Lochert, I. J.; Clarke, S. R., Investigation into the interaction of Dantocol in polymer bonded explosives and the impact on mechanical properties. *Parari 10th Australian Explosive Ordnance Symposium*, Brisbane, Australia, 2011; 9, pp 1-7.

Williams, C. A.; Walker, G. S.; Lochert, I. J.; Clarke, S. R., Application of Dantocol in polymer bonded explosives and determination of the mode of action. *2<sup>nd</sup> Australian energetic materials symposium*, Adelaide, Australia. 2010.

## 5.1 Introduction

Application of thermal analysis has found widespread use throughout the field of energetic materials.<sup>1</sup> This is commonly associated with Differential Scanning Calorimetry (DSC) and Thermogravimetric Analysis (TGA), which are applied to characterise thermal behaviour. Elucidation of thermograms provides information regarding polymorphic transitions and thermal decomposition kinetics. This also enables the evaluation of thermal stability and compatibility. Knowledge of such events is considered essential towards the safety and understanding of energetic materials.

Thermal techniques provide qualitative, and quantitative information regarding changes in chemical and physical behaviour. Quantitative analysis enables elucidation of compositional properties describing the mass fraction of coated particles. This is achieved by relating the heat of melting acquired for coated particles with that of individual components. Consequently, this method was applied by Suceka et al. to determine the composition of RDX mixtures.<sup>1</sup>

Various authors have employed thermoanalytical methods to characterise the behaviour of nitramine mixtures, including compositions involving trinitrotoluene,<sup>1</sup> nitroglycerine,<sup>2</sup> diazidonitrazapentane,<sup>2</sup> ammonium nitrate,<sup>3</sup> diethylenetriamine nitrate,<sup>4</sup> glycidyl azide polymer,<sup>5</sup> urea<sup>6</sup> and silicone rubber.<sup>7</sup> Investigations commonly applied DSC to provide qualitative information regarding the impact of coating agents towards nitramine decomposition. Quantitative analysis was also performed in terms of the activation energy and associated kinetic properties. This contributed towards the characterisation of coated particles, along with the elucidation of glass transition temperature, melting point, decomposition temperature and enthalpy values.



## 5.1.1 Differential Scanning Calorimetry

### 5.1.1.1 Glass Transition Temperature

Glass transition temperatures ( $T_g$ ) are influenced by the molecular mobility of cast cured energetic materials. Changes in molecular mobility stem from the addition of fillers, impacting the viscosity of composites, due to variation in crosslink density. Shifts in  $T_g$  are therefore able to provide an indication of interactions occurring at the filler-binder interface.<sup>8, 9</sup> Conversely, the absence of deviation in  $T_g$  signifies chain mobility imposes no effect on the transition temperature.<sup>10</sup>

The impact of bonding agents on the low temperature properties of propellants was investigated by Nema et al.<sup>9</sup> Adhesion of polar groups at the surface of oxidiser particles was deemed responsible for increasing  $T_g$  of the binder system. This was interpreted as disruption towards the propellants low temperature service range.

### 5.1.1.2 Melting Point

As previously alluded, the melting endotherm can be applied to quantify the composition of RDX mixtures.<sup>1</sup> This method has the advantage of rapidly establishing compositional properties, while simultaneously generating information regarding thermal behaviour. Elucidation of the mass fraction, initially involved heating mixtures above the melting point ( $T_m$ ) of RDX. From the DSC curve, integration of the melting endotherm was employed to determine the heat of fusion ( $\Delta H_{fus}$ ).

$$\Delta H_{fus} = \frac{AK}{m_s} \quad (5.1)$$

This relates the area ( $A$ ) of the endotherm to sample mass ( $m_s$ ), while ( $K$ ) represents the DSC calibration constant. The  $\Delta H_{fus}$  ratio of pure and coated RDX samples is then applied to calculate the mass percentage of coatings ( $m_{ct}$ ). This provides a quantitative representation of individual components according to Equation 5.2.

$$m_{ct}(\%) = \frac{\Delta H_{fusRDX/Coating}}{\Delta H_{fusRDX}} \times 100 \quad (5.2)$$

### 5.1.1.3 Sublimation

Sublimation is defined as the phase transition from solid to gaseous state, without passing through the liquid phase. Details regarding the heat of sublimation ( $\Delta H_s$ ) are considered one of the most valuable parameters in characterising the intensity of intermolecular interactions.<sup>11</sup> This provides a measure of intermolecular forces, as  $\Delta H_s$  represents the energy required to overcome interactions.<sup>12</sup> Energy contributions of hydrogen bonding, coulomb and van der Waals forces were investigated by Vávra et al. with regards to sublimation of energetic materials.<sup>13</sup> This identified the influence of intermolecular forces on the sublimation kinetics of participating materials.

Sublimation of RDX was initially investigated by Edwards in 1952, reporting a value of  $\Delta H_s = 112 \text{ kJ mol}^{-1}$ .<sup>14</sup> Dionne et al. later applied a vapour generator to determine the  $\Delta H_s$  of the nitramine, although this was considered highly laborious.<sup>15</sup> Consequently, an alternative method was developed involving DSC, providing improved capabilities for investigating sublimation properties.

The kinetics of sublimation are also used to provide an indication of volatile stability. Therefore  $\Delta H_s$  is often interpreted as a means for predicting stabilisation, in relation to constituent volatility. Evaluation of  $\Delta H_s$  was employed by Eslami et al. to investigate the impact of various organic coatings on the volatility of ammonium azide.<sup>16</sup> Along with data concerning the temperature of sublimation ( $T_s$ ), the effect of coating agents on sublimation behaviour is summarised in Table 5.1.

Sample	Composition (%)	$\Delta H_s$ ( $\text{J g}^{-1}$ )	$T_s$ ( $^{\circ}\text{C}$ )
Ammonium azide ( $\text{NH}_4\text{N}_3$ )	100	1471	116.2
$\text{NH}_4\text{N}_3$ :Viton	97:3	1323	117.5
$\text{NH}_4\text{N}_3$ :Steric acid	97:3	1680	121.5
$\text{NH}_4\text{N}_3$ :Nitrocellulose	97:3	1850	128.3

**Table 5.1.** Effect of coating agent on ammonium azides heat of sublimation.<sup>16</sup>

Investigations indicated treatment of ammonium azide resulted in a lower tendency to sublime. This was accompanied by decrease in volatility, confirmed according to the propellant's  $\Delta H_s$ . Related investigations involved the sublimation of ammonium perchlorate, and samples coated with ferrocenyl burn rate modifiers.<sup>17</sup> Interactions between ammonium perchlorate and ferrocenyl compounds were monitored by DSC, revealing contrary shifts towards lower  $\Delta H_s$  values.

#### **5.1.1.4 Thermal Stability and Compatibility**

Stability and compatibility of energetic materials in the presence of bonding agents is commonly determined by thermal analysis.<sup>18</sup> Vacuum thermal stability (VTS) is often applied, although a response is established using DSC or TGA to evaluate the effect on decomposition.<sup>7</sup> Eslami et al. demonstrated the influence of nitrocellulose coatings on the thermal properties of sodium azide particles.<sup>19</sup> This involved characterising the stability of decomposition temperatures, subsequent to coating of energetic particles. Kinetic parameters such as the activation energy ( $E_a$ ) was established using the Ozawa method, given in Equation 5.6. Investigations revealed a decline in  $E_a$  associated with coated particles. This method was also employed to investigate the influence of nitramine coatings.<sup>7</sup> The kinetic behaviour was again determined using the non-isothermal method to calculate  $E_a$  from both the Ozawa and Kissinger method. Establishing  $E_a$  via the Kissinger method is performed according to Equation 5.7

Chemically incompatible components are identified according to decline in  $E_a$  of decomposition. This is often accompanied by formation of low temperature exotherms. Other indications of incompatibility include shifts in the decomposition temperature of energetic fillers. Based on this response, bonding agents and other additives may be approved or prohibited from application in cast-cured energetic materials.

### 5.1.1.5 Critical Temperature

When chemical decomposition produces heat faster than can be dissipated to its surrounding, energetic materials undergo self-heating. The lowest temperature at which this event leads to ignition is considered the critical temperature ( $T_b$ ).<sup>5</sup> Interpretation of  $T_b$  provides insight into the thermal stability of energetic materials, identifying the ability to prevent chemical properties from transforming under thermal action. Calculation of  $T_b$  is typically established from the onset and  $E_a$  of thermal decomposition.

An et al. investigated the impact of polymer coatings on the  $T_b$  of RDX.<sup>20</sup> Negligible deviation in values suggests coatings imposed no effect on the nitramines thermal stability. Glycidyl azide polymers were similarly evaluated using non-isothermal DSC curves to determine the impact on nitramines.<sup>5</sup> Coated particles were found to display figures between that of individual components. This indicates significant decline in the  $T_b$  of nitramines, representing incompatibility of components. These results were similar for urea coatings, which also promote transition from thermal decomposition to ignition.<sup>6</sup> Conclusions were substantiated according to the decomposition onset and  $E_a$  of coated nitramine particles.

### 5.1.2 Thermogravimetric Analysis

Application of TGA provides a measure of change in mass as a function of temperature. This limits information to that involving mass, while the nature of transitions remain undetermined. Properties concerning decomposition and stability are therefore defined within the curve of TGA acquisitions. In contrast to DSC where heating is applied by conduction, temperatures are controlled through convection and irradiation. This provides the added benefits of measuring absolute temperature readings.<sup>21</sup>

Ticmanis et al. investigated the stability and compatibility of energetic mixtures based on kinetics derived from TGA.<sup>22</sup> Methodology involved a combination of isothermal and low heating rates in order to determine the value of  $E_a$ . This was supplemented by evaluation of thermal stability, defined according to the onset of decomposition and rate at which it

occurs.<sup>23</sup> Degradation in onset temperature was also used to convey the impact of alkyd and epoxy resin on the TGA curve of trinitrotoluene.<sup>24</sup>

The interaction of ferrocenyl compounds and ammonium perchlorate was similarly monitored by TGA.<sup>17</sup> This revealed a decrease in decomposition onset, following mixing of constituents. Conversely, the presence of hydrogen bonding amid *N*-guanylurea-dinitramide (FOX-12) was shown to stabilise the dinitramide ion in comparison with ammonium dinitramide.<sup>25</sup> The application of TGA throughout these investigations indicates its relevance towards characterising energetic mixtures.

## 5.2 Experimental

### 5.2.1 Differential Scanning Calorimetry

Thermal analysis of coated RDX was conducted by means of DSC. Preparation of coatings involved microencapsulation described in Section 2.2.2.6. This provided RDX particles displaying coating concentrations of 5–25% Dantocol. Analysis was performed using a TA Instruments MDSC-2930 differential scanning calorimeter. Samples (< 2mg) were sealed in aluminium nonhermetic pans and heated from ambient temperature to 280°C, under nitrogen purge. Heating rates of  $\beta = 5, 10, 15$  and  $20^\circ\text{C min}^{-1}$  were applied according to ASTM standard E698-11, in investigation of kinetic properties.<sup>26</sup>

Thermal analyses were performed in duplicate, with acquisitions interpreted using TA Instrument Universal Analysis 2000 software. The melting point was assigned to the maximum endothermic temperature, while  $\Delta H_{\text{fus}}$  was determined from the integral. Intersection between tangents of the exotherms leading edge and associated baseline was established as the onset of thermal decomposition.

### 5.2.2 Pressure Differential Scanning Calorimetry

Sublimation behaviour was investigated using a TA Instruments MDSC-2930 differential scanning calorimeter, equipped with high pressure cell. Constant pressure (*P*) was applied

over various settings of  $P = 1, 2, 3$  and 4MPa. Calibrations were performed prior to pressure change, using the  $T_m$  of indium to determine the cell constant. Samples ( $< 2\text{mg}$ ) were loaded into open aluminium pans and positioned within the Pressure Differential Scanning Calorimeter (PDSC). Compressed air was used to apply the desired pressure within the cell. Equilibrium was established at  $50^\circ\text{C}$ , before commencing heating at  $\beta = 10^\circ\text{C min}^{-1}$ . This was maintained until conclusion of vaporisation, as the PDSC curve returns to baseline. Calculation of  $\Delta H_s$  involved acquisition of four pressure-temperature points, necessary for fitting of the Antoine Equation.

### 5.2.3 Thermogravimetric Analysis

Thermogravimetric analysis was applied as a complementary technique, indicating weight loss as a function of temperature. The decomposition behaviour of coated RDX was determined by means of a TA Instruments TGA-2950 thermogravimetric analyser. Samples ( $< 2.0\text{mg}$ ) were transferred to aluminium pans and loaded within the furnace, using platinum trays. This was purged with nitrogen at a flow rate of  $100\text{ml min}^{-1}$ , followed by heating at a linear temperature ramp of  $5^\circ\text{C min}^{-1}$ . Associated weight loss was measured until the conclusion of decomposition at  $250^\circ\text{C}$ . Resulting TGA curves were analysed using TA Instruments Universal Analysis 2000 software.

## 5.3 Results

Thermoanalytical techniques were applied to encapsulated RDX particles, which upon heating results in chemical and physical change. Properties derived as a function of temperature were therefore investigated to determine the interrelationship of Dantocol coatings. This provided novel information regarding the bonding agents performance and mode of action.

### 5.3.1 Differential Scanning Calorimetry of Coated RDX

The characteristic DSC curve of RDX consists of two fundamental thermal events. An initial endothermic peak at 205°C which corresponds to the melting point ( $T_m$ ) and thermal decomposition ( $T_p$ ), involving a broad exothermic peak at 235°C. Of these events, the decrease in  $T_m$  for coated RDX is considered particularly significant. Blending of  $T_m$  within mixtures is known to originate from morphological effects and intermolecular interactions such as hydrogen bonding.<sup>27</sup> This indicates thermodynamic miscibility as depicted in Table 5.2. The response in  $T_m$  dictates the occurrence of intermolecular interactions involving surface coatings.<sup>28</sup> As deviation in temperatures increase, this implies improved strength of interactions.

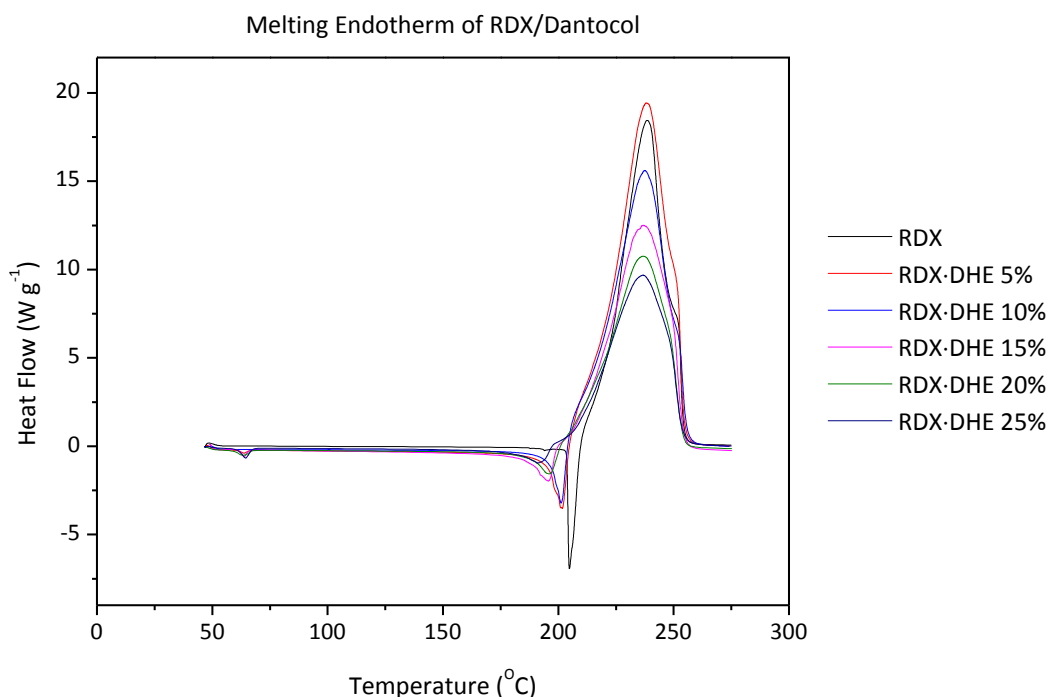


**Figure 5.1.** DSC curve of pure/coated RDX at  $\beta = 10^\circ\text{C min}^{-1}$ .

Sample	$T_m$ (°C)	$T_p$ (°C)	$\Delta H_{fus}$ (J g <sup>-1</sup> )
RDX	204.8	238.8	159.9
RDX·DHE 5%	201.5	238.1	162.2
RDX·DHE 10%	201.2	237.6	164.1
RDX·DHE 15%	197.8	236.5	169.2
RDX·DHE 20%	196.3	236.2	168.4
RDX·DHE 25%	191.0	235.8	168.8

**Table 5.2.** DSC data of pure/coated RDX at  $\beta = 10^\circ\text{C min}^{-1}$ .

The chemical potential of RDX is decreased in the presence of Dantocol, therefore leading to reduction in  $T_m$ . This is emphasized by the extent of constituents interaction. Immiscible systems in which intermolecular interactions are unable to occur, prevent this response in transition temperature. Consequently, depression in  $T_m$  is often referred to as a measure of constituent interaction, with various authors reporting a decrease in melting behaviour within thermodynamically miscible systems.<sup>27, 29, 30</sup> Painter et al. investigated mixtures participating in strong intermolecular interaction, with hydrogen bonding responsible for shifts in excess of  $\Delta T_m = 5-10^\circ\text{C}$ .<sup>29</sup> The occurrence of hydrogen bonding is renowned for influencing such properties,<sup>31</sup> as observed within the current system. These interactions were determined to increase with Dantocol concentration, resulting in further impact on  $\Delta T_m$ .

Integration of the melting endotherm was applied to determine  $\Delta H_{fus}$  of nitramine samples. This represents the work required for melting to occur, and is therefore influenced by intermolecular interactions.<sup>11, 32</sup> Jalový et al. previously employed  $\Delta H_{fus}$  to represent the extent of secondary bonding between compounds.<sup>33</sup> However it should be noted that bond length, magnitude and orientation also contribute towards  $\Delta H_{fus}$ . Data is therefore applied only as a prediction of intermolecular interaction. Zeman et al. went further to explain the impact of hydrogen bonding on the thermal behaviour of nitro compounds.<sup>32</sup> This detailed the relationship between  $\Delta H_{fus}$  and intermolecular forces.

Dantocol was found accountable for broadening the melting endotherm of RDX, resulting in variation of  $\Delta H_{fus}$ . Although increase in values were small, patterns emerged within results obtained in Table 5.2. This revealed increase in  $\Delta H_{fus}$  was proportional to the coating concentration, until reaching a maxima at 15% Dantocol coating. Thermal acquisitions were performed in duplicate, with trends persistent throughout the results. This provided insight into the magnitude of interaction occurring between constituents. As melting occurs, a resultant increase in surface area may intensify the effect on  $\Delta H_{fus}$ . This is due to additional active sites becoming capable of secondary bonding.



The impact of morphological effects is indicated by  $T_m$  susceptibility to changes in  $\beta$ .<sup>34</sup> In response, DSC was performed at sequential heating rates listed in Table 5.3. This displayed only minor deviation in  $T_m$ , as heating rates were increased. Therefore, the influence of intermolecular forces on thermal behaviour remains independent of morphological effects.

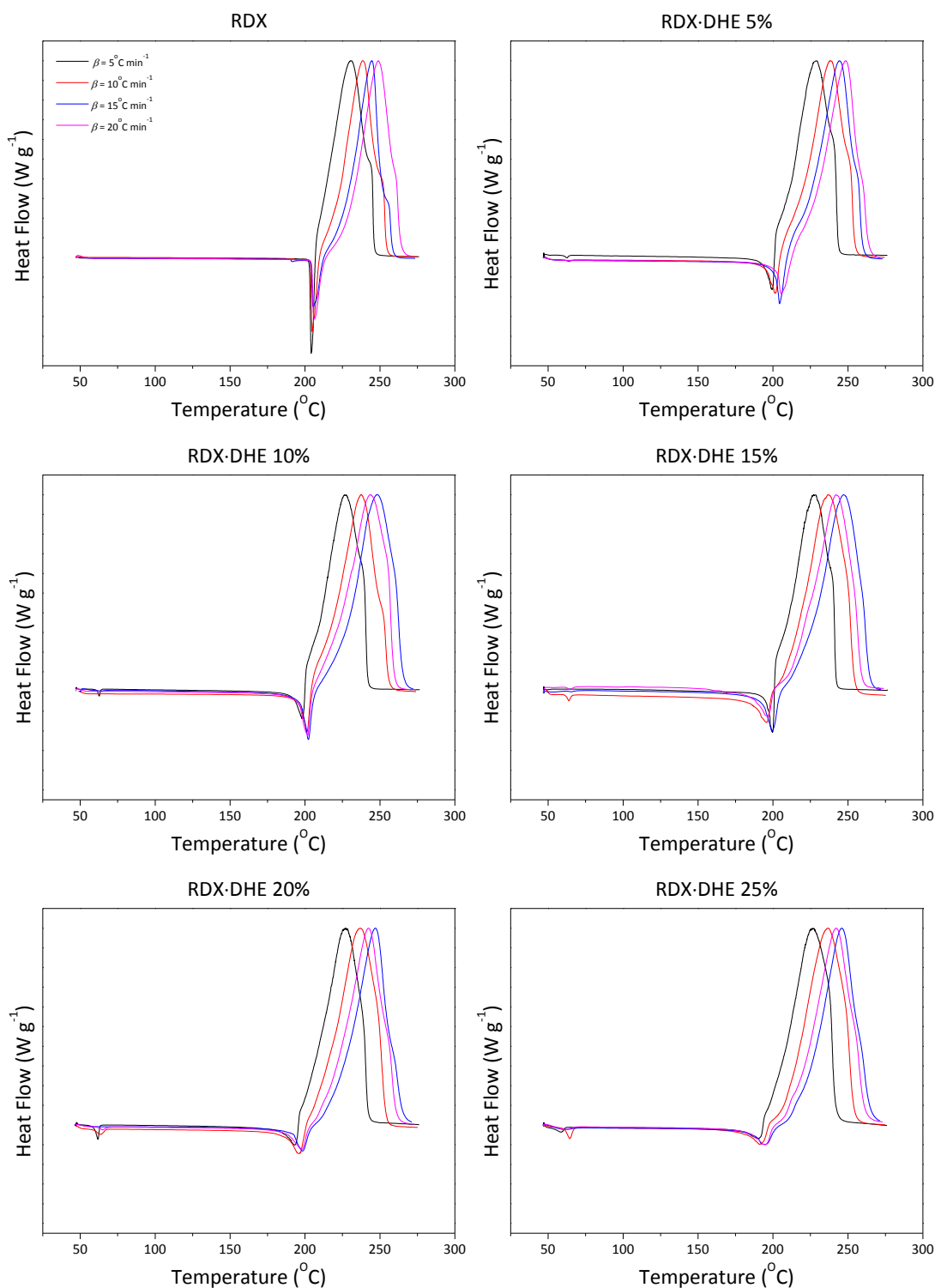


**Figure 5.2.** Normalised curve of pure/coated RDX at  $\beta = 5, 10, 15$  and  $20^\circ\text{C min}^{-1}$ .

Sample	Melting Point (K)			
	5°C min <sup>-1</sup>	10°C min <sup>-1</sup>	15°C min <sup>-1</sup>	20°C min <sup>-1</sup>
RDX	477.3	478.0	478.6	479.5
RDX·DHE 5%	472.9	474.6	477.5	478.6
RDX·DHE 10%	471.0	474.3	474.9	475.4
RDX·DHE 15%	469.6	470.9	471.7	472.6
RDX·DHE 20%	466.4	469.4	470.9	471.3
RDX·DHE 25%	463.8	464.2	467.7	468.2

**Table 5.3.** Melting point of pure/coated RDX at  $\beta = 5, 10, 15$  and  $20^\circ\text{C min}^{-1}$ .

### 5.3.1.1 Sublimation Temperature

Various experimental techniques have been applied to evaluate  $\Delta H_s$ , which are divided into direct and indirect methods. Direct methods engage the use of calorimeters, whilst indirect methods typically involve measurement of vapour pressure over a range of temperatures. Original methods were renowned for requiring extended operating times, large sample mass and an array of data points. In recent years, techniques involving PDSC were introduced, providing a reduction in run time and minimal sample size necessary for analysis of energetic material. This involves measurement of thermal events at temperatures upwards of  $600^\circ\text{C}$ , whilst maintained under pressure ( $\leq 7\text{MPa}$ ).

The PDSC curves of RDX and coated samples were generated at  $1\text{MPa}$  increments, over numerous pressure settings. These results were applied to the Antoine equation, establishing a relationship between Pressure ( $P$ ) and Temperature ( $T$ ).

$$\log_{10}P = A - B/(T + C) \quad (5.3)$$

Assignment of temperature was based on the thermal characterisation of RDX conducted by Infante-Castillo et al.<sup>35</sup> Typically, this involves thermal onset, however substitution of the maxima is also applicable. Selection of temperature neglects to impact results, provided methodology is consistent for each sample.<sup>36</sup> Reduction in error was achieved using the natural logarithm of pressures applied. This was employed to determine the regressed Antoine constants tabulated in Table 5.4.

Sample	Antoine Constants			
	A	B	C	R <sup>2</sup>
RDX	53.15	1795.72	-446.49	0.997
RDX·DHE 5%	46.64	1710.64	-442.32	0.999
RDX·DHE 10%	38.10	1547.01	-434.64	0.995
RDX·DHE 15%	31.92	1410.21	-427.31	0.993
RDX·DHE 20%	29.19	1334.70	-423.28	0.992
RDX·DHE 25%	30.94	1359.52	-425.60	0.992

**Table 5.4.** Antoine constants as determined by nonlinear least mean fit.

Substitution of constants in Equation 5.4, enables computation of the sublimation pressure temperature derivative. This adopted a temperature value of  $T = 298\text{K}$  according to previous work.<sup>12, 15</sup>

$$\left[ \frac{d(\text{Ln}P)}{d\left(\frac{1}{T}\right)} \right] = -2.3025851 \left[ \frac{BT^2}{(T+C)^2} \right] \quad (5.4)$$

$\Delta H_s$  was then determined from the Clapeyron Equation, whereby the Clausius-Clapeyron approximation was applied in preference to the Haggemacher approximation. This states the compressibility factor is equivalent to  $\Delta Z_s = 1.0$ , as applicable to Equation 5.5.

$$\Delta H_s = -R\Delta Z_s \left[ \frac{d(\text{Ln}P)}{d\left(\frac{1}{T}\right)} \right] \quad (5.5)$$

Results obtained for neat RDX were compared with literature values. This became problematic due to variation amongst published results. Deviations stem from the availability of numerous techniques and equations for determining sublimation kinetics. Irrespective of this, sublimation data remained consistent with work conducted by Rosen et al. which reported a value of  $\Delta H_s = 130.2\text{kJ mol}^{-1}$  for RDX.<sup>37</sup> Current methods generate a figure of  $\Delta H_s = 138.87\text{kJ mol}^{-1}$ , in agreement with this value. As investigations are focused on comparing the sublimation kinetics of pure and coated RDX particles, strict agreement with the literature is considered unnecessary. Of greater importance are the R<sup>2</sup> values associated with curve fitting of the Antoine equation constants. This exceeded R<sup>2</sup> > 0.99 across the range of constants depicted in Table 5.4. Based on these figures, the accuracy of results were confirmed.

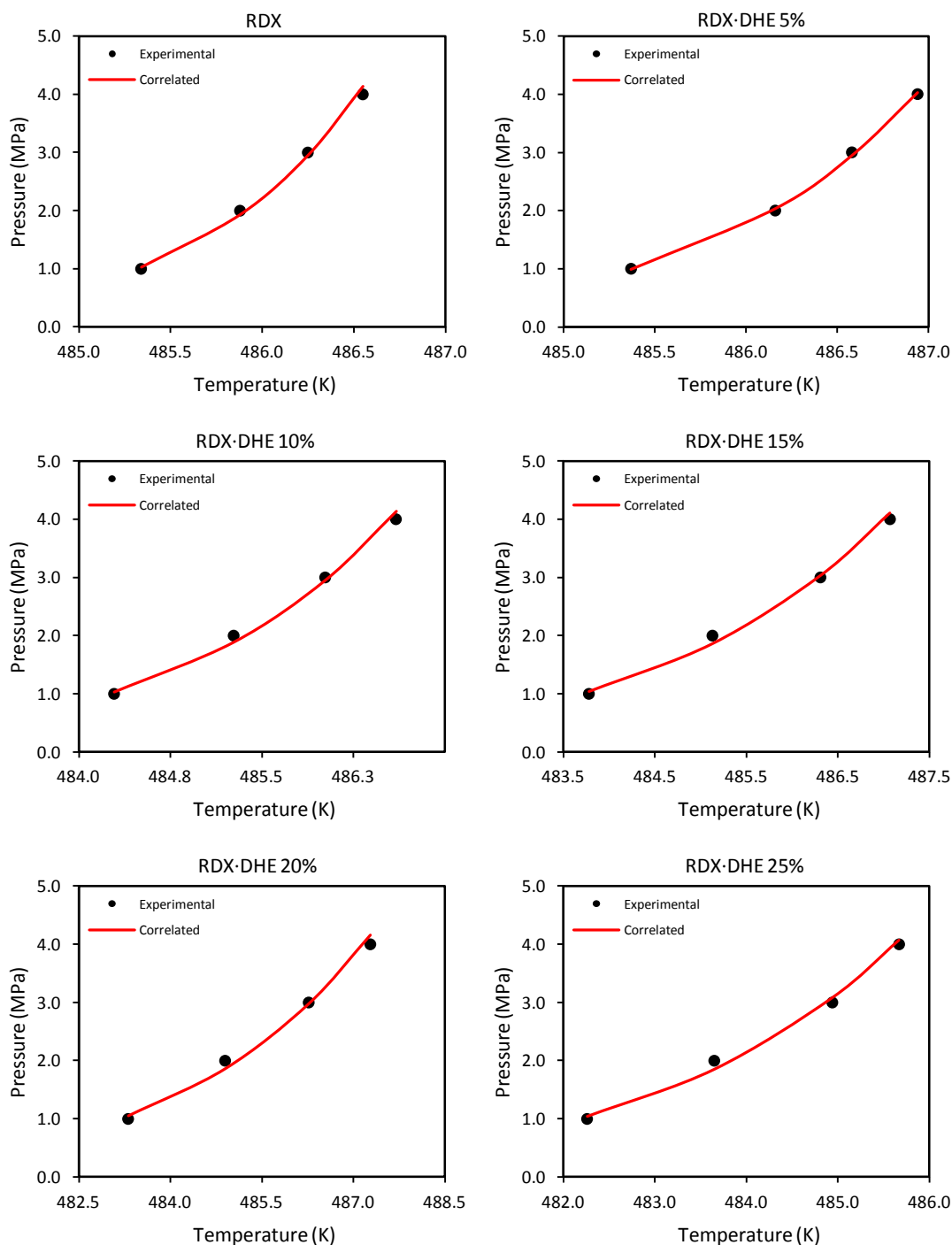


**Figure 5.3.** Vapour pressure curves of pure/coated RDX.

Plots expressing pressure versus temperature were examined for outliers, which can provide evidence of instability.<sup>38</sup> Figure 5.3 indicates the current system remains free of such data, representing sample stability and verifying the consistency of results. Overlaying the Antoine equation fit and experimental data points also serves to establish the accuracy of constants. This highlights the efficiency of the technique, as the curve of non-linear

regression pass through experimental data points. The results of curve fitting maintains a coefficient of determination above  $R^2 > 0.99$ , throughout the range of coatings.

Interaction of RDX and Dantocol surface coatings was characterised by  $\Delta H_s$ , according to the differential equation of the Clausius-Clapeyron approximation. In coherence with its definition as a measure of intermolecular forces,  $\Delta H_s$  is one of the most effective quantifiable parameters for characterising the intensity of intermolecular interactions.<sup>11, 12</sup> While spectroscopic techniques identify the nature of interactions, sublimation data is used to measure the intensity of such forces. The relationship between  $\Delta H_s$  of energetic materials and intermolecular hydrogen bonding was previously discussed by Rosen et al.<sup>37</sup> This detailed the manner in which hydrogen bonding results in increased values. As  $\Delta H_s$  represents the energy required to overcome intermolecular interactions, this reflects the degree of hydrogen bonding present.

The sublimation kinetics of RDX and coated particles is summarised in Table 5.5. As expected, results indicate an increase in intermolecular interaction following encapsulation in Dantocol. This occurrence is proportional to concentration of bonding agent, on account of the number of functional groups participating in secondary bonding.

Sample	$[d(\ln P)/d(1/T)]$ (K)	$\Delta Z_s$	$\Delta H_s$ (kJ mol <sup>-1</sup> )
RDX	-16702.99	1.00	138.87
RDX·DHE 5%	-16845.54	1.00	140.06
RDX·DHE 10%	-16996.54	1.00	141.31
RDX·DHE 15%	-17302.00	1.00	143.85
RDX·DHE 20%	-17449.11	1.00	145.08
RDX·DHE 25%	-17130.04	1.00	142.42

**Table 5.5.** Clausius-Clapeyron approximation of the heat of sublimation.

### 5.3.1.2 Thermal Stability and Compatibility

Interpretation of DSC provides an indication of thermal stability and compatibility. Stability is often defined by the onset of thermal decomposition and the velocity at which reaction occurs.<sup>39</sup> This enables thermal stability to be determined from the difference in onset

temperature and associated maxima. Consequently, increase in deviation indicates greater sensitivity to thermal stimuli. Meanwhile, decomposition of RDX exhibits a narrow exothermic peak, where less stable variants are prone to broadening. This classifies RDX as a thermostable explosive, along with its well-defined onset temperature. Additional stability can be provided through intermolecular interactions, often having a profound effect on the thermal behaviour of energetic particles. This is particularly relevant to systems participating in hydrogen bonding.

Evaluation of compatibility is necessary to identify additives contributing to increased sensitivity of energetic fillers.<sup>7</sup> This extends to the influence of Dantocol, which was assessed according to the kinetics of exothermic decomposition. Results were then applied to determine the effect on ignition behaviour. The activation energy ( $E_a$ ) of RDX and associated coatings was calculated using the Kissinger and Ozawa equation. Application of the Ozawa equation is based on the plot of  $\log \beta$  versus the reciprocal of  $T_p$ . The slope is then used to calculate  $E_a$ , according to ASTM test method E698-11.<sup>26</sup>

$$E_a = 2.303Rd \left[ \frac{\log \beta}{d\left(\frac{1}{T_p}\right)} \right] \quad (5.6)$$

where  $d[\log \beta/d(1/T_p)]$  is the slope of the plot. Alternatively, the Kissinger method is determined from the plot of  $\ln(\beta/T_p^2)$  versus the reciprocal of  $T_p$ . The activation energy is then determined according to Equation 5.7.

$$E_a = Rd \left[ \ln \left( \frac{\beta}{T_p} \right)^2 \right] / \left[ d \frac{1}{T_p} \right] \quad (5.7)$$

with  $d[\ln(\beta/T_p)^2]/[d(1/T_p)]$  equivalent to the slope. Values associated with the pre-exponential factor ( $A$ ) are then derived from the equation.

$$A = \left( \frac{\beta E_a \exp E_a}{RT_p} \right) / RT_p^2 \quad (5.8)$$

The kinetic behaviour of decomposition is summarised in Table 5.6, with results of both methods shown in agreement. This highlights comparisons in thermal data between RDX and that of increased surface coating.

Sample	$\beta$ (K min <sup>-1</sup> )	$T_p$ (K)	$E_a$ Ozawa (kJ mol <sup>-1</sup> )	$E_a$ Kissinger (kJ mol <sup>-1</sup> )	$\ln A$ (s <sup>-1</sup> )
RDX	5	503.22	152.32	148.92	26.55
	10	511.92			
	15	517.73			
	20	522.08			
RDX·DHE 5%	5	501.16	137.88	135.21	23.41
	10	511.20			
	15	517.53			
	20	521.64			
RDX·DHE 10%	5	500.60	138.65	136.37	23.76
	10	510.71			
	15	516.50			
	20	521.13			
RDX·DHE 15%	5	500.37	140.27	136.96	23.94
	10	509.67			
	15	515.80			
	20	520.64			
RDX·DHE 20%	5	500.20	140.71	137.69	24.15
	10	509.34			
	15	515.62			
	20	520.34			
RDX·DHE 25%	5	499.43	141.78	138.47	24.38
	10	508.90			
	15	515.40			
	20	519.08			

**Table 5.6.** Activation energies of pure/coated RDX.

In association with use of open pans, vaporisation is considered a prevalent process, whereby neat RDX demonstrates an activation energy of  $E_a$  Kissinger = 148.92 kJ mol<sup>-1</sup>. Confining samples to sealed pans promotes liquid state decomposition, generating an increase in energy release. This suggests scission of the N-N bond represents the primary decomposition step, due to consideration as the weakest covalent bond within the nitramines structure.<sup>40</sup> In response to experimental conditions, this occurrence remains independent of mass or heating rate. An absence in substantial deviation of  $T_p$  and  $E_a$  maintains support for system

compatibility.<sup>7, 24</sup> This highlights the rapport between Dantocol and RDX based composites, which has led to widespread use of the bonding agent.

### 5.3.1.3 Critical Temperature

The thermal stability of energetic materials can be defined as a measure of its ability to prevent chemical properties transforming under thermal stimulus.<sup>20</sup> This is often expressed in terms of the energetics critical temperature ( $T_b$ ). Values represent the lowest temperature above which materials self heat, causing ignition.<sup>41</sup> Evaluation of  $T_b$  is determined according to Equation 5.9.

$$T_b = \frac{E_a - \sqrt{E_a^2 - 4E_aRT_{i0}}}{2R} \quad (5.9)$$

whereby  $E_a$  is the activation energy,  $R$  is the gas constant ( $8.314\text{J mol}^{-1} \text{K}^{-1}$ ) and  $T_{i0}$  is the onset temperature at  $\beta = 0$ . The value for  $T_{i0}$  is obtained using linear regression of  $\beta$  and the onset temperature ( $T_i$ ).

$$T_i = T_{i0} + a\beta_i + b\beta_i^2 + c\beta_i^3 \quad (5.10)$$

where  $a$ ,  $b$  and  $c$  are coefficients. The slope of  $\beta$  verses  $T_i$  is therefore applied to determine the value of  $T_{i0}$ .

The critical temperature of pure RDX is consistent with the literature which reports figures from  $T_b = 482\text{K}$  to  $488\text{K}$ .<sup>42, 43</sup> Coated samples fail to increase values, therefore implying Dantocol is unable to improve  $T_b$  of RDX.<sup>6, 20</sup> This confirms benefits towards the mechanical properties of cast-cured energetic materials result from the bonding agents impact on interfacial adhesion.



Sample	$\beta$ (K min <sup>-1</sup> )	$T_i$ (K)	$T_{i0}$ (K)	$T_b$ (K)
RDX	5	480.6	471.4	484.5
	10	488.5		
	15	493.8		
	20	498.7		
RDX·DHE 5%	5	476.9	467.3	481.5
	10	485.0		
	15	491.1		
	20	495.9		
RDX·DHE 10%	5	476.3	467.4	481.4
	10	484.1		
	15	490.2		
	20	495.2		
RDX·DHE 15%	5	475.9	466.8	480.8
	10	483.5		
	15	489.9		
	20	494.5		
RDX·DHE 20%	5	475.5	465.9	479.9
	10	483.2		
	15	489.7		
	20	493.9		
RDX·DHE 25%	5	475.0	465.7	479.5
	10	482.8		
	15	488.9		
	20	493.4		

**Table 5.7.** Critical temperatures of RDX and coated samples.

### 5.3.2 Thermogravimetric Analysis

Investigation of the nitramines thermogravimetric behaviour indicates a single weight loss step, occurring over a temperature range of 150 - 235°C. This reveals almost residual-free decomposition of neat RDX. Comparisons with coated samples provide further clarification of the bonding agents impact on thermal stability. This is indicated by the onset of deformation and associated rate of occurrence. As deviation between peak and onset temperatures is increased, this represents greater sensitivity towards thermal stimuli. This effect is coherent with the understanding energetic materials are thermally unstable over this temperature range.

To emphasize the effect of Dantocol on RDX particles, coating concentrations were considerably increased. This was necessary to detect subtle differences otherwise difficult to observe at low concentrations. TGA curves acquired for RDX and coated samples are overlaid in Figure 5.4. Nitramine particles encapsulated in Dantocol exhibit minor shifts in decomposition towards lower temperature. As deviations are negligible, this confirms the systems thermal stability. These results are consistent with exothermic decomposition observed in the DSC curve.

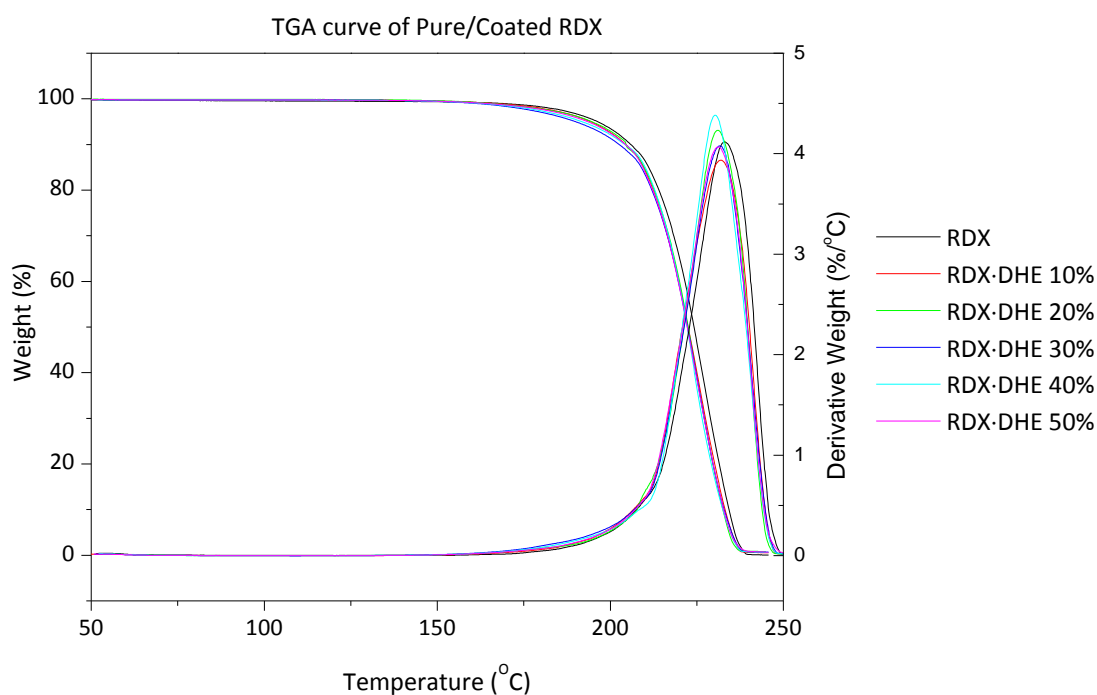


**Figure 5.4.** TGA curve of pure/coated RDX.

Data collated in Table 5.5 indicates maximum weight loss ( $T_{\max}$ ) and the percentage involved. Circumstances involving decline in  $T_{\max}$  signify a reduction in thermal stability. This occurrence is negligible within the current system, as coated samples show minimal deviation from  $T_{\max} = 226.94^{\circ}\text{C}$  of RDX. These results indicate the stability of components, which is substantiated by the percentage weight loss recorded.

Sample	$T_{\max}$ (°C)	Weight Loss (%)	Residue (%)
RDX	226.94	99.5	0.5
RDX·DHE 10%	225.52	99.5	0.5
RDX·DHE 20%	224.59	99.2	0.8
RDX·DHE 30%	225.28	99.3	0.7
RDX·DHE 40%	223.81	99.4	0.6
RDX·DHE 50%	224.69	99.3	0.7

**Table 5.8.** TGA data of pure/coated RDX.

## 5.4 Conclusion

Thermal analysis was successfully applied to elucidate the interaction of Dantocol and RDX. This provided additional information pertaining to the thermal stability and compatibility of constituents. DSC curves were initially interpreted to determine the melting behaviour of coated particles, with the intent of extrapolating data regarding interaction. Investigations revealed the melting endotherm broadened, whilst shifting towards lower temperature upon incorporation of Dantocol. Depression in melting point is recognised to reflect the thermodynamic miscibility of mixtures. This occurrence results from constituents undergoing intermolecular interaction between functional groups.<sup>28</sup>

Findings were confirmed by the heat of fusion, which is considered representative of intermolecular interactions.<sup>44</sup> Values were observed to increase in proportion to the concentration of Dantocol. This indicates additional work is required for melting to occur, as influenced by the presence of intermolecular interactions.<sup>11, 32, 33</sup> Interpretation of the melting endotherm was therefore able to provide an indication of the extent to which interaction occurs.

Kinetic parameters associated with thermal sublimation were established using PDSC. This was demonstrated to be effective in determining  $\Delta H_s$  for RDX and coated samples. Due to the intensity in thermal response, small sample size and slow heating rates were required. This was applied over a range of pressure settings, to determine  $\Delta H_s$  from the Antoine

equation. Sublimation kinetics of RDX were consistent with literature, which itself reported a range of values. As results for  $\Delta H_s$  represent the energy required to overcome intermolecular interactions, this assists in describing the extent of interaction between Dantocol and RDX. Given the values of  $\Delta H_s$  increased up to coatings of 25% Dantocol, the extent of secondary bonding was shown to increase. This also revealed improved volatile stability for encapsulated RDX samples.

Thermal Stability and compatibility was investigated according to the nitramines decomposition behaviour. Combined application of DSC and TGA succeeded in characterising the impact of Dantocol on exothermic decomposition of RDX. Inspection of results acquired for  $T_p$  and  $E_a$  assisted in establishing system compatibility. This was indicated according to limited deviation between RDX and coated samples. Decomposition results are also consistent with reduced sensitivity to thermal stimuli. Therefore, the ability of Dantocol to avoid impacting the decomposition behaviour of RDX confirms its suitability for nitramine based composites.

## 5.5 References

1. Suceska, M.; Rajic, M.; Culijak, R., Characterisation and quantitative determination of trinitrotoluene in mixtures with hexogen by differential scanning calorimetry. In *29th International Annual Conference of ICT, Fraunhofer-Institut fuer Chemische Technologie*; **1998**; pp 144/1 - 144/12.
2. Li, S.; Huang, W., Thermal characteristics of mixtures of cyclonite and nitroglycerine or diazidonitrazapentane. *Journal of thermal analysis* **1995**, *45* (1-2), 289-296.
3. Mathew, S.; Krishnan, K.; Ninan, K. N., A DSC Study on the Effect of RDX and HMX on the Thermal Decomposition of Phase Stabilized Ammonium Nitrate. *Propellants, Explosives, Pyrotechnics* **1998**, *23* (3), 150-154.
4. Denekamp, C.; Tomashy, A.; Shulman, H.; Klyman, D.; Hirshberg, B. *Thermal analysis of explosives - compatibility and relative stability*; Rafael Advanced Defence Systems, **2010**.
5. Huang, C.-C.; Wu, T.-S., A simple method for estimating the autoignition temperature of solid energetic materials with a single non-isothermal DSC or DTA curve. *Thermochimica Acta* **1994**, *239* (0), 105-114.
6. Rongzu, H.; Zhengquan, Y.; Yanjun, L., A study of reaction between RDX and urea by a single non-isothermal DSC curve. *Thermochimica Acta* **1988**, *134*, 429-434.
7. Lee, J.-S.; Hsu, C.-K.; Chang, C.-L., A study on the thermal decomposition behaviours of PETN, RDX, HNS and HMX. *Thermochimica Acta* **2003**, *392-392*, 173-176.
8. Diamant, Y.; Folman, M., Influence of dewetting on the damping properties of a filled polymer system: 1. Static characterization. *Polymer* **1979**, *20* (8), 1025-1033.
9. Nema, S. K.; Nair, P. R.; Francis, A. U., The effects of oxidizer bonding agents on the low temperature properties of HTPB. In *AIAA/SAE 13th Propulsion Conference*, AIAA: Florida, **1977**; Vol. 77, pp 1-6.
10. Kraus, G., Reinforcement of elastomers by carbon black. *Advances in Polymer Science* **1971**, *8* (Fortschritte der Hochpolymeren-Forschung), 156-237.
11. Zeman, S.; Krupka, M., New Aspects of Impact Reactivity of Polynitro Compounds, Part III. Impact Sensitivity as a Function of the Intermolecular Interactions. *Propellants, Explosives, Pyrotechnics* **2003**, *28* (6), 301-307.
12. Santos, L. M. N. B. F.; Schröder, B.; Fernandes, O. O. P.; Ribeiro da Silva, M. A. V., Measurement of enthalpies of sublimation by drop method in a Calvet type calorimeter: design and test of a new system. *Thermochimica Acta* **2004**, *415* (1-2), 15-20.
13. Vávra, P.; Pospíšil, M.; Repáková, J., Effect of intermolecular forces on some properties of explosives. In *5th New Trends in Research of Energetic Materials*, Pardubice, Czech Republic, **2002**; pp 357-368.
14. Edwards, G., The vapour pressure of cyclo-trimethylene-trinitramine (cyclonite) and pentaerythritol-tetranitrate. *Transactions of the Faraday Society* **1953**, *49*, 152-154.
15. Dionne, B. C.; Rounbehler, D. P.; Achter, E. K.; Hobbs, J. R.; Fine, D. H., Vapour pressure of explosives. *Journal of Energetic Materials* **1986**, *4*, 447-472.

16. Eslami, A.; Hosseini, S. G.; Shariaty, S. H. M., Stabilization of ammonium azide particles through its microencapsulation with some organic coating agents. *Powder Technology* **2011**, *208* (1), 137-143.
17. Tompa, A. S., DSC and TG study of the stability in vacuum of ferrocenyl compounds and their compatibility with ammonium perchlorate. *Thermochimica Acta* **1984**, *77* (1-3), 133-150.
18. Yueping, J.; Guangming, Q.; Yuxiang, Z.; Yi, Y., Synthesis and application of novel bonding agents. In *26th International Pyrotechniques Seminar*, Xi'an Modern Chemistry Research Institute: China, **1999**; pp 187-194.
19. Eslami, A.; Hosseini, S. G.; Asadi, V., The effect of microencapsulation with nitrocellulose on thermal properties of sodium azide particles. *Progress in Organic Coatings* **2009**, *65* (2), 269-274.
20. An, C. W.; Guo, X. D.; Song, X. L.; Wang, Y.; Li, F. S., Preparation and Safety of Well-Dispersed RDX Particles Coated with Cured HTPB. *Journal of Energetic Materials* **2009**, *27* (2), 118-132.
21. Tracton, A. A., *Coating Technology Handbook*. Third edition ed.; Taylor & Francis Group: Florida, **2006**; p 6/3.
22. Ticmanis, U.; Kaiser, M.; Pantel, G., Combined dynamic/isothermal TGA for stability and compatability testing. In *34th International Annual Conference of ICT*, Fraunhofer-Institut für Chemische Technologie.: Germany, **2003**; pp 76/1 - 76/9.
23. Kaderabek, V., Thermal stability of some nitramines and polynitroarenes determined by vacuum stability apparatus stabil. In *21st International Pyrotechniques Seminar*, **1995**; pp 345 -355.
24. Hemmilä, M. O., Use of thermal analysis in compatibility testing of 2, 4, 6-trinitrotoluene. *Journal of Thermal Analysis and Calorimetry* **1982**, *25* (1), 135-138.
25. Östmark, H.; Bemm, U.; Bergman, H.; Langlet, A., N-guanylurea-dinitramide: a new energetic material with low sensitivity for propellants and explosives applications. *Thermochimica Acta* **2002**, *384* (1-2), 253-259.
26. ASTM, Standard test method for arrhenius kinetic constants for thermally unstable materials using differential scanning calorimetry and the Flynn/Wall/Ozawa method. In *E698-11*, United States, **2011**; pp 1-8.
27. Aiman Eid Al-Rawajfaha; Hasan A. Al-Salahb; Al-Rhaelc, I., Miscibility, Crystallinity and Morphology of Polymer Blends of Polyamide-6/ Poly ( $\beta$ -hydroxybutyrate. *Jordan Journal of Chemistry* **2006**, *1* (2), 155-170.
28. Rostami, S., Crystallization behaviour of a semicrystalline miscible blend. *Polymer* **1990**, *31* (5), 899-904.
29. Painter, P. C.; Shenoy, S. L.; Bhagwagar, D. E.; Fishburn, J.; Coleman, M. M., Effect of hydrogen bonding on the melting point depression in polymer blends where one component crystallizes. *Macromolecules* **1991**, *24* (20), 5623-5629.
30. He, Y.; Zhu, B.; Inoue, Y., Hydrogen bonds in polymer blends. *Progress in Polymer Science* **2004**, *29* (10), 1021-1051.

31. Kuo, S.-W., Hydrogen-bonding in polymer blends. *Journal of Polymer Research* **2008**, *15* (6), 459-486.
32. Zeman, S.; Krupka, M., New Aspects of Impact Reactivity of Polynitro Compounds, Part II. Impact Sensitivity as “the First Reaction” of Polynitro Arenes. *Propellants, Explosives, Pyrotechnics* **2003**, *28* (5), 249-255.
33. Zeman, S.; Jalový, Z., Heats of fusion of polynitro derivatives of polyazaisowurtzitane. *Thermochimica Acta* **2000**, *345* (1), 31-38.
34. Nishi, T.; Wang, T. T., Melting Point Depression and Kinetic Effects of Cooling on Crystallization in Poly(vinylidene fluoride)-Poly(methyl methacrylate) Mixtures. *Macromolecules* **1975**, *8* (6), 909-915.
35. Infante-Castillo, R.; Pacheco-Londoño, L. C.; Hernández-Rivera, S. P., Monitoring the  $\alpha \rightarrow \beta$  solid–solid phase transition of RDX with Raman spectroscopy: A theoretical and experimental study. *Journal of Molecular Structure* **2010**, *970* (1–3), 51-58.
36. Back, D. D.; Grzyll, L. R.; Corrigan, M., DSC enthalpy of vaporization measurements of high temperature two-phase working fluids. *Thermochimica Acta* **1996**, *272* (0), 53-63.
37. Rosen, J. M.; Dickinson, C., Vapor pressures and heats of sublimation of some high-melting organic explosives. *Journal of Chemical & Engineering Data* **1969**, *14* (1), 120-124.
38. ASTM, Standard Test Method for Determining Vapour Pressure by Thermal Analysis. In *E1782-08*, United States of America, **2010**.
39. V, K. In *Thermal stability of some nitramines and polynitroarenes determined by vacuum apparatus*, 21st International Pyrotechnics Seminar, Moscow, Russia, Moscow, Russia, **1995**; pp 345-355.
40. Long, G. T.; Vyazovkin, S.; Brems, B. A.; Wight, C. A., Competitive Vaporization and Decomposition of Liquid RDX. *The Journal of Physical Chemistry B* **2000**, *104* (11), 2570-2574.
41. Harris, J., Autoignition temperatures of military high explosives by differential thermal analysis. *Thermochimica Acta* **1976**, *14* (1-2), 183-199.
42. Yi, X.; Rongzu, H.; Chaoqing, Y.; Guofu, F.; Jihua, Z., Studies on the critical temperature of thermal explosion for 3-Nitro-1,2,4-triazol-5-one (NTO) and its salts. *Propellants, Explosives, Pyrotechnics* **1992**, *17* (6), 298-302.
43. Tonglai, Z.; Rongzu, H.; Yi, X.; Fuping, L., The estimation of critical temperatures of thermal explosion for energetic materials using non-isothermal DSC. *Thermochimica Acta* **1994**, *244* (0), 171-176.
44. Zeman, S., The impact sensitivity of some nitramines. In *Proceedings of the 10th Symposium on Chemical Problems Connected with the Stability of Explosives*, Sweden, **1995**; Vol. 28, p 367.





# Chapter 6

---

Polymerisation of polyurethane binder system

---

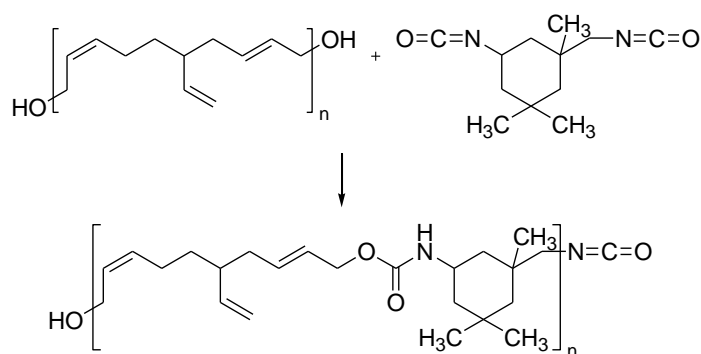
Sections of this chapter were published in: Williams, C. A.; Walker, G. S.; Lochert, I. J.; Clarke, S., Investigation into the interaction of Dantocol in polymer bonded explosives and bonding agent development. *16th New trends in energetic materials*, Pardubice, Czech Republic, 2013; Vol I, 399-406.

## 6.1 Introduction

Cast-cured PBXs typically comprise a complex mixture of filler, binder, metal fuel, catalyst, plasticiser, antioxidant and bonding agent. The effect of individual components on the properties of composite energetic material generates a complex system of functions. Additives may alter the cure kinetics of the binder system, along with the behaviour of remaining components.<sup>1</sup> These capabilities extend to impurities within ingredients, which likewise retain the potential to impact PBX properties. Consequently, the importance of understanding the function of each ingredient is critical in describing the overall process. In order to differentiate between individual effects, it is therefore necessary to investigate polymerisation of the binder system and the impact of additives on this process.

### 6.1.1 Polymerisation of Polyurethanes

The most widely used binder systems in current PBX formulations are those based on polyurethanes. Application of polyurethane binder systems have rapidly become standard throughout the munitions industry, in accordance with their performance characteristics, handleability and ease of manufacture.<sup>2</sup> Polyurethanes constitute an extremely versatile class of polymer, synthesised via reaction of an isocyanate curative and polyol to form urethane linkages. The design of urethanes requires consideration of compatibility, reactivity, viscosity and stability in optimising performance. Through conforming with these specifications, the cross-linking reaction of isophorone diisocyanate (IPDI) and hydroxyl-terminated polybutadiene (HTPB) has emerged as the leading polyurethane system. The resulting binder matrix shown in Scheme 6.1, imparts favourable mechanical properties. The rate of polyurethane formation is considered first order in terms of isocyanate and hydroxyl concentrations, therefore the overall reaction obeys second-order kinetics.<sup>3</sup>



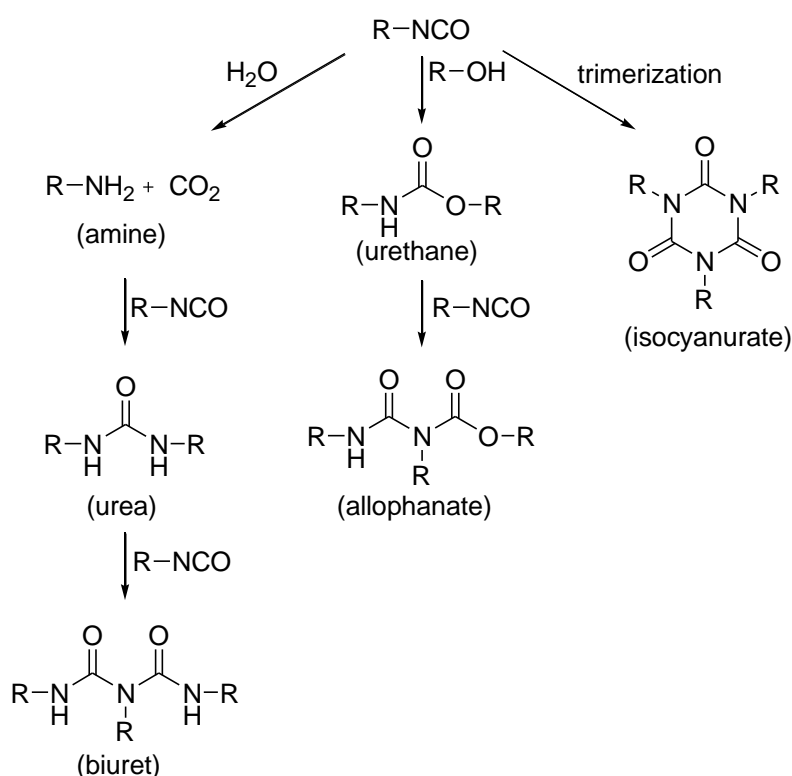
**Scheme 6.1.** Reaction of HTPB with IPDI to form a urethane linkage.

Polyol accounts for the greatest percentage of polyurethane content, and is therefore largely responsible for the polymer's physical properties. As HTPB exhibits good hydrolytic stability, viscosity and solid loading, these qualities are translated to the binder system.<sup>4</sup> This accounts for the extensive use of HTPB in composite solid propellants and cast-cured PBX formulations alike. Synthesis of the prepolymer is typically performed by hydrogen peroxide initiated free radical polymerisation of 1,3-butadiene.<sup>5</sup> Alternatively, anionic polymerisation is also employed, producing a narrow molecular weight distribution. The impact of increasing the molecular weight of HTPB influences hardness, modulus and crystallinity of the resulting polymer network. However, the cost of anionic polymerisation has resulted in adoption of free radical polymerisation for commercial application.

IPDI is commonly applied as the diisocyanate curative for polyurethane systems. The asymmetric cycloaliphatic diisocyanate consists of *cis* and *trans* units in a ratio of 3:1.<sup>6</sup> Isocyanate groups comprise of primary and secondary functionality, which generate contrasting reactivity. Steric hindrance of the primary isocyanate reduces reactivity due to the presence of quaternary  $\beta$ -methyl groups, whilst secondary isocyanates exhibit increased reactivity.<sup>6,7</sup> The secondary isocyanate is therefore responsible for tendency to participate in intermolecular interactions.<sup>8</sup> Still, the reaction of IPDI proceeds relatively slowly, compared with toluene diisocyanate and associated isocyanate curatives.<sup>9</sup> Aromatic isocyanates are recognised as exhibiting greater reactivity than aliphatic groups, due to the electron

withdrawing effect of the benzene ring.<sup>9</sup> Since rapid curing limits the pot life of insensitive munitions, application of IPDI is favourable as this improves processability.

Potentially the most detrimental factor associated with curing IPDI are the implications of moisture content. Atmospheric moisture undergoes side reactions with isocyanates to form urea as indicated in Scheme 6.2. Subsequent reaction of urea and isocyanate groups continue to produce allophanate and biuret side products.<sup>6</sup> Further propagation of the dimer uretidon and trimer isocyanurate are also known to occur during cure.



**Scheme 6.2.** Side reactions that may occur in isocyanate and hydroxyl systems.<sup>10</sup>

Once incorporated within the binder system, side products impose detrimental effects to the resulting polymers. Impurities continue to impact the stoichiometric ratio of NCO:OH, assuming such functionality is present. This is observed to influence the reaction's cure kinetics. If incorporated within the matrix, mechanical properties are substantially impaired, therefore control measures are required to ensure purity of the cure. This is achieved by eliminating exposure to atmospheric moisture, along with limiting the reaction temperature to 60°C, below which side reactions are inhibited.

During cure, polyurethane chains become entangled, providing mechanical strength. This is significantly improved by the addition of multifunctional prepolymers, enabling formation of cross-linking. When applied to manufacturing cast-cured PBX composites, this approach results in encapsulation of the energetic filler, producing a polymeric shell.<sup>11</sup> Encapsulating the energetic filler with cross-linked polyurethane is responsible for absorption and dissipation of energy, caused by hazardous stimuli. In terms of design, knowledge of mechanical, thermal and adhesive properties is critically important to cast-cured PBX composites.<sup>3</sup> Such properties are dependent on the degree of cross-linking introduced through reaction of polyfunctional groups.

The one-shot method is typically applied to the synthesis of PBX binder systems, through which the polyol, isocyanate and various other additives are blended. Upon reaction, HTPB forms the so called soft segment backbone, whilst the isocyanate and urethane linkages contribute towards the corresponding hard segment. Segmentation is responsible for the polyurethane's macroscopic properties. Hard segments function as the structural framework of the polyurethane, providing mechanical strength, whilst soft segments account for the polymers high elasticity. Therefore the soft segment is responsible for imparting the low temperature properties and improved flexibility of the resulting polyurethane.

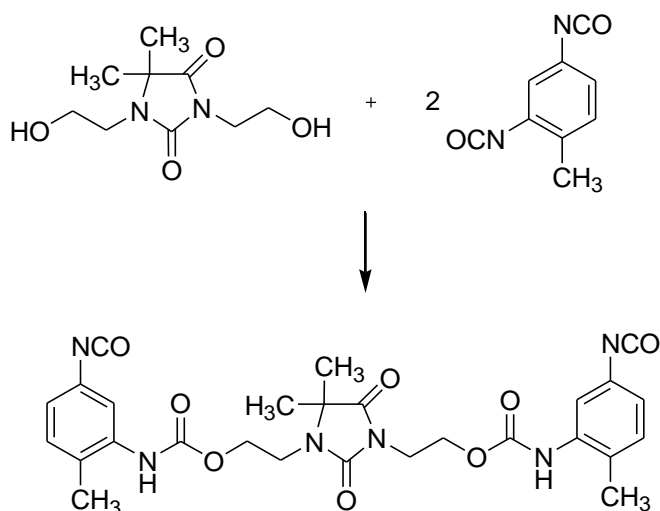
Within the current system, hydrogen bonding is nonexistent between hard and soft segments, due to the inability of HTPB to participate in such interaction following consumption of hydroxyl functionality. Hydrogen bonding is therefore limited to the urethane linkage, comprising both proton accepting carbonyls and proton donating amine groups.<sup>12</sup> This observation benefits investigation of Dantocol within the binder system, as this negates the existence of secondary bonding between segments.<sup>12</sup> Reaction is therefore limited to that propagating from Dantocol incorporated within the network structure, or secondary bonding between hard segments.

## 6.1.2 Polymerisation of Dantocol

Use of hydroxyalkylated hydantoin derivatives in polyurethane chemistry is described within the literature, involving reaction with 4,4'-diisocyanatodiphenylmethane.<sup>13</sup> This approach was used to prepare polyurethanes of reduced melting point and impeded tendencies towards low temperature crystallisation. Polymers were employed in the production of plastics, particularly within the field of mouldings. This provides urethane modified hydantoins of improved thermal stability, high flexibility, and high breaking elongation.

Alternative isocyanates applied in reaction with hydroxyalkylated hydantoins include; 2,4-diisocyanatotoluene, 2,6-diisocyanatotoluene and 1,2-bis-(4-isocyanatophenyl)-ethane.<sup>14</sup> Investigations also involved modification of the hydroxyalkyl chain length. This extended to straight or branched chains, preferably containing between two and six carbon atoms. Reaction conditions engaged a range of temperatures from 40°C to 120°C. This produced polyurethanes of typically rigid behaviour, whilst remaining soluble in organic solvents.

Morgan et al. prepared curable polymer compositions from Dantocol and isocyanates, reacted with thiol-containing monomers.<sup>15</sup> Application includes use in wire coatings, as result of the polymers thermal stability, flexibility and high elongation. Toluene-2,4-diisocyanate was identified as the preferred curative, reacting according to Scheme 6.3.



**Scheme 6.3.** Urethane reaction involving Dantocol and toluene-2,4-diisocyanate.

Adduct formation was also investigated, involving a two-step reaction process. This implicated the addition of Dantocol in an amount necessary to react with 0.5eq of the isocyanate functionality. Adduct-forming reactions were performed in moisture-free atmosphere at ambient pressure. The remaining isocyanate groups were then polymerised over a period of 10mins to 24 hours. This was also attempted in the presence of catalyst and inert solvent. Suitable catalysts include dibutyl tin dilaurate, stannous octate, triethylene diamine or *N,N,N',N'*-tetramethyl-1,3-butanediamine.

These results concur with descriptions provided by Coseri, indicating isocyanates react with almost any compound containing active hydroxyl groups.<sup>16</sup> Zeno et al. investigated the reaction of Dantocol and other hydroxyalkyl amide compounds.<sup>17</sup> Along with isocyanate reaction, the esterification of hydroxyalkyl alcohols was also described. While amide alcohols react more rapidly than standard alcohols, the reactivity of Dantocol contradicts this observation. Unlike acyclic amide alcohols, hydantoin conformations observe a lack of acid catalysis, according to the amides base strength.<sup>17</sup> This results in reduced reaction rate.

## **6.2 Experimental**

### **6.2.1 Polymerisation of Polyurethane Binder System**

Synthesis of polyurethane was based on a modified procedure described by Hamshere et al.<sup>18</sup> to ensure replication of PBX mixing conditions. Unfilled polyurethane gumstock was prepared by reaction of HTPB and stoichiometric equivalents of IPDI. Characterisation of HTPB was performed prior to cure, identifying hydroxyl functionality required for measurement of prepolymer equivalents. Elucidation of the hydroxyl equivalent weight (OH Eq. Wt) revealed a value of 1149.83g/eq. This was applied in calculating the stoichiometric ratio NCO:OH.

HTPB (1eq, 10g) was added to a 50mL two-necked flask, equipped with magnetic stirrer under vacuum. Multiple pots were prepared to investigate the effect of catalyst, with

triphenyl bismuth (0.233%, 25mg) combined to an isolated formulation. The prepolymer was heated for 1 hour at 60°C, followed by addition of IPDI (1eq, 0.97g). Constituents were mixed in vacuo for 15mins and the resulting polyurethane cast into 50mm Teflon moulds. Curing was promoted for 7 days at 60°C under continuous nitrogen purge. The resultant polyurethane was translucent and of rubbery consistency, indicating the formation of cross-linking.

### **6.2.2 Investigation of Dantocol and HTPB Blends**

The potential for interaction between Dantocol and HTPB was investigated subsequent to blending. This involved combining an equivalent alcohol content to that applied in PBX formulation ARX-2014. Dantocol (0.26g) and HTPB (7.346g) was charged to a 25mL round bottom flask and vigorously stirred for 1 hour. Preparation of a secondary blend was implemented, comprising an equivalent molar ratio of components. This focussed on increasing the intensity of Dantocol signals within spectroscopic techniques.

Additional energy was applied to blends via heating. This involved replicating PBX submix conditions to elucidate the impact of such environment. Hydroxyl blends were mixed under vacuum at 60°C over a period of several hours. Characterisation was then performed to determine the potential for interaction.

### **6.2.3 Polymerisation of Dantocol and Isophorone Diisocyanate**

Incorporation of Dantocol within the binder system was investigated in terms of reactivity associated with IPDI. This involved combining Dantocol (9.386g, 1.0eq) and IPDI (10.61g, 1.0eq) within a 50mL round bottom flask. Components were mixed at 60°C, whilst applying vacuum and sonication to remove gas. Upon completion of degassing, the polymer was cast into Teflon moulds and cured under nitrogen at 60°C for seven days. This procedure was repeated in the presence of catalyst to promote reaction completion. Triphenyl bismuth (0.2mg) was consequently added prior to isocyanate, and cured under identical conditions.



An alternative approach involving adduct formation was introduced to proceedings. The two step process involved mixing Dantocol (4.693, 0.5eq) and IPDI (10.61g, 1.0eq), within a moisture free environment. Reaction was conducted at 60°C over 24 hours, in acquisition of the desired adduct. The remaining Dantocol (4.693, 0.5eq) content was combined and mixing conditions re-established. Curing of polyurethane was again performed under nitrogen, at 60°C for seven days. This produced an inelastic polymer, brittle in property and of yellowing appearance.

## 6.2.4 Characterisation Techniques

### 6.2.4.1 Hydroxyl Number Determination

Hydroxyl concentration is typically expressed in terms of the hydroxyl equivalent weight. This was determined by a titrimetric approach developed by Manazara et al. in response to the reproducibility and reliability of methodology.<sup>11, 19</sup> The procedure involved esterification of HTPB, whereby hydroxyl groups were reacted with acetic anhydride in pyridine. Excess reagent was hydrolysed and titrated with potassium hydroxide to calculate the hydroxyl number according to the equation:

$$\text{OH Eq. Wt} = \frac{m \times 1000}{(V_{\text{blank}} - V_{\text{sample}}) \times N} \quad (6.1)$$

Where  $m$  is the mass of polymer and  $N$  being the normality of potassium hydroxide. The hydroxyl equivalent weight is subsequently applied to determining the OH number and OH value, outlined in the following equations:

$$\text{OH Number} = \frac{56.1 \text{ (mg KOH/eq)} \times 1000 \text{ (mg/g)}}{\text{OH Eq.Wt. (g/eq)}} \quad (6.2)$$

$$\text{OH Value} = \frac{1000 \text{ (meq/eq)}}{\text{OH Eq.Wt. (g/eq)}} \quad (6.3)$$

#### 6.2.4.2 Nuclear Magnetic Resonance

All spectra were acquired using a Bruker 600MHz NMR spectrometer.  $^1\text{H}$  and  $^{13}\text{C}$  spectra employed model parameters, comprising standard units of chemical shift (ppm) and J-coupling constant (Hz). Proton acquisitions were conducted in chloroform-*d*, referenced to  $\delta = 7.26\text{ppm}$  at concentrations of 1% (w/w) HTPB. This was increased to approximately 25% (w/w) for  $^{13}\text{C}$  spectra, applying a relaxation time of 12 seconds and 1800 pulses.<sup>20</sup>

Leachable fractions of linear polyurethane were prepared for NMR analysis by refluxing with chloroform-*d*. This involved heating polyurethane segments in deuterated solvent at 60°C. Reflux conditions were sustained overnight and the soluble component separated by filtration. Solutions were concentrated under distillation prior to NMR acquisition.

#### 6.2.4.3 Fourier Transform Infrared Spectroscopy

Reaction progress of polyurethanes was monitored by FTIR, using a Nicolet Nexus 8700 FT-IR Spectrophotometer. This focused on reduction of the isocyanate peak at  $2255\text{cm}^{-1}$ , coinciding with urethane formation. HTPB was simultaneously investigated to identify vibrational bands pertaining to the polyol. Spectra were acquired at a sample gain of 2.0 over 128 scans. Impinging light was recorded on a MCT/A detector cooled with liquid  $\text{N}_2$ . Resulting spectra were collected over a wavenumber range of  $650\text{-}4000\text{cm}^{-1}$ , at a resolution of  $2.0\text{ cm}^{-1}$ . OMNIC version 7.3 software was utilised to interpret spectra.

#### 6.2.4.4 Differential Scanning Calorimetry

The glass transition ( $T_g$ ) and melting temperatures ( $T_m$ ) of polyurethanes and HTPB prepolymer was investigated using a TA Instruments MDSC-2930 differential scanning calorimeter. Instrumentation was calibrated to the  $T_m$  endotherm of indium in determining the cell constant. Approximately 10mg of sample was sealed in aluminium hermetic pans and subjected to differential scanning calorimetry (DSC) analysis. The DSC cell was cooled using a liquid nitrogen cooling accessory (LNCA) under continuous  $\text{N}_2$  flow of  $100\text{mL}/\text{min}$ . Experimental parameters involved cooling the cell to  $-100^\circ\text{C}$  for 3mins, prior to heating at

10°C min<sup>-1</sup>. The heating rate was maintained until the conclusion of decomposition at temperatures upwards of 550°C. Interpretation of thermograms was performed using TA Instruments Universal Analysis software. Calculation of  $T_g$  values was defined as the temperature corresponding to the mid-point of the heat capacity change.

#### **6.2.4.5 Thermal Gravimetric Analysis**

Thermogravimetric analysis (TGA) was implemented to record the weight loss as a function of temperature. Decomposition behaviour was measured on a TA Instruments TGA-2950 thermogravimetric analyser, through conventional heating from room temperature to 600°C. Samples (~20mg) were exposed to a heating rate of 10°C min<sup>-1</sup>, under continuous nitrogen purge at 100mL min<sup>-1</sup>. The Curie-Point method was used to calibrate temperature relevant to the heating rate, using a nickel standard. Maximum weight loss and the onset temperature of decomposition was determined using TA Instruments Universal Analysis software.

#### **6.2.4.6 Rheology**

The rheological behaviour of polyurethane cure was investigated using a TA Instruments AR 2000 Advanced Rheometer. This employed a 20mm aluminium cone of 2°, operating in oscillatory time sweep mode. Stoichiometric equivalents of HTPB and IPDI were analysed at 60°C, to maintain consistency with PBX mixing. Isothermal conditions were maintained throughout cure using a peltier plate with an accuracy of ±0.2°C. Following temperature stabilization the diisocyanate curative was combined with HTPB and applied to the rheometer stage. Multiple experiments were performed to identify the impact of triphenyl bismuth addition at catalytic concentrations.

An oscillatory strain sweep was initially performed to identify the linear viscoelastic region (LVR) from which strain is selected. Based on results, 10% strain was applied to limit disruption to the network structure, following cross-linking. The adverse effects of applying excess strain extend to underestimation of viscosity build-up and storage modulus, resulting from shear thinning. Pre-shearing was performed prior to analysis, eliminating potential

shear or structural history. Curing of polyurethane was then examined by oscillatory time sweep at a frequency of 1Hz. Results were analysed using TA Instruments Data Analysis software to identify  $G'$ ,  $G''$ ,  $\eta^*$  and  $\tan \delta$  of the curing system.

#### **6.2.4.7 Gel Permeation Chromatography**

GPC analysis was conducted using a Shimadzu Prominence UFLC equipped with linear Phenomenex Phenogel GPC/SEC column. This employed multiple detectors including RI and fixed wavelength UV/Vis. Tetrahydrofuran was applied as the mobile phase, eluting at a flow rate of  $1\text{ mL min}^{-1}$ . Subsequent calibration was performed using polystyrene standards to generate the calibration curve. This was proceeded by injecting  $20\mu\text{L}$  aliquots of polyurethane ( $5\text{ mg mL}^{-1}$ ) at  $40^\circ\text{C}$ . Interpretation of chromatograms was performed using Shimadzu LC Solutions software to determine molecular weight data.

### **6.3 Results**

#### **6.3.1 Polymerisation of Polyurethane Binder System**

HTPB is known to exhibit multiple hydroxyl conformations, consisting of *cis*, *trans* and *vinyl* units.<sup>21</sup> Both *cis* and *trans* formations occur through 1,4-polymerisation of butadiene end groups. *Vinyl* content accounts for only a small percentage of HTPB and is derived from 1,2-polymerisation. Structural configuration imparts variation in the physical properties of HTPB and continue to impact polyurethanes derived from the prepolymer. Characterisation of HTPB is therefore required to understand polymer morphology, functionality and side reactions. This will later be applied in distinguishing a response towards incorporation of Dantocol within the binder. Preliminary investigation of HTPB, therefore provides background information necessary for interpreting interaction of Dantocol within blended systems.

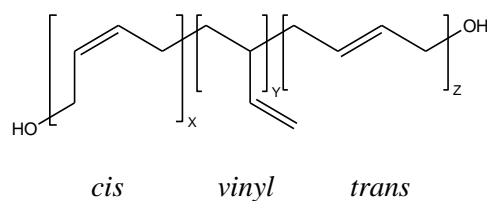


**Figure 6.1.** Structural configuration of HTPB.

### 6.3.1.1 Hydroxyl Number Determination

Functionality may be considered the single most important parameter in determining cross-linking of polymer networks.<sup>22</sup> Since formation of HTPB is of a statistically random nature, variation in polymer end groups are observed. Consequently, the hydroxyl equivalent weight must be determined to understand the functionality of HTPB. Polyol functionality is defined as the average number of hydroxyl groups per polymeric chain.<sup>23</sup> This is required to accurately determine the amount of polyol necessary to polymerise the isocyanate content. Elucidation of the equivalent weight, therefore ensures the precise stoichiometric ratio of binder components are combined to achieve reaction completion.

Hydroxyl numbers were determined in triplicate for HTPB prepolymer, according to chemical methodology. Data collated from titrations is represented in Table 6.1, indicating variations between the experimental data and manufactures specifications. Accuracy in the equivalent weight is critical in balancing the stoichmetric ratio of NCO:OH, necessary to form the desired network.

HTPB (R45HT LO)	OH Equivalent (g/eq)	OH Number (mg KOH/g)	OH Value (meq/g)
Manufactures data	1191.08	47.10	0.84
Experimental data	1149.83	48.79	0.87

**Table 6.1.** Hydroxyl functionality data for HTPB.

### 6.3.1.2 Nuclear Magnetic Resonance

#### 6.3.1.2.1 NMR Spectroscopy of Hydroxyl-Terminated Polybutadiene

NMR spectroscopy offers a precise means for identifying the structure and purity of HTPB, providing information related to triad configurations. Figure 6.2 depicts the  $^1\text{H}$  spectrum of HTPB, which yields broad signals on account of residual dipolar coupling.<sup>24</sup> Failure of proton-proton interactions to average out, stems entirely from the restricted molecular mobility of the polyols steric arrangement. The resulting residual interactions therefore produce the peak broadening observed. This is typical for polymeric compounds, which exhibit broad peaks compared to small molecules according to restricted segmental motion.<sup>25</sup> Under such circumstances, peaks are almost always singlets, due to the associated broadening.<sup>25</sup>

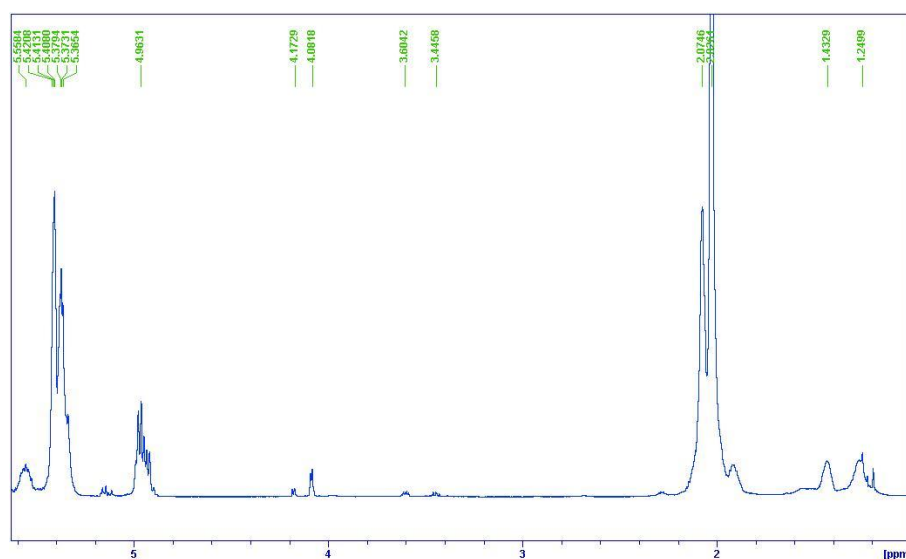


**Figure 6.2.**  $^1\text{H}$  NMR spectrum of HTPB in chloroform-*d*.

Inspection of HTPB's hydroxyl region indicates the presence of three terminal hydroxyl groups. Appearance of multiple  $\text{CH}_2\text{-OH}$  methylene peaks are assigned to *cis* (4.17ppm), *trans* (4.08ppm) and *vinyl* (3.60ppm) units. The signal of the adjacent *OH* proton is inherently weak, however its peak is subtly observed at  $\delta = 3.44\text{ppm}$ . Splitting of the hydroxyl end group is prompted by contributions from neighbouring units.

Peaks at  $\delta = 5.38$  and  $2.07\text{ppm}$  correlate with  $=\text{CH}-$  and  $-\text{CH}_2-$  protons of the *cis* units. Corresponding peaks of the *trans* units appear at  $\delta = 5.40$  and  $2.03\text{ppm}$  respectively. The 1,2-conformation of *vinyl* units generate additional peaks representing the tertiary alkane CH  $1.27\text{ppm}$  and terminal alkene  $=\text{CH}_2$   $4.95\text{ppm}$ . Signals coincide with the reoccurring  $=\text{CH}-$  and  $-\text{CH}_2-$  peaks located at  $\delta = 5.55$  and  $1.43\text{ppm}$ .

Units	Structure	Triad Sequence	$\delta$ (ppm)	Protons
<i>Cis</i>	1,4-saturated	$\underline{c}_t^c$	2.07	2H
	1,4-unsaturated	$\underline{tct}$	5.36	1H
		$\underline{cct}$	5.37	1H
		$\underline{ccc}$	5.38	1H
	OH end group	$\frac{c}{\underline{c}_v}$ $\underline{t}$	4.17	2H
<i>Vinyl</i>	1,4-saturated	$\underline{v}\underline{v}$	1.27	1H
		$\underline{v}\underline{v}_t^c$	1.43	2H
	1,4-unsaturated	trm $\underline{v}$	4.95	2H
		non-trm $\underline{v}$	5.55	1H
	OH end group	$\frac{c}{\underline{v}_v}$ $\underline{t}$	3.60	2H
<i>Trans</i>	1,4-saturated	$\underline{t}_t^c$	2.03	2H
	1,4-unsaturated	$\underline{ttt}$	5.40	1H
		$\underline{ttc}$	5.41	1H
		$\underline{ctc}$	5.42	1H
	OH end group	$\frac{c}{\underline{t}_v}$ $\underline{t}$	4.08	2H

$c = \text{cis}, v = \text{vinyl}, t = \text{trans}, \text{trm} = \text{terminal}$

**Table 6.2.**  $^1\text{H}$  spectral assignment of HTPB segments.<sup>26-28</sup>

The presence of *cis*, *vinyl* and *trans* units were confirmed by  $^{13}\text{C}$  NMR, with *trans* conformations favoured by free radical polymerisation. Conversely, the occurrence of *cis* configurations is known to dominant anionically synthesised HTPB.<sup>21</sup> The olefinic region depicted in Figure 6.3 includes contributions from all three monomer units. Principle signals of the unsaturated hydrocarbons occur at  $\delta = 114.2, 142.6\text{ppm}$  (*vinyl*),  $130.1\text{ppm}$  (*trans*) and  $129.4\text{ppm}$  (*cis*). Based on the integration values of these peaks, calculation of *vinyl* content is performed according to Equation 6.4:

$$\text{Vinyl content} = \frac{A+B}{(A+B+C)} \times 100\% \quad (6.4)$$

Where  $A$  and  $B$  is the area of the 1, 2-unsaturated CH and CH<sub>2</sub> *vinyl* peaks, and  $C$  is the area of both *cis* and *trans* peaks.<sup>23</sup> This identified the structural configuration of HTPB consists of 22.5% *vinyl* content. The remaining components were calculated from their respective integration values, indicating 56.4% *trans* and 21.1% *cis* contributions. Results were replicated in the CH<sub>2</sub>-OH chemical shift region 50–70ppm, with calculations reproduced to evaluate configurational content. These signals represent the chemical shift of *vinyl* (64.94ppm), *cis* (58.34ppm) and *trans* (63.48ppm) end groups. Splitting of the *cis* peak at 58.34ppm is attributed to the influence of neighbouring units.<sup>21</sup>

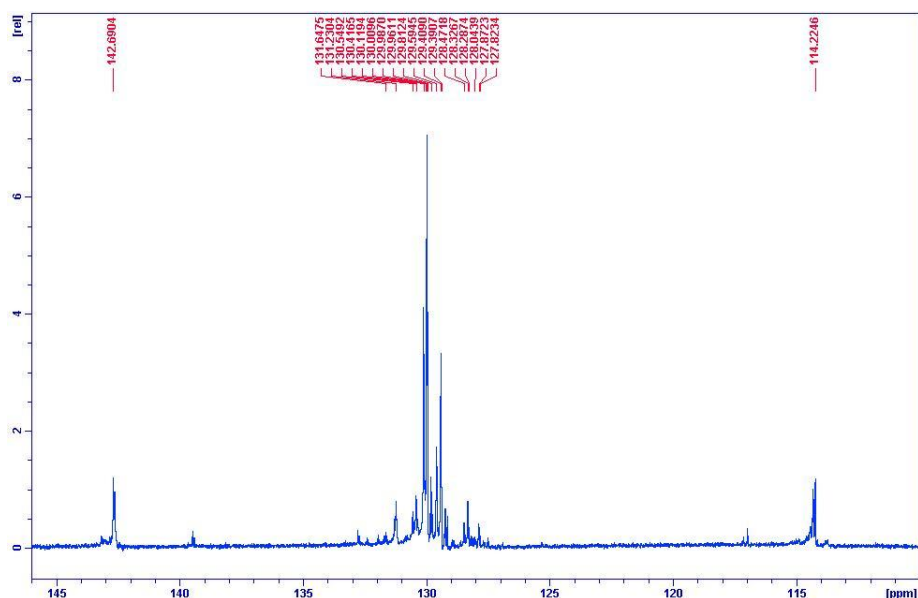


**Figure 6.3.** <sup>13</sup>C NMR spectrum of HTPB olefinic region in chloroform-*d*.

Consistent with the proton spectra of HTPB, inspection of the <sup>13</sup>C NMR also revealed contributions from triad sequences. This emerges from random addition of monomeric butadiene units, which form an array of configurations. The resultant HTPB chain consists of a combination of *cis*, *trans* and *vinyl* units, representing triad sequences. Figure 6.4 illustrates the presence of such morphology within the aliphatic region. Shifts in resonance signals result from the influence of neighbouring units on a central unit. Assignments of triad sequences in the olefinic and aliphatic region are detailed in Table 6.3. This was interpreted from Kanakavel et al.<sup>21</sup> describing the splitting of HTPB peaks due to *vinyl*, *cis* and *trans* centred triads.



Units	Position	Triad Sequence	$\delta$ (ppm)	Intensity
<i>Cis</i>	1,4-Unsaturated	V <u>c</u> v	130.55	0.59
		<u>c</u> <sub>t</sub> c <u>c</u>	129.59	1.63
		<u>c</u> <sub>t</sub> c <u>t</u>	129.41	3.27
		<u>c</u> <sub>t</sub> c <u>v</u>	129.39	1.59
		V <u>c</u> c	128.04	0.19
		V <u>c</u> t	127.87	0.40
		V <u>c</u> v	127.82	0.19
	1,4-saturated	r-v <u>v</u> <u>c</u>	33.49	0.08
		1,4-v <u>c</u>	32.70	13.29
		m-v <u>v</u> <u>c</u>	32.13	0.46
		<u>c</u> <sub>t</sub> <sup>c</sup>	27.37	9.09
		<u>C</u> v	24.85	1.19
	OH end group	<u>c</u> <sub>v</sub> <sup>c</sup>	58.57	0.17
		<u>c</u> <sub>t</sub>		
<i>Vinyl</i>	1,2-unsaturated	trm. <u>v</u>	114.22	1.15
		non trm. <u>v</u>	142.69	1.12
	1,2-saturated	1,4- <u>v</u> -1,4	43.46	0.70
		V <u>v</u> v	41.10	0.13
		V <u>v</u> v	39.02	0.08
		r-1,4- <u>v</u> v	35.62	0.13
	OH end group	1,4- <u>v</u> -1,4	33.92	0.92
		<u>v</u> <sub>v</sub> <sup>c</sup>	65.08	0.25
<i>Trans</i>	1,4-unsaturated	V <u>t</u> v	131.64	0.26
		<u>c</u> <sub>t</sub> <u>t</u> v	131.23	0.78
		v <u>t</u> <sub>t</sub> <sup>c</sup>	130.41	0.85
		c <u>t</u> <sub>t</sub> <sup>c</sup>	130.11	3.87
		t <u>t</u> <sub>t</sub> <sup>c</sup>	129.99	6.70
		<u>c</u> <sub>t</sub> <u>t</u> v	129.81	1.15
		V <u>t</u> c	128.47	0.40
		V <u>t</u> t	128.33	0.76
		V <u>t</u> v	128.28	0.46
		1,4-saturated	1,4-v <u>t</u>	38.17
	m-v <u>v</u> <u>t</u>		37.39	0.06
	<u>t</u> <sub>c</sub> <sup>t</sup>		32.70	13.3
	<u>T</u> v		30.12	2.15
	OH end group	<u>t</u> <sub>v</sub> <sup>c</sup>	63.79	0.50
		<u>t</u>		

*c* = cis, *v* = vinyl, *t* = trans, *r* = racemic, *m* = meso, *trm* = terminal

**Table 6.3.** <sup>13</sup>C NMR peak assignment of HTPB segments.<sup>21, 29, 30</sup>

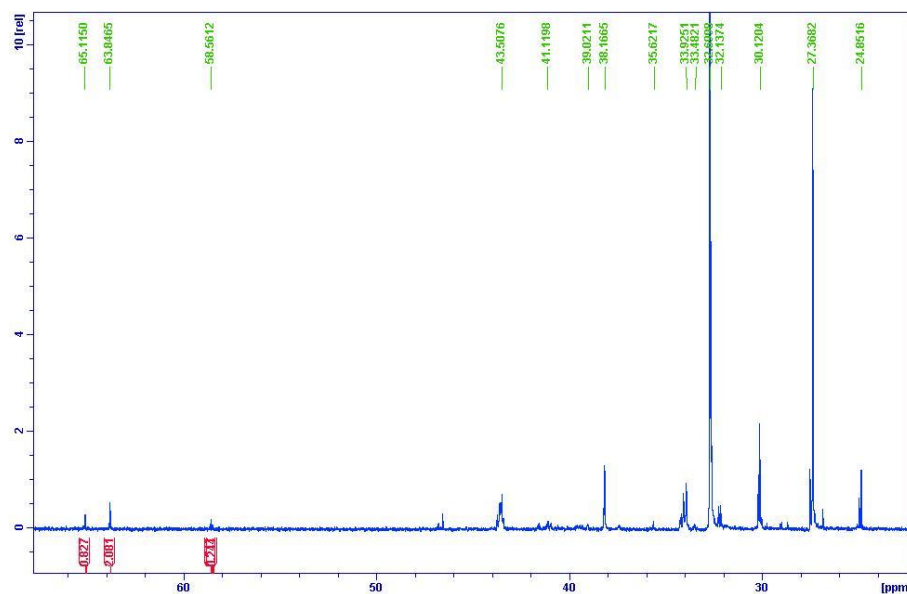


**Figure 6.4.**  $^{13}\text{C}$  NMR spectrum of HTPB aliphatic region in chloroform-*d*.

### 6.3.1.2.2 NMR Spectra of Polyurethane

Inspection of polyurethane solubility revealed that polymerisation of IPDI and HTPB generates a small percentage of linear strands. This occurs due to the distribution of HTPB functionality comprising monofunctional, bifunctional and trifunctional hydroxyl groups. Monofunctional prepolymer acts as a chain terminator, while difunctionals perform chain extension and trifunctionals produce cross-linking. Based on the relative quantities of these monomers, linear or low molecular weight polyurethane chains may occur. Removal of extractables using chloroform-*d* over heat, enables characterisation via solution NMR. Employing chloroform-*d* limits solvent interaction and eliminates the need for purification. Related techniques have previously been applied to extract comparable polyurethane systems. Harris et al.<sup>31</sup> performed extraction of soluble polyurethane fractions based on HTPB, whilst Kumar et al.<sup>32</sup> reported the extraction of low molecular weight leachable fractions of IPDI based polyurethanes. Observations agreed with the literature, having identified polyurethane extractables diffuse from the cross-linked network.

Inspection of  $^1\text{H}$  NMR confirms polyurethane formation, according to evolution of amide and alkoxy peaks, consistent with urethane groups. Chemical shifts for the respective protons

appear in Figure 6.5, along with saturated and unsaturated hydrocarbons of the polymer backbone. The characteristic amide functionality evolves as multiple resonances between  $\delta = 9.4$ - $10.0$ ppm. This represents duplicate amide groups produced via reaction of both primary and secondary isocyanates of IPDI.<sup>33</sup> Amides derived from the secondary isocyanates shift up-field, generating a chemical shift at 9.49ppm. The remaining down-field signal represents that of primary groups located at 9.80ppm.

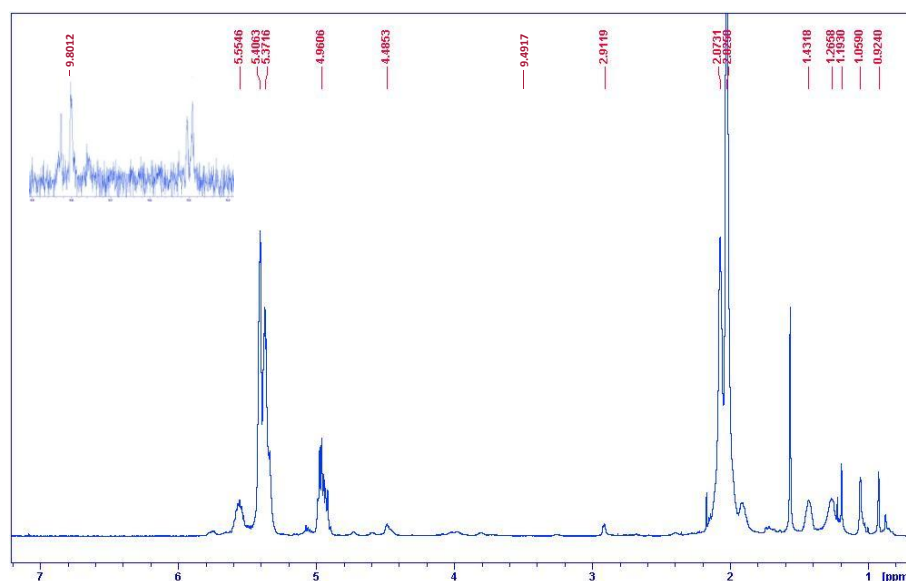


**Figure 6.5.**  $^1\text{H}$  NMR of polyurethane and superimposed amine region in chloroform-*d*.

The urethanes alkoxy group gives rise to multiple  $\text{CH}_2\text{-O}$  signals at  $\delta = 4.50$  and  $2.92$ ppm. This is accompanied by removal of the  $\text{CH}_2\text{-OH}$  and  $\text{OH}$  end groups of HTPB, as the oxygen forms covalent bonds with the isocyanate functionality. Alkoxy signals are reproduced in the  $^{13}\text{C}$  NMR, with the adjoining carbon producing chemical shifts at 66ppm and 54ppm. Neighbouring carbonyl groups develop weak signals at 156ppm and 154ppm. Due to the concentration of urethane linkages within polyurethane, the polymeric backbone dominates the NMR spectra. This emphasises the low intensity of the carbonyl group, along with the primary and secondary amide signals at 46ppm and 57ppm. Peak assignment was confirmed by 2D HMQC experiments, providing correlations between proton and carbon nuclei. The remaining peaks stem from triad sequences and IPDI incorporated within the polyurethane chain.

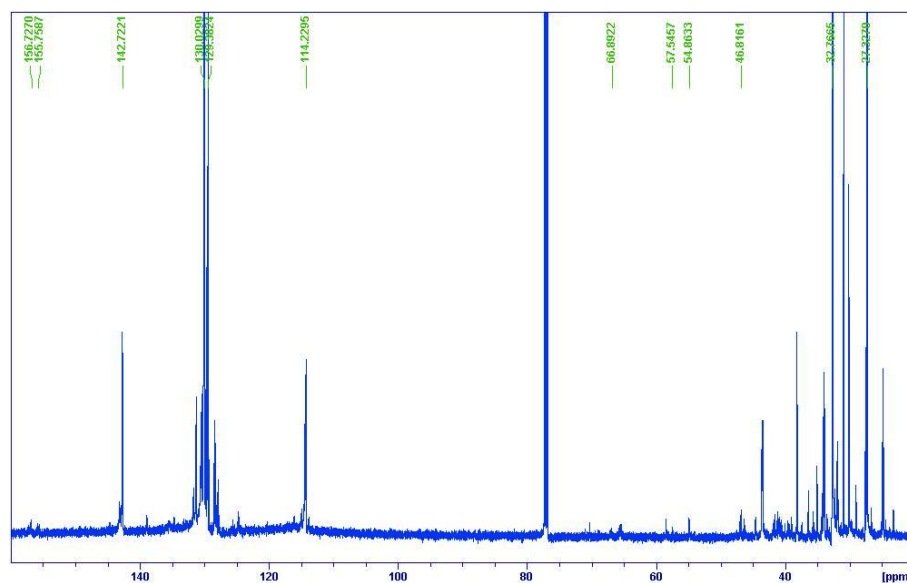


**Figure 6.6.**  $^{13}\text{C}$  NMR spectrum of polyurethane in chloroform-*d*.

### 6.3.1.3 Fourier Transform Infrared Spectroscopy

#### 6.3.1.3.1 FTIR Spectroscopy of Hydroxyl-Terminated Polybutadiene

The structure of HTPB was investigated by FTIR as a complementary technique to identify discrepancies between polyol and urethane bands. This will be utilised in determining the impact of Dantocol inclusion within future formulations. The presence of *cis*, *vinyl* and *trans* configurations within HTPB was confirmed in the FTIR spectra, with the assignment of isomer bands outlined in Table 6.4. The  $\text{CH}_2$  stretching bands of the *vinyl* units shows decreased intensity in comparison to that of the *trans* peaks. Based on the intensities of these bands, the *trans* units accounts for a higher percentage of the polyol, assuming similar absorptivities. Predominance of the *trans* configuration is supported by  $^{13}\text{C}$  NMR and is consistent with free radical polymerisation.

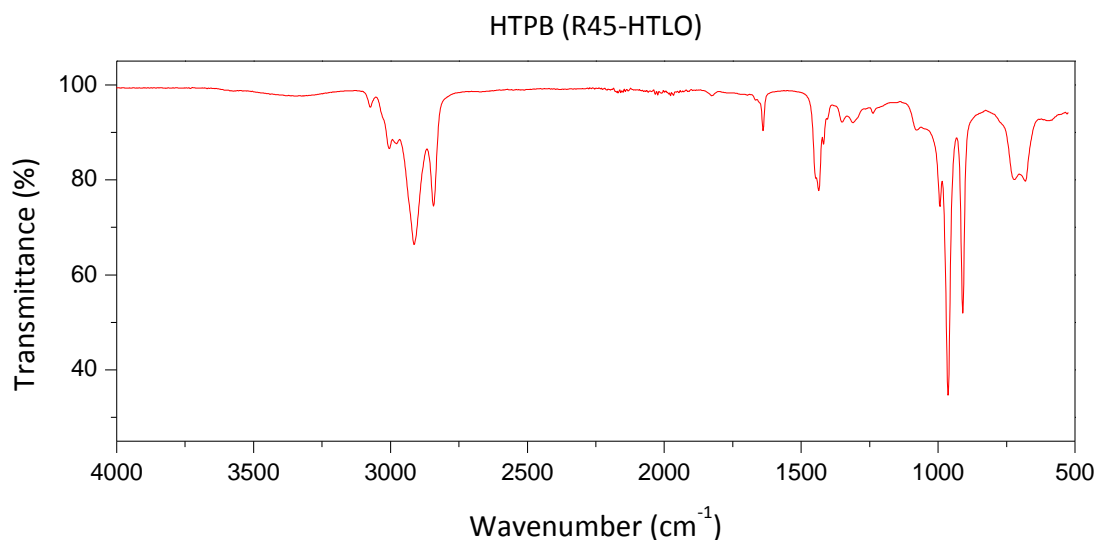


**Figure 6.7.** FTIR spectrum of HTPB (R45HT LO).

Wavenumber (cm <sup>-1</sup> )			Intensity	Assignment
<i>Cis</i>	<i>Trans</i>	<i>Vinyl</i>		
3660-3100	3660-3100	3660-3100	b	$\nu$ OH
		3073	m	$\nu_{as}$ CH <sub>2</sub> =
3004			m	$\nu$ (CH=CH)
		2977	m	$\nu_{sym}$ CH <sub>2</sub>
2913	2913	2913	s	$\nu_{as}$ CH <sub>2</sub>
	2843		s	$\nu_{sym}$ CH <sub>2</sub>
	1666		m	$\nu$ C=C
1654			w	$\nu$ C=C
		1639	s	$\nu$ C=C
1446, 1435			s	$\delta_{sym}$ CH <sub>2</sub>
	1435		s	$\delta_{sym}$ CH <sub>2</sub>
		1418	m	$\delta$ CH <sub>2</sub> =
1404			w	$\delta$ (=CH)
1350	1350	1350	b	CH <sub>2</sub> wag
	1310		m	$\delta$ (=CH <sub>2</sub> )
		993	m	CH wag
	963		s	CH wag
		909	s	CH wag

$\nu$  = stretch,  $\delta$  = deformation, s = strong, m = medium, w = weak, b = broad

**Table 6.4.** FTIR band assignment of HTPB segments.<sup>34</sup>

Separate from the saturated and unsaturated hydrocarbons, the hydroxyl terminated end groups appear as a broad band at 3660-3100cm<sup>-1</sup>. Low intensity associated with the OH

stretch, results from HTPBs hydroxyl equivalent weight. This imparts low hydroxyl concentration proportional to the polymeric hydrocarbons. Investigation of the hydroxyl contribution will be of future importance in distinguishing the impact of Dantocol interaction within blended systems.

### 6.3.1.3.2 FTIR Spectroscopy of Polyurethane

FTIR is often regarded as the most effective technique for monitoring reaction of polyurethanes. This has the advantage of rapidly producing high resolution spectra of curing polymers in either solid or liquid phase, depending on the stage of cure. Consequently, this method was employed to identify evolution of the C=O band at  $1730\text{cm}^{-1}$  and accompanying loss in intensity of the NCO band at  $2255\text{cm}^{-1}$ . Figure 6.8 indicates complete removal of the NCO peak, following seven days cure. This represents reaction completion, coinciding with the formation of carbonyl and amide vibrations.

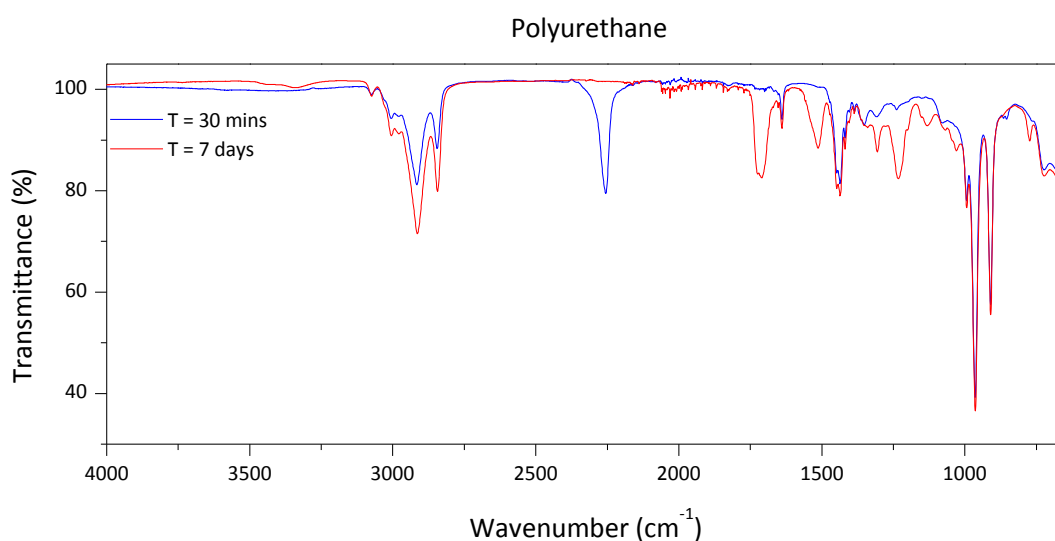


**Figure 6.8.** FTIR spectra of IPDI:HTPB based polyurethane.

Hydrogen bonding within the polyurethane system is limited to urethane linkages. This involves interaction of the amide functionality with either the carbonyl or alkoxy group. As urethane linkages contain the only available proton donor or acceptors, hydrogen bonding is therefore isolated to the hard segment.<sup>35</sup> This is represented in the carbonyl stretching vibration, consisting of two overlapping bands corresponding to free and hydrogen bonded

carbonyls. Evolution of free carbonyls occurs at  $1725\text{cm}^{-1}$ , whilst the hydrogen bonded equivalent undergoes bathochromic shift towards  $1712\text{cm}^{-1}$ . Simultaneous formation of amide bands, similarly exhibit shoulder formation indicative of hydrogen bonding. Overlaying bands remain unresolved unlike the proton acceptor, and are assigned a single wavenumber according to Table 6.5. As the reaction proceeds low intensity, hydroxyl peaks are replaced by a broad amine band between  $3430\text{-}3340\text{cm}^{-1}$ . The amine bending vibration confirms the presence of hydrogen bonding, with participating amide groups appearing at lower wavenumber.

Wavenumber ( $\text{cm}^{-1}$ )	Intensity	Assignment
3430-3340	m	$\nu\text{NH}$
2913	s	$\nu_{\text{as}}\text{CH}_2$
1725	s	$\nu\text{C=O}$
1712	s	$\nu\text{C=O}$
1639	s	$\nu\text{C=C}$
1517	m	$\nu\text{Amide I}$
1236	m	$\nu\text{Amide II}$

$\nu$  = stretch, s = strong, m = medium, w = weak

**Table 6.5.** Assignment of FTIR bands for IPDI:HTPB based polyurethane.<sup>34</sup>

In contrast to the evolution of urethane linkages, soft segment hydrocarbons remain unchanged throughout the curing process. Spectral overlay of the  $\nu_{\text{as}}\text{CH}_2$  band, pre and post cure, shows negligible deviation in intensity and wavenumber at  $2913\text{cm}^{-1}$ . This extends to the  $\nu\text{C=C}$  band at  $1639\text{cm}^{-1}$ , which also remains consistent during cure. These features facilitate normalisation of spectral data relative to the intensity of such peaks.

#### 6.3.1.4 Thermal Analysis

The thermal history of HTPB and its corresponding polyurethane was investigated by TGA and DSC. Analysis was conducted to identify the glass transition temperature ( $T_g$ ), melting temperature ( $T_m$ ), weight loss and decomposition point of the binder system. Such properties were examined to determine the extent of phase interaction, amid hard and soft segments. These implications are pivotal in defining the impact of Dantocol within PBX binder

systems. Furthermore the thermal stability of these systems provides a baseline for comparison after Dantocol addition.

#### 6.3.1.4.1 Differential Scanning Calorimetry of HTPB

Investigations into  $T_g$  of HTPB revealed the preliminary event occurs at  $-79.2^\circ\text{C}$ . This is depicted in the ensuing thermogram, acquired at a heating rate of  $10^\circ\text{C min}^{-1}$ . Interpretation of the DSC curve gives  $T_g$  as the half height of the tangent. Results reflect excessively low temperatures, indicating superior thermal stability. This is critical in optimising the operational temperature range of binder systems applied in PBX formulations.

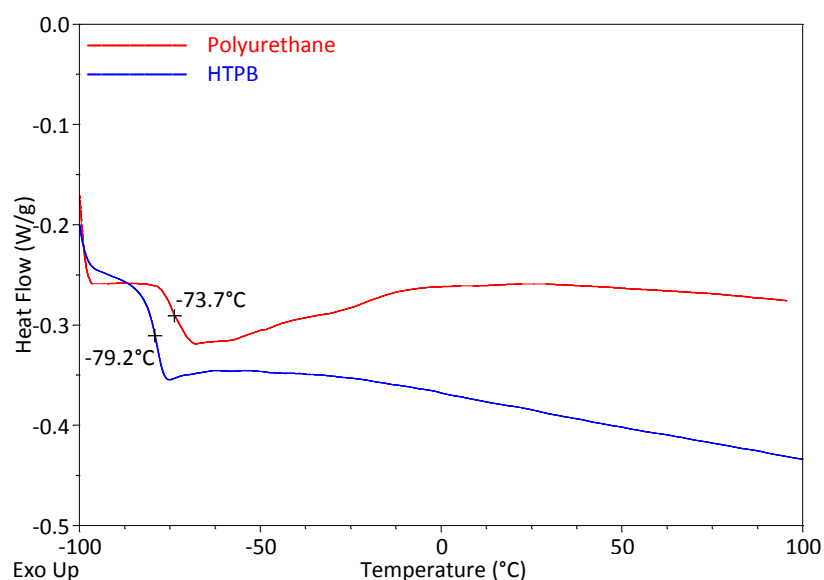


**Figure 6.9.** DSC overlay of HTPB and polyurethane glass transition temperature.

Thermal decomposition was measured from  $40\text{--}550^\circ\text{C}$ , at a heating rate of  $10^\circ\text{C min}^{-1}$ . Decomposition occurred in two steps, with an initial exothermic peak appearing at  $379.2^\circ\text{C}$ . This results from the positive energy balance of endothermic depolymerisation, together with exothermic cyclisation and cross-linking of residual HTPB.<sup>36</sup> The secondary decomposition step accounts for depolymerisation of cross-linked residue, formed during reactions in the first step.<sup>36</sup> This generates an endothermic peak, chiefly resulting from depolymerisation and desorption of fragments. Du et al.<sup>37</sup> reported the continued release of butadiene during the



initial stages of secondary decomposition. This indicates a small portion of unsaturated hydrocarbons remain present upon conclusion of the exothermic step.

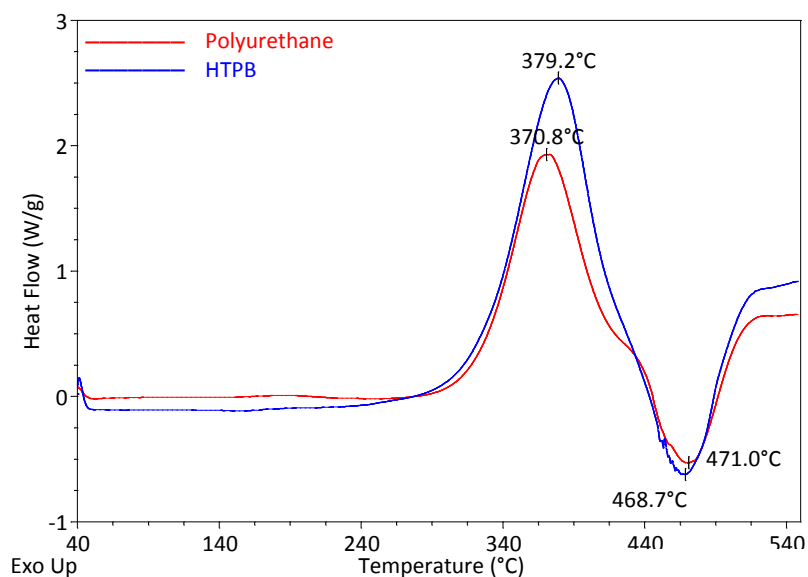


**Figure 6.10.** DSC overlay of HTPB and polyurethane thermal decomposition.

#### 6.3.1.4.2 Differential Scanning Calorimetry of Polyurethane

The thermal history of polyurethane and its HTPB derivative was interpreted according to Table 6.6. Segmentation observed within the polyurethane influences thermal properties of the binder system. Presence of hard segments is attributed to the extension of IPDI, providing physical cross-linking, as well as reinforcing soft segments. This is responsible for the high temperature performance of the polyurethane. Alternately the flexible soft segment is responsible for  $T_g$ , which determines the low temperature operational range of PBX composites. The  $T_g$  of polyurethane occurs at  $-73.7^\circ\text{C}$ , exhibiting minimal deviation of  $\Delta T_g = 5.5^\circ\text{C}$  from its HTPB starting material. This corresponds to phase separation due to polarity effects between highly polar hard segment and non-polar soft segment. Failure to undergo hydrogen bonding contributes to incompatibilities, resulting in domains composed primarily of individual segment.<sup>12</sup> This is represented in the DSC curve as a decrease in shift between the  $T_g$  of polyurethane and its polyol derivative.<sup>38</sup>

Sample	First stage			Second stage	
	$T_g$ (°C)	$T_d$ (°C)	$\Delta H$ (J g <sup>-1</sup> )	$T_d$ (°C)	$\Delta H$ (J g <sup>-1</sup> )
HTPB	-79.3	379.2	-768.7	469.7	341.9
Polyurethane	-73.7	370.8	-575.5	471.0	268.9

**Table 6.6.** Thermal properties of HTPB and polyurethane.

Insight into the kinetics and mechanism of decomposition is particularly important in the combustion of propellant systems. Thermal degradation of the binder system is critical in governing the performance of propellants, with decomposition contributing towards the fuel source during combustion.<sup>39</sup> The first decomposition step at 370.8°C represents cleavage of the urethane linkage as the polymers weakest bond. IPDI is then partially vaporised on account of its vapour pressure.<sup>36</sup> The polyol meanwhile experiences cross-linking and cyclisation, whilst undergoing depolymerising to produce volatile products. The magnitude of this exotherm is proportional to the number of double bonds present within the polyurethane.<sup>36</sup> This is immediately followed by the secondary stage, resulting from decomposition of the mainly saturated HTPB residue.<sup>37</sup> The kinetics of this endotherm remains independent of urethane cross-linking. Cleavage of the urethane which promotes vaporisation of IPDI in the first step causes the HTPB remaining to behave in the same manner prior to polymerisation.

#### 6.3.1.4.3 Thermal Gravimetric Analysis of HTPB

Weight loss was determined by TGA over a temperature range of 25-600°C. Data acquired for HTPB confirms decomposition occurs in two weight loss steps of indistinct separation. This is illustrated in Figure 6.11, representing a heating rate of 10°C min<sup>-1</sup>. Initial weight loss commences around 250°C, as low molecular weight hydrocarbons volatilisise. Maximum weight loss of this stage occurs at 377.0°C, accounting for 8.3% of the polyol's mass. The second stage of weight loss is attributed to decomposition of residue produced in the first stage. This is responsible for 91.4% of weight loss, with the maximum occurring at 467.1°C. Results indicate superior polymer stability, on account of nominal chain branching.<sup>23</sup> This

enables increased freedom of rotation within the polymeric backbone, thus improving thermal stability.

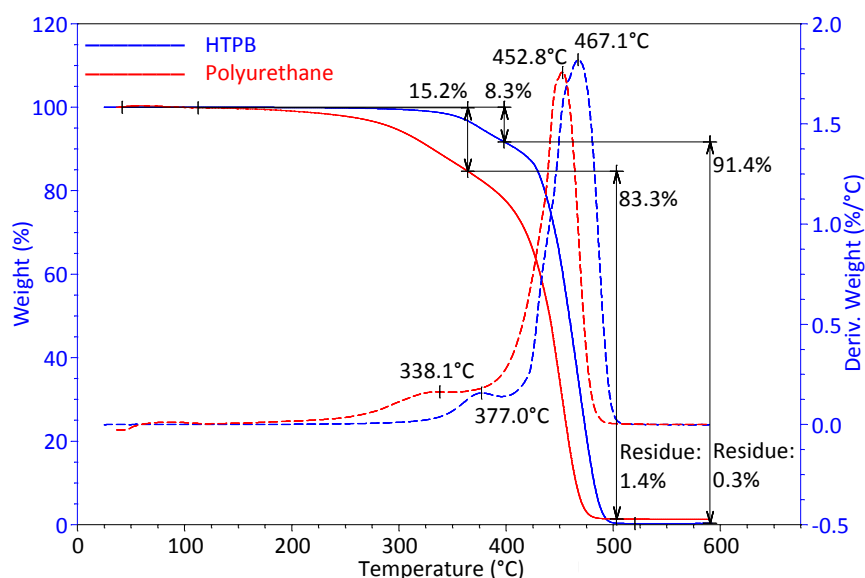


**Figure 6.11.** TGA overlay of HTPB and polyurethane.

#### 6.3.1.4.4 Thermal Gravimetric Analysis of Polyurethane

TGA analysis of the polyurethane reveals decomposition similarly occurs in two weight loss stages. Data pertaining to weight loss temperatures of polyurethane and its HTPB derivative are summarised in Table 6.7. Decomposition of polyurethane commences at lower temperature, according to the difference in degradation mechanisms. The details of both stages are described in full within Section 6.3.1.4.2. Weight loss pertaining to the initial stage is greater for polyurethane, as IPDI content vaporises along with low molecular weight residue, producing a loss of 15.2%. The secondary weight loss step observes a maximum at 452.8°C, accounting for 83.3% weight loss. Release of gaseous components during degradation includes contribution from carbon monoxide and methane.<sup>40</sup> This mirrors the decomposition mechanism of HTPB, following urethane cleavage in the first stage.

Sample	First stage		Second stage	
	Weight loss	Max weight loss	Weight loss	Max weight loss
HTPB	8.3%	377.0°C	91.4%	467.1°C
Polyurethane	15.2%	338.1°C	83.3%	452.8°C

**Table 6.7.** Thermal decomposition properties of HTPB and polyurethane.

### 6.3.1.5 Rheological Properties of Polyurethane Cure

Rheology is commonly applied in conjunction with thermal and spectroscopic techniques, to elucidate the mechanism of polymerisation. Rheological investigation of thermosets indicates critical points of conversion, including viscosity build-up and gel point. Gelation describes the formation of an infinite molecular network with initiation of cross-linking.<sup>41</sup> Meanwhile the viscosity of a curing system portrays network formation in the pre-gel stage, reflecting both chain extension and branching.<sup>42</sup> Points of conversion are dependent on the functionality of the monomers and its reactivity.<sup>41</sup> Investigation into rheological behaviour, therefore provides a unique insight into the reaction kinetics. This enables comparative analysis of kinetic parameters associated with urethane formation based on IPDI and respective alcohols. Knowledge of cure kinetics for systems comprising HTPB and Dantocol will assist in establishing the curing mechanism of polyurethane blends, following incorporation of the bonding agent.

Succeeding the addition of diisocyanate curative, the rheological behaviour of polyurethane cure was evaluated according to Figures 6.12 and 6.13. The connotations of  $\tan \delta$  indicate the incipient gelation point at its peak maximum. In relation to the catalysed system, this occurs at 39mins, whilst the uncatalysed equivalent displays a maximum at 169mins. Gelation according to  $\tan \delta$  occurs prior to the intercept of  $G'$  and  $G''$ , which is also a valid interpretation of the gel point. Values determined by the intercept method typically exceed that of the prior technique, as gelation of a thermosetting resin is not instantaneous and occurs over a period of time.<sup>43</sup> The gel point of a particular system may therefore vary depending on the method applied. Regardless of this, as gelation is approached, the viscosity of the systems deviates towards a higher value. This results from an increase in molecular weight, following polymerisation of HTPB and IPDI. The cross-linking reaction generates a rapid increase in molecular weight which translates to the rate of viscosity change.

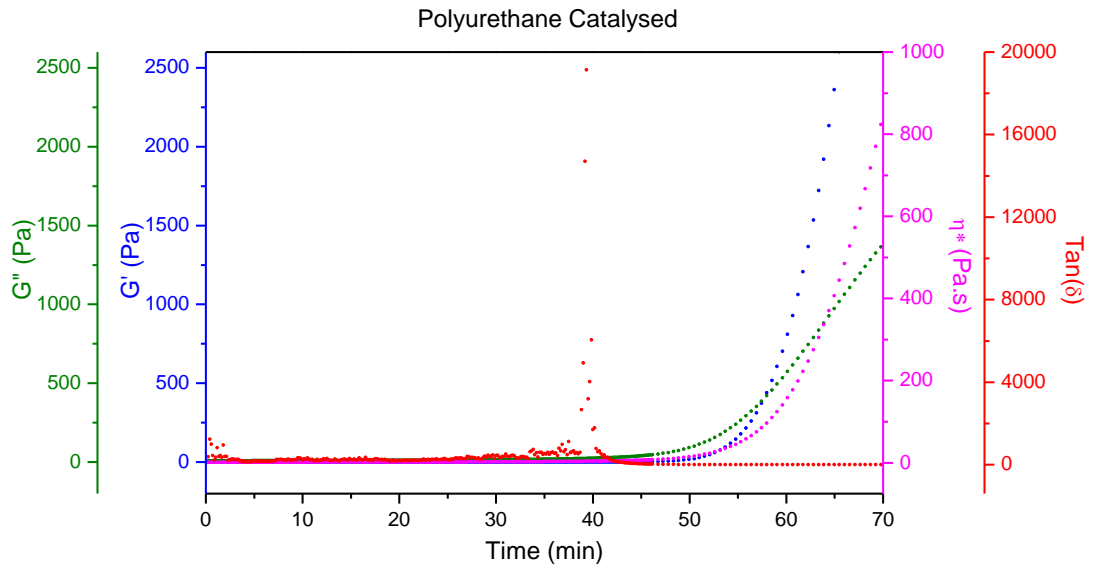


**Figure 6.12.**  $G'$ ,  $G''$ ,  $\eta^*$  and  $\tan \delta$  versus cure time for catalysed polyurethane.

The elastic modulus  $G'$  represents the build up of network formation within the polyurethane system.<sup>41</sup> This deviates from linearity at 45mins for the catalysed system, and proceeds to increase exponentially. Meanwhile, the loss of modulus  $G''$  which describes the flow behaviour of the system, appears to follow a sigmoidal curve. Initially, its rate of increase is greater than  $G'$ , until reaching an inflection point after which it decreases. This consequently creates an intersection at 58mins, which is often also interpreted as the gelation point.

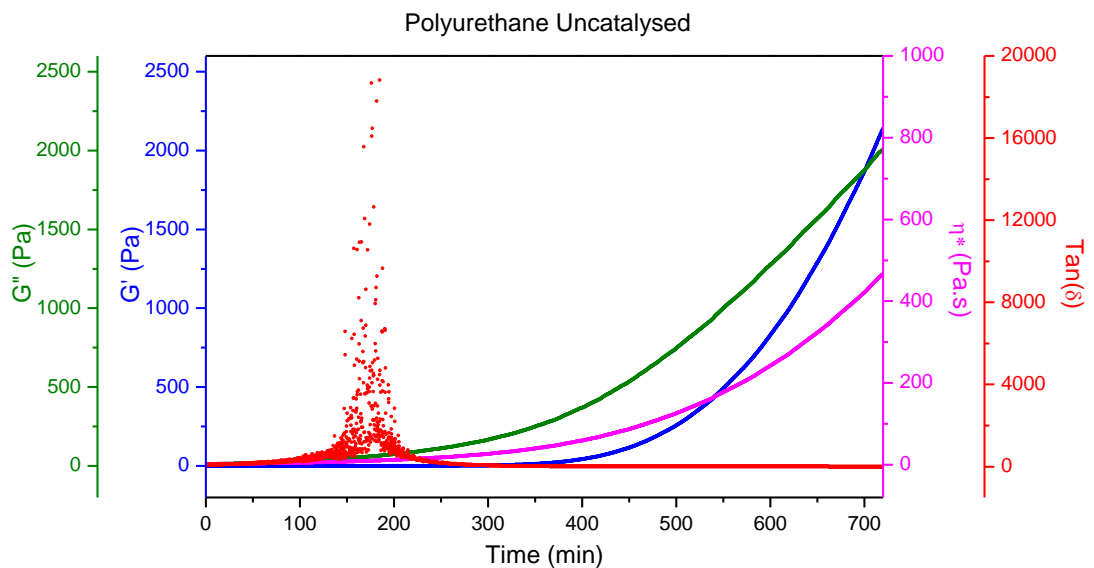


**Figure 6.13.**  $G'$ ,  $G''$ ,  $\eta^*$  and  $\tan \delta$  versus cure time for uncatalysed polyurethane.

Absence of catalyst imparts significant delay in the gelation time. This is observed to occur at 169mins, according to the maximum of  $\tan \delta$ . Further to this, the intercept at  $G' = G''$  appears after an extended delay, converging at 701mins. This indicates the impact of triphenyl bismuth on the cure kinetics of the binder system.

The complex viscosity increases exponentially with time during the polymerisation of HTPB and IPDI. This is influenced by the catalyst content, along with the functionality distribution of the prepolymer. The number of reaction sites affects the prepolymers ability to undergo reaction with the isocyanate, thus translating to the viscosity. The complex viscosity ( $\eta^*$ ) of the curing polyurethane at any given time ( $t$ ) can be expressed as the exponential function given in Equation 6.5.<sup>41, 42</sup>

$$\eta = \eta_o e^{k_\eta t} \quad (6.5)$$

Where  $\eta_o$  is the viscosity at  $t = 0$  and  $k_\eta$  is the rate constant for the viscosity increase. Plotting the natural logarithm of  $\eta$  against  $t$  yields a linear arrangement of slope equal to the rate of viscosity increase  $k_\eta$  according to Equation 6.6:

$$\ln \eta = \ln \eta_o + k_\eta t \quad (6.6)$$

This indicates viscosity build-up is a first-order process under the current set of conditions. Figure 6.14 illustrates the linearity of  $\ln \eta^*$  relating to the uncatalysed system. Conversely the catalysed system displays evidence of deviation from linearity. This may arise from the difference in chemical reactivity of functional groups, with the increased reactivity of isocyanate groups dominating viscosity build-up during initial stages.<sup>42</sup> The increased viscosity of the system causes retardation in reaction rates due to reduced freedom in chain mobility.<sup>42</sup> This manifests as deviation from linearity in the catalysed system at the time of gelation as defined by the maximum of  $\tan \delta$ .

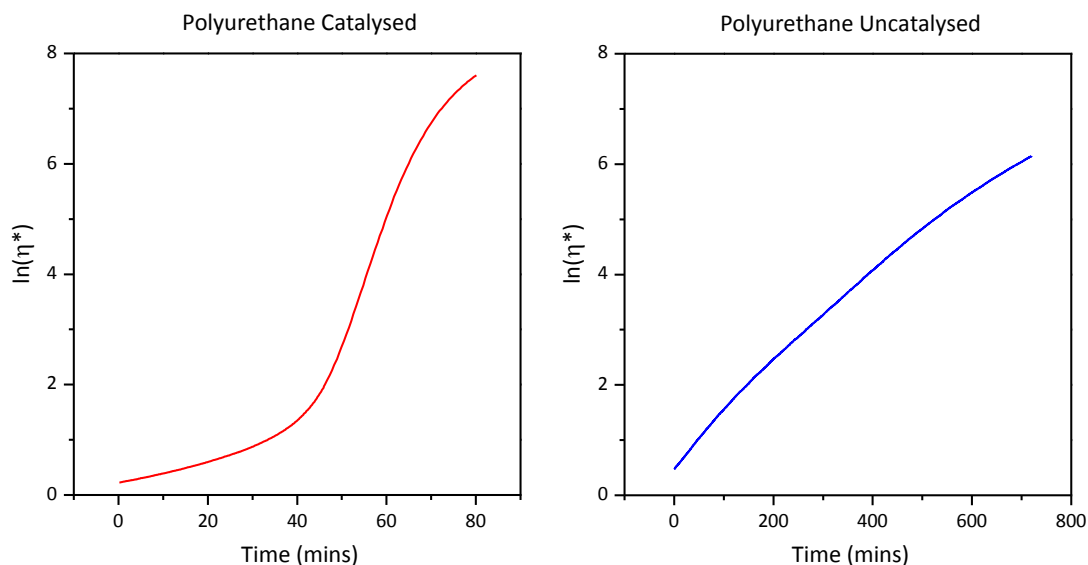


**Figure 6.14.** Plot of  $\eta^*$  vs time for catalysed/uncatalysed polyurethanes.

Altering the catalyst concentration and cure temperature, further impacts the viscosity build-up and subsequent rate constants. The effect of increasing the reaction rate is known to narrow the difference in rate constants.<sup>42</sup> This minimises the contrast in reactivity of the diisocyanates primary and secondary functionality. Thus inclusion of catalyst, while enhancing the reaction rate of both isocyanate groups, preferentially activates the less reactive group.

The uncatalysed reaction proceeds slowly, regardless of elevated cure temperature. Despite prolonged cure of 12 hours, reaction of the primary isocyanate is exclusively responsible for the rate constant. This generates the single linear plot for cure of the uncatalysed polyurethane. Similarly, increasing the temperature to 60°C increases the reactivity of both isocyanates, yet activation of the less reactive secondary group is greater in comparison. This reduces the difference in reactivity at higher temperatures, causing the rate constants to coalesce.

### 6.3.2 Investigation of Dantocol and HTPB Blends

The potential for interaction involving HTPB is limited to the prepolymer's hydroxyl functionality. As the hydroxyl equivalent weight determined was 1149.83g/eq, the

concentration of hydroxyl groups along the polymer chain is low. This limits the potential for hydrogen bonding, as substantiated by the immiscibility of Dantocol and HTPB. In the absence of reasonable association between components, the potential for hydrogen bonding is limited.<sup>44</sup> Coupled with the ability of Dantocol to migrate towards filler particles within the prepolymer, these observations suggest interaction with HTPB is negligible. To confirm this hypothesis and exclude unexpected reaction, characterisation of hydroxyl blends was performed.

### 6.3.2.1 Characterisation of Blends

Spectroscopic techniques were applied to investigate potential interaction of blends. This involved initial inspection of the  $^1\text{H}$  NMR spectrums characteristic hydroxyl region. Figure 6.15 indicates hydroxyl end groups associated with *cis* (4.17ppm), *trans* (4.08ppm) and *vinyl* (3.59ppm) units. Chemical shifts are consistent with neat HTPB, while hydroxyl bands at 2.92ppm and 2.68ppm represent Dantocol. Due to the concentration of bonding agent, peaks show reduced intensity. Absence of deviation within the hydroxyl region is reflective of earlier conclusions. This was reflected within the  $^{13}\text{C}$  NMR spectrum, indicating the chemical shifts associated with Dantocol. Along with peak consistency, negligible deviation was observed between the blend and individual components.

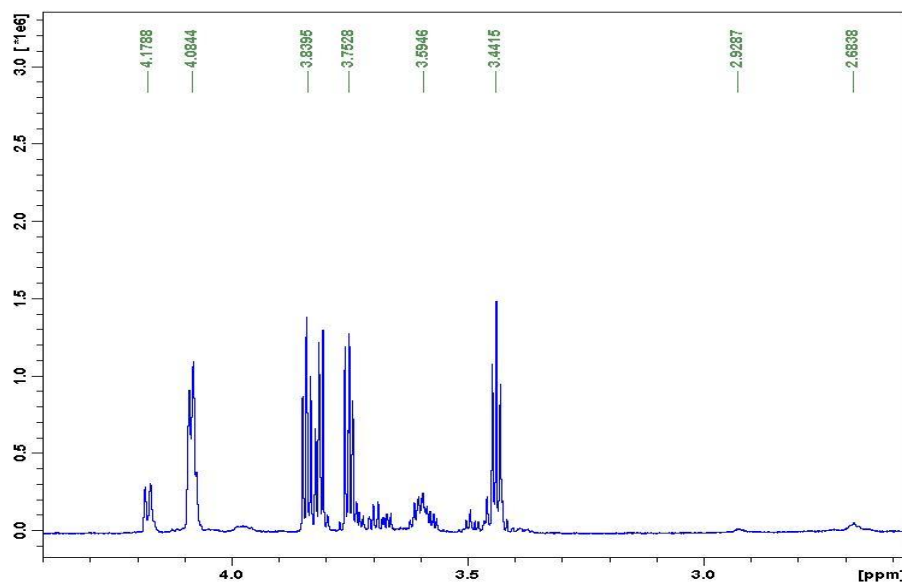


**Figure 6.15.**  $^1\text{H}$  NMR of Dantocol and HTPB blend hydroxyl region in chloroform-*d*.



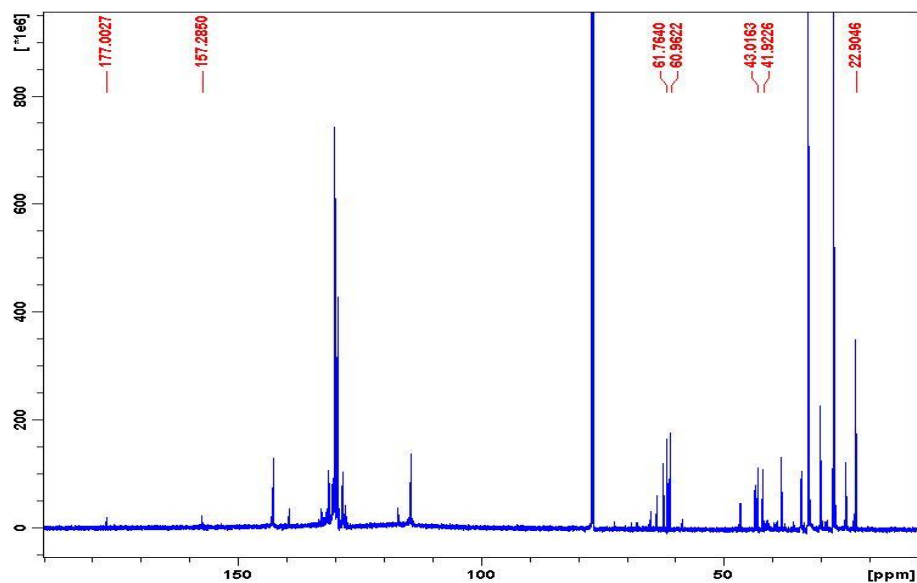


**Figure 6.16.**  $^{13}\text{C}$  NMR spectrum of Dantocol and HTPB blend in chloroform-*d*.

Results were confirmed by FTIR spectroscopy following overlay of HTPB and the comprising blend. Spectra appeared unchanged, with the exception of carbonyl vibrations associated with Dantocol. All remaining bands are consistent with HTPB, indicating the inability of elevated temperature to promote reaction. As expected, this confirms the polyol is unaccountable for incorporating Dantocol within the binder system. Furthermore, the potential for HTPB to participate in intermolecular interactions is dismissed following reaction with isocyanate. Consequently no further investigation of blends was required.

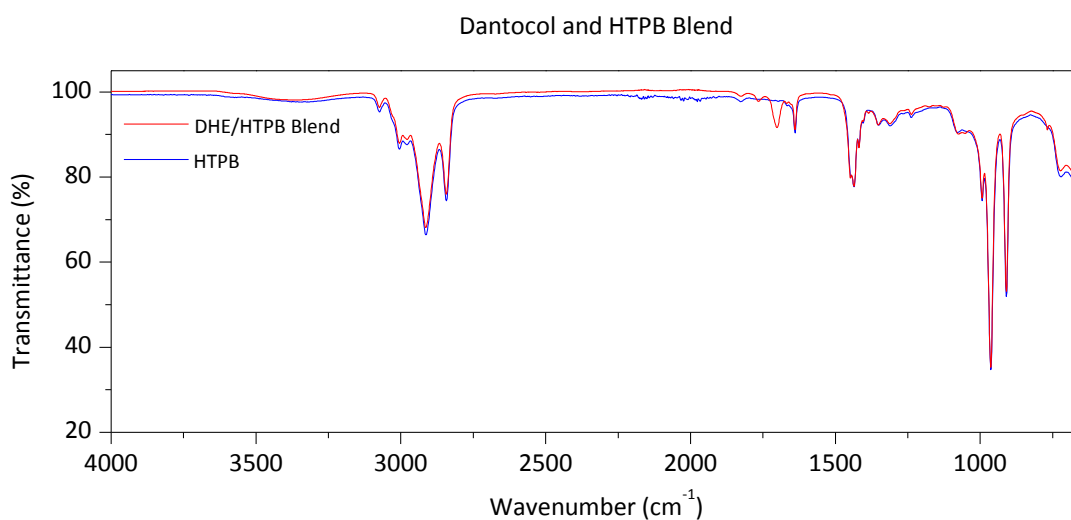
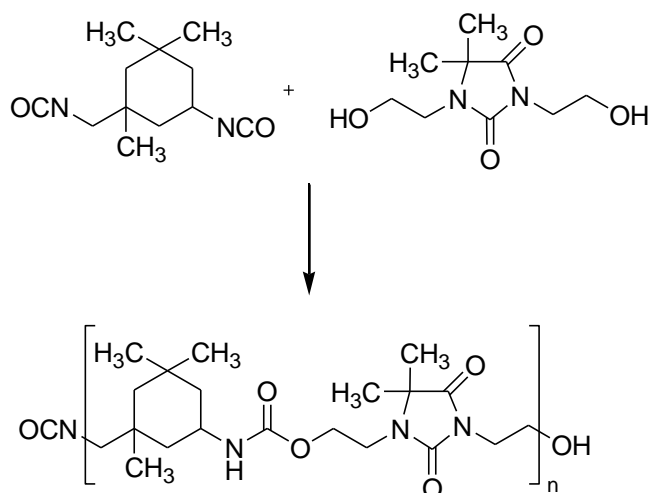


**Figure 6.17.** IR overlay of HTPB and Dantocol blend.

### 6.3.3 Polymerisation of Dantocol and Isophorone Diisocyanate

The likely method for incorporation of Dantocol within the binder system is through reaction with IPDI. This was investigated at an equivalent NCO:OH ratio, under standard PBX mixing conditions. Separation occurred following mixing of constituents, again indicating immiscibility. This impedes polymerisation with exception to that occurring at the interface region. Chemical reactivity between the bonding agent's hydroxyl groups and isocyanates is consequently regarded as slow. Despite this, prolonged curing enables urethane linkages formed at the interface to alter polarity, thus increasing solubility. This occurs via step polymerisation, described in reaction Scheme 6.4.



**Scheme 6.4.** Polymerisation of IPDI with Dantocol.

As immiscibility impedes curing and prevents polymerisation reaching completion, adduct formation was attempted to resolve the issue. Applying the two step addition process was proven effective in increasing solubility. This resolved previous difficulties to provide a linear polyurethane, rigid in structure and of high modulus. Rigidity was introduced by the absence of soft segments, otherwise derived from flexible long chain prepolymers. As Dantocol represents monomeric units, this is responsible for increasing the concentration of urethane linkages, which contribute towards hard segment formation. Segment representation is therefore accountable for the mechanical properties of polyurethanes.<sup>45</sup>

The impact of excess hard segments hinders the ability to achieve reaction completion, as unreacted isocyanates become confined.<sup>46</sup> Solvent addition was therefore applied in attempt to improve component miscibility. This functions to lower viscosity and concentration of reactive groups, thus reducing the rate of urethane formation.<sup>47</sup> Irrespective of this, viscosity build-up eventually reached a point at which no further reaction occurred. Therefore, conditions reverted to neat addition of Dantocol, IPDI and TPB, consistent with that observed for PBX formulations.

### 6.3.3.1 Catalyst

Reactivity between isocyanates and alcohols are dependent on several factors, including NCO:OH ratio and the temperature of reaction. Of further significance are the implications of catalyst addition. Catalysts are applied to PBX formulations with intent to control the rate of cure and minimise occurrence of side reactions.<sup>5</sup> The consequence of its omission may cause reactions to slow, resulting in incomplete cure. In this instance, knowledge of the kinetic behaviour for both catalysed and uncatalysed systems is important towards understanding the curing process.

The catalytic effect of triphenyl bismuth was investigated using the adduct forming technique. Cure of the polyurethane was monitored by FTIR, according to removal of the isocyanate band at  $2260\text{cm}^{-1}$ . Figure 6.18 indicates complete removal within the catalysed system, while residual isocyanate is observed amid the uncatalysed system. The ability of TPB to promote complete conversion demonstrates the efficiency of catalyst addition. This is accompanied by increased intensity of carbonyl bands, along with evolution of the amine stretch. Consequently the reaction of hydroxyl and isocyanate functionality represents a major pathway available for incorporation of Dantocol within the binder system.

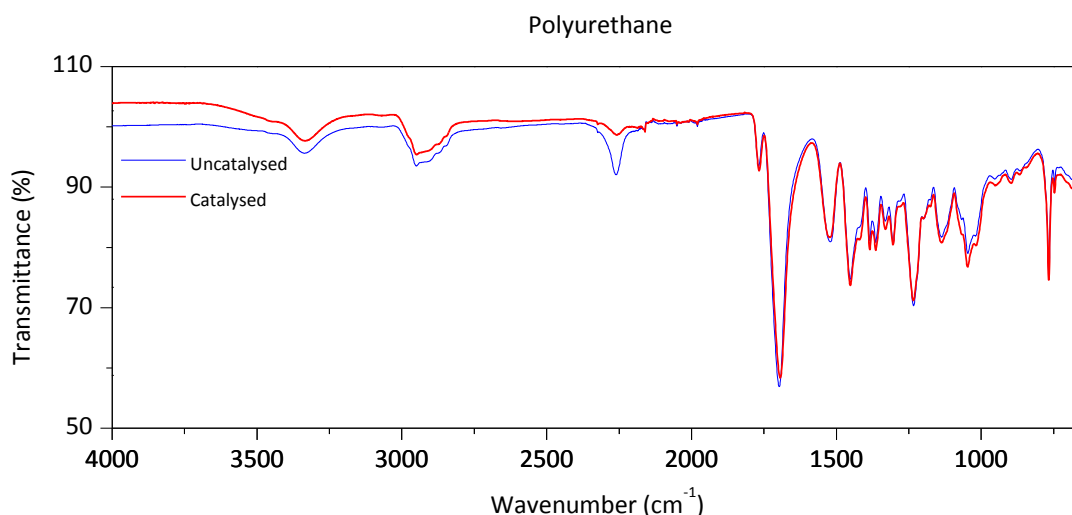


**Figure 6.18.** IR spectra of catalysed/uncatalysed polyurethane (Dantocol-IPDI).

### 6.3.3.2 Nuclear Magnetic Resonance

#### 6.3.3.2.1 NMR Spectroscopy of Isophorone Diisocyanate

IPDI consists of a mixture of *cis* and *trans* isomers, while its primary and secondary isocyanate functionality generates contrasting reactivity. This increases the complexity of reaction kinetics and subsequent polymer characterisation.<sup>48</sup> Initial polymerisation of the secondary isocyanate generates both *cis* and *trans* monourethanes. As reaction precedes, this occurs at the primary isocyanate, producing four monourethanes. These react to form diurethanes, which continue to polymerise into the polyurethane network. This complexity makes identifying isomeric configurations difficult.

Characterisation of IPDI isomers was therefore necessary to identify their contributions towards polymer morphology and reactivity. This provides a reference from which to interpret the reaction of IPDI and Dantocol. Chemical shifts associated with the diisocyanate are assigned in Table 6.8, while the occurrence of overlap was found to limit the interpretation of proton multiplicity. Consequently, IPDI peaks are often assigned to a spectra range, rather than individual appointment.<sup>49</sup> Despite this, interpretation of Figure 6.19 and 6.20 was able to identify isomers, along with their respective chemical shifts.

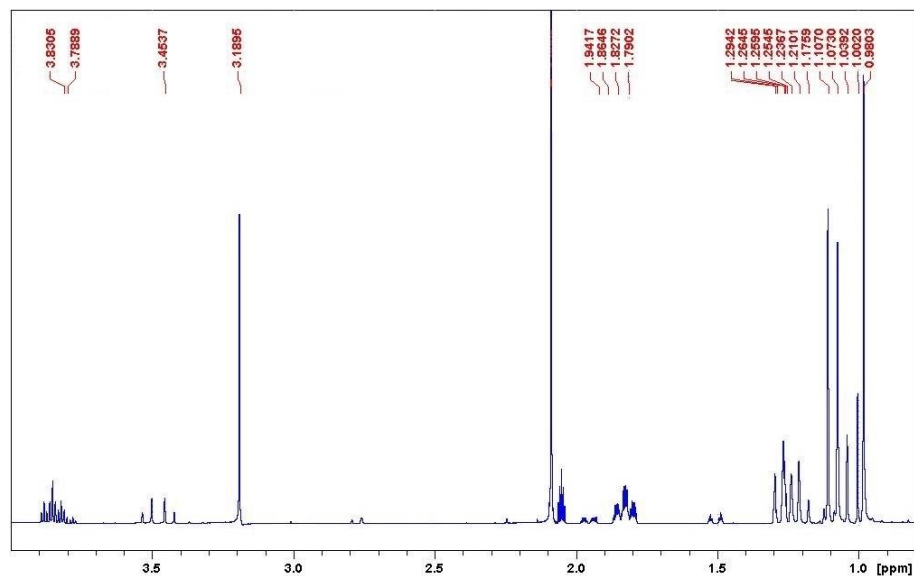


Figure 6.19.  $^1\text{H}$  NMR of isophorone diisocyanate in acetone- $d_6$ .

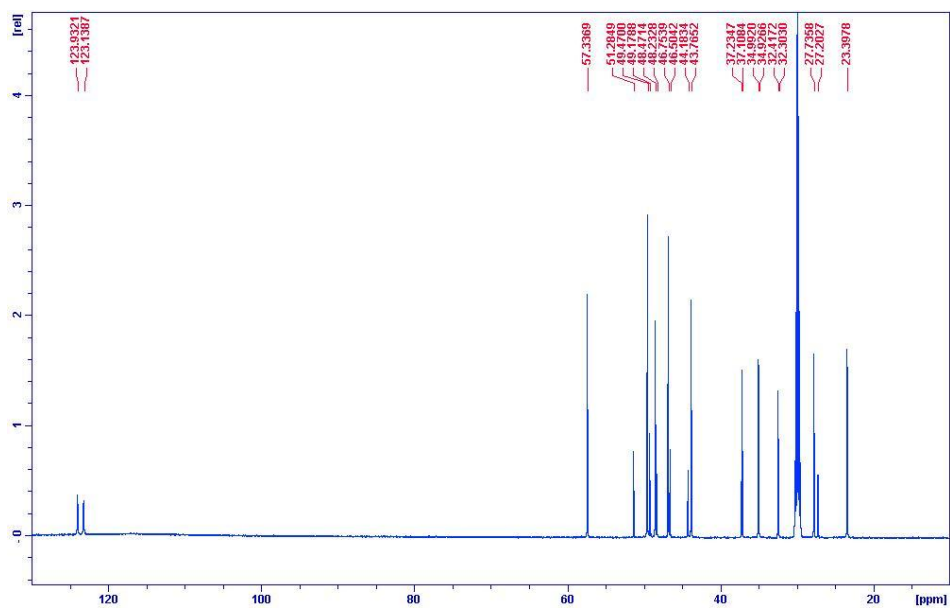
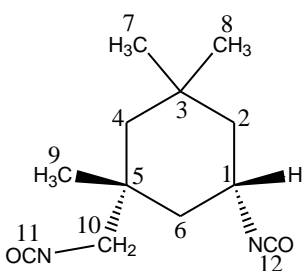
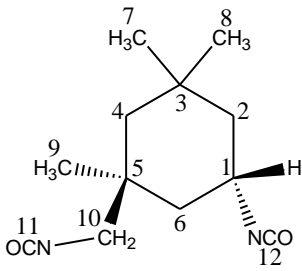


Figure 6.20.  $^{13}\text{C}$  NMR of isophorone diisocyanate in acetone- $d_6$ .

Structure	Position	$^1\text{H}$ NMR (ppm)	Position	$^{13}\text{C}$ NMR (ppm)
 <p><i>cis</i>-IPDI</p>	H-1	3.84	C-1	49.47
	H-2	1.82	C-2	48.47
	H-2'	1.21	C-3	32.41
	H-4	1.26	C-4	46.75
	H-4'	1.18	C-5	37.23
	H-6	1.79	C-6	43.76
	H-6'	1.24	C-7	27.73
	H-7	1.07	C-8	34.92
	H-8	0.98	C-9	23.39
	H-9	1.11	C-10	57.33
H-10	3.19	C-11	123.13	
			C-12	123.93
 <p><i>trans</i>-IPDI</p>	H-1	3.78	C-1	49.17
	H-2	1.94	C-2	48.23
	H-2'	1.26	C-3	32.30
	H-4	1.29	C-4	46.50
	H-4'	1.09	C-5	37.10
	H-6	1.86	C-6	44.18
	H-6'	1.25	C-7	27.20
	H-7	0.98	C-8	34.99
	H-8	1.00	C-9	29.95
	H-9	1.04	C-10	51.28
H-10	3.45	C-11	123.13	
			C-12	123.93

**Table 6.8.** Assignment of chemical shifts for IPDI isomers.<sup>6</sup>

### 6.3.3.2.2 NMR Spectroscopy of Polyurethane

Absence of cross-linking enabled solution NMR to be applied in characterisation of polyurethane configurations. Assignment of chemical shifts was possible due to prior investigation of monomer units. This assisted in identifying peaks associated with urethane linkages. Spectra also revealed broadening, consistent with dipolar coupling of polymers. This indicates the occurrence of increased geometrical constraints, which reduce molecular mobility and increase residual dipolar coupling between neighbouring proton spins.<sup>24, 41</sup> These observations are consistent with polymer formation, although prevent information being attained in reference to proton multiplicity.

Presence of polyurethane isomers become evident, due to the mass ratio of IPDI required to balance NCO:OH equivalents. This involves a tenfold increase in IPDI, compared with the mass ratio applied to HTPB based polyurethane. The difference in chemical environment associated with isomers creates minor deviation in chemical shifts. This manifests as multiple peaks, attributed to a particular proton/carbon position. These observations are evident within Table 6.9 and 6.10, depicting linear polyurethane isomers.

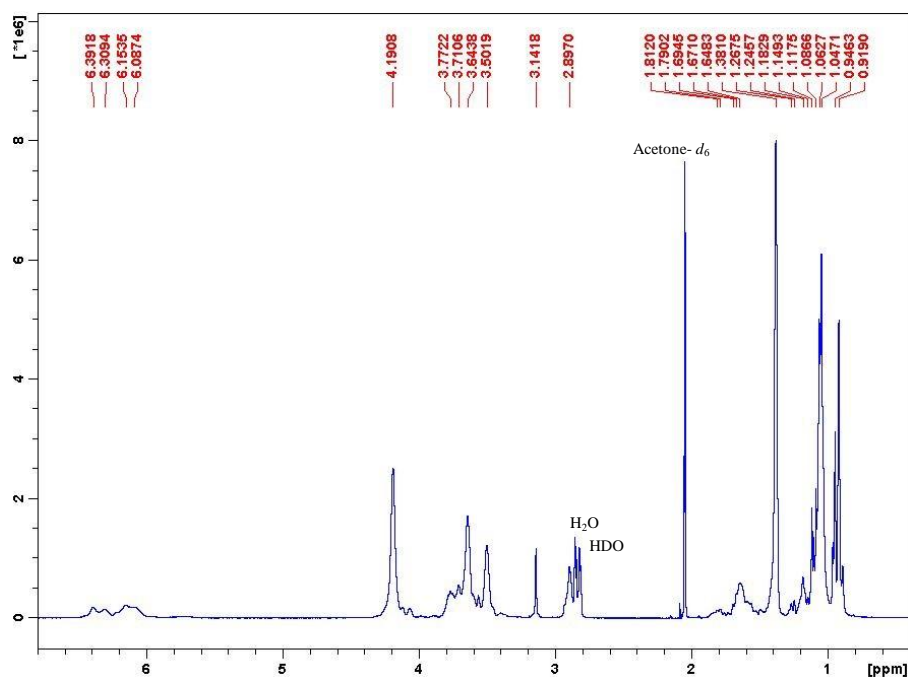


Figure 6.21.  $^1\text{H}$  NMR of Dantocol and IPDI based polyurethane in acetone- $d_6$ .

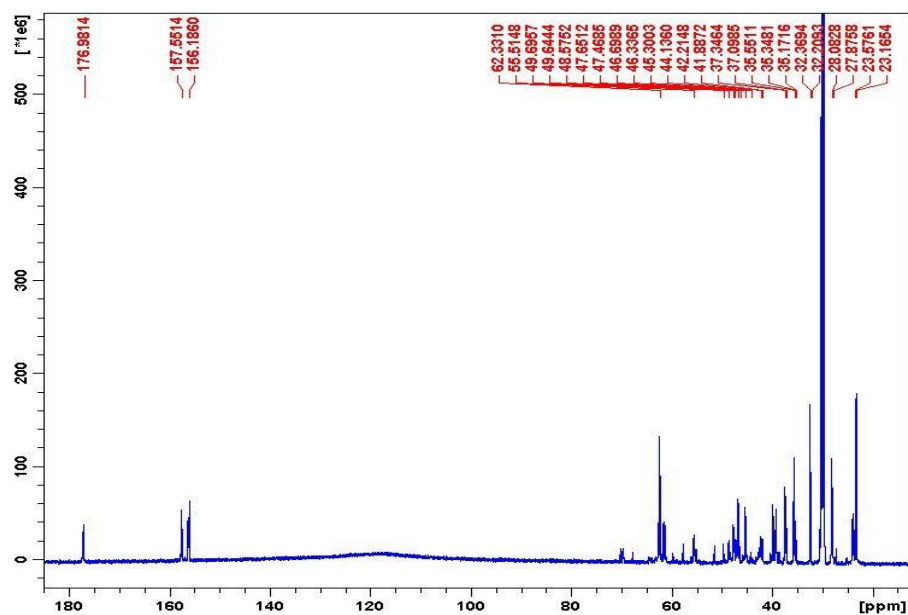
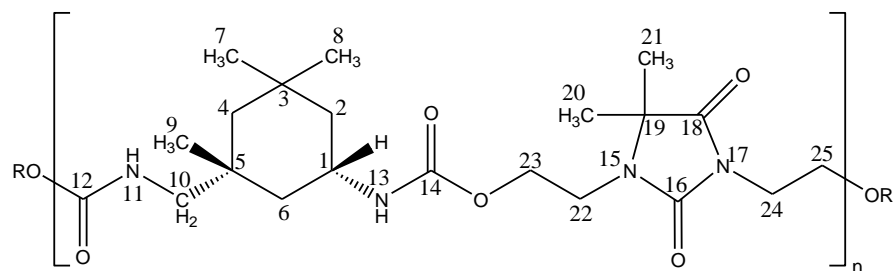


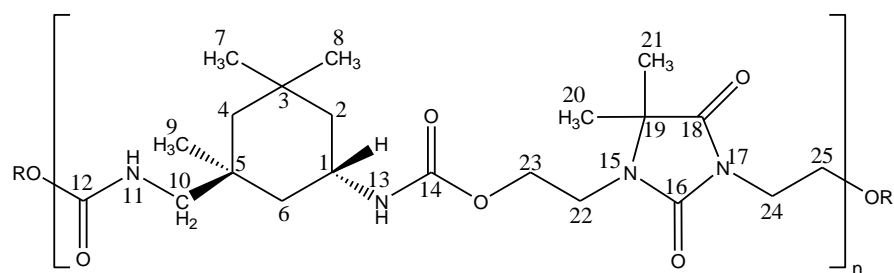
Figure 6.22.  $^{13}\text{C}$  NMR of Dantocol and IPDI based polyurethane in acetone- $d_6$ .



Position	$^1\text{H}$ NMR (ppm)	Position	$^{13}\text{C}$ NMR (ppm)
H-1	3.77	C-1	49.69
H-2	1.79	C-2	46.69
H-2'	1.24	C-3	32.36
H-4	1.69	C-4	46.69
H-4'	1.18	C-5	37.09
H-6	1.64	C-6	44.13
H-6'	1.08	C-7	27.87
H-7	1.08	C-8	35.34
H-8	0.91	C-9	23.57
H-9	1.06	C-10	55.51
H-10	2.89	C-12	156.18
H-11	6.39	C-14	156.18
H-13	6.15	C-16	176.98
H-20	1.38	C-18	156.55
H-21	1.38	C-19	62.33
H-22	3.64	C-20	23.16
H-23	4.19	C-21	23.16
H-24	3.50	C-22	42.21
H-25	4.19	C-23	47.65
		C-24	41.88
		C-25	47.46

**Table 6.9.** Assignment of chemical shifts for polyurethane based on *cis*-IPDI.<sup>6,50</sup>





Position	$^1\text{H}$ NMR (ppm)	Position	$^{13}\text{C}$ NMR (ppm)
H-1	3.71	C-1	49.64
H-2	1.81	C-2	46.33
H-2'	1.26	C-3	32.30
H-4	1.67	C-4	46.33
H-4'	1.14	C-5	37.34
H-6	1.64	C-6	45.30
H-6'	1.26	C-7	28.08
H-7	1.11	C-8	35.55
H-8	0.94	C-9	35.17
H-9	1.04	C-10	48.57
H-10	3.14	C-12	156.18
H-11	6.30	C-14	156.18
H-13	6.08	C-16	176.98
H-20	1.38	C-18	156.55
H-21	1.38	C-19	62.33
H-22	3.64	C-20	23.16
H-23	4.19	C-21	23.16
H-24	3.50	C-22	42.21
H-25	4.19	C-23	47.65
		C-24	41.88
		C-25	47.46

**Table 6.10.** Assignment of chemical shifts of polyurethane based on *trans*-IPDI.<sup>6, 50</sup>

Inspection of the amine region revealed peaks associated with urethane formation. Amines appearing at  $\delta = 6.10\text{ppm}$  represent reaction of the secondary isocyanate, while subsequent reaction of primary isocyanates produced the peak occurring at  $\delta = 6.30\text{ppm}$ . As these peaks evolve, removal of the bonding agent's hydroxyl peaks occur at  $\delta = 3.12\text{ppm}$  and  $3.26\text{ppm}$ . This region was monitored to provide an indication of reaction progress.

Polymerisation of the bonding agent's hydroxyethyl functionality prompted upfield shift in the  $\text{CH}_2$  attached to the urethane linkage. This was repeated for  $\text{CH}_2$  peaks associated with

the primary isocyanate, whereby shifts from 3.19 to 2.89ppm (*cis*) and 3.45 to 3.14ppm (*trans*) were observed. Methylene groups adjacent to urethane linkages also demonstrate broadening consistent with polymerisation.

Interpretation of the  $^{13}\text{C}$  NMR spectrum confirmed formation of linear polyurethane isomers. This was evident from the reduction of isocyanate peaks at 123.13ppm and 123.93ppm. Resonance associated with the secondary isocyanate occurs downfield from the primary group, resulting from lower electron density. This confirms suggestions the secondary isocyanate exhibits increased reactivity. Polymerisation is accompanied by carbonyl formation, appearing at 156.18ppm. The presence of urethane linkages also results in downfield shift of the adjoining  $\text{CH}_2$  peaks. This is consistent with  $^1\text{H}$  NMR, which indicates change in chemical environment, in comparison to starting material. These combined observations affirm incorporation of Dantocol proceeds via covalent bonding of the hydroxyl functionality and diisocyanate curative.

### 6.3.3.3 Fourier Transform Infrared Spectroscopy

Polymer characterisation also involved IR spectroscopy as a complementary technique to identify polyurethane formation. This confirmed the reaction of Dantocol according to vibrational bands associated with urethane linkages. Evolution of the amide I stretching vibration at  $1522\text{cm}^{-1}$  was characteristic of such reaction. This was accompanied by C=O formation, appearing at similar wavenumber to that of Dantocol. Impinging bands therefore limited information acquired from the carbonyl region.

Assignment	Intensity	Wavenumber ( $\text{cm}^{-1}$ )
$\nu\text{NH}$	m	3334
$\nu\text{C=O}$	s	1766
$\nu\text{C=O}$	s	1694
$\nu\text{Amide I}$	m	1522
$\nu\text{Amide II}$	m	1234

$\nu$  = stretch, s = strong, m = medium, w = weak

**Table 6.11.** Assignment of infrared bands for IPDI:DHE based polyurethane.<sup>34</sup>

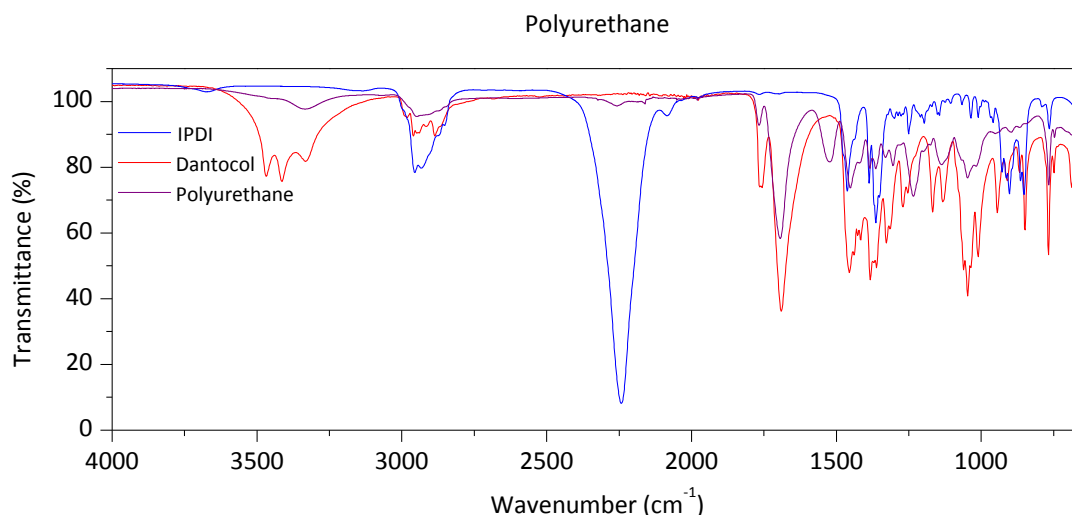


**Figure 6.23.** IR spectra of reactants IPDI, DHE and the resulting polyurethane.

Spectral overlay of starting material demonstrates the intensity of the isocyanate band. Although reactivity differs between primary and secondary functionality, the NCO stretching vibration of IPDI appears as a single band at  $2242\text{cm}^{-1}$ . This was monitored throughout the curing process as an indication of cure completion. Consumption of isocyanate groups during reaction with Dantocol results in declining intensity. This corresponds to an equivalent reduction in hydroxyl functionality. Both the removal and evolution of bands within the polyurethane spectrum therefore confirms polymerisation of Dantocol.

#### 6.3.3.4 Thermal Analysis

The polyurethane's DSC curve exhibits an initial endothermic peak at  $104^{\circ}\text{C}$ , representing the crystalline melting temperature. This occurs due to the presence of microcrystalline regions, consisting of short chain hard segments.<sup>51</sup> The major event at  $T_d = 363^{\circ}\text{C}$  depicts urethane cleavage, which initiates vaporisation of IPDI and Dantocol. In response to decomposition,  $\Delta H = 510.9\text{Jg}^{-1}$  was derived from the endothermic peak. These events are highlighted in Figure 6.24, illustrating the DSC curve of polyurethane.

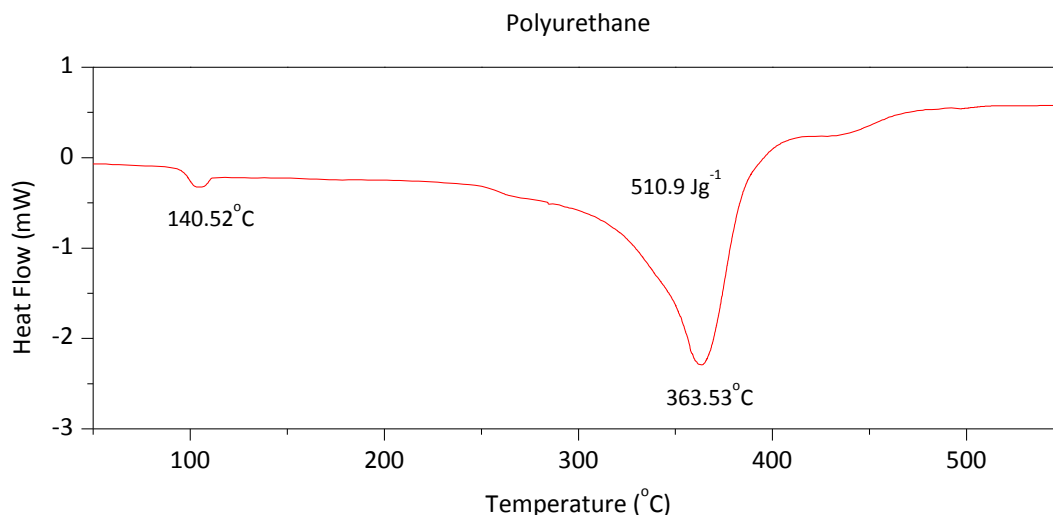


**Figure 6.24.** DSC curve of polyurethane based on Dantocol and IPDI.

Occurrence of the crystalline melting temperature provides an indication of morphological behaviour. Crystallisation of the matrix impedes polymerisation, which terminates upon hardness reaching a plateau.<sup>3</sup> Heating the polyurethane beyond this point enables movement allowing further reaction to occur. This is also observed in amorphous polymers, whereby reactions cease below the glass transition temperature.

The extent to which this enables reaction to occur is indicated by the presence of starting material, as represented by  $T_m$  peaks. Inspection of the bonding agent's characteristic melting point region reveals the absence of starting material from the polyurethane network. This typically appears as a sharp endothermic peak at  $T_m = 66^\circ\text{C}$ . As melting points are considered a reversible transition, this suggests unreacted Dantocol would be expected to generate an endothermic peak representing  $T_m$ .

### 6.3.3.5 Rheological Behaviour

Rheology was attempted to evaluate kinetics associated with urethane formation. This was complicated by adduct formation, involving stepwise addition of Dantocol. Irrespective of this, rheological behaviour was monitored at fixed intervals, while engaging oscillatory time sweep mode. The impact of urethane formation is known to have pronounced effects on molecular mobility, as monitored by changes in viscosity and elasticity.<sup>52</sup> In particular, the

reaction of short chain diols leads to aggregation of hard segment domains, causing oligomers to become less soluble within the monomer.<sup>53</sup> Heterogeneous mixtures may lead to minor deviation in exponential viscosity build-up, resulting from phase separation. Therefore, shear rate is often increased to promote dissociation of rigid urethane segments, thus enabling polymerisation to continue.

Within the current system, polymerisation of Dantocol is recognised as proceeding particularly slow. This is necessary to prevent dissociation of intermolecular forces within cast-cured PBX composites. Monomer reaction rate was reflected within the rheological behaviour, with viscosity build-up occurring over an extended period. This was such that gelation had yet to occur after curing for >12 hours at 60°C. The extended timeframe imposed limitations on the measurement of gel point at the intercept of  $G' = G''$ . These results concur with the rheological behaviour of polyurethanes derived from hydroxyl blends, investigated in Section 7.3.3. This established the addition of Dantocol to IPDI/HTPB caused prolonged gelation of the binder system.

Increasing the isocyanate concentration is known to reduce viscosity build-up of polyurethanes.<sup>41</sup> This is particularly relevant to the current system, which comprises a majority percentage of IPDI. Although 0.02% triphenyl bismuth was incorporated within formulations, the addition of catalyst was unable to sufficiently reduce the point of gelation. Irrespective of limitations encountered, results indicate significant reduction in reactivity by comparison to HTPB. This suggests reasoning as to how interactions between Dantocol and RDX remain intact within cast-cured PBX composites.

#### **6.3.3.6 Gel Permeation Chromatography**

The molecular weight of polyurethane was determined by GPC, enabling elucidation of the average number of repeat units. This is possible due to the absence of cross-linking, which facilitates solubility within the solvent phase. The resulting chromatogram demonstrates a single Gaussian peak, evident in Figure 6.25. This excludes the occurrence of low molecular

weight tailing, indicating an absence of unreacted starting material. Determining the number average molecular weight ( $M_n = 3461\text{Da}$ ) provides further evidence of polymerisation. This was used to calculate an average of eight repeating units, based on the molecular weight of starting material. Polydispersity ( $Pd$ ) was also found to remain relatively low, with the polyurethane displaying a value of  $Pd = 1.432$ .

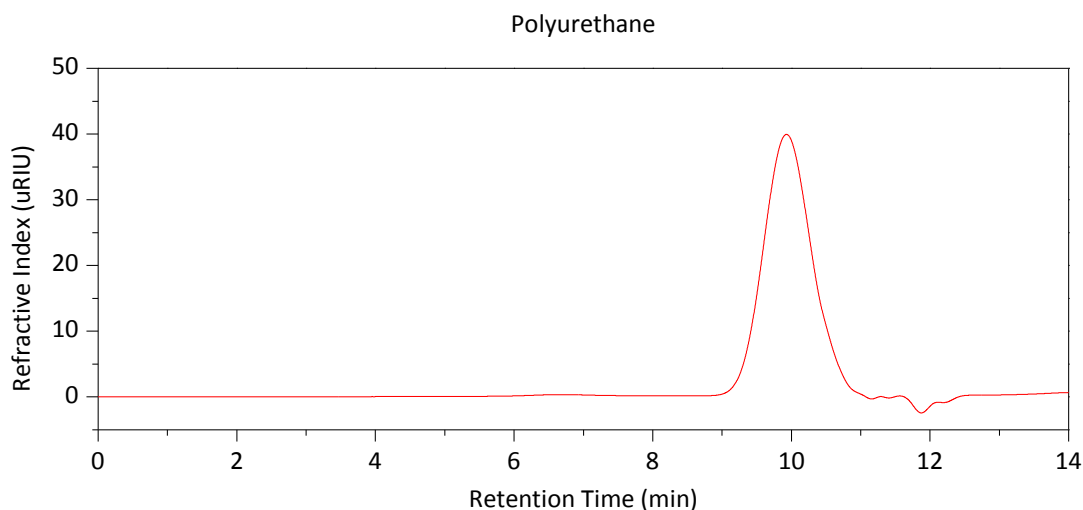


**Figure 6.25.** GPC chromatogram of polyurethane based on Dantocol and IPDI.

Peak Information	Daltons
Number Average Molecular Weight ( $M_n$ )	3461
Weight Average Molecular Weight ( $M_w$ )	4956
Z Average Molecular Weight ( $M_z$ )	6855
Z+1 Average Molecular Weight ( $M_{z1}$ )	9162
Polydispersity ( $Pd$ )	1.432

**Table 6.12.** GPC data for polyurethane based on Dantocol and IPDI.

## 6.4 Conclusion

Investigations involved a diverse approach to characterising the incorporation of Dantocol within the binder system. This initially called for the elucidation of polyurethane binder systems and their derivatives. The importance of understanding the properties of these components is critical in differentiating the mechanism involved in polymerisation of Dantocol. This also provides a reference from which to compare the impact of Dantocol upon the network's physical and chemical properties. The potential for bonding agent's

reaction was then investigated in terms of individual binder components. This succeeded in identifying covalent bonding occurring between Dantocol and IPDI.

### 6.4.1 Polyurethane Binder System

Polymerisation of HTPB and IPDI was characterised by numerous analytical techniques to evaluate the cure behaviour. The properties of HTPB were also evaluated, as it competes with Dantocol for isocyanate groups. Preliminary investigations of HTPB identified the hydroxyl equivalent weight, along with providing a background from which to interpret the impact of Dantocol. Spectroscopic analysis of HTPB and subsequent polyurethanes provided a crucial reference from which to identify the functional groups responsible for interaction between Dantocol and the binder system.

The NMR spectra of HTPB provided information regarding triad configurations, identifying the structural composition of the prepolymer. Investigation of the hydroxyl region indicated the presence of three terminal hydroxyl groups, representing *cis*, *trans*, and *vinyl* units. This was confirmed in the  $^{13}\text{C}$  spectra, revealing free radical polymerisation of HTPB favours *trans* conformations. Based on the integration values of CH-OH peaks the structural configuration of HTPB was found to comprise 56.4% *trans*, 22.5% *vinyl* and 21.1% *cis* contributions. Formation of triad sequences also emerged, resulting from random addition of monomeric butadiene units.

These results were replicated in the FTIR analysis, which also provides capabilities for determining the extent of cure. Evolution of the C=O band at  $1730\text{cm}^{-1}$  accompanied by removal of the NCO band at  $2255\text{cm}^{-1}$  provide an effective means of monitoring cure. This was applied in confirming reaction completion, following seven days curing of HTPB and IPDI.

Elucidation of thermal behaviour was investigated by TGA and DSC, identifying  $T_g$ ,  $T_m$ ,  $T_d$  and weight loss data pertaining to the binder system and prepolymer. Interpretation of these results denotes the extent of phase interaction between segments and thermal stability

required to quantify the influence of Dantocol addition. Both polyurethane and polyol exhibit low glass transition temperatures and high onset of decomposition. This reflects the thermal stability of constituents for which they're applied to cast-cured energetic material.

Decomposition of HTPB occurs in two stages, the first involving depolymerisation along with exothermic cyclisation and cross-linking of residual polyol. Secondary decomposition accounts for depolymerisation of cross-linked residue formed in the initial stage. Conversely the first stage of polyurethane decomposition represents cleavage of the urethane linkage. IPDI is subsequently vaporised, while HTPB replicates both stages of decomposition.

Investigations into the rheological behaviour of polyurethane cure provided unique insight into polymerisation of the binder system. This demonstrated critical points of conversion, including viscosity build-up, gel point and the influence of catalyst. Establishing the kinetic parameters of urethane formation provides information necessary to identify implications of bonding agent addition. This facilitates comparison of mechanisms involved in the polymerisation of IPDI and systems comprising dual alcohol components.

#### **6.4.2 Dantocol and HTPB Blends**

Preparation of the hydroxyl blend resulted in separation of components, indicating limited interaction between Dantocol and HTPB. This is inferred by the absence of reasonable association between components, thus negating the potential for hydrogen bonding.<sup>44</sup> Interpretation of spectroscopic techniques confirmed this observation as neither deviation or evolution of peaks occurred. Instead, this produced spectra consistent with overlaying individual components.

As the potential for interaction of HTPB is limited to its hydroxyl functionality, removal during polymerisation eliminates this possibility. Therefore the capacity to engage in hydrogen bonding is eliminated in respect to the polymeric chain. This leaves reaction with isocyanate as the available pathway for incorporation of Dantocol within the binder system.



### 6.4.3 Dantocol and IPDI Polymerisation

Polymerisation of Dantocol and IPDI was determined to yield linear polyurethane isomers of crystalline structure. This occurs independent of catalyst addition, although adduct formation was necessary to achieve reaction completion. The extent of conversion was determined by spectroscopic techniques, by monitoring the intensity of isocyanate peaks. This was accompanied by evolution of amine, amide and carbonyl bands associated with urethanes.

Thermal analysis of the polyurethane revealed a crystalline melting point at  $T_m = 104^\circ\text{C}$ . Crystalline behaviour reflects curing of monomeric compounds which contribute towards the formation of hard segments. This impedes polymerisation, as reactive groups are confined within rigid domains. Despite the issue, reaction completion was achieved according to removal of endothermic peaks from the  $T_m$  region of starting material. Cleavage of the urethane linkage at  $T_d = 363^\circ\text{C}$  was ultimately observed to demonstrate the polyurethanes high thermal stability.

The rate of urethane formation was investigated according to rheological behaviour. This confirmed polymerisation of Dantocol and IPDI occurs over an extended period, irrespective of catalyst addition. As urethane linkages are formed, polarity of components are altered, thus increasing solubility. The result of low reactivity enables intermolecular forces between Dantocol and RDX to remain intact following exposure to isocyanate. This is necessary for the bonding agent to achieve interfacial adhesion within cast-cured PBX composites.

The polyurethane chain was determined to comprise an average of eight repeat units, based on the GPC chromatogram. This was also used to establish the number average molecular weight ( $M_n = 3461\text{Da}$ ). Results of GPC substantiate the occurrence of covalent bonding between Dantocol and IPDI. This introduces a competing reaction between the hydroxyl functionality of HTPB. Therefore the proposed mechanism was investigated within a combined system, to identify the potential for Dantocol reaction. This is addressed in Chapter 7, describing the incorporation of Dantocol within cast-cured PBX composites.

## 6.5 References

1. Yee, R. Y.; Adicoff, A., Polymerization kinetics in propellants of the hydroxyl-terminated polybutadiene–isophorone diisocyanate system. *Journal of Applied Polymer Science* **1976**, *20* (4), 1117-1124.
2. Dr. Rudolf Meyer, J. K., Dr.-Ing. Axel Homburg, Explosives (Sixth Edition). sixth ed.; Wiley: Weinheim, 2007.
3. Haska, S. B.; Bayramli, E.; Pekel, F.; Özkar, S., Mechanical properties of HTPB-IPDI-based elastomers. *Journal of Applied Polymer Science* **1997**, *64* (12), 2347-2354.
4. Akira Iwama., K. H., Terue Takahashi., Kiyoshi Matsui., Kazunari Ishiura., Hydrogenated Hydroxy-Terminated Polyisoprene as a Fuel Binder for composite solid propellants. *Propellants, Explosives, Pyrotechnics* **1996**, *21* (1), 43-50.
5. Catherine, K.; Krishnan, K.; Ninan, K., A DSC Study on Cure Kinetics of HTPB-IPDI Urethane Reaction. *Journal of Thermal Analysis and Calorimetry* **2000**, *59* (1), 93-100.
6. Prabhakar, A.; Chattopadhyay, D. K.; Jagadeesh, B.; Raju, K. V. S. N., Structural investigations of polypropylene glycol (PPG) and isophorone diisocyanate (IPDI)-based polyurethane prepolymer by 1D and 2D NMR spectroscopy. *Journal of Polymer Science Part A: Polymer Chemistry* **2005**, *43* (6), 1196-1209.
7. Park, S. H.; Lee, J. S.; Suh, K. D., Low density polyethylene with an isocyanate functional group. *Journal of Materials Science* **1998**, *33* (21), 5145-5148.
8. Takada, K.; Matsuya, H.; Masuda, T.; Higashimura, T., Gas permeability of polyacetylenes carrying substituents. *Journal of Applied Polymer Science* **1985**, *30* (4), 1605-1616.
9. Korah Bina, C.; Kannan, K. G.; Ninan, K. N., DSC study on the effect of isocyanates and catalysts on the HTPB cure reaction. *Journal of Thermal Analysis and Calorimetry* **2004**, *78* (3), 753-760.
10. Dusek, K.; Spirkova, M.; Havlicek, I., Network formation of polyurethanes due to side reactions. *Macromolecules* **1990**, *23* (6), 1774-1781.
11. Daniel, M. A. *Polyurethane binder systems for polymer bonded explosives*; DSTO-GD-0492; DSTO: Weapons Systems Division, **2006**.
12. Brunette, C. M.; Hsu, S. L.; Rossman, M.; MacKnight, W. J.; Schneider, N. S., Thermal and mechanical properties of linear segmented polyurethanes with butadiene soft segments. *Polymer Engineering & Science* **1981**, *21* (11), 668-674.
13. Werner Rasshofer, R. P. Process for the production of urethane-modified polyisocyanate. 4587322, 1985.
14. Reiner, P.; Werner, R. Process for the production of urethane-modified polyisocyanate compositions using a hydantoin having two hydroxyl alkyl substituents. US Patent 4,587,322, **1987**.
15. Morgan, C. R. Hydantoin-containing polyene compositions. US Patent 4,112,233, **1978**.

16. Coseri, S., The Effect of Various Additives on the Kinetic and Reaction Mechanism between Ethanol and Phenylisocyanate. *High Performance Polymers* **2007**, *19* (5-6), 520-530.
17. Wicks, Z. W.; Appelt, M. R.; Soleim, J. C., Reaction of N-(2-hydroxyethyl) amido compounds. *Journal of Coatings Technology* **1985**, *57* (726), 51-61.
18. Hamshere, B. L.; Lochert, I. J.; Dexter, R. M. *Evaluation of PBXN-109: The explosive fill for the penguin anti-ship missile warhead*; DSTO-TN-0440; DSTO: Weapons Systems Division, **2003**.
19. Manazara, A. P., Johannessen, B., Denenholz, I.M., Characterisation of GAP Polyol and Plasticizer. In *25th International annual conference ICT*, Technologie, F.-I. F. C., Ed. Fraunhofer-Institut Fur Chemische Technologie: Germany, 1994.
20. Vilar, W. D.; Menezes, S. M. C.; Akcelrud, L., Characterization of hydroxyl-terminated polybutadiene. *Polymer Bulletin* **1995**, *35* (4), 481-488.
21. Kanakavel, M., Characterization of hydroxy-terminated polybutadienes by <sup>13</sup>C NMR. *Die Makromolekulare Chemie* **1987**, *188* (4), 845-854.
22. Ajaz, A. G., Hydroxyl-Terminated Polybutadiene Telechelic Polymer (HTPB): Binder for Solid Rocket Propellants. *Rubber chemistry and technology* **1995**, *68* (3), 481-506.
23. Provatas, A. *Characterisation and Polymerisation Studies of Energetic Binders*; DSTO-TR-1171; DSTO: Weapons Systems Division, **2001**.
24. Hailu, K.; Guthausen, G.; Becker, W.; König, A.; Bendfeld, A.; Geissler, E., In-situ characterization of the cure reaction of HTPB and IPDI by simultaneous NMR and IR measurements. *Polymer Testing* **2010**, *29* (4), 513-519.
25. Liu, K.-J.; Burlant, W., High-resolution NMR of crosslinked polymers: Effects of crosslinked density and solvent interaction. *Journal of Polymer Science Part A-1: Polymer Chemistry* **1967**, *5* (6), 1407-1413.
26. Rath, S. K.; Patri, M.; Khakhar, D. V., Structure–thermomechanical property correlation of moisture cured poly(urethane-urea)/clay nanocomposite coatings. *Progress in Organic Coatings* **2012**, *75* (3), 264-273.
27. Hatada, K.; Terawaki, Y.; Okuda, H.; Tanaka, Y.; Sato, H., Distribution of isomeric structure of CIS-trans equibinary poly(butadiene). *Journal of Polymer Science: Polymer Letters Edition* **1974**, *12* (6), 305-309.
28. Santee, E. R.; Chang, R.; Morton, M., 300 MHz proton NMR of polybutadiene: Measurement of cis-trans isomeric content. *Journal of Polymer Science: Polymer Letters Edition* **1973**, *11* (7), 449-452.
29. Elgert, K.-F.; Quack, G.; Stutzel, B., On the structure of polybutadiene: 4. <sup>13</sup>C n.m.r. spectrum of polybutadienes with cis-1,4-, trans-1,4- and 1,2-units. *Polymer* **1975**, *16* (3), 154-156.
30. Conti, F.; Delfini, M.; Segre, A. L.; Pini, D.; Porri, L., <sup>13</sup>C n.m.r. spectra of polybutadienes:2. *Polymer* **1974**, *15* (12), 816-818.

31. Harris, D. J.; Assink, R. A.; Celina, M., NMR Analysis of Oxidatively Aged HTPB/IPDI Polyurethane Rubber: Degradation Products, Dynamics, and Heterogeneity. *Macromolecules* **2001**, *34* (19), 6695-6700.
32. Kumar, N.; Jayabalan, M., Studies on the effect of extraction of isophorone diisocyanate-based segmented polyurethanes. *Journal of Chemical Sciences* **1989**, *101* (6), 455-465.
33. Sumi, M.; Chokki, Y.; Nakai, Y.; Nakabayashi, M.; Kanzawa, T., Studies on the structure of polyurethane elastomers. I. NMR spectra of the model compounds and some linear polyurethanes. *Die Makromolekulare Chemie* **1964**, *78* (1), 146-156.
34. Nagle, D. J.; Celina, M.; Rintoul, L.; Fredericks, P. M., Infrared microspectroscopic study of the thermo-oxidative degradation of hydroxy-terminated polybutadiene/isophorone diisocyanate polyurethane rubber. *Polymer Degradation and Stability* **2007**, *92* (8), 1446-1454.
35. Huang, S.-L.; Chao, M.-S.; Ruaan, R.-C.; Lai, J.-Y., Microphase separated structure and protein adsorption of polyurethanes with butadiene soft segment. *European Polymer Journal* **2000**, *36* (2), 285-294.
36. Chen, J. K.; Brill, T. B., Chemistry and kinetics of hydroxyl-terminated polybutadiene (HTPB) and diisocyanate-HTPB polymers during slow decomposition and combustion-like conditions. *Combustion and Flame* **1991**, *87* (3-4), 217-232.
37. Tingfa, D., Thermal decomposition studies of solid propellant binder HTPB. *Thermochimica Acta* **1989**, *138* (2), 189-197.
38. Bengtson, B.; Feger, C.; MacKnight, W. J.; Schneider, N. S., Thermal and mechanical properties of solution polymerized segmented polyurethanes with butadiene soft segments. *Polymer* **1985**, *26* (6), 895-900.
39. Assink, R. A.; Lang, D.; Celina, M. C., Condition Monitoring of a Thermally Aged HTPB/IPDI Elastomer by NMR CP Recovery Times. *Journal Name: Journal of Applied Polymer Science; Other Information: Submitted to Journal of Applied Polymer Science; PBD: 24 Jul 2000* **2000**, Medium: P; Size: 21 pages.
40. Huang, S.-L.; Chang, P.-H.; Tsai, M.-H.; Chang, H.-C., Properties and pervaporation performances of crosslinked HTPB-based polyurethane membranes. *Separation and Purification Technology* **2007**, *56* (1), 63-70.
41. Papadopoulos, E. Solutions to blistering: Modification of a poly(urea-co-urethane) coating applied to concrete surfaces. PhD Thesis, Flinders University, Adelaide, **2008**.
42. Sekkar, V.; Ambika Devi, K.; Ninan, K. N., Rheo-kinetic evaluation on the formation of urethane networks based on hydroxyl-terminated polybutadiene. *Journal of Applied Polymer Science* **2001**, *79* (10), 1869-1876.
43. Laza, J. M.; Vilas, J. L.; Mijangos, F.; Rodríguez, M.; León, L. M., Analysis of the crosslinking process of epoxy-phenolic mixtures by thermal scanning rheometry. *Journal of Applied Polymer Science* **2005**, *98* (2), 818-824.
44. Lee, J. Y.; Painter, P. C.; Coleman, M. M., Hydrogen bonding in polymer blends. 3. Blends involving polymers containing methacrylic acid and ether groups. *Macromolecules* **1988**, *21* (2), 346-354.

45. Tsai, Y.-M.; Yu, T.-L.; Tseng, Y.-H., Physical properties of crosslinked polyurethane. *Polymer International* **1998**, *47* (4), 445-450.
46. Henry, I.; Pascault, J.-P.; Taha, M.; Vigier, G.; Flat, J.-J., Structure and properties of polyurethane acrylate prepolymers based on hydroxy-terminated polybutadiene. *Journal of Applied Polymer Science* **2002**, *83* (2), 225-233.
47. Singh, M.; Kanungo, B. K.; Bansal, T. K., Kinetic studies on curing of hydroxy-terminated polybutadiene prepolymer-based polyurethane networks. *Journal of Applied Polymer Science* **2002**, *85* (4), 842-846.
48. Coutinho, F. M. B.; Rocha, M. C. G., Kinetic study of the reactions between hydroxylated polybutadiene and isocyanates in chlorobenzene—IV. Reactions with tolylene diisocyanate, 3-isocyanatomethyl-3, 5, 5-trimethylcyclohexyl isocyanate and hexamethylene diisocyanate. *European Polymer Journal* **1991**, *27* (2), 213-216.
49. Zhang, S.; Cheng, L.; Hu, J., NMR studies of water-borne polyurethanes. *Journal of Applied Polymer Science* **2003**, *90* (1), 257-260.
50. Bialas, N.; Höcker, H.; Marschner, M.; Ritter, W., <sup>13</sup>C NMR studies on the relative reactivity of isocyanate groups of isophorone diisocyanate isomers. *Die Makromolekulare Chemie* **1990**, *191* (8), 1843-1852.
51. Seymour, R. W.; Cooper, S. L., Thermal Analysis of Polyurethane Block Polymers. *Macromolecules* **1973**, *6* (1), 48-53.
52. Dimier, F.; Sbirrazzuoli, N.; Vergnes, B.; Vincent, M., Curing kinetics and chemorheological analysis of polyurethane formation. *Polymer Engineering & Science* **2004**, *44* (3), 518-527.
53. Navarchian, A. H.; Picchioni, F.; Janssen, L. P. B. M., Rheokinetics and effect of shear rate on the kinetics of linear polyurethane formation. *Polymer Engineering & Science* **2005**, *45* (3), 279-287.



# Chapter 7

---

Polymerisation of the binder system and PBX composites

---

Sections of this chapter were published in: Williams, C. A.; Walker, G. S.; Lochert, I. J.; Clarke, S., Investigation into the interaction of Dantocol in polymer bonded explosives and bonding agent development. *16th New trends in energetic materials*, Pardubice, Czech Republic, 2013; Vol. I, pp 399-406.

Williams, C. A.; Walker, G. S.; Lochert, I. J.; Clarke, S., Investigation into the Interaction of Dantocol in polymer bonded explosives and the Impact on Mechanical Properties. *3<sup>rd</sup> Australian energetic materials symposium*, Adelaide, Australia. 2012.

## 7.1 Introduction

Confirmation of Dantocol's ability to form urethane linkages presents the need to investigate polymerisation in the presence of HTPB. This is necessary to determine the impact of competing hydroxyl groups on the reaction with isocyanates. Subsequent characterisation of polyurethane blends, aims to identify the potential for alcohol components to form urethane linkages, in the presence of isocyanates. The occurrence of copolymerisation between components will effectively demonstrate the mechanism involved in incorporating Dantocol within the binder system.

Similar investigations were conducted by Kohga, involving reaction of glycerine within IPDI/HTPB binder systems.<sup>1</sup> The hydroxyl blend was cured upon addition of IPDI, confirming reaction of glycerine within the submix. Chemical reactivity between HTPB and IPDI was favoured over glycerine, prompting rapid formation of urethane linkages. Regardless of this, glycerine was found to react with IPDI, incorporating within the binder matrix.<sup>1</sup> The reaction pathway of polar glycerine molecules suggests a likely mechanism for that of Dantocol, as previously eluded to in Chapter 6. This is expected due to similarities between the polarity and hydroxyl functionality of both compounds.

Limitations were identified regarding glycerine's ability to undergo copolymerisation within the blend. Reaction of glycerine with IPDI was found to proceed below a mole ratio ( $\zeta$ ) equivalent to 10:1 (glycerine/HTPB). The properties of numerous blends satisfying  $\zeta \leq 10$  were investigated in terms of cure behaviour, mechanical properties and thermal decomposition.<sup>1</sup> Rheological behaviour indicted the rate of viscosity build-up decreased following addition of glycerine. This was deemed to improve the processing viscosity, and extend pot life. The extent of curing was monitored by FTIR, according to reduction of the isocyanate band. Spectra confirmed residual glycerine remaining unreacted, increased with  $\zeta$  of the triol. Thermal analysis revealed a decrease in decomposition temperature, compared to IPDI/HTPB linkages. This suggests the network structure is altered by the addition of

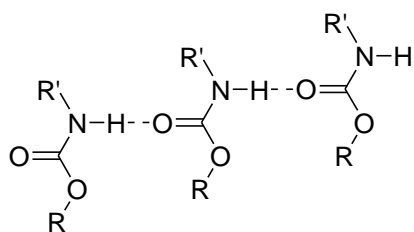


glycerine within the matrix. Incorporation of glycerine was also identified to improve the blends mechanical properties, particularly at low concentrations. An increase in tensile strength was observed due to chain extension of the binder, as glycerine contributes towards urethane linkages.

These techniques were replicated in characterising the bonding agent's reaction within polyurethane blends. The mechanism identified in the previous chapter, which involves Dantocol's multiple hydroxyl functionality and the diisocyanate curative, was investigated to determine the impact of HTPB on the potential for reaction. This is critical in determining whether the reaction proceeds in the presence of competing hydroxyl groups. The outcome of this will hopefully provide the first unequivocal evidence of Dantocol's mode of action within the binder system.

### 7.1.1 Influence of Hydrogen Bonding Within the Binder System

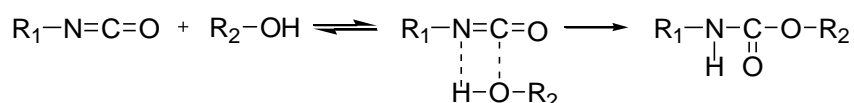
Considering the importance of hydrogen bonding towards interaction of Dantocol and filler particles, understanding the impact of intermolecular forces on the kinetics of urethane formation is crucial. Within the current binder system, hydrogen bonding occurs between the urethanes carbonyl and amide functionality, as indicated in reaction Scheme 7.1.



**Scheme 7.1.** Urethane linkages participating in hydrogen bonding.

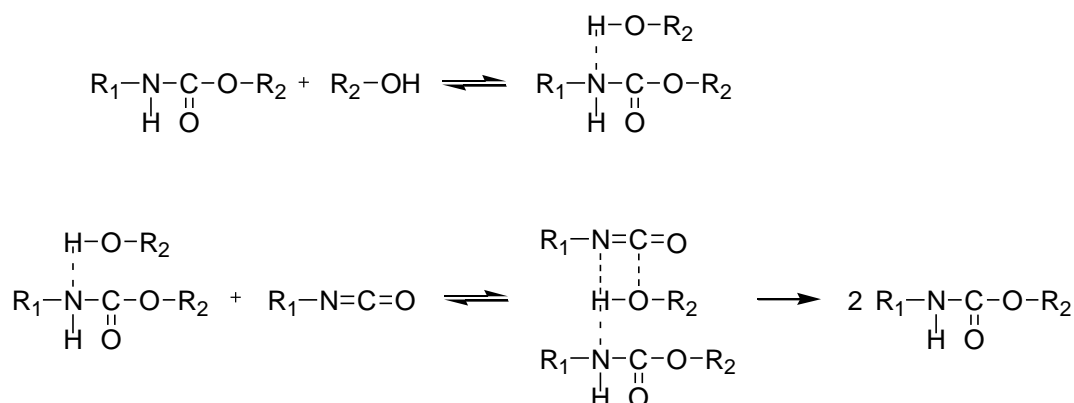
The influence of hydrogen bonding on the reaction mechanism is well documented, outlining the likely impact of intermolecular forces involving Dantocol.<sup>2-5</sup> Presence of interaction dictates the reactivity of hydroxyl groups towards isocyanates, depending on the strength of hydrogen bonding. In regards to the current system, the high chain flexibility of HTPB lends itself to strong hydrogen bonding, prior to reaction of hydroxyl groups. Polyols often impose

a catalytic effect on the rate of polyurethane formation. This was described by Baker et al. in concluding isocyanates first form an activated complex, which occurs through hydrogen bonding of hydroxyl groups.<sup>6</sup> Polarisation of hydroxyl functionality facilitates attack from the carbon atom of the activated isocyanate group. This reacts with the alcohol due to nucleophilic attack, forming a urethane linkage.<sup>5-8</sup> Rearrangement of the alcohol-isocyanate complex to produce polyurethane is acknowledged as the rate determining step, with polymerisation widely considered to follow second-order kinetics.<sup>5</sup>



**Scheme 7.2.** Reaction of alcohol and isocyanate to form polyurethane.

The degree of polarisation attributed to the reactivity of alcohols, is indicated by the magnitude of shifts observed in the IR spectra. Polarisation may also involve amine groups associated with urethane linkages. Therefore the later stages of reaction may be influenced by the autocatalytic effect of amine-alcohol complexes. Formation of hydrogen bonding and its resulting catalytic activity, is dependent on both steric factors and the basicity of the amine. Provided conditions permit arrangement of the amine-alcohol complex, polymerisation follows pathways described in reaction Scheme 7.3.



**Scheme 7.3.** Urethane catalysed reaction of polyurethane.<sup>9</sup>

The reaction rate of polyurethane formation is determined by two critical factors. Firstly the hydrogen bond association influences activation of isocyanates, while the nucleophilicity of the oxygen also contributes towards reaction rate. Therefore the rate of uncatalysed urethane reaction is largely dependent on the alcohol component.<sup>5,10</sup>

Conversely, hydrogen bonding may also contribute towards inhibiting urethane formation under separate circumstances.<sup>7</sup> Oberth and Bruenner studied the effect of hydrogen bond complexes formed within a range of chemical environments, on the rate of urethane formation.<sup>5</sup> Investigations classified solvent conditions into four groups, according to their impact on reaction rate. The first consists of alkanes and nonpolar solvents, which have no apparent effect on urethane formation. These behave as inert diluents, which enable hydrogen bonding between prepolymers to catalyse the reaction. Secondly, aromatic solvents including benzene and nitrobenzene were found to inhibit reaction of polyols. The third group consists of aprotic solvents, including ethers, ketones, nitriles and carboxylic acids. Strong interaction exists between these compounds and alcohols, which also impose an inhibiting effect. Lastly, amides, tertiary amines and dimethylsulfoxide were observed to polarise complexes, in order to catalyse reaction of polyurethanes. The strength of hydrogen bonding was most pronounced in tertiary amines, polarising hydroxyl groups of the polyol to promote increased reactivity.

Chang et al. confirmed these findings, in association with the strength of hydrogen bonding and its effect on the observed rate constant  $k_{\text{obs}}$ .<sup>7</sup> The inability of alkanes to participate in hydrogen bonding, negates their potential for impacting  $k_{\text{obs}}$ . Alternatively, aromatic solvents capable of weak hydrogen bonding, demonstrate decrease in  $k_{\text{obs}}$  of between 4 - 20 L mol<sup>-1</sup> min<sup>-1</sup>. As the strength of hydrogen bonding is increased for aprotic solvents,  $k_{\text{obs}}$  displays a decrease in magnitude of 120 - 400 L mol<sup>-1</sup> min<sup>-1</sup>. Formation of complexes involving hydrogen bonding of the alcohol and solvent result in reduced concentration of the isocyanate-alcohol complex. This imparts an inhibiting effect on polymerisation of the

binder system. Alternatively, the polarising effect of strong hydrogen bonding, such as amides, tertiary amines and dimethyl sulfoxide, produce a catalytic effect.

These effects suggest the potential implications of combining Dantocol and the binder system, along with identifying the contrasting response of hydrogen bonding towards the reaction rate. Of significance to later investigations, is the ability of hydrogen bonding to inhibit urethane formation under various conditions. This provides an early indication of theory enabling intermolecular forces between Dantocol and RDX to remain uninterrupted, in the presence of isocyanate.

### **7.1.2 Cast-Cured PBX Composites**

Since its introduction to nitramine-based composite energetic materials, Dantocol has experienced widespread use throughout the field. Despite this popularity, gaps exist within the literature regarding the bonding agent's mode of action. Consequently, the behaviour of Dantocol within cast-cured PBX composites has remained speculative until now. Investigations therefore represent the first to describe the mechanism in which Dantocol facilitates interfacial adhesion between the binder system and filler particles.

Initial investigations involving the interaction of Dantocol and individual PBX components, identified mechanisms available for achieving interfacial adhesion, within cast-cured energetic composites. This established hydrogen bonding and dipole interactions were responsible for intermolecular forces, between Dantocol and nitramine fillers. Further analysis confirmed Dantocol also participates in covalent bonding with isocyanates, thus forming urethane linkages within the binder system. Having identified the mechanisms facilitating adhesion amongst isolated components, the combined system was evaluated to shed light on competing reactions. As the bonding agent's multiple hydroxyl functionality is accountable for interaction with both filler particles and the binder system, understanding how this translates to PBX systems is pivotal to define function.

Attempts to characterise the cure chemistry of specific components within complex PBX formulations, poses significant analytical difficulty.<sup>11</sup> Under such conditions, investigations are limited to merely observing the removal of starting material, thus providing minimal understanding of relevant interactions. An alternative approach is to modify the system, such that the chemical environment is accurately mimicked. This method has the advantage of forming distinct reaction products, identifiable using analytical techniques. Consequently, the impact of RDX on reaction of Dantocol and IPDI, and the opposing effect of isocyanate on filler interaction, was evaluated with modified PBX formulations. This employed spectroscopy, microscopy and thermal analysis, to describe the behaviour of Dantocol within cast-cured PBX composites.

Perhaps the simplest method to observe the effects of bonding agent interaction, is through high resolution electron microscopy, as used by Dostanic et al. to investigate the efficiency of isocyanurate bonding agents within cast-cured composite propellants.<sup>12, 13</sup> The absence, or inefficiency of bonding agents was shown to promote dewetting, whereby oxidizer particles became separated from the binder system. This manifested as vacuole formation, exposing the oxidiser surface. While this provides evidence of bonding agent efficiency, supplementary techniques are required to characterise the mechanism of interaction.

With respect to characterising surface interactions, FTIR is recognised as a leading analytical technique, owing to its high sensitivity and signal to noise ratio.<sup>14</sup> Consequently, this was applied by Petkovic and Uscumlic, to elucidate the interaction between AP, HTPB, CTPB, HMX and a series of 1,3,5-trisubstituted isocyanurate bonding agents.<sup>14, 15</sup> Of particular relevance is the interaction of 1,3,5-*tris*(2-hydroxyethyl)isocyanurate within cast-cured composite propellants. Interpretation of FTIR spectra revealed fundamental changes occurred following the incorporation of bonding agent. Shifts in wavenumber indicated hydrogen bonding was responsible for interfacial adhesion, between the oxidizer and bonding agent. The intensity of carbonyl bands also confirmed copolymerisation of CTPB and 1,3,5-*tris*(2-hydroxyethyl)isocyanurate within the propellant system.

Alternatively, thermal analysis was applied by Kohga to investigate the potential interaction of HTPB/glycerine blends, with similar propellant composites.<sup>1</sup> Curing behaviour indicated polymerisation of IPDI and HTPB was favoured over the glycerine monomer. Although reactivity of the triols hydroxyl functionality appeared slow, urethane linkages were formed involving the diisocyanate curative. Upon incorporation within the network structure, glycerine contributed towards the formation of dangling ends. This enhanced the mobility of chain segments as indicated by the glass transition temperature. The polyurethane's increased mobility was found to enhance chain extension, thus improving the composites mechanical properties. Consequently, a similar approach was applied to the current system, identifying changes in thermal behaviour upon incorporation of Dantocol.

Based on techniques previously applied, the interaction of Dantocol within cast-cured PBX composites was evaluated. Investigations focused on fundamental spectral deviation, based upon which the bonding agents mode of action was interpreted. This follows elucidation of mechanisms involving Dantocol and individual components. Subsequent investigations therefore conclude the final stage of analysis, revealing the bonding agent's mode of action within combined systems.

## **7.2 Experimental**

### **7.2.1 Copolymerisation of Polyurethane Binder System**

Investigations involved characterisation of unfilled polyurethanes modelled on the binder system employed in PBX formulation PBXN-109. This called for reaction of IPDI and a blend of alcohols, consisting of HTPB and Dantocol. A primary blend was prepared, maintaining a NCO:OH ratio of 1.0 in accordance with PBXN-109. The alcohol content was modified to comprise equal parts HTPB and Dantocol, with the objective of identifying the bonding agent's reaction pathway within the binder system.

Copolymerisation of the blend involved mixing Dantocol (0.5eq, 0.430g) and HTPB (0.5eq, 4.570g) within a 50mL two-necked flask, equipped with magnetic stirrer and N<sub>2</sub> purge. The alcohol component was heated to 60°C, while stirring for 30 mins to achieve a homogenous mixture. IPDI (1eq, 0.884g) was charged to the reaction vessel and mixed under vacuum for 1 hour. Following this, the viscous solution was cast into 50mm Teflon moulds and cured at 60°C for 7 days under N<sub>2</sub> purge. Curing generates a translucent polymer of rubbery consistency.

In addition to the primary blend, a series of polyurethanes containing sequential HTPB/Dantocol equivalents were prepared. The molar ratio  $\zeta$  of supplementary formulations are detailed in Table 7.1, with each maintaining an equal NCO:OH ratio. Both processing and cure conditions were replicated from the original procedure. This involved mixing the alcohol blend at 60°C, followed by addition of IPDI under vacuum. Polyurethanes were cured for 7 days at 60°C under nitrogen purge. On inspection the resulting polymers displayed increased flexibility, proportional to the HTPB content. Contrary to this, Dantocol contributes towards the formation of hard segments, introducing rigidity within the system. Therefore, polyurethanes predominantly containing Dantocol as the alcohol component, exhibit increased brittleness.

Mole Ratio IPDI/HTPB/DHE	Mass Fraction (%)		
	IPDI	HTPB	DHE
1.0 : 1.0 : 0.0	8.81	91.19	-
1.0 : 0.8 : 0.2	10.56	87.39	2.05
1.0 : 0.6 : 0.4	13.16	80.65	5.12
1.0 : 0.5 : 0.5	15.02	77.68	7.31
1.0 : 0.4 : 0.6	17.48	72.32	10.20
1.0 : 0.2 : 0.8	25.99	53.78	20.23
1.0 : 0.0 : 1.0	50.69	-	49.31

**Table 7.1.** Mass fraction of polyurethane formulations.

Formulations were repeated in the presence of catalyst to evaluate its impact on polymerisation of the blend. Triphenyl bismuth was applied at concentrations of 0.02% w/w,

ensuring consistency with PBXN-109. Addition of catalyst occurred alongside HTPB and Dantocol, during the initial mixing stage. Vigorous stirring was required to ensure adequate distribution of triphenyl bismuth within the submix. Post cure characterisation indicates the addition of catalyst promotes reaction completion amongst the blends. This was monitored by FTIR to identify removal of the isocyanate peak, consumed during polymerisation.

## 7.2.2 Curing of Polymer Bonded Explosives

The composition of PBX formulations was modified to include the binder system, energetic filler, cure catalyst and bonding agent. This served to isolate spectral deviation to interactions propagating from components under investigation. All remaining conditions were replicated in line with DSTO formulation PBXN-109. This involved charging HTPB and Dantocol to a 50mL two-neck flask, equipped with magnetic stirrer. Having removed the metal fuel and other additives, the mass fraction of remaining components increased according to Table 7.2. Addition of catalyst was then performed, with 0.02% TPB mixed for 28mins within previously combined alcohols. Isothermal conditions were maintained through mixing, with temperatures of 60°C applied as stipulated in PBXN-109.<sup>16</sup>

Sample	Mass Fraction (%)					Bonding Agent (% Filler Mass)
	RDX	IPDI	HTPB	DHE	TPB	
PBXN-01	80	1.76	18.24	-	0.02	-
PBXN-02	80	1.94	17.85	0.21	0.02	0.26
PBXN-03	80	3.46	14.54	2.00	0.02	2.50
PBXN-04	80	5.16	10.84	4.00	0.02	5.00
PBXN-05	80	8.56	3.44	8.00	0.02	10.00
PBXN-06	80	10.14	-	9.86	0.02	12.30

**Table 7.2.** Formulation of cast-cured PBX composites.

The addition of RDX was performed in 50%, 25% and 25% increments, introduced at 13min intervals. This produced a well dispersed slurry, which after receiving an initial scrape down, was mixed for an additional 30mins. Diisocyanate curative was combined last to ensure adequate dispersal of constituents and avoid premature curing from exposure to moisture. The mass required was determined from the stoichiometric ratio of NCO:OH, along with the



combined mass of the binder system. This demanded the binder system account for 20% of the total mass. Removal of metal, plasticiser and other ingredients was responsible for increasing the value from 16% applied in PBXN-109. Upon addition of final ingredients, further mixing was performed, after which the vessel was scraped down and mixed for an additional 15mins.

The uncured submix was cast into Teflon moulds and heated at 60°C for 7 days under N<sub>2</sub>. Uniform distribution of constituents is necessary to ensure characterisation provides an accurate representation of cast-cured PBX composites. This avoids agglomeration, thus maintaining an even dispersal of RDX within the matrix. To ensure this occurs, curing must not be delayed, as this can result in settling of filler particles.<sup>17</sup> On completion of cure, resulting composites exhibit slight flexibility in response to network formation.

## **7.2.3 Characterisation of Composites**

### **7.2.3.1 Fourier Transform Infrared Spectroscopy**

Investigation of Dantocol's mode of action was conducted using a Nicolet Nexus 8700 FT-IR Spectrophotometer, equipped with MCT/A detector. This involved monitoring the reaction of Dantocol and IPDI amid presence of PBX components. Characterisation focused on evolution of features associated with urethane linkages, and corresponding removal of isocyanates. Presence of integration involving Dantocol and RDX, was also identified following deviation in participating bands. Spectra were acquired at a sample gain of 2.0 over a fixed number of 128 scans. Resulting spectra were collected between the range of 650 - 4000cm<sup>-1</sup>, at a resolution of 2.0 cm<sup>-1</sup>.

#### **7.2.3.1.1 Spectral Subtraction**

Interpretation of spectra involved application of the OMNIC version 7.3 software suite. This facilitated data manipulation, in order to distinguish between spectral features. Functionality associated with the reaction of Dantocol was consequently identified employing spectral

subtraction. This is commonly applied in removal of individual components, from that of complex spectra.<sup>18</sup> Algorithms require selection of the desired spectrum, along with a reference spectrum comprising the PBX component nominated for removal. The later is subtracted to establish the corresponding difference spectrum, after which adjustments are made to the subtraction factor.

### **7.2.3.2 Differential Scanning Calorimetry**

Thermal behaviour of PBX composites and associated binder system was investigated using a TA instruments MDSC-2930 differential scanning calorimeter. Instrumentation was calibrated to the  $T_m$  endotherm of indium to determine the cell constant. Cooling of the DSC cell was achieved using a liquid nitrogen cooling accessory (LNCA), under continuous  $N_2$  flow of  $100\text{mL min}^{-1}$ . Experimental parameters involved lowering the temperature to  $-100^\circ\text{C}$  for 3mins prior to heating at  $10^\circ\text{C min}^{-1}$ . Acquisitions were then interpreted using TA Instruments Universal Analysis software. Calculation of  $T_g$  was defined as the temperature corresponding to the midpoint of the heat capacity change.

### **7.2.3.3 Rheology**

Investigation of the binder systems rheological behaviour was determined using a TA Instruments AR 2000 Advanced Rheometer. This employed a  $2^\circ$  cone of length 20mm, operating in oscillatory time sweep mode. Polymerisation of the binder system was investigated at  $60^\circ\text{C}$  to maintain consistency with PBXN-109. Isothermal conditions were maintained throughout cure, using a Peltier plate accurate to  $\pm 0.2^\circ\text{C}$ .

Oscillatory strain sweep mode was used to identify the Linear Viscoelastic Region (LVR) from which strain was selected. Based on these results, 10% strain was applied to limit disruption to the network structure during cross-linking. Pre-shearing was performed prior to analysis, eliminating shear and structural history. The curing behaviour of the binder system was then examined in oscillatory time sweep mode, at a frequency of 1Hz. Information collated was analysed using TA Instruments Data Analysis software.

#### **7.2.3.4 Scanning Electron Microscopy**

The surface morphology of cast-cured PBX composites was investigated using a CamScan MX2500 SEM, equipped with Energy Dispersive X-ray (EDX). Composites were pretreated with 5nm of platinum, deposited utilising a Quorumtech K757X Sputter Coater. Conductive samples were then exposed to an acceleration voltage of 10kV, over a spot size of 4.00nm. The adjustment of settings was controlled using MaXim 4 software to produce high resolution images. This indicated the presence of surface deformations and subsequent impact of Dantocol addition.

### **7.3 Results**

#### **7.3.1 Copolymerisation of Polyurethane Blend**

Polymerisation of IPDI and hydroxyl blends was investigated in regards to determining the mechanism involving Dantocol and the binder system. The primary polyurethane blend was based on a gum stock version of PBXN-109, prepared using a modified procedure described by Hamshere et al.<sup>16</sup> Replication of reaction conditions was necessary to provide an accurate representation of the environment encountered during processing and cure of cast-cured PBX composites. This required polyurethane blends maintain a NCO:OH ratio of 1:1. The stoichiometric equivalence impacts crosslink density, as IPDI reacts with hydroxyl groups to generate a three dimensional structure composed of urethane linkages.<sup>19</sup> The formation of polar linkages introduces intermolecular attraction between hard segments, involving hydrogen bonding of the carbonyl and amine functionality.

Throughout curing, the bonding agent's hydroxyl functionality may participate in hydrogen bonding with the amine or carbonyl groups that compose urethane linkages. Instances where the strength of interaction is sufficient to cause polarising effects, the reaction is catalysed according to Section 7.1.1. This is important in understanding the mechanism involved in polymerisation of the blend.

### 7.3.1.1 Fourier Transform Infrared Spectroscopy of Polyurethane blend

Reaction of polyurethane was monitored through the consumption of isocyanate groups, as indicated by decrease in the intensity of  $\nu_{\text{NCO}} = 2262\text{cm}^{-1}$ . This is evident in Figure 7.1, revealing a steep decline in the  $\nu_{\text{NCO}}$  intensity as polymerisation proceeds. Unlike the catalysed system, the isocyanate band remains visible after curing of the uncatalysed system. In the absence of catalyst the activation energy is greater; therefore requiring additional energy to reach completion. Furthermore, as the reaction of Dantocol and IPDI proceeds the reduction in local molecular motion impedes reaction during the later stages of cure.

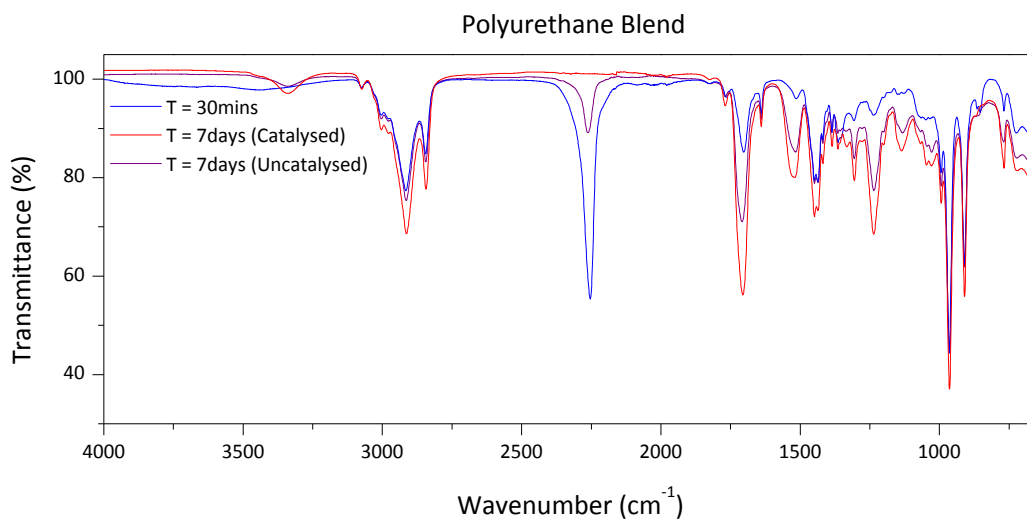


**Figure 7.1.** FTIR spectra of the IPDI/HTPB/DHE polyurethane blend.

Thermal energy is required for urethane segments to move in respect to one another, thus enabling reaction of the remaining prepolymer. Inadequate temperatures to promote movement consequently result in reaction termination.<sup>20</sup> This contributes towards isocyanate groups becoming trapped within the polyurethanes hard segments. Contrary to the polymeric structure of HTPB, the bonding agents short chain causes the diol to incorporate within the hard segment, following reaction with IPDI. Therefore as the concentration of Dantocol increases, hard segments expand trapping unreacted isocyanates. This appears in the IR spectra as a residual isocyanate peak, common at increased bonding agent concentrations.

Curing of polyurethanes is largely dependent on the isocyanate applied to the binder system. Polyurethanes containing IPDI are recognised for slow curing, thus requiring the addition of

catalyst to increase reaction rate. PBXN-109 contains 0.02% triphenyl bismuth, added in the initial mixing stage to activate hydroxyl groups.<sup>17</sup> This was investigated by repeating polymerisation of blends, using an equivalent catalyst concentration. Addition of triphenyl bismuth enabled complete conversion of the isocyanate functionality. Figure 7.1 shows the overlay of catalysed and uncatalysed blends, with the inclusion of TPB resulting in removal of isocyanate bands.

The assignment of peaks in Table 7.3, indicates functional groups associated with urethane formation. Inspection of the carbonyl region reveals multiple bands, with the peak at  $1768\text{cm}^{-1}$  attributed to the bonding agents hydantoin ring. Polyurethanes also display a characteristic  $\nu\text{C}=\text{O}$  stretch, which evolves due to formation of urethane linkages. This accounts for the remaining band at  $1708\text{ cm}^{-1}$ , consisting of free and hydrogen bonded moieties. Hydrogen bonded carbonyls correspond to those located within the interior of hard segments, while appearing at lower wavenumber than observed for free bands.<sup>21</sup> Following reaction of the HTPB end groups, non-polar soft segments are unable to participate in hydrogen bonding.<sup>21, 22</sup> Removal of hydroxyl groups subsequently limits interaction between hard and soft segments, therefore simplifying characterisation of the bonding agent interaction. Along with imparting either catalytic or stabilising activity, hydrogen bonds also influence physical properties such as tensile strain, strength and elongation.

Wavenumber ( $\text{cm}^{-1}$ )	Intensity	Assignment
3490-3205	m	$\nu\text{NH}$
2914	s	$\nu\text{CH}_2$
2262	w	$\nu\text{NCO}$
1768	w	$\nu\text{C}=\text{O}_{\text{hydantoin}}$
1708	s	$\nu\text{C}=\text{O}_{\text{urethane}}$
1516	m	$\nu\text{Amide I}$
1235	m	$\nu\text{Amide II}$

$\nu$  = stretch, s = strong, m = medium, w = weak

**Table 7.3.** Assignment of infrared bands for polyurethane blend.

Presence of hydrogen bonding within the polyurethane network is qualitatively, and to some extent, semi-quantitatively determined by FTIR. This manifests as an increase in the intensity of hydrogen bonded N-H and C=O bands, which shift towards lower wavenumber.<sup>23</sup> Consequently, the magnitude of shifts are proportional to the strength of hydrogen bonding. Variation in wavenumber also indicates the contrast in proton acceptors involved in hydrogen bonding between the NH functionality.<sup>24</sup> The relative strength of intermolecular forces present within polyurethanes, remains subject to debate. Meanwhile the separation of hard and soft segments is acknowledged to arise from the degree of hydrogen bonding between hard segments. This subsequently affects the mechanical and thermal properties of the resulting polymer.

The NH stretching vibration is recognised to consist of two major bands attributed to free and hydrogen bonded moieties.<sup>24, 25</sup> Appearance of the free  $\nu_{\text{NH}}$  manifests as a shoulder at  $3438\text{cm}^{-1}$ , which is caused to diminish in intensity due to hydrogen bonded NH groups. The hydrogen bonded  $\nu_{\text{NH}}$  stretch centred at  $3336\text{cm}^{-1}$  experiences a corresponding increase in intensity, representative of the interaction strength. Additionally, the intensity of the carbonyl band at  $1708\text{cm}^{-1}$  also produces an overtone within this region, typically located around  $3362\text{cm}^{-1}$ .

The amide I stretch appearing at  $1516\text{cm}^{-1}$  is recognised for its complexity amongst other bands. This contains spectral features attributed to free moieties, along with those engaged in hydrogen bonding within crystalline and amorphous domains.<sup>26</sup> All three bands contribute towards the morphology of the amide I vibration. Separate from this is the amide II vibration at  $1235\text{cm}^{-1}$ , often considered the NH in-plane bending vibration.<sup>25</sup> Likewise, the composition of the amide II band remains sensitive to hydrogen bonding, consistent with the NH and amide I peaks.

Both the location and conformation of amide bands are of particular relevance to the outcome of investigations. Overlaying the amide region of polyurethanes based on single alcohols with that of the blend, reveals contributions from both HTPB and Dantocol towards

urethane linkages. This is particularly apparent within the amide I region depicted in Figure 7.2. Amide bands associated with the blend are observed to broaden, whilst shifting towards a midway point between the two systems based on HTPB and Dantocol. This is characteristic of vibrational bands resulting from copolymerisation of both alcohols and the diisocyanate curative. Failure of Dantocol to react accordingly, would result in formation of amide bands resembling that of IPDI/HTPB described in Chapter 6.

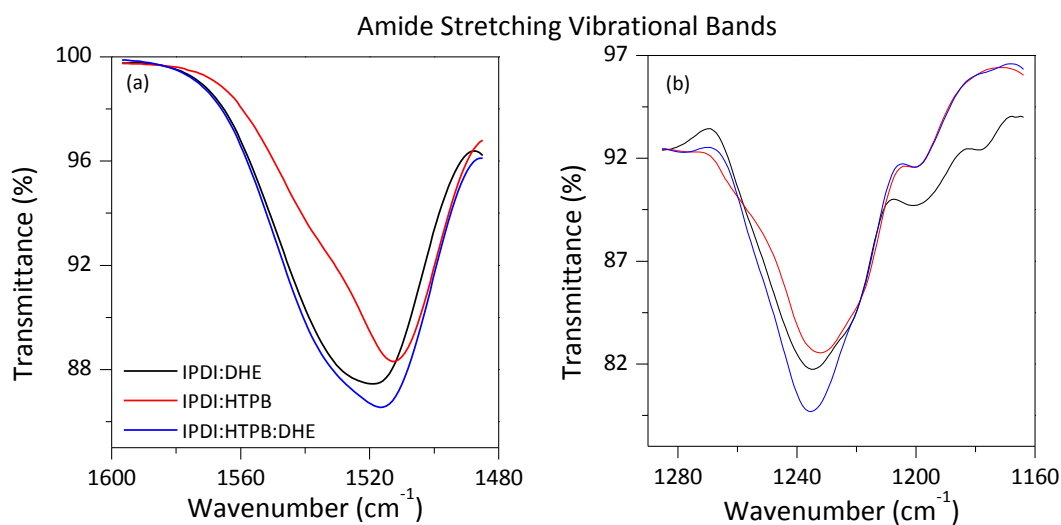


**Figure 7.2.** FTIR spectra of (a) amide I (b) amide II peaks for polyurethanes.

Although less pronounced, the amide II region substantiates evidence of copolymerisation involving both alcohols and the isocyanate. Again the amide band represents contributions from separate urethane linkages, which are distinguished according to their chemical environment. As minor variation occurs between the peak maxima of urethanes based on either HTPB or Dantocol, a similar trend is expected for the polyurethane blend. Consequently, the overlaying bands of linkages derived from alcohols and the diisocyanate, impose a reinforcing effect, causing peak shifts and broadening. These subtle deviations in bands were further investigated by spectral subtraction, to identify contributions from individual alcohol components.

### 7.3.1.1.1 Spectral Subtraction

Incorporation of Dantocol within the blend was investigated by removing bands associated with IPDI/HTPB linkages. Interpretation of subtraction spectra focused on the sign of peak intensity, with negative bands reflecting an overall loss in functional groups, while positive bands indicate an increase. The subtraction spectrum generated in Figure 7.3, displays positive peaks associated with the carbonyl region. This is expected as Dantocol's carbonyl functionality overlays that of urethane linkages, therefore increasing the concentration of carbonyl groups. Alternatively the  $\text{CH}_2$  stretch residing at  $2911\text{cm}^{-1}$  reflects negative peaks, indicating decrease in functionality. This occurs in response to the subtraction of HTPB responsible for alkenyl groups.

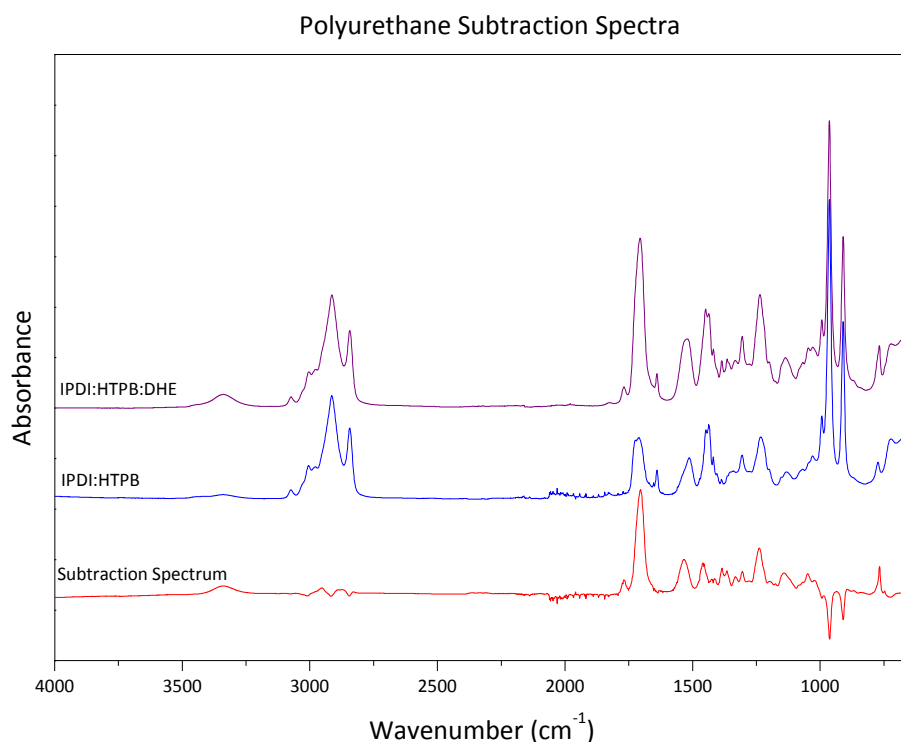


**Figure 7.3.** FTIR spectra of IPDI/HTPB/DHE – IPDI/HTPB = subtraction spectrum.

Of particular relevance to investigations are the implications associated with the subtraction spectrums NH and amide region. Results confirm previous findings, indicating both Dantocol and HTPB participate in reaction with the diisocyanate curative. This is implied by formation of positive bands representing  $\nu_{\text{amide}}$  and  $\nu_{\text{NH}}$ . With exception of both alcohols



reacting with IPDI, subtraction of linkages derived from HTPB would otherwise fail to produce positive peaks. Evolution of positive bands therefore indicates reaction of Dantocol and IPDI, as regions remain free of impinging bands.

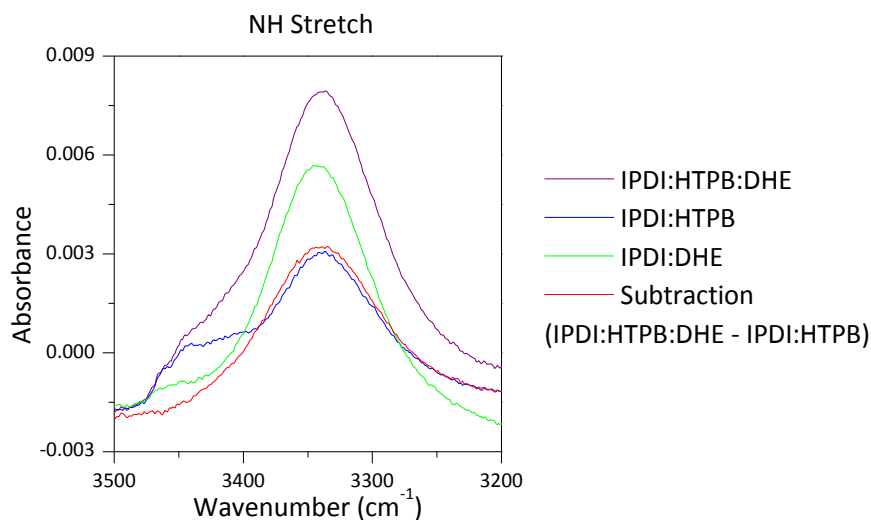


**Figure 7.4.** FTIR spectra of polyurethane blend NH region.

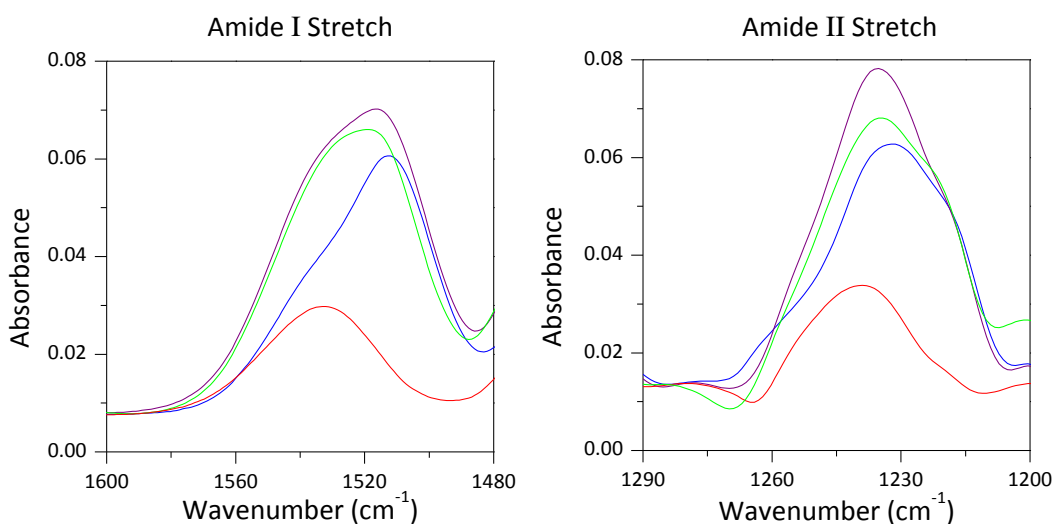


**Figure 7.5.** FTIR spectra of polyurethane blend amide I and II region.

Interpretation of the amide region revealed additional findings, providing conclusive evidence of the bonding agents reaction mechanism. Complementary to the formation of positive amide peaks, the wavenumber of subtraction band indicates contributions from linkages derived from Dantocol. Amide bands appear at greater wavenumber than those observed for polyurethanes based on HTPB. This coincides with the wavenumber of

polyurethanes derived from Dantocol, indicating reaction with the diisocyanate curative. Dantocol linkages are therefore responsible for contributions at the high wavenumber end of amide bands associated with the blend.

### 7.3.1.2 Polyurethane of Increasing Dantocol concentration

A series of polyurethane blends were prepared comprising increased mole ratios of the bonding agent. Polymerisation of alcohol blends in the presence of IPDI was evaluated in terms of spectral features depicted in Figure 7.6. In addition, the extent of curing was monitored by removal of isocyanate peaks at  $\nu_{\text{NCO}} \approx 2260\text{cm}^{-1}$ . Spectra representing the starting material, were collected following mixing to provide a reference from which to compare the initial isocyanate content. The intensity of peaks at  $T = 30\text{min}$  indicates an increase proportional to the concentration of IPDI, which is altered in balancing the NCO:OH ratio. As the urethane reaction proceeds, isocyanate groups are consumed resulting in reduced intensity. This confirms the occurrence of polymerisation throughout the series of hydroxyl blends.

IPDI:HTPB:DHE Mole Ratio	NH		Amide I		Amide II	
	$\nu$ ( $\text{cm}^{-1}$ )	Area	$\nu$ ( $\text{cm}^{-1}$ )	Area	$\nu$ ( $\text{cm}^{-1}$ )	Area
1.0 : 1.0 : 0.0	3340	167	1513	412	1232	338
1.0 : 0.8 : 0.2	3340	304	1516	536	1235	451
1.0 : 0.6 : 0.4	3340	320	1516	609	1235	464
1.0 : 0.5 : 0.5	3340	343	1517	641	1235	470
1.0 : 0.4 : 0.6	3339	453	1521	778	1235	594
1.0 : 0.2 : 0.8	3338	475	1522	810	1235	633
1.0 : 0.0 : 1.0	3338	539	1521	875	1232	650

**Table 7.4.** Polyurethane peak data of amine, amide I and II vibrational bands.

Evolution of amide bands, coupled with the broad NH stretch verifies formation of urethane linkages. Details regarding the area and wavenumber of the identified peaks are collated in Table 7.4. All three bands display an increase in peak area proportional to the concentration of Dantocol. Due to the bonding agents low hydroxyl equivalent weight in comparison to HTPB, the concentration of urethane linkages is increased with Dantocol content. Flow on

effects impact the degree of hard segments, which participate in hydrogen bonding. Increasing the molar ratio of Dantocol, therefore causes the intensity of hydrogen bonded NH and amide bands to increase relative to free moieties.

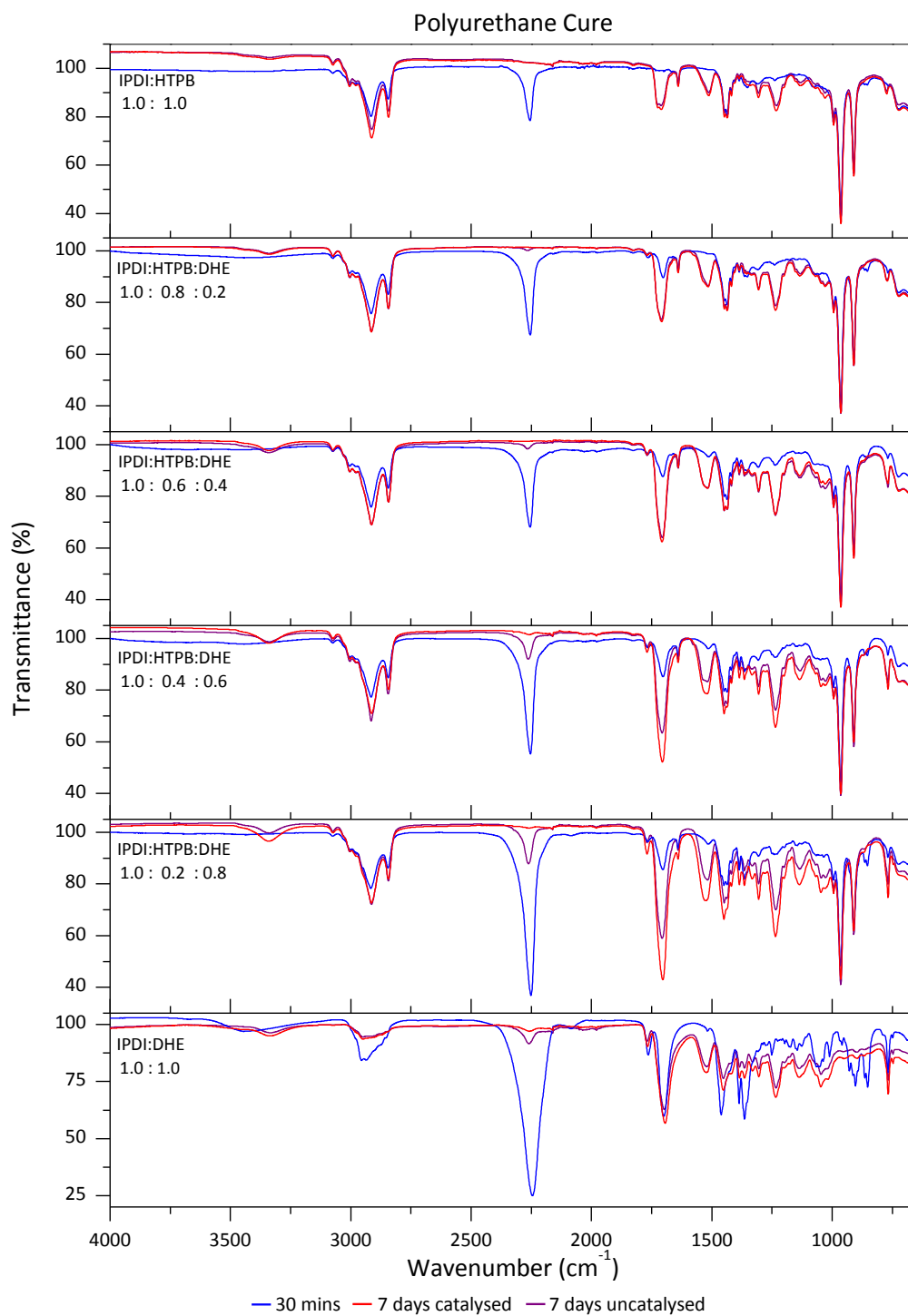


**Figure 7.6.** FTIR spectra of polyurethane blends.

As previously alluded, the NH vibrational band consists of free and hydrogen bonded amine groups, contributing towards a collective band.<sup>25</sup> Free NH groups appear as a shoulder at higher wavenumber, observed in Figure 7.7 at  $\nu_{\text{NH}} = 3438\text{cm}^{-1}$ . This is perhaps most apparent in the polyurethane spectrum of IPDI/HTPB. Sequential increase in Dantocol content, causes the free NH shoulder to decrease over successive blends. In contrast, hydrogen bonded NH bands appearing at  $3340\text{cm}^{-1}$ , increase in relation to the diminishing intensity of free NH moieties. This represents the strength of hydrogen bonding between polyurethane hard segments. Evidently, the incorporation of Dantocol within the matrix contributes towards hard segments, which corroborate this observation.

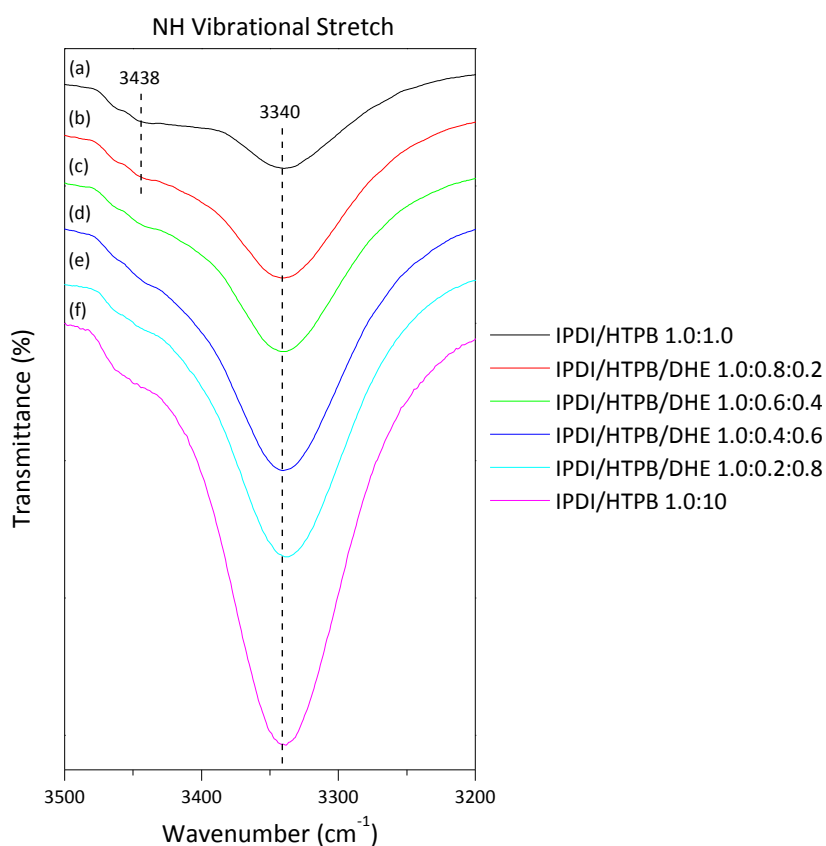


**Figure 7.7.** FTIR spectra of NH region for polyurethanes blends.

Shifts observed in  $\nu_{\text{amide I}}$ , arise from copolymerisation of HTPB and Dantocol with the diisocyanate curative. This generates peak broadening, due to formation of multiple linkages derived from IPDI/Dantocol and IPDI/HTPB. The wavenumber of the collective band provides an indication of each components input towards the matrix. Along with the assignment of bands pertaining to blends, Table 7.4 highlights the amide vibrations of

polyurethanes based on single alcohols. Deviation in wavenumber corresponds to the mole ratio of HTPB and Dantocol. Bands shift towards lower wavenumber as the concentration of HTPB is increased, while addition of Dantocol provides greater wavenumbers. This trend remains consistent throughout the series of blends, indicating the mole ratio of alcohols is responsible for determining peak maximum.

### 7.3.1.3 Thermal Analysis of Polyurethane Blend

Thermal behaviour of polyurethane blends was investigated via DSC, to determine the impact of Dantocol on the binder system. Acquisition of DSC curves in Figure 7.8, indicates the  $T_g$  of respective polyurethane systems. The value of  $T_g$  was derived from the half height of the line between intersecting tangents. This occurs at  $T_g = -73^\circ\text{C}$  for both the blend and IPDI/HTPB based polyurethane. Similarities exist between the  $T_g$  of these examples and the HTPB starting material, which occurs at  $T_g = -78^\circ\text{C}$ , accounting for an increase of  $\Delta T_g = 5^\circ\text{C}$ . This is indicative of phase separation, resulting from the polarity effects between polar IPDI and nonpolar HTPB. Evidently, the implications of decreasing  $T_g$  values represent a reduction in segment mixing.<sup>27, 28</sup> The driving force behind separation stems from incompatibilities between segments, owing to the inability of HTPB soft segments to participate in hydrogen bonding.

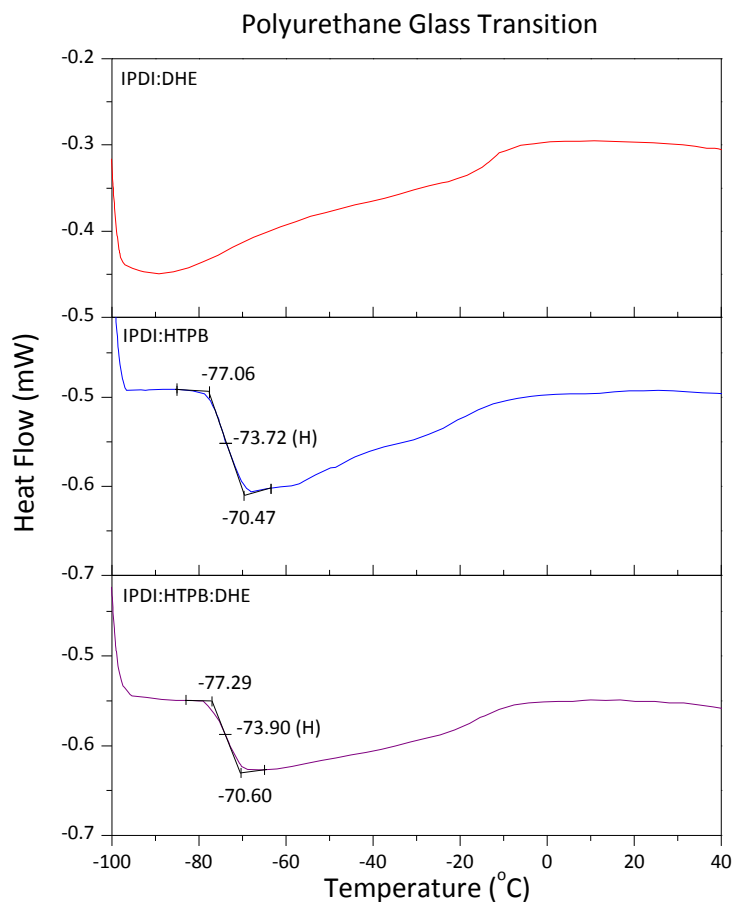


**Figure 7.8.** DSC curve of polyurethanes  $T_g$ .

Evidence of phase separation is consistent with FTIR findings, which suggest the absence of interaction between segments. This generates domains composed primarily of individual segments, appearing as regions of hard segments dispersed within a matrix of soft segments.<sup>22</sup> These characteristics enable  $T_g$  to provide an indication of hard and soft segment interaction. Current studies indicate negligible deviation between the  $T_g$  of polyurethane blends and that based on IPDI/HTPB. This indicates the addition of Dantocol fails to increase interaction involving HTPB soft segments. The implications of this negate the potential for interaction between Dantocol and HTPB to account for the bonding agents mode of action. This provides further support for covalent bonding as being responsible for reaction of Dantocol and the binder systems isocyanate content.

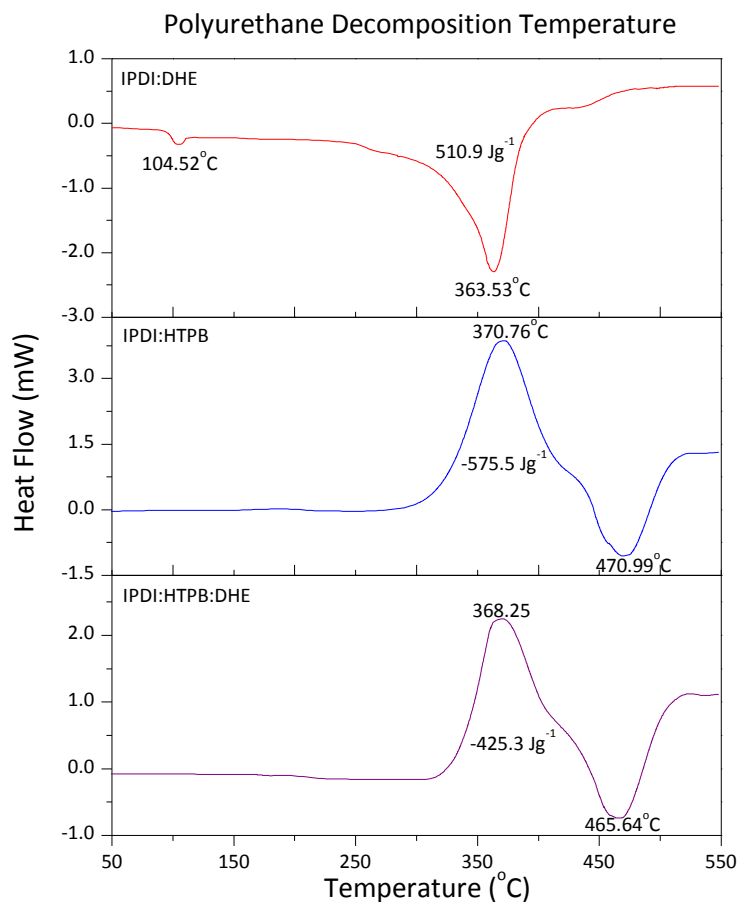


**Figure 7.9.** DSC curve of polyurethanes thermal decomposition.

Thermal decomposition was investigated from 50°C to 500°C, at  $\beta = 10^\circ\text{C min}^{-1}$ . The resulting polyurethane thermograms are represented in Figure 7.9. Compositions containing HTPB produce an initial decomposition step depicting urethane cleavage. This is immediately followed by crosslinking and cyclisation of the remaining polyol. Thermal events proceed via the double bonds of the HTPB backbone, therefore energy release is dependent on the polyol concentration.<sup>29</sup> This was investigated via enthalpy change ( $\Delta H$ ), with the exotherm of IPDI/HTPB displaying a value of  $\Delta H = -575.5\text{Jg}^{-1}$ . Addition of Dantocol to the polyurethane blend generates a positive increase in enthalpy, with the integration revealing  $\Delta H = -425.3\text{Jg}^{-1}$ . This is consistent with reduction in HTPB content required to balance the NCO:OH ratio. Although the mole ratio of HTPB is decreased, the polyols mass exceeds that of Dantocol, lending itself to greater representation within the DSC curve.

Initial decomposition of the polyurethane blend occurs at  $T_d = 368.25^\circ\text{C}$ , while appearing at  $T_d = 370.76^\circ\text{C}$  for IPDI/HTPB. Minor variation in peak maxima suggests repetition of the decomposition mechanism, involving cleavage of the urethane linkage. The second stage represents endothermic decomposition of the HTPB residue, formed during depolymerisation.<sup>30</sup> Similarly, the discrepancy between the two polymers again appears minimal, with peaks associated with the polyurethane blend and IPDI/HTPB occurring at  $T_d = 465.65^\circ\text{C}$  and  $470.99^\circ\text{C}$  respectively. This occurs as the endotherm represents decomposition exclusive of HTPB, with additional components vaporising during the initial decomposition step.

In comparison to previous networks, polyurethanes based on Dantocol and the diisocyanate curative, understandably contributes towards contrasting thermograms. An initial endotherm appears at  $104^\circ\text{C}$ , representing the polymers crystalline melting temperature. Absence of microcrystalline regions within systems comprising HTPB, occurs due to incorporation of soft segments, imparting flexibility within the network. The consecutive event at  $T_d = 363^\circ\text{C}$  represents urethane cleavage, which initiates vaporisation of both IPDI and Dantocol. Additional inspection of the bonding agents characteristic melting point region, also indicated an absence of starting material from the polyurethane network.

Investigations of the melting behaviour identified conditions necessary to observe the  $T_m$  of Dantocol, which can exist as liquid or solid at room temperature. Although crystallisation is reversible under ideal conditions, this behaviour often requires cooling to promote occurrence. This involved cooling liquid Dantocol to temperatures of  $-100^\circ\text{C}$  for a period of 3 mins. Following isothermal conditions, the DSC cell was heated at  $\beta = 5^\circ\text{C min}^{-1}$  towards a maximum of  $80^\circ\text{C}$ . The combination of low temperature and slow heating rate promotes recrystallisation, ensuring  $T_m$  is observed within the DSC curve. Conditions were replicated for polyurethanes based on IPDI/HTPB/Dantocol and IPDI/Dantocol, without evidence of the otherwise well defined  $T_m$  endotherm. This implies participation of Dantocol in covalent



bonding, as the alternative involving suspension within the matrix would otherwise replicate the melting endotherm.<sup>1</sup>

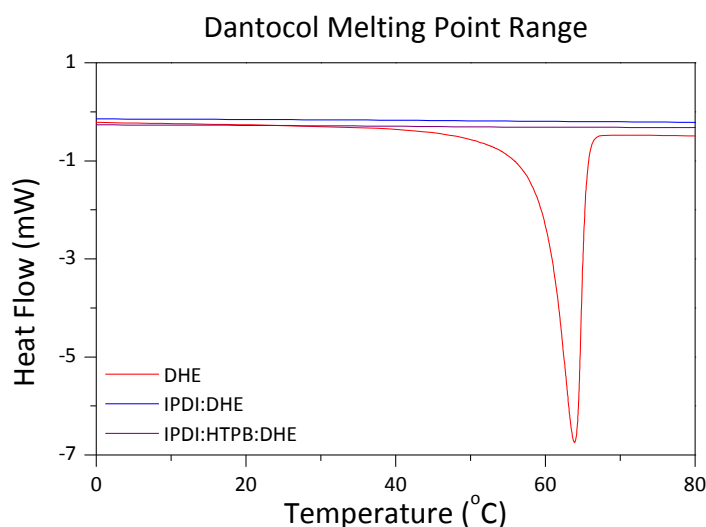


**Figure 7.10.** DSC curve of polyurethanes over the  $T_m$  range of Dantocol.

#### 7.3.1.4 Rheology of Polyurethane Blend

Rheo-kinetic studies of the polyurethane blend were performed to identify cure behaviour. The functionality distribution and subsequent reactivity of alcohol components plays a critical role in the kinetics of network formation. Details of these attributes provide insight into the curing mechanism of Dantocol within the submix. Unlike spectroscopic techniques which are limited to indentifying removal or evolution of functional groups, rheological investigations provide the capability to determine branching status of the cross-linking reaction. Rheology is also commonly applied to describe the kinetics of viscosity build-up, along with monitoring pot-life and point of gelation.<sup>31</sup>

As polymerisation proceeds, the viscosity of the system increases with time. Viscosity build-up is attributed to increase in molecular weight, resulting from polymer chain growth and branching. As the reaction of HTPB and IPDI is favoured over Dantocol, the rate of viscosity build-up is reduced with respect to the blend. This is accompanied by prolonged gelation, as indicated by the intercept of  $G'$  and  $G''$ . Observation of the gelation point occurs after 79mins, compared with 58mins for the IPDI/HTPB system.

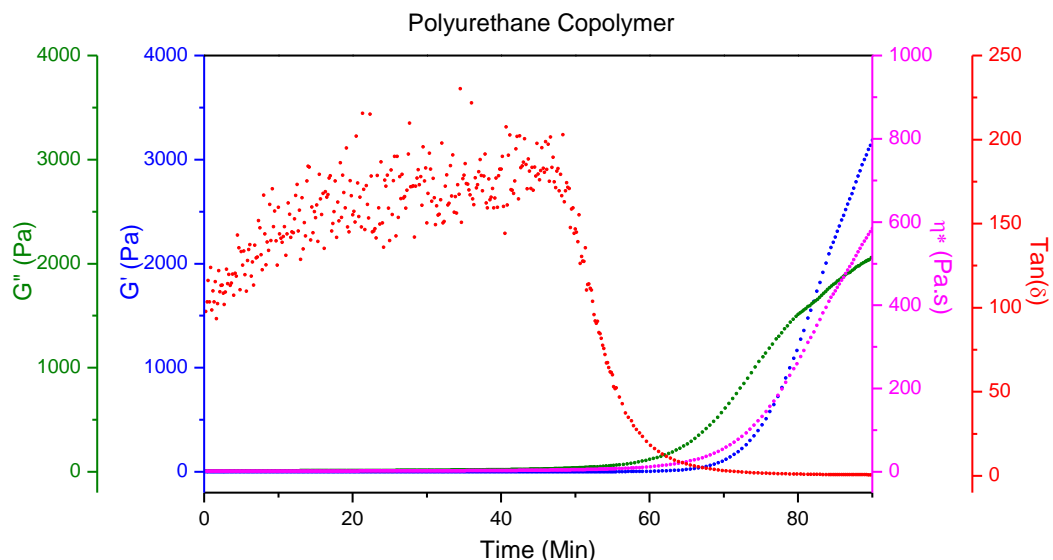


**Figure 7.11.** Rheological behaviour of polyurethane copolymer.

Evaluation of Figures 7.11 and 7.12 indicates curing occurs in two stages, with the formation of dual rate constants. Plotting the natural logarithm of  $\eta^*$  against time, yields multiple linear functions of slope equivalent to the rate of viscosity increase. As the viscosity of the curing system increases, minor deviations in linearity occur due to reduced freedom of chain mobility.<sup>31</sup> Irrespective of this, formation of linear functions indicates the difference in reactivity imposed by the blend's multiple OH components. This is responsible for defining rate constants  $k_1$  and  $k_2$ , which account for the kinetic behaviour of the blend. The chemical reactivity of HTPB dominates the initial viscosity build-up, while Dantocol accounts for the less favoured hydroxyl groups.

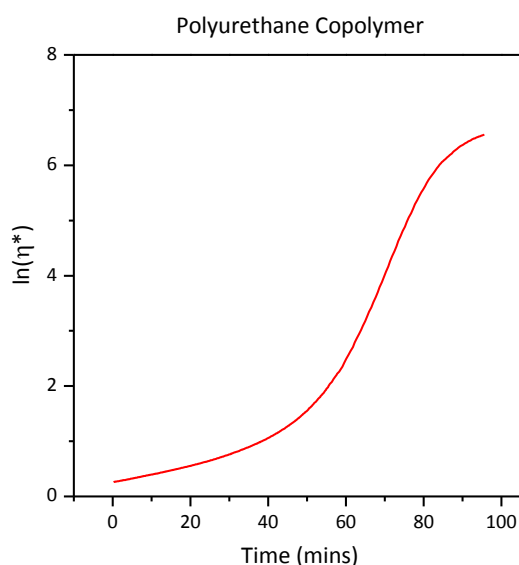


**Figure 7.12.** Plot of  $\eta^*$  vs time for polyurethane blend.

### 7.3.2 Cast-Cured PBX Composites

Prior investigation of Dantocol's hydroxyl functionality revealed the capacity to engage in covalent bonding with IPDI, along with hydrogen bonding involving nitramines. These competing mechanisms were evaluated within PBX formulations, consisting of sequential Dantocol concentrations. Further investigation of cure involved differentiating between polymerisation of IPDI and the hydroxyl functionality of Dantocol and HTPB. This was assessed by comparison to polyurethanes defined in Chapter 6, comprising a single hydroxyl component. Previous investigation of the network structure therefore provides a baseline from which to compare current hydroxyl blends. This highlights the contribution of Dantocol and HTPB towards formation of urethane linkages.

#### 7.3.2.1 Scanning Electron Microscopy

The morphological characteristics of dewetting, and subsequent impact of Dantocol upon dewetting phenomena were examined by SEM. Investigation of length, area and angle of non-bonded RDX particles, was used to assess the efficiency of Dantocol within PBX composites. This provides an initial indication of mechanical properties in regards to the concentration of bonding agent. In order to evaluate bonding agent efficiency, formulations were compared to that without Dantocol. The consequence of bonding agent omission is evident in Figure 7.13, depicting the presence of surface dewetting and agglomeration of filler particles. This represents poor interfacial adhesion, thus exposing the surface of RDX. Deformations also extend to the formation of crevices within the region adjacent to filler particles. The width of such abnormalities measured approximately 1-2 $\mu$ m in length.

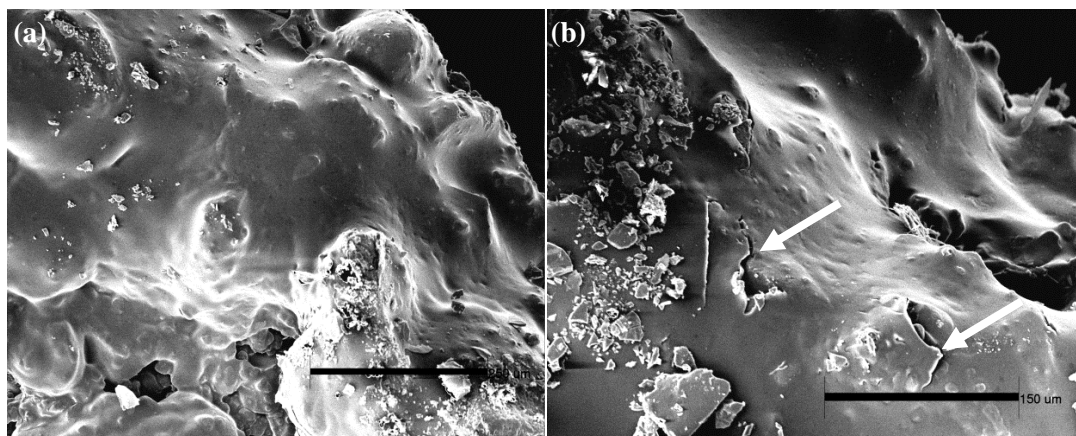


**Figure 7.13.** SEM image of PBXN-01 (a) particle agglomeration and (b) crack formation.

Limited dewetting is observed in formulations comprising Dantocol. This indicates strong interaction exists at the filler/binder interface, preventing onset of deformation mechanisms. As the concentration of bonding agent is increased, the presence of cracks, voids and peeling cease to occur within the observable region. Elimination of defects, provides unequivocal evidence of Dantocol's ability to improve interfacial adhesion through formation of bonds involving RDX and the binder system.

Distribution of RDX within the binder also appears to improve, with particles evenly dispersed throughout the matrix. This is reflected upon comparison of topography, with decline in crystal protrusions representing uniform filler dispersal. Application of Dantocol as the sole hydroxyl content, brings about deviation in surface morphology. This demonstrates a comparatively abrasive surface, following exclusion of HTPB from PBXN-06. Polymerisation of HTPB otherwise contributes to formation of soft segments, as differs from segmentation derived from Dantocol. Consequently, the occurrence of smoothening associated with HTPB's polymeric backbone is therefore omitted. This generates increased surface deviation observed in Figure 7.14.(f), resulting from hard segment formation.

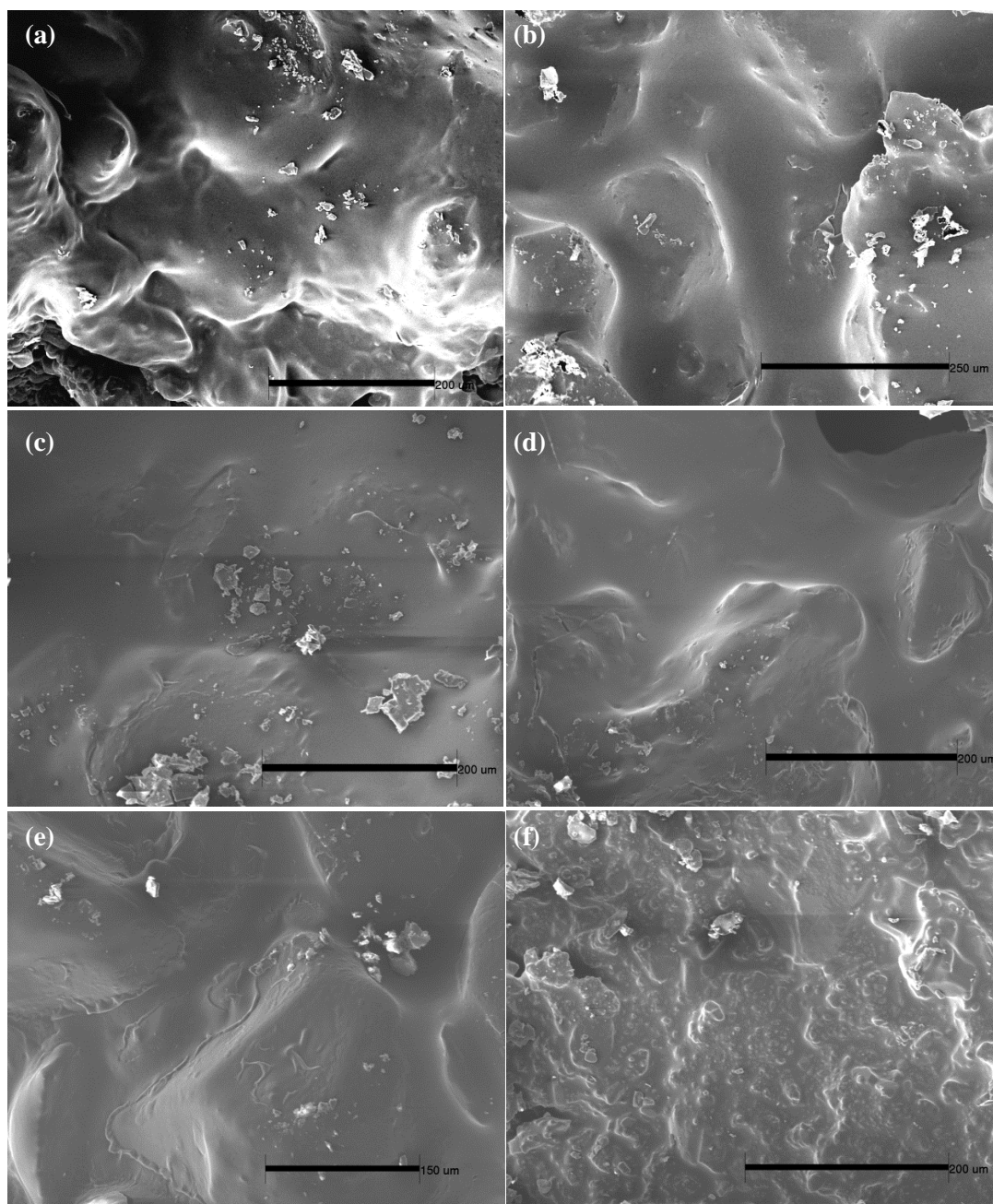


**Figure 7.14.** SEM images of PBX formulations (a) PBXN-01 (b) PBXN-02 (c) PBXN-03 (d) PBXN-04 (e) PBXN-05 (f) PBXN-06.

### 7.3.2.2 Fourier Transform Infrared Spectroscopy

#### 7.3.2.2.1 Intermolecular Interaction of Dantocol

Common throughout the study of polyurethane kinetics, is the elucidation of isocyanate content via application of FTIR.<sup>32</sup> In order to clarify the bonding agents mode of action, the potential for Dantocol to react with IPDI was investigated in the presence of RDX. This was

monitored by observing bands associated with urethane linkages and corresponding isocyanate reduction. Application of FTIR is equally as effective in describing the surface chemistry of filler particles. Simultaneous investigation of the proposed interactions involving Dantocol and RDX was therefore conducted. This serves to identify the mechanism in which competing interactions occur, thus revealing the final key to understanding Dantocol's mode of action.

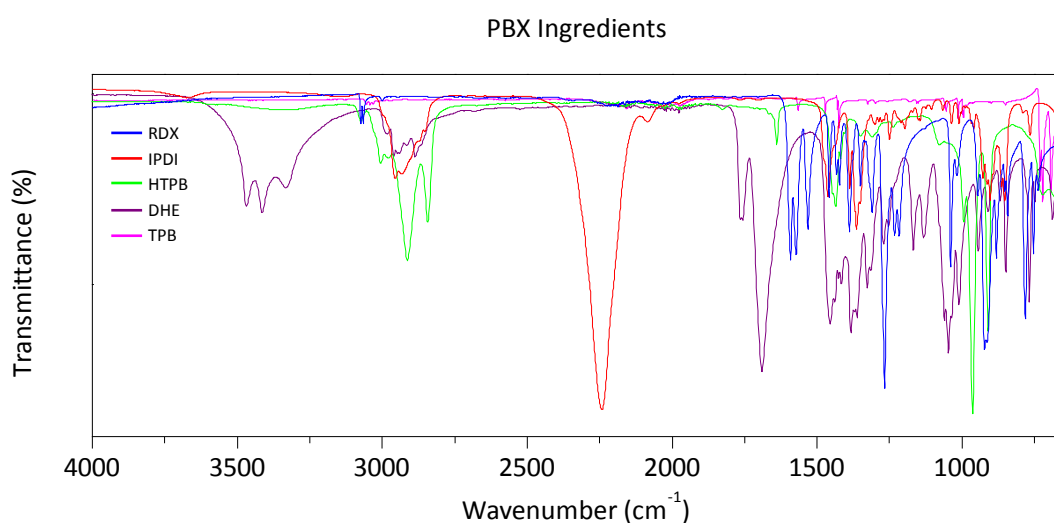


**Figure 7.15.** FTIR spectra of PBX ingredients.

Spectra pertaining to precursors were initially acquired, identifying overlay and providing a reference from which to establish shifts. The characteristic bands of the applied starting materials are highlighted in Figure 7.15, with IPDI ( $\nu_{\text{NCO}} = 2242\text{cm}^{-1}$ ) and RDX ( $\nu_{\text{as}}\text{NO}_2 = 1532\text{cm}^{-1}$ ) considered of primary significance. Dantocol's multiple C=O bands also present implications, and appear at  $1687.9\text{cm}^{-1}$  and  $1761.8\text{cm}^{-1}$ . Both impede upon C=O vibrations associated with urethane linkages, therefore complicating the wavenumber region. This dictates the interpretation of C=O peaks is limited to contributing general information. Consequently, the amine and amide bands are utilised to obtain definitive spectral data.

Following investigation of starting materials, spectra pertaining to PBX composites were acquired. Interpretation of vibrational bands identified bonding agent interactions occurring amidst formulations. The effect of increasing Dantocol concentration was employed to confirm these observations, with FTIR, DSC and SEM applied in the characterisation of

primary and secondary bonding. Spectroscopic data revealed fundamental changes occurred in the FTIR spectra of formulations comprising Dantocol. This is observed in Figure 7.16, depicting cast-cured PBX composites of increasing bonding agent concentration.

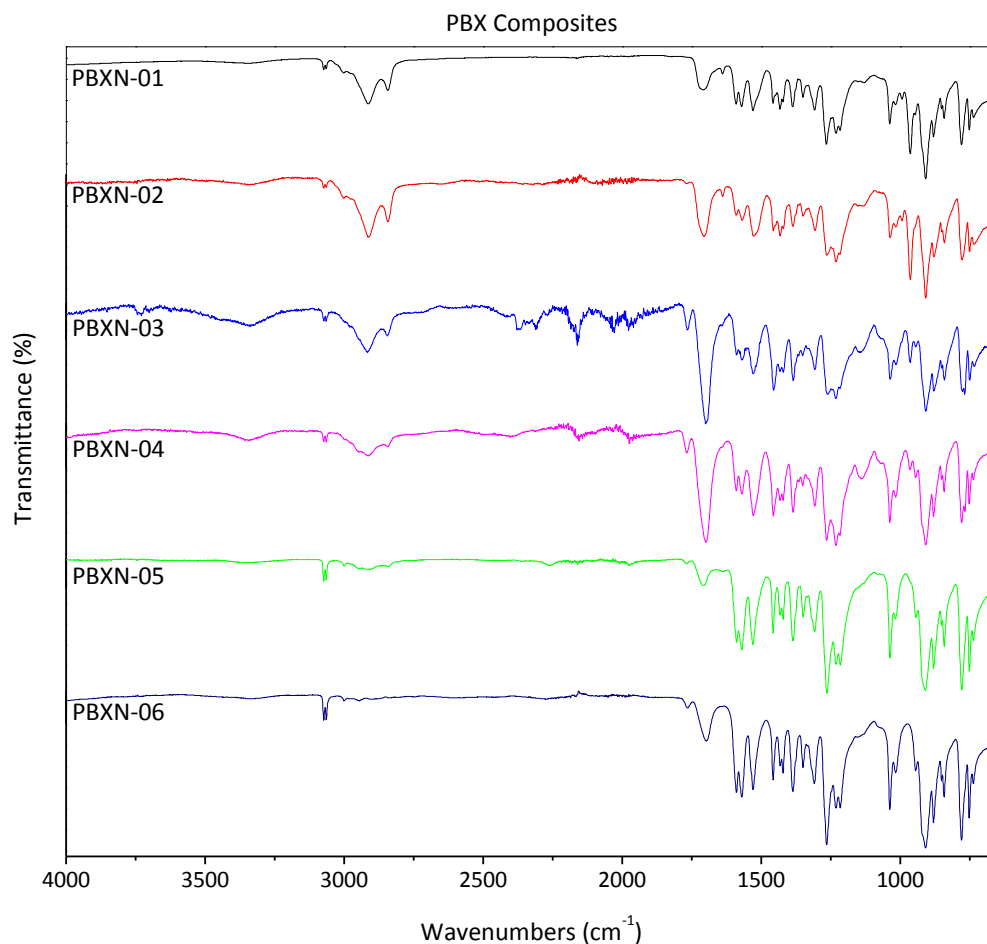


**Figure 7.16.** FTIR spectra of PBX composites.

#### 7.3.2.2.2 Hydrogen Bonding of Dantocol and RDX

Hydrogen bonding observed in Chapter 3 was assessed to determine its stability within energetic composites. Based on the spectral shift of hydrogen bonded nitro groups, the relative strength of intermolecular forces remain unimpeded. This was established by comparison of hydrogen bonded  $\nu_{as}NO_2$  bands, to that observed in previous RDX coatings. The magnitude of bathochromic shifts confirms the competing reaction of IPDI has limited impact on hydrogen bond dissociation. Prevention of dissociation is known to occur due to the influence of proton acceptors.<sup>5, 33, 34</sup> Dependent on the imposed polarising effects,

reaction of hydroxyl and isocyanate groups may be inhibited by participation of polyols in secondary bonding.

Investigation of the focal nitro region is complicated by evolution of amides associated with urethane formation. Fortuitously, the offset of vibrational bands and concentration of filler particles is sufficient to enable interpretation of free/bonded  $\nu_{as}NO_2$  bands. As RDX accounts for 80% of the total mass, this ensures minimal influence of the amide I vibration, causing appearance as minor tailing. This is confirmed by comparison with amide II bands, consisting of equally low intensity.

Shifts associated with the asymmetrical nitro stretching vibration are highlighted in Table 7.5, reflecting deviation from neat RDX ( $\nu_{as}NO_2 = 1532cm^{-1}$ ). Potentially the most definitive evidence of interaction between Dantocol and RDX, concerns the failure of PBXN-01 to display appreciable shift. Removal of Dantocol negates the potential for hydrogen bonding to occur, thus preventing interaction of nitro groups. Conversely, the incorporation of Dantocol within formulations generates increasing  $\Delta\nu_{as}NO_2$ , proportional to bonding agent concentration. This also confirms the amide I band is unaccountable for spectral shifts.

Sample	HTPB:DHE	Vibrational Bands ( $cm^{-1}$ )					
		$\nu NH$	$\nu_{as}CH_2$	$\nu C=O$	$\nu C=O$	$\nu_{as}NO_2$	$\nu AmideII$
PBXN-01	1.0 : -	3480-3200	2914	-	1709	1531	1232
PBXN-02	0.8 : 0.2	3480-3200	2914	1767	1706	1526	1231
PBXN-03	0.6 : 0.4	3480-3200	2916	1766	1700	1525	1232
PBXN-04	0.4 : 0.6	3480-3200	2916	1767	1699	1523	1231
PBXN-05	0.2 : 0.8	3480-3200	2916	1768	1701	1521	1231
PBXN-06	- : 1.0	3480-3200	-	1765	1697	1520	1231

**Table 7.5.** Assignment of IR bands for PBX formulations.

Shifts in  $\nu_{as}NO_2$  indicate negligible variation in the extent of interaction between isolated coatings and energetic composites. This is evident at corresponding Dantocol concentrations, whereby both systems demonstrate similar  $\Delta\nu_{as}NO_2$  results. Maximum shift in wavenumber was subsequently observed for PBXN-06, recording a magnitude of  $\Delta\nu_{as}NO_2 = 12cm^{-1}$ . This represents the greatest concentration of nitro groups participating in secondary bonding.



### 7.3.2.2.3 Dipole Interaction of Dantocol and RDX

The dipole moment associated with Dantocol's carbonyl functionality was previously shown to engage in interaction with RDX. Presence of dipole interactions occurred in synergy with hydrogen bonding, thus increasing interfacial adhesion. This observation was repeated for PBX composites, with shifts developing within the carbonyl region. Spectral complexity presents difficulties identifying shifts associated with dipole interactions. As the effects are subtle, shifts are easily influenced by resonances associated with urethane linkages. Therefore, the potential for bands to impinge upon Dantocol's carbonyl region must be considered.

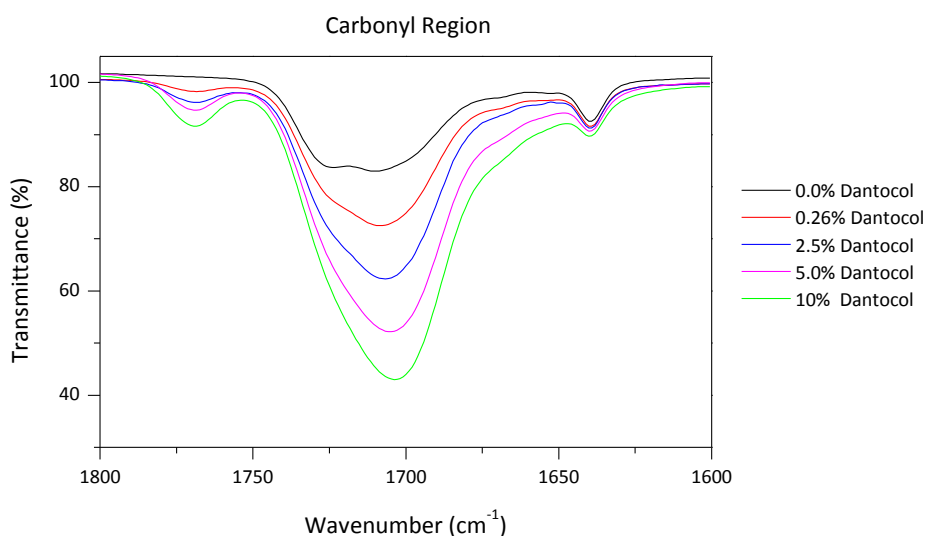


**Figure 7.17.** FTIR spectra of PBX composites C=O region.

Inspection of the carbonyl region highlights shifts associated with Dantocol addition. As the concentration of bonding agent is increased, so too does the magnitude of carbonyl shifts. This is consistent with observations in Section 3.3.4, providing support for the occurrence of dipole interactions. The extent of shifts is observed to plateau at approximately  $\nu\text{C=O}$  1700cm<sup>-1</sup>. This suggests delocalised electrons within the ring structure have completed interaction with RDX. Evolution of shifts is consistent with previous investigation of Dantocol and RDX coatings. This represents deviations in excess of  $\Delta\nu\text{C=O}$  9cm<sup>-1</sup>, following the plateauing of spectral shifts. The implications of these results infer consistency

in the strength of dipole interactions, comparing isolated coatings and energetic composites. Consequently, the presence of weak interaction associated with dipole forces further substantiates this occurrence.

Additional investigations were required to confirm, beyond doubt, the existence of dipole interactions is responsible for shifts associated with C=O vibrations. This was achieved by adduct incorporation, whereby Dantocol was reacted with isocyanate prior to addition in PBX formulations. Protection of the bonding agent's hydroxyl functionality served to limit secondary bonding to that involving dipole interactions. Details of the investigation are discussed throughout Section 9.3.3.3.

#### **7.3.2.2.4 Copolymerisation of Urethane Linkage**

The second phase of investigations involved the elucidation of covalent bonding between Dantocol and IPDI. Interpretation of Figure 7.16 depicts features associated with urethane formation, as present throughout compositions. Following cure, PBX composites reveal almost complete removal of isocyanate ( $\nu\text{NCO} = 2242\text{cm}^{-1}$ ), which is consumed during polymerisation. This confirms IPDI reacts with both HTPB and Dantocol, to produce the polyurethane binder system. Although less reactive than HTPB, polymerisation of the hydantoin is indicated by removal of isocyanate from formulations consisting primarily of Dantocol hydroxyl equivalents. Under these conditions, failure to react alternatively to HTPB would incur negligible impact on the intensity of  $\nu\text{NCO}$ . Complete removal of HTPB from PBXN-06 confirms incorporation of bonding agent within the network, as Dantocol represents the sole hydroxyl content.

Inspection of regions associated with urethane functionality, confirms evolution of carbonyl, amine and amide bands. This occurs throughout the series of PBX composites, indicating cure of the binder system. As previously eluded, the bonding agent's carbonyl functionality impinges upon that associated with urethane formation. Consequently, this appears as a

complex band limiting spectral interpretations. The occurrence of overlay meanwhile confirms evolution of carbonyls associated with polyurethane formation.

Similarly, the amide I vibration also observes partial overlay, due to the asymmetrical nitro stretch associated with RDX. In response, the amide II peak was deemed of particular significance, as this provides additional details concerning polymerisation of urethane linkages. Unlike previous bands, the absence of overlay contributes to acquiring definitive evidence of copolymerisation. This appears at  $\nu_{\text{amide II}} \approx 1231\text{cm}^{-1}$  throughout formulations, which is consistent with polyurethane gumstocks. Comparison of PBXN-01 and PBXN-06 indicates negligible deviation in amide II bands, irrespective of the difference in hydroxyl starting material. This is consistent with hydroxyl blends, while intensity increases proportional to Dantocol content. Conversely, if covalent bonding was unable to occur, this would be expected to result in decreased intensity. These combined observations therefore confirm the polymerisation of Dantocol.

Evolution of amine vibrations conclude that associated with urethane formation. This appears as broad vibrations occurring at  $\nu_{\text{NH}} = 3480\text{-}3200\text{cm}^{-1}$ . Bands also exhibit low intensity throughout the series of PBX composites. This is accompanied by negligible deviation in wavenumber, creating bands of which approximately align. Consistency between the NH stretch of energetic composites and polyurethane gumstocks was also observed. This confirmed polymerisation, with evolution of  $\nu_{\text{NH}}$  bands corresponding to  $\nu_{\text{NCO}}$  removal. Results demonstrate the major pathway available for incorporation of Dantocol within the binder system involves reaction with IPDI.

### **7.3.2.3 Thermal Analysis**

Although the thermal behaviour of RDX is well documented, limited details exist in relation to cast-cured PBX composites.<sup>35, 36</sup> Investigation of thermal degradation and glass transition temperature, was therefore conducted in elucidation of composites and the effects of Dantocol addition. This involved interpretation of thermograms acquired through application

of DSC analysis. These results were considered effective in describing urethane linkages, as relate to the reaction of Dantocol.

Polyurethane segmentation consists of soft and hard segments, with the later contributing towards increased  $T_g$ .<sup>37</sup> Depending on the ratio of these segments, the binder system is subject to deviation in  $T_g$ . This is influenced by reaction of Dantocol, effecting the formation of hard segment domains, chain mobility and segment organisation.<sup>1, 37</sup> The implications of uniform filler loading (RDX = 80% w/w), ensured the presence of RDX wasn't accountable for shifts in  $T_g$ .<sup>38</sup> Consequently, the increase in  $T_g$  reflects incorporation of Dantocol within the binder system. This observed deviation from  $T_g = -71^\circ\text{C}$  to  $-67^\circ\text{C}$  following increase in bonding agent concentration.

Variation in transition temperature confirms the network structure of polyurethane is altered upon addition of bonding agent.<sup>1</sup> Covalent bonding is responsible for such occurrence, with the mechanism involving Dantocol and IPDI described in Chapter 6. Failure of Dantocol to incorporate within the binder system would otherwise reflect consistency in  $T_g$ , irrespective of concentration. In excess of 5% (w/w) Dantocol concentration (PBXN-04), the reduction in total chain mobility promotes increased crystallinity, limiting the amorphous region such that  $T_g$  becomes difficult to observe.

Investigation of melting behaviour is illustrated in Figure 7.18, along with the decomposition of cast-cured PBX composites. Previous characterisation of RDX identified  $T_m$  appears as an endotherm occurring at  $204^\circ\text{C}$ . This was apparent within PBX composites, representing the presence of energetic filler. Conversely, the characteristic  $T_m$  of Dantocol remained absent, indicating incorporation within the network structure. As described in Section 7.3.1.3, this negates the potential for Dantocol to remain unreacted within the matrix.

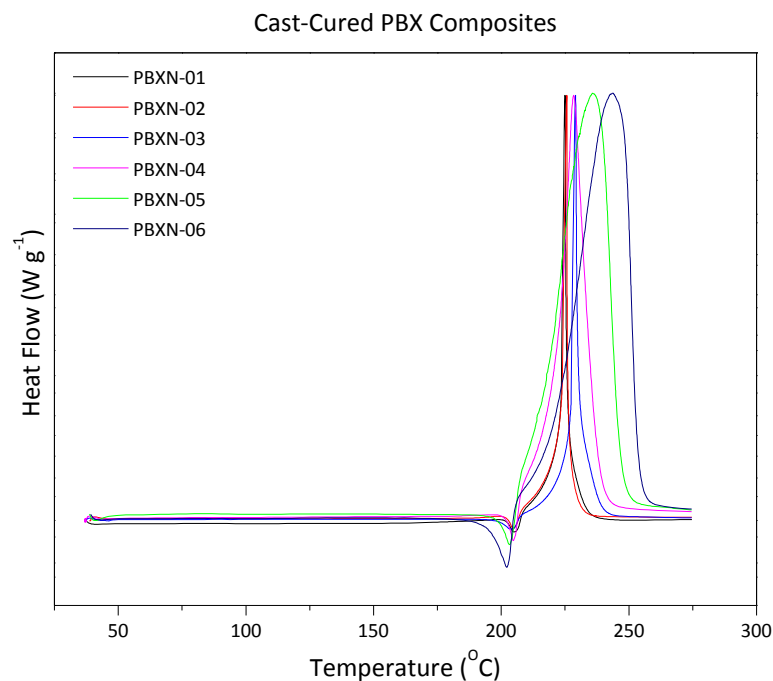


**Figure 7.18.** Normalised DSC curve of cast-cured PBX composites indicating  $T_m$  and  $T_d$ .

Decomposition of polyurethane proceeds in unison with RDX. The resulting exotherm occurs in immediate succession to  $T_m$ , with decomposition generating a sharp response in heat flow. This reflects the rate at which decomposition of RDX eventuates. Energy released in association with RDX, is significant by comparison to decomposition of polyurethane. This is further exaggerated due to the mass fraction of polyurethane (binder system = 20% w/w), comprising a small percentage of the overall weight. Increasing the contribution of Dantocol within the binder system results in shift towards higher  $T_d$ . This is accompanied by broadening, in response to changes in polyurethane structure. Deviation in  $T_d$  is highlighted in Table 7.6, with shifts in excess of  $\Delta T_d = 19.41^\circ\text{C}$  observed following incorporation of Dantocol. Elucidation of thermochemical behaviour confirms previous conclusions, outlining the formation of covalent bonds between Dantocol's hydroxyl functionality and isocyanates.

Sample	DHE (%)	$T_g$ (°C)	$T_m$ (°C)	$T_d$ (°C)
PBXN-01	-	-71.13	205.15	224.16
PBXN-02	0.26	-68.69	204.97	225.68
PBXN-03	2.50	-68.07	204.61	227.07
PBXN-04	5.00	-67.83	204.36	229.85
PBXN-05	10.00	-	203.54	236.14
PBXN-06	12.30	-	202.30	243.57

**Table 7.6.** DSC assignment of cast-cured PBX composites.

#### 7.3.2.4 Theoretical Chemistry Behind Resistance to Hydrogen Bond Dissociation

Polyurethanes are recognised for self-associating through intermolecular hydrogen bonding.<sup>39</sup> To facilitate hydrogen bonding between the polyurethanes amide functionality and other additives, favourable conditions are required in terms of intra- and intermolecular association. Despite this possibility, conditions within the current system prohibit urethane linkages from participating in hydrogen bonding with energetic fillers. This explains poor interfacial adhesion between the filler/binder system, resulting in propagation of dewetting. Confirmation is provided by the binder systems failure to promote shift in the nitramines asymmetrical nitro stretch, subsequent to removal of Dantocol.

In contrast, the application of Dantocol exhibits strong hydrogen bonding in conjunction with RDX. The strength of this interaction is such that bonding remains unimpeded by the binder system. This is highlighted in the IR spectra of Figure 7.16, revealing limited disruption to shifts in  $\nu_{as}NO_2$  participating in hydrogen bonding. The strength of this interaction impedes movement of Dantocol's participating hydroxyl functionality, providing initial resistance to dissociation. This is further assisted by steric hindrance and pH, which contribute to inhibiting dissociation of hydrogen bonding.<sup>5</sup> The influence of pH results in basic conditions, causing hydroxyls to become more nucleophilic and thus avoided.

Potentially the most important factor in prevention of hydrogen bond dissociation, stems from the influence of proton acceptors. This may determine the potential for reaction to occur between participating hydroxyl groups and diisocyanate curatives. Fundamental work by Oberth et al.<sup>5</sup> described the means by which proton acceptors engaged in hydrogen

bonding with prepolymers, are capable of lowering the rate constant of polyurethanes. This occurred in ethers, ketones, nitriles, carboxylic acids and nitro compounds, which compete with isocyanates for hydroxyl binding sites. Implications result in the inhibition of urethane formation.<sup>5</sup> Conversely, the reaction of polyurethane was assisted by amides, tertiary amines and dimethyl sulfoxide, according to polarising effects which catalyse the reaction. Inert compounds have no discernible impact on the reaction rate and act only as diluents. This indicates the reaction is sensitive to small differences in the hydrogen bonding capacity of its chemical environment.

Ephraim et al.<sup>34</sup> and Zaplatin<sup>33</sup> supported these observations, with previously identified functionality again disrupting the reaction of alcohol and isocyanate. Importantly, the impact of nitro compounds was found to decrease the reaction rate of polyurethanes. This occurs as strong hydrogen bonding between hydroxyl and nitro functionality remains unable to cause sufficient polarisation of the associated alcohol.<sup>5, 7, 9</sup> Therefore unlike the urethanes amine functionality which exhibits an autocatalytic effect, nitramines inhibit polymerisation of polyurethane. This enables the complex formed between RDX and Dantocol to remain intact following addition of IPDI.

### **7.3.2.5 Promotion of Bonding Agent Interaction**

#### **7.3.2.5.1 Isocyanate Selectivity**

IPDI is recognised to exhibit selectivity in terms of reaction involving hydroxyl functionality. This assumes a critical role within the polymerisation of polyurethanes. Consequently, the differential reactivity of primary and secondary isocyanates, is partially responsible for extensive use of IPDI throughout cast-cured energetic materials. This offers the potential for synthesising controlled polyurethane structures, by means of selective sequential reactions.<sup>40</sup> The implication of this enables IPDI to achieve selectivity ratios in excess of 10:1, through application of mild conditions.<sup>41</sup>

The diisocyanate comprises primary aliphatic and secondary cycloaliphatic groups, which are responsible for variation in reactivity.<sup>42</sup> This is recognised as critical for achieving sequential formation of polyurethanes.<sup>43</sup> Consequently, the selectivity of IPDI is detailed throughout the literature, revealing the influence of temperature, coreactant, stoichiometry, catalyst and experimental methods.<sup>32, 41-49</sup> Such occurrence is ultimately derived from shielding of the primary isocyanate, in response to quaternary  $\beta$ -methyl groups.<sup>50</sup>

Reactivity of the isocyanate functionality is also largely dependent on the presence of catalyst. Upon its omission, or the inclusion of Lewis acids, secondary isocyanate demonstrates greater reactivity. Alternatively, the addition of Lewis bases such as 1,4-diazabicyclo (2,2,2) octane, are known to favour the primary isocyanate.<sup>49</sup> In the case of metal catalysts, increased selectivity can be explained by the catalytic mechanism. Metals function as Lewis acids, activating the isocyanate group by coordination of carbonyl groups. The additional demand on space required by the activated transition state, is therefore responsible for preferential catalysis. This lowers the activation energy of the secondary isocyanate in response to reduced steric hindrance. These conditions have been shown to increase reactivity in excess of twelve times that of the primary isocyanate.<sup>50</sup> Alternatively, the addition of Lewis base catalyses polymerisation through activation of the hydroxyl functionality, resulting in inversion of selectivity. The implications of catalyst addition must therefore be considered when investigating IPDI selectivity.

The defined characteristics of IPDI are considered highly desirable for controlled synthesis of polyurethanes.<sup>46</sup> Following polymerisation of the initial isocyanate, reactivity of the remaining group is impeded.<sup>49</sup> As the affinity of HTPB for IPDI favours reaction involving the secondary isocyanate, incorporation of Dantocol within the binder system involves the least reactive isocyanate. The mobility of reactive functionality is also influenced following initial polymerisation of IPDI and HTPB. Combined with the inhibition effect of nitramine interaction, this ensures reaction of isocyanate is limited to Dantocol's free hydroxyl groups.

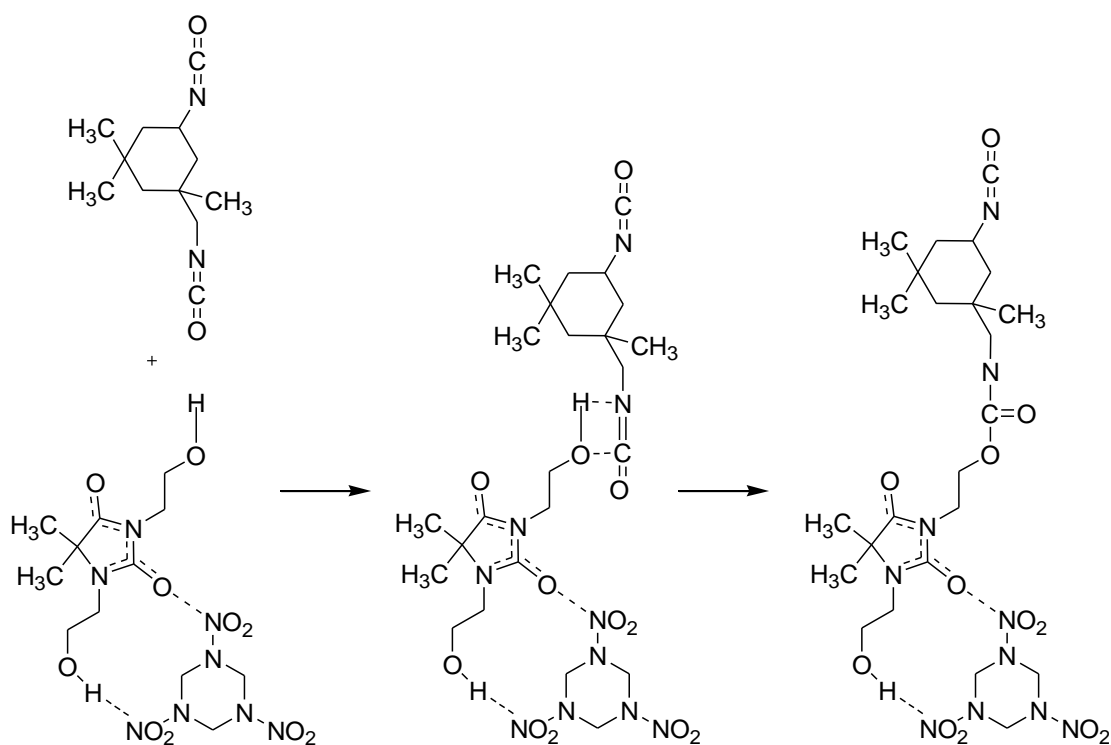


These implications account for the mechanism by which IPDI selectivity prevents dissociation of hydrogen bonding between Dantocol and RDX.

#### **7.3.2.5.2 Implications of Mixing Procedure**

The process involved in mixing cast-cured PBX composites assists in promoting the bonding agents mode of action. This is achieved by the order of its addition, temperature of mixing and timeframe over which RDX is combined. Typically, the procedure involves addition of polyol, plasticiser, antioxidant, cure catalyst and bonding agent, prior to onset of mixing. Isothermal conditions are applied, exceeding  $T_m$  of Dantocol to ensure adequate dispersal within the submix. This is followed by stepwise addition of RDX, resulting in the formation of a viscous slurry. The polarity of HTPB promotes migration of Dantocol towards filler particles, whereby it adheres to the surface through secondary bonding. Interaction is improved at elevated temperature, as additional energy is introduced to the system. This is supported by the prolonged addition of energetic filler, which assists in dispersal whilst providing the opportunity for encapsulation to occur.

Alongside the polarity of the system, the addition of isocyanate is decisive in Dantocol's ability to participate in interaction. Dependent on the order in which IPDI is combined, this may impede the bonding agents mode of action. As the diisocyanate is incorporated last, this permits interaction of Dantocol and RDX prior to its addition. Isocyanates are then able to react with Dantocol's free hydroxyls groups. This occurs as depicted in Scheme 7.4, representing incorporation within the binder system. The increased affinity of IPDI and HTPB further limits dissociation of Dantocol interaction. Flexibility introduced by HTPB then assists in providing the molecular mobility necessary to promote covalent bonding of Dantocol and isocyanate. These combined conditions ensure filler interaction is maintained, whilst the bonding agent remaining hydroxyl functionality reacts to form urethane linkages.



**Scheme 7.4.** Interfacial adhesion involving Dantocol at the filler/binder system interface.

## 7.4 Conclusion

### 7.4.1 Copolymerisation of Polyurethane Blend

Characterisation of the mechanism involving Dantocol and the binder system, confirmed formation of urethane linkage following polymerisation with the isocyanate. This was established from the IR spectra, which identified evolution of bands responsible for polymerisation of Dantocol. These results were substantiated using rheological and thermal analysis to investigate polyurethane blends. The connotations of these findings have advanced knowledge of the mechanism involved in reaction of Dantocol and the binder system, whilst aiding in the design of novel systems.

Investigations conclude the occurrence of covalent bonding between Dantocol's multiple hydroxyl groups and the isocyanate, remains favourable over secondary bonding. This discredits the potential for hydrogen bonding between Dantocol's carbonyl groups and the hydroxyl functionality of HTPB, due to the polyol's reactivity with isocyanate groups.

Although hydrogen bonding may arise between amines formed during polymerisation of Dantocol, this is only possible following urethane formation. Suspension of Dantocol within the binder matrix was subsequently disproved, with covalent bonding confirmed responsible for incorporation of Dantocol.

Copolymerisation of HTPB and Dantocol with the diisocyanate was established using spectroscopic techniques, through evolution of characteristic urethane bands. This was accompanied by reduction of the isocyanate stretch as polymerisation occurs. Vibrational bands were further scrutinised through implementing spectral subtraction. This involved removal of bands associated with the IPDI/HTPB linkage, present within the polyurethane blend. The resulting subtraction spectra displayed bands consistent with IPDI/Dantocol linkages, as observed in the mono-alcohol system. These bands were found to appear at longer wavenumber compared with those associated with IPDI/HTPB linkages. This enables qualitative analysis of contributions from individual components.

In addition to spectroscopic techniques, the thermal behaviour of polyurethane blends was evaluated by DSC. Elucidation of the decomposition behaviour and glass transition temperature, confirmed incorporation of Dantocol within the binder matrix. Results inferred intermolecular forces between hard and soft segments were unaided by the addition of Dantocol within hard segments. Along with removal of  $T_m$  associated with unreacted Dantocol, these findings negate the potential for suspension of bonding agent within the binder system.

Knowledge of the rheo-kinetic properties involved in network formation provides insight into variations in alcohol reactivity. Investigations identified reaction of HTPB remains favourable over that involving Dantocol and the isocyanate. Consequently, this invokes multiple rate constants, which contribute towards kinetic behaviour of the blend. Along with the viscosity build-up and point of gelation, elucidation of rheological data confirms copolymerisation of blends and identifies the processability and pot-life of the binder system.

### 7.4.2 Cast-Cured PBX Composites

Investigations confirm Dantocol functions to increase the crosslink density in the area adjacent to filler particles. This occurs through covalent bonding with isocyanates, resulting in formation of urethane linkages. Incorporation of Dantocol within the binder system proceeds whilst simultaneously engaging in secondary bonding with RDX. Participating intermolecular forces include hydrogen bonding and dipole interactions, appearing in synergy to improve interfacial adhesion. This demonstrates the significance of Dantocol's multiple hydroxyl groups in facilitating both filler interaction and covalent bonding with IPDI.

Hydrogen bonding between free hydroxyl groups and isocyanates experience an autocatalytic effect described in Section 7.1.1. This occurs in contrast to inhibition imposed upon urethane formation, due to the influence of proton acceptors such as nitro compounds. Reaction inhibition is dependent on the polarising effect experienced between participating compounds.<sup>7</sup> This is evident within the current system, enabling hydrogen bonding between Dantocol and RDX to remain intact upon exposure to IPDI.

Dantocol remaining hydroxyl functionality is responsible for incorporation within the binder system. Characterisation of the polyurethane network revealed fundamental changes in chemical structure, subsequent to Dantocol addition. This identified the mechanism involved in bonding agent reaction, upon which contributes to hard segment formation. Evolution of urethane linkages therefore account for Dantocol's mode of action, coupled with the occurrence of filler interaction. The combined mechanism facilitates interfacial adhesion between the energetic filler and binder system. Consequently, the relative bond strength is accountable for prevention of dewetting, and improvement in mechanical properties.

## 7.5 References

1. Kohga, M., From Cross-linking to Plasticization – Characterization of Glycerin/HTPB Blends. *Propellants, Explosives, Pyrotechnics* **2009**, *34* (5), 436-443.
2. Sacher, E., A re-examination of the polyurethane reaction. *Journal of Macromolecular Science, Part B* **1979**, *16* (4), 525-538.
3. Satchell, D. P. N.; Satchell, R. S., Acylation by ketens and isocyanates. A mechanistic comparison. *Chemical Society Reviews* **1975**, *4* (2), 231-250.
4. Caraculacu, A. A.; Coseri, S., Isocyanates in polyaddition processes. Structure and reaction mechanisms. *Progress in Polymer Science* **2001**, *26* (5), 799-851.
5. Oberth, A. E.; Bruenner, R. S., Effect of hydrogen bonding on the kinetics of the urethane reaction. *The Journal of Physical Chemistry* **1968**, *72* (3), 845-855.
6. Baker, J. W.; Gaunt, J., The mechanism of the reaction of aryl isocyanates with alcohols and amines. Part II. The base-catalysed reaction of phenyl isocyanate with alcohols. *Journal of the Chemical Society* **1949**, 9-18.
7. Chang, M.-C.; Chen, S.-A., Kinetics and mechanism of urethane reactions: Phenyl isocyanate–alcohol systems. *Journal of Polymer Science Part A: Polymer Chemistry* **1987**, *25* (9), 2543-2559.
8. Coseri, S., The Effect of Various Additives on the Kinetic and Reaction Mechanism between Ethanol and Phenylisocyanate. *High Performance Polymers* **2007**, *19* (5-6), 520-530.
9. Han, J. L.; Yu, C. H.; Lin, Y. H.; Hsieh, K. H., Kinetic study of the urethane and urea reactions of isophorone diisocyanate. *Journal of Applied Polymer Science* **2008**, *107* (6), 3891-3902.
10. Sergiu, C., Contributions to the Mechanism of the Reactions of Isocyanates with Alcohols and Glycols. In *5th International Electronic Conference on Synthetic Organic Chemistry* **2001**; pp 1-7.
11. Broline, B. M. *Acylaziridine Reactivity in the Liner and Propellant Environments*; Boeing Aerospace Co: Seattle, **1985**.
12. Dostanić, J.; Husović, T. V.; Ušćumlić, G.; Heinemann, R. J.; Mijin, D., The influence of bonding agents in improving interactions in composite propellants determined using image analysis. *Journal of Microscopy* **2008**, *232* (3), 530-533.
13. Dostanić, J.; Ušćumlić, G.; Husović, T. V.; Heinemann, R. J.; Mijin, D., The use of image analysis for the study of interfacial bonding in solid composite propellant. *Journal of the Serbian Chemical Society* **2007**, *72* (10), 1023-1030.
14. Petković, J.; Wali, A.; Mijin, D.; Ušćumlić, G., The Influence of Bonding Agents in Improving Interactions in Composite Propellants, Determined Using the FTIR Spectra. *Scientific Technical Review* **2009**, *59* (3-4), 12-16.
15. Ušćumlić, G. S.; Zreigh, M. M.; Mijin, D. Z., Investigation of the interfacial bonding in composite propellants. 1,3,5-trisubstituted isocyanurates as universal bonding agents. *Journal of Serbian Chemistry Society* **2006**, *71* (5), 445-458.

16. Hamshere, B. L.; Lochert, I. J.; Dexter, R. M. *Evaluation of PBXN-109: The explosive fill for the penguin anti-ship missile warhead*; DSTO-TN-0440; DSTO: Weapons Systems Division, **2003**.
17. Daniel, M. A. *Polyurethane binder systems for polymer bonded explosives*; DSTO-GD-0492; DSTO: Weapons Systems Division, **2006**.
18. *Omnic user's guide, Version 7.3*. Thermo Electron Corporation: Madison, USA, **2006**; p 1-471.
19. Takada, K.; Matsuya, H.; Masuda, T.; Higashimura, T., Gas permeability of polyacetylenes carrying substituents. *Journal of Applied Polymer Science* **1985**, *30* (4), 1605-1616.
20. BillMeyer, F. W., *Textbook of Polymer Science*. 3rd ed.; Wiley-Interscience: New York, **1984**.
21. Huang, S.-L.; Lai, J.-Y., On the gas permeability of hydroxyl terminated polybutadiene based polyurethane membranes. *Journal of Membrane Science* **1995**, *105* (1–2), 137-145.
22. Brunette, C. M.; Hsu, S. L.; Rossman, M.; MacKnight, W. J.; Schneider, N. S., Thermal and mechanical properties of linear segmented polyurethanes with butadiene soft segments. *Polymer Engineering & Science* **1981**, *21* (11), 668-674.
23. Senich, G. A.; MacKnight, W. J., Fourier Transform Infrared Thermal Analysis of a Segmented Polyurethane. *Macromolecules* **1980**, *13* (1), 106-110.
24. Xingjun, L., Study of hydrogen bonds in polyester-polyurethanes by solution n.m.r. *Polymer* **1994**, *35* (11), 2315–2320.
25. Coleman, M. M.; Lee, K. H.; Skrovanek, D. J.; Painter, P. C., Hydrogen bonding in polymers. 4. Infrared temperature studies of a simple polyurethane. *Macromolecules* **1986**, *19* (8), 2149-2157.
26. Skrovanek, D. J.; Painter, P. C.; Coleman, M. M., Hydrogen bonding in polymers. 2. Infrared temperature studies of nylon 11. *Macromolecules* **1986**, *19* (3), 699-705.
27. Bengtson, B.; Feger, C.; MacKnight, W. J.; Schneider, N. S., Thermal and mechanical properties of solution polymerized segmented polyurethanes with butadiene soft segments. *Polymer* **1985**, *26* (6), 895-900.
28. Sung, C. S. P.; Schneider, N. S., Infrared Studies of Hydrogen Bonding in Toluene Diisocyanate Based Polyurethanes. *Macromolecules* **1975**, *8* (1), 68-73.
29. Chen, J. K.; Brill, T. B., Chemistry and kinetics of hydroxyl-terminated polybutadiene (HTPB) and diisocyanate-HTPB polymers during slow decomposition and combustion-like conditions. *Combustion and Flame* **1991**, *87* (3–4), 217-232.
30. Tingfa, D., Thermal decomposition studies of solid propellant binder HTPB. *Thermochimica Acta* **1989**, *138* (2), 189-197.
31. Sekkar, V.; Ambika Devi, K.; Ninan, K. N., Rheo-kinetic evaluation on the formation of urethane networks based on hydroxyl-terminated polybutadiene. *Journal of Applied Polymer Science* **2001**, *79* (10), 1869-1876.

32. Cunliffe, A. V.; Davis, A.; Farey, M.; Wright, J., The kinetics of the reaction of isophorone di-isocyanate with mono-alcohols. *Polymer* **1985**, *26* (2), 301-306.
33. Zaplatin, A. A.; Samigullin, F. K.; Zharkov, V. V.; Nikitina, L. N.; Kafeengauz, A. P., Kinetics of the reaction of phenyl isocyanate with butanol in bipolar aprotic solvents *Kinetika I Kataliz* **1974**, *16* (6), 1382
34. Ephraim, S.; Woodward, A. E.; Mesrobian, R. B., Kinetic Studies of the Reaction of Phenyl Isocyanate with Alcohols in Various Solvents1. *Journal of the American Chemical Society* **1958**, *80* (6), 1326-1328.
35. Zhao, F.-Q.; Chen, P.; Li, S.-W., Effect of ballistic modifiers on thermal decomposition characteristics of RDX/AP/HTPB propellant. *Thermochimica Acta* **2004**, *416* (1-2), 75-78.
36. Lee, J.-S.; Hsu, C.-K., Thermal properties and shelf life of HMX-*HTPB* based plastic-bonded explosives. *Thermochimica Acta* **2002**, *392-393* (0), 153-156.
37. Tsai, Y.-M.; Yu, T.-L.; Tseng, Y.-H., Physical properties of crosslinked polyurethane. *Polymer International* **1998**, *47* (4), 445-450.
38. Provatas, A. *Characterisation and Polymerisation Studies of Energetic Binders*; DSTO-TR-1171; DSTO: Weapons Systems Division, **2001**.
39. Coleman, M. M.; Skrovanek, D. J.; Hu, J.; Painter, P. C., Hydrogen bonding in polymer blends. 1. FTIR studies of urethane-ether blends. *Macromolecules* **1988**, *21* (1), 59-65.
40. Koshiha, M.; Hwang, K. S.; Foley, S.; Yarusso, D.; Cooper, S., Properties of ultra-violet curable polyurethane acrylates. *Journal of Materials Science* **1982**, *17* (5), 1447-1458.
41. Ono, H.-K.; Jones, F. N.; Pappas, S. P., Relative reactivity of isocyanate groups of isophorone diisocyanate. Unexpected high reactivity of the secondary isocyanate group. *Journal of Polymer Science: Polymer Letters Edition* **1985**, *23* (10), 509-515.
42. Lomölder, R.; Plogmann, F.; Speier, P., Selectivity of isophorone diisocyanate in the urethane reaction influence of temperature, catalysis, and reaction partners. *Journal of Coatings Technology* **1997**, *69* (868), 51-57.
43. Bialas, N.; Höcker, H.; Marschner, M.; Ritter, W., <sup>13</sup>C NMR studies on the relative reactivity of isocyanate groups of isophorone diisocyanate isomers. *Die Makromolekulare Chemie* **1990**, *191* (8), 1843-1852.
44. Prabhakar, A.; Chattopadhyay, D. K.; Jagadeesh, B.; Raju, K. V. S. N., Structural investigations of polypropylene glycol (PPG) and isophorone diisocyanate (IPDI)-based polyurethane prepolymer by 1D and 2D NMR spectroscopy. *Journal of Polymer Science Part A: Polymer Chemistry* **2005**, *43* (6), 1196-1209.
45. Spyrou, E.; Metternich, H. J.; Franke, R., Isophorone diisocyanate in blocking agent free polyurethane powder coating hardeners: analysis, selectivity, quantumchemical calculations. *Progress in Organic Coatings* **2003**, *48* (2-4), 201-206.
46. Hatada, K.; Ute, K.; Peter Pappas, S., E,Z assignments of isophorone diisocyanate (IPDI) and their implications on the relative reactivity of the isocyanate groups. *Journal of Polymer Science Part C: Polymer Letters* **1987**, *25* (12), 477-480.

47. Gerard, J.-F.; Percec, P. L.; Pham, Q. T., Polyuréthanes à propriétés émulsifiantes et électrolytiques, 2. Cinétique de polycondensation en solution des alkylimino-2,2' diéthanol avec le diisocyanate d'isophorone. Etude par  $^1\text{H}$  et  $^{13}\text{C}$  NMR. *Die Makromolekulare Chemie* **1988**, 189 (7), 1719-1737.
48. Lorenz, O.; Decker, H.; Rose, G., NCO-prepolymere aus diisocyanaten mit unterschiedlich reaktiven NCO-gruppen. *Die Angewandte Makromolekulare Chemie* **1984**, 122 (1), 83-99.
49. Surivet, F.; Lam, T. M.; Pascault, J.-P., Control synthesis of isocyanate and alkoxy-silane terminated macromers. *Journal of Polymer Science Part A: Polymer Chemistry* **1991**, 29 (13), 1977-1986.
50. Hatada, K.; Ute, K.; Oka, K.-I.; Pappas, S. P., Unambiguous  $^{13}\text{C}$ -NMR assignments for isocyanate carbons of isophorone diisocyanate and reactivity of isocyanate groups in Z - and E-stereoisomers. *Journal of Polymer Science Part A: Polymer Chemistry* **1990**, 28 (11), 3019-3027.







# Chapter 8

---

Synthesis of novel bonding agents

---

Sections of this chapter were published in: Williams, C. A.; Walker, G. S.; Lochert, I. J.; Clarke, S., Investigation into the interaction of Dantocol in polymer bonded explosives and bonding agent development. *16th New trends in energetic materials*, Pardubice, Czech Republic, 2013; Vol. I, pp 399-406.

Williams, C. A.; Walker, G. S.; Lochert, I. J.; Clarke, S. R.; Kirkbride, P.K, Investigation into the interaction of Dantocol in polymer bonded explosives and bonding agent development. *4<sup>th</sup> Australian energetic materials symposium*, Adelaide, Australia. 2014.

## 8.1 Introduction

Few organic compounds are recognised to improve the interfacial adhesion of nitramine based PBX composites. The search for bonding agents capable of achieving this function therefore remains an active area of research. Given the benefits relayed to cast-cured energetic materials, expanding the range of available bonding agents is acknowledged as highly desirable. Amongst the limited number of current products, most experience issues associated with basicity, evolution of gas, destruction of the energetic plasticizer, low density and poor strain capabilities. This reflect the need for advances in bonding agent technology.

Development of novel bonding agents which overcome limitations encountered amongst commercial examples, evidently presents a substantial benefit to cast-cured energetic materials. Upon attempt to improve bonding agent design, considerations should be made to ensure proposed compounds contribute towards decreased sensitivity, appropriate mixing times, improved mechanical properties, lower costs and decreased mixing viscosity. To satisfy these requirements specific properties must be realised to ensure functionality is observed.

An effective bonding agent should be soluble within the submix, at temperatures exceeding that encountered upon mixing. This enables dispersal throughout the submix, whereby functionality adheres to the surface of filler particles. Bonding agents regarded as too soluble consequently fail to undergo phase separation, causing retention within the binder system. The solubility parameter should therefore lie between values associated with the filler/binder system. Amid presence of non-polar binder systems, polar bonding agents undergo adsorption at the surface of nitramine particles. This requires the bonding agents affinity for polar nitro groups to exceed that of additional PBX components. Evidently, the bonding agents polar functionality is therefore responsible for migration towards filler particles, and subsequent surface interaction.

The implications of pH are also significant in terms of bonding agent compatibility and function. Both acidic and basic compounds tend to migrate towards filler particles more readily than neutral examples. However, the effect of excessive increase or decrease in pH may also result in inhibition of cure, or degradation of filler/binder components.<sup>1</sup> Basic conditions are also avoided due to issues arising from gassing and the effect on bonding agents hydroxyl functionality. This causes the proton donor to exhibit increased nucleophilicity. The inclusion of acidic protons is also known to impose significant compatibility issues. This involves functionally such as amines which engage in reaction with nitramine particles, thus rendering potential bonding agent incompatible.

Selection of bonding agent functionality is partially dependant on the binder system, as components must be capable of covalent bonding. As polyurethane binder systems are commonly applied, compatible bonding agents often comprise hydroxyl functionality. Hydroxyalkyl amides have been shown to esterify more rapidly than conventional alcohols, providing an explanation for Dantocol's cross-linking efficiency. The reactivity of bonding agent towards isocyanates is therefore decisive in its ability to incorporate within polyurethane based composites. To improve reactivity of hydroxyalkyl amides and diisocyanate curatives, previous investigations were conducted into the effects of acid and base catalysis. Lomax et al. reported variable success in catalysing the urethane reaction.<sup>2</sup>

Bonding agents must also comprise functionality available to participate in secondary bonding, involving the energetic filler applied. Hydantoin derivatives represent a class of bonding agent capable of providing a means for such interaction. Since the initial application, various hydantoin derivatives have emerged according to their efficiency as bonding agents. This is owing to the heterocycles unique structure, which facilitates interfacial adhesion to achieve tightly bound cast-cured energetic materials.<sup>3</sup> Alternative side chains were investigated by Consaga et al. identifying hydroxyalkyl functionality as the most efficient in terms of bonding agent performance.<sup>4,5</sup> This also recognised hydroxyl, epoxy or isocyanate terminated chains as preferable for application in HTPB-based binder systems.

Preparation of hydantoin derivatives involved substitution of functionality indicated in Figure 8.1.

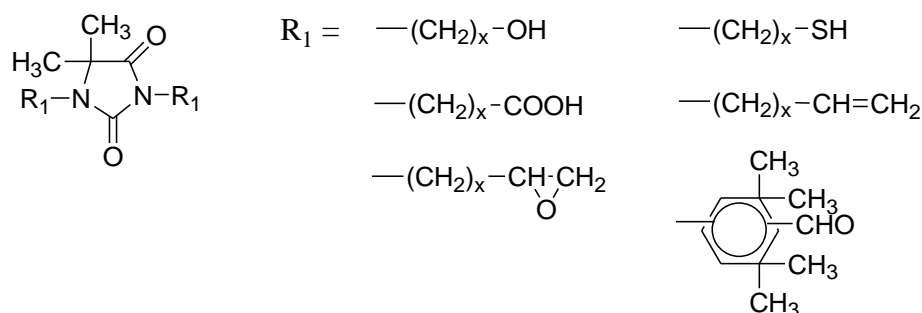


**Figure 8.1.** Substitution of hydantoin functionality.

Based on the success of hydroxyalkyl hydantoin, variation in chain length was investigated to optimise bonding agent efficiency. Hydantoin comprising hydroxyalkyl side chains of between 1 - 10 carbons were identified as necessary to facilitate function. Meanwhile, optimal conditions were achieved following substitution of chains spanning 1 - 5 carbons in length. Resultant bonding agents were incorporated within cast-cured energetic material, revealing improved elongation and modulus.<sup>6</sup> In addition, the instability of hydroxymethyl imides was similarly characterised by Vail et al.<sup>7</sup>

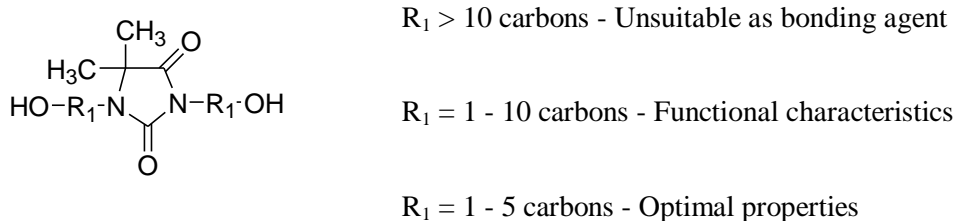


**Figure 8.2.** Variation of hydroxyalkyl chain length.

The addition of alternative polar groups is nonessential to function, as hydroxyls remain capable of bonding with both the filler and binder system. Dehm et al. investigated a series of polyols including 1,2-propanediol, 1,3-propanediol, 1,4-butanediol, 1,3-hexanediol, 1,8-octanediol and glycerol, concerning application in nitramine-based composites.<sup>8</sup> This involved encapsulating filler particles with the proposed diols, followed by reaction with isocyanates in the presence of catalyst. The mechanical properties of composites acquired

were found to improve upon addition of bonding agent. This confirmed the ability of hydroxyls to undergo cross-linking with the binder system, whilst engaging in hydrogen bonding between filler particles. Fundamental work by Kim et al. also concluded compounds containing one or more functional groups were capable of satisfying bonding agent criteria.<sup>9</sup>

10

Application of N-heterocyclic compounds amid organic polymers demonstrates the capability to improve thermal stability.<sup>11</sup> This presents the opportunity to address limitations associated with the upper temperature range of cast-cured energetic materials. Common examples of thermostable N-heterocycles include hydantoin, isocyanuric acid, barbituric acid, 5,5-diethylbarbituric acid, uric acid, adenine, parabanic acid and melamine.<sup>11</sup> Each exhibit thermal decomposition in excess of  $T_d > 300^\circ\text{C}$ , thus improving thermal stability upon incorporation within the network. This is pertinent to satisfying the requirements of insensitive munitions and therefore a consideration amid bonding agent design. Consequently, isocyanuric acid and parabanic acid were selected as starting materials for the synthesis of novel bonding agents.

Increasing the size of bonding agent molecules provides the potential to introduce additional binding sites, with studies suggesting macromolecules often outperform smaller molecules.<sup>9</sup> The purpose of increasing the end-group concentration serves to enable greater adsorption at dilute concentrations. This also introduces greater flexibility in modifying the solubility characteristics of bonding agents.<sup>12</sup> In response, the use of dendrimers was proposed for bonding agent application. This presents significant potential, as dendrimers are suited to most applications where low viscosity and excess functional groups are advantageous.<sup>13</sup> Despite these characteristics, dendrimers have observed limited application within cast-cured energetic materials until now.

Due to the many requirements demanded of an effective bonding agent, few compounds are available for application in nitramine based composites.<sup>5</sup> This includes the obligation to improve mechanical properties through occurrence of interfacial adhesion. In addition to

forming bonds between the highly dissimilar filler/binder system, bonding agents are required to overcome issues associated with the nitramines smooth inert surface. This is necessary to prevent dissociation of intermolecular forces, responsible for the propagation of dewetting. Bonding agents must also remain chemically and thermally stable, while preferably displaying compatibility within a range of energetic fillers and binder systems. With emphasis on satisfying these requirements, novel compounds were proposed for incorporation within cast-cured PBX composites. The composition of bonding agents was determined based on the results of previous chapters and fulfilment of these conditions.

## 8.2 Experimental

### 8.2.1 Adduct Characterisation

#### 8.2.1.1 Difunctional Isocyanate Terminated Bonding Agent

Difunctional isocyanate terminated bonding agent (DITBA) describes a hydantoin and meta-tetramethylxylene diisocyanate (TMXDI) adduct. This comprises 65% isocyanate-terminated hydantoin and 35% TMXDI curative. The diisocyanate monomer contains two tertiary aliphatic isocyanates which polymerise with hydroxyl-terminated prepolymers, forming a polyurethane network. This provides unique characteristics upon comparison to IPDI and its primary/secondary isocyanates. Reaction of TMXDI and Dantocol results in the diisocyanate terminated hydantoin highlighted in Figure 8.3. This accounts for the principle component of DITBA, producing a viscous adduct of slight acidity (pH = 5.5).

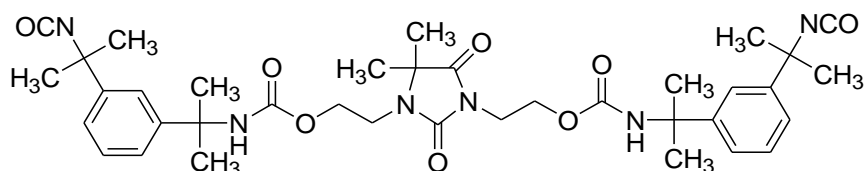


**Figure 8.3.** Difunctional isocyanate terminated bonding agent.



$^1\text{H}$  NMR 600MHz, Chloroform-*d*,  $\delta$  (ppm): 1.36 (s, 6H,  $2\text{CH}_3$ ); 1.70 (s, 12H,  $2\text{C}(\text{CH}_3)_2$ ); 3.46 (t, 2H,  $\text{CH}_2\text{-N}$ ); 3.70 (t, 2H,  $\text{CH}_2\text{-N}$ ); 4.17 (t, 4H,  $2\text{CH}_2\text{-O}$ ); 5.08-5.44 (br, 1H, *NH*); 7.25-7.34 (m, 3H,  $3\text{CH}$  arom); 7.47 (s, 1H, *CH* arom).

$^{13}\text{C}$  NMR 600MHz, Chloroform-*d*,  $\delta$  (ppm): 22.47 ( $2\text{CH}_3$ ); 28.93, 29.64 ( $2\text{CH}_3$ ); 38.14, 38.63 ( $\text{CH}_2\text{-N}$ ); 54.54, 61.27 (C); 54.92 ( $2\text{CH}_2\text{-O}$ ); 120.02-127.99 (4CH arom); 123.63 (NCO); 145.56 ( $2\text{C}$  arom); 155.63 ( $2\text{NHCOO}$ ); 154.86, 176.16 ( $2\text{C}=\text{O}$ ).

FTIR,  $\nu$  ( $\text{cm}^{-1}$ ): 3343.45 $\text{cm}^{-1}$  ( $\nu$  *NH*); 3055.71( $\nu$  aromatic ring); 2974.67 $\text{cm}^{-1}$  ( $\nu$  aliphatic  $\text{CH}_2$ ); 2249.58 ( $\nu$  NCO); 1652.59, 1704.62 $\text{cm}^{-1}$  ( $\nu$   $\text{C}=\text{O}$ ); 1525.54 ( $\nu$  AmideI); 1455.75, 1382.52 $\text{cm}^{-1}$  ( $\nu_{\text{as}}$   $\text{CH}_2\text{-N}$ ); 1230.97 ( $\nu$  AmideII); 767.44 $\text{cm}^{-1}$  ( $\nu$   $\text{CH}_2$ ); 703.81 ( $\nu$  aromatic ring).

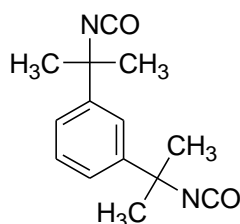


**Figure 8.4.** Meta-tetramethylxylylene diisocyanate.

$^1\text{H}$  NMR 600MHz, Chloroform-*d*,  $\delta$  (ppm): 1.74 (s, 12H,  $2\text{C}(\text{CH}_3)_2$ ); 7.34 (m, 3H, *CH* arom); 7.52 (s, 1H, *CH* arom).

$^{13}\text{C}$  NMR 600MHz, Chloroform-*d*,  $\delta$  (ppm): 32.62 ( $4\text{CH}_3$ ); 60.44 ( $2\text{C}$ ); 120.40, 123.24, 128.17 (4CH arom); 123.63 (NCO); 146.74 ( $2\text{C}$  arom).

### 8.2.1.2 Trifunctional Isocyanate Terminated Bonding Agent

Trifunctional isocyanate terminated binding agent (TITBA) alternatively consists of an isocyanurate and TMXDI adduct. This constitutes 65% isocyanate-terminated isocyanurate and 35% TMXDI curative. Consequently, the structure of isocyanurate introduces addition functionality responsible for the triisocyanate. This is depicted in Figure 8.5, such as occurs

in TITBA. The resulting adduct again demonstrates high viscosity and low acidity, consistent with that of the difunctional adaptation.

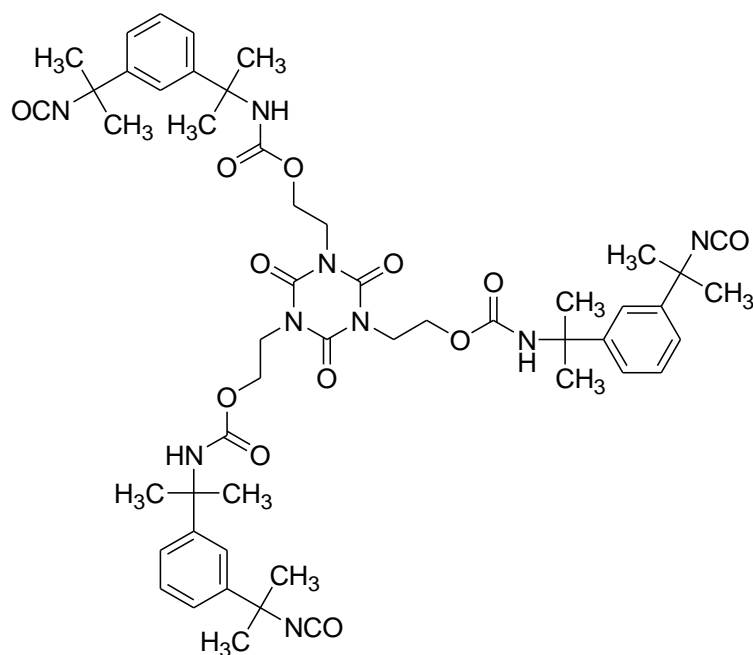


**Figure 8.5.** Trifunctional isocyanate terminated bonding agent.

$^1\text{H}$  NMR 600MHz, Chloroform-*d*,  $\delta$  (ppm): 1.70 (s, 12H,  $2\text{C}(\text{CH}_3)_2$ ); 4.11 (t, 6H,  $3\text{CH}_2\text{-N}$ ); 4.26 (t, 6H,  $3\text{CH}_2\text{-O}$ ); 5.08-5.59 (br, 3H,  $3\text{NH}$ ); 7.25-7.34 (m, 3H,  $3\text{CH}$  arom); 7.46 (s, 1H,  $\text{CH}$  arom).

$^{13}\text{C}$  NMR 600MHz, Chloroform-*d*,  $\delta$  (ppm): 29.54, 30.33 ( $2\text{CH}_3$ ); 42.66 ( $3\text{CH}_2\text{-N}$ ); 55.25 ( $3\text{CH}_2\text{-O}$ ); 55.52 ( $2\text{C}$ ); 121.16-128.54 ( $4\text{CH}$  arom); 123.51 (NCO); 147.37 ( $2\text{C}$  arom); 149.19 ( $3\text{C}=\text{O}$ ); 154.53 (NHCOO).

FTIR,  $\nu$  ( $\text{cm}^{-1}$ ): 3347.01 ( $\nu$  NH); 3060.49 ( $\nu$  aromatic ring); 2971.86 ( $\nu$  aliphatic  $\text{CH}_2$ ); 2261.84 ( $\nu$  NCO); 1689.27 ( $\nu$   $\text{C}=\text{O}$ ); 1521.65 ( $\nu$  AmideI); 1454.65, 1382.06 ( $\nu_{\text{as}}$   $\text{CH}_2\text{-N}$ ); 1231.21 ( $\nu$  AmideII); 762.75 ( $\nu$   $\text{CH}_2$ ); 703.58 ( $\nu$  aromatic ring).

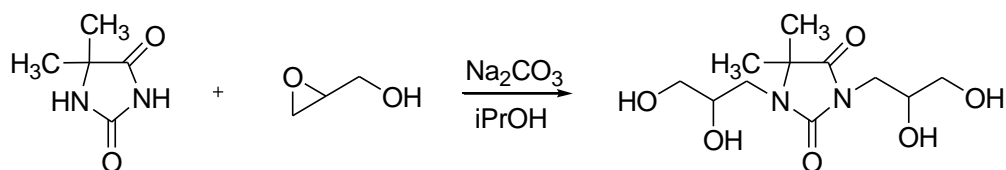
#### Meta-Tetramethylxylylene Diisocyanate

$^1\text{H}$  NMR 600MHz, Chloroform-*d*,  $\delta$  (ppm): 1.73 (s, 12H,  $2\text{C}(\text{CH}_3)_2$ ); 7.34 (m, 3H,  $3\text{CH}$  arom); 7.52 (s, 1H,  $\text{CH}$  arom).

$^{13}\text{C}$  NMR 600MHz, Chloroform-*d*,  $\delta$  (ppm): 33.32 (4CH<sub>3</sub>); 61.15 (2C); 121.45, 123.08, 128.56 (4CH aromat); 123.54 (2NCO); 146.28 (2C aromat).

### 8.2.2 Synthesis of 1,3-Bis(2,3-dihydroxypropyl)-5,5-dimethylhydantoin

Based on the hydantoin structure, 1,3-*bis*(2,3-dihydroxypropyl)-5,5-dimethylhydantoin was prepared via attachment of dihydroxypropyl side chains. This involved combining 5,5-dimethylhydantoin (0.05mol, 6.41g) and sodium carbonate (0.05mol, 5.30g) in propan-2-ol (100mL). Constituents were mixed at 70°C under N<sub>2</sub> purge to form a homogenous solution. Glycidol (0.11mol, 8.15g) was then added dropwise, whilst increasing the temperature to 80°C. The solution was left to reflux overnight, after which the product was filtered to remove catalyst. Solvent was then evaporated, and the remaining contents washed in diethyl ether to remove excess glycidol. This was dried with potassium carbonate to provide 1,3-*bis*(2,3-dihydroxypropyl)-5,5-dimethylhydantoin in 94% yield.



**Scheme 8.1.** Synthesis of 1,3-*bis*(2,3-dihydroxypropyl)-5,5-dimethylhydantoin.

$^1\text{H}$  NMR 600MHz, Acetone-*d*<sub>6</sub>,  $\delta$  (ppm): 1.38, 1.41 (s, 3H, CH<sub>3</sub>); 3.47, 3.50 (d, 4H, 2CH<sub>2</sub>-OH); 3.55, 3.58 (d, 2H, CH<sub>2</sub>-N); 3.74 (t, 2H, 2CH<sub>2</sub>-OH); 3.86 (m, 2H, 2CH-OH); 4.11, 4.16 (d, 1H, CH-OH).

$^{13}\text{C}$  NMR 600MHz, Acetone-*d*<sub>6</sub>,  $\delta$  (ppm): 25.06, 25.08 (CH<sub>3</sub>); 42.10, 42.55 (CH<sub>2</sub>-N); 59.04 (C); 64.62, 64.88 (CH<sub>2</sub>-OH); 70.20, 70.38 (CH-OH); 157.18, 178.60 (C=O).

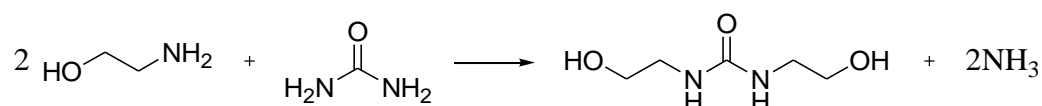
FTIR,  $\nu$  (cm<sup>-1</sup>): 770.35 ( $\nu$  CH<sub>2</sub>); 1096.72, 1042.50 ( $\nu$ OH); 1447.97 ( $\nu_{\text{as}}$ CH<sub>2</sub>-N); 1692.78, 1651.81 ( $\nu$ C=O); 2933.54 ( $\nu$ CH<sub>2</sub> aliphatic); 3334.53 ( $\nu$ OH).

### 8.2.3 Synthesis of Hydroxyalkyl Ureas

Hydroxyalkyl urea bonding agents were prepared from aminoalcohols and a single urea equivalent. The design of bonding agents incorporates two or more hydroxyl groups, forming linear, branched or substituted configurations. This was achieved by the aminoalcohol applied, which extended to the use of various such combinations. Reaction of constituents proceeds in the absence of both solvent and catalyst, providing favourable conditions from which limited purification was required.

#### 8.2.3.1 Synthesis of 1,3-Bis(2-hydroxyethyl)urea

Ethanolamine (0.02mol, 1.22g) and urea (0.01mol, 0.60g) were charged to a 50mL round bottom flask equipped with stirrer and condenser. Reactants were heated at 120°C for 8 hours, whilst engaged in mixing of the solution. As the reaction proceeds ammonia was produced requiring N<sub>2</sub> purge to effect its removal. The resulting low viscosity liquid was purified under vacuum, driving off ammonia dissolved in residual water to provide 1,3-bis(2-hydroxyethyl)urea at 97% yield.



**Scheme 8.2.** Synthesis of 1,3-bis(2-hydroxyethyl)urea.

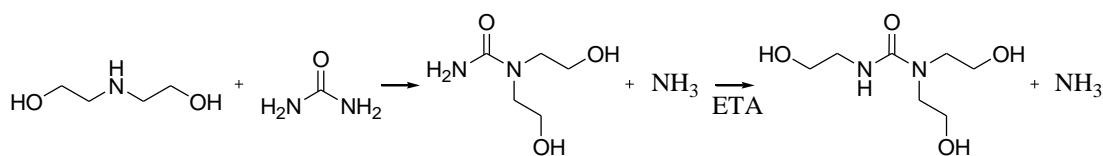
<sup>1</sup>H NMR 600MHz, Deuterium oxide, δ (ppm): 2.69, 3.20 (t, 2H, CH<sub>2</sub>-N); 3.55, 3.57 (t, 2H, CH<sub>2</sub>-OH).

<sup>13</sup>C NMR 600MHz, Deuterium oxide, δ (ppm): 41.85, 42.24 (NH-CH<sub>2</sub>); 60.63, 60.80 (CH<sub>2</sub>-OH); 160.76 (C=O)

FTIR, ν (cm<sup>-1</sup>): 1059.54, 1042.40 (νOH); 1263.89 (νAmide); 1562.06 (νNH bend); 1625.41 (νC=O); 2935.83, 2864.21 (νCH<sub>2</sub>); 3287.31 (νOH).

### 8.2.3.2 Synthesis of 1,1,3-*Tris*(2-hydroxyethyl)urea

Synthesis of 1,1,3-*tris*(2-hydroxyethyl)urea involves a two-step process, involving initial reaction of diethanolamine (0.01mol, 1.05g) and an equivalent urea (0.01mol, 0.60g) molarity. Constituents were mixed at 120°C for 8 hours under N<sub>2</sub> purge. This was followed by reaction with ethanolamine (0.01mol, 0.61g), occurring at the remaining amine group. The resulting triol was purified under vacuum to remove ammonia, thus revealing 1,1,3-*tris*(2-hydroxyethyl)urea of yield 86%.



**Scheme 8.3.** Synthesis of 1,1,3-*tris*(2-hydroxyethyl)urea.

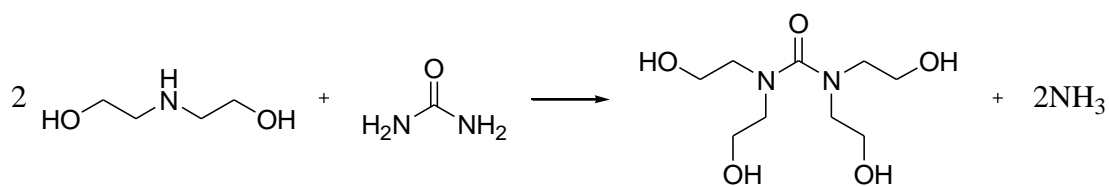
<sup>1</sup>H NMR 600MHz, Deuterium oxide,  $\delta$  (ppm): 2.70, 3.19, 3.41 (t, 2H, CH<sub>2</sub>-N); 3.58, 3.65, 3.69 (t, 2H, CH<sub>2</sub>-OH).

<sup>13</sup>C NMR 600MHz, Deuterium oxide,  $\delta$  (ppm): 41.35 (NH-CH<sub>2</sub>); 49.29 (2NH-CH<sub>2</sub>); 59.05, 59.70, 60.14 (CH<sub>2</sub>-OH); 161.00 (C=O).

FTIR,  $\nu$  (cm<sup>-1</sup>): 765.21 ( $\nu$ CH<sub>2</sub>); 1045.31 ( $\nu$ OH stretch); 1548.43 ( $\nu$ NH bend); 1648.46 ( $\nu$ C=O); 2927.73, 2871.60 ( $\nu$ CH<sub>2</sub>); 3299.21 ( $\nu$ OH).

### 8.2.3.3 Synthesis of 1,1,3,3-*Tetrakis*(2-hydroxyethyl)urea

Using the previously described method, diethanolamine (0.02mol, 2.10g) and urea (0.01mol, 0.60g) were refluxed at 120°C for 8 hours under N<sub>2</sub> purge. The addition of two diethanolamine equivalents facilitates attachment to urea's multiple amine moieties. This results in the tetraol depicted in reaction Scheme 8.4. Purification was performed under vacuum to acquire 1,1,3,3-*tetrakis*(2-hydroxyethyl)urea at 94% yield.



**Scheme 8.4.** Synthesis of 1,1,3,3-tetrakis(2-hydroxyethyl)urea.

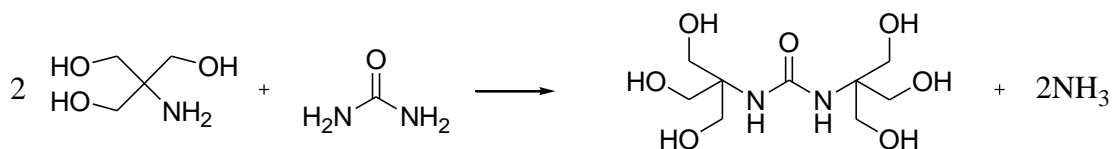
$^1\text{H}$  NMR 600MHz, Deuterium oxide,  $\delta$  (ppm): 2.69, 3.40 (t, 4H,  $2\text{CH}_2\text{-N}$ ); 3.63, 3.68 (t, 4H,  $2\text{CH}_2\text{-OH}$ ).

$^{13}\text{C}$  NMR 600MHz, Deuterium oxide,  $\delta$  (ppm): 49.80 ( $4\text{CH}_2\text{-N}$ ); 59.54, 60.23 ( $2\text{CH}_2\text{-OH}$ ); 161.51 ( $\text{C}=\text{O}$ ).

FTIR,  $\nu$  ( $\text{cm}^{-1}$ ): 770.79 ( $\nu\text{CH}_2$ ); 1037.62 ( $\nu\text{OH}$ ); 1245.53 ( $\nu\text{Amide}$ ); 1587.45 ( $\nu\text{NH}$  bend); 1649.81 ( $\nu\text{C}=\text{O}$ ); 2925.75, 2843.39 ( $\nu\text{CH}_2$ ); 3269.64 ( $\nu\text{OH}$ ).

#### 8.2.3.4 Synthesis of 1,3-Bis[3-hydroxy-1,1-bis(2-hydroxyethyl)propyl]urea

Following similar methodology, 2-amino-2-hydroxymethyl-propane-1,3-diol (0.02mole, 2.42g) was substituted in the reaction involving urea (0.01mol, 0.60g) amine functionality. Reactants were charged to a 50mL round bottom flask, equipped with condenser and magnetic stirrer. The solution was heated to  $140^\circ\text{C}$  under  $\text{N}_2$  purge, and stirred over a period of 8 hours. 1,3-bis[3-hydroxy-1,1-bis(2-hydroxyethyl)propyl]urea was acquired following in vacuo removal of ammonia, resulting in 76% yield.



**Scheme 8.5.** Synthesis of 1,3-bis[3-hydroxy-1,1-bis(2-hydroxyethyl)propyl]urea.

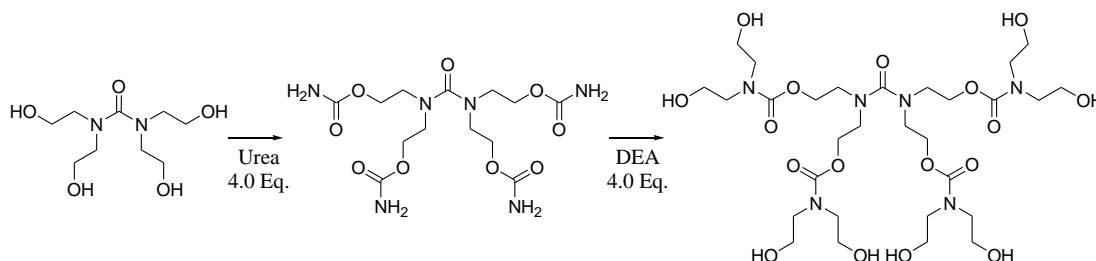
$^1\text{H}$  NMR 600MHz, Deuterium oxide,  $\delta$  (ppm): 3.51 (s, 12H,  $6\text{CH}_2\text{-OH}$ ).

$^{13}\text{C}$  NMR 600MHz, Deuterium oxide,  $\delta$  (ppm): 55.83 ( $2\text{C-N}$ ); 62.56 ( $6\text{CH}_2\text{-OH}$ ); 161.09 ( $\text{C}=\text{O}$ ).

FTIR,  $\nu$  ( $\text{cm}^{-1}$ ): 769.59 ( $\nu\text{CH}_2$ ); 1020.12 ( $\nu\text{OH}$ ); 1279.80 ( $\nu\text{Amide}$ ); 1586.53 ( $\nu\text{NH bend}$ ); 1721.98 ( $\nu\text{C=O}$ ); 2920.84, 2846.23 ( $\nu\text{CH}_2$ ); 3234.86 ( $\nu\text{OH}$ ).

## 8.2.4 Synthesis of Polycarbamate Dendrimer

An alternative synthetic approach was applied in the preparation of polycarbamate dendrimers. This involved engaging urea (0.01mol, 0.60g) as an initiator core, amid reaction with diethanolamine (0.02mol, 2.10g) described in Section 8.2.3.3. Assembly of second generation architecture was initiated upon repeat urea addition (0.04mol, 2.40g), producing carbamate linkages according to reaction Scheme 8.6. Conditions involve refluxing constituents at 120°C for 8 hours under  $\text{N}_2$  purge. The polycarbamate (0.002mol, 0.81g) intermediate was then reacted with diethanolamine (0.008mol, 0.84g) at 120°C for an additional 12 hours. This resulted in acquisition of the second generation polycarbamate dendrimer. Purification was performed at each stage of preparation, involving removal of ammonia and unreacted compounds.



**Scheme 8.6.** Synthesis of dendrimeric polycarbamate.

$^1\text{H}$  NMR 600MHz, Deuterium oxide,  $\delta$  (ppm): 2.74 (t, 8H,  $4\text{CH}_2\text{-N}$ ); 3.44 (t, 16H,  $4\text{OCN}(\text{CH}_2)_2$ ); 3.68 (t, 8H,  $4\text{CH}_2\text{-O}$ ); 3.73 (t, 16H,  $8\text{CH}_2\text{-OH}$ ).

$^{13}\text{C}$  NMR 600MHz, Deuterium oxide,  $\delta$  (ppm): 49.28, 49.37 ( $2\text{CH}_2\text{-N}$ ); 59.05 ( $8\text{CH}_2\text{-OH}$ ); 59.68 ( $8\text{CH}_2\text{-N}$ ); 62.70 ( $4\text{CH}_2\text{-O}$ ); 160.50 ( $\text{C=O}$ ); 161.00 ( $4\text{C=O}$ ).

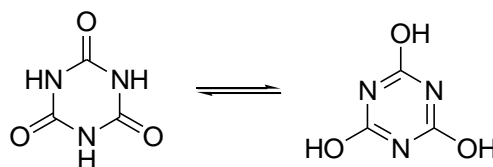
FTIR,  $\nu$  ( $\text{cm}^{-1}$ ): 764.16 ( $\nu\text{CH}_2$ ); 1027.89 ( $\nu\text{OH}$ ); 1272.23 ( $\nu\text{Amide}$ ); 1584.79 ( $\nu\text{NH bend}$ ); 1725.89, 1645.40 ( $\nu\text{C=O}$ ); 2928.81, 2874.59 ( $\nu\text{CH}_2$ ); 3270.49 ( $\nu\text{OH}$ ).

## 8.2.5 Hydroxyalkylation of Heterocyclic Compounds

Heterocyclic compounds comprising hydroxyethyl side chains were proposed for application as novel bonding agents. This involved reaction of nitrogen containing heterocycles and ethylene oxide to produce desired compounds. Base-catalysed hydroxyalkylation of heterocyclic amides is often problematic due to vulnerability towards ring opening.<sup>7</sup> Consequently, reaction was performed either neat or in the presence of polar solvents, unreactive to ethylene oxide.

### 8.2.5.1 Preparation of 1,3,5-*Tris*(2-hydroxyethyl)isocyanurate

The trifunctional isocyanurate was purchased from Sigma Aldrich and purified prior to application. This involved recrystallisation from isopropanol, followed by drying at 80°C under vacuum. Characterisation was subsequently performed by spectroscopic techniques to confirm purity. The preparation of 1,3,5-*tris*(2-hydroxyethyl)isocyanurate is readily performed in high yield, via reaction of isocyanuric acid and ethylene oxide. This is conducted in the presence of an inert solvent and alkaline catalyst, preventing the occurrence of side reactions.<sup>14</sup> The cyanuric acid derivative exists as tautomers, interconverting between cyanuric acid and isocyanuric acid. Tautomers differ in the location of hydrogen atoms, while aromaticity contributes to the stability of triple lactam-lactim tautomerism. Reaction with ethylene oxide results in protons forming the hydroxyl functionality. This amounts to hydroxyethyl attachment, upon which 1,3,5-*tris*(2-hydroxyethyl)isocyanurate is acquired.



**Scheme 8.7.** Isocyanurate acid and cyanuric acid tautomers.

<sup>1</sup>H NMR 600MHz, Dimethyl sulfoxide-*d*<sub>6</sub>,  $\delta$  (ppm): 3.53 (m, 6H, 3CH<sub>2</sub>-OH); 3.82 (t, 6H, 3CH<sub>2</sub>-N); 4.76 (t, 3H, 3OH).

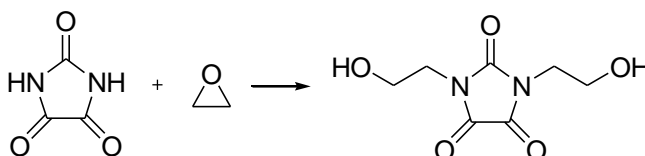


$^{13}\text{C}$  NMR 600MHz, Dimethyl sulfoxide- $d_6$ ,  $\delta$  (ppm): 44.22 (3 $\text{CH}_2\text{-N}$ ); 57.46 (3 $\text{CH}_2\text{-OH}$ ); 149.07 (3 $\text{C=O}$ ).

FTIR,  $\nu$  ( $\text{cm}^{-1}$ ): 763.36 ( $\nu\text{CH}_2$ ); 1054.86, 1035.62 ( $\nu\text{OH}$  stretch); 1453.63 ( $\nu_{\text{as}}\text{CH}_2\text{-N}$ ); 1671.32 ( $\nu\text{C=O}$ ); 2884.50 ( $\nu\text{CH}_2$  aliphatic); 3241.49-3482.34 ( $\nu\text{OH}$ ).

### 8.2.5.2 Synthesis of 1,3-Bis(2-hydroxyethyl)parabanate

Hydroxyalkylation of parabanic acid was performed by reaction with ethylene oxide in the presence of triethylamine. Parabanic acid (0.01mol, 1.14g) and catalytic triethylamine ( $3 \times 10^{-4}$ mol, 0.03g) was charged to a 100mL Young's vessel equipped with magnetic stirrer. Reactants were heated to  $35^\circ\text{C}$  under  $\text{N}_2$  purge, thus removing atmospheric moisture. facilitate the removal of moisture. Ethylene oxide (0.02mol, 0.88g) was then introduced in its gaseous state, via Masterflex Chem-Durance™ tubing. This was measured according to gain in weight of the reaction vessel. The solution was stirred overnight (12-15 hours), after which triethylamine was removed at  $80^\circ\text{C}$  under vacuum. Recrystallisation of 1,3-bis(2-hydroxyethyl)parabanate was promoted upon cooling in isopropanol. This was isolated by means of filtration and the remaining solvent removed under vacuum.



**Scheme 8.8.** Synthesis of 1,3-bis(2-hydroxyethyl)parabanate.

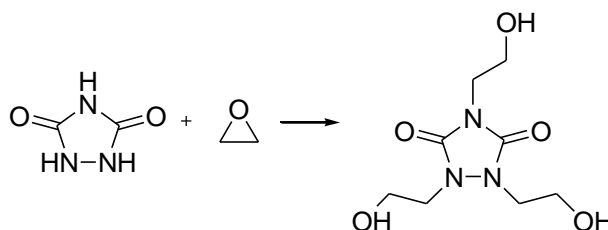
$^1\text{H}$  NMR 600MHz, Dimethyl sulfoxide- $d_6$ ,  $\delta$  (ppm): 4.81 (t, 2H, 2 $\text{CH}_2\text{-OH}$ ); 3.56 (t, 4H, 2 $\text{CH}_2\text{-N}$ ); 3.56 (t, 4H, 2 $\text{CH}_2\text{-OH}$ ).

$^{13}\text{C}$  NMR 600MHz, Dimethyl sulfoxide- $d_6$ ,  $\delta$  (ppm): 41.25 (2 $\text{CH}_2\text{-N}$ ); 57.45 (2 $\text{CH}_2\text{-OH}$ ); 154.26 ( $\text{C=O}$ ); 157.55 (2 $\text{C=O}$ );

FTIR,  $\nu$  ( $\text{cm}^{-1}$ ): 751.69 ( $\nu\text{CH}_2$ ); 1054.22, 1033.22 ( $\nu\text{OH}$  stretch); 1403.19 ( $\nu_{\text{as}}\text{CH}_2\text{-N}$ ); 1771.34, 1720.11 ( $\nu\text{C=O}$ ); 2865.87 ( $\nu\text{CH}_2$  aliphatic); 3086.49-3447.96 ( $\nu\text{OH}$ ).

### 8.2.5.3 Synthesis of 1,2,4-*Tris*(hydroxyethyl)urazole

Urazole (0.01mol, 1.01g) and triethylamine ( $1 \times 10^{-4}$ mol, 0.01g) were charged to a 100mL Young's vessel equipped with magnetic stirrer. The reactant was then dissolved in dimethylformamide (3mL), and ethylene oxide (0.03mol, 1.32g) introduced via Masterflex Chem-Durance™ tubing. This was heated to 120°C and stirred overnight (12-15 hours). Following reaction completion, both the solvent and catalyst were removed under vacuum to reveal a viscous liquid which crystallised upon standing. 1,2,4-*Tris*(hydroxyethyl)urazole was then recrystallised from isopropanol, and cooled overnight to promote precipitation. Crystals were filtered and dried under vacuum, thereupon yielding the desired product.



**Scheme 8.9.** Synthesis of 1,2,4-*tris*(hydroxyethyl)urazole.

$^1\text{H}$  NMR 600MHz, Dimethyl sulfoxide- $d_6$ ,  $\delta$  (ppm): 3.28 (t, 1H, OH); 3.39 (t, 2H, 2OH); 3.502 (t, 6H, 3CH<sub>2</sub>-N); 3.505 (t, 6H, 3CH<sub>2</sub>-OH).

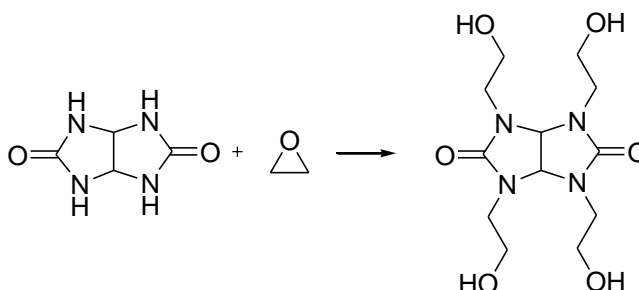
$^{13}\text{C}$  NMR 600MHz, Dimethyl sulfoxide- $d_6$ ,  $\delta$  (ppm): 46.62, 47.55 (3CH<sub>2</sub>-N); 57.40, 57.64 (3CH<sub>2</sub>-OH); 156.03 (2C=O).

FTIR,  $\nu$  (cm<sup>-1</sup>): 747.60 ( $\nu\text{CH}_2$ ); 1042.52, 1033.40 ( $\nu\text{OH}$  stretch); 1456.78 ( $\nu_{\text{as}}\text{CH}_2\text{-N}$ ); 1692.18, 1794.64 ( $\nu\text{C=O}$ ); 2750.77 ( $\nu\text{CH}_2$  aliphatic); 3264.31 ( $\nu\text{OH}$ ).

### 8.2.5.4 Synthesis of 1,3,4,6-*Tetra*(2-hydroxyethyl)glycoluril

Hydroxalkylation of glycoluril (0.01mol, 1.42g) was conducted using a 100mL Young's vessel, to which dimethylformamide (14mL) and potassium hydroxide ( $1.4 \times 10^{-4}$ mol, 0.014g) were combined. The vessel was purged with N<sub>2</sub> prior to introducing ethylene oxide (0.04mol, 1.76g), thereby preventing the occurrence of side reactions. Heating was then

applied at a temperature of 95°C, for 24 hours. Upon conclusion of synthesis, the catalyst was removed by filtration and solvent evaporated under vacuum. This provided 1,3,4,6-*tetra*(2-hydroxyethyl)glycoluril in the form of a brown, viscous liquid.



**Scheme 8.10.** Synthesis of 1,3,4,6-*tetra*(2-hydroxyethyl)glycoluril.

$^1\text{H}$  NMR 600MHz, Dimethyl sulfoxide- $d_6$ ,  $\delta$  (ppm): 3.21 (t, 4H, 4OH); 3.41 (t, 8H, 4 $\text{CH}_2\text{-N}$ ); 3.51 (t, 8H, 4 $\text{CH}_2\text{-OH}$ ); 5.48 (s, 2H, 2CH aromat).

$^{13}\text{C}$  NMR 600MHz, Dimethyl sulfoxide- $d_6$ ,  $\delta$  (ppm): 44.91 (4 $\text{CH}_2\text{-N}$ ); 58.97 (4 $\text{CH}_2\text{-OH}$ ); 64.54 (2CH aromat); 161.18 (2C=O).

FTIR,  $\nu$  ( $\text{cm}^{-1}$ ): 762.35 ( $\nu\text{CH}_2$ ); 1056.27, 1033.08 ( $\nu\text{OH}$  stretch); 1493.00 ( $\nu_{\text{as}}\text{CH}_2\text{-N}$ ); 1678.65, 1759.13 ( $\nu\text{C=O}$ ); 2844.22 ( $\nu\text{CH}_2$  aliphatic); 3150.38 ( $\nu\text{OH}$ ).

### 8.3 Results

Based on the collective finding of investigations, novel bonding agents were proposed for incorporation within PBX formulations. This focussed on delivering improvements in mechanical properties, insensitivity, cross-linking, cost efficiency and mixing viscosity. In pursuit of satisfying these requirements, both structure and functionality were manipulated accordingly. This entailed emphasis upon design, applicable to which also enabled integration of additional functions. In response to the potential for bonding agents to perform secondary functions, further benefits are incurred upon application within energetic composites.

The ability to engage in the process of filler reinforcement is primarily dependent on bonding agent composition. Reinforcing agents require functionality available to participate in cross-linking with the binder system, resulting in encapsulation of filler particles. Although improving mechanical properties, application offers limited potential to resolve issues associated with poor filler/binder interaction.<sup>5</sup> Bonding agents are consequently required to behave as wetting agents, thereby lowering the surface tension in order to strengthen adhesion. Implications also result in reduced separation between the binder system and filler particles. This assists in compounding the spatial arrangement of energetic composites, supported by the ability of bonding agents to participate in interfacial bonding.

These characteristics also introduce the potential for compounds to perform as scavengers for soluble metal impurities. Additional functionality is therefore required, enabling this to coincide with previous behaviour. The connotations associated with increased functionality also allow compounds to assume the role of cross-linking agents. Combining the effects upon cross-link density with that of supporting functions therefore provides superior capabilities. This assists in establishing bonding agents adept at improving the mechanical properties and insensitivity of cast-cured energetic materials.

### **8.3.1 Bonding Agent Adducts**

#### **8.3.1.1 Difunctional Isocyanate Terminated Bonding Agent**

Investigation of DITBA was conducted to determine the potential for Dantocol's delocalised electrons to participate in dipole interactions with RDX's nitro functionality. This called upon protection of Dantocol's hydroxyl functionality, isolating intermolecular forces between that emerging from carbonyl groups. The occurrence of dipole interactions within cast-cured PBX composites was initially described within Section 7.3.2.2.3. Evaluation of adduct performance will serve to confirm the existence of such interaction in the absence of hydrogen bonding.

Prior to investigating the potential interaction of DITBA, elucidation of the adduct was necessary to understand both physical and chemical properties. This included the aliphatic isocyanate from which the bonding agents derived. TMXDI exists as a liquid at room temperature and readily reacts with polyols in the presence of catalyst. The diisocyanate was first applied as a commercial adduct in 1986 by the American Cyanamid Company.<sup>15</sup> This consisted of TMXDI and trimethylpropane, which was originally developed for high performance surface coatings. As the adduct undergoes polymerisation, this contributes towards the formation of hard segment domains. Hydroxyl-terminated prepolymers of low glass transition temperature are therefore applied to impart softness and flexibility within resulting polyurethanes.

Reaction of Dantocol and TMXDI prior to incorporation within PBX formulations ensures participation in covalent bonding with the binder system. Attachment of isocyanate-terminated side chains thereby engage in polymerisation with HTPB to form urethane linkages. TMXDI was selected based on its unsymmetrical structure, which upon curing impedes crystallisation of hard segments, increases phase mixing and reduces the modulus. Hourston et al. confirmed these observations, with polyurethanes containing TMXDI hard segments found to exhibit minimal tendency towards phase separation.<sup>16</sup> The diisocyanate is also recognised as less moisture sensitive than IPDI, reducing the potential for urea formation. Further side-products are additionally prevented by steric hindrance, avoiding self-condensation otherwise resulting in allophanate, biuret or isocyanurate.

Comprising an NCO functionality of 2.0, the equivalent weight of DITBA was found to measure 352g eq<sup>-1</sup>. This accounted for an isocyanate percentage of 20.85% by weight of constituents. Elucidation of isocyanate content was necessary to determine the quantities of PBX ingredients required to balance the NCO:OH ratio. The percentage of TMXDI within the adduct was consistent with that applied by Wolfgang et al. in the production of an universal adhesive.<sup>17</sup> Minimising the TMXDI content was found to provide polyurethanes capable of superior adhesion. This dictated adducts comprising 35% TMXDI were

considered preferable for general application.<sup>17</sup> The remaining 65% of DITBA accounts for the diisocyanate-terminated hydantoin depicted in Figure 8.3.

### 8.3.1.2 Trifunctional Isocyanate Terminated Bonding Agent

Implementation of TITBA is applicable to adhesives, sealants, plastics and coatings, consistent with that of the difunctional adduct. This constitutes a homogenous solution representing 65% isocyanate-terminated isocyanurate and 35% TMXDI curative. Not unlike the difunctional isocyanate, attachment of TMXDI ensures the bonding agent reacts to become an inherent part of the binder system. This is accountable for an equivalent weight of 331g eq<sup>-1</sup> and NCO functionality of 2.65. These specifications imply an isocyanate weight percentage of 20.26% is observed in relation to TITBA. As the isocyanate functionality is greater than 2.0, this is also responsible for the introduction of cross-linking.

According to the structure of TMXDI, self-condensation of TITBA is subsequently avoided. This enables polymerisation to be conducted at temperatures in excess of 130°C, whilst evading common isocyanate impurities. Similar conditions promote branching of IPDI, resulting in observation of side-reactions. TMXDI resolves the issue according to steric hindrance introduced by the dimethyl functionality. This also ensures potential reaction of isocyanate and carboxylic acid groups is impeded.<sup>18</sup> These conditions are favourable in terms of limiting impurities known to influence the stoichiometric ratio of polyurethanes, and subsequent mechanical properties.

### 8.3.2 Synthesis of 1,3-Bis(2,3-dihydroxypropyl)-5,5-dimethylhydantoin

Synthesis of 1,3-bis(2,3-dihydroxypropyl)-5,5-dimethylhydantoin proceeds via reaction of glycidol and 5,5-dimethylhydantoin. This involves ring opening of the epoxide due to attack of secondary amides.<sup>19, 20</sup> The influence of strain imposed upon the three-membered ring, coupled with polarisation of the C-O bond ensures the tendency of glycidol to react.<sup>21</sup> Covalent bonding between the amide and epoxide moieties occurs when reactants are present in equal molar equivalents. However, slight excess of glycidol is recommended to ensure

reaction completion is achieved. Increasing the molar ratio beyond this point may inadvertently promote reaction of the product and epoxide.<sup>22</sup> This typically involves the hydroxypropyl side chains primary hydroxyl group.

Ring opening of the epoxide proceeds at the least substituted carbon atom, according to the Markovnikov rule. This requires addition of acid or base catalyst, with suitable examples including inorganic acids, Lewis acids, amines, alcoholates and alkali metal hydroxides. The implications associated with acid catalysis resulted in products consisting of 2,3- and 1,3-dihydroxypropyl-5,5-dimethylhydantoin. Synthesis of 1,3-bis(2,3-dihydroxypropyl)-5,5-dimethylhydantoin was found to result from nucleophilic ring opening. This contrasts with 1,3-bis(1,3-dihydroxypropyl)-5,5-dimethylhydantoin, according to which is derived from electrophilic ring opening.<sup>22</sup> Addition of strong Lewis acids may also result in decomposition of reaction products. Consequently, weak Lewis acids are often added to catalyse the reaction of glycidol and amine containing compounds. This previously observed  $\text{BF}_3$ ,  $\text{BF}_3\text{O}(\text{C}_2\text{H}_5)_2$ ,  $\text{SnCl}_4$ ,  $\text{SbCl}_3$  and  $\text{LiCl}$  applied to catalyse the reaction, through means of proton transfer.<sup>23</sup>

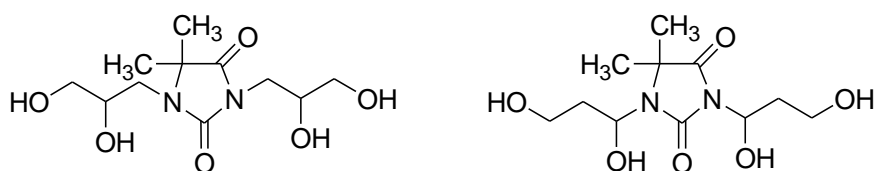
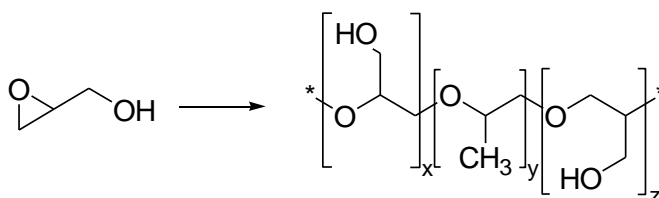


**Figure 8.6.** Structure of 2,3- and 1,3-dihydroxypropyl-5,5-dimethylhydantoin.

Due to problems arising from acid catalysis, sodium carbonate was added to obtain a single configuration. This promoted base catalysis, with sodium carbonate performing the task of acid-binding agent.<sup>22-25</sup> Application also offered the advantage of replacing chloride containing catalyst, whilst eliminating the need for ion exchange resins with regards to purification. Selection of catalyst was further based on sodium carbonate's insolubility amongst reactants, therefore benefiting removal.

Preventing self-polymerisation of glycidol was accomplished by dropwise addition, combined with limiting the maximum reaction temperature. This ensured low concentrations were maintained amongst 5,5-dimethylhydantoin, therefore inhibiting the formation of polyglycidol.<sup>22</sup> Reaction then commenced at the heterocycles 3'-nitrogen position, with adjacent carbonyls resulting in the amines increased acidity. This was followed by reaction at the 1'-nitrogen position, as the molar equivalents of glycidol was gradually increased. Upon attachment of multiple hydroxypropyl chains, the reaction was quenched to prevent propagation of side products.



**Scheme 8.11.** Self-polymerisation of glycidol to polyglycidol.

Purification involved the removal of sodium carbonate following precipitation in acetone. This was achieved by filtration of catalyst, along with residual polyglycidol. Solvent was then removed by distillation at temperatures below 120°C. Further increase in temperature resulted in discolouration of 1,3-bis(2,3-dihydroxypropyl)-5,5-dimethylhydantoin due to heat degradation. Investigation of thermal behaviour revealed  $T_b$  is accompanied by thermal decomposition, preventing distillation of the product. Excess glycidol was therefore removed by washing in diethyl ether, and the purity of 1,3-bis(2,3-dihydroxypropyl)-5,5-dimethylhydantoin confirmed by NMR and FTIR.

### 8.3.3 Synthesis of Hydroxyalkyl Ureas

A series of hydroxyalkyl urea compounds containing two or more hydroxyl groups were synthesised from urea and various aminoalcohols. This was applied in preparation of bis, tris, tetrakis and hexakis-hydroxyethyl monoureas. The preferred method of synthesis involved neat addition of reagents, heated under reflux conditions. Reactions may



alternatively be conducted in an aqueous environment, as a means of removing ammonia evolved during synthesis.

The linear conformation of 1,3-*bis*(2-hydroxyethyl)urea contains dual hydroxyl functionality, capable of facilitating interfacial adhesion. This meanwhile prevents contributions towards cross-linking, limiting its capacity to improve mechanical properties compared to derivatives comprising  $\text{OH} > 2$ . Introduction of branched configurations enables hydroxyalkyl ureas to perform the additional obligations of cross-linking agents. The ability to promote cross-linking within the binder system succeeds in meeting a preferred embodiment of bonding agent design. This is demonstrated in 1,1,3-*tris*(2-hydroxyethyl)urea, whereby the asymmetrical structure provides functionality capable of improving interfacial adhesion whilst contributing to cross-linking. Increasing the molar equivalents of diethanolamine to acquire 1,1,3,3-*tetrakis*(2-hydroxyethyl)urea eliminates hydrogens associated with secondary amines. This is otherwise known to impart issues involving the compatibility of acid protons and energetic filler particles.

Substitution of 2-amino-2-hydroxymethyl-propane-1,3-diol contributes towards variation in chain length. This comprises a tertiary carbon, covalently bonded to amine functionality. Also attached to the central carbon exist three hydroxethyl side-chains, facilitating an increase in hydroxyl functionality. Subsequent reaction of 2-amino-2-hydroxymethyl-propane-1,3-diol and urea resulted in the 6-arm configuration indicated in Scheme 8.5. The increase in melting transition of 2-amino-2-hydroxymethyl-propane-1,3-diol requires elevated temperatures to ensure a homogenous solution is acquired. This produced 1,3-*bis*[3-hydroxy-1,1-*bis*(2-hydroxyethyl)propyl]urea, which unlike other derivatives was observed to crystallise upon cooling. Introduction of branching also provided an increase in hydroxyl functionality, as confirmed by spectra of hydroxyalkyl ureas within the Appendix (Figures A.4 - A.7).

### 8.3.4 Synthesis of Dendrimeric Bonding Agents

Dendrimer application has aroused considerable interest throughout the past decade, owing to performance in drug delivery, catalysis, hybrid systems and nanotechnology.<sup>26</sup> This stems from the unique architecture of dendrimeric molecules, according to which enables a high degree of surface functionality. Assembly is performed through repetitive monomer addition, originating from an initiator core.<sup>27</sup> This results in a three-dimensional macromolecule, synonymous with high end-group concentration. The implications in surface activity suggest the potential for dendrimeric bonding agents to dramatically improve interfacial adhesion. Consequently, a hydroxyl functionalised polycarbamate dendrimer was prepared for application. This contributes to high polarity from which interfacial adhesion is established.

The capacity for commercial dendrimers to perform as bonding agents was initially investigated by Zarras et al.<sup>27, 28</sup> This involved application of polyamidoamine (PAMAM), *tetrakis*(5-cyano-2-oxa-butyl)methane (tetranitrile), *tetrakis*(5-carboxy-2-oxabutyl)methane (tetraacid) and *tetrakis*(5-hydroxy-2-oxapentyl)methane (tetraol). Investigations involved the comparison of mechanical properties pertaining to cast-cured propellant composites, based on formulations containing dendrimeric bonding agents. Hydroxyl-functionalised dendrimers were determined to improve mechanical properties upon comparison to composites removed of bonding agent. Substitution of cyano end-groups was alternatively unable to improve mechanical properties, following incorporation of tetranitrile. This further substantiates the proficiency of hydroxyl groups, with regards to bonding agent application.

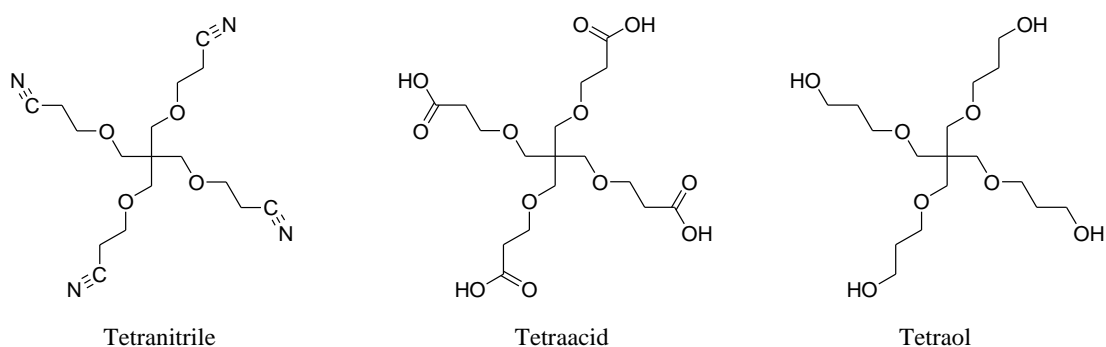


**Figure 8.7.** Commercial dendrimers applied as bonding agents.<sup>28</sup>

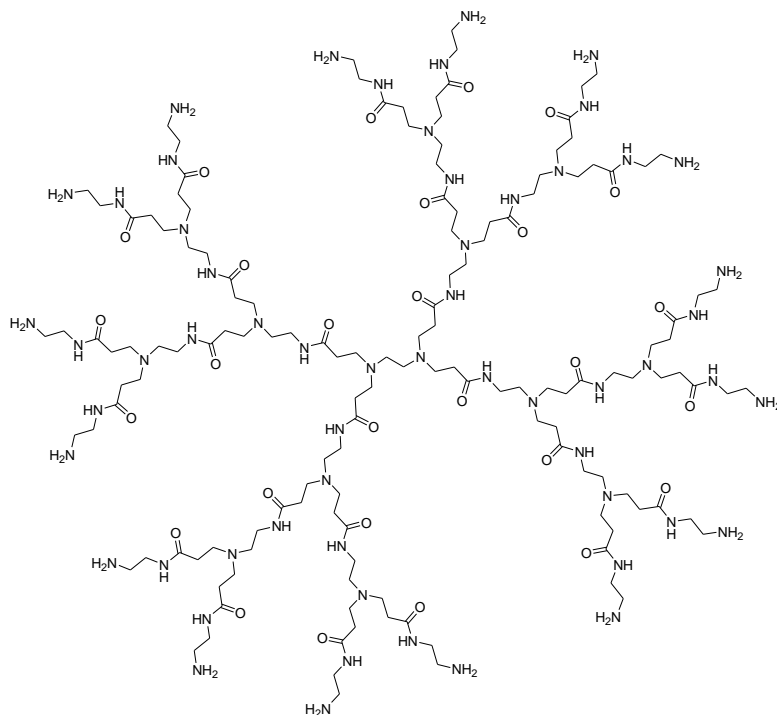


**Figure 8.8.** Second generation polyamidoamine.

Pan et al. identified hydrogen bonding was responsible for interaction between hydroxyl-terminated dendrimers and ammonium perchlorate.<sup>29</sup> X-ray photoelectron spectroscopy and micro-infrared spectroscopy was applied to identify the presence of hydrogen bonding.<sup>29</sup> Preparation involved forming a dendrimer coating upon which encapsulated the surface of ammonium perchlorate. These techniques were similarly applied to investigate intermolecular forces involving HMX.<sup>30, 31</sup> Interaction between the filler and hydroxyl-terminated PAMAM revealed the development of hydrogen bonding indicated in Figure 8.9. This was confirmed according to shifts observed in the asymmetrical nitro stretching vibration.

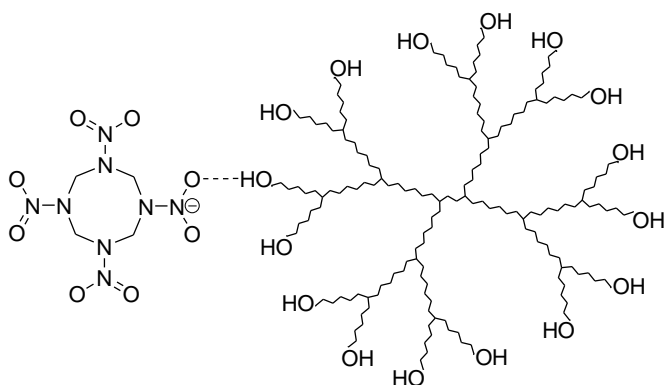


**Figure 8.9.** Hydrogen bonding between HMX and hydroxyl-functionalised dendrimer.<sup>30</sup>

Synthesis of the polycarbamate dendrimer differed from previously prepared bonding agents, involving multiple iterations to establish an increase in branching. Typically the assembly of dendrimers is recognised for its complexity and time duration. These issues were addressed according to the yield of polycarbamate, and ease in which purification was performed. Reaction progress was monitored by NMR to confirm the development of dendrimer growth. This also verified the bonding agents monodispersity, as indicated in the Appendix (Figures A.8). Circumstances known to influence the degree of monodispersity include the occurrence of dendrimer fragmentation and incomplete removal of diethanolamine. These conditions may promote reactants to function as independent initiator cores, thereby broadening the molecular weight distribution.<sup>32</sup> Dendrimer bridging may also occur in response to the quantity of sequencing reagent, or exposure to temperatures in excess of 150°C.

Potential obstacles were avoided to obtain the desired polycarbamate structure. This consisted of eight hydroxyl moieties, as occur within the macromolecules outer shell. The implications associated with increase in end-group concentration thereby supports the development of cross-linking, subsequent to polymerisation with isocyanate. Expanding upon the hydroxyl content is also responsible for establishing the dendrimer's hydrogen bonding rich structure. This functions to increase surface activity, thereby improving interfacial adhesion. Additional advantages include the omission of acidic protons, which are known to impede filler compatibility. This was identified as problematic in relation to amines incorporated within PAMAM. Secondary amines were therefore replaced with carbamate functionality, in attempt to resolve compatibility issues.

Combined with the bonding agents high end-group concentration, the solubility and low viscosity characteristics of polycarbamate satisfy the conditions necessary for application in high solid coatings.<sup>13</sup> However, complications may also arise in connection with increased functionality, resulting in rapid cross-linking of the binder system. This influences the molecular mobility, thus preventing reaction completion as functional groups are encapsulated within the matrix. The number of reactive groups must therefore be considered

to avoid such occurrence, with third and fourth generation dendrimers excluded from investigations.

### 8.3.5 Synthesis of Hydroxyalkyl Heterocycles

Hydroxyalkylation of nitrogen containing heterocycles was performed according to ring opening of ethylene oxide in the presence of catalyst. The quantity of epoxide introduced was regulated to prevent runaway ethoxylation, upon exposure to reaction conditions.<sup>33</sup> This ensured the heterocyclic component remained in excess, avoiding side reactions indicated in Scheme 8.12.<sup>34</sup> The occurrence of alcohol ethoxylates prevents hydroxyalkyl heterocycles from crystallising during the later stages of purification. This raises complications with regards to purity, thus requiring consideration.



**Scheme 8.12.** Side reaction of hydroxyalkyl groups and unreacted ethylene oxide.

Base catalysis is considered favourable regarding the hydroxyalkylation of N-heterocycles, as acid catalyst demonstrate reduced efficiency and incur impurities. Application therefore extended to alkali metal hydroxides and tertiary amines, present at concentrations ranging from 0.05-6.0% (w/w). These examples may be applied neat, provided the heterocyclic content exists as liquid under reaction conditions.<sup>35</sup> Alternatively, polar solvents are applied to form a homogenous solution, with those applicable remaining inert in the presence of ethylene oxide. Application of dimethylformamide was therefore recognised as preferable within current examples. This led to adopting the polar aprotic solvent in quantities necessary to promote dissolution.

Although the temperature of hydroxyalkylation reactions is often varied between 25°C and 140°C, higher temperatures can be applied under pressure. This may be necessary to prevent splitting of heterocyclic structures, causing observation of colour change.<sup>33, 36</sup> Once incorporated within the reaction mixture, aliphatic impurities are unable to be removed by

standard means of purification. Conducting the reaction at elevated temperature and pressure also presents advantages in terms of the epoxides solubility and boiling point.<sup>14, 37</sup> This results in significant increase in reaction rate, while prolonged exposure to such conditions favours the occurrence of side products.

#### **8.3.5.1 Preparation of 1,3,5-*Tris*(2-hydroxyethyl)isocyanurate**

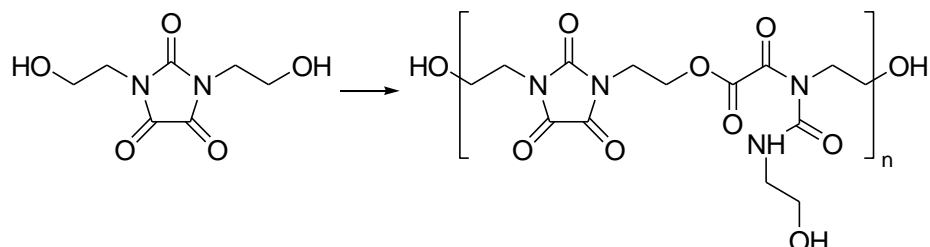
Isocyanurates have previously observed application in the field of polymer chemistry.<sup>38-40</sup> These identified materials exhibit good hardness and thermal resistance, while often appearing in coatings, inks and adhesives. Vanhoye et al. previously described a process for curing polyurethanes based on 1,3,5-*tris*(2-hydroxyethyl)isocyanurate and diisocyanate curatives.<sup>39</sup> Due to the high decomposition temperature of 1,3,5-*tris*(2-hydroxyethyl)isocyanurate, resulting polymers were found to exhibit superior thermal stability. This translated to application in high temperature materials, suggesting the potential for incorporation within cast-cured PBX composites.<sup>38, 41</sup>

Recrystallisation of 1,3,5-*tris*(2-hydroxyethyl)isocyanurate from isopropanol resulted in the acquisition of white precipitate. Spectroscopic techniques confirmed crystal purity, along with the effective removal of water. This limits the potential for moisture to react with isocyanate, thus promoting urea formation. The removal of trace impurities also presents benefits to achieving bonding agent compatibility. This is required prior to incorporation of 1,3,5-*tris*(2-hydroxyethyl)isocyanurate within cast-cured PBX composites.

#### **8.3.5.1 Synthesis of 1,3-*Bis*(2-hydroxyethyl)parabanate**

Parabanic acid is a crystalline solid, melting with decomposition at 242°C. The polar compound exhibits solubility within polar solvents, along with undergoing dissolution in the presence of ethylene oxide. Reaction is therefore able to occur neat, or in the presence of an appropriate solvent. Upon combining ethylene oxide under mild condition, reaction with parabanic acid produces 1,3-*bis*(2-hydroxyethyl)parabanate. Triethylamine was added to catalyse the reaction, creating a parabanic anion of increased reactivity towards ethylene

oxide. This proceeds via adduct formation, enabling proton transfer from the imide to epoxide functionality.<sup>42</sup> Increasing the catalyst concentration or introducing excess ethylene oxide may promote polymerisation of the product. This occurs due to ring opening of parabanic acid, yielding the linear configuration indicated in reaction Scheme 8.13.



**Scheme 8.13.** Polymerisation of 1,3-*bis*(2-hydroxyethyl)parabanate.

Reaction conditions were maintained at  $T = 35^{\circ}\text{C}$ , preventing formation of impurities apparent at higher temperature. Interpretation of spectra illustrated in the Appendix (Figures A.10) confirmed polymerisation of 1,3-*bis*(2-hydroxyethyl)parabanate and ethylene oxide was avoided. This was evident from the  $^1\text{H}$  NMR spectrum, indicating an absence of peaks associated with the imide region. Hydroxyalkylation of parabanic acids imide functionality was further substantiated by the integration value of the hydroxyl peak ( $\delta = 4.82\text{ppm}$ ).

Application of parabanic acid derivatives in polymer chemistry is recognised to produce materials of high thermal stability, resistance to abrasion, mechanical strength, elasticity and superior adhesion.<sup>43, 44</sup> Display of such characteristics has prompted use in the manufacture of foams, films, fibres and construction elements.<sup>43, 44</sup> These materials are consequently applied to produce coatings directed towards laminates, electro-insulation and metallic/ceramic surfaces.

Polymers containing parabanic acid are often prepared by ring closure, occurring upon polymerisation with cyanofornamidyl isocyanate and other monomers. Alternative examples incorporating the N-heterocyclic structure include various polyureas and polycarboiimides. This provides an initial indication of the potential for 1,3-*bis*(2-hydroxyethyl)parabanate to satisfy the requirements of an effective bonding agent.

### 8.3.5.2 Synthesis of 1,2,4-*Tris*(2-hydroxyethyl)urazole

Synthesis of 1,2,4-*tris*(2-hydroxyethyl)urazole was achieved following reaction of urazole and ethylene oxide in the presence of triethylamine. Application of catalyst was necessary to avoid the impact of basic conditions associated with urazoles amide functionality, according to which contrasting reactivity is incurred between the two moieties. The implications of catalyst removal therefore accounts for reaction of ethylene oxide and the products hydroxyethyl side chains. Addition of the epoxide was also limited to three molar equivalents per mole of urazole introduced. This prevented reaction beyond that involving hydroxyalkylation of the heterocycles amine functionality, thereby yielding high purity 1,2,4-*tris*(2-hydroxyethyl)urazole.

The reaction temperature was maintained between 80-150°C, to prevent the occurrence of unwanted side products. Ideal conditions meanwhile involved overnight stirring at 120°C. This was performed in the presence of polar solvents, although aqueous and other inert solvent conditions were also feasible. The addition of dimethylformamide prompted urazole to form a suspension, assisting to determine reaction completion as 1,2,4-*tris*(2-hydroxyethyl)urazole was observed to form a homogenous solution. The time taken for this to occur varied dependant on reaction conditions, although typically proceeding overnight.

Purification of 1,2,4-*tris*(2-hydroxyethyl)urazole involved the initial removal of triethylamine and solvent under vacuum. Recrystallisation from isopropanol was then performed, requiring elevated temperature to form a homogenous solution. This was quenched to enable precipitation of 1,2,4-*tris*(2-hydroxyethyl)urazole in the form of white crystals. Characterisation of crystals was applied, producing spectra depicted in the Appendix (Figures A.11). This successfully confirmed hydroxyalklation of urazoles amide functionality.



#### 8.3.5.4 Synthesis of 1,3,4,6-Tetra(2-hydroxyethyl)glycoluril

Hydroxyalkylation of glycoluril was implemented to provide a highly polar N-heterocyclic structure, comprising four hydroxyethyl side chains. Synthesis of the starting material is described throughout the literature, involving reaction of glyoxal and optically substituted urea.<sup>45</sup> This is typically prepared in the presence of acid catalyst, including that of hydrochloric acid. Subsequent reaction of glucoluril and ethylene oxide alternatively employed potassium hydroxide to facilitate base catalysis. Introduction of the epoxide proceeded with four molar equivalents accounting for each mole of glycoluril. Excess ethylene oxide was avoided to prevent the occurrence of high molecular weight impurities.

Reaction conditions were maintained at temperatures between 50-150°C, whilst heating at 95°C was identified as favourable. This acts to prevent ethoxylation, along with the production of other impurities. Due to the boiling point of dimethylformamide exceeding that of the reaction temperature, this was applied as the solvent component. Selection also reflected the solvents ability to remain inert in the presence of ethylene oxide, and efficiency upon which the product was dissolved. Further to achieving reaction completion, potassium hydroxide and residual alkali metal salts were removed by filtration. Dimethylformamide was then evaporated under vacuum, yielding 1,3,4,6-tetra(2-hydroxyethyl)glycoluril as confirmed in spectra depicted in the Appendix (Figures A.12).

Polymers comprising glycouril and its derivatives have previously constituted polyesters, polyamides and alkyd resins. Variations of these examples were applied in the development of surface active agents, lubricants, foams and flameproofing composites.<sup>46, 47</sup> This suggests the potential for glycouril derivatives to promote interfacial adhesion, based on prior application as surfactants. Coupled with the ability to undergo polymerisation, connotations in surface activity allude to the possibility for advancing bonding agent technology.

## 8.4 Conclusion

The development of novel bonding agents presents the potential to dramatically improve the safety and mechanical properties of cast-cured energetic materials. Currently, few compounds are considered capable of achieving this task, with fewer still compatible with nitramine based composites. This requires the ability to participate in filler interaction, while simultaneously engaging in covalent bonding between the binder system. To satisfy these requirements, various properties must be addressed to ensure interfacial adhesion is achieved.

Effective bonding agents are required to remain soluble within the submix, at temperatures exceeding than encountered upon mixing. This facilitates dispersal amongst PBX components, thereby enabling migration towards filler particles. The bonding agents affinity for nitramines and other such fillers must therefore exceed that displayed for auxiliary components. This ensures adhesion occurs at the surface of filler particles in response to intermolecular forces. Additional functionality is therefore required to promote incorporation within the binder system. This dictates reactivity towards network components is observed.

Given the efficiency with which Dantocol satisfies these requirements, expanding the range of hydroxyalkyl heterocycles presents a likely approach to improving performance. This motivated the synthesis of novel bonding agents, including that derived from 1,3-*bis*-substituted-5,5-dimethylhydantoin. Substitution of Dantocol's hydroxyethyl side chains involved the attachment of dihydroxypropyl moieties, functioning to increase the hydroxyl functionality. This additionally aimed to enable 1,3-*bis*(2,3-dihydroxypropyl)-5,5-dimethylhydantoin to perform the role of cross-linking agent, while simultaneously increasing the hydrogen bonding capacity.

The thermal stability of nitrogen containing heterocycles is known to improve the thermal decomposition behaviour of polyurethanes upon incorporation within the network.<sup>11</sup> This applies to Dantocol's characteristic ring structure, from which variations were investigated to

provide thermal stability. Comparison of bonding agents illustrated in Figure 8.10 details the extent of modifications applied, following attempts to exploit the hydantoins known performance. This involved the collective synthesis of 1,3-*bis*(2-hydroxyethyl)parabanate, 1,2,4-*tris*(2-hydroxyethyl)urazole and 1,3,4,6-*tetra*(2-hydroxyethyl)glycoluril. Proposed bonding agents offer additional functionality capable of engaging in interfacial adhesion. This aims to improve bonding agent performance, thereby benefiting explosive ordnance.

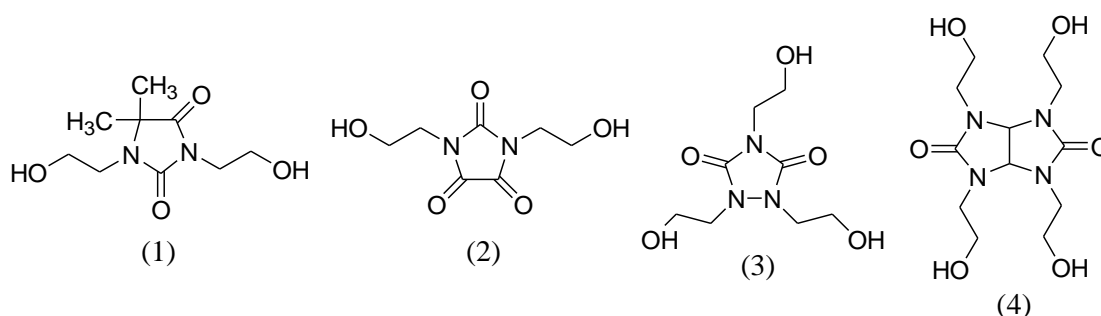


**Figure 8.10.** Bonding agent structures of (1) Dantocol (2) 1,3-*bis*(2-hydroxyethyl)parabanate (3) 1,2,4-*tris*(2-hydroxyethyl)urazole and (4) 1,3,4,6-*tetra*(2-hydroxyethyl)glycoluril.

The presence of bulky side groups is known to inhibit secondary bonding, as responsible for filler adhesion. This occurs due to the attached functionalities limited ability to orientate in such a manner as to prevent dissociation.<sup>48</sup> Consequently, incorporating an increase in chain length is often able to improve the stability of intermolecular forces. This functions to limit the development of steric hindrance, ensuring greater accessibility in relation to active sites. Subsequent increase in flexibility also provides benefits towards secondary bond formation. The implications in concern to chain extension were investigated by Vail et al. identifying hydroxyethyl side chains to optimise interaction.<sup>7</sup> This prompted the synthesis of (hydroxyethyl)urea derivatives, through which the extent of hydroxyethyl branching was increased.

Reaction of aminoalcohols and a single urea moiety was employed amid preparation of hydroxyalkyl ureas. This involved sequential increase in hydroxyethyl attachment, based upon the aminoalcohol applied. Synthesis of proposed bonding agents thereby accounted for

acquisition of 1,3-*bis*(2-hydroxyethyl)urea, 1,1,3-*tris*(2-hydroxyethyl)urea, 1,1,3,3-*tetrakis*(2-hydroxyethyl)urea, 3-[3-hydroxy-1,1-*bis*(2-hydroxyethyl)propyl]-1,1-*bis*(2-hydroxyethyl)urea and 1,3-*bis*[3-hydroxy-1,1-*bis*(2-hydroxyethyl)propyl]urea.

Based on the applied synthetic pathway, repetitive addition of urea and diethanolamine was performed in fulfilment of polycarbamate dendrimer assembly. Architecture associated with the second generation dendrimer presented an increase in functionality, with eight hydroxyl end-groups constituting the polycarbamates outer shell. This served to elucidate the effect of additional surface activity, with respect to bonding agent performance. Prior to conducting these investigations, proposed bonding agents were submitted to compatibility testing involving energetic composites. This constitutes a requirement for application of novel compounds within cast-cured energetic materials.

## 8.5 References

1. Kim, C. S. Filler Reinforcement of Polyurethane Binder Using a Neutral Polymer Bonded Explosive. 4915755, 1987.
2. Lomax, J.; Swift, G., Hydroxyalkylamides, low polluting crosslinkers for carboxyl containing polymers. *Journal of Coatings Technology* **1978**, *50* (643), 49-55.
3. Ušćumlić, G.; Kshad, A. A.; Mijin, D., Synthesis and investigation of solvent effects on the ultraviolet absorption spectra of 1,3-bis-substituted-5,5-dimethylhydantoin. *Journal of Serbian Chemistry Society* **2003**, *68* (10), 699-706.
4. Consaga, J. P. Dimethyl hydantoin bonding agents in solid propellants. US Patent 4,214,928, **1980**.
5. Consaga, J. P. Bonding agents for composite propellants. US Patent 4,944,815, **1990**.
6. Reilly, C. B.; Rossi, R. K. Hydantoin produced polyurethane. US Patent 3,928,289, **1975**.
7. Vail, S. L.; Pierce, A. G., Limitations for the addition of amides to formaldehyde and glyoxal. *The Journal of Organic Chemistry* **1972**, *37* (3), 391-393.
8. Dehm, H. C. Composite modified double-base propellant with filler bonding agent. US Patent 4,038,115, **1977**.
9. Kim, C. S.; Youn, P. H.; Noble, P. N.; Gao, A., Development of neutral polymeric bonding agents for propellants with polar composites filled with organic nitramine crystals. *Propellants, Explosives, Pyrotechnics* **1992**, *17* (1), 38-42.
10. Kim, C. S.; Noble, P. N.; Youn, C. H.; Tarrant, D.; Gao, A., The mechanism of filler reinforcement from addition of neutral polymeric bonding agents to energetic polar propellants. *Propellants, Explosives, Pyrotechnics* **1992**, *17* (2), 51-58.
11. Lubczak, J., Polyhydroxyalkyl derivatives and polyetherols obtained from azacyclic compounds. *Polimery* **2011**, *56* (5), 360-358.
12. Weishang, Y.; Wenhui, W.; Zhanning, J.; Jianwu, D.; Huiming, T., Investigation on interfacial bonding in HMX-containing model propellant composite. *Propellants, Explosives, Pyrotechnics* **1995**, *20* (6), 327-329.
13. Voit, B., New developments in hyperbranched polymers. *Journal of Polymer Science Part A: Polymer Chemistry* **2000**, *38* (14), 2505-2525.
14. Little, E. D. Production of tris-2-hydroxyalkyl isocyanurates. US Patent 3,088,948, **1963**.
15. Fiori, D. E., m-TMXDI/TMP Adduct: A New Aliphatic Isocyanate Cross-Linking Agent for the Coatings Industry. *Surface Coatings Australia* **1989**, *26* (3), 13-18.
16. Hourston, D. J.; Schäfer, F.-U.; Bates, J. S.; Gradwell, M. H. S., TMXDI-based poly(ether urethane)/polystyrene interpenetrating polymer networks: 1. Morphology and thermal properties. *Polymer* **1998**, *39* (15), 3311-3320.

17. Wolfgang, K.; Gerhard, G.; Roland, G.; Rainer, H.; Wolfgang, M. Polyurethane-based universal household adhesive. US Patent 5,270,433, **1993**.
18. Kobylansk, I.; Ley, D.; Venkatesan, J., Hotter performance: tertiary isocyanate monomer improves thermal adhesion properties of adhesive. *European Coatings Journal* **2009**, *1*, 26-31.
19. Fedoseev, M. S.; Spiridonov, A. A.; Novoselova, M. N.; Osipova, G. F., Synthesis of hydroxyalkyl-5,5-dimethylhydantoins and some aspects of their application. *Russian Journal of Applied Chemistry* **1995**, *68* (2), 262-264.
20. Fedoseev, M. S.; Spiridonov, A. A.; Novoselova, M. N.; Osipova, G. F. Electrically insulating polyester varnish for enameling of electric conductors. RU Patent 2,035,774, **1995**.
21. Cossy, J.; Bellosta, V.; Hamoir, C.; Desmurs, J.-R., Regioselective ring opening of epoxides by nucleophiles mediated by lithium bistrifluoromethanesulfonimide. *Tetrahedron Letters* **2002**, *43* (39), 7083-7086.
22. Plavac, F. Glycidol modified succinimides. US Patent 4,617,137, **1986**.
23. Beata Barbara, K. o., Possibilities for Application of 2,3-Epoxypropanol-1 in Surfactant Synthesis. In *Proceedings of the 3rd World Conference on Detergents*, AOCS Publishing: **1994**; pp 240-244.
24. Nordal, V.; Holtermann, H. Chemical Compounds. US Patent 4,250,113, **1981**.
25. Kottler, A.; Scheffler, H. Tertiary N-(dioxypopyl)-amines and methods of making the same. US Patent 2,784,233, **1957**.
26. Chen, C.-P.; Dai, S. A.; Chang, H.-L.; Su, W.-C.; Wu, T.-M.; Jeng, R.-J., Polyurethane elastomers through multi-hydrogen-bonded association of dendritic structures. *Polymer* **2005**, *46* (25), 11849-11857.
27. Zarras, P.; Dean, D.; Ciaramitaro, D.; Nguyen, S.; Dodson, F. J.; Cambrea, L. R.; Baldwin, L., Dendritic-based bonding agents for high density insensitive munitions (IM) propellant formulations. *Polymer Preprints* **2008**, *49* (1), 27-28.
28. Zarras, P.; Ciaramitaro, D.; Dean, D. L.; Hawkins, S.; Lormand, K. D.; Baldwin, L. C., Dendrimers for improved mechanical properties of composite propellants. *Polymeric Materials: Science & Engineering* **2006**, *94*, 258-259.
29. Pan, B.-f.; Luo, Y.-j.; Tan, H.-m., Study on Interaction between AP and Dendritic Bonding Agent. *Energetic Materials* **2004**, *12* (1), 6-9.
30. Pan, B.-f.; Luo, Y.-j.; Tan, H.-m., Interaction between HMX and dendritic bonding agent. *Chinese Journal of Explosives & Propellants* **2004**, *27* (3), 25-28.
31. Pan, B.-f.; Luo, Y.-j.; Tan, H.-m., Study on interaction between RDX and dendritic bonding agent. *Journal of Propulsion Technology* **2003**, *24* (5), 470-473.
32. Tomalia, D. A.; Baker, H.; Dewald, J.; Hall, M.; Kallos, G.; Martin, S.; Roeck, J.; Ryder, J.; Smith, P., A new class of polymers: starburst-dendritic macromolecules. *Polymer Journal* **1985**, *17* (1), 117-132.

33. Macfadyen, D. E. Fatty and benzoic acid esters of ethoxylated di-lower-alkyl hydantoins GB Patent 1,460,652, **1973**.
34. Zarzyka-Niemiec, I.; Lubczak, J., Kinetics and mechanism of addition of parabanic acid (imidazolidine-2,4,5-trione) to oxiranes. *International Journal of Chemical Kinetics* **2003**, 35 (2), 73-80.
35. Woellner, J.; Heinemann, K.-H. Process for the alkylation of hydantoins. DE Patent 1,912,026, **1970**.
36. Macfadyen, D. E. Fatty and benzoic acid esters of ethoxylated hydantoins substituted or not in the 5-position. US Patent 4,028,378, **1977**.
37. Ericks, W. P. Condensation products of triazines and substitute triazines with alkylene oxides. US Patent 2,381,121, **1945**.
38. Kuehn, E. Isocyanurates from unsaturated monohydric alcohols and polyisocyanates. US Patent 4,159,376, **1979**.
39. Grosius, P.; Vanhoye, D. Precursors of polymers containing isocyanurate units. US Patent 5,256,748, **1993**.
40. Abuelyaman, A. S.; Mitra, S. B. Polymerizable isocyanurate monomers and dental compositions. US Patent 2013/0012614, **2013**.
41. Preston, J. A. THEIC-hydantoin-ester resins for wire coatings. US Patent 3,889,036, **1975**.
42. Lubczak, J., Hydroxyalkylation of Cyclic Imides with Oxiranes. Part II. The Mechanism of Reaction in Presence of Triethylamine. *Open Journal of Physical Chemistry* **2012**, 2 (2), 97-102.
43. Patton, T. L. Iminoimidazolidinedione and parabanic acid polymers containing imide groups. US Patent 3,933,758, **1976**.
44. Kraft, K.; Reese, J. Process for preparing triketoimidazolidines. US Patent 4,018,743, **1977**.
45. Merten, R.; Michael, D.; Rottmaier, L.; Tima, M. J. Flame-proof polyamide moulding compositions. US Patent 4,409,347, **1983**.
46. Rottmaier, L.; Merten, R., Glycoluril salts and a process for the preparation thereof. Google Patents: **1984**.
47. Rottmaier, L.; Merten, R.; Tima, M. J.; Michael, D., Flame-proof polyamide moulding compositions. Google Patents: **1983**.
48. He, Y.; Zhu, B.; Inoue, Y., Hydrogen bonds in polymer blends. *Progress in Polymer Science* **2004**, 29 (10), 1021-1051.





# Chapter 9

---

## Mechanical Properties of PBXs

---

Sections of this chapter was presented at: Williams, C. A.; Walker, G. S.; Lochert, I. J.; Clarke, S. R.; Kirkbride, P.K, Investigation into the interaction of Dantocol in polymer bonded explosives and bonding agent development. *4<sup>th</sup> Australian energetic materials symposium*, Adelaide, Australia. 2014.

## 9.1 Introduction

The mechanical behaviour of energetic materials is fundamentally responsible for safety and performance. This is driven by physical processes and the complicated microstructure occurring within the system, as emphasised upon mechanical loading. Potentially the most detrimental failure mechanism occurring within cast-cured energetic materials is that of dewetting.<sup>1, 2</sup> Poor adhesion at the filler/binder interface causes deterioration of mechanical properties due to the propagation of dewetting. Subsequent detachment of filler particles induces weakening of the material, decrease in modulus, susceptibility towards breakage and the formation of vacuoles. Within cast-cured propellant systems, vacuoles may cause an immediate rise in pressure, capable of resulting in catastrophic failure.<sup>3</sup> This may also promote transition to detonation within PBX composites, as voids are known to act as initiation sites if adiabatically compressed.<sup>4</sup>

Application of bonding agents restricts the violence in response to hazardous stimuli, which is limited to an acceptable level specified by sensitiveness testing.<sup>5</sup> This contributes towards the development of insensitive munitions, characterised according to reduced sensitivity. The importance of bonding agents within cast-cured energetic materials, therein drives the demand for novel compounds capable of improving mechanical properties. To achieve this requirement, effective bonding agents must exhibit the capacity to interact with energetic fillers, whilst engaging in covalent bonding with the binder system. This enables the application of high filler loading, thereby improving energetic performance and establishing filler reinforcement.

Improvement in interfacial adhesion requires low bonding agent concentrations are applied to cast-cured energetic materials. Optimisation of mechanical properties demands the addition of bonding agent is limited to that necessary to produce a monolayer coating. The effect of excess bonding agent contributes towards the formation of hard segments within the binder system, thus increasing rigidity and impeding mechanical properties. This also

reduces interfacial adhesion in response to altering the concentration of polar groups. Electropositive and negative atoms consequently engage in hydrogen bonding within the polymer phase, prior to interaction with filler particles. This decreases the extent of polar groups adjacent to the surface, thereby inhibiting bonding agent interaction.<sup>6</sup> Residual stress is also accrued within the binder phase in response to excess bonding agent. This constitutes the potential to initiate deformation mechanisms, impeding the resultant mechanical properties.

Gercel et al. investigated the effect of aziridine bonding agents on the adhesive and mechanical properties of HTPB/AP based cast-cured propellant composites.<sup>7</sup> This compared the performance of BITA and MAPO with regard to bonding agent concentration. Mechanical properties were determined by tensile and hardness tests, with concentrations of 1.0, 1.5, and 2.0% w/w, found to optimise bonding agent performance. Further increase in concentration initiated the rearrangement of aziridines, lowering the bonding agents performance due to lack of hydrogen bonds between AP.<sup>7</sup> Amongst the applied aziridine-containing compounds, available functionality was then observed to participate in covalent bonding with the binder system. This enhanced adhesive forces due to network incorporation and secondary dipole attraction, or hydrogen bonding between the bonding agent and filler particles.<sup>7,8</sup>

Similar investigations were conducted by Tüzün et al. involving variation in the TEPANOL content applied to AN/HTPB based propellants.<sup>9</sup> Bonding agent concentrations of 0.2, 0.3 and 0.35% w/w, revealed significant improvement in mechanical properties. Systems containing 0.35% TEPANOL were observed to exhibit the lowest burning rate amongst propellants investigated. This occurred in response to the decline in HTPB content, following further addition of TEPANOL. Such adjustments in hydroxyl compounds were necessary to balance the NCO:OH equivalent ratio. Alternatively, Cucksee et al. employed a combination of bonding agents to improve the mechanical properties of propellants, demonstrated at upper and lower service temperatures.<sup>10</sup> This involved variation in the ratio

of MT4, HX-752 and BIDE, incorporated within AP/HTPB based composites. Formulations observed improved physical properties, as determined by the stress-strain curves acquired between -40°C and 60°C.

## **9.2 Experimental**

### **9.2.1 Processing of Polymer Bonded Explosives**

#### **9.2.1.1 Mixing Procedure**

Initial mixes were prepared in 50g quantities using a Baker Perkins planetary action mixer. This provides sufficient material for assessing the sensitiveness and processing properties of novel PBX formulations. Upon satisfying these requirements, larger quantities were prepared using a 500g planetary action mixer. All mixes were conducted under vacuum (<10torr) whilst heating at  $T = 60^{\circ}\text{C}$ . Ingredients applied were sourced from consistent batches, limiting the potential for variability. These conditions functioned to enable direct comparisons between the performance of proposed bonding agents.

Mixing was performed in accordance with conventional practice, based upon formulation ARX-2014. This consists of 64% RDX, 20% aluminium and 16% binder, whilst comprising an equivalent NCO:OH molar ratio. The exact composition of PBX formulations is dependent upon the equivalent weights of binder ingredients. This extends to include HTPB, IPDI, DOA and prospective bonding agents. Substitution of bonding agents therefore requires adjustment in formulations according to Tables 9.1 and 9.2.

Material	ARX-2014		ARX-2014.CW1		ARX-2014.CW2	
	Wt (%)	Wt (g)	Wt (%)	Wt (g)	Wt (%)	Wt (g)
Aluminium	20	100.00	20	100.00	20	100.00
RDX Type I Class 1	59	295.00	59	295.00	59	295.00
RDX Type I Class 5	5	25.00	5	25.00	5	25.00
HTPB	7.18	35.90	7.424	37.12	7.18	35.90
Diocetyl adipate	7.445	37.23	7.69	38.45	7.445	37.23
Isophorone Diisocyanate	1	5.00	0.771	3.86	1	5.00
Antioxidant-2246	0.1	0.50	0.1	0.50	0.1	0.50
Dantocol (Commercial)	0.26	1.30	-	-	-	-
Dantocol (Purified)	-	-	-	-	0.26	1.30
Triphenyl Bismuth	0.015	0.075	0.015	0.075	0.015	0.075

**Table 9.1.** PBX Formulations comprising 0.0% and 0.26% Dantocol.

Material	ARX-2014.CW3		ARX-2014.CW4		ARX-2014.CW5	
	Wt (%)	Wt (g)	Wt (%)	Wt (g)	Wt (%)	Wt (g)
Aluminium	20	100.00	20	100.00	20	100.00
RDX Type I Class 1	59	295.00	59	295.00	59	295.00
RDX Type I Class 5	5	25.00	5	25.00	5	25.00
HTPB	7.172	35.86	6.995	34.98	7.031	35.16
Diocetyl adipate	7.431	37.16	7.246	36.23	7.284	36.42
Isophorone Diisocyanate	1.022	5.11	-	-	-	-
Antioxidant-2246	0.1	0.50	0.1	0.50	0.1	0.50
THEIC	0.26	1.30	-	-	-	-
DITBA	-	-	1.644	8.22	-	-
TITBA	-	-	-	-	1.57	7.85
Triphenyl Bismuth	0.015	0.075	0.015	0.075	0.015	0.075

**Table 9.2.** PBX formulations comprising THEIC, DITBA or TITBA.

Binder precursors were thoroughly mixed and degassed prior to addition of solid ingredients. This comprised a bimodal RDX distribution, consisting of 60% RDX Type I Class 1 and 40% RDX Type I Class 5, to maximise cast density. The stepwise addition of RDX is indicated in Table 9.3, along with the duration of mixing and in vacuo requirements. Inclusion of the diisocyanate curative was added last to prevent reaction with moisture and provide an appropriate pot-life. This is responsible for initiating cure, consecutive to which casting was performed.

Material/Action	Mix time (min)	
	No Vacuum	Vacuum
HTPB + DOA + Bonding agent + AO + TPB	2	28
Aluminium	2	13
RDX (50%)	2	13
RDX (25%)	2	13
RDX (25%)	2	13
Scrape down	-	-
Mix	0	60
Isocyanate curative	1	4
Scrape down	-	-
Mix	0	15

**Table 9.3.** PBX mixing procedure.

### 9.2.1.2 Casting

Upon completion of the mixing cycle, PBX slurries were vacuum cast into 5" x 3.5" x 1.5" moulds. During this operation, vibrations were applied to the assembly, in order to facilitate degassing. This assisted in the removal of trapped gas pockets, otherwise responsible for deformations. Following transfer to moulds, the composite was cured for seven days at  $T = 60^{\circ}\text{C}$ . PBXs were then machined into slabs and stamped into standardised dimensions for Instron mechanical testing.

Preparation of dogbone specimens involved the use of a remotely operated pneumatic press and cutter. The JANNAF class C dogbone cutter was assembled according to attachment of the appropriate blade. This comprised a gauge length of 69mm and sample centre equivalent to 10.5mm x 12.5mm. PBX slabs are then positioned directly below the steel blade, in preparation for cutting. This was performed using a Bellows-Valvair pneumatic press at  $P \approx 40\text{Psi}$ , stipulated according to composite strength. The resulting dogbone specimen consist of external dimensions measuring 125mm x 27mm, as specified by ASTM standards.

## 9.2.2 Compatibility Testing

### 9.2.2.1 Differential Scanning Calorimetry

Novel bonding agents are required to avoid compatibility issues associated with energetic fillers. This specifically applies to fillers selected for use within prospective formulations. Initial evaluation of the compatibility between bonding agents and RDX was performed according to thermal analysis. This involved DSC to determine the impact of bonding agents on the onset of nitramine decomposition.

Thermal compatibility was investigated using a TA Instruments MDSX-2930 DSC. Sample preparation involved mixing 3.0mg of equal parts filler/bonding agent, within aluminium hermetic pans. The DSC cell was purged with 100mm min<sup>-1</sup> nitrogen, prior to heating at  $\beta = 5^{\circ}\text{C min}^{-1}$  from 50°C to 280°C. Experiments were conducted in duplicate and analysed using TA Instruments Universal Analysis 2000 software. Decomposition onset ( $T_i$ ) was taken as the point at which the baseline tangent intersects that correlating with the slope. Under the circumstances that  $T_i$  of RDX was significantly decreased, the investigated bonding agent was deemed incompatible and no further testing should be conducted.

### 9.2.2.2 Vacuum Thermal stability

The definitive measurement of bonding agent compatibility involved application of Vacuum Thermal Stability (VTS) testing. This provides a measure of nitramine stability, based upon the volume of gas liberated following in vacuo heating.<sup>11</sup> Analysis was performed using a TNO Pressure Vacuum Stability Test unit, equipped with pressure transducers, thermostatic oil bath and digital manometer. Procedural methods involve heating 2.5g of RDX and an equivalent mass of bonding agent within a TNO glass tube. Evolution of gas under vacuum was compared to that observed for individual components, investigated under otherwise identical conditions. This was measured using a pressure transducer to determine the volume according to Equation 9.1.<sup>12</sup>

$$V = \left( V_b + V_d - \left( \frac{m_1}{d_1} + \frac{m_2}{d_2} \right) \right) * \left[ \left( \frac{P_2 * 273.15}{273.15 + T_2} \right) - \left( \frac{P_1 * 273.15}{273.15 + T_1} \right) \right] * \frac{1}{1013} \quad (9.1)$$

Whereby  $V$  is the gas production by sample mass, while  $V_b$  and  $V_d$  indicate the tube and pressure transducer volume. The mass of sample 1 and 2 is represented by  $m_1$  and  $m_2$ , along with their respective densities  $d_1$  and  $d_2$ .  $P_1$  denotes the original pressure registered within the tube, and  $P_2$  the pressure upon conclusion of the experiment. Finally,  $T_1$  and  $T_2$  represent the initial and final room temperature recorded. The formula used to calculate compatibility of the combined system is then determined according to Equation 9.2.

$$V_R = M - (E + S) \quad (9.2)$$

Where  $V_R$  is the gas generated between the two components, and  $M$  depicts the gas production of the 5g mixture. The gas associated with individual components is then indicated by  $E$  and  $S$ , which respectively correspond to the energetic filler and bonding agent. All calculations were performed using PVST software, with results obtained in duplicate.

## 9.2.3 Sensitiveness Testing

### 9.2.3.1 Rotter Impact Sensitiveness

Impact sensitiveness was determine using a Rotter Impact apparatus. This involved preparation of samples by weighing out 25 brass caps, each containing 30mg of PBX composite. These were stored over silica gel for approx 12hrs to facilitate the remove of moisture. Loaded caps were then assembled over a polished steel anvil and impacted by 5kg drop weight. The was released from predetermined height, as dictated according to the Bruceton procedure. Ignition was established in response to evolution of gas, with the figure of insensitiveness (F of I) quoted relative to RDX, Grade F = 80.



### 9.2.3.2 BAM - Friction Test

The BAM test was applied to measure the response to frictional forces, through subjecting PBXs to hazardous stimuli between two surfaces. Instrument setup involves attachment of the lower ceramic tile in parallel with the platform. Approximately 25mg of powdered PBX was then distributed across the surface in preparation for applying friction. Meanwhile the upper frictional peg was lowered into contact and loading adjusted via positioning of the test arm. The peg was then dragged across the sample surface while observing for signs of ignition, spark or evolution of gas. Loadings are subsequently reported as the minimum force required to promote ignition.

### 9.2.3.3 Temperature of Ignition

Temperature of ignition (T of I) was determined by heating PBX samples at  $\beta = 5^{\circ}\text{C min}^{-1}$ , until observation of rapid burn or ignition. Samples were prepared in borosilicate test tubes of dimensions; length  $100\pm 3\text{mm}$ , external diameter  $12.5\pm 0.5\text{mm}$  and wall thickness  $1.0\pm 0.25\text{mm}$ . PBX composites (200mg) were dispensed into tubes, and inserted within a compatible heating mantle. Constant increase in temperature is then applied at the previously defined heating rate. The resulting T of I is recorded as the lowest temperature at which smoke, flame or audible sign of ignition occurs. Those materials demonstrating a T of I less than  $140^{\circ}\text{C}$  were classified as intrinsically sensitive to stimuli.

### 9.2.3.4 Electrostatic Discharge

The effect of electrostatic discharge (ESD) on energetic materials is known to raise severe safety concerns. Hazardous conditions arise as charge reaches the potential ( $U$ ) at which material breakdown occurs, or subsequent to grounding conditions enabling discharge of existing energy upon the material.<sup>13</sup> Resultant investigation of ESD involves the addition of PBX to indentations located within a polyethylene sample disc. To each, a small portion of copper foil was individually applied to promote conductivity. The disc was then connected on one side of a non-inductive capacitor, and a second brass terminal connected to the

opposing side of the capacitor. This was positioned in such a manner, as to enable the brass terminal to contact the copper foiling of the initial sample. A capacitor (from 0.001 to 0.1mF) was then selected using a switch upon which connects the earth. The capacitor was charged to a potential of  $U = 9.5\text{kV}$ , providing a stored energy equivalent to 4.5, 0.45 or 0.045J. ESD testing was initiated following pulse application, causing  $U$  of the selected capacitor to form across the sample spark gap. The energy at which ignition occurs was indicated according to evolution of smoke, flame or other audible sign.

### **9.2.4 Mechanical Testing**

Uniaxial tensile testing was conducted on cast-cured PBX composites using an Instron 5500R1185 Universal Test Instrument. Standardised JANNAF Class C specimen were loaded by means of the upper/lower grips and subjected to continuous strain in order to evaluate mechanical properties.<sup>14</sup> This involved operating a 1kN load cell, whilst maintaining ambient temperature ( $T = 25^{\circ}\text{C}$ ). Loadings engaged a strain rate of  $50\text{mm min}^{-1}$ , pending the rupture of PBX specimen. Acquisition of data throughout mechanical loading, reveals both the materials stress and strain performance. This enables calculation of Young's modulus as determined from 5% to 100% maximum load.

## **9.3 Results**

### **9.3.1 Compatibility Testing**

In addition to forming bonds between the highly dissimilar surface of filler particles and the binder system, bonding agent must also remain chemically and thermally stable.<sup>15</sup> Novel bonding agents are therefore required to demonstrate compatibility with existing PBX ingredients. This stipulates compatibility testing is performed, prior to incorporation of novel compounds.

### 9.3.1.1 Differential Scanning Calorimetry

The thermal behaviour of bonding agent/RDX mixtures was measured by DSC to determine the onset ( $T_i$ ) and peak decomposition temperature ( $T_p$ ) of RDX. Incompatibility is indicated by  $\Delta T_i \geq 5^\circ\text{C}$ , following which no further testing should be conducted. This occurs if the mixture exhibits instability upon exposure to heat, or presuming components engage in undesirable reactions at elevated temperatures. Decomposition often leads to the formation of gases, typically comprising  $\text{CO}_2$ ,  $\text{H}_2\text{O}$  and  $\text{N}_2$ . In response to the accompanying exotherm, the thermal stability of RDX and novel bonding agents was evaluated according to Table 9.4.

RDX and Bonding Agents (1:1)	Decomposition Temperature	
	$T_i$ ( $^\circ\text{C}$ )	$T_p$ ( $^\circ\text{C}$ )
Dantocol	206.50	229.78
1,3- <i>Bis</i> (2-hydroxyethyl)urea	91.07	122.79
1,1,3- <i>Tris</i> (2-hydroxyethyl)urea	94.93	125.34
1,1,3,3- <i>Tetrakis</i> (2-hydroxyethyl)urea	139.87	183.90
1,3- <i>Bis</i> [3-hydroxy-1,1- <i>bis</i> (2-hydroxyethyl)propyl]urea	135.53	165.16
Polycarbamate dendrimer gen 2	141.60	178.01
1,3,5- <i>Tris</i> (2-hydroxyethyl)isocyanurate	206.38	228.49
1,3- <i>Bis</i> (2-hydroxyethyl)parabanate	204.62	229.11
1,2,4- <i>Tris</i> (hydroxyethyl)urazole	204.01	228.23
1,3,4,6- <i>Tetra</i> (2-hydroxyethyl)glycoluril	201.49	227.94
1,3- <i>Bis</i> (2,3-dihydroxypropyl)-5,5-dimethylhydantoin	193.18	224.37
Difunctional isocyanate terminated bonding agent	206.12	229.98
Trifunctional isocyanate terminated bonding agent	207.23	230.46

**Table 9.4.** Thermal decomposition of RDX and novel bonding agents at  $\beta = 5^\circ\text{C min}^{-1}$ .

#### 9.3.1.1.1 Hydroxyalkyl Ureas

Compatibility of RDX was initially evaluated with regards to 1,3-*bis*(2-hydroxyethyl)urea (BHU), 1,1,3,3-*tetrakis*(2-hydroxyethyl)urea (THU), 1,3-*bis*[3-hydroxy-1,1-*bis*(2-hydroxyethyl)propyl]urea (BHPU) and the polycarbamate dendrimer (PCD). Interpretation of the resulting DSC curves featured in Figure 9.1, reveal premature decomposition of blends. Based on the initial exotherm produced between RDX and hydroxyalkyl ureas, decomposition was observed to occur below that of neat RDX. This identified

incompatibility, preventing the application of hydroxyalkyl urea bonding agents. To further characterise reactions occurring between components, BHU and THU were submitted to VTS testing.

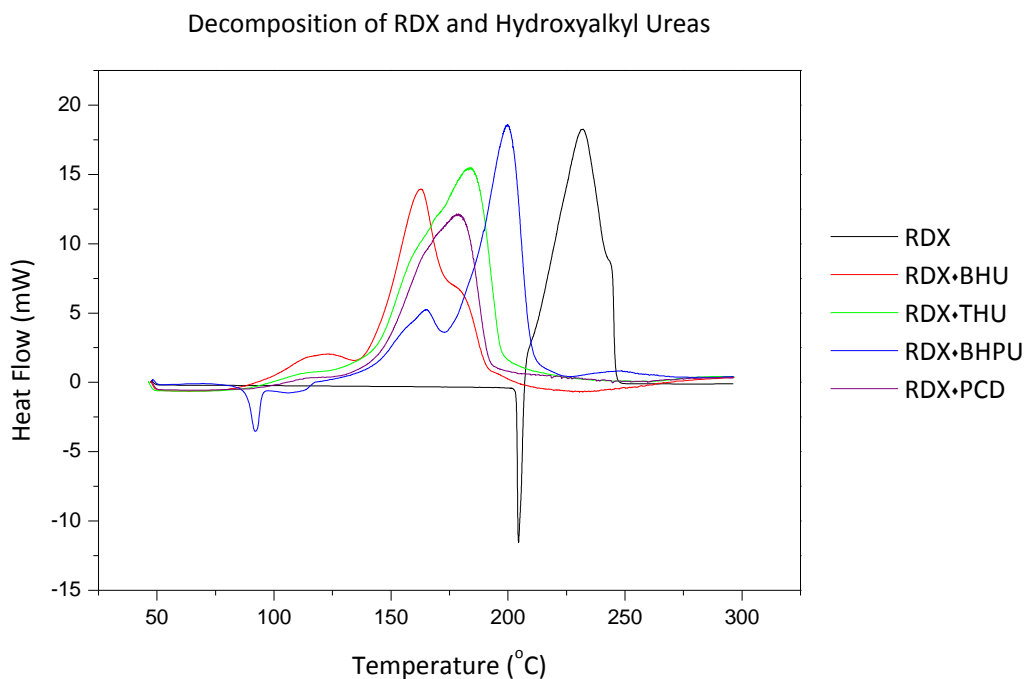


**Figure 9.1.** Thermal compatibility of RDX and hydroxyalkyl ureas.

### 9.3.1.1.2 Hydroxyalkyl Heterocycles

Hydroxyalkyl heterocycles were subjected to thermal compatibility testing, inclusive of 1,3,5-*tris*(2-hydroxyethyl)isocyanurate (THEIC), 1,3-*bis*(2,3-dihydroxypropyl)-5,5-dimethylhydantoin (DHP), 1,3-*bis*(2-hydroxyethyl)parabanate (HEP), 1,2,4-*tris*(2-hydroxyethyl)urazole (HEU) and 1,3,4,6-*tetra*(2-hydroxyethyl)glycoluril (HEG). Unlike the previous series of compounds, hydroxyalkyl heterocycles were without NH functionality, often responsible for compatibility issues.

Initial investigation of Dantocol for comparative purposes, revealed minor variation in the decomposition behaviour of RDX. This observed a decline in onset temperature ( $T_i = 206.50^\circ\text{C}$ ), representing reduced thermal stability. The extent of  $\Delta T_i$  associated with the commercial bonding agent reflects that of marginal compliance, regarding the acceptable limits. Evaluation of novel heterocycles, similarly revealed bonding agents to boarder upon

the limitations of compatibility. Minimal variation in the magnitude of  $\Delta T_i$  was evident between examples, with THEIC demonstrating marginally improved thermal stability. DHP produced the greatest shift in decomposition temperature, with onset occurring at  $T_i = 193.18^\circ\text{C}$ . Due to temperatures residing within the range of compatibility, hydroxyalkyl heterocycles were approved for VTS testing.

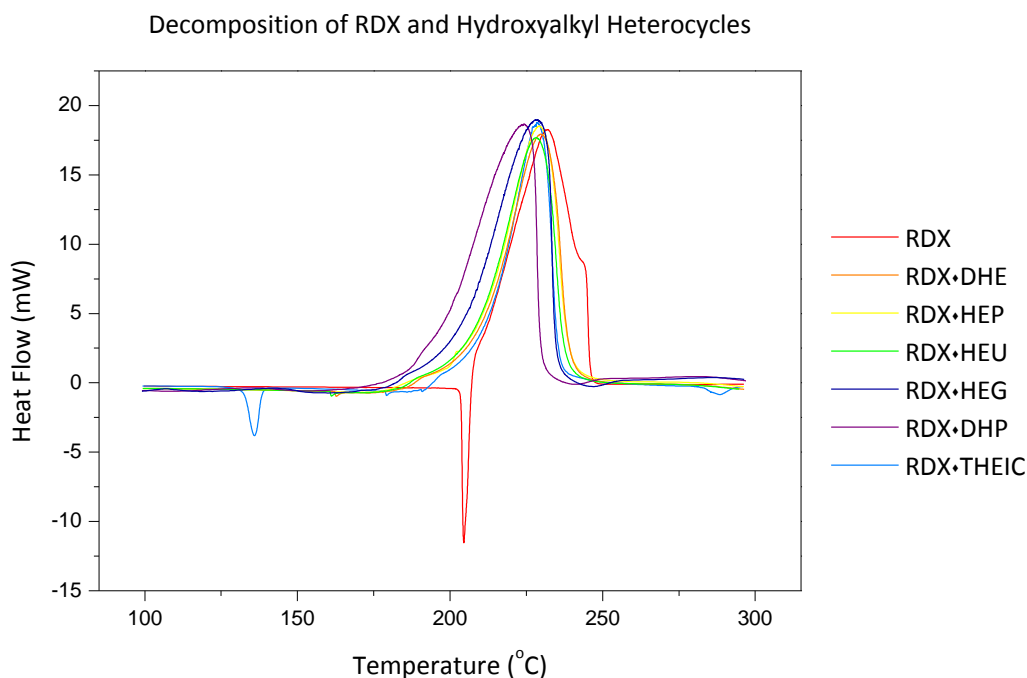


**Figure 9.2.** Thermal compatibility of RDX and hydroxyalkyl heterocycles.

### 9.3.1.1.3 Bonding Agent Adducts

Similar results were observed for the difunctional isocyanate terminated bonding agent (DITBA) and trifunctional isocyanate terminated bonding agent (TITBA). Mixtures involving either adduct combined with RDX produced minimal exothermic deviation. This is conveyed in Figure 9.3, with DITBA and TITBA accountable for minor shifts toward  $T_i = 206.12^\circ\text{C}$  and  $207.23^\circ\text{C}$ . These results depict thermal compatibility between RDX and bonding agent adducts, pending the outcome of VTS testing.

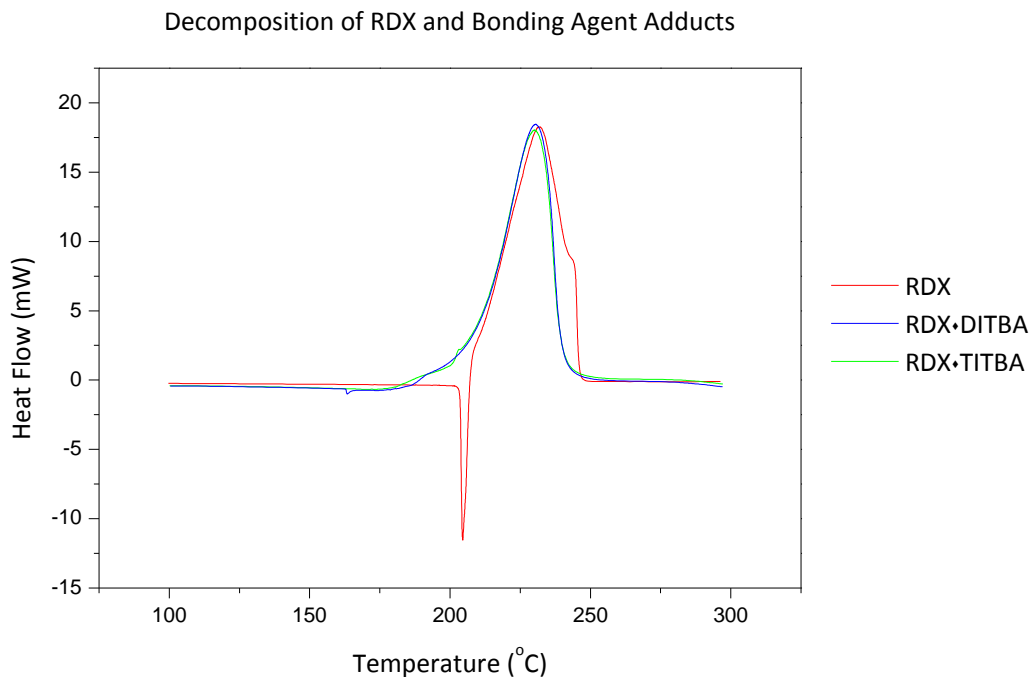


**Figure 9.3.** Thermal compatibility of RDX and bonding agent adducts.

### 9.3.1.2 Vacuum Thermal Stability Testing

Bonding agents which satisfied initial compatibility requirements, were submitted to further VTS testing. This rigorous procedure was used to establish a conclusive response to bonding agent stability. To avoid issues associated with nitramine decomposition, bonding agents are required to occur as neutral or slightly acidic compounds. Molecules exhibiting increased acidity are responsible for lowering the onset of RDX decomposition, rendering potential bonding agent incompatible.

This was investigated according to application of BHU, comprising secondary amine functionality. The hydroxyalkyl urea was assessed along with THU, which alternatively contains tertiary amines. Although the structure of THU may appear suitable for application within nitramine based formulations, both hydroxyalkyl ureas were observed to promote excess gas production. This denotes reactivity with RDX, thereby preventing bonding agent application. The relatively low boiling point of applied compounds was consequently approached upon exposure to VTS conditions. Interpretation of gas production amongst isolated components served to highlight this occurrence, with BHU and THU demonstrating

respectively values of  $V = 2.05\text{mL g}^{-1}$  and  $1.145\text{mL g}^{-1}$ . This was accompanied by discolouration of hydroxyalkyl ureas, suggesting decomposition occurs in conjunction with boiling.

Bonding Agents	Vacuum Thermal Stability	
	$V$ (mL g <sup>-1</sup> )	$V_R$ (mL)
Dantocol	0.055	4.36
1,3- <i>Bis</i> (2-hydroxyethyl)urea	2.05	*
1,1,3,3- <i>Tetrakis</i> (2-hydroxyethyl)urea	1.145	*
1,3,5- <i>Tris</i> (2-hydroxyethyl)isocyanurate	0.246	0.219
1,3- <i>Bis</i> (2-hydroxyethyl)parabanate	0.043	5.432
1,2,4- <i>Tris</i> (hydroxyethyl)urazole	0.052	5.613
1,3,4,6- <i>Tetra</i> (2-hydroxyethyl)glycoluril	0.034	6.134
1,3- <i>Bis</i> (2,3-dihydroxypropyl)-5,5-dimethylhydantoin	0.009	8.693
Difunctional isocyanate terminated bonding agent	0.220	0.940
Trifunctional isocyanate terminated bonding agent	0.220	0.482

\*Excess gas production.

**Table 9.5.** VTS data of RDX and novel bonding agents.

Substitution of tertiary amides and the increased boiling point of N-heterocyclic compounds, contributed towards greater potential for satisfying requirements. This was verified according to the results of Table 9.5, comparing the VTS of hydroxyalkyl heterocycles and alternative bonding agents. Investigations included an initial evaluation of Dantocol, to enable comparisons to be made between the commercial product. Surprisingly, this was discovered to narrowly comply with VTS requirements ( $V_R \leq 5.0\text{mL}$ ), thus generating a value of  $V_R = 4.36\text{mL}$ . Similar results were observed amongst novel N-heterocyclic compounds, as several examples marginally exceeded the defined limit. This specifically included 1,2,4-*tris*(hydroxyethyl)urazole and 1,3-*bis*(2-hydroxyethyl)parabanate, displaying consecutive figures of  $V_R = 5.613\text{mL}$  and  $5.432\text{mL}$ . Interpretation of these results suggest both examples verge upon the acceptable limit. In contrast to these results, 1,3,5-*tris*(2-hydroxyethyl)isocyanurate was found to meet the necessary criteria, demonstrating compliancy according to  $V_R = 0.219\text{mL}$  and  $V = 0.246\text{mL g}^{-1}$ .

Bonding agent adducts were also observed to avoid compatibility issues, with data residing within the acceptable limits. This appeared to improve upon results associated with Dantocol, as DITBA and TITBA demonstrated a reduction in  $V_R$  towards respective figures of 0.940mL and 0.482mL. Therefore the volume of gas evolved due to reaction with RDX constitutes decline. This enabled bonding agents to experience inclusion within small scale PBX formulations.

### 9.3.2 Sensitiveness Testing

Small scale sensitiveness testing was conducted prior to preparing  $\geq 500$ g PBX batches. This involved investigation of thermal stability and ignition sensitivity according to procedures outlined in Table 9.6. Previous evaluation of ARX-2014 was conducted by the DSTO, at their facility in Edinburgh, South Australia. This established formulations comprising 0.26% wt Dantocol, satisfied the appropriate sensitivity criteria, enabling commission of large scale production.

Hazard Data Test	ARX-2014		
	CW3	CW4	CW5
Rotter impact <sup>1</sup> (mL)	120 (2.8)	110 (2.8)	100 (1.8)
BAM -friction test (N)	360	324	288
Temperature of ignition (°C)	204	208	210
Electrostatic discharge-ignition (J)	4.5	4.5	4.5
Electrostatic discharge - no ignition (J)	0.45	0.45	0.45

<sup>1</sup>Figure of insensitiveness, evolved gas volumes (mL) in parentheses.

**Table 9.6.** Sensitiveness testing of novel PBX formulations.

Remaining formulations were evaluated according to the inclusion of novel bonding agents. Interpretation of sensitiveness testing, identified bonding agents to exhibit compatibility with all remaining PBX ingredients. This was evident from the results depicted in Table 9.6, suggesting similar levels of insensitivity. Consequently, formulations were recognised to display superior impact sensitivity, in accordance with the figure of insensitiveness. Ignition due to electrostatic discharge was also observed to occur above the required limit, as did results pertaining to the temperature of ignition. Compliance with sensitivity criteria was



ultimately achieved following data regarding the frictional force necessary to promote ignition. Observation of such response to hazardous stimuli, thereby enabled the application of THEIC, DITBA and TITBA within large scale PBX batches.

### **9.3.3 Mechanical Testing**

To elucidate the effect of novel bonding agents on mechanical properties, PBX formulations were subjected to standardised stress-strain conditions. Bonding agent performance was assessed by characteristics including maximum load, therein providing an indication of the strength associated with interfacial adhesion. The energy required to promote occurrence of dewetting, also constitutes an informative quantity.<sup>16</sup> This is determined by the composites ability to transfer, or distribute stress upon exposure to mechanical loading. Results therefore provide an indication of both performance and failure criteria associated with materials.<sup>17</sup>

#### **9.3.3.1 Dantocol**

The performance of Dantocol was initially assessed according to a comparative investigation, involving the omission of bonding agent. This was compared to a standard formulation (ARX-2014) comprising 0.26% wt Dantocol. Subsequent removal of bonding agent provided a baseline from which to compare the impact of Dantocol addition. This also functioned to evaluate the potential of amines associated with the urethane linkage to participate in RDX interaction.

Removal of bonding agent from ARX-2014.CW1, was accompanied by the extensive decline in strain at maximum load. The degree of variability depicted in Figure 9.4, reflects premature dewetting, as filler particles detach from the binder system. This corresponds to an inherent loss of filler reinforcement, generating decline in Young's modulus  $E = 8.846\text{MPa}$ . Degradation of mechanical properties is also accountable for 72% reduction in maximum load. This reflects the significance of Dantocol addition within current formulations. An important assertion from this response pertains to the inability of urethane linkages to provide secondary bonding responsible for adhesion. This negates the possibility of the NH

moiety from engaging in hydrogen bonding with RDX, thereby influencing the onset of dewetting.

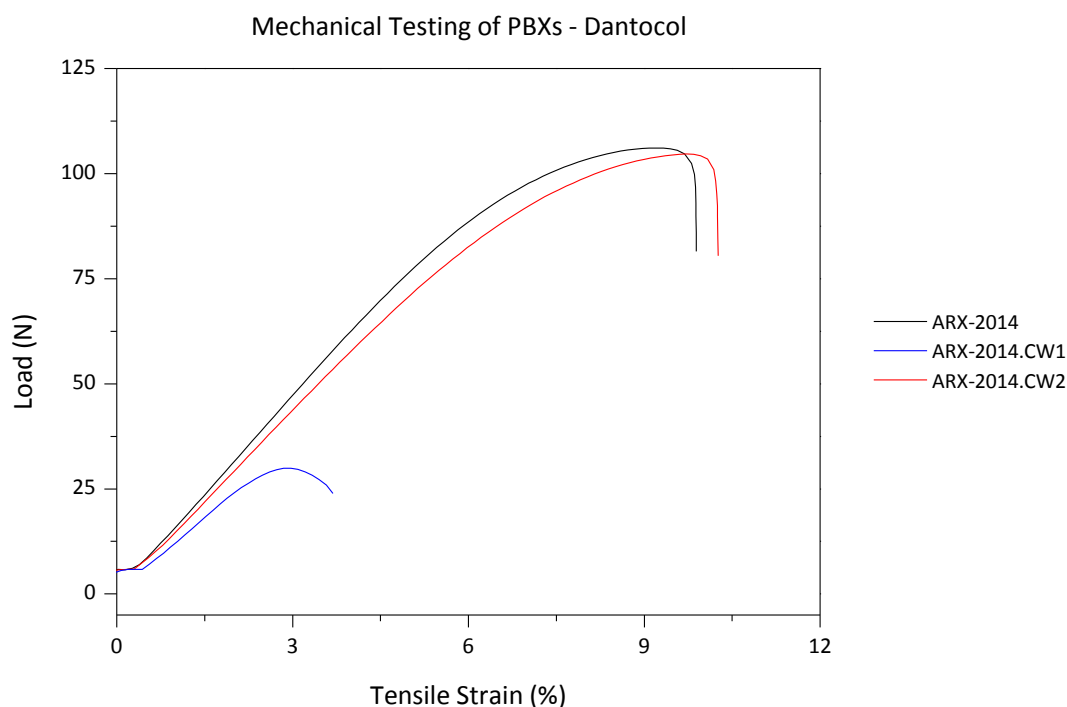


**Figure 9.4.** Load vs tensile strain of PBXs containing Dantocol/no bonding agent.

Incorporation of 0.26% Dantocol prompts the occurrence of filler reinforcement, accompanied by increase in tensile and compressive strain. The mechanism of filler reinforcement occurs via interfacial effects, as opposed to overall increase in crosslink density.<sup>18</sup> These results are collated in Table 9.7, outlining the degree of bonding agent efficiency. Comparison of commercial and purified Dantocol revealed negligible deviation between respective formulations. Based on chemical purity, the mechanical properties of ARX-2014 and ARX-2014.CW2 remained fundamentally consistent, with experimental error likely responsible for minor variation in data.

Mechanical Properties	ARX-2014		ARX-2014.CW1		ARX-2014.CW2	
	Mean	STD (%)	Mean	STD (%)	Mean	STD (%)
Maximum Load (N)	108.439	2.043	30.065	0.182	103.592	1.320
Tensile stress at max load (MPa)	0.813	0.012	0.225	0.002	0.782	0.009
Tensile strain at max load (mm/mm)	0.092	0.003	0.030	0.001	0.096	0.003
Axial strain at max load (mm/mm)	0.070	0.007	0.011	0.004	0.072	0.004
Modulus (MPa)	12.084	0.411	8.742	0.390	10.898	0.264
Modulus (Youngs 5%-100%) (MPa)	12.133	0.480	8.846	0.504	10.952	0.277

**Table 9.7.** Mechanical properties of PBXs containing Dantocol/no bonding agent.

### 9.3.3.2 1,3,5-Tris(2-hydroxyethyl)isocyanurate

The structure of THEIC comprises an additional amide and hydroxyethyl moiety, compared to that of Dantocol. This was expected to provide increased adhesive energy per molecule, consistent with the addition of bonding sites. The extent of adhesion was therefore anticipated to exceed that of small molecules exerting similar polarity. Conversely, the incorporation of 0.26% THEIC, failed to promote interfacial adhesion within PBX formulation ARX-2014.CW3. Interpretation of mechanical properties revealed values consistent with that acquired following the removal of bonding agent. This is conveyed in the plot of load versus tensile strain illustrated in Figure 9.5.

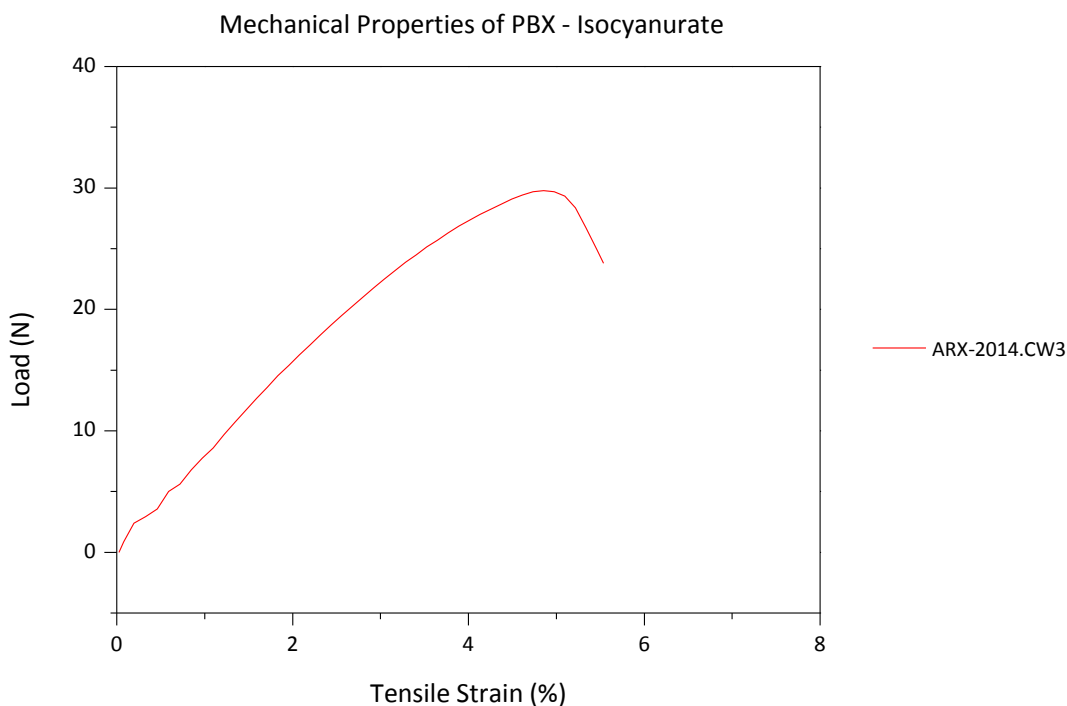


**Figure 9.5.** Load vs tensile strain of PBX comprising THEIC.

Solubility within the submix is predicted to account for the isocyanurates inability to establish interfacial adhesion. Coupled with the increased melting point of THEIC ( $T_m = 136-140^{\circ}\text{C}$ ), this prevents the occurrence of phase transfer at the required processing temperature. THEIC therefore remains a solid, inhibiting both filler interaction and incorporation within the binder system. Polymerisation of THEIC is typically performed at elevated temperatures to promote urethane formation.<sup>19</sup> Application of energetic materials

prevents the use of temperatures exceeding 60°C, in the interest of avoiding hazardous conditions. This presents limitations concerning the potential adoption of THEIC within nitramine based PBX composites.

### 9.3.3.3 Bonding Agent Adducts

Application of bonding agent adducts was investigated as an alternative approach to achieving interfacial adhesion. This involved the use of adducts to perform tasks otherwise associated with bonding agents and isocyanate curatives. The composition of DITBA was based upon Dantocol and TMXDI, with the later representing an aliphatic diisocyanate curative. Investigation of the difunctional adduct was also conducted to determine the potential for Dantocol's delocalised electrons to participate in dipole interaction. This called upon hydroxyl protection to isolate intermolecular forces between that involving RDX and the bonding agents carbonyl functionality.

The composition of TITBA was alternatively derived from THEIC and TMXDI, according to which is responsible for the adducts triisocyanate functionality. This addressed issues previously encountered upon application of THEIC within PBX formulations. Improvement of solubility parameters, thereby enabled TITBA to perform as required, facilitating the development of interfacial adhesion. This was assessed following incorporation of the trifunctional adduct within ARX-2014.CW5. The resulting mechanical properties were investigated by uniaxial tensile testing, with data acquisition interpreted in Table 9.8.

Mechanical Properties	ARX-2014.CW3		ARX-2014.CW4		ARX-2014.CW5	
	Mean	STD (%)	Mean	STD (%)	Mean	STD (%)
Maximum load (N)	29.825	0.464	115.154	2.971	103.192	2.586
Tensile stress at max load (MPa)	0.235	0.004	0.907	0.023	0.813	0.020
Tensile strain at max load (mm/mm)	0.046	0.010	0.064	0.009	0.050	0.001

**Table 9.8.** Mechanical properties of PBX formulations.

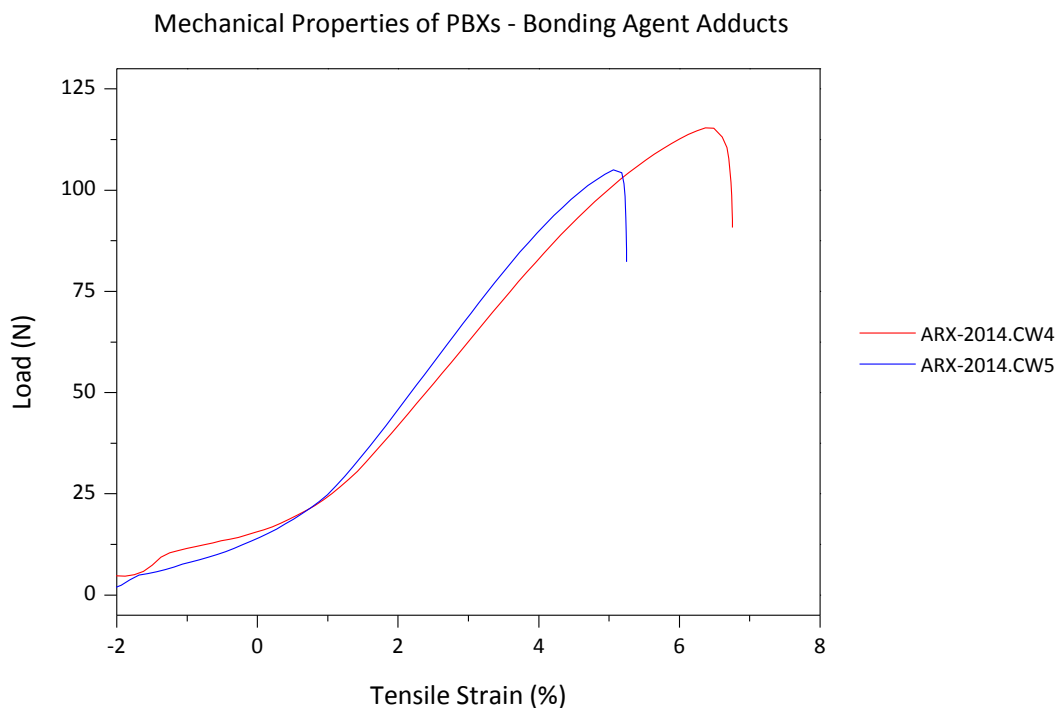


**Figure 9.6.** Load vs tensile strain of PBXs comprising bonding agent adducts.

#### 9.3.3.3.1 Difunctional Isocyanate Terminate Bonding Agent

Isocyanate terminated bonding agents follow a divergent approach to improving interfacial adhesion between the filler and binder system. Unlike standard bonding agent which adhere to the filler surface and engage in covalent bonding with the binder system, these examples are reacted with diisocyanate prior to submix addition. This provides the advantage of ensuring DITBA becomes incorporated within the binder system. The bonding agent must then demonstrate the capacity to interact with filler particles, subsequent to network addition.

Based on the results of mechanical testing, interaction of DITBA was identified at the filler/binder interface. This provides similar stress and strain behaviour to that observed upon incorporation of Dantocol within formulation ARX-2014. Comparisons between the performance of DITBA and Dantocol, substantiates the occurrence of dipole interactions involving the hydantoin delocalised carbonyl groups. This assists to achieve a maximum load of 115.154N, otherwise unattainable based upon the removal of hydroxyl functionality. The increase in molecular weight also provides the advantage of reducing solubility with

respect to HTPB. This readily enables the migration of bonding agent toward filler particles, whereby surface adhesion then occurs.

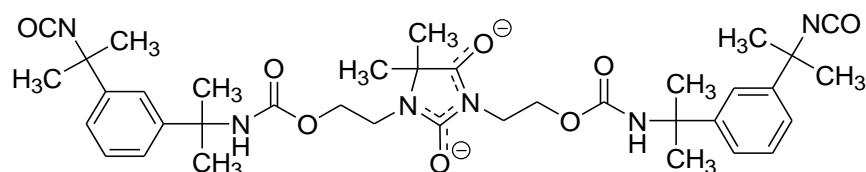


**Figure 9.7.** Delocalised electrons associated with the hydantoin structure.

As the diisocyanate bonding agent facilitates replacement of IPDI, this also contributes towards the materials mechanical properties. Unlike IPDI, the diisocyanate structure of TMXDI promotes equivalent isocyanate reactivity, while the dimethyl functionality lowers reactivity according to steric hindrance. This also inhibits reaction with water, otherwise responsible for the production of urea and self-condensation leading to branching. Further comparison identified TDXDI to contribute towards softer polyurethane composites, while generating higher elongation.<sup>20</sup>

Ducote et al. first introduced TMXDI as an alternative to IPDI within polyurethane based propellants.<sup>21</sup> The mechanical properties of cast-cured propellant composites displayed equal or improved stress, strain and modulus results, compared with IPDI based formulations.<sup>21-23</sup> Similar outcomes were observed in both catalysed and non-catalysed systems, involving the addition of 0.03% TPB. This suggests substitution of TMXDI within the current formulation is likely to contribute towards DITBA performance.

### 9.3.3.3.2 Trifunctional Isocyanate Terminated Bonding Agent

Evaluation of the trifunctional bonding agent also confirmed participation in interfacial adhesion, thereby delaying the onset of deformation. The adducts additional isocyanate moiety contributes towards increasing the cross-link density of the binder system. This presents the potential to strengthen the polyurethane network, whilst introducing additional hard segments. The resulting impact on mechanical properties is represented in Table 9.7, identifying visible deviation between the difunctional adaptation. This is predominately

evident within the maximum load, according to which observed a 10.3% decrease. These findings provide support for DITBA within the current series of formulations.

Importantly, the adduct remained within the liquid phase throughout the mixing process, permitting TITBA to engage in interfacial adhesion. This contrasts with the results of Section 9.3.3.2, which described the inability of THEIC to participate in interaction. Subsequent reaction with TMXDI in the synthesis of TITBA, also substantiates the occurrence of dipole interactions. This involves the electronegative carbonyls indicated in Figure 9.8, based upon which are responsible for intermolecular forces. Coupled with the adducts ability to engage in covalent bonding with HTPB, this addressed the implications associated with dewetting.

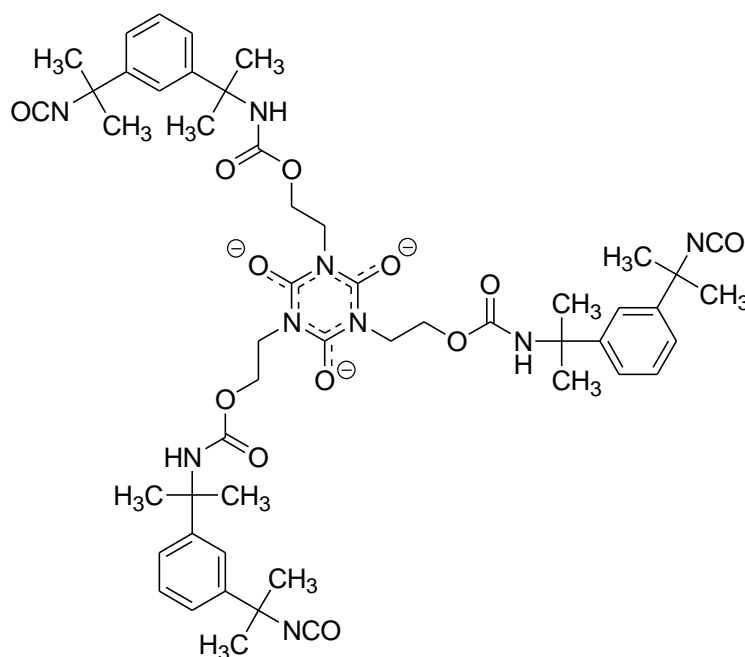


**Figure 9.8.** Delocalised electrons associated with the isocyanurate structure.

## 9.4 Conclusion

Satisfying the energetic performance criteria of cast-cured PBX composites is achieved by incorporation of high filler loading. This requires further adhesion at the filler/binder interface, preventing the onset of dewetting and other deformation mechanisms.<sup>24</sup> Propagation of dewetting results from an initial micro-vacuole, also known as nucleation.<sup>18</sup> The redistribution of stress then incurs tear, causing filler particles to dewet from the binder

system.<sup>18</sup> This leads to the formation of sensitised zones, which act as initiation sites if adiabatically compressed by impact or shockwave.

Bonding agents are therefore applied to resolve issues associated with poor interfacial adhesion, enabling high filler loading without compromising the risk of mechanical failure. This assists in incorporating filler particles within the polymeric binder system, thus improving mechanical properties and preventing degradative mechanisms. The implications of strengthening adhesion at the filler/binder interface is directly accountable for inhibition of aging, resistance to moisture diffusion, reduction in rigidity and improved stress-strain characteristics.<sup>25</sup> This results in cast-cured PBX composites displaying vastly improved mechanical properties.<sup>18</sup>

#### **9.4.1 Compatibility and Sensitiveness Testing**

Given the benefits apparent in mechanical properties, expanding the range of available bonding agents is therefore considered highly desirable. Novel bonding agents were assessed for compatibility and sensitivity prior to incorporation within PBX formulations. This initially entailed the investigation of thermal stability to identify characteristics including weight loss, phase change, gassing and the rate of decomposition. The thermal response between hydroxyalkyl ureas and RDX was found to expedite nitramine decomposition. Alternatively, hydroxyalkyl heterocycles and bonding agent adducts were observed to avoid associated issues. This was achieved through introduction of neutral or slightly acidic pH, thus preventing early onset of thermal decomposition.

Successive VTS investigations revealed evidence of incompatibility between hydroxyalkyl heterocycles and RDX. Although fulfilling the initial VTS criteria ( $V \leq 2.0\text{mL g}^{-1}$ ), compatibility results were observed to marginally exceed the required limit ( $V_R \leq 5.0\text{mL}$ ). Bonding agents satisfying these requirements were consequently submitted to small scale sensitiveness testing. This involved investigation of cast-cured PBX composites, establishing compliance in response to impact, friction, heat and electrostatic discharge. The range of



formulations evaluated were deemed unanimously compliant, with each satisfying the necessary requirements. This enabled the preparation of large scale batches required for investigation of mechanical properties, due to the results of sensitiveness testing.

### **9.4.2 Mechanical Properties**

Evaluation of Dantocol performance was investigated by comparative analysis, involving the removal of bonding agent from PBX formulations. The omission of Dantocol was accompanied by premature dewetting, thus producing a significant drop in tensile strength. This results in adverse effect upon the composites energetic performance and sensitivity to hazardous stimuli.<sup>18</sup> Following incorporation of 0.26% Dantocol, substantial improvement in mechanical properties was observed. Comprehensive increase in maximum load therefore reflects the influence of dewetting, along with the efficiency in which Dantocol improves interfacial adhesion.

The mechanical properties observed following application of bonding agent adducts, revealed the capacity of carbonyls to participate in dipole interactions. Hydroxyl protection inevitably required delocalised electrons to demonstrate the ability to engage in intermolecular forces. This occurred in correlation with the nitramine's NO<sub>2</sub> functionality, enabling DITBA and TITBA to enhance adhesion at the filler/binder interface. In response to the efficiency in which this function was performed, the mechanical properties of derived formulations improved accordingly.

The adduct formed between THEIC and TMXDI, also resolved issues previously encountered upon application of THEIC. Solubility of the precursor, otherwise prevented dispersal and subsequent interaction within PBX formulations. This produced mechanical properties comparable to that acquired following the removal of bonding agent. Alternatively reacting THEIC with the aliphatic diisocyanate prior to application, presents an adduct capable of interfacial adhesion. This implies the preparation of TITBA holds the potential to provide benefits in explosive ordnance.

## 9.5 References

1. Lohrmann, M.; Hubner, C. In *The influence of the matrix-filler-interaction on the mechanical properties of filled elastomers*, 27th International Annual Conference of ICT, Fraunhofer-Institut für Chemische Technologie: **1996**; pp 140/1-140/7.
2. Geibler, E.; Eisenreich, N.; Geibler, A.; Hubner, C., Analysis and test methods for service life prediction of energetic materials. In *31st International Annual Conference of ICT*, Fraunhofer-Institut für Chemische Technologie: **2000**; pp 149/1 - 149/11.
3. Hubner, C.; Geibler, E., Finite element modelling of matrix-filler debonding of energetic materials. In *30th International Annual Conference of ICT*, Fraunhofer-Institut für Chemische Technologie: **1999**; pp 99/1 - 99/15.
4. Bellerby, J. M.; Kiriratnikom, C., Explosive-binder adhesion and dewetting in nitramine-filled energetic materials. *Propellants, Explosives, Pyrotechnics* **1989**, *14* (2), 82-85.
5. Provatas, A. *Formulation and performance studies of polymer bonded explosives (PBX) containing energetic binder systems. Part I*; DSTO-TR-1397; DSTO: Weapons Systems Division, **2003**.
6. Hori, K., On the adhesion between hydroxyl-terminated polybutadiene fuel binder for composite solid propellants. *Propellants, Explosives, Pyrotechnics* **1985**, *21* (1), 43-50.
7. Gercel, B. O.; Uner, D. O.; Pekel, F.; Ozkar, S., Improved adhesion properties and bonding performance of HTPB-based polyurethane elastomer by using aziridine-type bond promoter. *Journal of Applied Polymer Science* **2001**, *80*, 806-814.
8. Hori, K.; Iwama, A., FTIR spectroscopic study on the interaction between ammonium perchlorate and bonding agents. *Propellants, Explosives, Pyrotechnics* **1990**, *15* (3), 99-102.
9. Tüzün, F. N.; Uysal, B. Z., The Effect of Ammonium Nitrate, Coarse/Fine Ammonium Nitrate Ratio, Plasticizer, Bonding Agent, and Fe<sub>2</sub>O<sub>3</sub> Content on Ballistic and Mechanical Properties of Hydroxyl Terminated Polybutadiene Based Composite Propellants Containing 20 % AP. *Journal of ASTM International* **2005**, *2* (6), 1-13.
10. Cucksee, M. T.; Allen, H. C. Bonding Agent System for Improved Propellant Aging and Low Temperature Physical Properties. US Patent 4,090,893, **1978**.
11. Baker, J. W.; Gaunt, J., The mechanism of the reaction of aryl isocyanates with alcohols and amines. Part II. The base-catalysed reaction of phenyl isocyanate with alcohols. *Journal of the Chemical Society* **1949**, 9-18.
12. Wall, C. *TNO pressure vacuum stability test (PVST)*; EI 437; Defence Science and technology Organisation: Weapons System Division, **2012**.
13. Mellor, A. M.; Boggs, T. L.; Convino, J.; Dickinson, C. W.; Dreitzler, D.; Thorn, L. B.; Frey, R. B.; Gibson, P. W.; Roe, W. E.; Kirshenbaum, M.; Mann, D. M., Hazard initiation in solid rocket and gun propellants and explosives. *Progress in energy and combustion science* **1988**, *14* (3), 213-244.
14. Hamilton, R. S.; Wardle, R. B.; Hinshaw, J. C. Vinyl ethers as nonammonia producing bonding agents in composite propellant formulations. US Patent 5,336,343, **1994**.

15. Consaga, J. P. Bonding agents for composite propellants. US Patent 4,944,815, **1990**.
16. Zorll, U., Adhesion testing. In *Coatings Technology: Fundamentals, Testing, and Processing Techniques*, Taylor and Francis Group: **2006**.
17. Chaffee, K. P.; Rusek, J. J. *Surface Science for Advanced Propulsion*; Phillips Laboratory Propulsion Directorate: Edwards Air Force Base, **1996**; p 313.
18. Kim, C. S.; Noble, P. N.; Youn, C. H.; Tarrant, D.; Gao, A., The mechanism of filler reinforcement from addition of neutral polymeric bonding agents to energetic polar propellants. *Propellants, Explosives, Pyrotechnics* **1992**, *17* (2), 51-58.
19. Kuehn, E. Isocyanurates from unsaturated monohydric alcohols and polyisocyanates. US Patent 4,159,376, **1979**.
20. Cytec *TMXDI® (META) aliphatic isocyanate the choice for aqueous polyurethane dispersions*; UPT-796-B; New Jersey, **2008**.
21. Ducote, M. E. TMXDI, curing agent for hydroxy terminated propellant binders. US Patent 4,913,753, **1990**.
22. Doll, D. W.; Lund, G. K. Processing and curing aid for composite propellants. US Patent 5,942,720, **1999**.
23. Wallace, I. A. Ambient temperature mix, cast, and cure composite propellant formulations. US Patent 5,472,532, **1995**.
24. Diamant, Y.; Folman, M., Influence of dewetting on the damping properties of a filled polymer system: 1. Static characterization. *Polymer* **1979**, *20* (8), 1025-1033.
25. Sciamareli, J.; Holanda, J. A. S.; Dutra, R. C. L.; Lourenco, V. L.; Iha, K., RX bonding agent - study of its natural aging. In *34th International Annual Conference of ICT*, Fraunhofer-Institut fuer Chemische Technologie: **2003**; pp 63/1 - 63/11.



# Chapter 10

---

Conclusion

## 10.1 Introduction

The addition of bonding agents to cast-cured energetic materials is recognised to provide significant benefits towards mechanical properties. This is confirmed in response to its extensive use throughout the field, with the majority of modern formulation comprising a bonding agent component.<sup>1</sup> The reputation surrounding bonding agents is derived from their ability to enhance interfacial adhesion, thereby promoting filler reinforcement. This provides a solution to issues occurring from poor compatibility between the binder and filler particles.

As bonding agents possess the capacity to prevent dewetting and other deformation mechanisms, this is considered fundamentally important to the insensitivity of energetic composites. The propagation of dewetting is often regarded as the most destructive deformation mechanism occurring within energetic materials.<sup>2, 3</sup> This is recognised to promote weakening of materials, decrease in modulus, increased potential for fracture and the production of voids, which act as initiation sites if adiabatically compressed.<sup>4</sup> Therefore the incorporation of compatible bonding agents provide the ability to prevent such issues, thus contributing to the development of insensitive munitions.

## 10.2 Interaction of Dantocol and RDX

Irrespective of the significance associated with bonding agents, limited literary content exists discussing the additive's mode of action. Consequently, the selection of bonding agents for application within energetic materials is largely considered speculative. In providing a comprehensive understanding of mechanisms occurring, this stands to benefit both the selection and development of novel bonding agents. This primarily involves the characterisation of bonding arising at the filler/binder interface.

Due to the surface sensitivity associated with infrared spectroscopy, this is widely considered the preferred method for the study of hydrogen bonding. The majority of information regarding hydrogen bonding relates to measurement of NMR and FTIR peak shifts, thermal

analysis, or acidities.<sup>5</sup> Still, the investigation of interface regions is often problematic, depending on the content of individual layers and depth at which the region resides. As the interface exists within a finite region between two layers, isolating interactions occurring at this point presents significant difficulties. According to most surface and interfacial techniques, a trade-off therefore exists between depth resolution and sensitivity.<sup>6</sup>

### **10.2.1 Coatings and Characterisation of Dantocol**

Prior to characterising Dantocol interaction, preparation involved encapsulating filler particles within a thin film of bonding agent. This required the development of an effective method to maximise interactions occurring at the interface. The process was also called upon to provide individually coated particles, resistant to aggregation, while imposing negligible impact on crystal morphology. These properties were dependent on the applied conditions, along with influencing coating thickness, particle size distribution and surface conditions.<sup>7</sup>

The established microencapsulation procedure was found to provide superior coatings in preparation for sample analysis. This involved suspending RDX in a bonding agent solution, whereby the removal of solvent caused the precipitation of Dantocol. Further to delivering uniform coatings, microencapsulation had no measurable impact on the structure, crystal morphology or particle size of nitramine crystals. This is required to characterise the interaction of Dantocol and RDX as it occurs in PBX formulations.

### **10.2.2 Characterisation of interfacial interactions by FTIR**

FTIR spectroscopy was applied to evaluate interfacial interactions, owing to its high sensitivity to noise ratio and suitability for solid analyse. Application of FTIR techniques consisting of differing surface sensitivities, thus provided the means necessary to evaluate secondary bonding, as it occurs between Dantocol and RDX. The combined capabilities of ATR, DRIFTS, PAS and transmission spectroscopy, therefore implemented various penetration depths, invaluable in characterising the interface region.

The combination of FTIR results revealed the presence of spectral shifts, consistent with the nitramines  $\nu_{\text{as}}\text{NO}_2$  peak. This indicated that  $\text{NO}_2$  groups participate in hydrogen bonding between the bonding agent's OH functionality. The strength of hydrogen bonding was indicated by the magnitude of  $\nu_{\text{as}}\text{NO}_2$  shifts. These observations correspond to deviation in the bonding agent's broad OH band. This confirmed hydrogen bonding occurs between the nitramine's proton accepting nitro group and Dantocol. These conclusions are consistent with the literature, which describes the participation of alternate nitro compounds in hydrogen bonding, with appropriate proton donors.<sup>8-16</sup>

The superior surface sensitivity of DRIFTS offered benefits towards the evaluation of surface interactions. This is often capable of detecting interactions other techniques are unable to identify.<sup>17</sup> Examples include weak interactions such as dipole interaction, which were revealed within coated RDX samples. Although minor evidence of dipole interactions was identified within supporting techniques, DRIFTS provided conformation of this interaction. Shifts in the C=O bands indicate the dipole moment responsible for interaction, which functions to complement that of hydrogen bonding.

### **10.2.3 Hydroxyl protection of Dantocol**

Hydroxyl protection was applied to confirm the functionality responsible for Dantocol interaction. Manipulation of the bonding agent's hydroxyl functionality, provided a means to differentiate between the occurrence of hydrogen bonding and supplementary dipole interactions. This was achieved through silylation of Dantocol, thereby controlling the ability to engage in hydrogen bonding. Disilylation involved reaction with trimethylsilyl chloride, while selective protection was required to yield the monosilylated alternative. Substitution of *tert*-butyldimethylsilyl chloride was necessary to limit attachment to the less hindered hydroxyl moiety.

Characterisation of hydroxyl-protected bonding agents revealed silylation impeded interaction with RDX. This confirmed the nitramine's polar  $\text{NO}_2$  groups undergoes hydrogen



bonding with Dantocol's proton donating hydroxyl groups. Meanwhile, spectroscopic techniques also confirmed weak interactions occur in the absence of hydrogen bonding. This is consistent with dipole interactions, involving the hydantoin's electronegative carbonyl groups.

Interfacial adhesion is significantly reduced in the absence of acid-base interactions.<sup>18</sup> Energy associated with hydrogen bonding is dependent upon the acidity of proton donor and basicity of the proton acceptor.<sup>19</sup> The attractive force associated with hydroxyl groups, therefore exceeds that achieved in response to dipole interactions. Contributions towards adhesion is consequently reduced, as dipole-dipole interactions generate an endothermic heat of mixing and enhance cohesive interactions at the interface.<sup>19-21</sup> Although comparatively weak, local dipoles remain capable of supplementing the occurrence of hydrogen bonding.

#### **10.2.4 Thermal analysis of bonding agent interaction**

Thermal analysis was applied to further elucidate intermolecular forces between Dantocol and RDX. This also provided supplementary information regarding the thermal stability and compatibility of constituents. Interpretation of DSC curves identified the melting behaviour of coated particles, with the melting endotherm observed to broaden and shift towards lower temperature upon the addition of Dantocol. Decrease in melting point is known to reflect the thermodynamic miscibility of mixtures, resulting from intermolecular forces.<sup>22</sup> These findings were confirmed according to the heat of fusion, which also reflects interaction.<sup>23</sup> This indicated additional work was required to promote melting, as influenced by the presence of intermolecular forces.<sup>24-26</sup> Characterisation of the melting endotherm was therefore able to provide a semi-quantitative response to the extent in which interaction occurs.

Application of PDSC was employed to establish the kinetic parameters associated with thermal sublimation. Results were consistent with the  $\Delta H_s$  reported within the literature for neat RDX crystals. This represents the energy required to overcome intermolecular

interactions, thereby assisting to describe the extent of bonding agent interaction. Given the increase in  $\Delta H_s$  following addition of Dantocol, the extent of secondary bonding was therefore demonstrated to increase.

### **10.3 Polymerisation of Dantocol and the Binder System**

Incorporation of Dantocol within the binder system was investigated using a diverse approach to characterise the reaction. This involved an initial analysis of the polyurethane binder system and its precursors. The importance of understanding the characteristics of these components, is integral to differentiating between the mechanism of bonding agent reaction. This also sufficed as a reference, from which to compare the network's physical and chemical properties upon polymerisation of Dantocol. The bonding agent's involvement in covalent bonding, was then investigated in relation to binder precursors. Finally, the reaction was characterised in association with the integrated binder system, identifying the impact of competing reactions.

#### **10.3.1 Polyurethane Binder System**

Polymerisation of HTPB and IPDI, was characterised by spectroscopic, thermoanalytical and rheological techniques, to elucidate curing behaviour. Preliminary investigation of HTPB, identified the hydroxyl equivalent weight, isomer content, triad configurations and molecular weight, necessary to establish the impact of Dantocol. Coupled with the results of polyurethanes derived from HTPB, this provided a critical reference from which to identify the participation of Dantocol in covalent bonding.

Investigation into the polyurethane's rheological behaviour provided further insight regarding the cure kinetics. This identified critical points of conversion, including viscosity build-up, gel point and the impact of catalyst addition. Establishing the rheo-kinetic properties of urethane formation, also provides data from which the influence of Dantocol

can be compared. This was required to interpret the rheological behaviour associated with the reaction of competing hydroxyl components.

### **10.3.2 Dantocol and HTPB Blends**

The possibility of interaction between Dantocol and HTPB, was investigated through means of a hydroxyl blend. Negligible interaction was inferred by the absence of reasonable association between components, thereby negating the potential for hydrogen bonding.<sup>27</sup> This was reflected amongst spectroscopic techniques, with neither deviation or evolution of peaks observed. Spectra were therefore consistent with the combined overlay of Dantocol and HTPB. As the potential for interaction of HTPB is limited to its hydroxyl functionality, consumption during polymerisation with IPDI eliminates the possibility of this occurring. This leaves reaction with isocyanate as the only credible mechanism for incorporation of Dantocol.

### **10.3.3 Dantocol and IPDI Polymerisation**

Polymerisation of Dantocol and IPDI was found to yield linear polyurethane isomers, consisting of crystalline appearance. This initially required adduct preparation, with the intermediate facilitating reaction completion in conjunction with catalyst addition. The extent of conversion was monitored by spectroscopic techniques, according to the decline in NCO peak intensity. Removal of NCO was accompanied by evolution of amine, amide and carbonyl bands, correlating with the formation of urethane linkages.

Thermal analysis identified exhibition of the polyurethanes crystalline melting point ( $T_m = 104^\circ\text{C}$ ). Crystalline behaviour reflects curing of monomeric compounds, contributing towards the formation of hard segment domains. This results in confinement of reactive groups, therefore hindering reaction completion. These circumstances also reduce the observed reactivity, as indicated according to rheological analysis. Low reactivity contributes towards inhibiting dissociation of intermolecular forces between Dantocol and

RDX, in the presence of isocyanate. This must endure the attack of IPDI, if interfacial adhesion is to persist within cast-cured PBX composites.

### **10.3.4 Copolymerisation of Polyurethane Blend**

Confirmation of Dantocol's ability to produce urethane linkages, required further investigation in the presence of HTPB. This is necessary to identify the impact of competing hydroxyl groups, in regards to reaction involving IPDI. Copolymerisation of HTPB and Dantocol with the diisocyanate was confirmed using spectroscopic techniques, aimed at establishing the presence of amine, amide and carbonyl peaks. Potentially the most revealing observation, was the removal of isocyanate from polyurethane spectra. This occurred at various ratios of HTPB and Dantocol, signifying the polymerisation of both hydroxyl components.

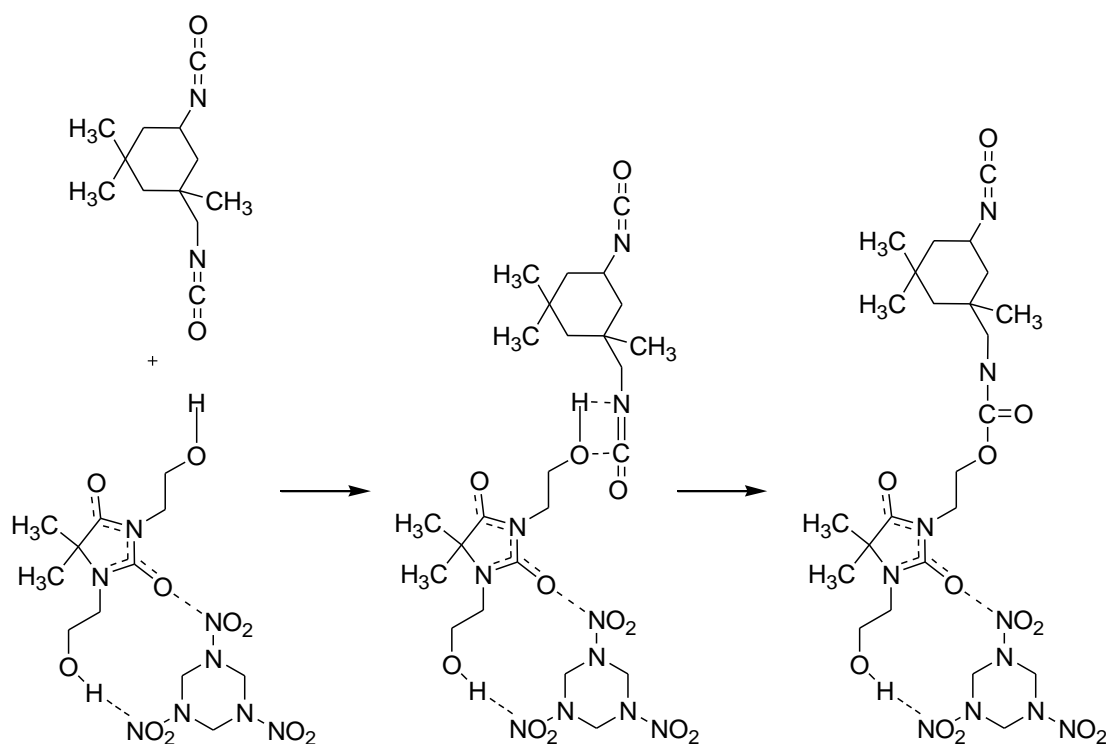
Complementary to spectroscopic techniques, DSC was applied to investigate the thermal behaviour of polyurethane blends. Interpretation of decomposition and the glass transition temperature, confirmed incorporation of Dantocol within the binder system. Results also demonstrated the addition of bonding agent neglected to impact the occurrence of intermolecular forces, between hard and soft segments. The implications of this rule out the potential for Dantocol to remain suspended within the binder system.

The reactivity of hydroxyl components was determined, according to the rheological behaviour observed during network formation. This identified the improved reactivity of HTPB, in comparison to Dantocol and IPDI. In response, this produced multiple rate constants, contributing towards the kinetic behaviour. The investigation also revealed the point of gelation and viscosity build-up, along with confirming blend copolymerisation. This described the ability of Dantocol to form covalent bonds with the curative's diisocyanate functionality, producing urethane linkages in competition with HTPB.

## 10.4 Dantocols mode of action

Investigation of Dantocol within the binder system, revealed the bonding agent functions to increase crosslink density adjacent to filler particles. Details involved the incorporation of Dantocol within the network, whilst simultaneously participating in filler interaction. Intermolecular forces involved in RDX interaction consist of hydrogen bonding and dipole interactions, appearing in synergy to improve adhesion. This reflects the significance of Dantocol's multiple hydroxyl groups, which account for both filler interaction and covalent bonding with IPDI.

Hydrogen bonding is recognised to introduce an autocatalytic effect, occurring between isocyanates and free hydroxyl groups. This contrasts with the inhibiting effect proton acceptors, inclusive of nitro compounds, are known to impose upon urethane formation. Reaction inhibition is dependant upon the polarising effect incurred between participating compounds.<sup>28</sup> This prevents dissociation of hydrogen bonding between Dantocol and RDX, irrespective of isocyanate content.



**Scheme 10.1.** Interfacial adhesion involving Dantocol at the filler/binder system interface.

The bonding agent's remaining hydroxyl functionality is responsible for incorporation within the binder system, as indicated according to reaction Scheme 10.1. This was established following characterisation of the polyurethane network, revealing fundamental changes in chemical structure due to Dantocol. These results confirmed the mechanism involved in bonding agent reaction, according to which accounts for hard segment formation. Coupled with the interaction involving RDX, the urethane reaction concludes that responsible for Dantocol's mode of action. This facilitates interfacial adhesion to prevent deformation mechanisms, thereby contributing towards IM compliance.

## **10.5 Synthesis of Novel Bonding Agents**

Bonding agents development presents the potential to significantly improve the safety and mechanical properties of cast-cured energetic materials. Few compounds are currently available that display the ability to function as an effective bonding agent. To ensure this occurs, numerous properties must be incorporated to provide interfacial adhesion. This includes defined conditions pertaining to solubility, pH, polarity, functionality, molecular weight, chain flexibility, filler compatibility and thermal stability. Addressing these demands provides the ability to overcome issues associated with the filler/binders highly dissimilar surfaces, engaging in bond formation between both components.

### **10.5.1 Synthesis of 1,3-*bis*(2,3-dihydroxypropyl)-5,5-dimethylhydantoin**

Given the efficiency in which Dantocol satisfies these requirements, expanding the range of hydroxyalkyl heterocycles represents potential for improving performance. This eventuated in the synthesis of novel bonding agents, derived from the original hydantoin structure. Substitution of dihydroxypropyl side chains was performed to increase the hydroxyl functionality. This involved reaction of 5,5-dimethylhydantoin and glycidol, yielding 1,3-*bis*(2,3-dihydroxypropyl)-5,5-dimethylhydantoin. Additional hydroxyl functionality served to increase the hydrogen bonding capacity, while facilitating the role of cross-linking agent.

### 10.5.2 Synthesis of Hydroxyalkyl Ureas

The ability of hydroxyethyl chains to promote bonding agent interaction, was exploited amid preparation of hydroxyalkyl ureas. Reaction of aminoalcohols and a single urea moiety, was employed to produce a series of bonding agents, containing sequential increase in hydroxyethyl functionality. This was achieved based upon the aminoalcohol applied, with reactions performed neat and absent of catalyst. Synthesis resulted in the acquisition of 1,3-*bis*(2-hydroxyethyl)urea, 1,1,3-*tris*(2-hydroxyethyl)urea, 1,1,3,3-*tetrakis*(2-hydroxyethyl)urea, 3-[3-hydroxy-1,1-*bis*(2-hydroxyethyl)propyl]-1,1-*bis*(2-hydroxyethyl)urea and 1,3-*bis*[3-hydroxy-1,1-*bis*(2-hydroxyethyl)propyl]urea.

### 10.5.3 Synthesis of Polycarbamate Dendrimer

Based upon the previous synthetic pathway, repetitive addition of urea and diethanolamine was applied to produce a polycarbamate dendrimer assembly. This introduced high end-group concentration, associated with the development of second generation architecture. Consequently, the polycarbamate's outer shell was designed to terminate in the occurrence of eight hydroxyl moieties. Bonding agent performance was therefore investigated according to the dendrimers additional surface activity. This combination of high end-group concentration, low viscosity and solubility parameters, is recognised to contribute towards the conditions necessary for high solid coatings.<sup>29</sup>

### 10.5.4 Synthesis of Hydroxyalkyl Heterocycles

Nitrogen containing heterocycles are recognised to improve the thermal decomposition behaviour of polyurethanes, subsequent to network incorporation.<sup>30</sup> This applies to Dantocols characteristic ring structure, based upon which derivatives were investigated to achieve thermal stability. Variations in regard to the heterocyclic structure are depicted in Figure 10.2, outlining modifications applied to exploit the hydantoin's known performance. This involved the synthesis of 1,3-*bis*(2-hydroxyethyl)parabanate, 1,2,4-*tris*(2-

hydroxyethyl)urazole and 1,3,4,6-*tetra*(2-hydroxyethyl)glycoluril. Proposed bonding agents again offered additional functionality, focussed upon improving interfacial adhesion. This was achieved following hydroxyalkylation of N-heterocycles, amid the presence of base catalysis.

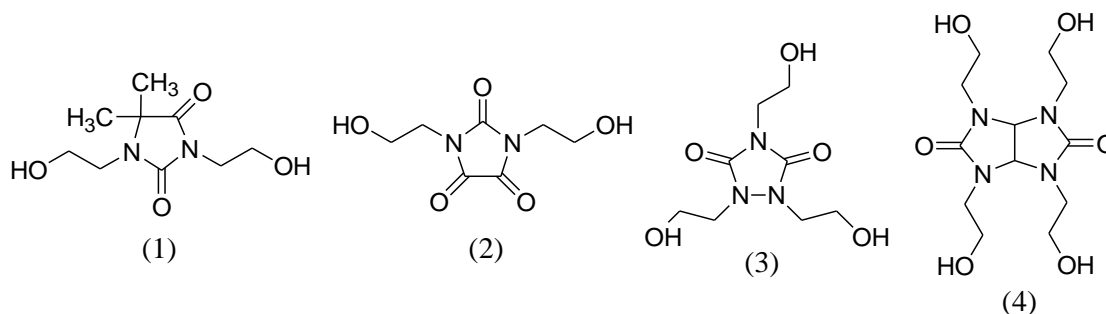


**Figure 10.1.** Bonding agent structures of (1) Dantocol (2) 1,3-*bis*(2-hydroxyethyl)parabanate (3) 1,2,4-*tris*(2-hydroxyethyl)urazole and (4) 1,3,4,6-*tetra*(2-hydroxyethyl)glycoluril.

## 10.6 Mechanical Properties of PBXs

### 10.6.1 Compatibility and Sensitiveness Testing

Bonding agent compatibility and sensitivity was assessed in regards to RDX, prior to incorporation within PBX formulations. This involved the investigation of thermal stability, identifying characteristics including weight loss, phase change, gassing and the rate of decomposition. Thermal decomposition of RDX was observed to deviate towards reduced temperatures, amid the presence of hydroxyalkyl urea bonding agents. Meanwhile, hydroxyalkyl heterocycles and bonding agent adduct's, produced minimal deviation in decomposition onset, thereby satisfying stability criteria. This was achieved through the introduction of neutral or slightly acidic pH, and improved thermal resistance of the isolated bonding agent.

Further assessment by means of VTS testing, alluded to minor incompatibility between hydroxyalkyl heterocycles and RDX. While initial VTS criteria ( $V \leq 2.0\text{mL g}^{-1}$ ) was satisfied, compatibility results were discovered to narrowly exceed the required limit ( $V_R \leq$



5.0mL). Small scale sensitiveness testing was then performed on those bonding agents which fulfilled these requirements. This entailed investigation of cast-cured PBX composites to establish the response to impact, friction, heat and electrostatic discharge. All formulations involved were found to comply with sensitiveness testing criteria, thereby displaying an acceptable response to hazardous stimuli. These results enabled the preparation of large scale batches, required for investigating mechanical properties.

### **10.6.2 Mechanical Properties**

The performance of Dantocol was investigated following a comparative study, involving the additives removal from PBX formulations. Bonding agent omission was accompanied by early onset of dewetting, creating a significant drop in tensile strength. This detracts from the composite's sensitivity to hazardous stimuli, as well as performance.<sup>31</sup> The addition of 0.26% Dantocol, conveyed significant improvement in the mechanical properties of PBXs. This constituted a 78.37N increase in maximum load, thus reflecting the influence of dewetting, along with efficiency in which Dantocol improves interfacial adhesion.

Similar results were observed following the application of bonding agent adducts. This revealed the capacity of electronegative carbonyls to participate in dipole interactions, following the protection of hydroxyl functionality. Interaction of delocalised electrons correlated with the nitramines NO<sub>2</sub> functionality, enabling DITBA and TITBA to enhance interfacial adhesion. The efficiency with which this occurred was reflected throughout the mechanical properties of those formulations comprising either adduct example.

Preparation of TITBA following the reaction of THEIC and TMXDI, also resolved issues involving the application of THEIC within cast-cured PBX composites. The solubility associated with THEIC, led to prevention of bonding agent dispersal and subsequent interaction within the submix. Consequently, the mechanical properties were observed to deteriorate, reflecting results equivalent to that acquired upon bonding agent removal. Failure to undergo interaction was therefore resolved, following reaction of THEIC with the

aliphatic diisocyanate, prior to PBX application. This provided an adduct capable of interfacial adhesion, thus presenting benefits towards the development of insensitive munitions.

## **10.7 Future Developments**

The development of novel bonding agents successfully identified the potential for improvement in mechanical properties and insensitivity of cast-cured PBX composites. Whilst these compounds satisfied the requirements of an effective bonding agent, optimisation of concentration within PBX formulation may provide further improvement in bonding agent performance. This was previously applied to determine the concentration of Dantocol required to achieve optimal performance, however these results may vary between compounds. Application of novel bonding agents within cast-cured propellant composites may additionally provided an indication of compatibility within alternative composites. Further investigation may also include the substitution of alternative fillers and binder systems.

Elucidation of Dantocol's mode of action has paved the way for future research into the design and synthesis of novel bonding agents. Having developed a range of bonding agents focussed on exceeding the performance characteristics of Dantocol, further expanding upon the selection of available bonding agents presents the potential for additional improvements. This may provide viable alternatives for incorporation within cast-cured energetic materials, with flow-on benefits for explosive ordnance.

## 10.8 References

1. Klager, K., Polyurethanes, the most versatile binder for solid composite propellants. In *20th Joint Propulsion Conference*, American Institute of Aeronautics and Astronautics: Cincinnati, Ohio, **1984**.
2. Geibler, E.; Eisenreich, N.; Geibler, A.; Hubner, C., Analysis and test methods for service life prediction of energetic materials. In *31st International Annual Conference of ICT*, Fraunhofer-Institut für Chemische Technologie: **2000**; pp 149/1 - 149/11.
3. Lohrmann, M.; Hubner, C. In *The influence of the matrix-filler-interaction on the mechanical properties of filled elastomers*, 27th International Annual Conference of ICT, Fraunhofer-Institut für Chemische Technologie: **1996**; pp 140/1-140/7.
4. Bellerby, J. M.; Kiriratnikom, C., Explosive-binder adhesion and dewetting in nitramine-filled energetic materials. *Propellants, Explosives, Pyrotechnics* **1989**, 14 (2), 82-85.
5. Hadzi, D., Spectroscopic and structural aspects of very strong hydrogen bonds. *Chimia* **1972**, 26, 7-13.
6. Chaffee, K. P.; Rusek, J. J. *Surface Science for Advanced Propulsion*; Phillips Laboratory Propulsion Directorate: Edwards Air Force Base, **1996**; p 313.
7. Eerligh, R.; Van Gool, M. A.; Kramer, R. E.; Van Ham, N. H. A., Investigation of the result of coating techniques of high explosives with the aid of scanning electron microscope / energy-dispersive X-ray spectrometry. *17th Annual International ICT Conference* **1986**, 10-1.
8. Forlani, L., Hydrogen Bonding and Complex Formation Involving Compounds with Amino, Nitroso and Nitro Groups. In *PATAI'S Chemistry of Functional Groups*, John Wiley & Sons, Ltd: **2009**.
9. Li, F.; Ye, L.; Nie, F.; Liu, Y., Synthesis of boron-containing coupling agents and its effect on the interfacial bonding of fluoropolymer/TATB composite. *Journal of Applied Polymer Science* **2007**, 105 (2), 777-782.
10. Granzhan, V. A.; Semenenko, S. V.; Zaitsev, P. M., The susceptibility of the nitro group to hydrogen bond formation. *Journal of Applied Spectroscopy* **1968**, 9 (3), 929-932.
11. Granzhan, V. A.; Semenenko, S. V.; Zaitsev, P. M., Sensitivity of a nitro group to the formation of a hydrogen bond. I Intramolecular hydrogen bonding in phenols. *Zhurnal Prikladnoi Spektroskopii* **1968**, 9 (3), 407-411.
12. Urbański, T., A study of the hydrogen bonds between the nitro-group and the hydroxyl or amino-groups in substituted nitroparaffins. *Tetrahedron* **1959**, 6 (1), 1-9.
13. Baitinger, W. F.; Schleyer, P. v. R.; Murty, T. S. S. R.; Robinson, L., Nitro groups as proton acceptors in hydrogen bonding. *Tetrahedron* **1964**, 20 (7), 1635-1647.
14. Kamlet, M. J.; Taft, R. W., Linear solvation energy relationships. 20. Intra- vs. intermolecular hydrogen bonding by some 2-nitroaniline and 2-nitrophenol derivatives. *The Journal of Organic Chemistry* **1982**, 47 (9), 1734-1738.
15. Johnstone, R. A. W.; Loureiro, R. M. S.; Cristiano, M. L. S.; Labat, G., Bond energy/bond order relationships for N-O linkages and a quantitative measure of ionicity: the

role of nitro groups in hydrogen-bonding. *Archieve of Organic Chemistry* **2010**, (5), 142-169.

16. T. Dubis, A.; Lotowski, Z.; Siergiejczyk, L.; Z. Wilczewska, A.; W. Morzycki, J., Study of Hydrogen Bonding in Nitro Enamides. *Journal of Chemical Research, Synopses* **1998**, (4), 170-171.

17. Hapner, G.; Nease, A. *Study of explosives by diffuse reflectance FT-IR spectroscopy*; Monsanto Research Corp., Miamisburg, OH (USA). Mound: **1985**.

18. Drago, R. S.; Vogel, G. C.; Needham, T. E., Four-parameter equation for predicting enthalpies of adduct formation. *Journal of the American Chemical Society* **1971**, 93 (23), 6014-6026.

19. Fowkes, F. M., Role of acid-base interfacial bonding in adhesion. *Journal of Adhesion Science and Technology* **1987**, 1 (1), 7-27.

20. Mittal, K. L., *Acid-base interactions: relevance to adhesion science and technology*. **1991**.

21. Fowkes, F. M., Attractive forces at interfaces. *Industrial & Engineering Chemistry* **1964**, 56 (12), 40-52.

22. Rostami, S., Crystallization behaviour of a semicrystalline miscible blend. *Polymer* **1990**, 31 (5), 899-904.

23. Zeman, S., The impact sensitivity of some nitramines. In *Proceedings of the 10th Symposium on Chemical Problems Connected with the Stability of Explosives*, Sweden, **1995**; Vol. 28, p 367.

24. Zeman, S.; Krupka, M., New Aspects of Impact Reactivity of Polynitro Compounds, Part II. Impact Sensitivity as "the First Reaction" of Polynitro Arenes. *Propellants, Explosives, Pyrotechnics* **2003**, 28 (5), 249-255.

25. Zeman, S.; Krupka, M., New Aspects of Impact Reactivity of Polynitro Compounds, Part III. Impact Sensitivity as a Function of the Intermolecular Interactions. *Propellants, Explosives, Pyrotechnics* **2003**, 28 (6), 301-307.

26. Zeman, S.; Jalový, Z., Heats of fusion of polynitro derivatives of polyazaisowurtzitane. *Thermochimica Acta* **2000**, 345 (1), 31-38.

27. Lee, J. Y.; Painter, P. C.; Coleman, M. M., Hydrogen bonding in polymer blends. 3. Blends involving polymers containing methacrylic acid and ether groups. *Macromolecules* **1988**, 21 (2), 346-354.

28. Chang, M.-C.; Chen, S.-A., Kinetics and mechanism of urethane reactions: Phenyl isocyanate-alcohol systems. *Journal of Polymer Science Part A: Polymer Chemistry* **1987**, 25 (9), 2543-2559.

29. Voit, B., New developments in hyperbranched polymers. *Journal of Polymer Science Part A: Polymer Chemistry* **2000**, 38 (14), 2505-2525.

30. Lubczak, J., Polyhydroxyalkyl derivatives and polyetherols obtained from azacyclic compounds. *Polimery* **2011**, 56 (5), 360-358.

31. Kim, C. S.; Noble, P. N.; Youn, C. H.; Tarrant, D.; Gao, A., The mechanism of filler reinforcement from addition of neutral polymeric bonding agents to energetic polar propellants. *Propellants, Explosives, Pyrotechnics* **1992**, *17* (2), 51-58.



# Appendix

---

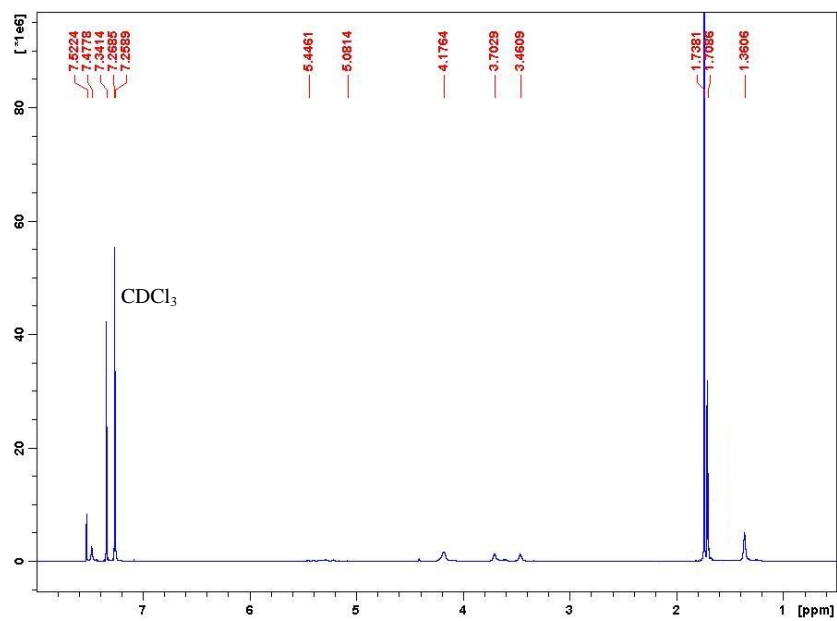


Figure A.1.1  $^1\text{H}$  NMR of difunctional isocyanate terminate bonding agent in chloroform-*d*.

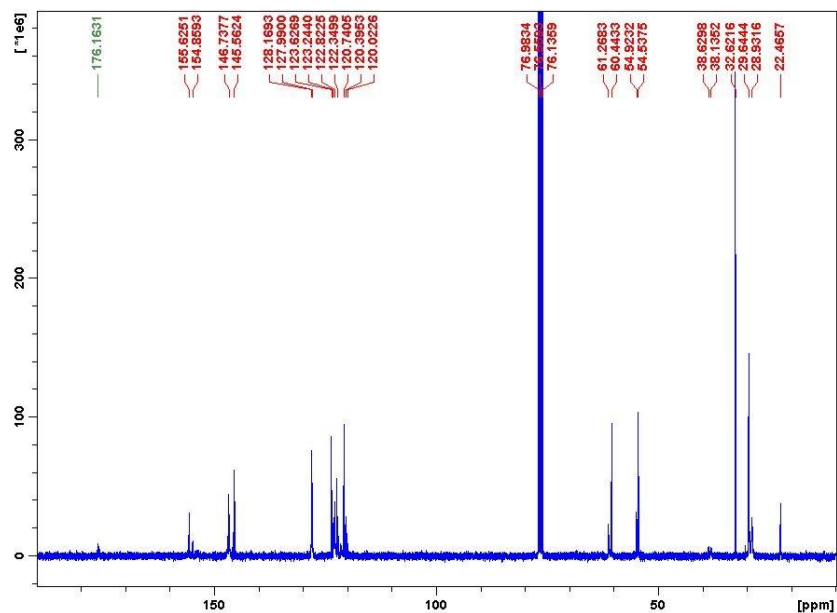


Figure A.1.2  $^{13}\text{C}$  NMR of difunctional isocyanate terminate bonding agent in chloroform-*d*.

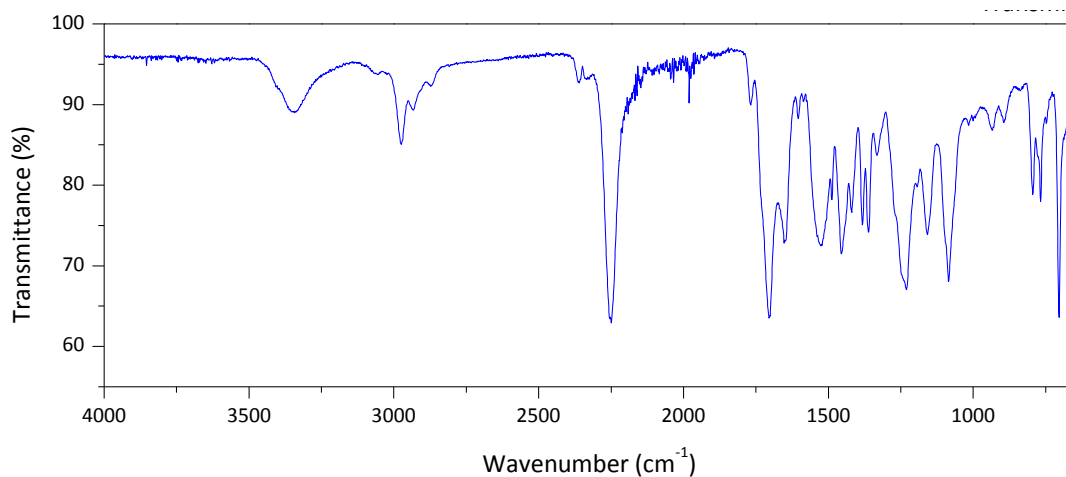


Figure A.1.3 FTIR spectrum of difunctional isocyanate terminate bonding agent.



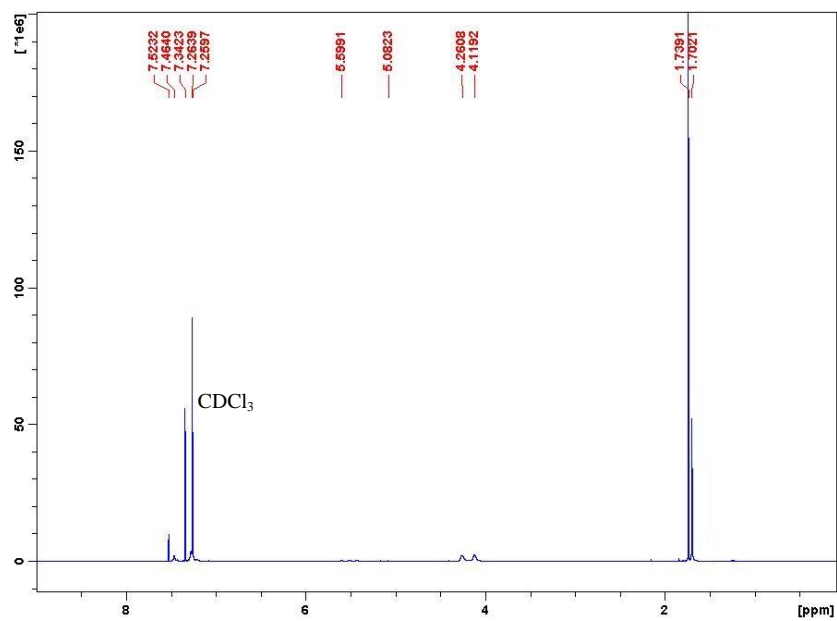


Figure A.2.1  $^1\text{H}$  NMR of trifunctional isocyanate terminate bonding agent in chloroform-*d*.

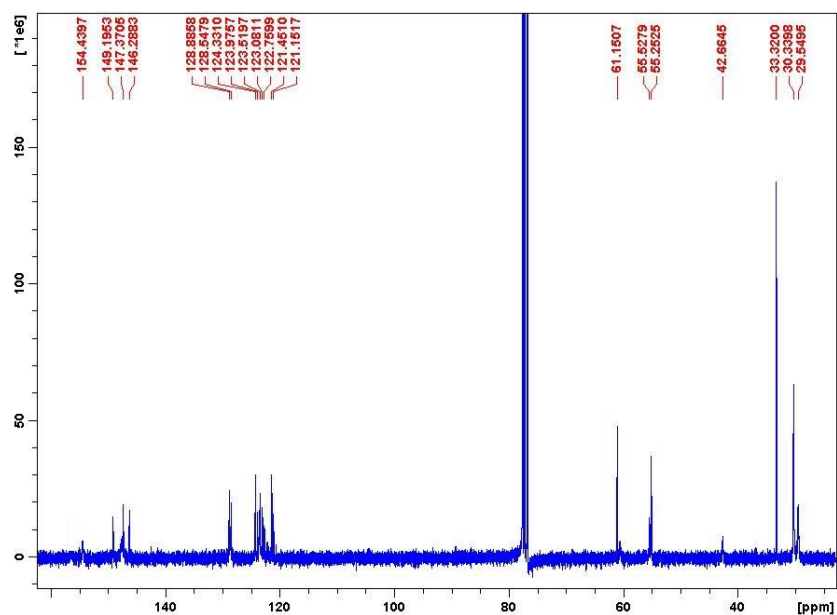


Figure A.2.2  $^{13}\text{C}$  NMR of trifunctional isocyanate terminate bonding agent in chloroform-*d*.

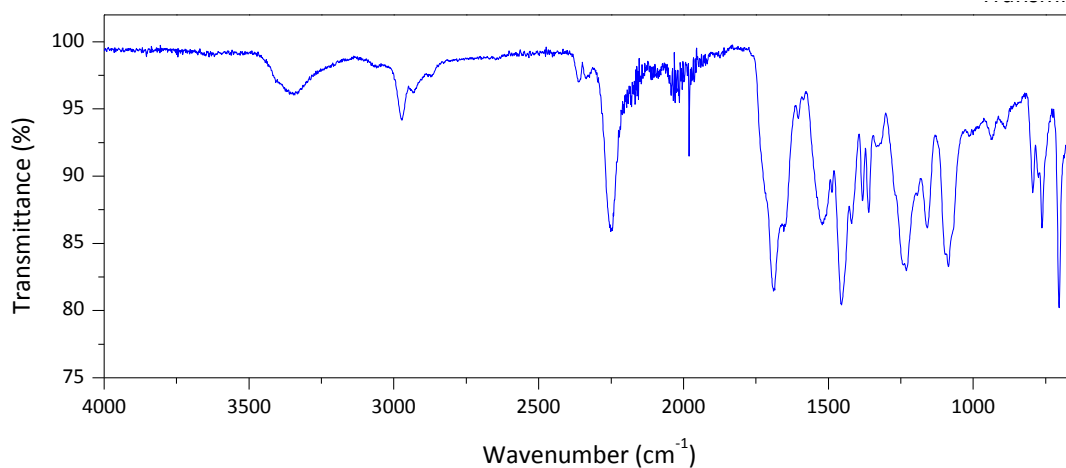


Figure A.2.3 FTIR spectrum of trifunctional isocyanate terminate bonding agent.

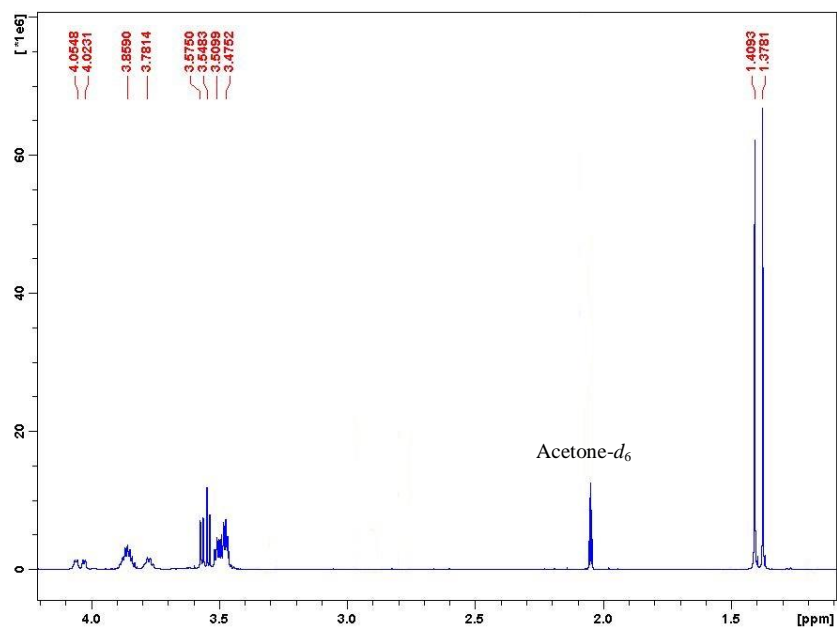


Figure A.3.1  $^1\text{H}$  NMR of 1,3-bis(2,3-dihydroxypropyl)-5,5-dimethylhydantoin in acetone- $d_6$

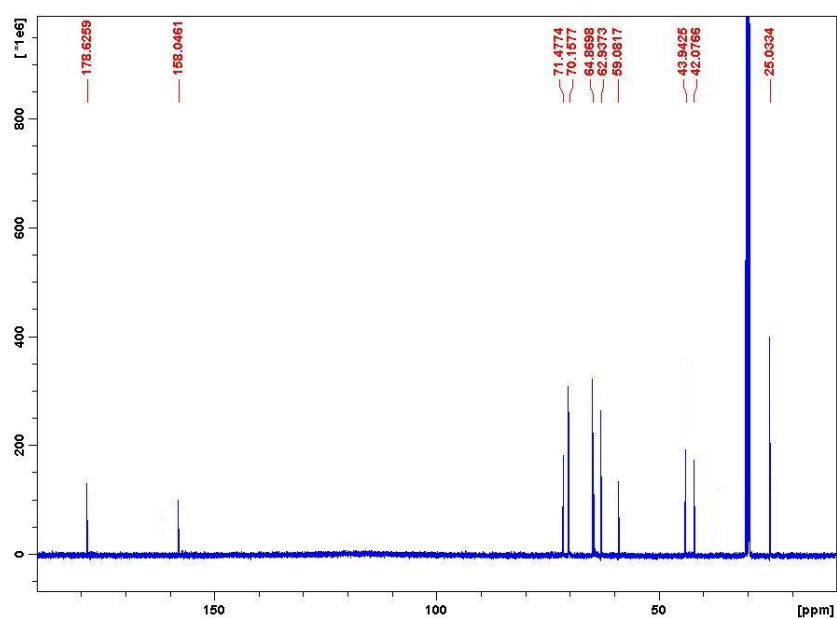


Figure A.3.2  $^{13}\text{C}$  NMR of 1,3-bis(2,3-dihydroxypropyl)-5,5-dimethylhydantoin in acetone- $d_6$

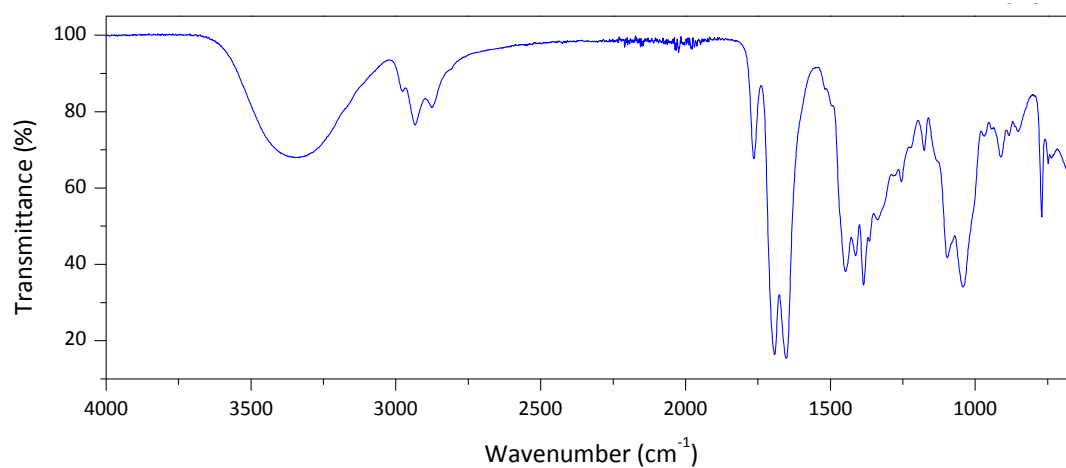


Figure A.3.3 FTIR spectrum of 1,3-bis(2,3-dihydroxypropyl)-5,5-dimethylhydantoin.

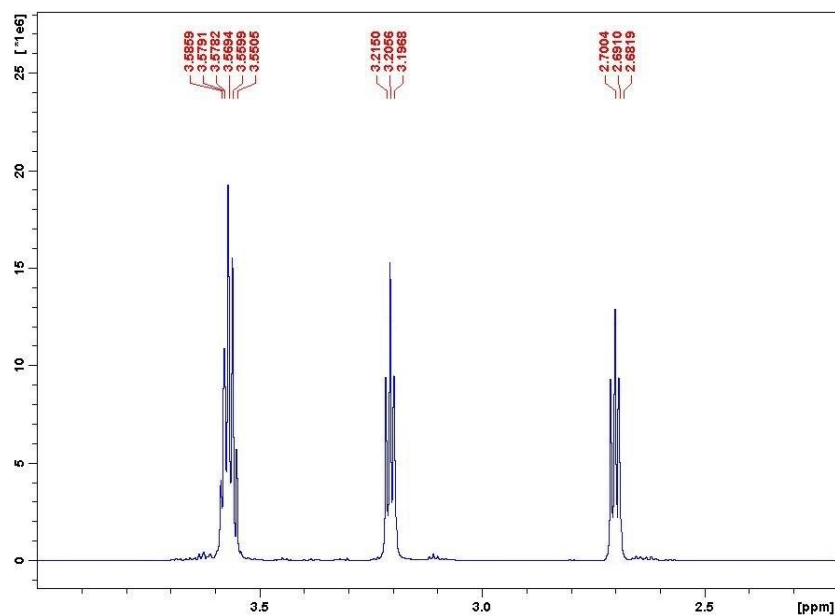


Figure A.4.1  $^1\text{H}$  NMR of 1,3-bis(2-hydroxyethyl)urea in deuterium oxide.

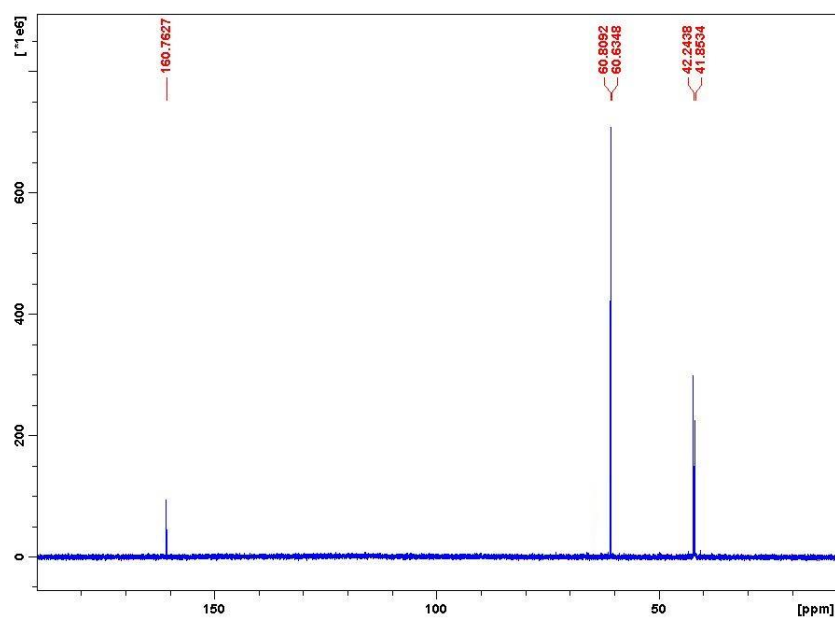


Figure A.4.2  $^{13}\text{C}$  NMR of 1,3-bis(2-hydroxyethyl)urea in deuterium oxide.

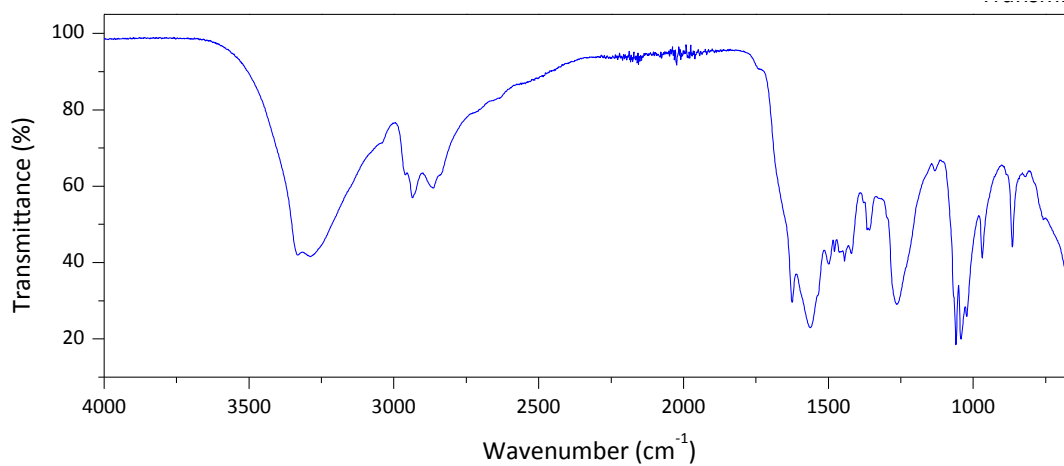


Figure A.4.3 FTIR spectrum of 1,3-bis(2-hydroxyethyl)urea.

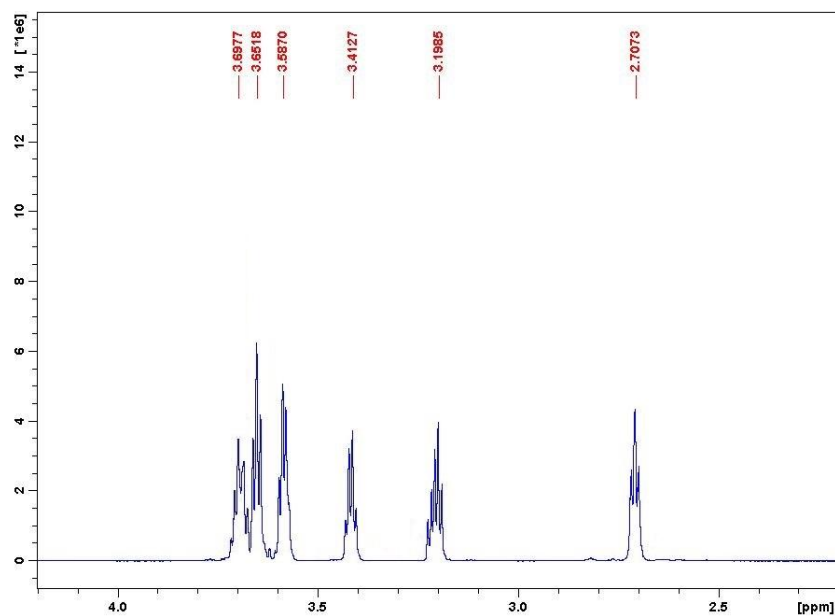


Figure A.5.1  $^1\text{H}$  NMR of 1,1,3-*tris*(2-hydroxyethyl)urea in deuterium oxide.

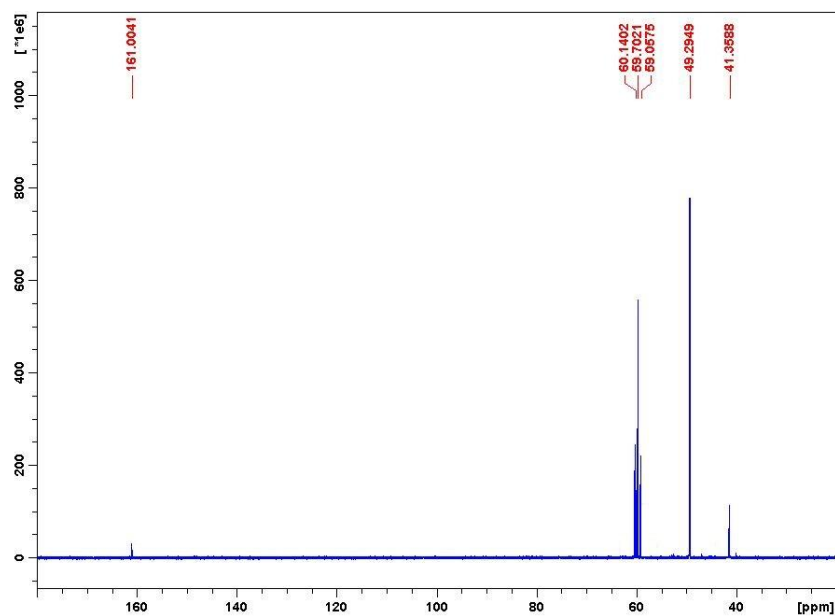


Figure A.5.2  $^{13}\text{C}$  NMR of 1,1,3-*tris*(2-hydroxyethyl)urea in deuterium oxide.

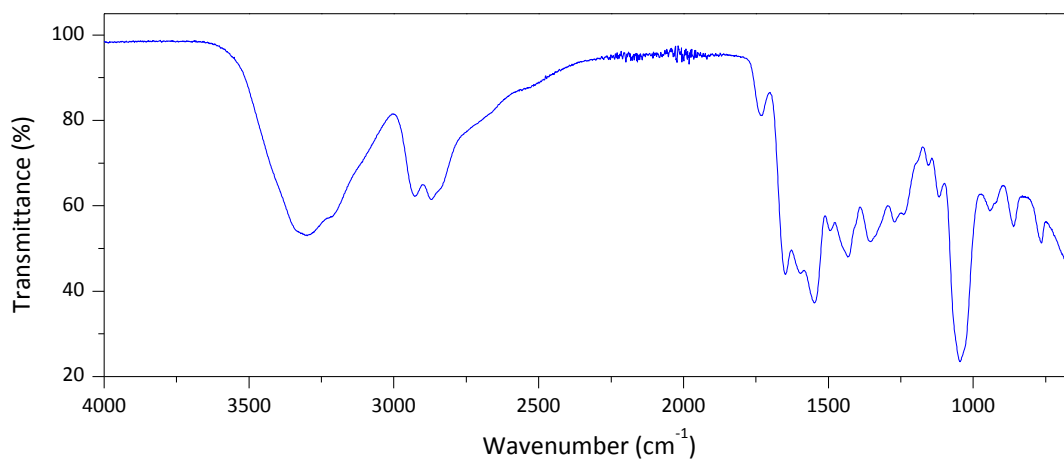


Figure A.5.3 FTIR spectrum of 1,1,3-*tris*(2-hydroxyethyl)urea.

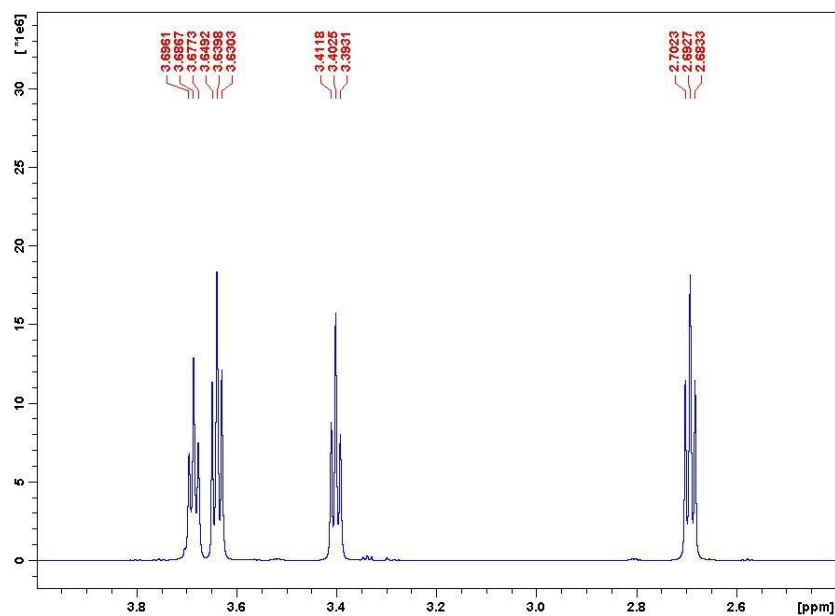


Figure A.6.1  $^1\text{H}$  NMR of 1,1,3,3-tetrakis(2-hydroxyethyl)urea in deuterium oxide.

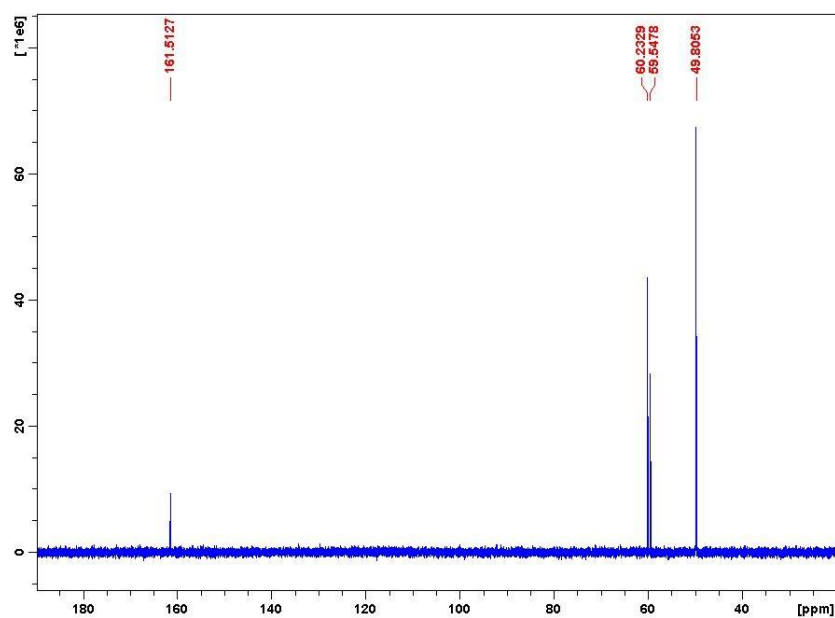


Figure A.6.2  $^{13}\text{C}$  NMR of 1,1,3,3-tetrakis(2-hydroxyethyl)urea in deuterium oxide.

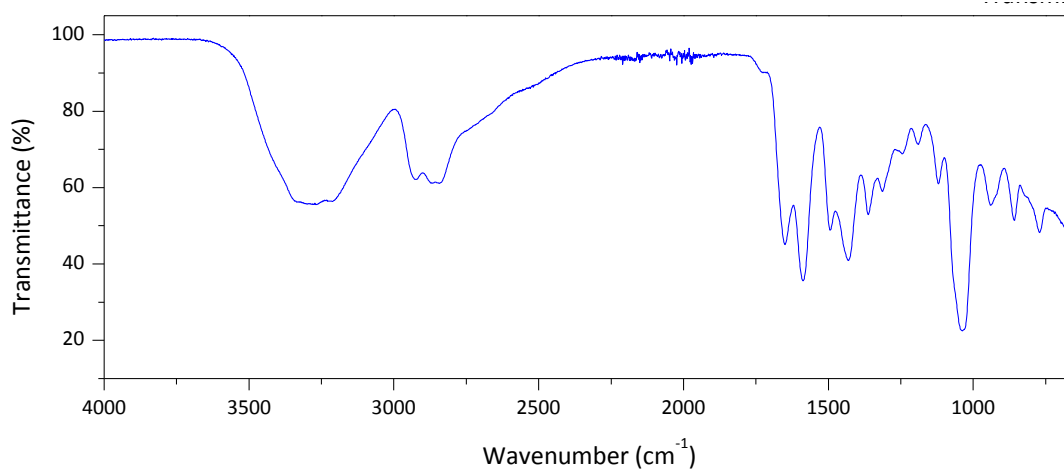


Figure A.6.3 FTIR spectrum of 1,1,3,3-tetrakis(2-hydroxyethyl)urea.

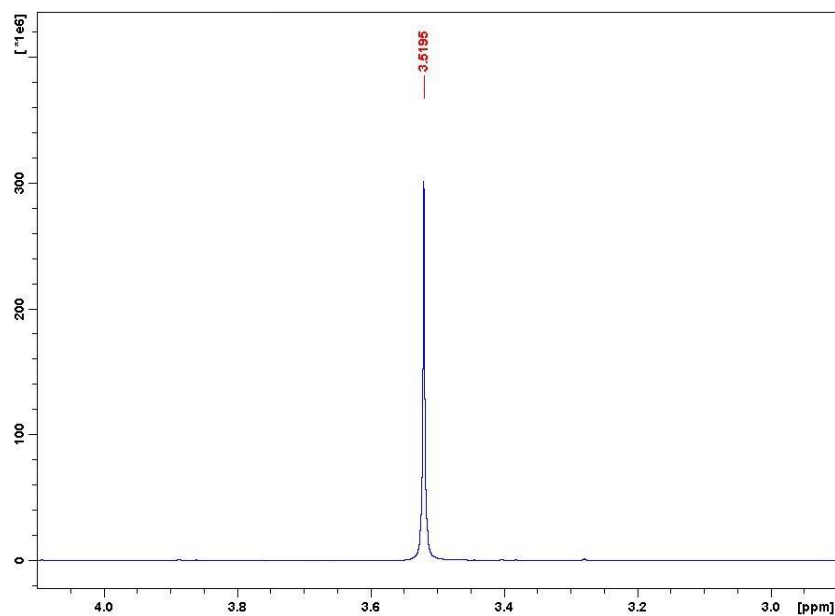


Figure A.7.1  $^1\text{H}$  NMR of 1,3-bis[3-hydroxy-1,1-bis(2-hydroxyethyl)propyl]urea in  $\text{D}_2\text{O}$ .

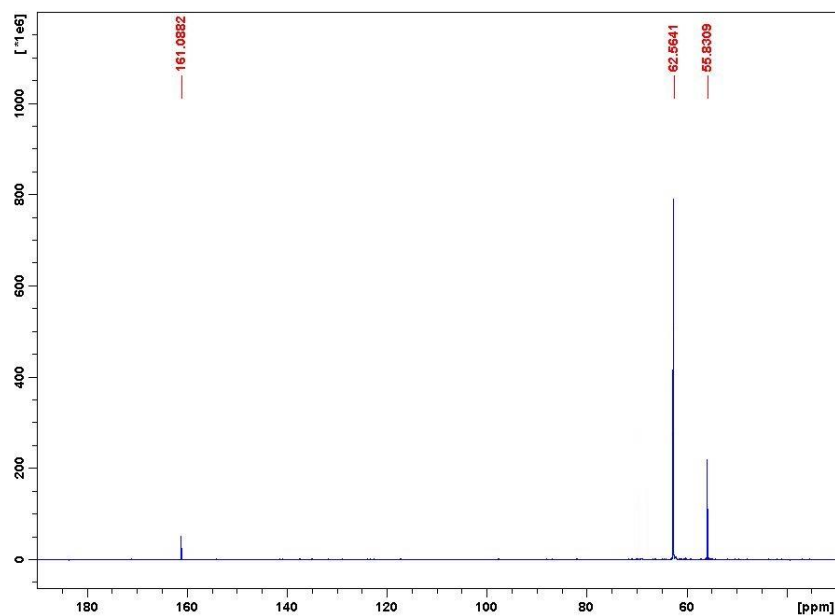


Figure A.7.2  $^{13}\text{C}$  NMR of 1,3-bis[3-hydroxy-1,1-bis(2-hydroxyethyl)propyl]urea in  $\text{D}_2\text{O}$ .

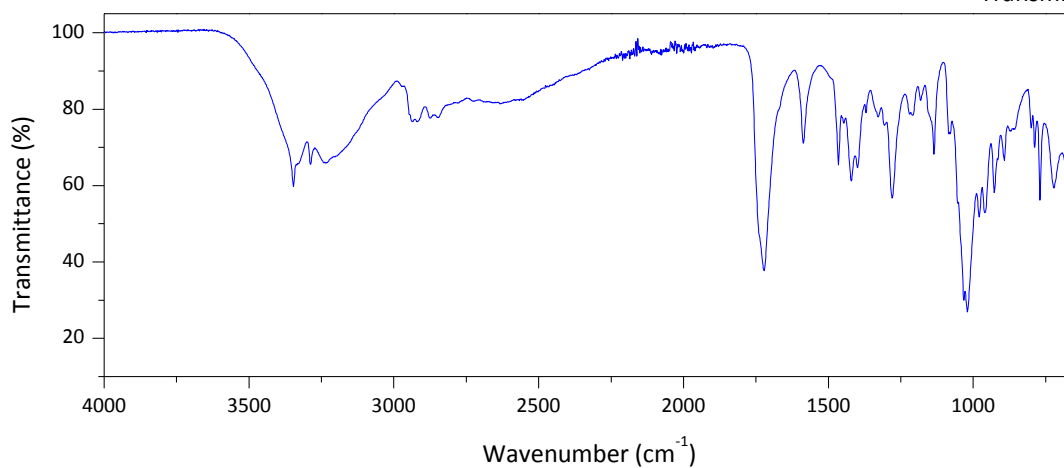


Figure A.7.3 FTIR spectrum of 1,3-bis[3-hydroxy-1,1-bis(2-hydroxyethyl)propyl]urea.

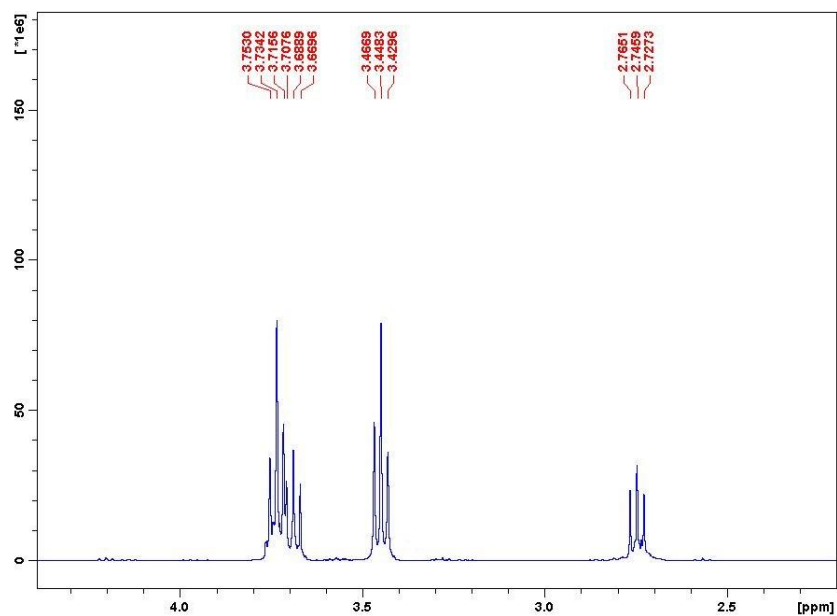


Figure A.8.1  $^1\text{H}$  NMR of polycarbamate dendrimer in deuterium oxide.

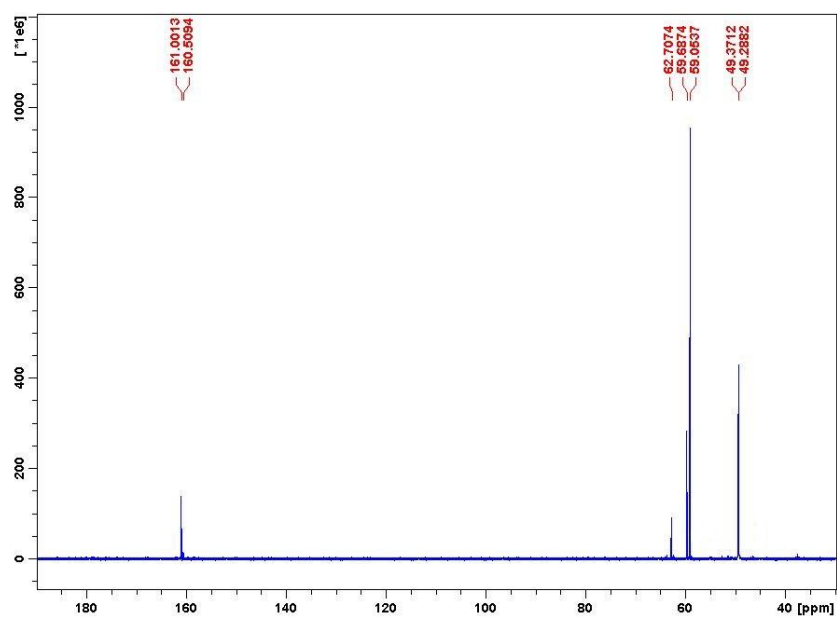


Figure A.8.2  $^{13}\text{C}$  NMR of polycarbamate dendrimer in deuterium oxide.

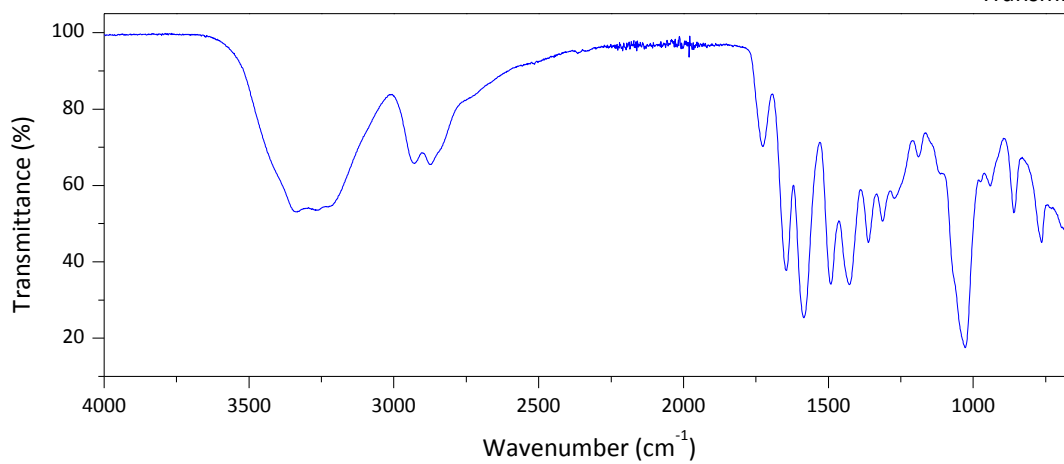


Figure A.8.3 FTIR spectrum of polycarbamate dendrimer.

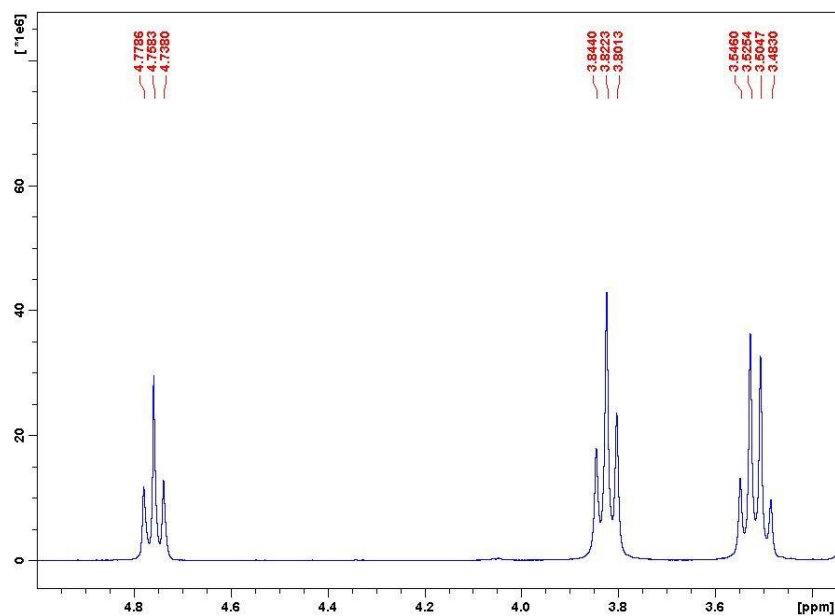


Figure A.9.1  $^1\text{H}$  NMR of 1,3,5-tris(2-hydroxyethyl)isocyanurate in dimethyl sulfoxide- $d_6$ .

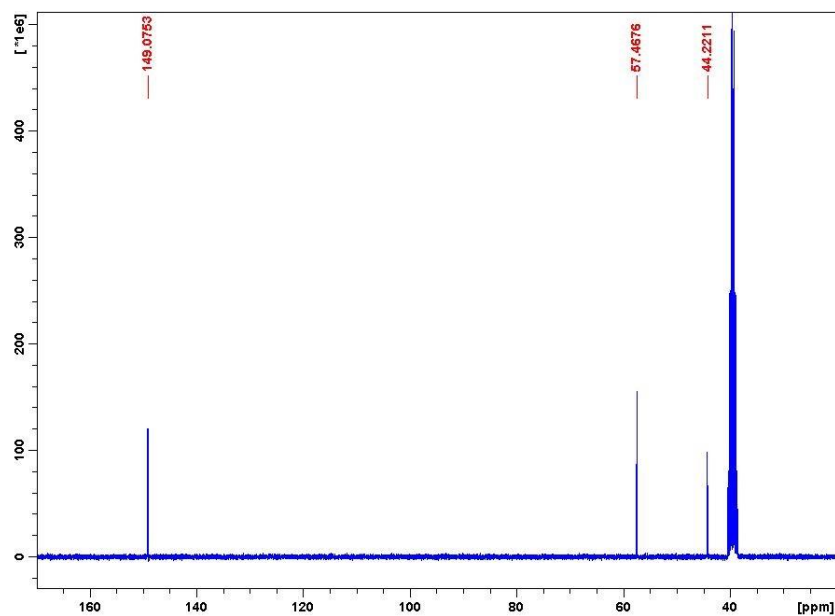


Figure A.9.2  $^{13}\text{C}$  NMR of 1,3,5-tris(2-hydroxyethyl)isocyanurate in dimethyl sulfoxide- $d_6$ .

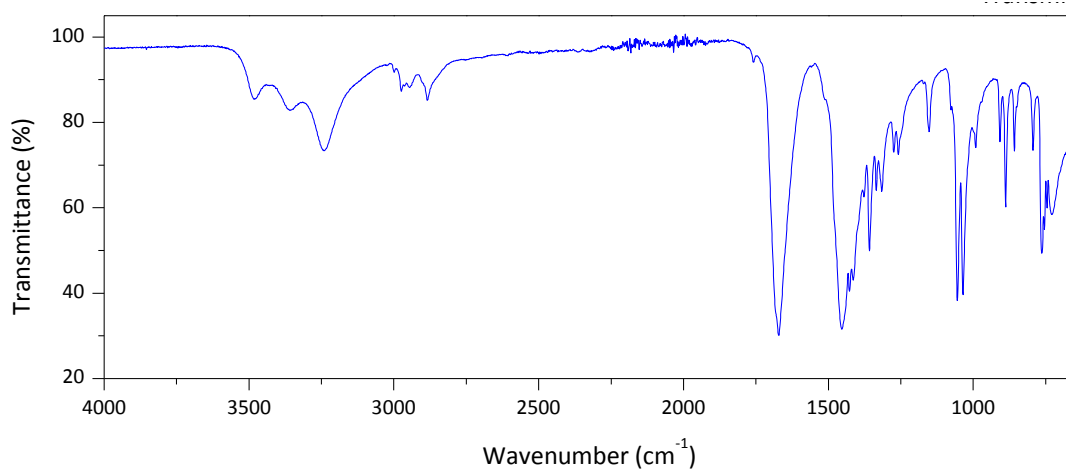


Figure A.9.3 FTIR spectrum of 1,3,5-tris(2-hydroxyethyl)isocyanurate.



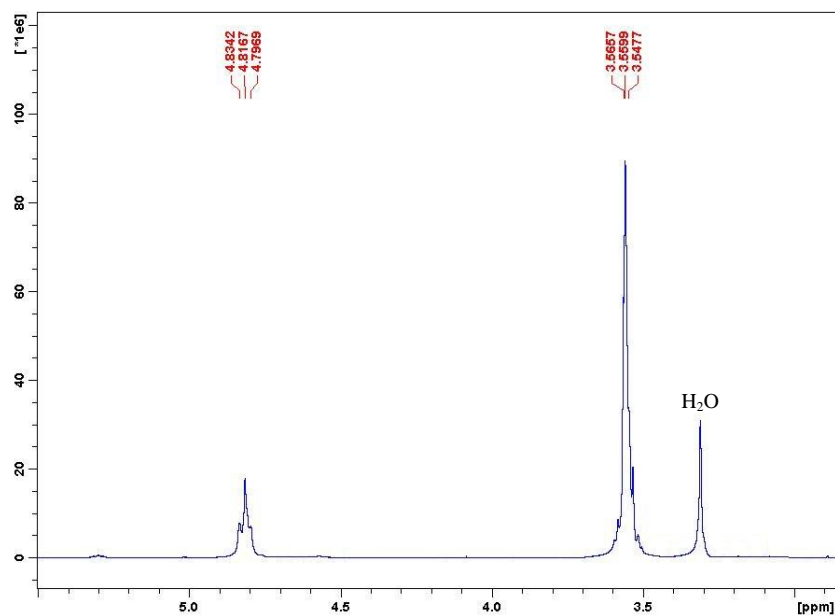


Figure A.10.1  $^1\text{H}$  NMR of 1,3-bis(2-hydroxyethyl)parabonate in dimethyl sulfoxide- $d_6$ .

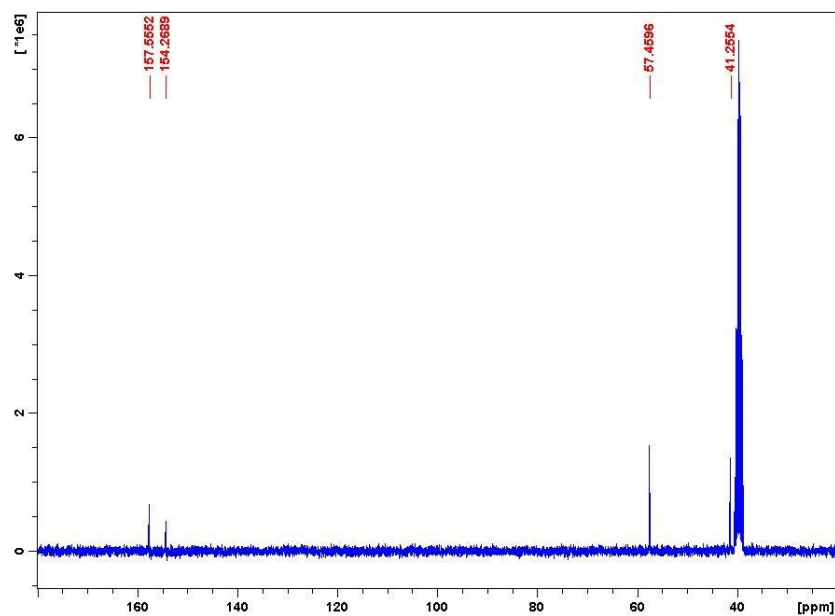


Figure A.10.2  $^{13}\text{C}$  NMR of 1,3-bis(2-hydroxyethyl)parabonate in dimethyl sulfoxide- $d_6$ .

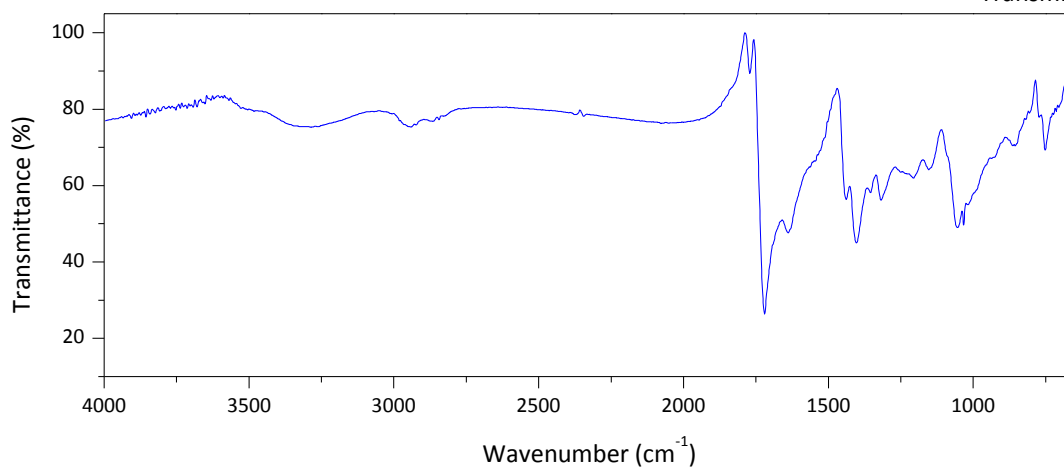


Figure A.10.3 FTIR spectrum of 1,3-bis(2-hydroxyethyl)parabonate.

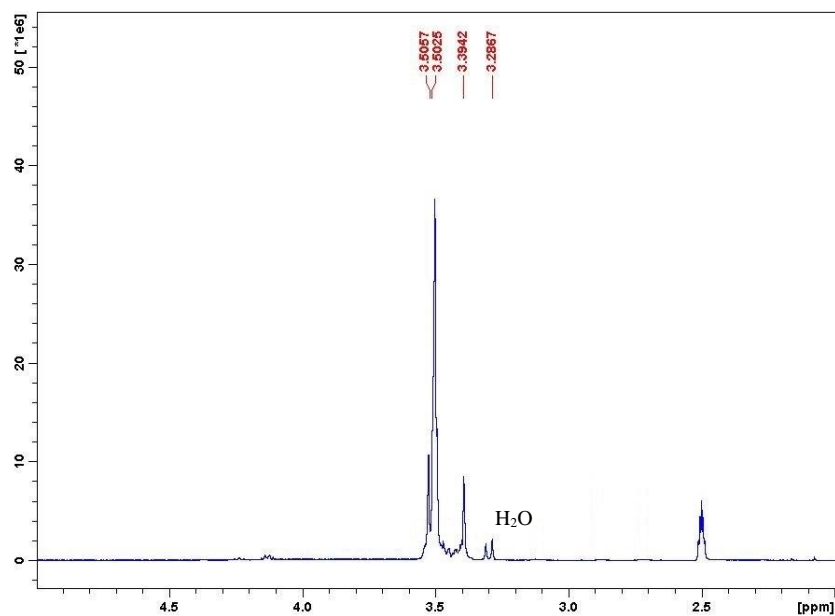


Figure A.11.1  $^1\text{H}$  NMR of 1,2,4-*tris*(hydroxyethyl)urazole in dimethyl sulfoxide- $d_6$ .

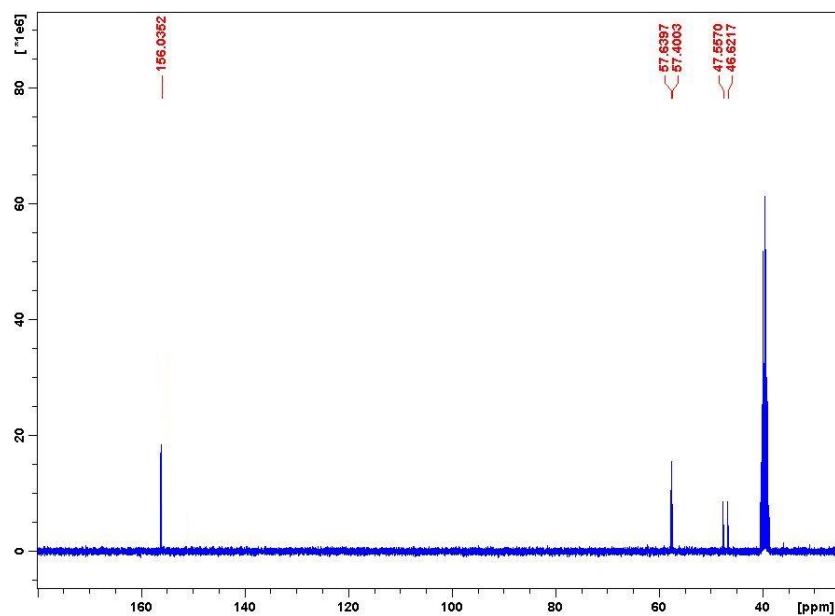


Figure A.11.2  $^{13}\text{C}$  NMR of 1,2,4-*tris*(hydroxyethyl)urazole in dimethyl sulfoxide- $d_6$ .

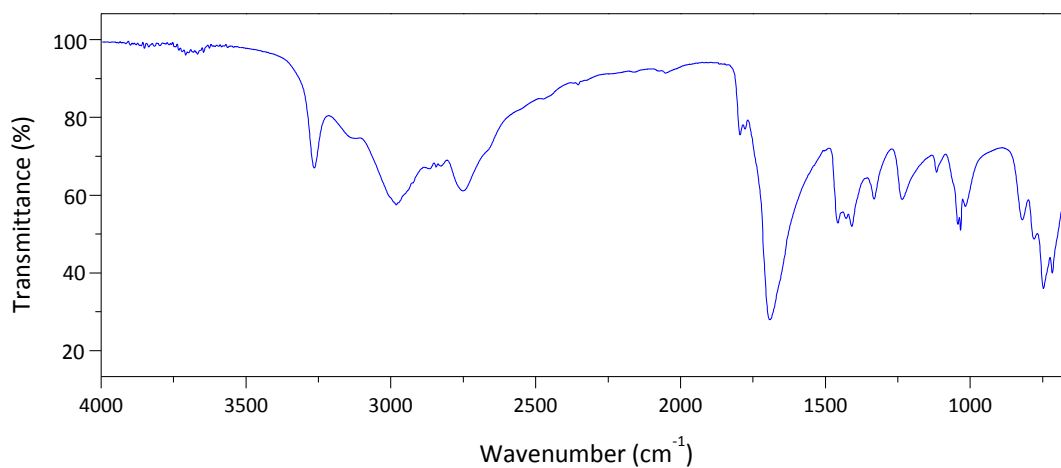


Figure A.11.3 FTIR spectrum of 1,2,4-*tris*(hydroxyethyl)urazole.

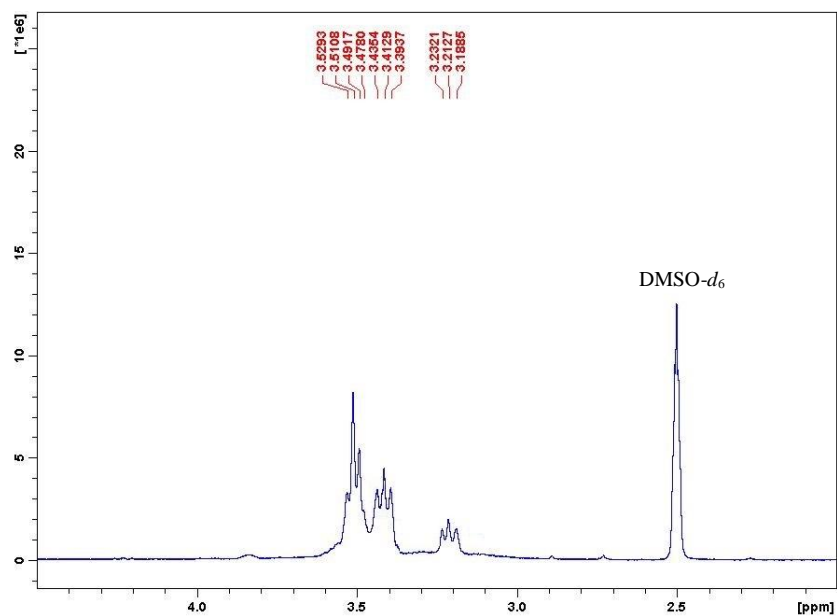


Figure A.12.1  $^1\text{H}$  NMR of 1,3,4,6-*tetra*(2-hydroxyethyl)glycoluril in dimethyl sulfoxide- $d_6$ .

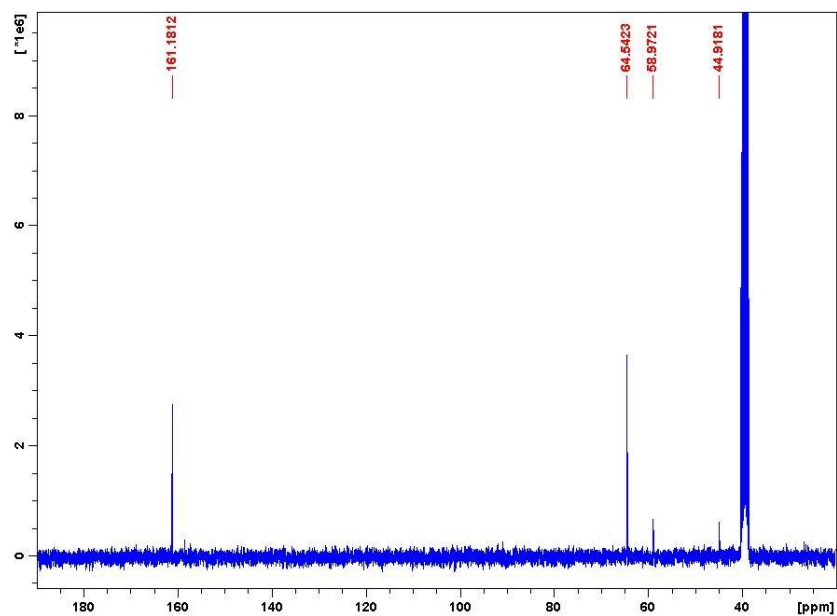


Figure A.12.2  $^{13}\text{C}$  NMR of 1,3,4,6-*tetra*(2-hydroxyethyl)glycoluril in dimethyl sulfoxide- $d_6$ .

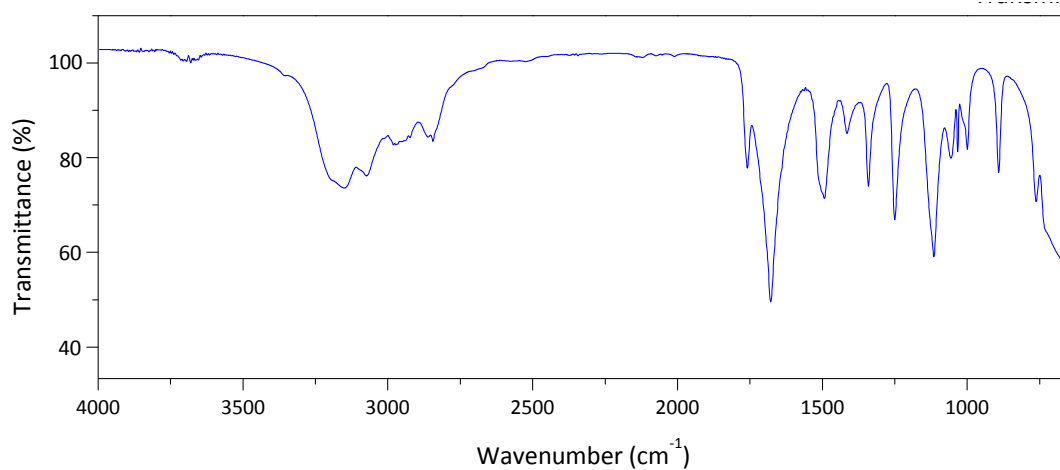


Figure A.12.3 FTIR spectrum of 1,3,4,6-*tetra*(2-hydroxyethyl)glycoluril.

**Abbreviations**

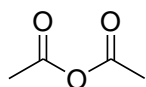
$\delta$	Chemical shift
$\beta$	Heating rate
$\xi$	Molar ratio
$\eta$	Complex viscosity
AO 2246	2, 2'-Methylene- <i>bis</i> [6- <i>t</i> -butyl-4-methyl phenol]
AFM	Atomic force microscope
AN	Ammonium nitrate
AP	Ammonium perchlorate
ATR	Attenuated total reflectance
BI	Bonding index
BIDE	Butyliminodiethanol
BITA	1,1',1''-(1,3,5-Benzenetriyltricarbonyl) <i>tris</i> (2-ethylaziridine)
BHPU	1,3- <i>Bis</i> [3-hydroxy-1,1- <i>bis</i> (2-hydroxyethyl)propyl]urea
BHU	1,3- <i>Bis</i> (2-hydroxyethyl)urea
BTMF	1,1'- <i>Bis</i> (trimethylsiloxymethyl) ferrocene
CEEM	Centre of expertise in energetic materials
CDCl <sub>3</sub>	Chloroform- <i>d</i>
d	Density
DAFS	1,1-Diacetylferrocene disemicarbazone
DAFT	1,1'-Ferrocenediyl-diethylidene <i>bis</i> (thiocarbonohydrazide)
Dantocol	1,3- <i>Bis</i> (2-hydroxyethyl)-5,5-dimethylhydantoin
DBTDL	Dibutyltin bismuth
DHP	1,3- <i>Bis</i> (2,3-dihydroxypropyl)-5,5-dimethylhydantoin
DITBA	Difunctional isocyanate terminated bonding agent
DMF	Dimethylformamide
DOA	Dioctyl adipate
DRIFT	Diffuse reflectance infrared fourier transform

DSC	Differential scanning calorimetry
DSTO	Defence science and technology organisation
$\Delta E$	Enthalpy change
$E_a$	Activation energy
EDX	Energy dispersive x-ray
ESD	Electrostatic discharge
FDBAH	1,1-Diacetylferrocenebenzoyl hydrazone
FDNBAH	1,1-Diacetylferrocene- <i>p</i> -nitrobenzoyl hydrazone
F of I	Figure of insensitiveness
FOX-12	<i>N</i> -guanylurea-dinitramide
FSD	Fourier self-deconvolution
FTIR	Fourier transform infrared spectroscopy
GPC	Gel permeation chromatography
$\Delta H_{\text{fus}}$	Heat of fusion
HDI	Hexamethylene diisocyanate
HEG	1,3,4,6- <i>Tetra</i> (2-hydroxyethyl)glycoluril
HEP	1,3- <i>Bis</i> (2-hydroxyethyl)parabanate
HEU	1,2,4- <i>Tris</i> (2-hydroxyethyl)urazole
HMDI	<i>Bis</i> (4-isocyanatocyclohexyl)methane
HMX	Cyclotetramethylene tetranitramine
$\Delta H_s$	Heat of sublimation
HTCE	Hydroxy-terminated (poly)caprolactone ether
HTPB	Hydroxyl-terminated polybutadiene
HTPE	Hydroxy-terminated polyether
HX-752	1,1'-(1,3-Phenylenedicarbonyl) <i>bis</i> -2-methyl-aziridine
IDP	Isodecyl pelargonate
IM	Insensitive munitions
IPDI	Isophorone diisocyanate
JANNAF	Joint Army Navy NASA Air Force

LNCA	Liquid nitrogen cooling accessory
IR	Infrared
LVR	Linear viscoelastic region
m	Mass
M	Molar mass
MAPO	<i>Tris</i> -1-(2-methyl aziridiny) phosphine oxide
MDI	Diphenylmethan-4,4'-diisocyanate
MT4	2.0 moles of <i>tris</i> -1(2 methylaziridiny)phosphine oxide, 0.7 mole adipic acid, and 0.3 mole tartaric acid
N 100	Poly(hexamethylene diisocyanate)
NMR	Nuclear magnetic resonance
NPBA	Neutral polymeric bonding agent
NTO	3-Nitro-1,2,4-triazol-5-one
P	Pressure
PAS	Photo-acoustic spectroscopy
PAMAM	Polyamidoamine
PBX	Polymer bonded explosive
PCD	Polycarbamate dendrimer gen 2
P <sub>d</sub>	Polydispersity
PDSC	Pressure differential scanning calorimetry
RDX	Cyclotrimethylene trinitramine
SEM	Scanning electron microscope
STD	Standard deviation
TATB	Triaminotrinitro-benzene
T <sub>b</sub>	Critical temperature
TBS	<i>Tert</i> -Butyldimethylsilyl
TBSDHE	<i>N</i> -(2-hydroxyethyl)- <i>N</i> -(2- <i>tert</i> -butyldimethylsilyloxy-ethyl)-5,5-dimethylhydantoin
TDI	Toluene diisocyanate
TEM	Transmission electron microscope

Tepan	Cyanoacrylated tetraethylenepentamine
Tepanol	Tetraethylenepentaamine acrylonitrile glycidol adduct
Tetraacid	<i>Tetrakis</i> (5-carboxy-2-oxabutyl)methane
Tetranitrile	<i>Tetrakis</i> (5-cyano-2-oxa-butyl)methane
Tetraol	<i>Tetrakis</i> (5-hydroxy-2-oxapentyl)methane
TFDD	<i>P</i> -toluenesulfonic acid 1,1'-ferrocenediylldiethylidene dihydrazide
T <sub>g</sub>	Glass transition temperature
TGA	Thermal gravimetric analysis
THEIC	1,3,5- <i>Tris</i> (2-hydroxyethyl)isocyanurate
THU	1,1,3,3- <i>Tetrakis</i> (2-hydroxyethyl)urea
T <sub>i</sub>	Decomposition onset temperature
TITBA	Trifunctional isocyanate terminated bonding agent
T <sub>m</sub>	Melting point
T <sub>max</sub>	Maximum weight loss temperature
TMP	Trimethylolpropane
TMS	Trimethylsilyl
TMSDHE	1,3- <i>Bis</i> (2-trimethylsilyloxyethyl)-5,5-dimethylhydantoin
TMXDI	Meta-tetramethylxylene diisocyanate
T of I	Temperature of ignition
T <sub>p</sub>	Peak decomposition Temperature
TPB	Triphenyl bismuth
T <sub>s</sub>	Temperature of sublimation
<i>U</i>	Potential
<i>v</i>	Vibrational band
<i>V</i>	Volume
V <sub>R</sub>	Volume of gas produced due to reaction between two components
VoD	Velocity of detonation
VTS	Vacuum thermal stability
XPS	X-ray photoelectron spectroscopy

## Laboratory Reagents



Acetic Anhydride (ACS reagent,  $\geq 98.0\%$ )

Supplier: Sigma-Aldrich Chemical Company

Molecular Formula:  $(\text{CH}_3\text{CO})_2\text{O}$

Molecular Weight:  $102.09\text{g mol}^{-1}$

Boiling Point:  $139.8^\circ\text{C}$



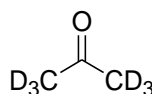
Acetone (ACS reagent,  $99.5\%$ )

Supplier: Sigma-Aldrich Chemical Company

Molecular Formula:  $\text{CH}_3\text{COCH}_3$

Molecular Weight:  $58.08\text{g mol}^{-1}$

Boiling Point:  $56^\circ\text{C}$



Acetone- $d_6$  ("100%",  $99.96$  atom % D)

Supplier: Cambridge Isotope Laboratories, Inc

Molecular Formula:  $\text{CD}_3\text{COCD}_3$

Molecular Weight:  $58.08\text{g mol}^{-1}$

Boiling Point:  $56^\circ\text{C}$



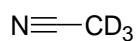
Acetonitrile (ACS reagent,  $99.5\%$ )

Supplier: Sigma-Aldrich Chemical Company

Molecular Formula:  $\text{CH}_3\text{CN}$

Molecular Weight:  $41.05\text{g mol}^{-1}$

Boiling Point:  $81^\circ\text{C}$



Acetonitrile- $d_3$  ("100%",  $99.96$  atom % D)

Supplier: Cambridge Isotope Laboratories, Inc

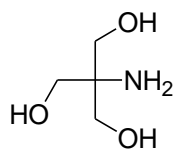
Molecular Formula:  $\text{CD}_3\text{CN}$

Molecular Weight:  $41.05\text{g mol}^{-1}$

Boiling Point:  $81^\circ\text{C}$



2-Amino-2-hydroxymethyl-propane-1,3-diol (puriss. p.a.,  $\geq 99.7\%$ )



Supplier: Sigma-Aldrich Chemical Company

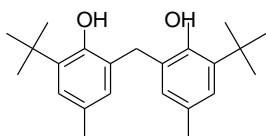
Molecular Formula:  $\text{NH}_2\text{C}(\text{CH}_2\text{OH})_3$

Molecular Weight:  $121.14\text{g mol}^{-1}$

Boiling Point:  $219^\circ\text{C}$

Antioxidant-2246 (Lowinox)

Supplier: Sigma-Aldrich Chemical Company



Molecular Formula:  $\text{CH}_2[\text{C}_6\text{H}_2[\text{C}(\text{CH}_3)_3](\text{CH}_3)\text{OH}]_2$

Molecular Weight:  $340.50\text{g mol}^{-1}$

Melting Point:  $123\text{-}127^\circ\text{C}$

Aluminium (Grade 75S)

Supplier: Ecka Granules Australia PTY Ltd

Al

Molecular Formula: Al

Molecular Weight:  $26.98\text{ mol}^{-1}$

Melting Point:  $660.32^\circ\text{C}$

Benzene (ACS reagent, 99.0%)



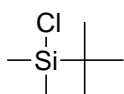
Supplier: Sigma-Aldrich Chemical Company

Molecular Formula:  $\text{C}_6\text{H}_6$

Molecular Weight:  $78.11\text{g mol}^{-1}$

Boiling Point:  $80^\circ\text{C}$

*tert*-Butyldimethylsilyl chloride (reagent grade, 97%)

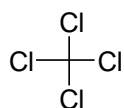


Supplier: Sigma-Aldrich Chemical Company

Molecular Formula:  $(\text{CH}_3)_3\text{CSi}(\text{CH}_3)_2\text{Cl}$

Molecular Weight:  $150.72\text{g mol}^{-1}$

Boiling Point:  $125^\circ\text{C}$



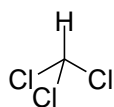
Carbon tetrachloride (Reagent grade, 99.9%)

Supplier: Sigma-Aldrich Chemical Company

Molecular Formula: CCl<sub>4</sub>

Molecular Weight: 153.82g mol<sup>-1</sup>

Boiling Point: 76.72°C



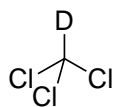
Chloroform (ACS reagent, 99.8%)

Supplier: Sigma-Aldrich Chemical Company

Molecular Formula: CHCl<sub>3</sub>

Molecular Weight: 119.38g mol<sup>-1</sup>

Boiling Point: 61.2°C



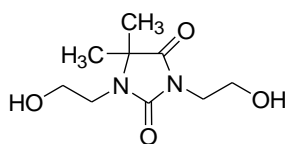
Chloroform-*d* ("100%", 99.96 atom % D, contains 0.5% silver foil)

Supplier: Cambridge Isotope Laboratories, Inc

Molecular Formula: CDCl<sub>3</sub>

Molecular Weight: 120.38g mol<sup>-1</sup>

Boiling Point: 60.9°C



Dantocol (Lonza)

Supplier: Interchem PTY Ltd

Molecular Formula: C<sub>9</sub>H<sub>16</sub>O<sub>4</sub>N<sub>2</sub>

Molecular Weight: 216.25g mol<sup>-1</sup>

Melting Point: 62-65°C



Deuterium oxide ("100%", 99.96 atom % D)

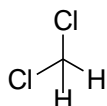
Supplier: Cambridge Isotope Laboratories, Inc

Molecular Formula: D<sub>2</sub>O

Molecular Weight: 20.03g mol<sup>-1</sup>

Boiling Point: 101.4°C

Dichloromethane (anhydrous,  $\geq 99.8\%$ , 50-150ppm amylene)



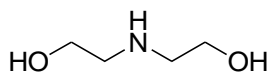
Supplier: Sigma-Aldrich Chemical Company

Molecular Formula:  $\text{CH}_2\text{Cl}_2$

Molecular Weight:  $84.93\text{g mol}^{-1}$

Boiling Point:  $39.8^\circ\text{C}$

Diethanolamine (ACS reagent,  $\geq 98.5\%$ )



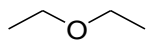
Supplier: Sigma-Aldrich Chemical Company

Molecular Formula:  $\text{HN}(\text{CH}_2\text{CH}_2\text{OH})_2$

Molecular Weight:  $105.14\text{g mol}^{-1}$

Boiling Point:  $280^\circ\text{C}$

Diethyl ether (ACS reagent, anhydrous,  $\geq 99.0\%$ , BHT as inhibitor)



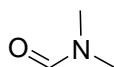
Supplier: Sigma-Aldrich Chemical Company

Molecular Formula:  $(\text{CH}_3\text{CH}_2)_2\text{O}$

Molecular Weight:  $74.12\text{g mol}^{-1}$

Boiling Point:  $34.6^\circ\text{C}$

Dimethylformamide (anhydrous, 99.8%)



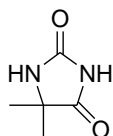
Supplier: Sigma-Aldrich Chemical Company

Molecular Formula:  $\text{HCON}(\text{CH}_3)_2$

Molecular Weight:  $73.09\text{g mol}^{-1}$

Melting Point:  $153^\circ\text{C}$

5,5-Dimethylhydantoin (97%)



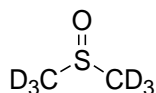
Supplier: Sigma-Aldrich Chemical Company

Molecular Formula:  $\text{C}_5\text{H}_8\text{N}_2\text{O}_2$

Molecular Weight:  $128.13\text{g mol}^{-1}$

Melting Point:  $174-177^\circ\text{C}$

Dimethyl sulfoxide-*d*<sub>6</sub> ("100%", 99.96 atom % D)



Supplier: Cambridge Isotope Laboratories, Inc

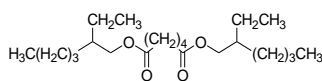
Molecular Formula: (CD<sub>3</sub>)<sub>2</sub>SO

Molecular Weight: 84.17g mol<sup>-1</sup>

Boiling Point: 189°C

Dioctyl adipate

Supplier: Corflex

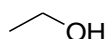


Molecular Formula: CH<sub>3</sub>(CH<sub>2</sub>)<sub>7</sub>OCO(CH<sub>2</sub>)<sub>4</sub>COO(CH<sub>2</sub>)<sub>7</sub>CH<sub>3</sub>

Molecular Weight: 370.57g mol<sup>-1</sup>

Boiling Point: 404.84°C

Ethanol (200 proof, ACS reagent, ≥99.5%)



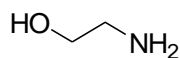
Supplier: Sigma-Aldrich Chemical Company

Molecular Formula: CH<sub>3</sub>CH<sub>2</sub>OH

Molecular Weight: 46.07g mol<sup>-1</sup>

Boiling Point: 78.3°C

Ethanolamine (ACS reagent, ≥99.0%)



Supplier: Sigma-Aldrich Chemical Company

Molecular Formula: NH<sub>2</sub>CH<sub>2</sub>CH<sub>2</sub>OH

Molecular Weight: 61.08g mol<sup>-1</sup>

Boiling Point: 170°C

Ethylene oxide (≥99.5%)



Supplier: Sigma-Aldrich Chemical Company

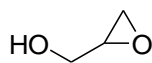
Molecular Formula: C<sub>2</sub>H<sub>4</sub>O

Molecular Weight: 44.05g mol<sup>-1</sup>

Boiling Point: 10.7°C

Glycidol (96%)

Supplier: Sigma-Aldrich Chemical Company



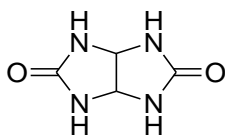
Molecular Formula: C<sub>3</sub>H<sub>6</sub>O<sub>2</sub>

Molecular Weight: 74.08g mol<sup>-1</sup>

Boiling Point: 61-62 °C (15mmHg)

Glycoluril (97%)

Supplier: Sigma-Aldrich Chemical Company



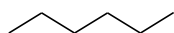
Molecular Formula: C<sub>4</sub>H<sub>6</sub>N<sub>4</sub>O<sub>2</sub>

Molecular Weight: 142.12g mol<sup>-1</sup>

Melting Point: 144-146°C

Hexane (Laboratory Reagent, ≥95%)

Supplier: Sigma-Aldrich Chemical Company



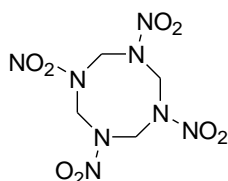
Molecular Formula: CH<sub>3</sub>(CH<sub>2</sub>)<sub>4</sub>CH<sub>3</sub>

Molecular Weight: 86.18g mol<sup>-1</sup>

Boiling Point: 69°C

HMX (Type I, Class 1 and 5)

Supplier: ADI Ltd



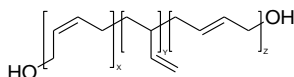
Molecular Formula: C<sub>4</sub>H<sub>8</sub>N<sub>8</sub>O<sub>8</sub>

Molecular Weight: 296.155g mol<sup>-1</sup>

Boiling Point: 276°C

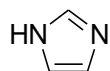
Hydroxyl-terminated polybutadiene (R45-HTLO)

Supplier: Sartomer



Molecular Formula: OH(CH<sub>2</sub>CHCHCH<sub>2</sub>)<sub>n</sub>OH

Molecular Weight: 1149.83g mol<sup>-1</sup>



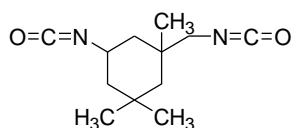
Imidazole (ACS reagent,  $\geq 99\%$ )

Supplier: Sigma-Aldrich Chemical Company

Molecular Formula:  $C_3H_4N_2$

Molecular Weight:  $68.08\text{g mol}^{-1}$

Boiling Point:  $256^\circ\text{C}$



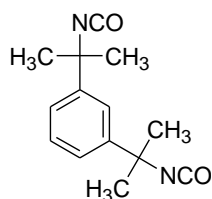
Isophorone diisocyanate (98%)

Supplier: Sigma-Aldrich Chemical Company

Molecular Formula:  $\text{OCNC}_6\text{H}_7(\text{CH}_3)_3\text{CH}_2\text{NCO}$

Molecular Weight:  $222.28\text{g mol}^{-1}$

Boiling Point:  $158^\circ\text{C}$



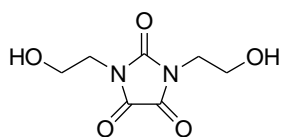
meta-Tetramethylxylylene diisocyanate (97%)

Supplier: Sigma-Aldrich Chemical Company

Molecular Formula:  $C_6H_4[\text{C}(\text{CH}_3)_2\text{NCO}]_2$

Molecular Weight:  $244.29\text{g mol}^{-1}$

Boiling Point:  $106^\circ\text{C}$  (0.9mmHg)



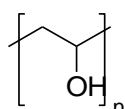
Parabanic acid (99%)

Supplier: Sigma-Aldrich Chemical Company

Molecular Formula:  $C_3H_2N_2O_3$

Molecular Weight:  $114.06\text{g mol}^{-1}$

Melting Point:  $249^\circ\text{C}$



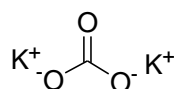
Polyvinyl Alcohol (LR)

Supplier: Chem-Supply

Molecular Formula:  $(\text{CH}_2\text{CHOH})_n$

Average Molecular Weight:  $100,000\text{g mol}^{-1}$

Potassium Bromide (FT-IR grade,  $\geq 99\%$  trace metals basis)  
Supplier: Sigma-Aldrich Chemical Company  
 $K^+Br^-$  Molecular Formula: KBr  
Molecular Weight:  $119.00\text{g mol}^{-1}$   
Melting Point:  $734^\circ\text{C}$



Potassium Carbonate (ACS reagent,  $\geq 99.0\%$ )  
Supplier: Sigma-Aldrich Chemical Company  
Molecular Formula:  $K_2CO_3$   
Molecular Weight:  $138.21\text{g mol}^{-1}$   
Melting Point:  $891^\circ\text{C}$

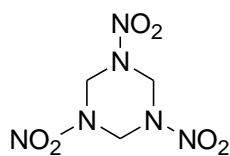
Potassium hydroxide (reagent grade, 90%)  
Supplier: Sigma-Aldrich Chemical Company  
 $K^+OH^-$  Molecular Formula: KOH  
Molecular Weight:  $56.11\text{g mol}^{-1}$   
Melting Point:  $361^\circ\text{C}$



2-Propanol (ACS reagent,  $\geq 99.5\%$ )  
Supplier: Sigma-Aldrich Chemical Company  
Molecular Formula:  $(CH_3)_2CHOH$   
Molecular Weight:  $60.10\text{g mol}^{-1}$   
Boiling Point:  $82^\circ\text{C}$



Pyridine (ACS reagent,  $\geq 99.0\%$ )  
Supplier: Sigma-Aldrich Chemical Company  
Molecular Formula:  $C_5H_5N$   
Molecular Weight:  $79.10\text{g mol}^{-1}$   
Boiling Point:  $115^\circ\text{C}$



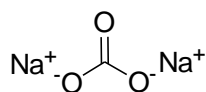
RDX (Type I, Class 1 and 5)

Supplier: ADI Ltd

Molecular Formula:  $C_3H_6N_6O_6$

Molecular Weight:  $222.12\text{g mol}^{-1}$

Boiling Point:  $234^\circ\text{C}$



Sodium carbonate (ACS reagent, anhydrous,  $\geq 99.5\%$ )

Supplier: Sigma-Aldrich Chemical Company

Molecular Formula:  $\text{Na}_2\text{CO}_3$

Molecular Weight:  $105.99\text{g mol}^{-1}$

Melting Point:  $851^\circ\text{C}$



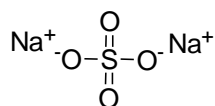
Sodium Chloride (ACS reagent,  $\geq 99.0\%$ )

Supplier: Sigma-Aldrich Chemical Company

Molecular Formula:  $\text{NaCl}$

Molecular Weight:  $58.44\text{g mol}^{-1}$

Melting Point:  $801^\circ\text{C}$



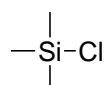
Sodium Sulphate (ACS reagent,  $\geq 99.0\%$ , anhydrous)

Supplier: Sigma-Aldrich Chemical Company

Molecular Formula:  $\text{Na}_2\text{SO}_4$

Molecular Weight:  $142.04\text{g mol}^{-1}$

Melting Point:  $884^\circ\text{C}$



Trimethylsilyl Chloride ( $\geq 97\%$ )

Supplier: Sigma-Aldrich Chemical Company

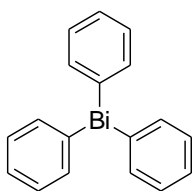
Molecular Formula:  $(\text{CH}_3)_3\text{SiCl}$

Molecular Weight:  $108.64\text{g mol}^{-1}$

Boiling Point:  $57^\circ\text{C}$



Triphenylbismuth (98%, 99.9% trace metals basis)



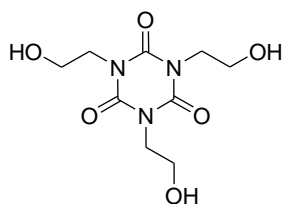
Supplier: Sigma-Aldrich Chemical Company

Molecular Formula:  $\text{Bi}(\text{C}_6\text{H}_5)_3$

Molecular Weight:  $440.29 \text{ g mol}^{-1}$

Melting Point:  $76\text{-}81^\circ\text{C}$

1,3,5-Tris(2-hydroxyethyl)isocyanurate (97%)



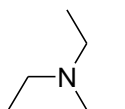
Supplier: Sigma-Aldrich Chemical Company

Molecular Formula:  $\text{C}_9\text{H}_{15}\text{N}_3\text{O}_6$

Molecular Weight:  $261.23 \text{ g mol}^{-1}$

Melting Point:  $136\text{-}140^\circ\text{C}$

Triethylamine ( $\geq 99\%$ )



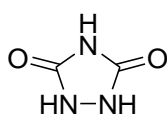
Supplier: Sigma-Aldrich Chemical Company

Molecular Formula:  $(\text{C}_2\text{H}_5)_3\text{N}$

Molecular Weight:  $101.19 \text{ g mol}^{-1}$

Boiling Point:  $88.8^\circ\text{C}$

Urazole (97%)



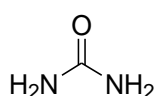
Supplier: Sigma-Aldrich Chemical Company

Molecular Formula:  $\text{C}_2\text{H}_3\text{N}_3\text{O}_2$

Molecular Weight:  $101.06 \text{ g mol}^{-1}$

Melting Point:  $240\text{-}245^\circ\text{C}$

Urea (ACS reagent, 99.0-100%)



Supplier: Sigma-Aldrich Chemical Company

Molecular Formula:  $\text{NH}_2\text{CONH}_2$

Molecular Weight:  $60.06 \text{ g mol}^{-1}$

Melting Point:  $133^\circ\text{C}$

## List of Figures

<b>Figure 1.1.</b> Polyol prepolymers. ....	5
<b>Figure 1.2.</b> Triisocyanate/Diisocyanate curatives. ....	7
<b>Figure 1.3.</b> Nitramine fillers. ....	7
<b>Figure 1.4.</b> Hydantoin bonding agent. ....	10
<b>Figure 1.5.</b> Plasticisers. ....	10
<b>Figure 1.6.</b> Cure catalyst. ....	11
<b>Figure 1.7.</b> Antioxidant. ....	11
<b>Figure 1.8.</b> SEM image outlining (a) dewetting of AP from the binder matrix, and contrasting (b) incorporation of AP within the matrix. ....	16
<b>Figure 1.9.</b> $\beta$ -HMX crystal fracture (f) due to deformation twinning (t). ....	19
<b>Figure 1.10.</b> Mechanism of molecular slippage and reformation. ....	20
<b>Figure 1.11.</b> Tetraethylenepentamine, acrylonitrile and glycidol adduct. ....	24
<b>Figure 1.12.</b> Tetraethylenepentamine and acrylonitrile adduct. ....	24
<b>Figure 1.13.</b> Structures of ferrocene based bonding agents. ....	27
<b>Figure 1.14.</b> Interface cohesive model. ....	33
<b>Figure 2.1.</b> Coating mechanism of particles suspended in an emulsion. ....	55
<b>Figure 2.2.</b> IR spectrum of purified Dantocol. ....	62
<b>Figure 2.3.</b> $^1\text{H}$ NMR of purified Dantocol in chloroform- <i>d</i> . ....	62
<b>Figure 2.4.</b> $^1\text{H}$ NMR of recrystallised RDX in acetonitrile- <i>d</i> <sub>3</sub> . ....	63
<b>Figure 2.5.</b> Slurry coating of RDX in 10% Dantocol. ....	65
<b>Figure 2.6.</b> Slurry coating of RDX in 10% Dantocol, through subtle drying. ....	65
<b>Figure 2.7.</b> Slurry coating of RDX in 10% Dantocol using gyratory mixer. ....	66
<b>Figure 2.8.</b> Slurry coating of RDX in 10% Dantocol using centrifugation. ....	66
<b>Figure 2.9.</b> Reverse slurry coating of RDX in 10% Dantocol. ....	67
<b>Figure 2.10.</b> Reverse slurry coating of RDX in 10% Dantocol, post recrystallisation. ....	68
<b>Figure 2.11.</b> Starved addition coating of RDX in 10% Dantocol. ....	68
<b>Figure 2.12.</b> Starved addition coating of RDX in 10% Dantocol using alternative solvent conditions. ....	69

<b>Figure 2.13.</b> Solvent/antisolvent coating of RDX in 10% Dantocol.....	70
<b>Figure 2.14.</b> Solvent/antisolvent coating of RDX in 10% Dantocol, involving chloroform/tetrahydrofuran.....	70
<b>Figure 2.15.</b> Aqueous suspension/melting coating of RDX in 10% Dantocol.....	71
<b>Figure 2.16.</b> IR spectra of RDX washed in solvent.....	73
<b>Figure 2.17.</b> RDX crystals washed in (a) chloroform and (b) ethanol.....	74
<b>Figure 2.18.</b> RDX washed in (a) carbon tetrachloride and (b) methylene chloride.....	74
<b>Figure 2.19.</b> RDX coated with 10% Dantocol in ethanol, applying mixing times of $T =$ (a) 15mins (b) 30mins (c) 60mins.....	76
<b>Figure 2.20.</b> RDX coated with 10% Dantocol in chloroform, applying mixing times of $T =$ (a) 15mins (b) 30mins (c) 60mins.....	76
<b>Figure 2.21.</b> RDX coated with 10% Dantocol in methylene chloride, applying mixing times of $T =$ (a) 15mins (b) 30mins (c) 60mins.....	76
<b>Figure 2.22.</b> Coating of RDX in 10% Dantocol, involving use of (a) filtration/heat and (b) distillation to remove solvent.....	77
<b>Figure 2.23</b> Coatings of RDX in 10% Dantocol (a) before and (b) after surfactant addition.....	78
<b>Figure 2.24.</b> Microencapsulation of RDX in 10% Dantocol.....	79
<b>Figure 3.1.</b> IR spectra of RDX and dichloromethane washed RDX.....	93
<b>Figure 3.2.</b> IR spectra of RDX and Dantocol 5-25% coated samples.....	94
<b>Figure 3.3.</b> Cumulative offset of asymmetrical $\text{NO}_2$ stretching vibration.....	95
<b>Figure 3.4.</b> Normalised OH peak data of RDX and Dantocol 10-100%.....	96
<b>Figure 3.5.</b> FTIR spectra of RDX and Dantocol 5-25% coated samples.....	98
<b>Figure 3.6.</b> Fourier self-deconvolution of asymmetrical nitro stretching vibration.....	101
<b>Figure 3.7.</b> Peak resolution of $\text{NO}_2$ groups.....	103
<b>Figure 3.8.</b> Relationship between BI and Dantocol coating concentration of RDX.....	106
<b>Figure 3.9.</b> PAS spectra of RDX•DHE 20% conc at increasing mirror velocities.....	107
<b>Figure 3.10.</b> PAS spectra of pure and Dantocol coated RDX ( $vel = 0.9494\text{cm s}^{-1}$ ).....	108
<b>Figure 3.11.</b> DRIFT spectrum of pure RDX.....	111
<b>Figure 3.12.</b> DRIFT spectra of RDX•DHE (5-25%) carbonyl region.....	111
<b>Figure 3.13.</b> DRIFT spectra of pure and coated RDX at Dantocol conc 5-25%.....	112

<b>Figure 3.14.</b> Spectra of Class 5 and recrystallised RDX coated with 5% Dantocol.....	116
<b>Figure 3.15.</b> Spectra of pure and coated HMX of 5-25% Dantocol conc.....	118
<b>Figure 4.1.</b> $^1\text{H}$ NMR of 1,3- <i>bis</i> (2-trimethylsilyloxyethyl)-5,5-dimethylhydantoin $\text{CDCl}_3$ ..	135
<b>Figure 4.2.</b> $^{13}\text{C}$ NMR of 1,3'- <i>bis</i> (2-trimethylsilyloxyethyl)-5,5-dimethylhydantoin $\text{CDCl}_3$ ..	136
<b>Figure 4.3.</b> FTIR spectrum of 1,3- <i>bis</i> (2-trimethylsilyloxyethyl)-5,5-dimethylhydantoin.....	137
<b>Figure 4.4.</b> SEM of RDX coated in TBSDHE (a) before and (b) after electron ablation..	137
<b>Figure 4.5.</b> SEM images of (a) RDX at coating concentrations of (b) 5% TMSDHE (c) 10% TMSDHE (d) 15% TMSDHE (e) 20% TMSDHE (f) 25% TMSDHE.....	138
<b>Figure 4.6.</b> IR spectra of RDX coated in TMSDHE 5-25%.....	139
<b>Figure 4.7.</b> $^1\text{H}$ NMR of <i>N</i> -(2-hydroxyethyl)- <i>N</i> -(2- <i>tert</i> -butyldimethylsilyloxyethyl)-5,5-dimethylhydantoin in chloroform- <i>d</i> .....	141
<b>Figure 4.8.</b> $^{13}\text{C}$ NMR of <i>N</i> -(2-hydroxyethyl)- <i>N</i> -(2- <i>tert</i> -butyldimethylsilyloxyethyl)-5,5-dimethylhydantoin in chloroform- <i>d</i> .....	142
<b>Figure 4.9.</b> FTIR spectrum of <i>N</i> -(2-hydroxyethyl)- <i>N</i> -(2- <i>tert</i> -butyldimethylsilyloxy-ethyl)-5,5-dimethylhydantoin.....	143
<b>Figure 4.10.</b> SEM images of (a) RDX at coating concentrations of (b) 5% TBSDHE (c) 10% TBSDHE (d) 15% TBSDHE (e) 20% TBSDHE (f) 25% TBSDHE.....	144
<b>Figure 4.11.</b> FTIR spectra of RDX coated in TBSDHE 5-25%. .....	145
<b>Figure 4.12.</b> Hydrogen bonding of Dantocol and RDX.....	146
<b>Figure 4.13.</b> Dipole interaction of Dantocol and RDX.....	147
<b>Figure 5.1.</b> DSC curve of pure/coated RDX at $\beta = 10^\circ\text{C min}^{-1}$ .....	161
<b>Figure 5.2.</b> Normalised curve of pure/coated RDX at $\beta = 5, 10, 15$ and $20^\circ\text{C min}^{-1}$ .....	163
<b>Figure 5.3.</b> Vapour pressure curves of pure/coated RDX.....	166
<b>Figure 5.4.</b> TGA curve of pure/coated RDX.....	172
<b>Figure 6.1.</b> Structural configuration of HTPB.....	191
<b>Figure 6.2.</b> $^1\text{H}$ NMR spectrum of HTPB in chloroform- <i>d</i> .....	192
<b>Figure 6.3.</b> $^{13}\text{C}$ NMR spectrum of HTPB olefinic region in chloroform- <i>d</i> .....	194
<b>Figure 6.4.</b> $^{13}\text{C}$ NMR spectrum of HTPB aliphatic region in chloroform- <i>d</i> .....	196
<b>Figure 6.5.</b> $^1\text{H}$ NMR of polyurethane and superimposed amine region in chloroform- <i>d</i> .....	197
<b>Figure 6.6.</b> $^{13}\text{C}$ NMR spectrum of polyurethane in chloroform- <i>d</i> .....	198
<b>Figure 6.7.</b> FTIR spectrum of HTPB (R45HT LO).....	199

<b>Figure 6.8.</b> FTIR spectrum of IPDI:HTPB based polyurethane.....	200
<b>Figure 6.9.</b> DSC overlay of HTPB and polyurethane glass transition temperature.....	202
<b>Figure 6.10.</b> DSC overlay of HTPB and polyurethane thermal decomposition.....	203
<b>Figure 6.11.</b> TGA overlay of HTPB and polyurethane.....	205
<b>Figure 6.12.</b> $G'$ , $G''$ , $\eta^*$ and $\tan \delta$ versus cure time for catalysed polyurethane.....	207
<b>Figure 6.13.</b> $G'$ , $G''$ , $\eta^*$ and $\tan \delta$ versus cure time for uncatalysed polyurethane.....	207
<b>Figure 6.14.</b> Plot of $\eta^*$ vs time for catalysed/uncatalysed polyurethanes.....	209
<b>Figure 6.15.</b> $^1\text{H}$ NMR of Dantocol and HTPB blend hydroxyl region in chloroform- $d$ .....	210
<b>Figure 6.16.</b> $^{13}\text{C}$ NMR of Dantocol and HTPB blend in chloroform- $d$ .....	211
<b>Figure 6.17.</b> IR overlay of HTPB and Dantocol blend.....	211
<b>Figure 6.18.</b> IR spectra of catalysed/uncatalysed polyurethane (Dantocol-IPDI).....	214
<b>Figure 6.19.</b> $^1\text{H}$ NMR of isophorone diisocyanate in $d_6$ -acetone.....	215
<b>Figure 6.20.</b> $^{13}\text{C}$ NMR of isophorone diisocyanate in $d_6$ -acetone.....	215
<b>Figure 6.21.</b> $^1\text{H}$ NMR of Dantocol and IPDI based polyurethane in $d_6$ -acetone.....	217
<b>Figure 6.22.</b> $^{13}\text{C}$ NMR of Dantocol and IPDI based polyurethane in $d_6$ -acetone.....	217
<b>Figure 6.23.</b> IR spectra of reactants IPDI, DHE and the resulting polyurethane.....	221
<b>Figure 6.24.</b> DSC curve of polyurethane based on Dantocol and IPDI.....	222
<b>Figure 6.25.</b> GPC chromatogram of polyurethane based on Dantocol and IPDI.....	224
<b>Figure 7.1.</b> FTIR spectra of the IPDI/HTPB/DHE polyurethane blend.....	246
<b>Figure 7.2.</b> FTIR spectra of (a) amide I (b) amide II peaks for polyurethanes.....	249
<b>Figure 7.3.</b> FTIR spectra of IPDI/HTPB/DHE – IPDI/HTPB = subtraction spectrum.....	250
<b>Figure 7.4.</b> FTIR spectra of polyurethane blend NH region.....	251
<b>Figure 7.5.</b> FTIR spectra of polyurethane blend amide I and II region.....	251
<b>Figure 7.6.</b> FTIR spectra of polyurethane blends.....	253
<b>Figure 7.7.</b> FTIR spectra of NH region for polyurethanes blends.....	254
<b>Figure 7.8.</b> DSC curve of polyurethanes $T_g$ .....	256
<b>Figure 7.9.</b> DSC curve of polyurethanes thermal decomposition.....	257
<b>Figure 7.10.</b> DSC curve of polyurethanes over the $T_m$ range of Dantocol.....	259
<b>Figure 7.11.</b> Rheological behaviour of polyurethane copolymer.....	260

<b>Figure 7.12.</b> Plot of $\eta^*$ vs time for polyurethane blend. ....	260
<b>Figure 7.13.</b> SEM image of PBXN-01 (a) particle agglomeration and (b) crack formation. ....	262
<b>Figure 7.14.</b> SEM images of PBX formulations (a) PBXN-01 (b) PBXN-02 (c) PBXN-03 (d) PBXN-04 (e) PBXN-05 (f) PBXN-06. ....	263
<b>Figure 7.15.</b> FTIR spectra of PBX ingredients. ....	264
<b>Figure 7.16.</b> FTIR spectra of PBX composites. ....	265
<b>Figure 7.17.</b> FTIR spectra of PBX composites C=O region. ....	267
<b>Figure 7.18.</b> Normalised DSC curve of cast-cured PBX composites indicating $T_m$ and $T_d$ . ....	271
<b>Figure 8.1.</b> Substitution of hydantoin functionality. ....	288
<b>Figure 8.2.</b> Variation of hydroxyalkyl chain length. ....	288
<b>Figure 8.3.</b> Difunctional isocyanate terminated bonding agent. ....	290
<b>Figure 8.4.</b> Meta-tetramethylxylylene diisocyanate. ....	291
<b>Figure 8.5.</b> Trifunctional isocyanate terminated bonding agent. ....	292
<b>Figure 8.6.</b> Structure of 2,3- and 1,3-dihydroxypropyl-5,5-dimethylhydantoin. ....	305
<b>Figure 8.7.</b> Commercial dendrimers applied as bonding agents. ....	308
<b>Figure 8.8.</b> Second generation polyamidoamine. ....	309
<b>Figure 8.9.</b> Hydrogen bonding between HMX and hydroxyl-functionalised dendrimer. ....	309
<b>Figure 8.10.</b> Bonding agent structures of (1) Dantocol (2) 1,3- <i>bis</i> (2-hydroxyethyl)parabanate (3) 1,2,4- <i>tris</i> (2-hydroxyethyl)urazole and (4) 1,3,4,6- <i>tetra</i> (2-hydroxyethyl)glycoluril. ....	317
<b>Figure 9.1.</b> Thermal compatibility of RDX and hydroxyalkyl ureas. ....	334
<b>Figure 9.2.</b> Thermal compatibility of RDX and hydroxyalkyl heterocycles. ....	335
<b>Figure 9.3.</b> Thermal compatibility of RDX and bonding agent adducts. ....	336
<b>Figure 9.4.</b> Load vs tensile strain of PBXs containing Dantocol/no bonding agent. ....	340
<b>Figure 9.5.</b> Load vs tensile strain of PBX comprising THEIC. ....	341
<b>Figure 9.6.</b> Load vs tensile strain of PBXs comprising bonding agent adducts. ....	343
<b>Figure 9.7.</b> Delocalised electrons associated with the hydantoin structure. ....	344
<b>Figure 9.8.</b> Delocalised electrons associated with the isocyanurate structure. ....	345
<b>Figure 10.1.</b> Bonding agent structures of (1) Dantocol (2) 1,3- <i>bis</i> (2-hydroxyethyl)parabanate (3) 1,2,4- <i>tris</i> (2-hydroxyethyl)urazole and (4) 1,3,4,6- <i>tetra</i> (2-hydroxyethyl)glycoluril. ....	362

**List of Tables**

<b>Table 1.1.</b> Commercially available bonding agents.....	9
<b>Table 3.1.</b> RDX peak shifts of OH and asymmetrical stretching NO <sub>2</sub> vibration (cm <sup>-1</sup> ).....	95
<b>Table 3.2.</b> Transmission assignment of asymmetrical NO <sub>2</sub> stretching vibration.....	99
<b>Table 3.3.</b> FSD data for asymmetrical nitro stretching vibration. ....	102
<b>Table 3.4.</b> Bonding index of Dantocol coated RDX.....	105
<b>Table 3.5.</b> PAS assignment of pure and Dantocol coated RDX ( <i>vel</i> = 0.9494cm s <sup>-1</sup> ).....	109
<b>Table 3.6.</b> Peak assignment of RDX and Dantocol coated samples.....	113
<b>Table 3.7.</b> DRIFT Spectra of RDX·DHE carbonyl region at resolution 2cm <sup>-1</sup> .....	114
<b>Table 3.8.</b> Assignment of OH, C=O and NO <sub>2</sub> peaks displaying spectral shift.....	117
<b>Table 4.1.</b> Molar attraction constants of functional groups at 25°C.....	130
<b>Table 4.2.</b> FTIR assignment of TMSDHE microencapsulated RDX.....	140
<b>Table 4.3.</b> FTIR assignment of TBSDHE microencapsulated RDX.....	146
<b>Table 5.1.</b> Effect of coating agent on ammonium azides heat of sublimation.....	156
<b>Table 5.2.</b> DSC data of pure/coated RDX at $\beta = 10^{\circ}\text{C min}^{-1}$ .....	161
<b>Table 5.3.</b> Melting point of pure/coated RDX at $\beta = 5, 10, 15$ and $20^{\circ}\text{C min}^{-1}$ .....	164
<b>Table 5.4.</b> Antoine constants as determined by nonlinear least mean fit. ....	165
<b>Table 5.5.</b> Clausius-Clapeyron approximation of the heat of sublimation. ....	167
<b>Table 5.6.</b> Activation energies of pure/coated RDX.....	169
<b>Table 5.7.</b> Critical temperature of RDX and coated samples.....	171
<b>Table 5.8.</b> TGA data of pure/coated RDX.....	173
<b>Table 6.1.</b> Hydroxyl functionality data for HTPB.....	191
<b>Table 6.2.</b> <sup>1</sup> H spectral assignment of HTPB segments.....	193
<b>Table 6.3.</b> <sup>13</sup> C NMR peak assignment of HTPB segments.....	195
<b>Table 6.4.</b> FTIR band assignment of HTPB segments.....	199
<b>Table 6.5.</b> Assignment of FTIR bands for IPDI:HTPB based polyurethane.....	201
<b>Table 6.6.</b> Thermal properties of HTPB and polyurethane.....	204
<b>Table 6.7.</b> Thermal decomposition properties of HTPB and polyurethane.....	205

<b>Table 6.8.</b> Assignment of chemical shifts for IPDI isomers.....	216
<b>Table 6.9.</b> Assignment of chemical shifts for polyurethane based on <i>cis</i> -IPDI.....	218
<b>Table 6.10.</b> Assignment of chemical shifts of polyurethane based on <i>trans</i> -IPDI.....	219
<b>Table 6.11.</b> Assignment of infrared bands for IPDI:DHE based polyurethane.....	220
<b>Table 6.12.</b> GPC data for polyurethane based on Dantocol and IPDI.....	224
<b>Table 7.1.</b> Mass fraction of polyurethane formulations.....	241
<b>Table 7.2.</b> Formulation of cast-cured PBX composites.....	242
<b>Table 7.3.</b> Assignment of infrared bands for polyurethane blend.....	247
<b>Table 7.4.</b> Polyurethane peak data of amine, amide I and II vibrational bands.....	252
<b>Table 7.5.</b> Assignment of IR bands for PBX formulations.....	266
<b>Table 7.6.</b> DSC assignment of cast-cured PBX composites.....	272
<b>Table 9.1.</b> PBX Formulations comprising 0.0% and 0.26% Dantocol.....	327
<b>Table 9.2.</b> PBX formulations comprising THEIC, DITBA or TITBA.....	327
<b>Table 9.3.</b> PBX mixing procedure.....	328
<b>Table 9.4.</b> Thermal decomposition of RDX and novel bonding agents at $\beta = 5^{\circ}\text{C min}^{-1}$ .....	333
<b>Table 9.5.</b> VTS data of RDX and novel bonding agents.....	337
<b>Table 9.6.</b> Sensitiveness testing of novel PBX formulations.....	338
<b>Table 9.7.</b> Mechanical properties of PBXs containing Dantocol/no bonding agent.....	340
<b>Table 9.8.</b> Mechanical properties of PBX formulations.....	342



## List of Schemes

<b>Scheme 1.1.</b> Reaction of HTPB with IPDI to form a Urethane linkage.....	6
<b>Scheme 1.2.</b> Reaction of isocyanates and moisture forming carbon dioxide and urea.....	18
<b>Scheme 1.3.</b> Synthesis of HX-752.....	22
<b>Scheme 1.4.</b> Proposed intermolecular interaction between AP and HX-752.....	23
<b>Scheme 1.5.</b> Synthesis of MAPO.....	25
<b>Scheme 1.6.</b> Proposed intermolecular interaction between AP and MAPO.....	25
<b>Scheme 1.7.</b> Synthesis of 1,1',1''-(1,3,5-benzenetriyltricarboxyl) <i>tris</i> (2-ethylaziridine).....	26
<b>Scheme 1.8.</b> Interaction of BTMF with AP and HTPB.....	28
<b>Scheme 1.9.</b> Synthesis of 1,3'- <i>bis</i> (2-hydroxyethyl)-5,5-dimethylhydantoin.....	29
<b>Scheme 4.1.</b> Hydroxyl protection via formation of trimethylsilyl imodazole.....	129
<b>Scheme 4.2.</b> Synthesis of 1,3- <i>bis</i> (2-trimethylsilyloxyethyl)-5,5-dimethylhydantoin.....	131
<b>Scheme 4.3.</b> Synthesis of <i>N</i> -(2-hydroxyethyl)- <i>N</i> -(2- <i>tert</i> -butyldimethylsilyloxyethyl)-5,5-dimethylhydantoin.....	133
<b>Scheme 6.1.</b> Reaction of HTPB with IPDI to form a urethane linkage.....	181
<b>Scheme 6.2.</b> Side reactions that may occur in isocyanate and hydroxyl systems.....	182
<b>Scheme 6.3.</b> Urethane reaction involving Dantocol and toluene-2,4-diisocyanate.....	184
<b>Scheme 6.4.</b> Polymerisation of IPDI with Dantocol.....	212
<b>Scheme 7.1.</b> Urethane linkages participating in hydrogen bonding.....	235
<b>Scheme 7.2.</b> Reaction of alcohol and isocyanate to form polyurethane.....	236
<b>Scheme 7.3.</b> Urethane catalysed reaction of polyurethane.....	236
<b>Scheme 7.4.</b> Interfacial adhesion involving Dantocol at the filler/binder system interface.....	276
<b>Scheme 8.1.</b> Synthesis of 1,3- <i>bis</i> (2,3-dihydroxypropyl)-5,5-dimethylhydantoin.....	293
<b>Scheme 8.2.</b> Synthesis of 1,3- <i>bis</i> (2-hydroxyethyl)urea.....	294
<b>Scheme 8.3.</b> Synthesis of 1,1,3- <i>tris</i> (2-hydroxyethyl)urea.....	295
<b>Scheme 8.4.</b> Synthesis of 1,1,3,3- <i>tetrakis</i> (2-hydroxyethyl)urea.....	296
<b>Scheme 8.5.</b> Synthesis of 1,3- <i>bis</i> [3-hydroxy-1,1- <i>bis</i> (2-hydroxyethyl)propyl]urea.....	296
<b>Scheme 8.6.</b> Synthesis of dendrimeric polycarbamate.....	297
<b>Scheme 8.7.</b> Isocyanurate acid and cyanuric acid tautomers.....	298

<b>Scheme 8.8.</b> Synthesis of 1,3- <i>bis</i> (2-hydroxyethyl)parabanate.....	299
<b>Scheme 8.9.</b> Synthesis of 1,2,4- <i>tris</i> (hydroxyethyl)urazole.....	300
<b>Scheme 8.10.</b> Synthesis of 1,3,4,6- <i>tetra</i> (2-hydroxyethyl)glycoluril.....	301
<b>Scheme 8.11.</b> Self-polymerisation of glycidol to polyglycidol. ....	306
<b>Scheme 8.12.</b> Side reaction of hydroxyalkyl groups and unreacted ethylene oxide.....	311
<b>Scheme 8.13.</b> Polymerisation of 1,3- <i>bis</i> (2-hydroxyethyl)parabanate.....	313
<b>Scheme 10.1.</b> Interfacial adhesion involving Dantocol at the filler/binder system interface.....	359



